Volume 2

PART D

IMPACTS DURING THE KNITTING OPERATION

CHAPTER 11.

PRELIMINARY

11.1 Needle Damage at High Machine Speed.

As the rotational speed of a knitting machine is increased, the incidence of needle fracture at the head and butt also increases. The time spent in replacing the broken elements offsets any advantages that could be obtained from running the machine at high speed in an attempt to obtain an increased fabric production rate. Until the mechanisms of needle fracture are thoroughly understood it will be impossible to design machine elements that can operate satisfactorarily at high speed.

Needles break at the beginning of the hook bend, at the butt, and, less frequently, across the latch pivot, as indicated in Fig 11.1. Fig 11.2 is a diagram showing a typical sample of fractured needles.

Later experiments, discussed more fully in chapter 19 and 20, were to demonstrate that the majority of the butt fractures originate from the top of the butt and only occasionally from the bottom. Fig 11.2 shows the fracture in a transition stage before the butt is completely separated from the shank.

The head fracture occurs at the beginning of the hook bend, at the thinnest section of the needle shank. The results of measurements carried out at the Bentley Machine Development Co. Ltd. have indicated that head fracture occurs at approximately the same rate, independently whether the machine is knitting or the needles are passing through the cams without knitting. These experiments also

indicated that latch impact is not the primary cause of head fracture, although it certainly could be a contributory factor at high knitting speeds.

A metallurgical examination of the fracture surfaces of a sample of latch needles, that had broken at the hook bend during normal service, was carried out at the Bentley Machine Development Co. Ltd. The metallurgist suggested that the fracture surface was characteristic of pure tensile failure and he could not determine any evidence to suggest a fatigue failure.

11.2 Reasons for Impact Measurements.

The major reasons for embarking upon a detailed analysis of the cam-needle impact, and its effect upon needle fracture, are summarised below :-

(i) Petrow[33 to 37 inc] predicted theoretically that an impact between the cams and knitting elements would generate a stress wave that would reach damaging proportions just at the beginning of the bend of the hook. Subsequent to his analysis, he redesigned some needles and successfully increased the normal operating speed of the knitting machine.

(ii) Measurements using the tranducer mark (III) see Fig 8.16 (b) section 8.5.4, indicated that there was an impact just at the point where the needle first contacted the stitch-cam. This impact became more prominent as the machine speed was increased.

(iii) As machine speed increased the fracture rate also increased and it was difficult to see how the steady level of cam-force, as measured with the transducer mark (III), could be responsible for this. Experiments, see Fig 8.16 (b) section 8.5.4, indicated that the cam-force did not

change very much as machine speed was increased, unless a heavy addition of oil was applied to the trick.

(iv) At high machine speed, needle head fracture occurred, even if the needles were running through the cams without yarn being fed to the hooks. Other than stress-wave propagation or hook vibration, there was no other constraint or force acting on the needle hook. Stress-waves or hook vibration could only be generated by a rapidly applied impact force.

11.3 Inability of the Cam-force Transducer Mark III to Measure the Impact.

As an initial approximation, the transducer beam was idealised as a simple spring mass system with the spring stiffness and mass analogous to the beam stiffness and mass. When two elastic systems collide, the force pulse that instantaneously exists at the impact point is often a half-sinusoidal pulse as shown in Fig 11.3. The response of the transducer beam to a half sine-wave of duration π/ω seconds, where ω is the pulse frequency in rads/sec, can be represented by the equation :-

$$\frac{d^2y}{dt^2} + \omega_n^2 = F(t) \quad \ldots \quad (50),$$

where: $\omega_n^2 = \frac{k}{m}$,

k and m are defined in Fig 11.3.

$$F(t) = F_0 \sin(\omega t) \qquad 0 \leqslant t \leqslant \pi/\omega,$$

$$F(t) = 0 \qquad t \geqslant \pi/\omega,$$

and $\frac{d^2y}{dt^2}$ = the acceleration of mass m,

The solution of the equation is the sum of the complementary function and the particular integral. It has the form shown below :-

$$y = A\sin(\omega_n t + \phi) + \frac{F_o \sin(\omega t)}{k\left(1 - \left(\omega/\omega_n\right)^2\right)}.$$

The constants A and ϕ can be determined from the initial conditions :-

$$\ddot{y} = \frac{d^2y}{dt^2} = 0,$$

when $t = 0$.

The following equation is then derived :-

$$y = \frac{F_o}{k\left(1 - \left(\omega/\omega_n\right)^2\right)}\left(\sin(\omega t) - \left(\omega/\omega_n\right)\sin(\omega_n t)\right) \qquad (51).$$

If the beam natural frequency ω_n is several magnitudes higher than the pulse frequency ω ,

then y is approximately equal to $\frac{F_o}{k}\sin\omega t$,

$$\text{or} \quad k y_{max} = F_o,$$

and static calibration of the beam can therefore be used with a good degree of accuracy.

However, if ω_n is not very much larger, or even smaller, than the pulse frequency ω , then the pulse shape recorded by the strain-guages would be considerably different from the actual forcing pulse shape, and there would be a large amount of beam resonant frequency after the impact.

An experiment was carried out to determine the response of the cam-force transducer mark III to the impact at the instant of needle stitch-cam contact. The filters illustrated in Fig 5.5 were not connected into the circuit. The experimental traces obtained, showed severe beam natural frequency

oscillation, and a low magnitude initial pulse at the moment of contact. From these results it was concluded that the pulse frequency was either similar to, or considerably higher than, the beam natural frequency.

The cam-force transducer mark III was therefore not considered to be a suitable instrument for the measurement of the impact process because the beam natural frequency was to low.

11.4 Requirements of an Impact Measuring Device.

A successful impact measuring transducer must satisfy two basic requirements :-

(i) It must have a natural frequency considerably higher than the highest significant frequency component of the pulse.

(ii) The measuring system attached to the transducer must be capable of recording a signal in response to the impact.

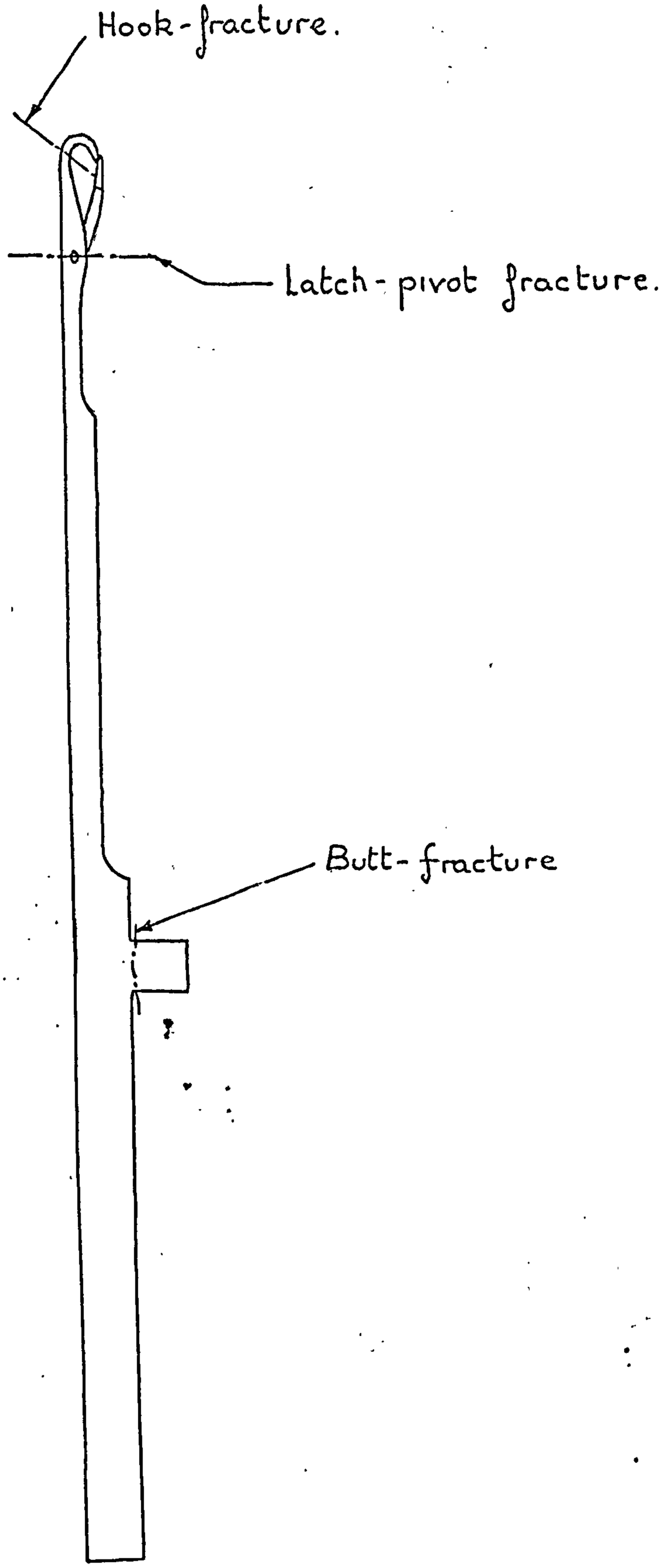

POSITIONS OF THE MOST FREQUENT NEEDLE FRACTURES

Fig 111

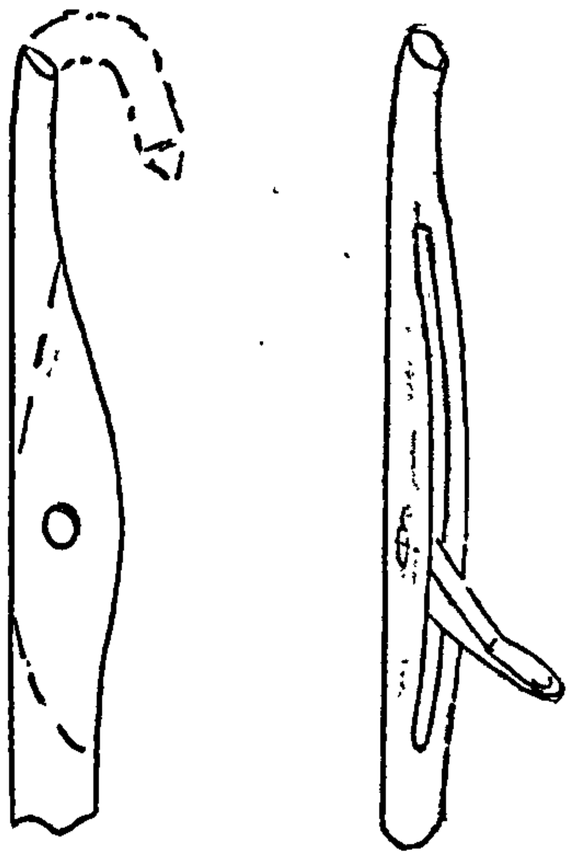

Breakage at
hook bend

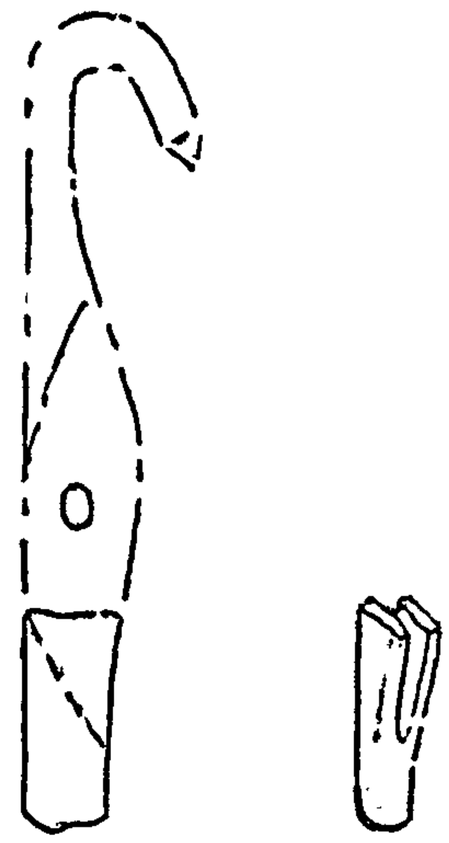

Breakage below
latch pivot.

Breakage at Butt
originating at base
before complete fracture

Breakage at Butt
originating at top
before complete fracture

FRACTURE POSITIONS ON KNITTING NEEDLE.

FIG 11.2

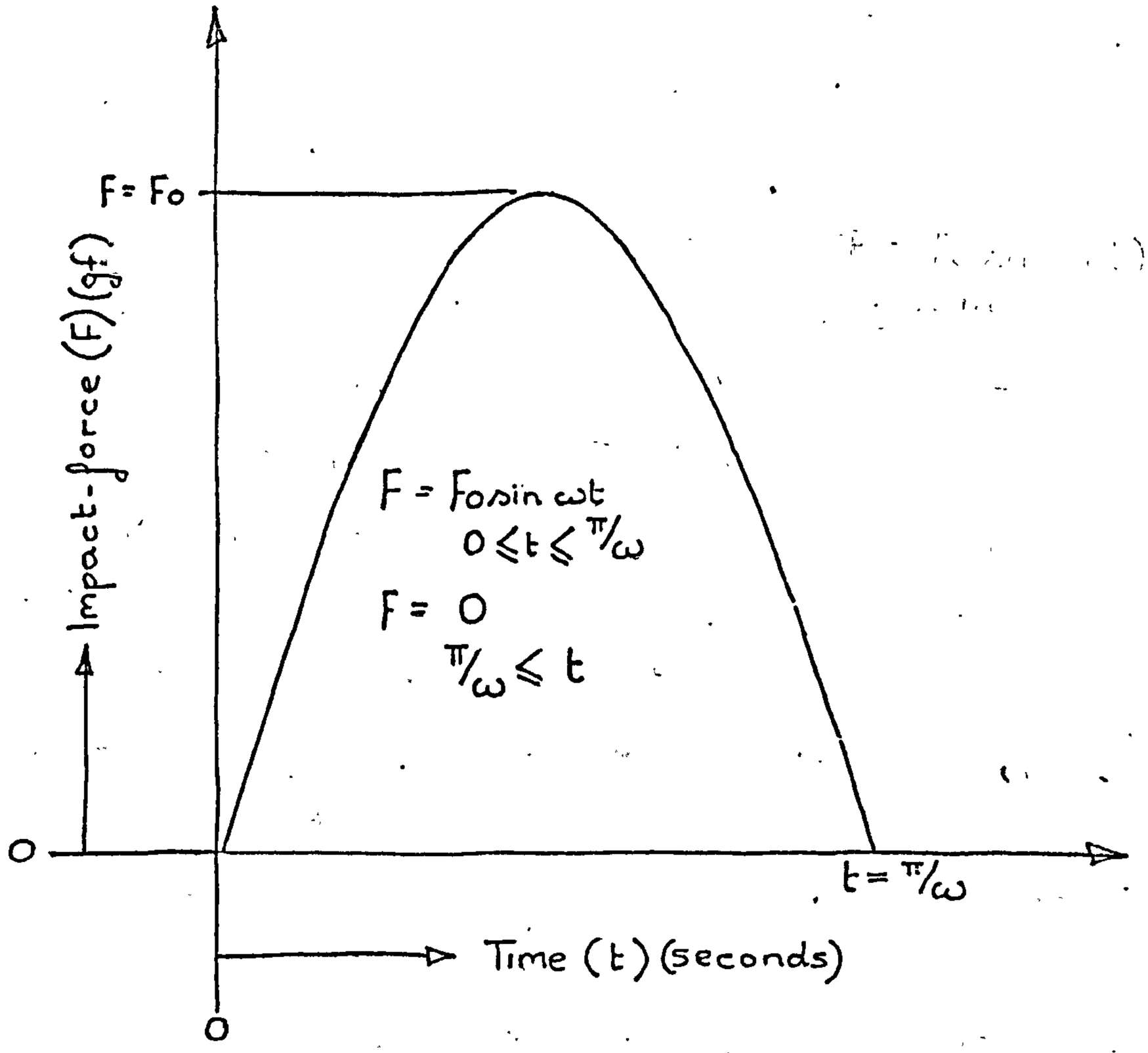

Where ω = pulse frequency
F = impact force

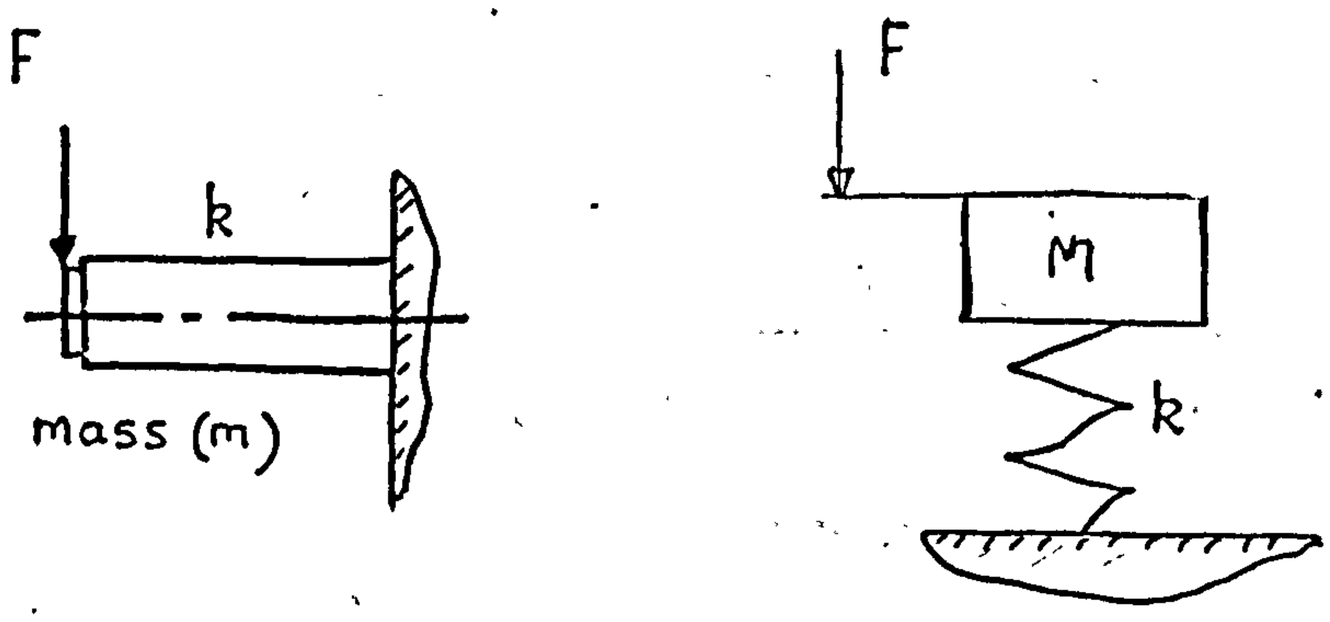

m = idealised beam mass.
k = beam stiffness.

Half-sine impact pulse.

FIG 11.3

CHAPTER 12

STITCH-CAM IMPACT

12.1 The Need for an Understanding of the Impact before an Instrument can be Designed.

Before an impact measuring device is designed it is essential that some knowledge of the impact pulse shape and magnitude is obtained since, without this knowledge, it is impossible to know what natural frequency and strain sensitivity the measuring instrument must have. Additionally, a theoretical analysis is desirable, because it would indicate the manner in which the various parameters influence the impact process, and because it would offer guidance as to the manner in which subsequent experiments should be carried out. However, it is dangerous as well as unscientific, to assume that any initial hypothesis is automatically valid, because frequently experimental results demand that fundamental changes should be made to the theory before it can become a reasonably true representation of the impact process.

12.2 Theoretical Prediction of Stitch-cam Impact.

A theoretical examination of the impact process was undertaken and the results of the analysis formed the subsequent basis for the design of a measuring instrument.

The forces acting upon the needle at the instant it contacts the stitch cam are shown in Fig 12.1, and the nomenclature used in this theoretical analysis is defined in Fig 12.2.

Initially, when the needle first contacts the cam, the butt deflects and bends until the vertical component of the cam-needle reaction force reaches a value that will

just overcome the static trick resistance and start the needle's acceleration downwards.

The limiting value of the vertical force just before vertical motion begins, can be determined from the force relationship shown on Fig 12.1.

$$R_y = k\mu_1 Q + k_1\mu_1 (R_k + S) + P_s - mg, \quad \ldots \quad (52),$$

$$R_x = \frac{bS}{a}, \quad \ldots \quad (53),$$

and $R_k + R_s = S$,

where $R_y = R(\cos\theta - k_2\mu_2 \sin\theta)$, $\ldots$ (54),

and $R_x = R(\sin\theta + k_2\mu_2 \cos\theta)$. $\ldots$ (55).

Let $H_s = P_s + k_1\mu_1 Q - mg$,

therefore from the above equations (52) to (55) the following equation for R can be derived :

$$R = \frac{H_s}{\cos\theta\,(1 - \alpha k_1 k_2 \mu_1 \mu_2) - \sin\theta\,(k_2\mu_2 + \alpha k_1\mu_1)}, \quad (56),$$

where $\alpha = \frac{2a}{b} - 1$.

As soon as the needle begins to move downwards an accelerating force exists :-

$$R_y - \mu_1 Q - \mu_1 (R_k + S) - P_d - F + mg = m\frac{d^2y}{dt^2}. \quad (57).$$

A great simplification in the analysis can be made if, at this initial stage, the viscous resistance F is assumed negligible, (note: further work concerning the effect of the viscous drag upon the impact is contained in section 12.3.2.)

In equation(57), if we say :

$$R_x = \frac{bS}{a}, \quad . \quad . \quad . \quad . \quad . \quad (58),$$

$$H_d = \mu_1 Q + P_d - mg, \quad . \quad . \quad . \quad (59),$$

and $R_k + R_x = S$, ... (60),

then equation(57) simplifies to a form :-

$$R_y - H_d - \mu_1 \propto R_x = m \frac{d^2y}{dt^2} \quad . \quad . \quad . \quad (61).$$

Fig 12.3 shows the motion of the needle butt just as it begins to move vertically downwards, and from this the following equations can be derived :-

$$x - \delta v = y \cot an \theta, \quad . \quad . \quad (62),$$

$$\text{but } x = vt,$$

and therefore $$\delta v = vt - y \cot an \theta. \quad . \quad . \quad (63).$$

At this stage in the analysis it was important to determine the relationship between the horizontal force acting on the butt and the resulting butt deflection. However, this is not at all easy to predict theoretically, because a large number of parameters influence the butt deflection under load, some of which are summarised as follows :-

(i) the clearance between the needle shank and the trick-walls,

(ii) the stiffness of the trick walls,

and (iii) whether there are needles in tricks immediately adjacent to the needle under load.

It was considered a simpler and more reliable operation to measure the butt deflection by experiment and then

attempt a theoretical analysis of butt deflection under load.

The experimental and theoretical analysis of butt deflection is detailed in section 12.4. A close fit to the experimental result can be obtained using the theoretical expression :-

$$R_x = K\delta v\left(1 - e^{-B\delta v}\right), \quad . \quad . \quad . \quad (64),$$

where K and B = constants.

The resulting analysis using equation (64) became highly complex and non-linear differential equations resulted. Consequently, for an initial examination, it was decided to approximate the shape of the butt deflection graph to a form that would serve to simplify the analysis.

A reasonable approximation to the shape is shown in Fig 12.4, which is represented by an equation of the form :-

$$R_x = K(\delta v - G) \qquad \delta v \geqslant G \quad . \quad . \quad (65)$$

and $$R_x = 0 \qquad \delta v \leqslant G$$

where K and G are cam-angle dependent.

It was considered that the simplification would involve maximum error at low speed when the butt deflection at impact is small.

Using the simplification :

$$K\delta v = R_x + KG \quad . \quad . \quad . \quad . \quad (66),$$

let $$K\delta v = N_x \quad . \quad . \quad . \quad (67).$$

Where N_x is a horizontally applied force,

and hence $$N = N_x(\sin\Theta + \mu_2\cos\Theta) \quad . \quad . \quad (68),$$

The response y was evaluated for a slope deflection graph that is linear and of slope K to the origin. The force N_x can be determined from the response and corrected using equation (66). If the term $K(\delta v - G)$ had been used in the analysis, then it would have been difficult to define y and $\frac{dy}{dt}$ at $t = 0$ because equation (65) is only defined for: $\delta v \geq G$.

Using equation (61), and substituting N for R, the following equation is derived :-

$$N(\cos\theta - \mu_2 \sin\theta) - H_d - \mu_1 \propto N(\sin\theta + \mu_2 \cos\theta) = m\left(\frac{d^2y}{dt^2}\right), \quad (69),$$

which becomes :-

$$N(\cos\theta(1 - \propto\mu_1\mu_2) - \sin\theta(\mu_2 + \propto\mu_1)) - H_d = m\left(\frac{d^2y}{dt^2}\right), \quad (70).$$

Therefore from equations (70), (67) and (68):

$$\frac{K(\delta v)}{\sin\theta + \mu_2\cos\theta}\left(\cos\theta(1 - \propto\mu_1\mu_2) - \sin\theta(\mu_2 + \propto\mu_1)\right) - H_d = m\left(\frac{d^2y}{dt^2}\right), \quad (71).$$

Let

$$\frac{K\left(\cos\theta(1 - \propto\mu_1\mu_2) - \sin\theta(\mu_2 + \propto\mu_1)\right)}{\sin\theta + \mu_2\cos\theta} = D, \quad (72),$$

then

$$D(\delta v) - H_d = m\left(\frac{d^2y}{dt^2}\right), \quad (73),$$

and from equations (73) and (63):

$$D(vt - y\,\mathrm{cotan}\,\theta) - H_d = m\left(\frac{d^2y}{dt^2}\right). \quad (74).$$

Finally

$$\frac{d^2y}{dt^2} + \left(\frac{D\,\mathrm{cotan}\,\theta}{m}\right)y = \frac{Dv\,t}{m} - \frac{H_d}{m} \quad (75).$$

The solution of equation(75)has the form :-

$$y = vt\tan\theta - \left(\frac{H_d}{D}\right)\tan\theta - a\sin(nt+\phi), \quad . \quad . \quad (76),$$

where n is a frequency term given by :-

$$n = \sqrt{\frac{D\cot an\theta}{m}} \quad rads/sec. \quad . \quad . \quad (77).$$

When

$$t = 0, \quad y = 0, \quad \frac{dy}{dt} = 0,$$

then

$$\sin\phi = -\frac{1}{a}\left(\frac{H_d}{D}\right)\tan\theta \quad . \quad . \quad . \quad . \quad (78),$$

$$\cos\phi = \frac{v\tan\theta}{na} \quad . \quad . \quad . \quad . \quad (79),$$

and hence

$$a^2 = \tan^2\theta\left(\left(\frac{v}{n}\right)^2 + \left(\frac{H_d}{D}\right)^2\right) \quad . \quad . \quad . \quad . \quad (80).$$

The reaction force R can also be derived from equation(66) :-

$$N = \frac{K\delta v}{\sin\theta + \mu_2\cos\theta} \quad . \quad . \quad . \quad . \quad (81).$$

Using equation(63), equation (81) becomes :-

$$N = \frac{K(vt - y\cot an\theta)}{\sin\theta + \mu_2\cos\theta} \quad . \quad . \quad . \quad . \quad (82),$$

and substituting equation (76) for y, equation (82) becomes :-

$$N = \frac{K\left(\frac{H_d}{D} + a\cot an\theta\sin(nt+\phi)\right)}{\sin\theta + \mu_2\cos\theta} \quad . \quad . \quad (83),$$

and

$$N_x = K\left(\frac{H_d}{D} + a\cot an\theta\sin(nt+\phi)\right) \quad . \quad . \quad (84).$$

As $$R_x + KG = N_x \quad . \quad . \quad . \quad (85),$$

then $$R_x = K\left(\frac{H_d}{D} + a\cot\theta\sin(nt+\phi) - G\right) \quad (86).$$

Finally

$$R = \frac{K\left(\frac{H_d}{D} + a\cot\theta\sin(nt+\phi) - G\right)}{\sin\theta + \mu_2\cos\theta} \quad (87),$$

$$\text{for } vt - y\cot\theta \geqslant G$$

and $$R = 0 \quad \text{for } vt - y\cot\theta < G.$$

The equations governing the motion of the needle-butt, and the force instantaneously created between the butt and the cams, are summarised below :-

$$y = vt\tan\theta - \left(\frac{H_d}{D}\right)\tan\theta - a\sin(nt+\phi) \quad (88),$$

where

$$n = \sqrt{\frac{D\cot\theta}{m}} \quad . \quad . \quad . \quad (89),$$

and

$$\cos\phi = \frac{v\tan\theta}{na} \quad . \quad . \quad . \quad (90),$$

and

$$a^2 = \tan^2\theta\left(\left(\frac{v}{n}\right)^2 + \left(\frac{H_d}{D}\right)^2\right) \quad . \quad . \quad (91),$$

and finally using the approximate butt-deflection graph:-

$$R = \frac{K\left(\frac{H_d}{D} + a\cot\theta\sin(nt+\phi) - G\right)}{\sin\theta + \mu_2\cos\theta} \quad (92),$$

$$\text{for } vt - y\cot\theta > G,$$

and

$$R = 0 \quad \text{for } vt - y\cot\theta < G.$$

Fig 12.5 is a diagram intended to provide a physical interpretation of the needle motion on the cam at the instant of impact, but a more detailed analysis is carried out in chapter 14, where the theoretical and experimental results are compared.

12.3 Omissions and Simplifications contained in the theory.

Some assumpticns and modifications were made to the theory in order to simplify the analysis. It was important that the effects of these simplifications were clearly understood before the theory was used for the design of an impact transducer. A brief summary of the major assumptions is as follows :-

(i) The butt deflection under load.

(ii) The viscous damping term.

(iii) The surface profile of the cam. Each of these is treated individually in the following subsections.

12.3.1 Butt-Deflection under Load.

The major simplification of the analysis is the linearisation of the graph of butt deflection against horizontal load. The effect of this simplification upon the analysis is examined in chapter 14.

The butt deflection was measured during a static examination and it is possible that an inertial component of force exists when the machine is running at high speed.

As an approximation which is reasonably accurate for determining the fundamental frequency, the beam can be represented as a simple spring mass system. The spring stiffness and the mass is analogous to an equivalent butt stiffness and mass.

If a force is applied to the spring mass system the

following equation can be derived :-

$$\frac{d^2(\delta v)}{dt^2} + \frac{K}{m_v}(\delta v) = R_x(t) \quad . \quad . \quad . \quad . \quad (93),$$

where δv = butt deflection.

$\Omega = \sqrt{K/m_v}$ = butt natural frequency.

$R_x(t)$ = horizontal applied force as a function of time.

K = butt stiffness.

m_v = equivalent butt mass.

From equation (93):

$$M.F = \frac{1}{1 - \left(\omega/\Omega\right)^2} \quad . \quad . \quad . \quad (94),$$

where $M.F$ = the magnification factor (defined as the ratio of the amplitude to the deflection that a static force of magnitude F would produce)

An estimation of the butt natural frequency was carried out using an approximate value for m_v, from which it was obvious that the frequency was considerably higher than the pulse frequency which is measured and examined in chapter 14. Using this result M.F is very nearly equal to 1 and a static calibration is therefore justified.

12.3.2 The Viscous Damping Term.

To simplify the analysis, the effect of the oil upon the impact was neglected. The final solution, obtained from the theory, predicted an undamped oscillation of frequency h rads/sec. It was expected that the oil would act as a damper and eventually reduce the amplitude of the oscillation to zero. The stitch-cam impact transducer, which is detailed in chapter 13 was used in an experiment to determine the effect

of the oil upon the impact process.

A fuller explanation of experimental method using this transducer is left until chapter 14. However, initially a trick, a 0.443 mm needle and the cam were thoroughly cleaned with solvent and dried. The machine was then run and a photographic trace was taken. A large amount of oil was then applied to the trick, the machine was re-run at the same speed, and another trace was obtained.

Inall, a range of similar tests were carried out at a wide range of machine speeds. Typical samples are included in Figs 12.5 (a) and (b).

From the results the following conclusions were drawn :-

(i) The oil had a negligible effect upon the magnitude of the primary impact.

(ii) The oil shortened the time of needle bounce on the stitch-cam.

(iii) The oil tended to decay the oscillation magnitude.

The terms "primary impact" and "bounce" are discussed in more detail in chapter 13 and 14.

12.3.3 Effect of the Surface Profile of the Cam upon the Impact.

The theory assumes that the cam surface at the point of impact is defined by the cam angle, θ, and, in practice, wear takes place to a far greater extent at the point of impact than at other points on the cam surface. Because such excessive wear alters the cam angle, the theory must be modified to allow for this change of cam-shape.

12.4 Measurement of the Butt-Deflection under Load.

A special cam shaped as shown in Fig 12.7 was

fitted to the beam of the stitch cam impact transducer detailed in chapter 13. A needle positioned in a cleaned trick was forced against the cam. As the butt deflected under load the cylinder moved forward slightly, and a 0.0001 inch, dial gauge fitted to the stationary machine mounting recorded the cylinder movement, as shown in Fig 12.7. As further load was applied to the cam, the output voltage from the transducer was recorded on the Tektronix Storage Oscilloscope. An explanation of the circuitry used in conjunction with the stitch-cam impact transducer is given in chapter 13.

The butt deflection characteristic was measured for the four different circumstances, detailed below :-

(i) A test carriedout on a standard 0.443 mm needle, with needles fitted in the tricks on each side of the necdle under test.

(ii) A test carried out on a standard 0.443 mm needle, with the tricks on each side of the test needle left empty.

(iii) A test carried out on a crimped 0.406 mm needle, the crimp being as shown in Diagram I of Fig 12.8.

(iv) A test carried out on a modified 0.443 mm needle, the butt shape being as shown in Diagram II of Fig 12.8.

Four experimental graphs were plotted of butt-deflection against oscilloscope trace deflection, for each of the conditions (i) to (iv) and these are shown in Figs 12.9 to 12.12 respectively.

A possible explanation for the shape of the butt deflection graph is that initially, when load is applied,

the needle is being deformed into the trick, as illustrated in Fig 12.13. The force deflection characteristic in this region would be highly variable because no needle or trick has precisely the same shape. When tests were carried out on a large number of needles in various tricks, it was discovered that the initial low force region was highly variable while the high-force characteristic was much more constant (see Fig 12.9). When the needle with the modified butt shown in Fig 12.8 diagram II was tested (with backing needles in adjacent tricks) the butt stiffness (Fig 12.12) was reduced; however the lowest value of K was obtained when the standard 0.443 mm needle was tested (Fig 12.10) with the backing needles removed from the tricks immediately around the test needle. These two experiments, and others, indicated that the largest contribution to the butt deflection under load was actually trick wall deflection, the butt contributing only a relatively small amount to the total deflection under high loads.

The slope of the graph (Fig 12.11) when loading the 0.406 mm crimped needle shown in diagram I of Fig 12.8, was not very much different to the deflection slope under load for the standard 0.443 mm needle. Initially, when loading the crimped needle, a large deflection occurred for only a small load; this region corresponded to the straightening out of the needle crimp.

12.4.1 Theoretical Estimate of Butt Deflection under Loads.

Fig 12.14 is a diagram of the forces acting on the needle butt, from which it is obvious that, when the

cam-cylinder clearance is small, the butt deflection is very small. From the geometry of the drawing the trick wall would deflect most when the butt was loaded. The major difficulty with any form of theoretical approach to the problem is that it is very difficult to determine how much of the verge wall is taking part in the bending process. However, treating the trick wall as a cantilever in simple bending, it would need to be 2.45 in. wide to produce a force per unit deflection of 6000 lbf/in. The derivation of the figure (2.45 in.) is shown in Fig 12.14.

12.4.2 The Dependence of K and G upon the Cam Angle.

To simplify the theoretical analysis an approximation was made to the shape of the butt-deflection against load characteristic. As shown in section 12.2 the shape of the graph was represented by the equation :-

$$R_x = K(\delta v - G) \quad . \quad . \quad . \quad . \quad . \quad (95),$$

where R_x = the horizontal component of cam reaction force

K = the graph slope

δv = butt deflection

G = intersept of graph with vertical axis.

It was obvious from the theoretical analysis, that during normal service, the horizontal force acting on the needle butt for steep-angled cams would be considerably larger than when shallower-angled cams were used. It was decided to weight the factors K and G according to cam-angle. The manner in which this weighting was carried out is shown in Fig 12.15, which is a butt deflection against load graph for a standard 0.443 mm needle, with needles fitted in the surrounding tricks; this particular needle and its trick were used for the majority of experiments detailed in chapter

14.

From Fig 12.15, the following values of K and G were determined :-

(i) Cam-angle $\theta = 60^{\circ}$ $K = 5,980$ lbf/inch, $G = 11.36 \times 10^{-4}$ in.

Using these values the theoretical solution should be accurate for horizontally applied loads above 1000 gf. The maximum error occurs at very small values of horizontal load.

(ii) Cam-angle $\theta = 45^{\circ}$ $K = 4,070$ lbf/inch, $G = 8.35 \times 10^{-4}$ in.

Using these values the theoretical solution should be accurate for horizontally applied loads of between 450 and 1,900 gf. Maximum errors should occur at very small and very large values of horizontally applied load.

(iii) Cam-angle $\theta = 30^{\circ}$ $K = 2,600$ lbf/inch, $G = 5.36 \times 10^{-4}$ in.

Using these values the theoretical solution should be accurate for horizontally applied loads of between 236 and 1,000 gf. Maximum errors occur at very small and very large loads.

Values of K and G were selected for other cam angles and a graph was drawn of the K and G variation as shown in Fig 12.16.

12.5 Measurements of the Coefficients of Friction.

Before the theoretical analysis could be used to determine the required natural frequency of the stitch-cam impact transducer, and for comparison with experimental results, it was important that the coefficients of friction should be measured as accurately as possible.

The coefficients of friction between the needle and the cam, and the needle and trick were measured in section

9.3. Because the needle was now being run in a different trick, and the cams were different to those used in section 9.3 it was decided to remeasure the coefficients. The tests were carried out using the same method detailed in section 9.3. First, the coefficient of cam-needle friction, μ_2, was calculated from the experimental traces of vertical and horizontal impact, and then independent tests were carried out using the tilting table shown in Fig 9.4. The measurements were carried out with a light smear of oil on the cam surface. The actual values determined were slightly lower than those quoted in section 9.3. Although the coefficient of cam-needle friction, measured using the tilting table was only very slightly less than that determined in section 9.3, the value obtained from the trace was much less. A mean-value of the cam-needle coefficient was assumed to be $\mu_2 = 0.08$, and the value of the trick-needle coefficient used was $\mu_1 = 0.10$.

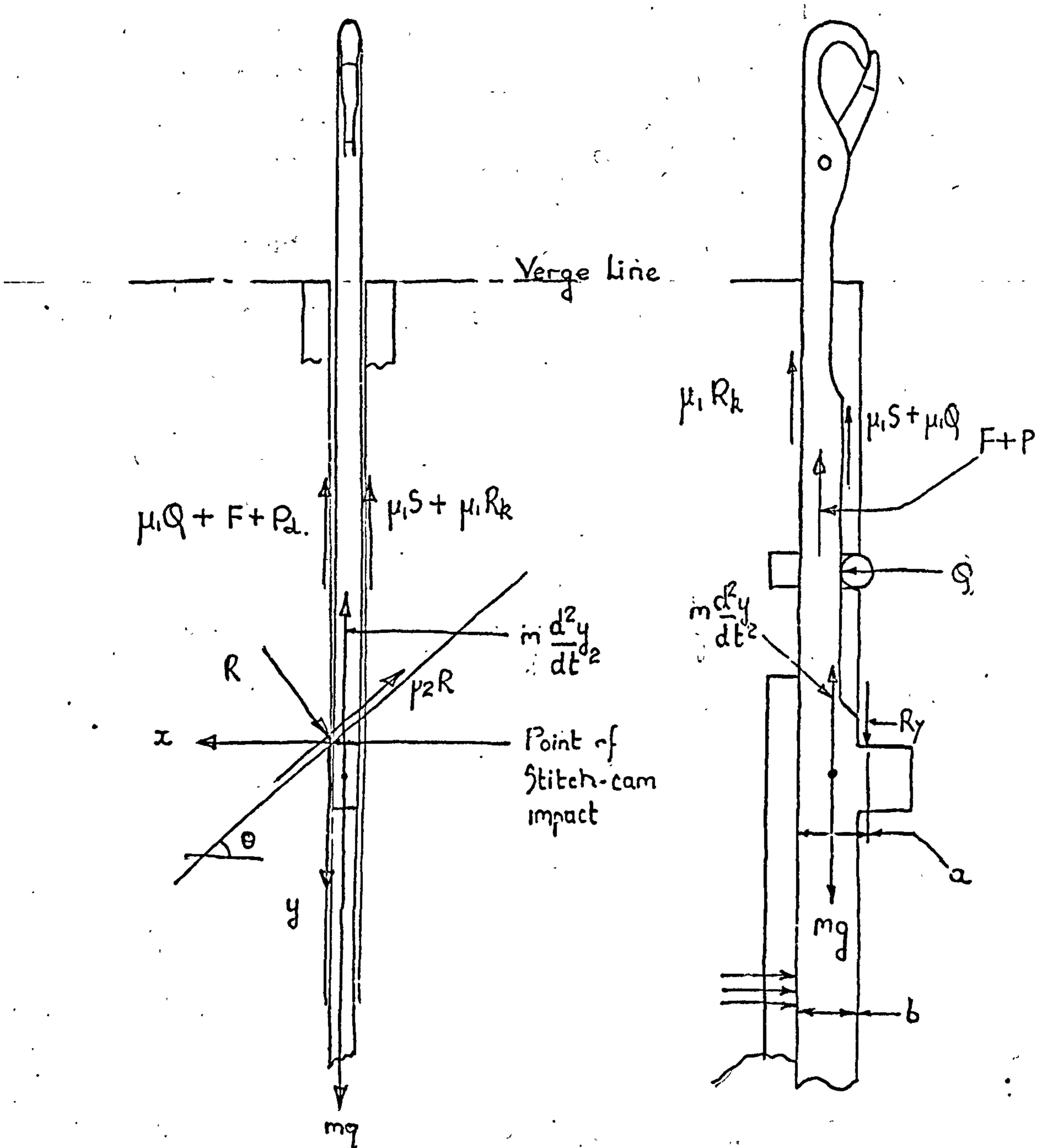

Forces on the Needle
at the Instant of Stitch Cam Impact. FIG 12.1
(for nomenclature used see FIG 12.2)

F = viscous drag from oil

P_d = trick clamping force (dynamic)

S = side reaction force

μ_2 = coefficient of friction (cam to needle) } dynamic

μ_1 = " " " (trick to needle) }

m = needle mass

mg = needle weight

t = time

$M \frac{d^2y}{dt^2}$ = inertial force

$\frac{dy}{dt} = v$ = vertical velocity

$\frac{dx}{dt}$ = machine peripheral horizontal velocity

$\frac{d^2y}{dt^2}$ = vertical acceleration

δv = butt deflection

R = cam-needle reaction force

R_x = horizontal component of R

R_y = vertical component of R

R_k = side reaction force }

a = reaction force (R) moment arm } see Fig 12.1 for further explanation

b = reaction force (S) moment arm }

Q = band-spring force

θ = cam-angle

$k_1\mu_1$ = static coefficient of friction trick to needle

$k_2\mu_2$ = " " " " cam to needle

P_s = trick clamp force (static)

H_s, α, H_d, N } defined in text

K = butt-deflection against load graph-slope

G = " " " " " intersect with axis

n, a, D, ϕ } defined in text

— Nomenclature used in Impact Analysis (section 12.2) (see also Fig 12.1)

Fig 12.2

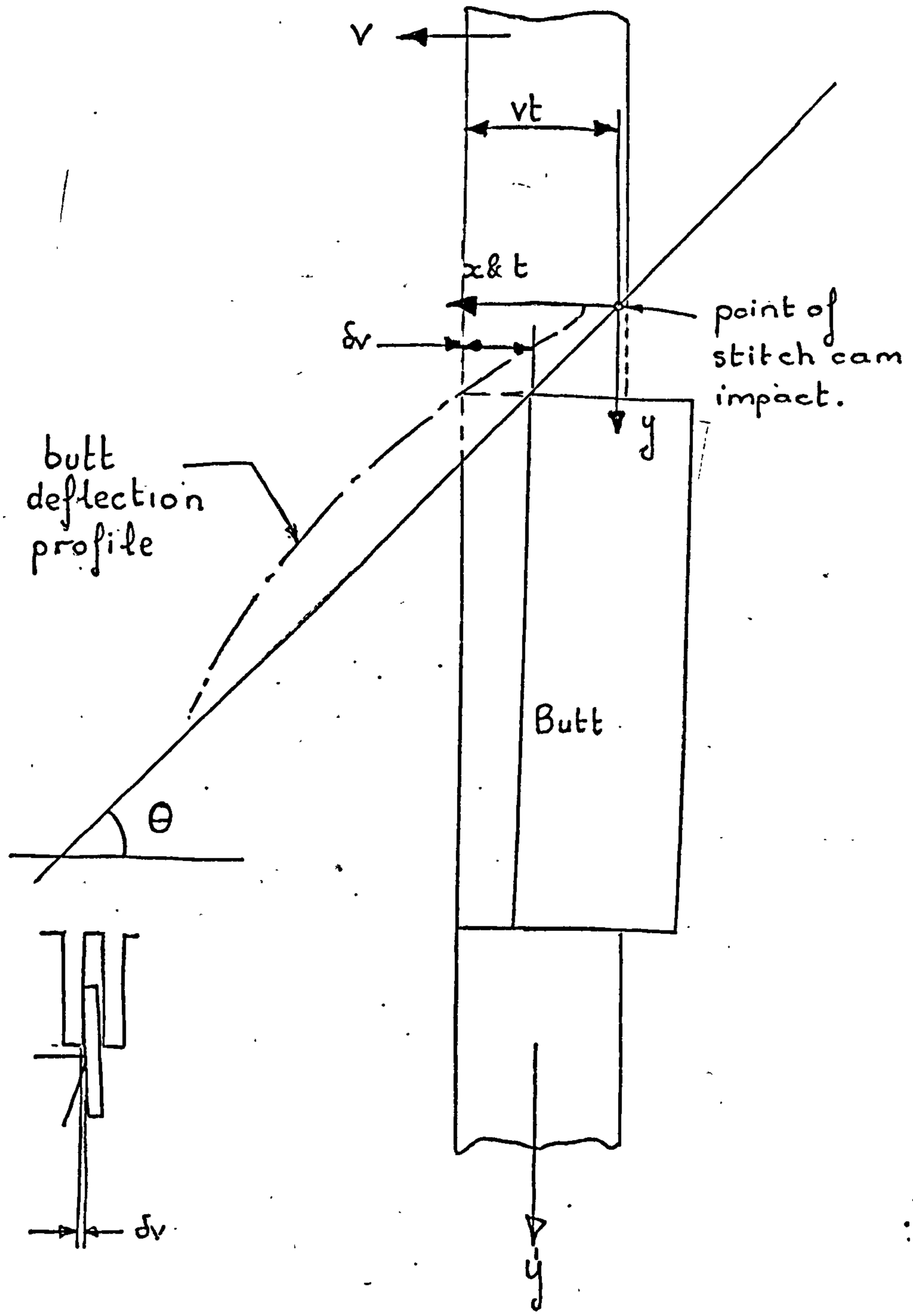

Motion of Needle on
Stitch Cam at Instant of Impact.

Fig 12.3

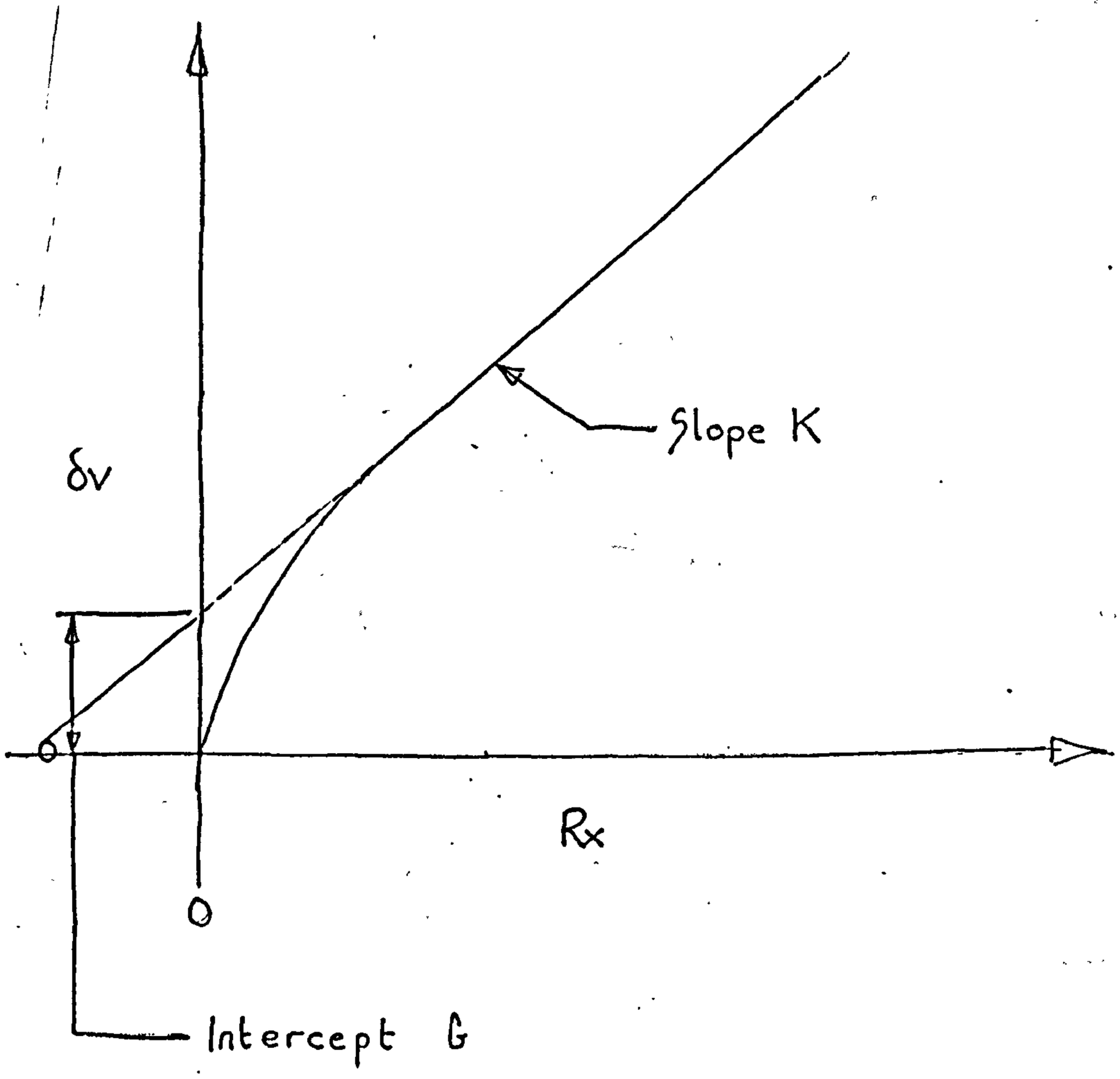

Load (R_x) against
butt deflection (δv).

FIG 12.4

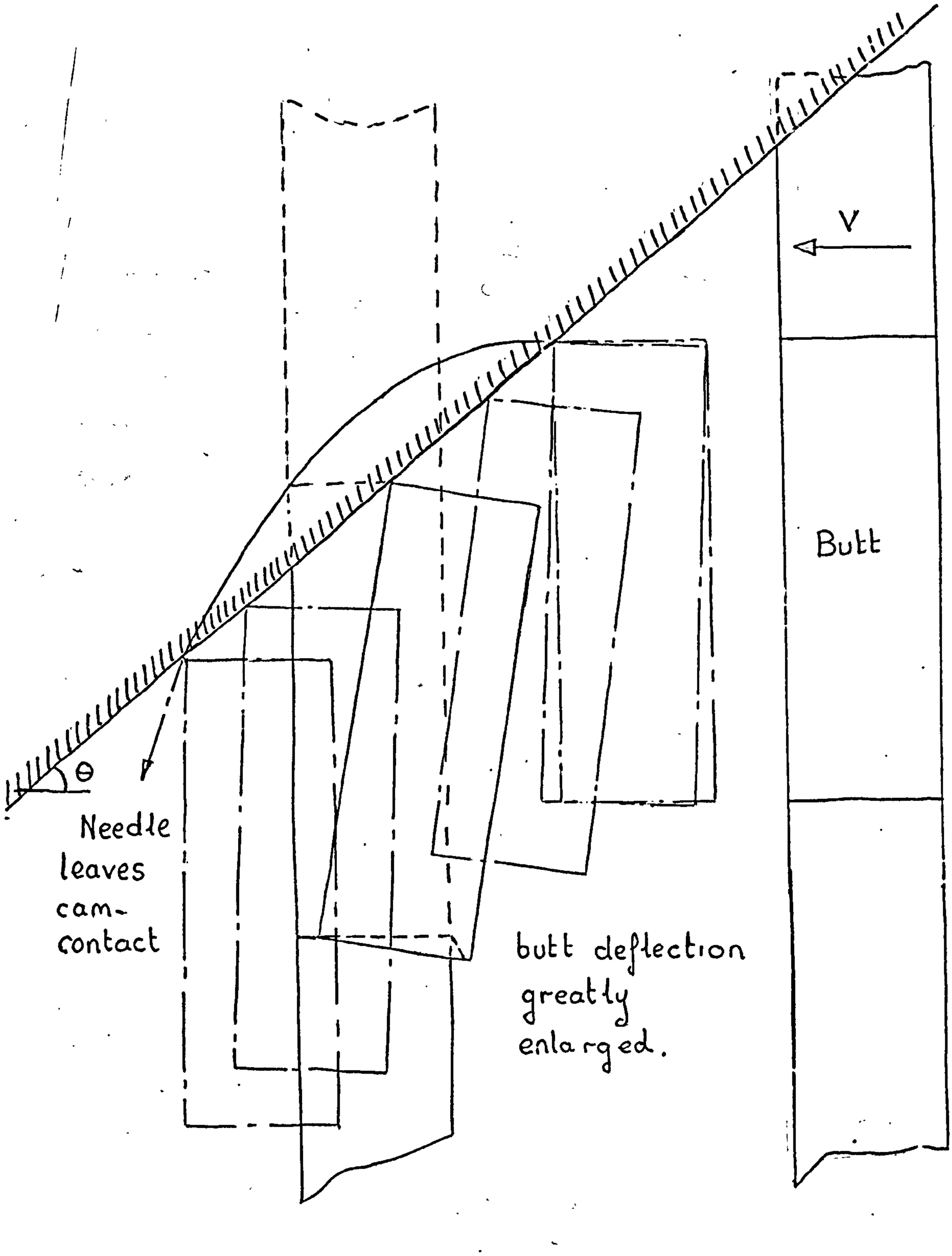

MOTION OF BUTT ON STITCH CAM.

FIG. 12.5

The Damping Effect of the Oil

Parameters

Time = 2×10^{-4} Secs/8.5 mm (H)

Machine Speed = 0.86 m/sec (31.5 in./sec)

Scales

Horizontal impact scale = 69.4 gf/mm (V)

Vertical impact scale = 76.4 gf/mm (V)

Cam angle = 49° linear

Diagram I = No oil

Diagram II = Heavy addition of oil

(H) = Horizontal scale deflection

(V) = Vertical scale deflection

Needle type - 0.443 mm see Fig 3.2

Parameters for traces shown in Fig 12.6(b)

Fig 12.6(a)

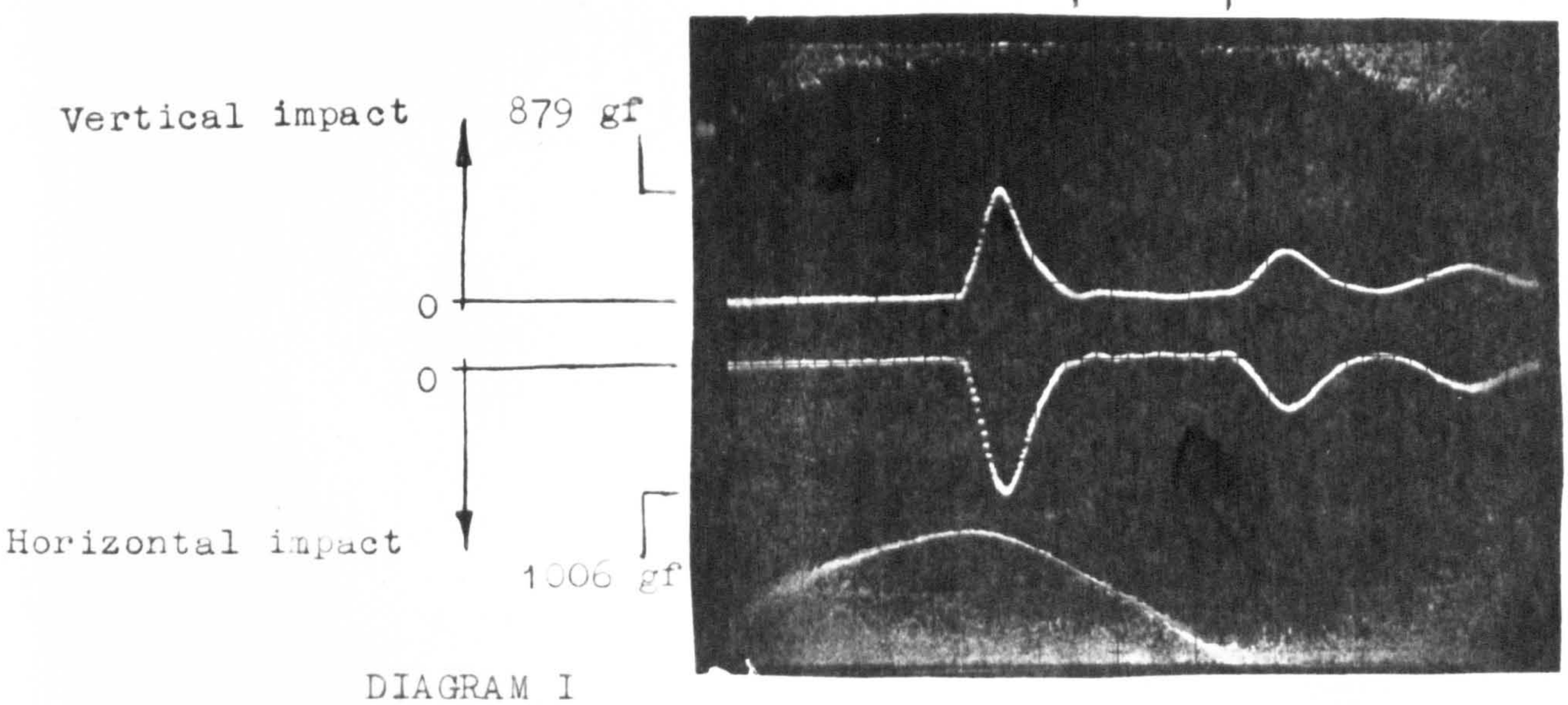

DIAGRAM I

No Oil

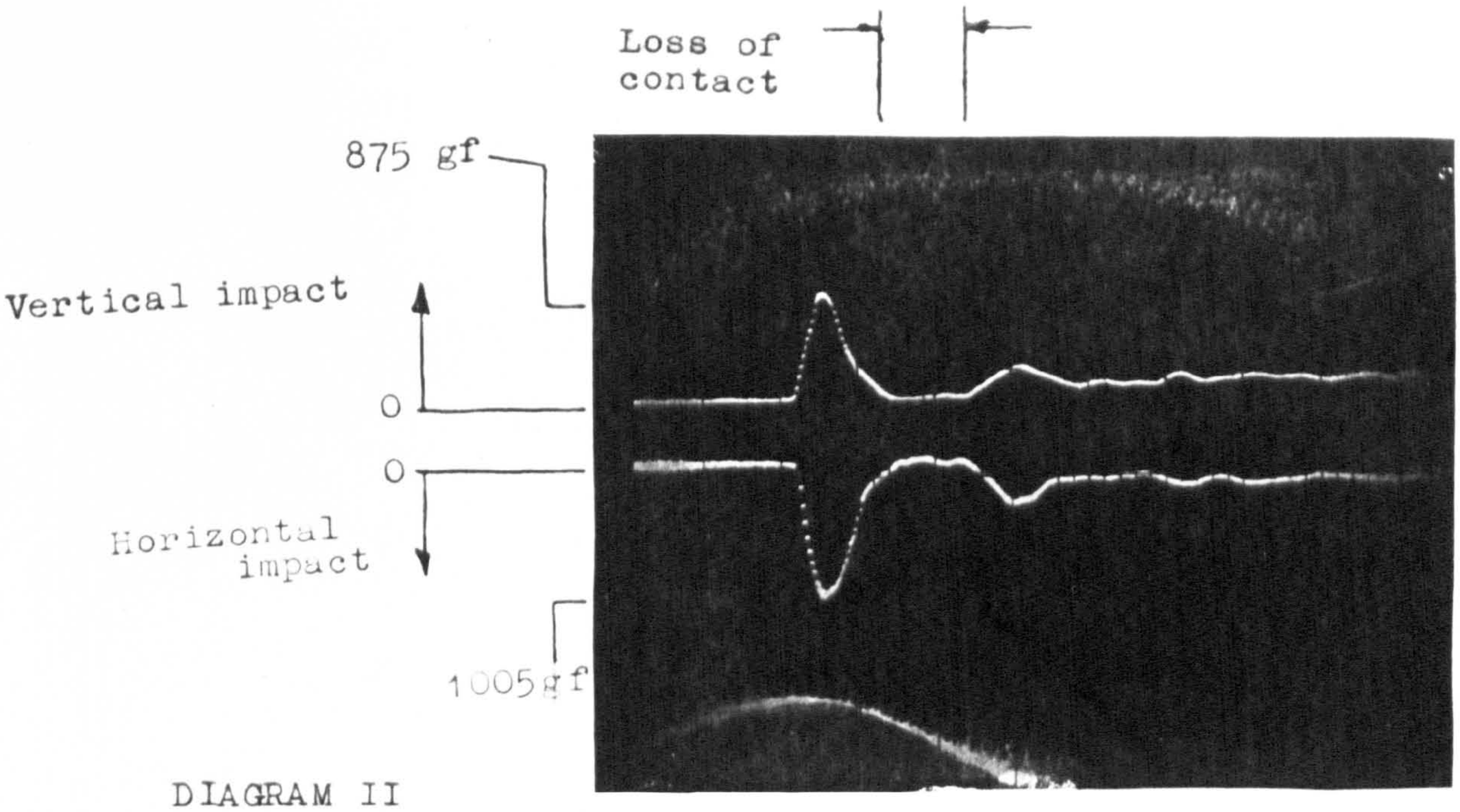

DIAGRAM II

Heavy addition of Oil

Effect of the Oil upon the Impact Force

Fig 12.6(b)

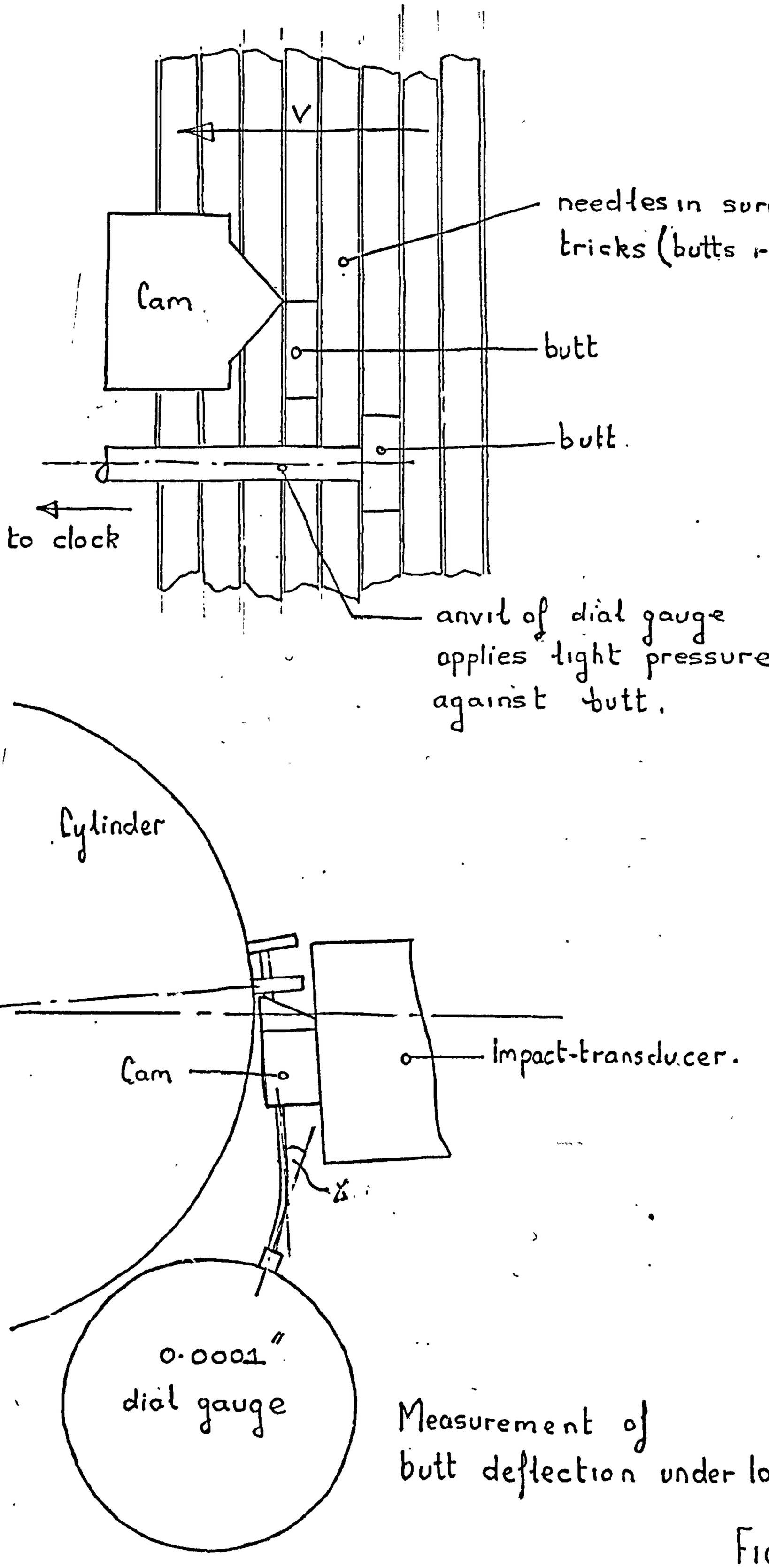

Measurement of butt deflection under load.

FIG 12.7

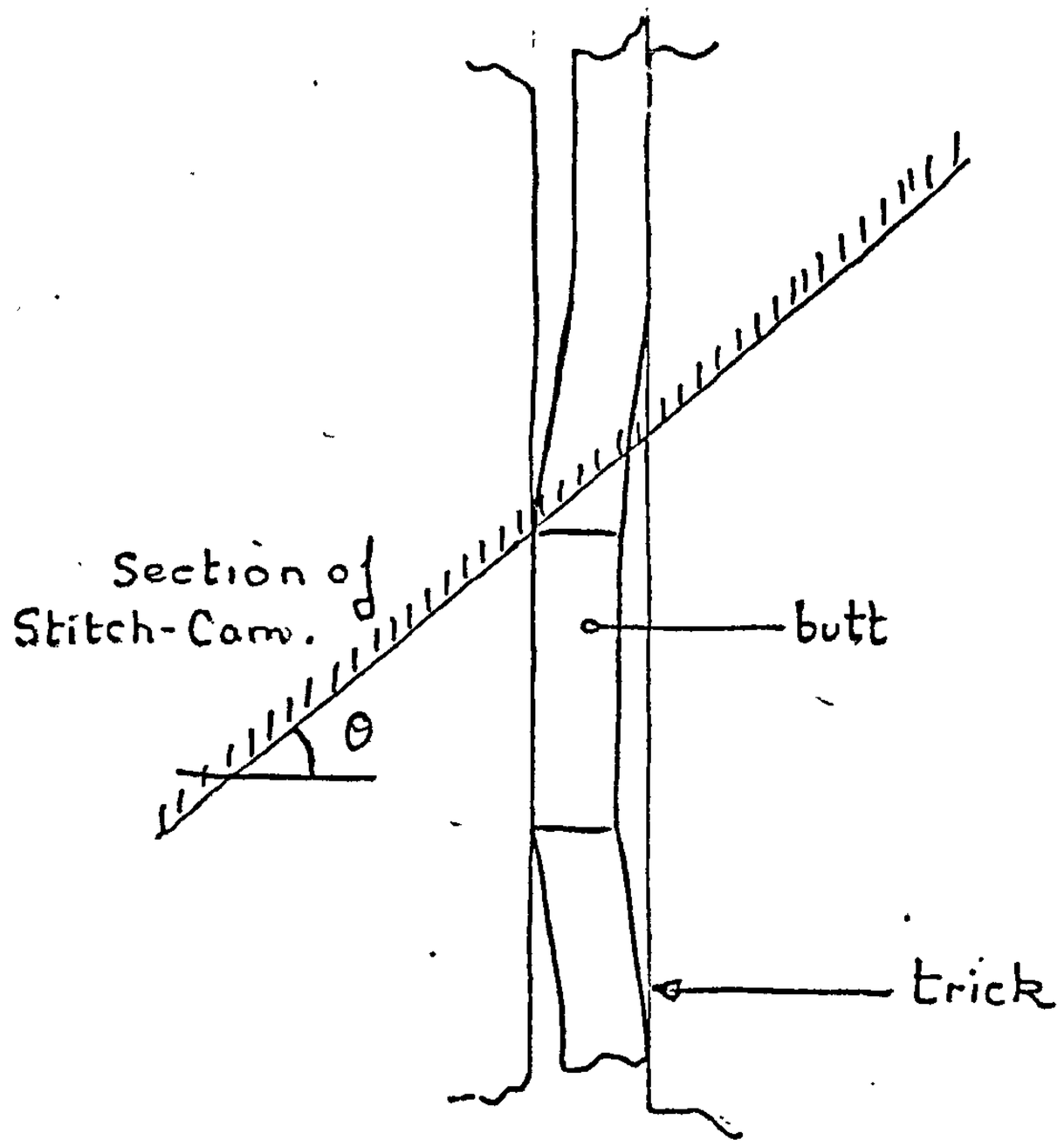

Diagram I
Crimped 0·406mm needle

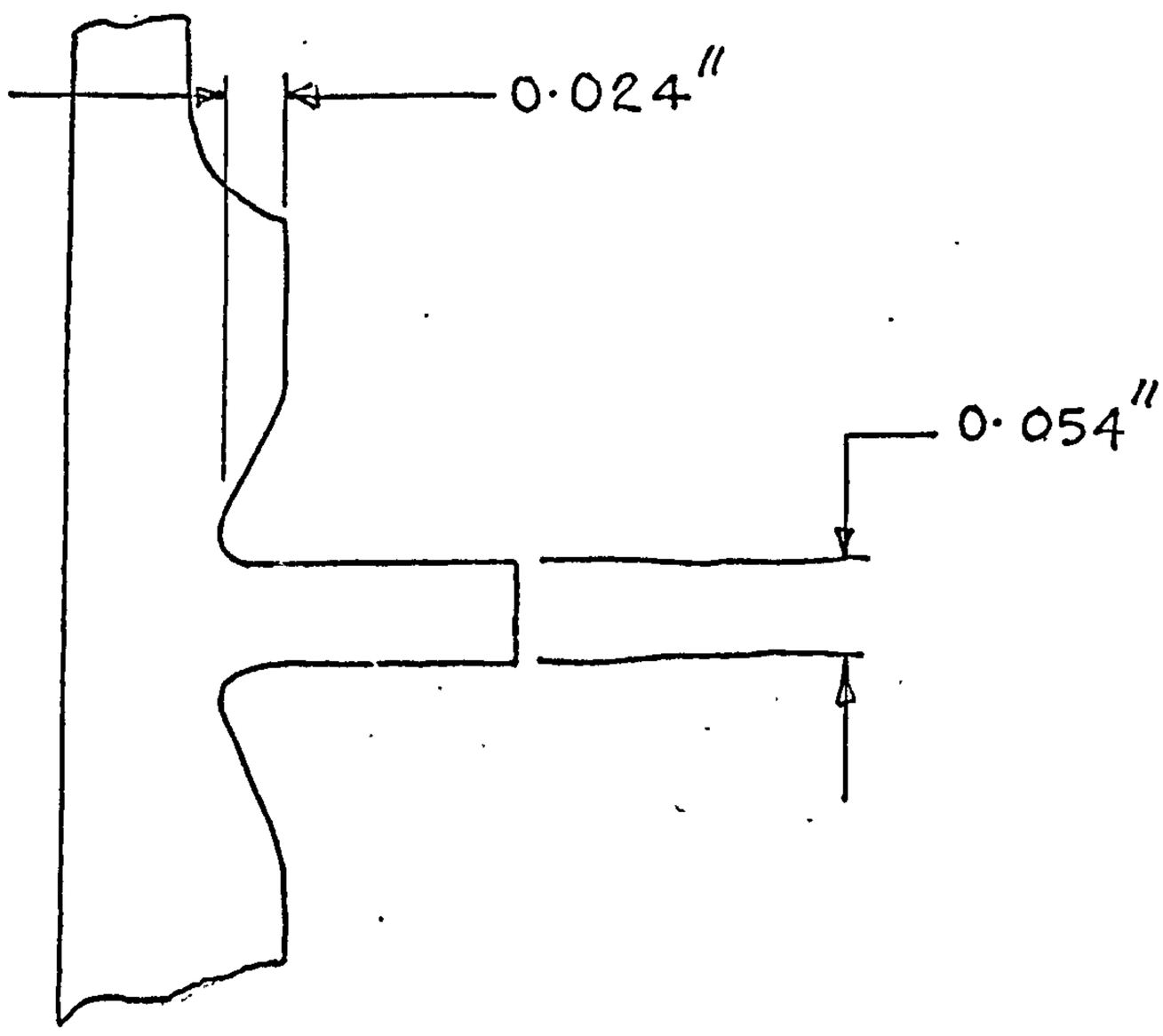

Diagram II 0·443mm needle modified butt.

Needles for butt deflection tests

FIG 12.8

* The correction

The correction consisted of modifying results for angle χ in Fig 12.7

In the diagram the displacement registered by the dial gauge equals d, (referred to as uncorrected butt deflection)

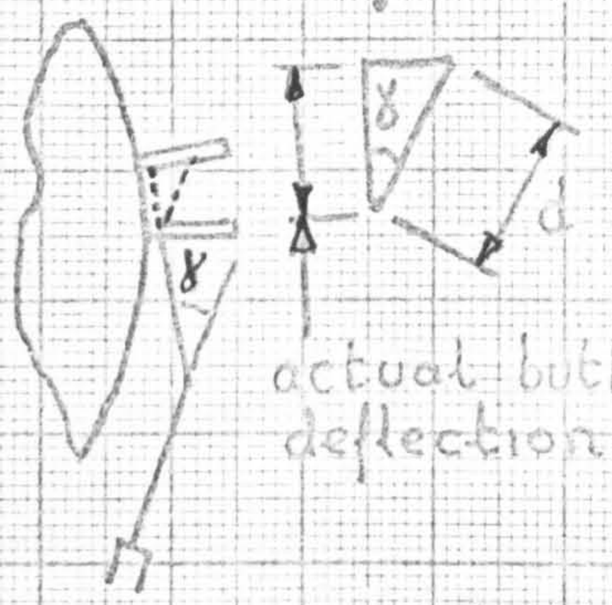

Therefore corrected butt deflection
$= d \cos \chi$
In Fig 12.7
$\cos \chi = 0.9336$

Slope (uncorrected) $= 9 \times 10^{-4}$ cm/kgf

Slope (corrected)
$\frac{1}{K} = 9 \times 10^{-4} \times 0.9336$ *
$\frac{1}{K} = 8.4 \times 10^{-4}$ cm/kgf
$K = 1190$ kgf/cm (6,600 lb/inch)

Can-cylinder clearance = 0.006 in.

0 1180 2360 3540 4720 5900 7080
horizontally applied load (gf)

THE BUTT DEFLECTION CHARACTERISTIC OF 0.443 mm NEEDLE (NEEDLES FITTED IN ADJACENT TRICKS)

FIG 12.9

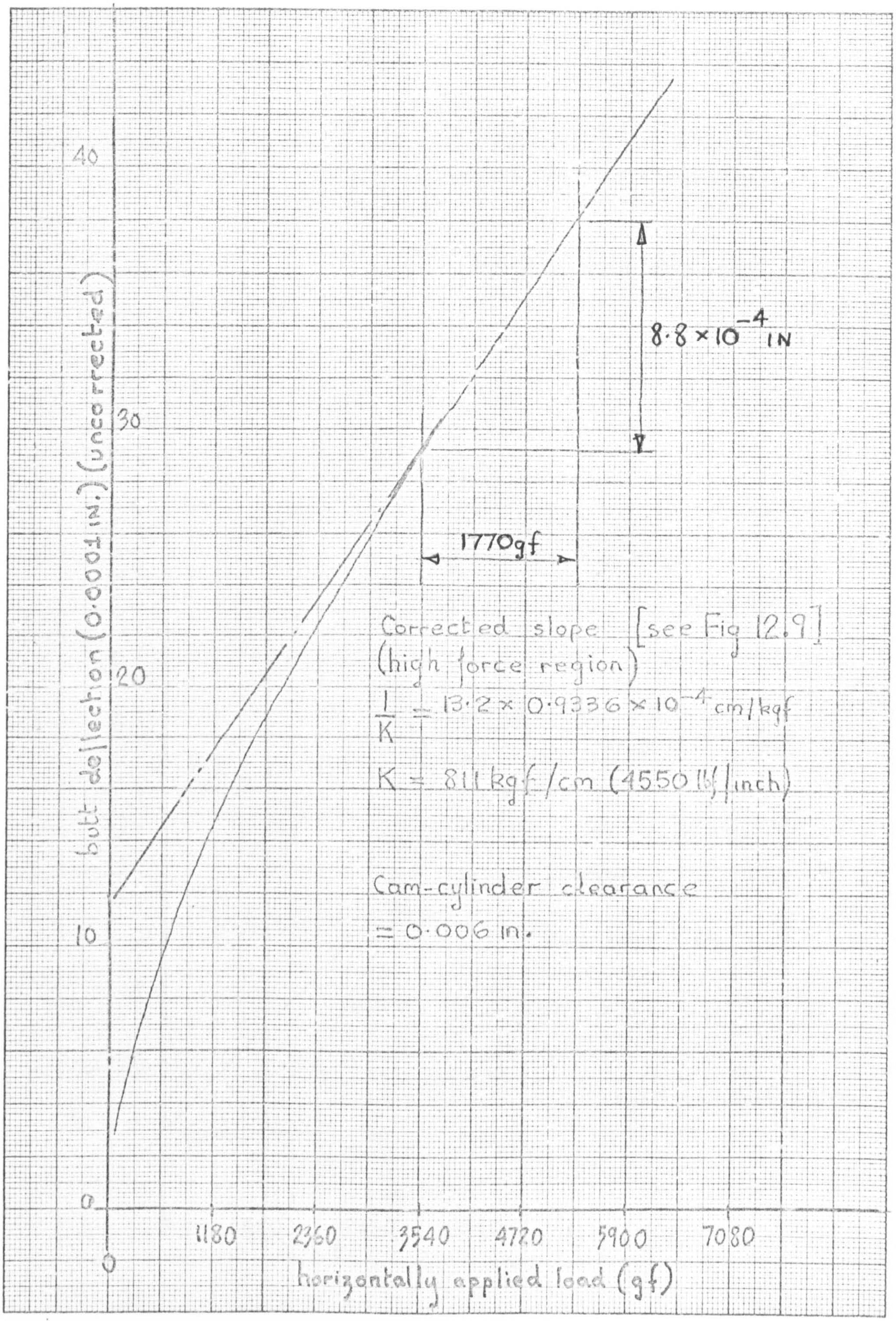

BUTT DEFLECTION CHARACTERISTIC OF 0.443 mm NEEDLE
(NEEDLES REMOVED FROM ADJACENT TRICKS)

FIG 12.10

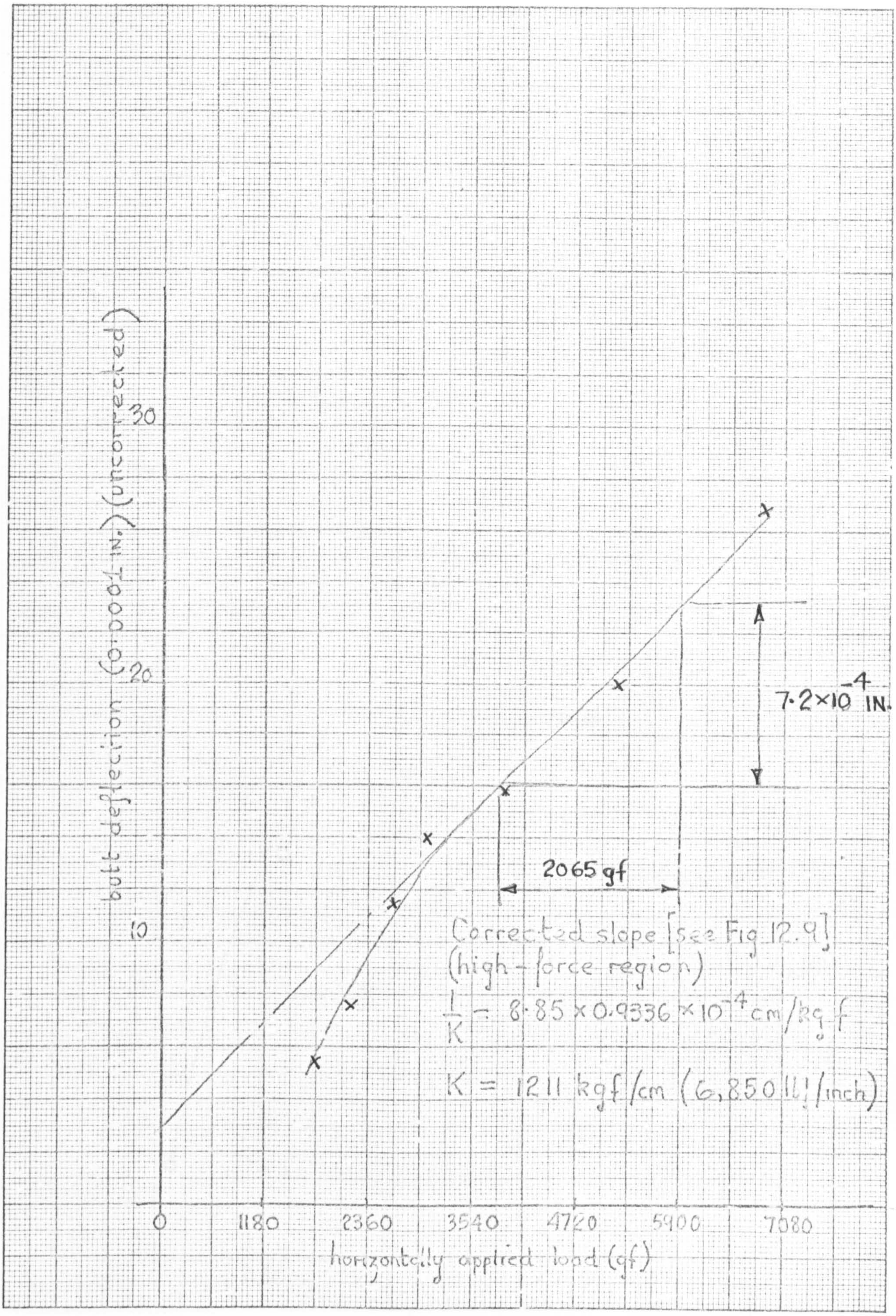

BUTT DEFLECTION CHARACTERISTIC OF 0·406 mm CRIMPED NEEDLE (DIAGRAM I. FIG 12.8)

FIG 12.1

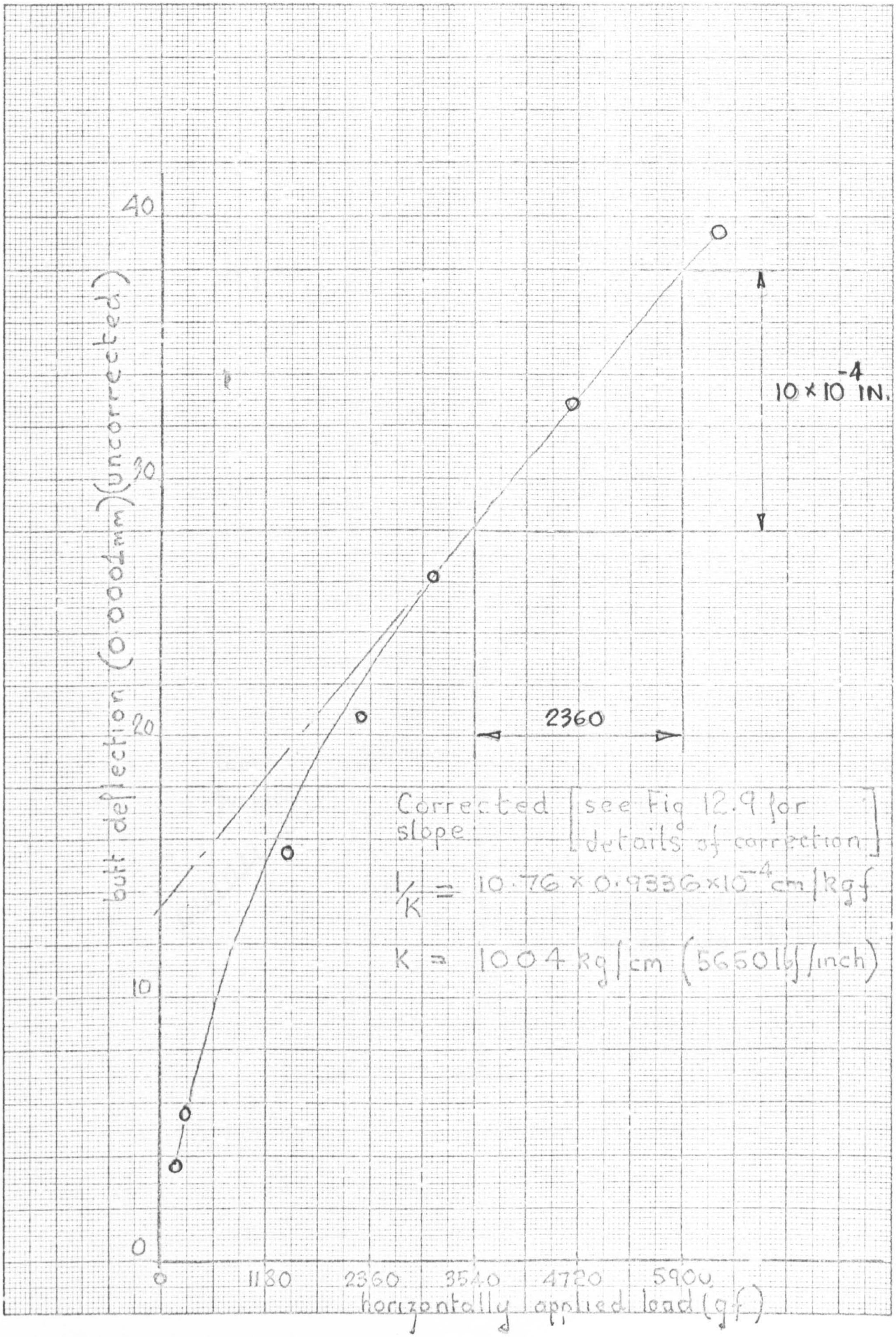

BUTT DEFLECTION CHARACTERISTIC OF 0.443mm NEEDLE WITH MODIFIED BUTT (DIAGRAM II FIG 12.8.) FIG 12.12

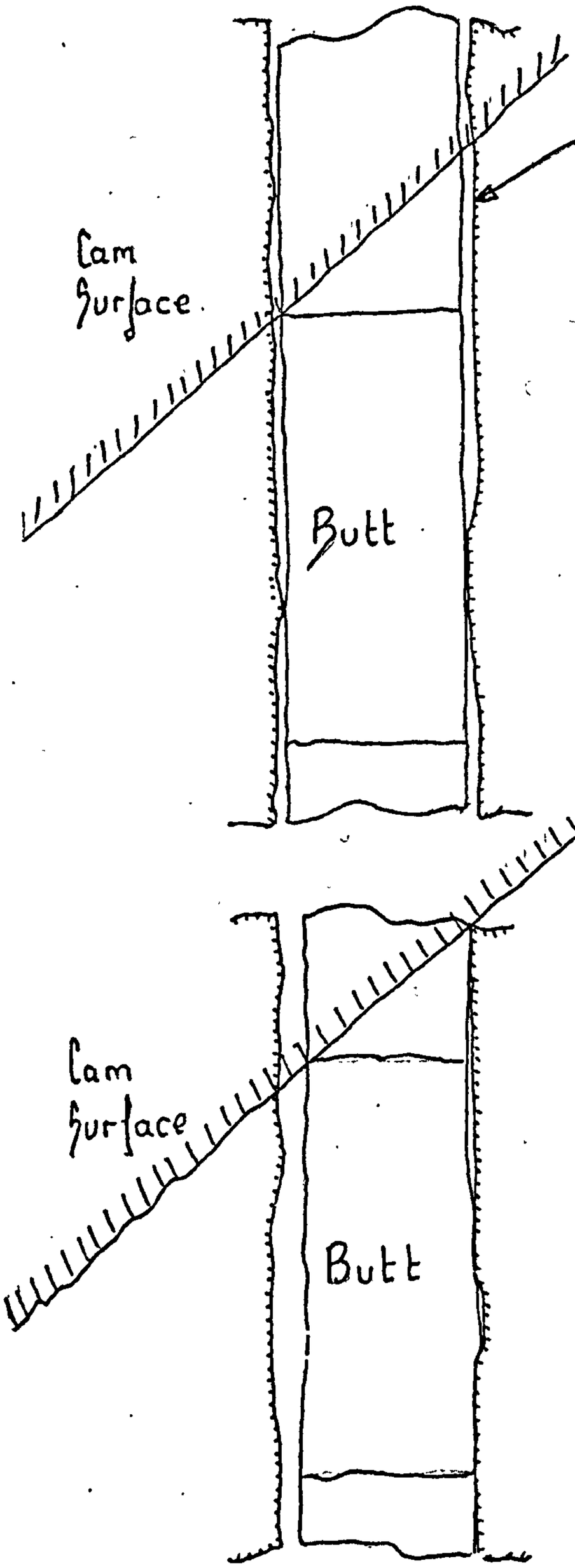

enlarged view of surface irregularity on trick wall

before heavy loading

after loading butt forced against trick wall.

Needle deformation into trick

Fig 12.13.

Vertical view of needle in trick

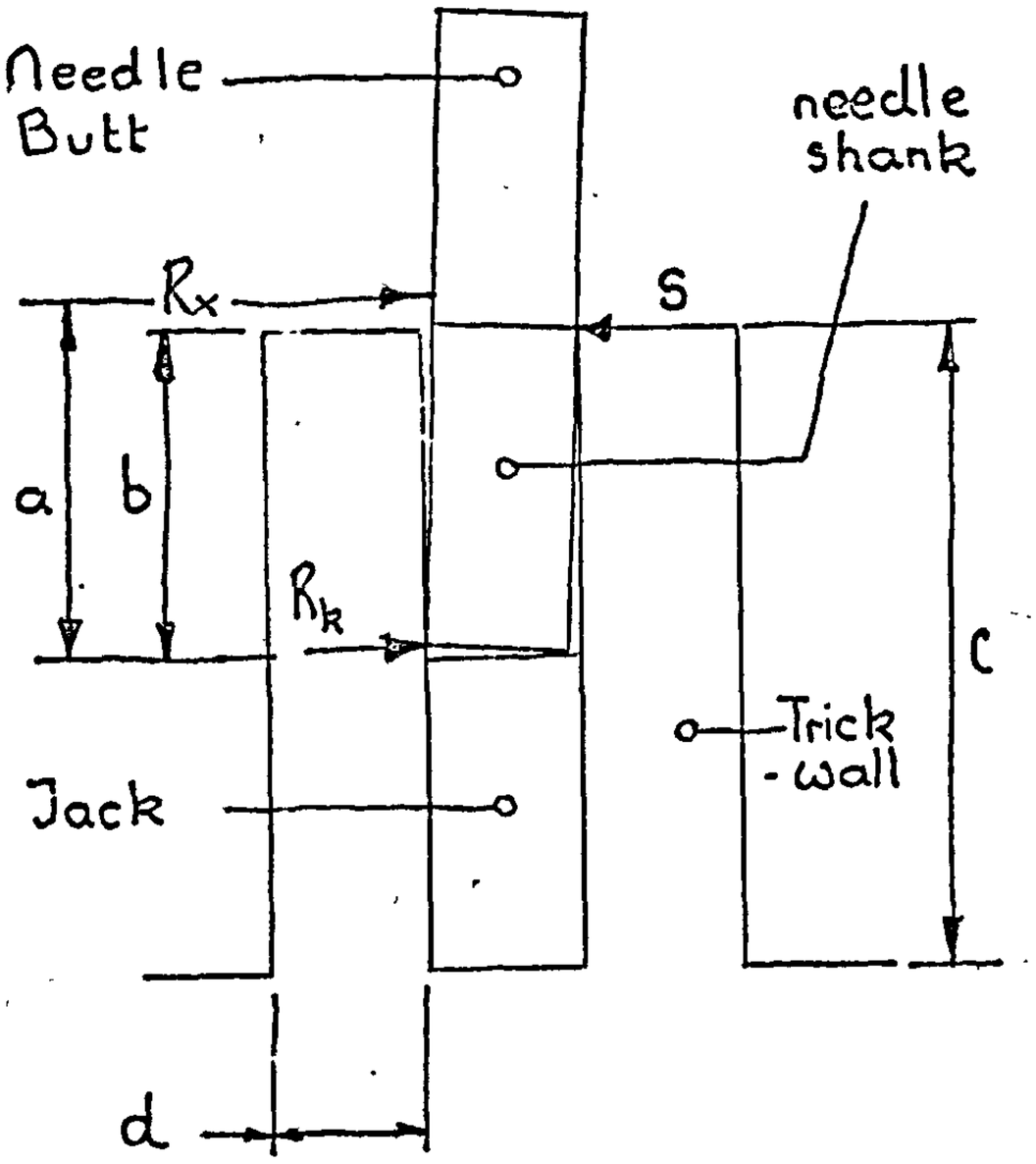

Radial view of needle in trick (not to same scale)

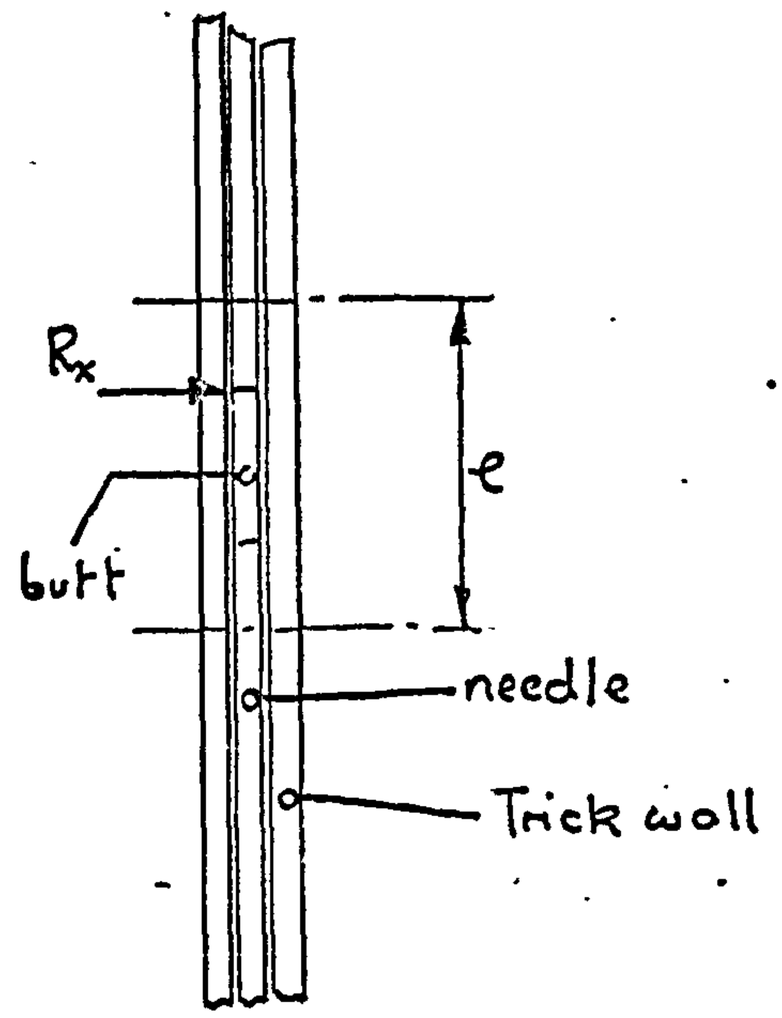

E = youngs modulus for verge,
R_x = horizontal force,
S = side reaction force,
R_K = side reaction force,
e = an effective cantilever verge width,
d = verge thickness,
δ = deflection at verge end,
I = verge 2nd moment of area,
c, a, b } Moment arms,
$K = R_x/\delta$.

From the diagram above assuming simple bending theory with an effective width cantilever.

$$EI\delta = \frac{Sc^3}{3} \quad \text{and} \quad R_K + R_x = S \quad \text{and} \quad I = \frac{ed^3}{12}$$

$$\text{then } \delta = \frac{4aR_xc^3}{Ebed^3}$$

As an example if $\frac{R_x}{\delta} = 6000$ lbf/in

d = 0.0175 in
b = 0.125 in
E = 30×10^6 lbf/in
c = 0.25 in.
a = 0.131 in (cam-cyl clear = 0.006 in

$$\text{For example } e = \frac{4(0.131 \times 6000 \times (0.25)^3)}{30 \times 10^6 \times (0.0175)^3 \times 0.125}$$

$$e = 2.45 \text{ in}$$

Therefore if the trick wall could be treated as a cantilever of width e, using simple bending theory for K = 6,000 lbf/in, e = 2.45 in

FORCES ACTING ON NEEDLE BUTT FIG 12.14

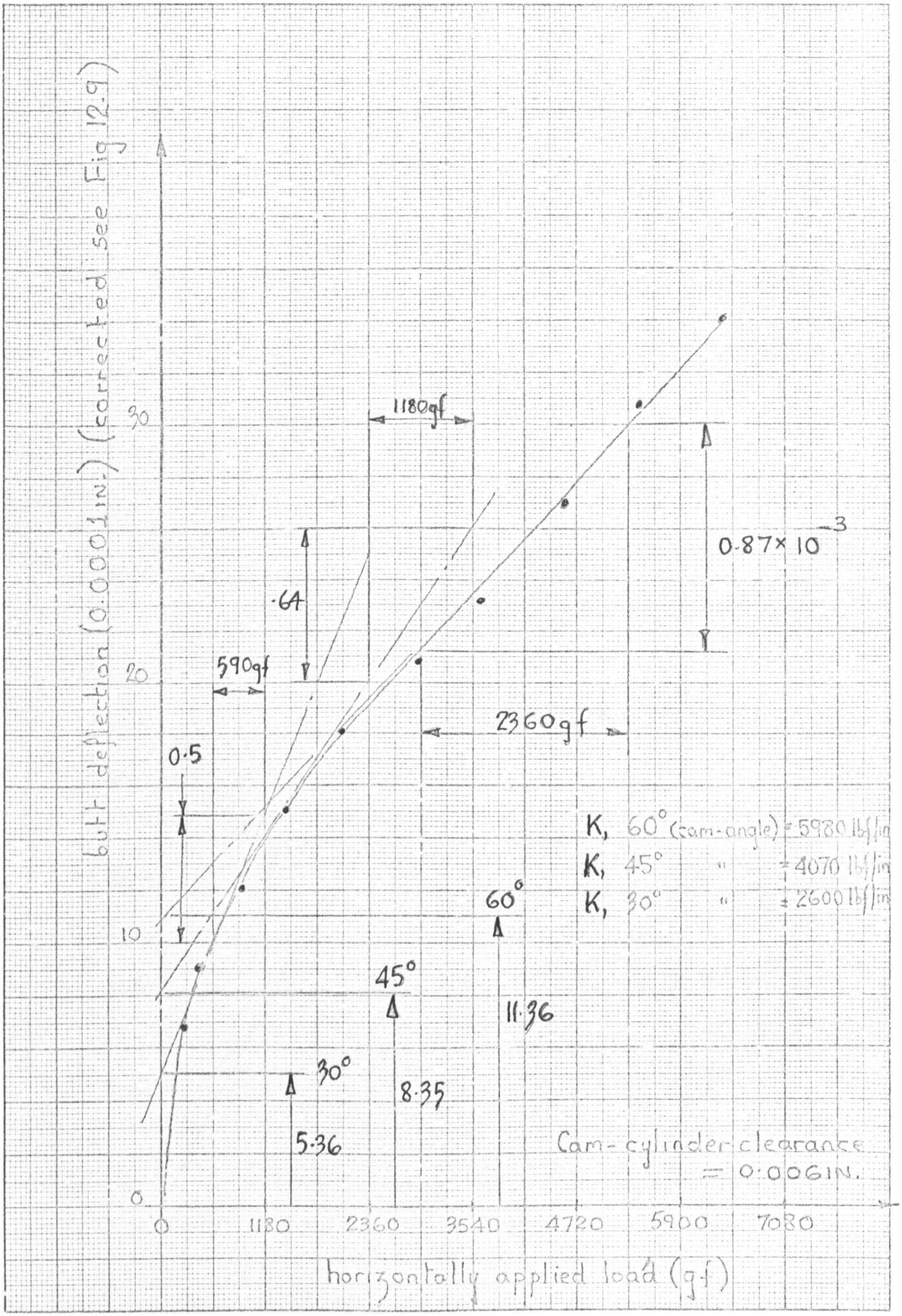

THE BUTT DEFLECTION CHARACTERISTIC OF A 0.443 mm NEEDLE (NEEDLES FITTED IN ADJACENT TRICKS)

Fig 12.15

Selected values of K and G for various cam angles

G (Intersect with zero load axis see Fig 12.15

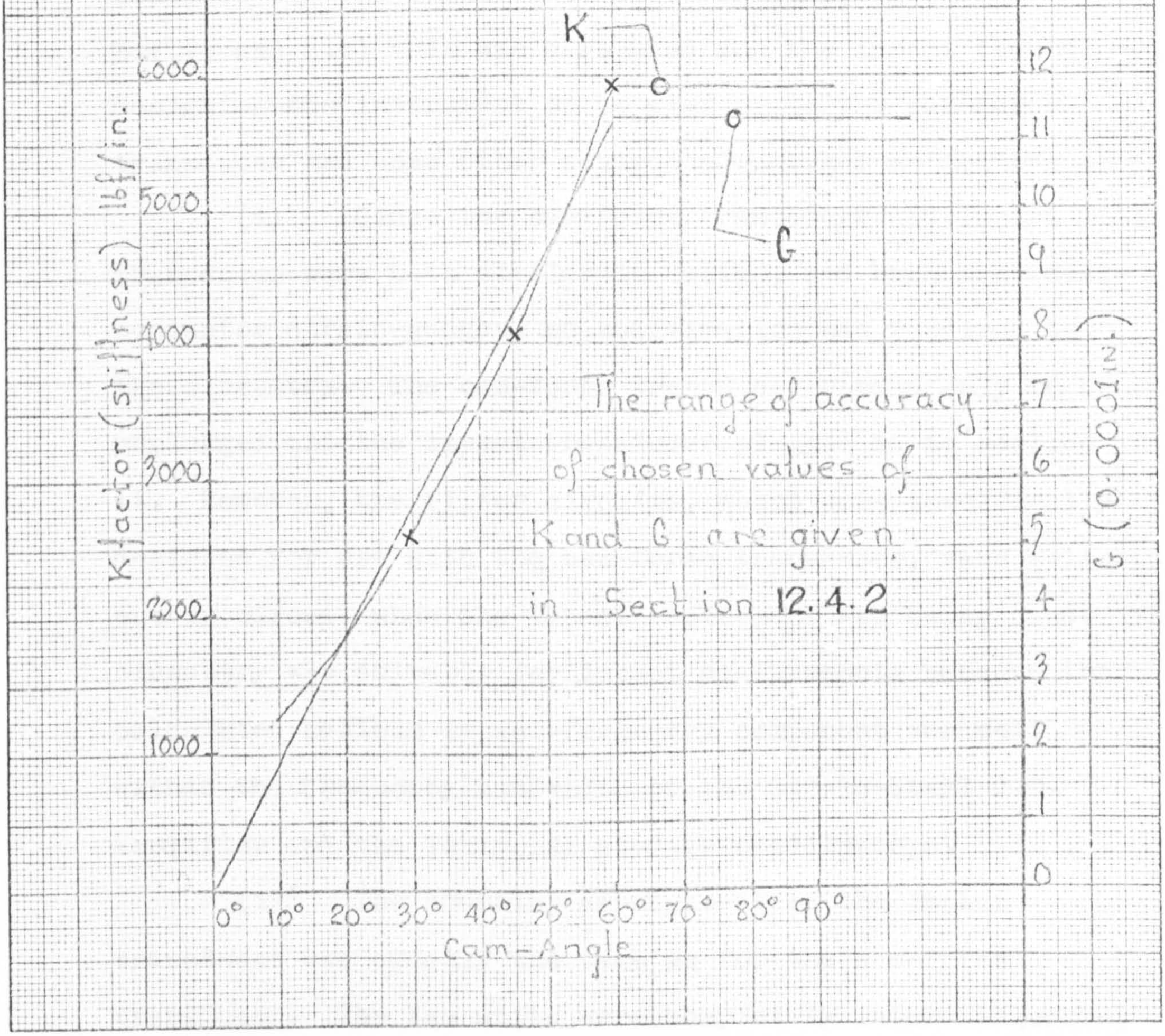

The range of accuracy of chosen values of K and G are given in Section 12.4.2

GRAPH OF K (Stiffness term) AGAINST CAM-ANGLE

FIG 12.16

CHAPTER 13

STITCH-CAM IMPACT INSTRUMENTATION

13.1 Design and Manufacture of a Stitch-Cam Impact Transducer.

The stitch-cam impact transducer necessitated a much higher natural frequency than had the earlier cam-force transducers (marks I to III). As a basic force measuring instrument however, its mode of operation was similar to the cam-force transducers, and for the same reasons that the transverse bending mode of operation was selected for the semi-conductor strain-gauging (see sections 3.1.1, and 4.1) this was also used for the impact transducer. Designing the instrument to be similar to the cam-force transducer had some other obvious advantages as follows :-

(i) Since the cam-force transducer and impact transducer were both similar in design, and both used semi-conductor strain-gauges, no modification was required to the circuitry. The cam-force transducer needed only to be unplugged and the impact transducer plugged in to replace it. However, the filter circuits, which were specifically designed for use with the cam-force transducer, were switched out of circuit when the impact instrument was being used. The circuitry was suitable for impact measurements because the calculated maximum impact-frequency component was well within the frequency bandwidth of the Strain-Stall D.C. Amplifier and the Tektronix storage oscilloscope.

(ii) The mounting arrangement of the impact transducer was exactly the same as for the cam-force transducer. The two units were completely interchangeable, the clamping mechanism and bolt holes being the same for both.

(iii) The impact transducer was calibrated in exactly similar manner, as for the cam-force transducer. The same apparatus used for calibration on the bench and machine could be used for both instruments. Further information on the calibration proccdure was given in section 4.5 and Fig 4.10, the only difference being that the load applied to the cams of the impact transducer were much higher, i.e. up to 20 kgf, when compared to those used for calibrating the experiments of chapter 8.

(iv) The strain-gauging techniques established during the design of the cam-force transducer mark III were repeated with the stitch-cam impact transducer. Semi-conductor strain gauges were used, and these were bonded to the surface, as described in section 4.4.1.

Recommendations contained in chapter 10 for the future design of a cam-force transducer were applied to the design of the impact measuring instrument. The beam and supporting bracket were as a single part out of aluminium. Further details of the design are given in the diagram Fig 13.1.

Using the impact analysis, and the measured coefficients of friction, the impact pulse was calculated to be sinusoidal in shape with a frequency of approximately 3,000 Hz. It was considered that a suitable natural frequency for the impact measuring instrument was approximately five times the maximum pulse frequency, i.e. 15,000 Hz. Since the impact magnitude was calculated to be much higher than the magnitude of the cam-force (chapter 8), it was considered that an instrument with a natural frequency of 15,000 Hz would still have adequate sensitivity to record

the impact.

An instrument was designed having the beam proportions shown in Fig 13.1. The beam was so stiff and thick that it was more like a stiff-boss than a conventional beam and therefore simple beam theories could not be used in the calculation of the natural frequencies. Subsequent to the completed design, it was considered that, no matter what measuring method was used, it would be very difficult to increase the natural frequency any more because the beam becomes so thick and short that it is no longer a practical measuring method. With such a thick beam, a linear load-to-strain relationship cannot be assumed, and the calibration procedure becomes very important. It does not really matter what is the relationship between force applied to the cams and the resulting strain, provided that calibration graphs can be obtained before and after experiments and they are always repeatable. However, when calibration tests were carried out on the impact transducer, the relationship between strain and the applicd force to the cams was found to be linear for the force range of 0 to 20 kgf.

If such a high natural frequency was to be achieved it was important that the mass of the cams at the end of the beam should be minimised. It was impossible to use the cams originally fitted to the cam-force transducer mark II because they were far too heavy, and the cams actually designed for use with the instrument were very small and of low mass; they were, however, of the same material, hardness and finish as conventional circular knitting machine cams.

During the design stage the natural frequency of the beam was calculated using a strain-energy method. When the transducer was built and in use, the natural

frequency was found to be lower than the calculated value and equalled approximately 13,000 Hz. Fig 13.1, shows the method of clamping the transducer to the knitting machine.

The design of the cams for the impact measuring transducer was considerably different to that used for the cam-force transducer, and this meant a major alteration in the method of carrying out measurements as discussed in more detail in section 14.1.

The cams used with the transducer were of a very simple design, and to increase the measuring range of the instrument a large number were made, with a range of various cam angles. A facility was also designed into the impact transducer to enable it to be used for guard cam impact measurement; this is discussed more fully in chapter 15.

13.2 Design of an Instrument to Measure the Bounce of a Needle on the Cams.

Researchers using high-speed photography[31,50] have observed that many needles after the point of initial stitch-cam contact follow a bouncing path down the cam with only intermittent cam needle contacts. Irregular motion of the needle near the loop forming region could have serious disadvantages for stitch uniformity, but it may have some advantages on the stitch-cam, particularly in respect of heat generated at high speeds. There were obvious advantages in building a needle bounce detector that could be used in conjunction with the stitch-cam impact transducer as follows:-

(i) It could be used to determine the parameters that effect needle bounce, the extent of the bouncing, and the effect of guard-cam bounce upon loop formation.

(ii) It could be used for an independent examination

of the theory derived in section 12.2.

(iii) When used in conjunction with the stitch-cam impact transducer it would define regions of the impact force trace where there should or should not be an impact.

A very simple device consisting of a battery and a high resistance was used as shown in Fig 13.2. The device had the advantage of containing no delay elements in the circuit, capacitors, inductors etc., and consequently its response was very fast, having a rise time of less than 1×10^{-6} seconds.

To use the bounce detector, the impact transducer had to be electrically isolated from the rest of the knitting machine, by placing sheets of bakelite between the transducer and the clamps and bakelite washers round all the clamping bolts. One of the wires from the bounce detector was then connected to the transducer and the other wire to the knitting machine. As soon as the needle contacted the cams, the circuit was closed and a 1.5 volt signal appeared across the oscilloscope terminals; however, when the needle and cams lost contact the voltage across the oscilloscope collapsed. The nature of needle bounce could thus be easily observed at exactly the same instant as force measurements were obtained from the stitch-cam impact transducer. The high resistance in the circuit ensured that, when the circuit was closed, the current flow through the needle and cam was an absolute minimum i.e. in the order of micro-amps.

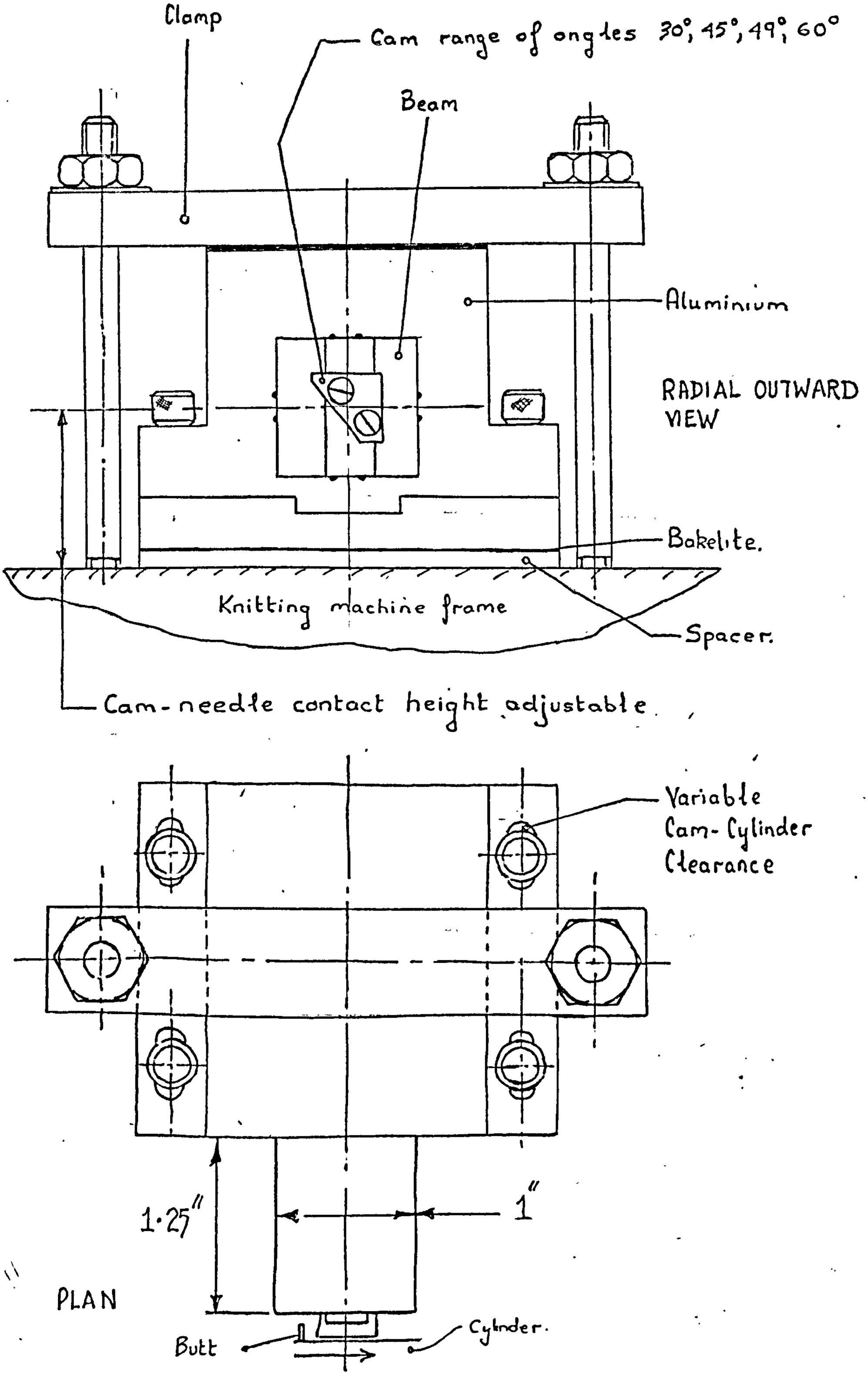

STITCH-CAM IMPACT TRANSDUCER

FIG. 13.1

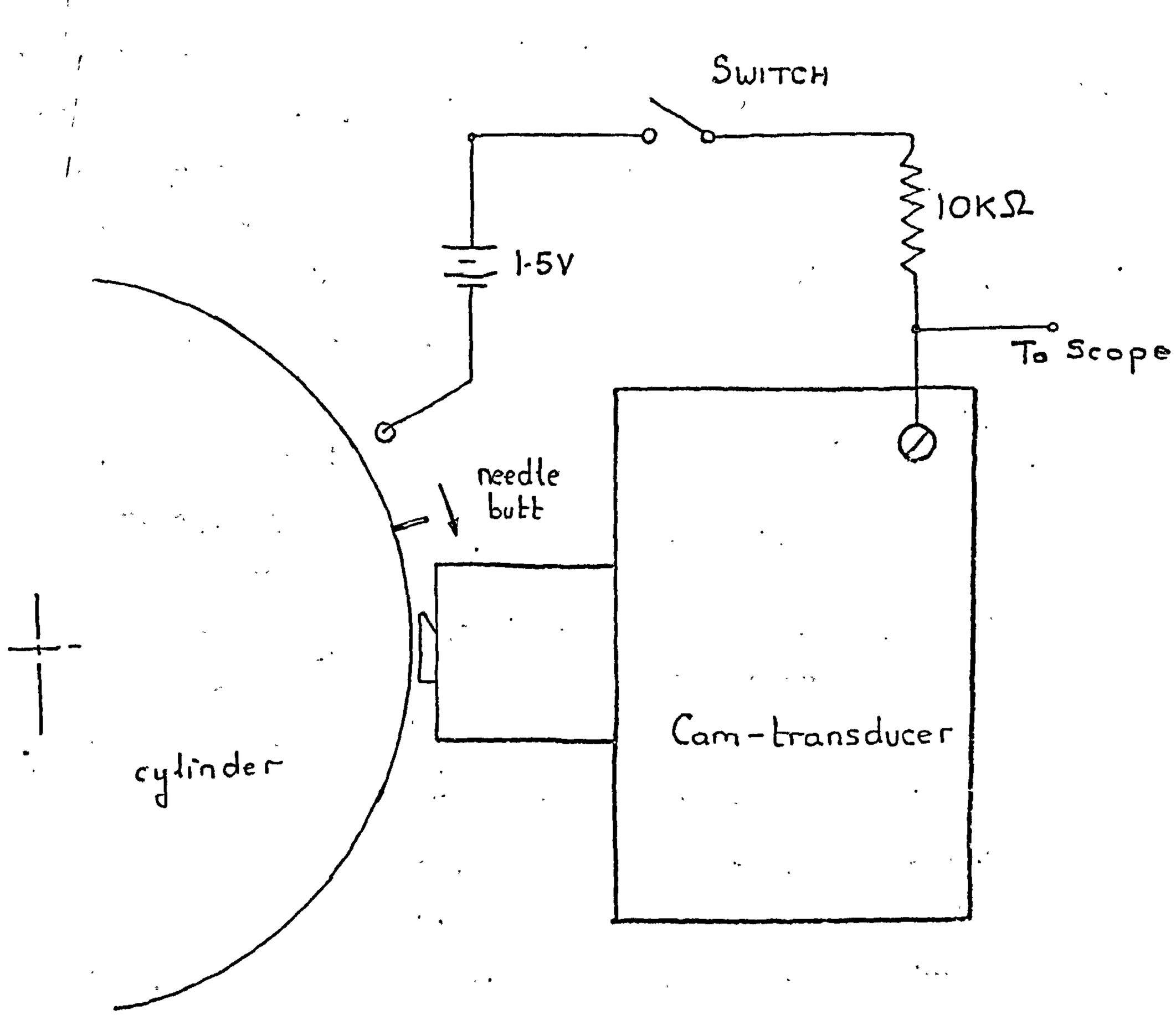

CIRCUIT DIAGRAM
BOUNCE DETECTOR.

FIG 13.2

CHAPTER 14

STITCH-CAM IMPACT EXPERIMENTATION

14.1 Introduction.

Detailed in this chapter are the results of experiments, using the stitch-cam impact transducer, for investigating the effect of various parameters upon the impact. A comparison of these with the theory (derived in section 12.2) is also detailed in this chapter.

All the results derived in chapters 14,16and 17 are summarised in chapter 18, and the relevance of the results to the design of the needles, tricks and cams, is discussed in chapters 23 and 24.

14.2 Experimental Method.

It was not possible to carry out the normal knitting process whilst obtaining stitch-cam impact measurements. Two important reasons for changes in the experimental method, from the system used with the cam-force transducer mark III, as detailed in section 8.1,are stated below :-

(i) The requirement of a high natural frequency for the impact transducer meant that the cams attached to the instrument had to be small in order to reduce the mass at the end of the beam. To carry out the normal knitting process, the cams would need to be much larger and heavier.

(ii) In section 8.5.4 it was noted that the stitch cam impact became more prominent as machine speed was increased. The relationship between speed and impact is very important because future machines will probably run much faster than those of the present day. For this reason impact measurements were carried out over a range from

0 to 450 ft/min (2.28 m/sec). During the experiments detailed in chapter 8, it was found difficult to operate the knitting machine above 250 ft/min (1.27 m/sec) without very frequent stops to remove damaged needles and repair fabric holes. Obviously, impact measurements would be very difficult to obtain if the speed was such that the machine could not satisfactorily knit and very frequent stops had to be made.

The experimental arrangement for the impact measurements is shown in Fig 14.1. Before measurements could be carried out, all the needles and cams were removed from the cylinder, and a standard needle, which for most experiments was a 0.443 mm needle illustrated in Fig 3.2, was fitted in a thoroughly cleaned trick. Several similar needles, but with their butts removed, were positioned each side of the standard needle; at the opposite side of the cylinder, and at several intermediate positions, single needles, without butts, were fitted. The purpose of fitting so many needles around the circumference was two-fold; firstly, the equal distribution of needles balanced the cylinder during rotation, and secondly, the band-spring acting on an equally distributed mass of needles maintained its correct normal operating tension on the standard needle under test.

The stitch cam impact transducer was fitted and lightly clamped to the knitting machine. A 0.15 mm shim was then placed between the cam and the cylinder, and the transducer was pushed towards the cylinder until it lightly clamped the shim. The transducer was then tightened down and the shim was removed.

After the standard needle impacted the stitch cam, the

needle moved down and it was necessary to raise the needle again for it to hit the stitch cam at the next revolution. A raising cam with an angle of 25^{o} was fitted on the other side of the cylinder. After stitch-cam impact, the raising cam lifted the needle, until it was at a height equivalent to that of the stitch-cam impact point during normal knitting. There was a danger, especially at high speed, that one of the needles would lift out of the trick slightly, and foul the cams, thus causing considerable damage. To remove this risk, lead-in cams were fitted, just before the stitch and raising cams, these being illustrated in Fig 14.1.

The standard needle thus impacted the stitch-cam at the same height and in a similar manner as the impact during normal knitting. However, there was one difference in that, during normal knitting, a loop of yarn, tensioned by the fabric weight, is held around the needle shank. To similate this effect of the fabric take-down, yarn was looped around the standard needle shank, and small weights, to represent the take-down tension, were attached to the loop as shown in Fig 14.2.

The experimental procedure was very similar to that used with the cam-force transducer mark III as detailed in section 8.1. However, for all the impact experiments, the filters detailed in section 5.2 were switched out of the circuit. Calibration of the transducer was initially carried out on the bench and frequent re-checks were made on the machine.

The photo-diode trigger circuit was connected into channel 1 of the Tektronix Oscilloscope. The horizontal and vertical impact signals were fed into channels 2 and 3, and the bounce transducer output into channel 4. The bounce

transducer was fitted onto the side of the impact transducer and, when bounce measurements were required, it was switched on, a trace being recorded on the oscilloscope screen in conjunction with the impact traces and the timing pulse.

The trigger was set to fire the oscilloscope just before the needle contacted the stitch-cam, the procedure for setting the trigger being identical to that detailed im section 8.1.1. Further information concerning the experimental technique is contained in Fig 14.1.

14.3 Theoretical Interpretation of the Impact Process.

A theoretical description of the stitch-cam impact process can be formulated from the relationships detailed in section 12.2. Initially, when the needle contacts the stitch cam the force rises to a value at which its vertical component is just large enough to initiate motion to the needle. The impact force then follows a sinusoidal change in magnitude. When the force reaches a value where :-

$$a\cot an\,\Theta \sin(nt+\phi) = -\left(\frac{H_d}{D} - G\right) \quad \ldots\ldots \quad (96),$$

the reaction-force R becomes equal to zero, and the needle butt loses contact with the cam. A theoretical examination of needle motion subsequent to loss of cam contact was not undertaken, but it was obvious that the duration of the bounce between contacts was very dependent on the resistance to needle motion in the trick, and on the amount of oil in the trick. Subsequent experiments, detailed in section 14.5.2 and 14.6, showed that when the trick resistance was very Low, the loss of contact was considerably longer than the impact duration and a large number of bounces occurred. Theoretically, the $\frac{H_d}{D}$ term defines the

steady level of cam-force, and at high speed, if $\frac{H_d}{D}$ is very low, then it follows from equation (96) that loss of cam contact occurs at a relatively low value of the term. $a\cot an\,\theta \sin(nt+\phi)$ consequently, a large number of bounces and secondary impacts would occur at high speed. When the term $\frac{H_d}{D}$ is larger, there are not so many losses of contacts; but the primary impact magnitude will be larger due to the increased amplitude and the larger value of $\frac{H_d}{D}$. Further information on this point is contained in 14.5.2.

When the needle recontacted the cam, a secondary impact of lower magnitude than the primary developed, particularly as machine speed was further increased. The secondary impact also followed a sinusoidal force relationship. A graph showing the theoretical impact as it varies with speed is shown in Fig 14.3. If a theoretical analysis had been carried out using the experimentally-obtained graph of butt-deflection, then the frequency of the impact pulse would have been variable depending upon the load and deflection. The resulting force developed at impact would not be a sine wave, but would be an addition of waves approximately similar in shape to a sine-wave.

14.4 Comparison of Theoretical and Experimental Results.

Experimental measurements detailed in this section were primarily concerned with the effects which the yarn-loop around the needle shank, the machine speed, and the cam-angle have upon the impact.

14.4.1 Effect of the Yarn-Loop around the Needle Shank.

Experiments were carried out to determine the effect the yarn around the needle shank has upon the impact. Initially, traces were obtained with no yarn around the shank at a range

of machine speeds. Yarn was then looped around the needle, and weights were hung on the yarn to simulate a take-down load of 5 gf per needle. The experiment was repeated at a similar range of machine speeds. Finally, weights were attached to simulate a load of 13.5 gf and the experiment was repeated. The yarn had very little effect upon the stitch-cam impact and, for the majority of subsequent experiments detailed in this chapter, the simulation of the fabric take-down tension by looping yarn around the shank, was unnecessary. A typical experimental result is shown in Fig 14.4 (a) and (b).

14.4.2 Effect of Machine Speed and Cam-Angle upon Stitch-Cam Impact.

Analysis of the impact process is detailed in section 12.2. The equation for the reaction force R is given below:-

$$R = \frac{K\left(\frac{H_d}{D} + a\cot\theta\sin(nt+\phi) - G\right)}{\sin\theta + \mu_2\cos\theta} \quad (97),$$

i.e. for $vt - y\cot\theta \geqslant G$,

and $$R = 0 \quad \text{for } vt - y\cot\theta \leqslant G \quad . \quad (98).$$

The coefficients in the above equation have been defined in Fig 12.2. The parameters a, v and n are defined by the three equations shown below :-

$$n = \sqrt{\frac{D\cot\theta}{m}} \quad \text{rads/sec} \quad . \quad (99),$$

$$a^2 = \tan^2\theta\left(\left(\frac{v}{n}\right)^2 + \left(\frac{H_d}{D}\right)^2\right) \quad . \quad . \quad (100),$$

and $$\sin\phi = \frac{1}{a}\left(\frac{H_d}{D}\right)\tan\theta \quad . \quad . \quad . \quad (101).$$

In equation (97) a large value for the term $\frac{H_d}{D}$ occurs, when H_d is large and D small. An approximation to H_d can

be obtained by measuring the force required to lift the needle vertically upwards in the trick when the cylinder is stationary; the method used was similar to that detailed in section 9.5. It was considered that for an average needle-trick combination the value of H_d was between 20 and 40 gf. The term D hac a low value with a 60^o cam and for this angle was calculated to be 413 kgf/cm.

For an average needle and trick $\frac{H_d}{D}$ would rarely exceed 100×10^{-6} cm.

A lesser value of $\frac{V}{n}$ occurs when V is small. For the 60^o cam, when $V = 15$ m/min (49 ft/min) and the calculated frequency term $n = 18,720$ rads/sec, then $\frac{V}{n} = 1,336 \times 10^{-6}$ cm. Therefore the term $\frac{H_d}{D}$ is small compared to $\frac{V}{n}$ under all conditions, except when :-

(i) H_d is large, ie>40 gf.

(ii) V is very small.

if the $\frac{H_d}{D}$ term is ignored, then equation(97) can be simplified to the following form :-

$$R = \frac{Kv\sin(nt) - KGn}{n(\sin\theta + \mu_2\cos\theta)}, \quad \text{for } t \geqslant \frac{1}{n}\sin^{-1}\left(\frac{Gn}{V}\right) \qquad (102)$$

and $$R = 0, \quad \text{for } t \geqslant \frac{1}{n}\sin^{-1}\left(\frac{Gn}{V}\right) \qquad (103)$$

From equation (102):-

$$R_{max} = \frac{Kv - KGn}{n(\sin\theta + \mu_2\cos\theta)} \quad t \geqslant \frac{1}{n}\sin^{-1}\left(\frac{Gn}{V}\right) \qquad (104)$$

Equation (104) was evaluated for varying cam-angles.

the results being as follows :-

(i) Θ = 30° } see section 12.4.2
K = 2,600 lbf/inch (463 kgf/cm)
G = 5.36 x 10^{-4} inch (13.62 x 10^{-4} cm)

μ_1 = 0.1 } see section 12.5
μ_2 = 0.08

D = 3,595 lbf/inch (641 kgf/cm)
n = 40,400 rads/sec.
pulse time π/n = 0.078 x 10^{-3} secs.

$$R_{max} = 0.1146V - 2.525 \quad \ldots \quad (105),$$

where: V is in inches/sec and R is in lbf.

defined for $0.1146V \geqslant 2.525$

(ii) Θ = 45° } see section 12.4.2
K = 4070 lbf/inch (729 kgf/cm)
G = 8.35 x 10^{-4} inch (21.20 x 10^{-4} cm)

μ_1 = 0.1 } see section 12.5
μ_2 = 0.08
D = 3,130 lbf/inch (558 kgf/cm)
n = 28,700 rads/sec.
pulse time π/n = 0.110 x 10^{-3} secs

$$R_{max} = 0.1874V - 4.49 \quad \ldots \quad (106),$$

defined for $0.1874V \geqslant 4.49$

(iii) Θ = 49°,
K = 4,450 lbf/inch (794 kgf/cm),
G = 9.1 x 10^{-4} inch (23.1 x 10^{-4} cm),
μ_1 = 0.1,
μ_2 = 0.08,
D = 2,910 lbf/inch (519 kgf/cm)
n = 25,700 rads/sec.
Time for pulse π/n = 0.122 x 10^{-3} secs.

$$R_{max} = 0.216V - 5.05 \quad \ldots \quad (107)$$

where: V is in inches/sec and R_{max} is in lbf

defined $0.216V \geqslant 5.05$

(iv) Θ = 60° } see section 12.4.2
K = 5,980 lbf/inch (1,043 kgf/cm)
G = 11.36 x 10^{-4} inches

$\mu_1 = 0.1$,
$\mu_2 = 0.08$,
$D = 2,315$ lbf/inch (413 kgf/cm),
$n = 18,720$ rads/sec.
} see section 12.5

Time for pulse $\pi/n = 0.17 \times 10^{-3}$ secs.

$$R_{max} = 0.354v - 7.52 \quad . \quad . \quad . \quad (108)$$

where: V is in inches/sec and R is in lbf.

defined $0.354v \geqslant 7.52$

Experiments were carried out to measure the stitch-cam impact. Initially, a 30° cam was fitted to the transducer which was then clamped down to the machine, the transducer position being set so that the cam was only 0.15 mm from the cylinder. The bounce transducer and its circuitry were allowed to warm up for a short time after switching on and the machine was very lightly oiled and run for several minutes before any traces were taken. Photographic traces were taken at a large number of machine speeds, and from these, the peak values of horizontal and vertical impact were measured and plotted. The theoretical values obtained from equation(105) were also plotted on the same graph. The experimental procedure was repeated with the 45°, 49° and 60° cams. The 30°, 45°, 49° and 60° cam results are shown respectively on Figs 14.5 to 14.8 inclusive. Fig 14.9 shows the experimentally measured impact force plotted against cam-angle at two speeds, namely 200 ft/min (1.00 m/sec) and 350 ft/min (1.77 m/sec). Fig 14.10 shows the horizontal component of the impact force for all the cam angles plotted against machine speed. Fig 14.11 shows typical traces obtained during the experiments using the 49° cam, and Fig 14.12 illustrates the stitch-cam impact and the steady level of cam-force.

These experimental and theoretical results are discussed in chapter 18.

14.5 Further Experimental Measurements.

A series of experiments was designed to investigate the effects of some important parameters upon the stitch cam impact. The experiments are detailed individually in the following subsections.

14.5.1 Effect of Needle Modifications.

A crimped 0.406 mm needle was fitted in a thoroughly cleaned trick. A diagram of this needle is shown in Fig 12.8 diagram I, and Fig 12.11 is the butt-deflection graph. Stitch-cam impact and bounce traces were obtained at varying machine speeds. The method of carrying out the measurements was the same as that detailed in section 14.2. The machine was very lightly oiled and run for approximately ten minutes before traces were taken. A typical sample of traces is included in Fig 14.13, and Fig 14.14 is a graphical plot of impact force against machine speed.

It is seen that for the 0.406 mm crimped needle, that the impact-force is not very much different to results obtained for the 0.443 mm needle on the 49^{o} stitch-cam given in section 14.4. However Fig 14.13 shows the impact delayed after initial stitch-cam contact, this apparently being the effect of the cam un-bending the needle crimp.

A 0.443 mm needle with a very much modified butt was fitted in a thoroughly cleaned trick. The butt shape is shown in Fig 12.8 diagram II and the appropriate butt deflection-against-load graph is given in Fig 12.12. Experiments followed the same procedure as detailed in section 14.1, and a graphical plot of impact force against butt deflection is shown in Fig 14.15. The experimental results clearly illustrate that a major modification to the butt shape had relatively little effect upon the stitch-cam impact.

A standard needle was fitted in a thoroughly cleaned trick. Following the procedure detailed in section 14.2 the impact force was measured, a typical result being presentcd below :-

At a speed of 307 ft/min (1.57 m/sec),
with cam-cylinder clearance = 0.15 mm,
and cam-angle = 49°,

then the maximum horizontal component
of cam-needle reaction force = 1,830 gf,

and the maximum vertical component of
cam-needle reaction force = 1,508 gf.

The needles each side of the standard needle under test were then removed from the tricks, the experiment repeated and a typical result was as follows :-

Machine speed = 307 ft/min,

maximum horizontal component
of cam-needle reaction force = 1,665 gf,

and maximum vertical component of
cam-needle reaction force = 1,398 gf.

The results showed that the impact magnitude decreased when the tricks each side of the standard needle were empty.

The experiments detailed in this subsection showed that major modifications in butt design had little effect upon the stitch-cam impact. However, the small change in the flexibility of the trick-walls, resulting from the removal of the surrounding needles, acted to reduce the magnitude of the stitch-cam impact.

Further discussion concerning these results is included in chapter 18.

14.5.2 Effect of Trick Resistance to Needle Motion.

If a trick becomes damaged during normal operation, or the needle is bent, it is possible that the force required to move the needle vertically in its trick can become very large. An examination of the trick resistance to motion

was carried out on a large number of needles in the knitting machine tricks. It was found that there was a large degree of variation in the force required to move the needles, and, although most were reasonably free, there were some very free in the tricks, and a few very tight.

A 0.443 mm needle was inserted in a cleaned trick, and the trick was then tightened up considerably. Following the experimental procedure detailed in section 14.1, a series of experimental results were obtained at varying speed, typical samples of results being shown in Fig 14.16 (a) and (b). Fig 14.17 is a graphical plot of the experimental horizontal and vertical impact forces.

An experiment to measure the butt deflection of the test needle under horizontal loads followed, the test procedure being as detailed in section 12.3.1. The graphical plot of butt-deflection against load is shown in Fig 14.18. Since the experimentally measured forces were high, it was decided that maximum values of K and G should be used in the theoretical analysis, i.e. 4,780 lbf/in. (852 kgf/cm) and 13.8×10^{-4} in. (35.1×10^{-4} cm).

Using the theory derived in chapter 9 for very low speed measurements.

$$R = \frac{H_d}{\cos\Theta(1-\alpha\mu_1\mu_2) - \sin(\mu_2+\alpha\mu_1)} \quad \ldots (109),$$

where $$H_d = P_d + \mu_1 Q - mg \quad \ldots (110).$$

All the terms are defined in equation (22) chapter 9.

When the cam-cylinder clearance is small α is approximately equal to 1, and when $\mu_2 = 0.08$, $\mu_1 = 0.1$, and $\Theta = 49^\circ$, then equation (109) reduces to :-

$$R = \frac{H_d}{0.523} \quad . \quad . \quad . \quad . \quad (111)$$

The machine was run at low speed and an experimental trace obtained is shown in diagram II Fig 14.16. From this and using equation (111), the value of H_d was determined as 1,650 gf.

Using this value of H_d , the magnitude of the impact force was calculated. The values of the parameters, and the equations used, are shown below :-

$K =$ 4,780 lbf/inch (854 kgf/cm)
$\mu_2 =$ 0.08
$\mu_1 =$ 0.10
$G =$ 13.8×10^{-4} in. (35.1×10^{-4} cm)
$D =$ 3,115 lbf/inch (550 kgf/cm)
$\theta =$ 49°
$n =$ 26,630 rads/sec
$H_d =$ 1,650 gf

$$a^2 = \frac{0.00187v^2 + 1.81}{10^6} \quad . \quad . \quad . \quad (112)$$

$$R_{max} = \frac{K\left(a\cot an\,\theta + \frac{H_d}{D} - G\right)}{\sin\theta + \mu_2 \cos\theta} \quad . \quad . \quad (113)$$

Theoretical curves of horizontal and vertical camforce are superimposed on the experimental results in Fig 14.17. These showed a reasonable degree of agreement particularly when one considereś the nature of the theoretical approximations. Further discussion concerning the effect of trick resistance to motion is contained in chapter 18.

14.5.3 Effect of Needle Mass upon the Impact.

Equation (104), derived in section 14.4.2, had the form:-

$$R_{max} = \frac{K\left(\frac{v}{n} - G\right)}{\sin\theta + \mu_2 \cos\theta} \qquad t \gtrsim \frac{1}{n} \sin^{-1}\left(\frac{Gn}{v}\right) \quad . \quad (114)$$

The equation was considered reasonably valid provided

that :-

(i) $H_d < 40$ gf,

and (ii) $v > 10$ in/sec (0.25 m/sec).

If the needle mass is changed, the most important effect upon equation (114) is the change in the frequency term η . For a needle of mass m_1 the frequency n_1 is defined by the equation :

$$n_1 = \sqrt{\frac{D \cot an \theta}{m_1}} \quad . \quad . \quad (115),$$

if m_1 is changed to be equivalent to a value m_2 then :-

$$n_2 = n_1 \sqrt{\frac{m_1}{m_2}} \quad . \quad . \quad . \quad (116),$$

and the reaction force R is defined by the following equation :

$$\left(\begin{matrix}\text{for needle} \\ \text{mass } m_2\end{matrix}\right) R_{max} = \frac{K\left(\left(\sqrt{\frac{m_2}{m_1}}\left(\frac{v}{n_1}\right)\right) - G\right)}{\sin\theta + \mu_2 \cos\theta} \quad . \quad (117).$$

From equation (117), if m_2 is larger than m_1 , then R_{max} increases; if m_2 is smaller than m_1 , then R_{max} decreases.

Two special needles of differing masses were prepared, (Fig 14.19), one needle with a small piece of metal fixed to the needle head and the other with cut-outs at the back. The masses of the needles were 1.36 g and 0.43 g respectively. Apart from these changes in the needle mass, they were identical to a standard 0.443 mm needle, which had a mass of 0.67 g. Using equation (117), theoretical graphs of R_{max} against machine speed were plotted using the following parameters :-

(i) $\Theta = 49^{\circ}$,
$m = 0.43$ g,

Cam-cylinder
clearance = 0.15 mm

$K =$ 4,450 lbf/inch (794 g/cm)
$G =$ 9.1×10^{-4} in. (23.1×10^{-4} cm)
$\mu_1 =$ 0.1
$\mu_2 =$ 0.08
$D =$ 2,920 lbf/inch (519 kgf/cm)
$n =$ 32,050 rads/sec.
$R_{max} = 0.1723v - 5.05$

(ii) $\theta = 49^{\circ}$,
$m = 1.36$ g,

Cam-cylinder
clearance = 0.15 mm

$K =$ 4,450 lbf/inch (794 kgf/cm)
$G =$ 9.1×10^{-4} in. (23.1×10^{-4}cm)
$\mu_1 =$ 0.1
$\mu_2 =$ 0.08
$D =$ 2,910 lbf/inch (519 kgf/cm)
$n =$ 18,000 rads/sec
$R_{max} = 0.309v - 5.05$

The theoretical plots for both needles are shown on the graph in Fig 14.20.

Experiments were carried out to measure the impact force against machine speed for each of the needles. Initially, the high-mass needle was fitted in a cleaned trick, and the experiment was carried out following the procedure detailed in section 14.2. The needle was then removed from the trick and the experiment repeated with a standard 0.67 g needle. Finally, the low-mass needle was tested. Fig 14.21 shows a typical pair of traces obtained during the experiments. Diagram I shows the impact for the 1.36 g needle at 116 ft/min (0.59 m/sec) and Diagram II the impact for the standard 0.67 g needle at 116 ft/min. The experimental results for the 1.36 and 0.43 g needle are

superimposed upon the theoretical results in Fig 14.20, and Fig 14.22 shows the horizontal components of impact obtained from the experiment.

The results show that the mass of the needle has a large effect upon the stitch-cam impact. Further discussion concerning the effect of needle mass is contained in chapter 18.

14.5.4 Effect of Increasing the Cam-Cylinder Clearance.

From the theoretical analysis, equation(104) derived in section 14.4.2 had the form :-

$$R_{max} = \frac{\frac{Kv}{n} - KG}{(\sin\theta + \mu_2\cos\theta)} \quad -t \geqslant \frac{1}{n}\sin^{-1}\left(\frac{Gn}{v}\right) \quad . \qquad (118)$$

$$\text{where} \qquad n = \sqrt{\frac{K(\cos(1-\alpha\mu_1\mu_2) - \sin\theta(\mu_2+\alpha\mu_1))\operatorname{cotan}\theta}{m(\sin\theta+\mu_2\cos\theta)}} \qquad (119)$$

$$\text{and} \qquad \alpha = \frac{2a}{b} - 1$$

All the terms in the above equation were previously defined in Fig 12.2

When the cam-cylinder clearance is changed, the most important parameters affected are K and α . If the cam-cylinder clearance is changed by only a small amount, then K and α change very little and the impact force will be little different. This conclusion was confirmed by an experiment. Fig 14.23 shows the impact force with a cam-cylinder clearance of 0.15 mm superimposed over results obtained with

a cam-cylinder clearance of 0.38 mm, from which it can be seen that there was little difference between them.

Detailed experimentation to determine the effect of increasing the cam-cylinder clearance by a large amount was not undertaken. However, observation of equations (118) and (119) shows that as both the clearance and $\propto$ become larger, then η rapidly becomes smaller due to the term :-

$$\cos\theta\,(1-\propto\mu_1\mu_2) - \sin\theta\,(\mu_2+\propto\mu_1).$$

As η becomes smaller, R_{max} increases, and when

$$\cos\theta\,(1-\propto\mu_1\mu_2) = \sin\theta\,(\mu_2+\propto\mu_1),$$

R_{max} is theoretically infinite.

14.6 <u>Measurements of Needle Bounce down the Stitch-Cam.</u>

Alternately 30°, 60° and 45° cams were fitted to the impact transducer, which was positioned each time so that the cam was only 0.15 mm from the cylinder. Before each set of results was taken, the bounce transducer was switched on for a short warming-up period, and the machine was very lightly oiled.

Four typical results for the 45° cam are shown in Fig 14.24, and Fig 14.25 is a graph of the time interval between primary and secondary impacts, and the total time involved in bouncing for a range of machine speeds.

During the experiments, the following conclusions were reached :-

(i) When the needle was very free in the trick bouncing started earlier, there were more losses of contact, and bounce extended further down the cam.

(ii) As machine speed was increased, the tendency for loss of contact, and the number of bounces, increased.

Further discussion concerning the bounce process

is contained in chapter 18, together with a summary of results.

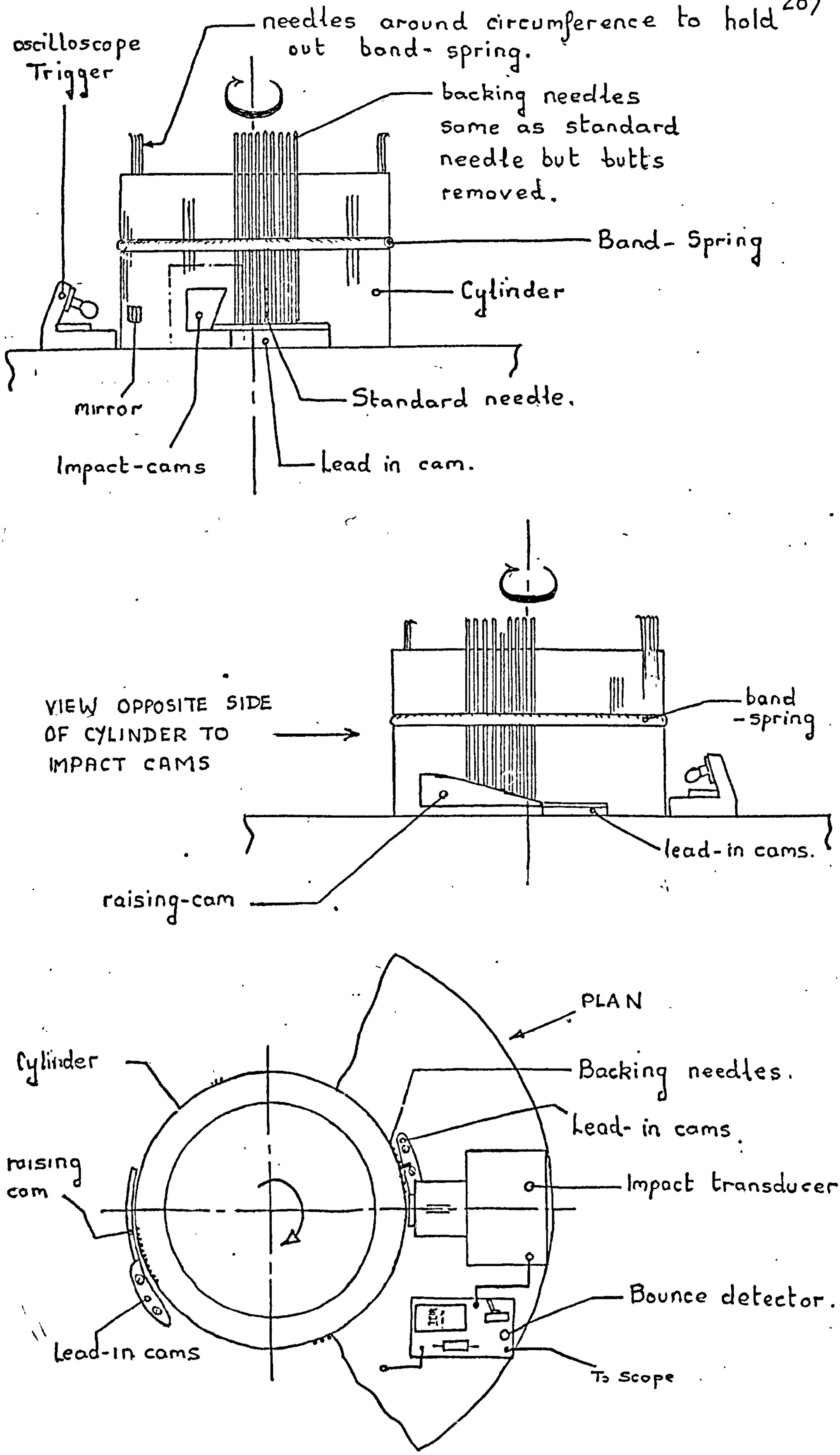

STITCH-CAM-IMPACT EXPERIMENTAL ARRANGEMENT

FIG 14.1

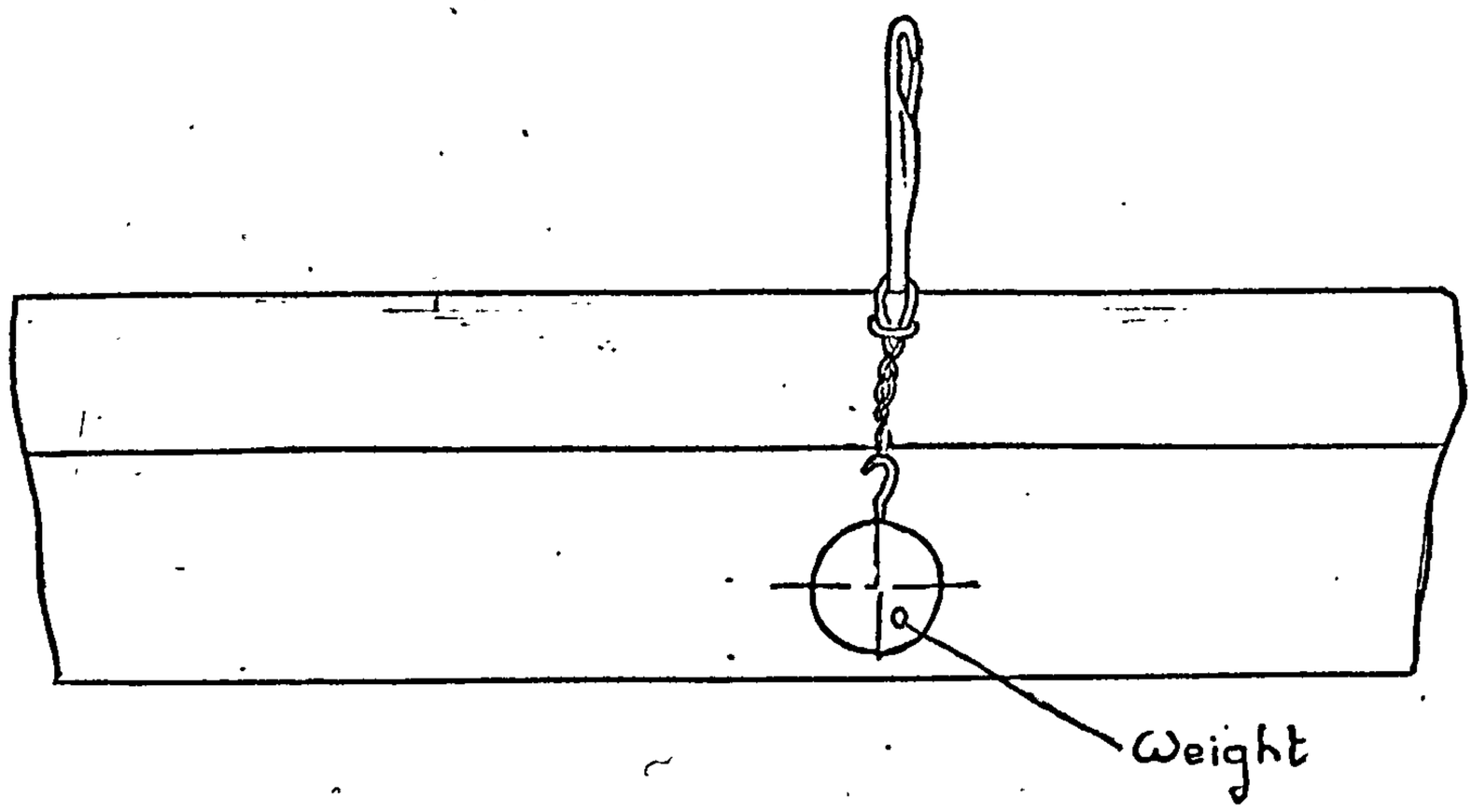

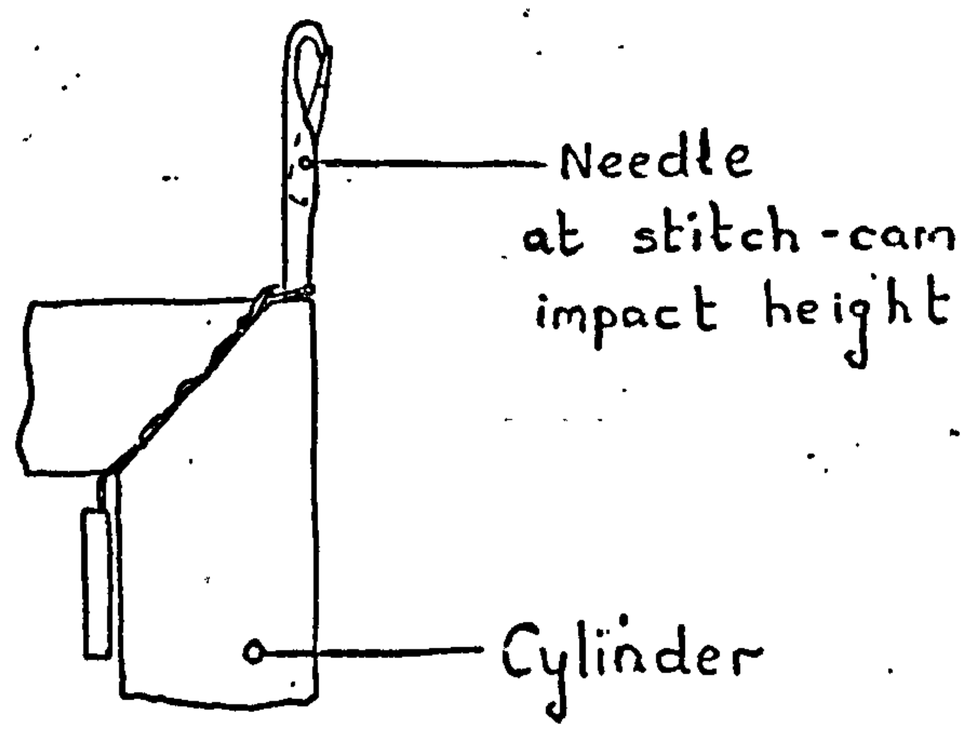

EXPERIMENTAL SIMULATION
OF FABRIC TAKE-DOWN TENSION

FIG 14.2

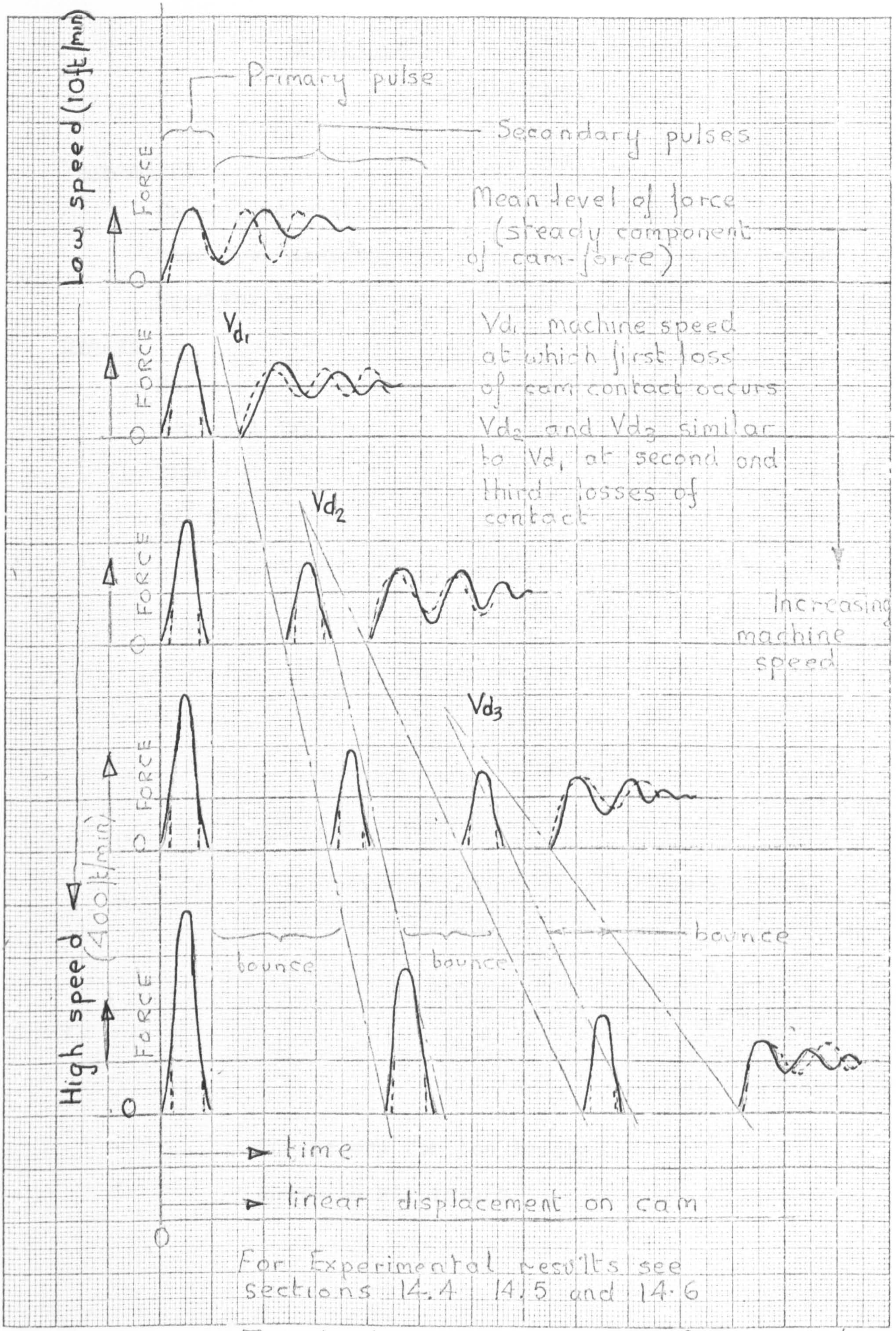

THEORETICAL AND PRACTICAL IMPACT FORCE AND PULSE SHAPE DUE TO THE IMPACT PROCESS

FIG 14.3

Effect of the Yarn-Loop around the Needle Shank

Parameters

Cam-cylinder clearance	= 0.15 mm (0.006 in.)
Take-down tension	= 13.6 gf/needle
Speed for both traces	= 391 ft/min (2 m/sec)

Scales

Horizontal Impact	= 69.4 gf/mm
Vertical Impact	= 76.5 gf/mm
Time	= 0.2×10^{-3} secs/8.5 mm
49° Cam	

Parameters for the traces shown in Fig 14.4(b)

Fig 14.4(a)

DIAGRAM I

Yarn around Shank

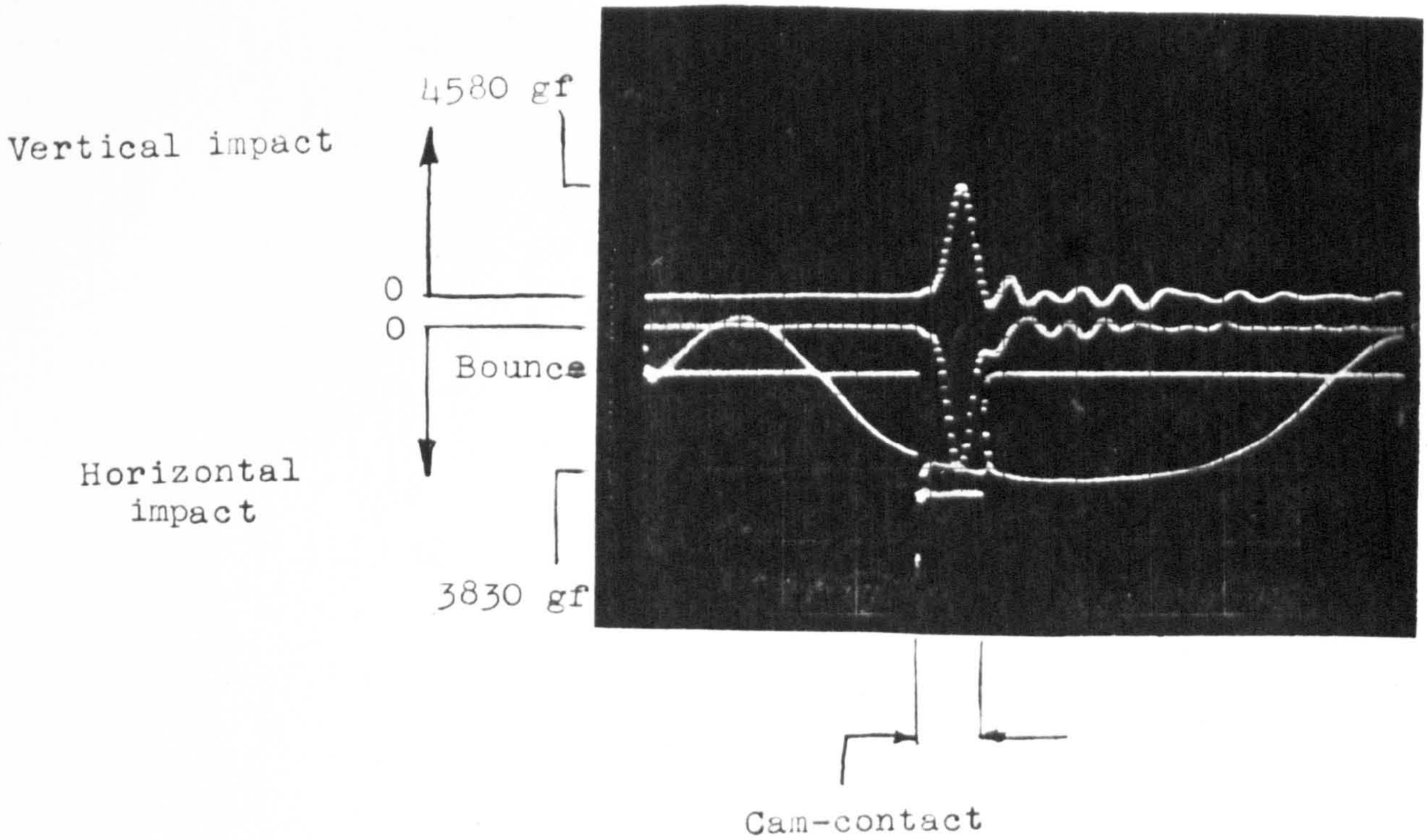

DIAGRAM II

No Yarn around Shank

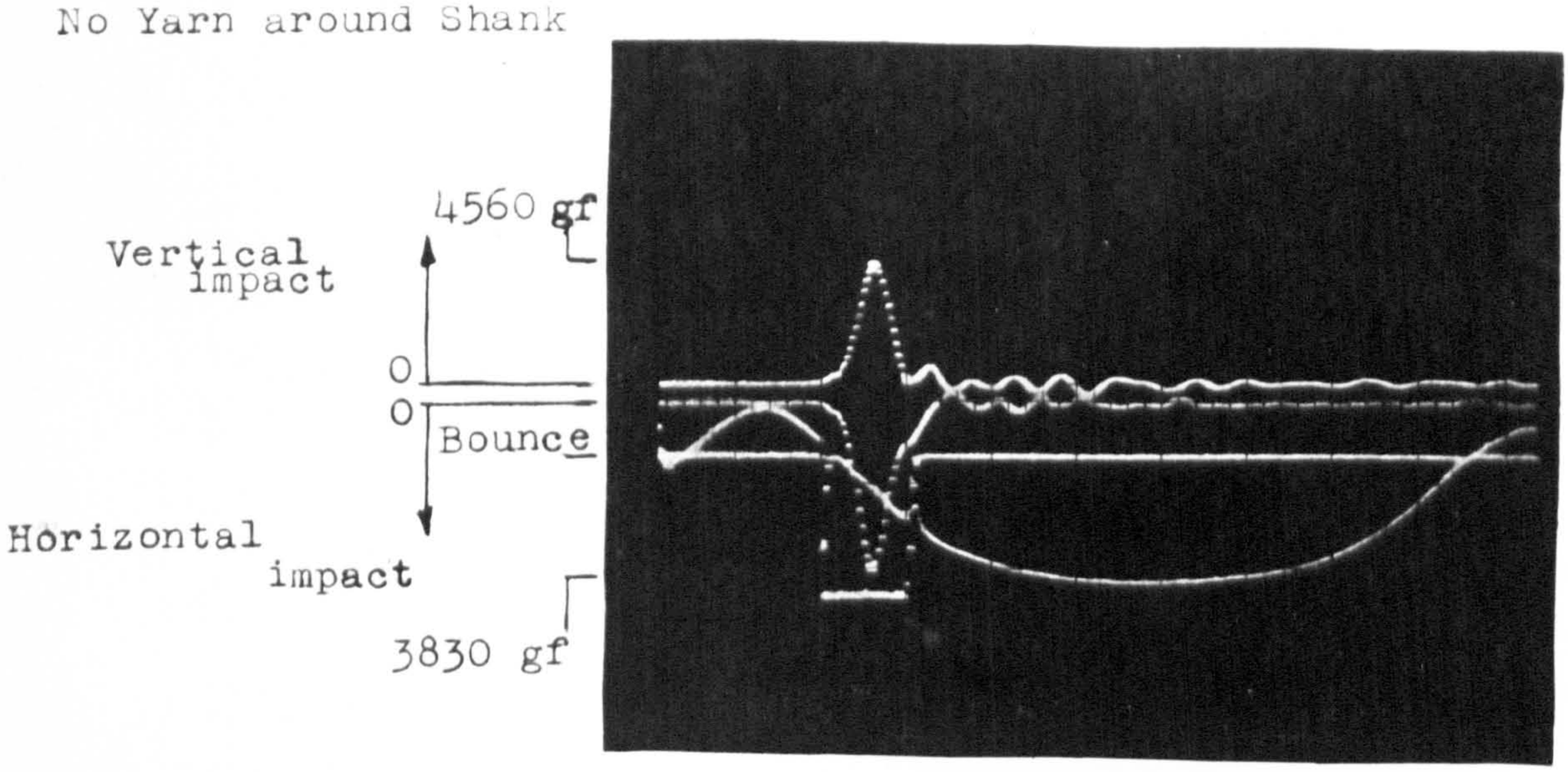

Effect of the Yarn-Loop around the Needle Shank

Fig 14.4(b)

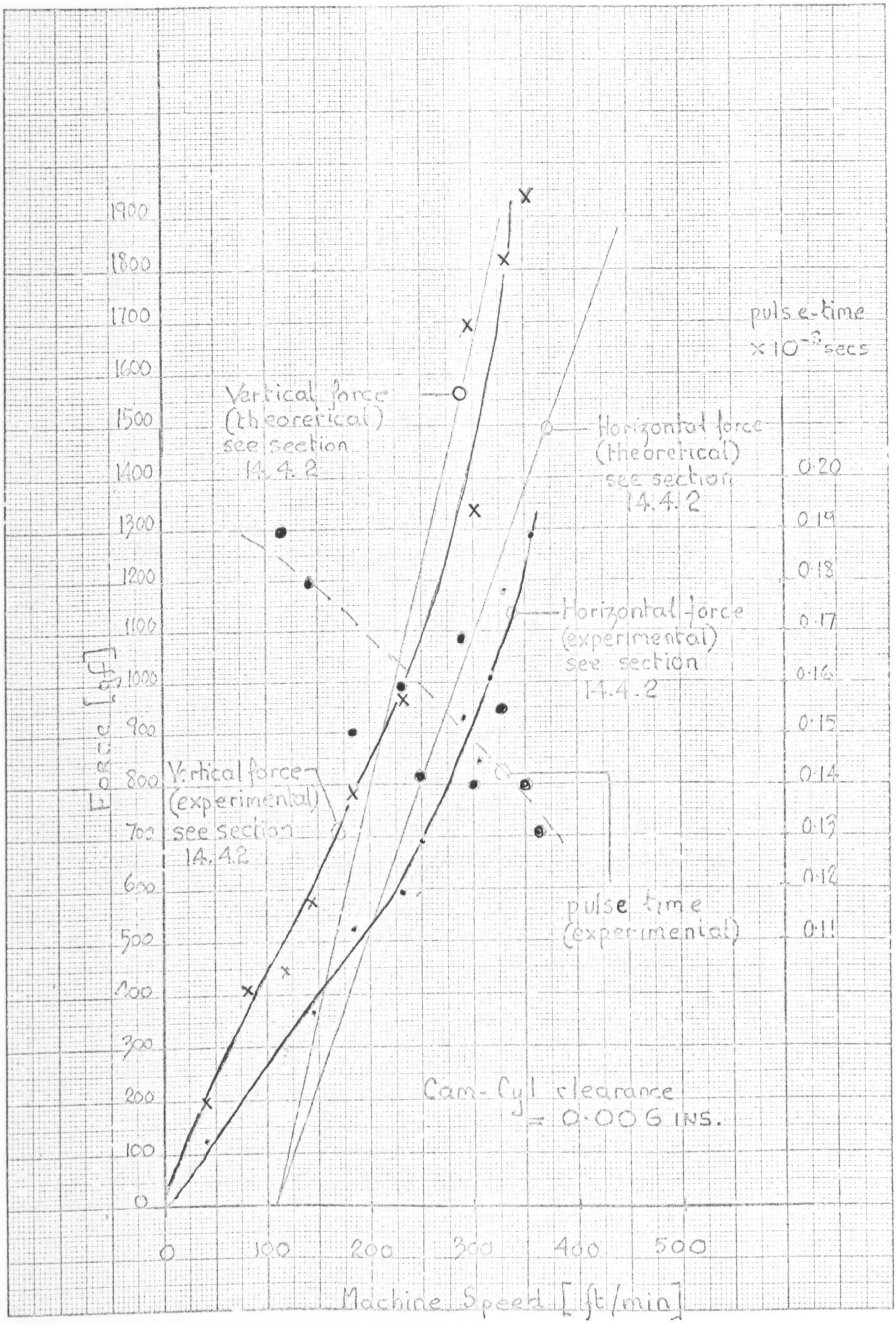

THEORETICAL AND EXPERIMENTAL IMPACT FORCE (0·443 mm NEEDLE) 30° Cam.

FIG 14.5

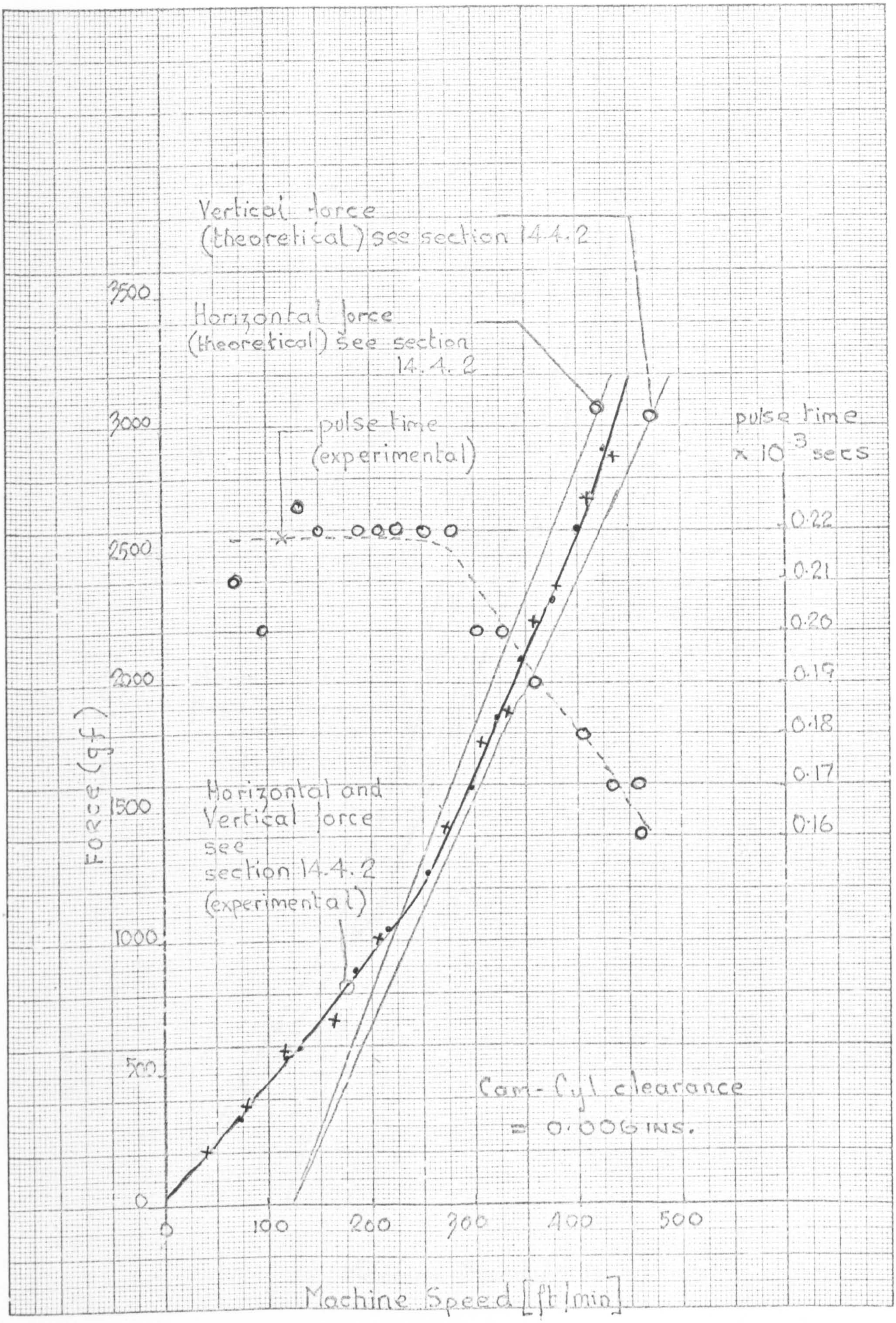

THEORETICAL AND EXPERIMENTAL IMPACT FORCE
(0.443mm NEEDLE) 45° CAM

FIG 14.6

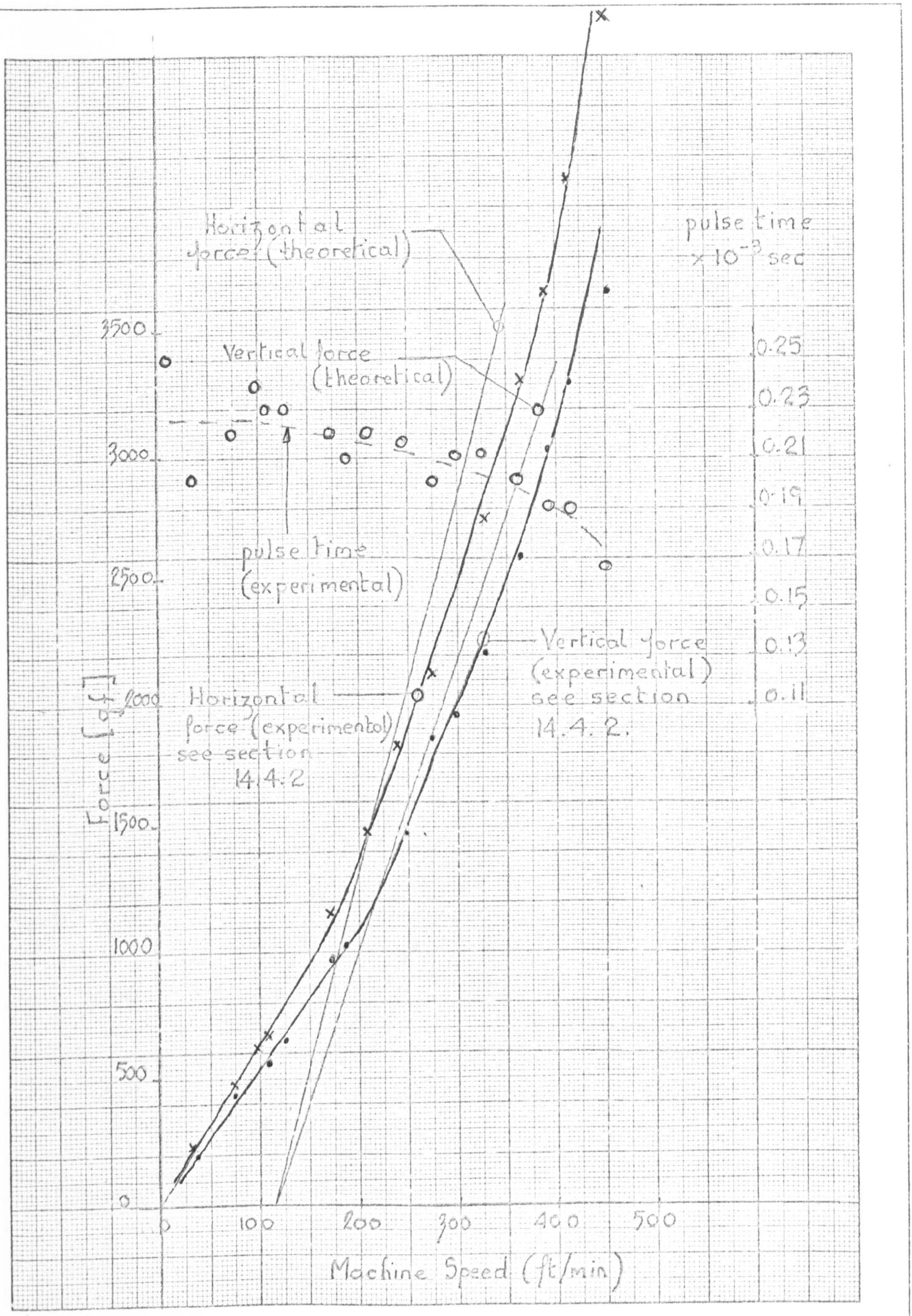

THEORETICAL AND EXPERIMENTAL IMPACT FORCE (0·443 mm NEEDLE) 49° CAM

FIG 14.7

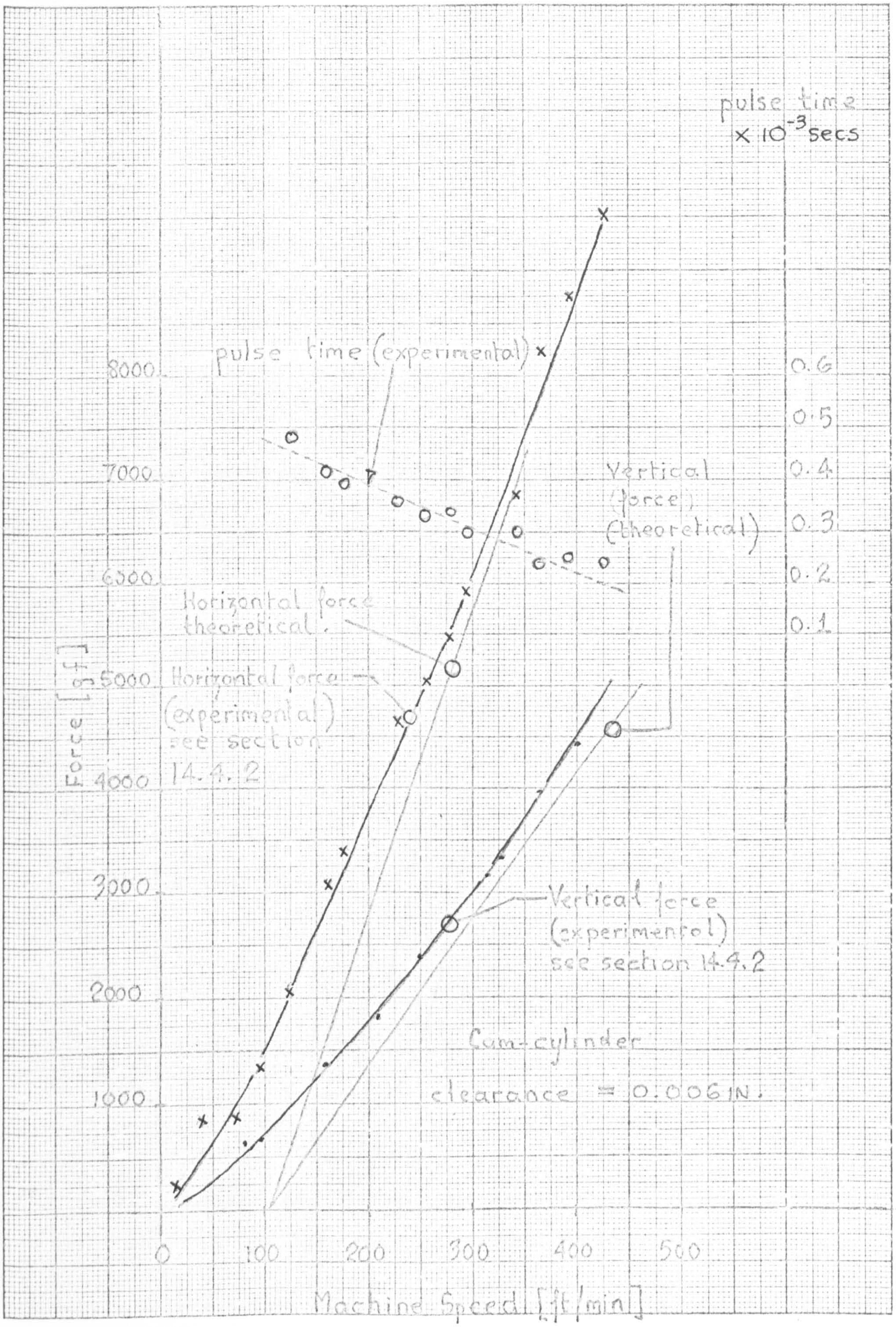

THEORETICAL AND EXPERIMENTAL IMPACT FORCE
(0.443 mm NEEDLE) 60° CAM

FIG 14.8

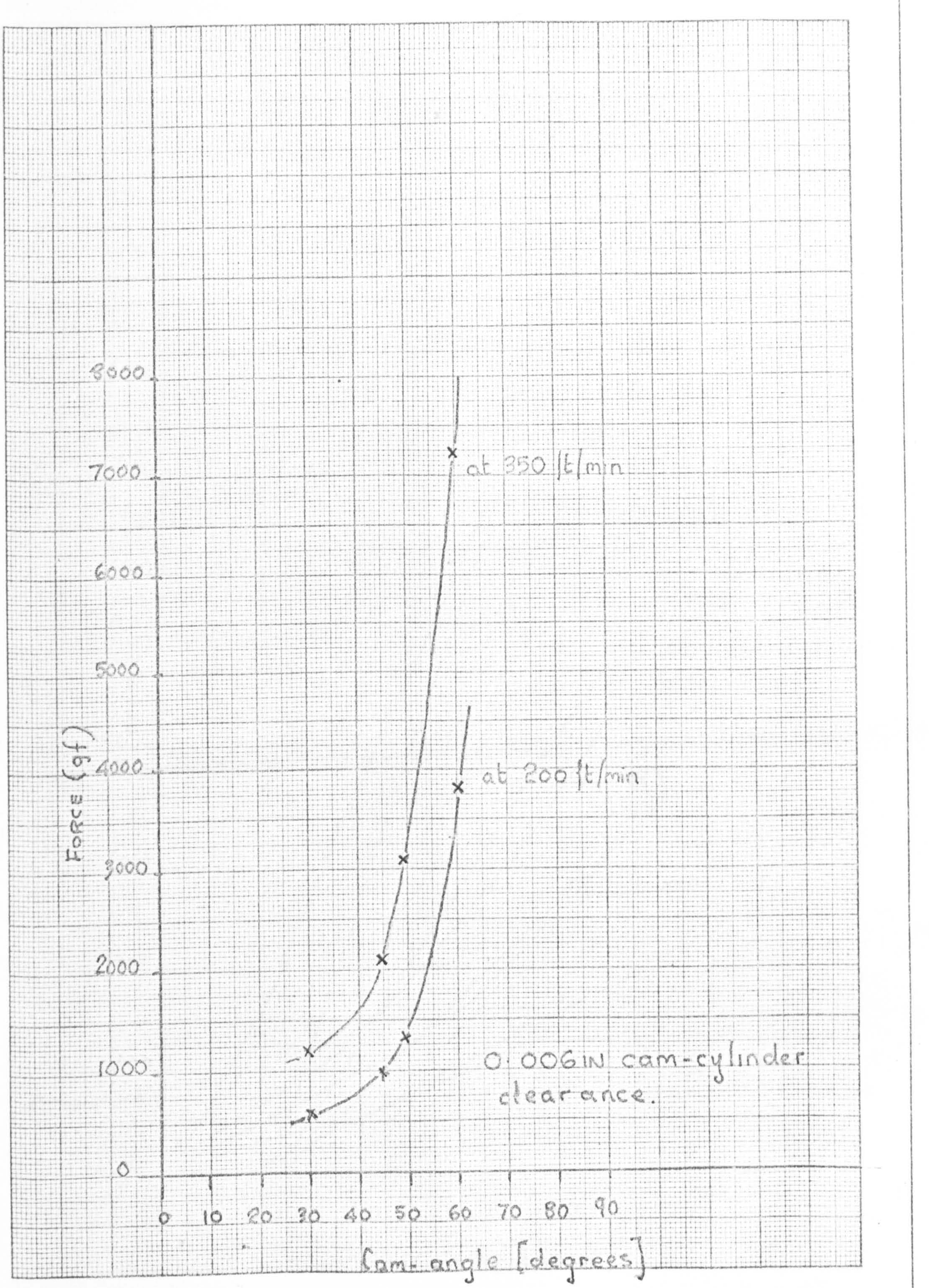

EXPERIMENTAL IMPACT FORCE AGAINST CAM-ANGLE (0.443 mm NEEDLE)

FIG 14.9.

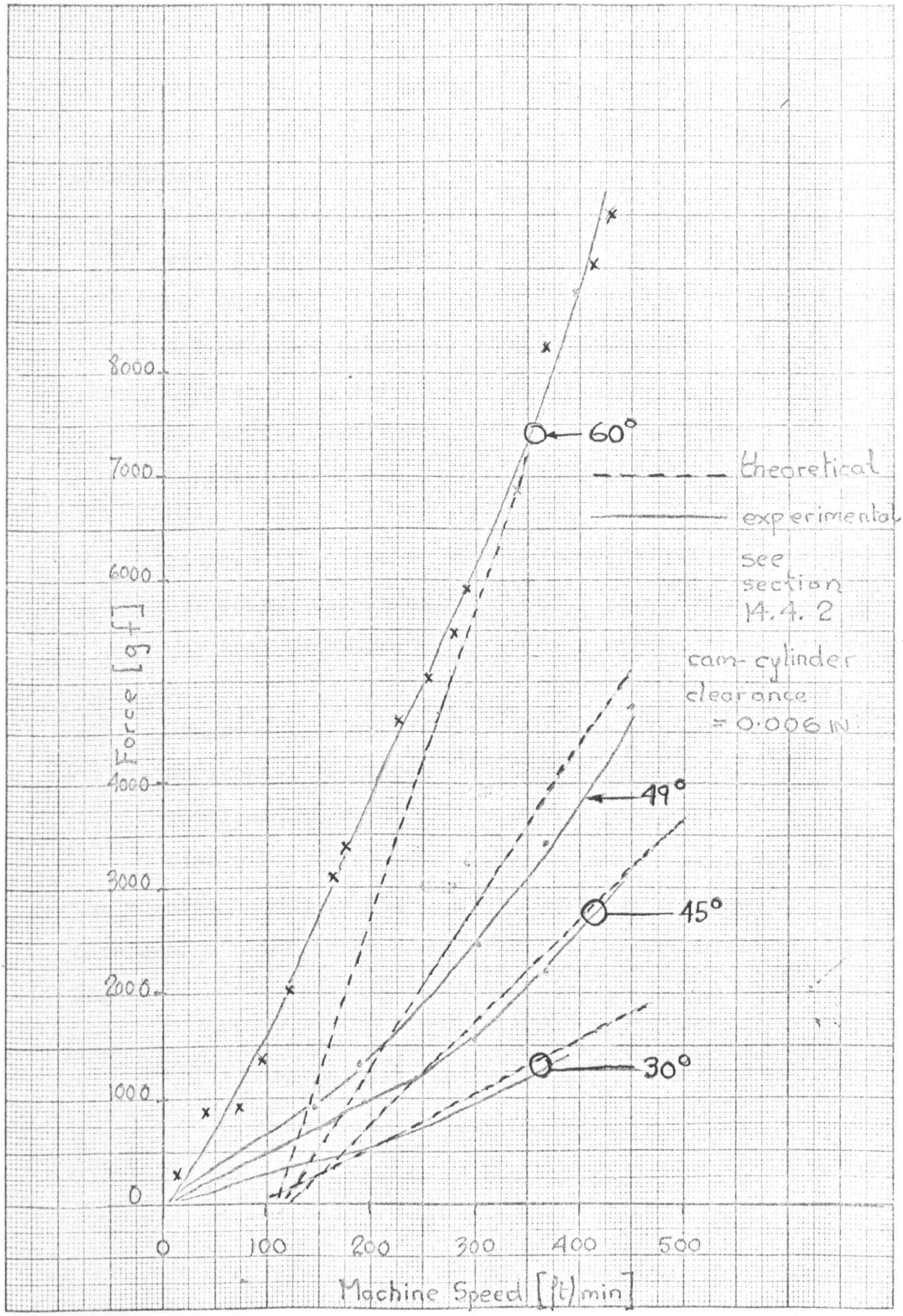

HORIZONTAL COMPONENT OF IMPACT (THEORY AND EXPERIMENT) 30°, 45°, 49° and 60° CAMS.

FIG 14.10

Effect of Machine Speed upon Impact Force

Parameters

0.443 mm standard needle

very little oil added

49^{o} Cam

Cam-cylinder clearance = 0.15 mm

Diagram I speed = 46.6 ft/min

Horizontal Cam-force = 27.8 gf/mm

Vertical Cam-force = 67.4 gf/mm

Time = 0.5×10^{-3} secs/8.5 mm

Diagram II speed = 204 ft/min

Horizontal Cam-force = 69.5 gf/mm

Vertical Cam-force = 67.4 gf/mm

Time = 0.2×10^{-3} secs/8.5 mm

Diagram III speed = 256 ft/min

Horizontal Cam-force = 69.5 gf/mm

Vertical Cam-force = 67.4 gf/mm

Time = 0.2×10^{-3} secs/8.5 mm

The results shown in Fig 14.11(b) were not obtained for the same needle trick arrangement used for the graphical results in Fig 14.7.

Parameters for the traces shown in Fig 14.11(b)

Fig 14.11(a)

DIAGRAM I
Speed = 46.6 ft/min

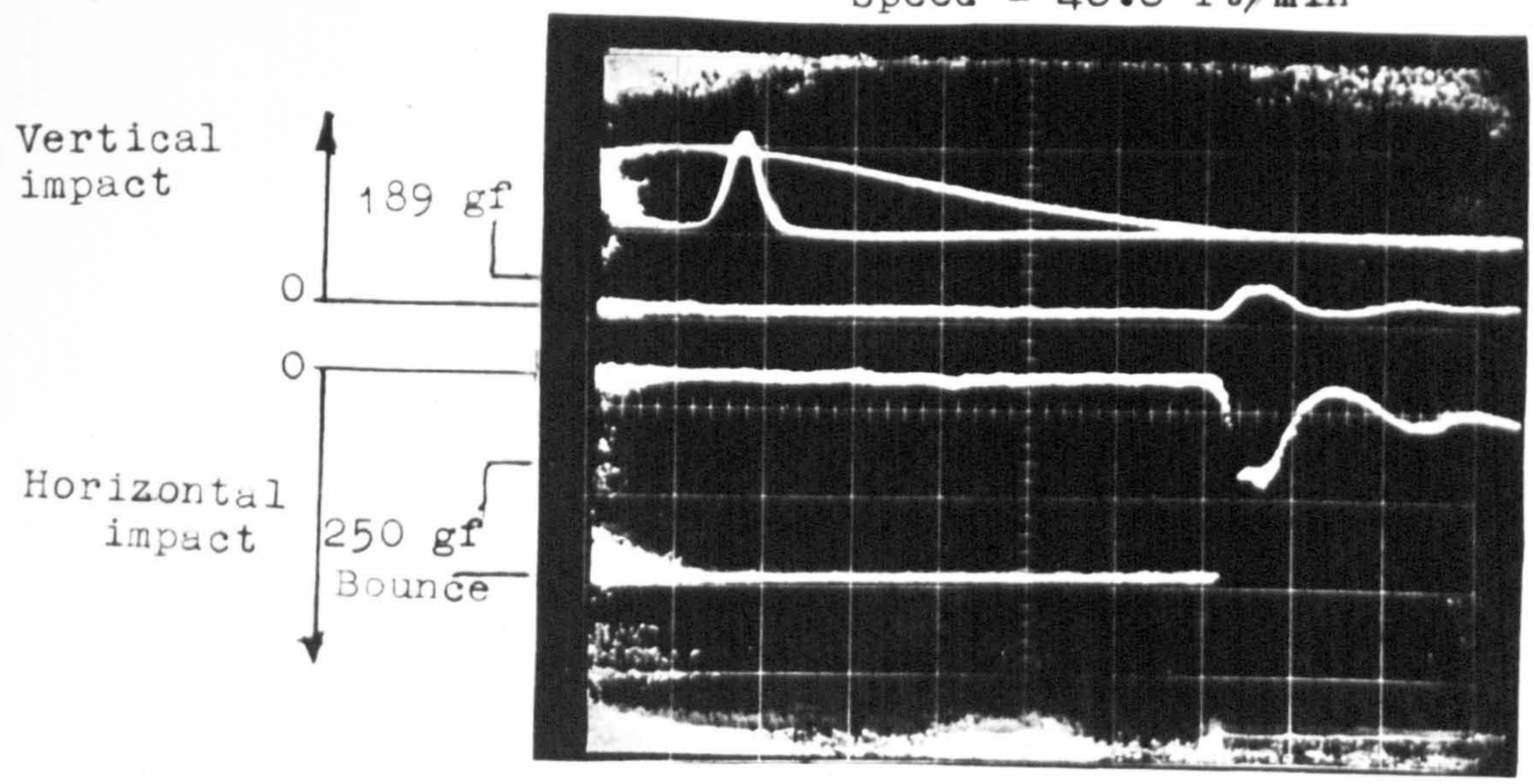

DIAGRAM II
Speed = 204 ft/min

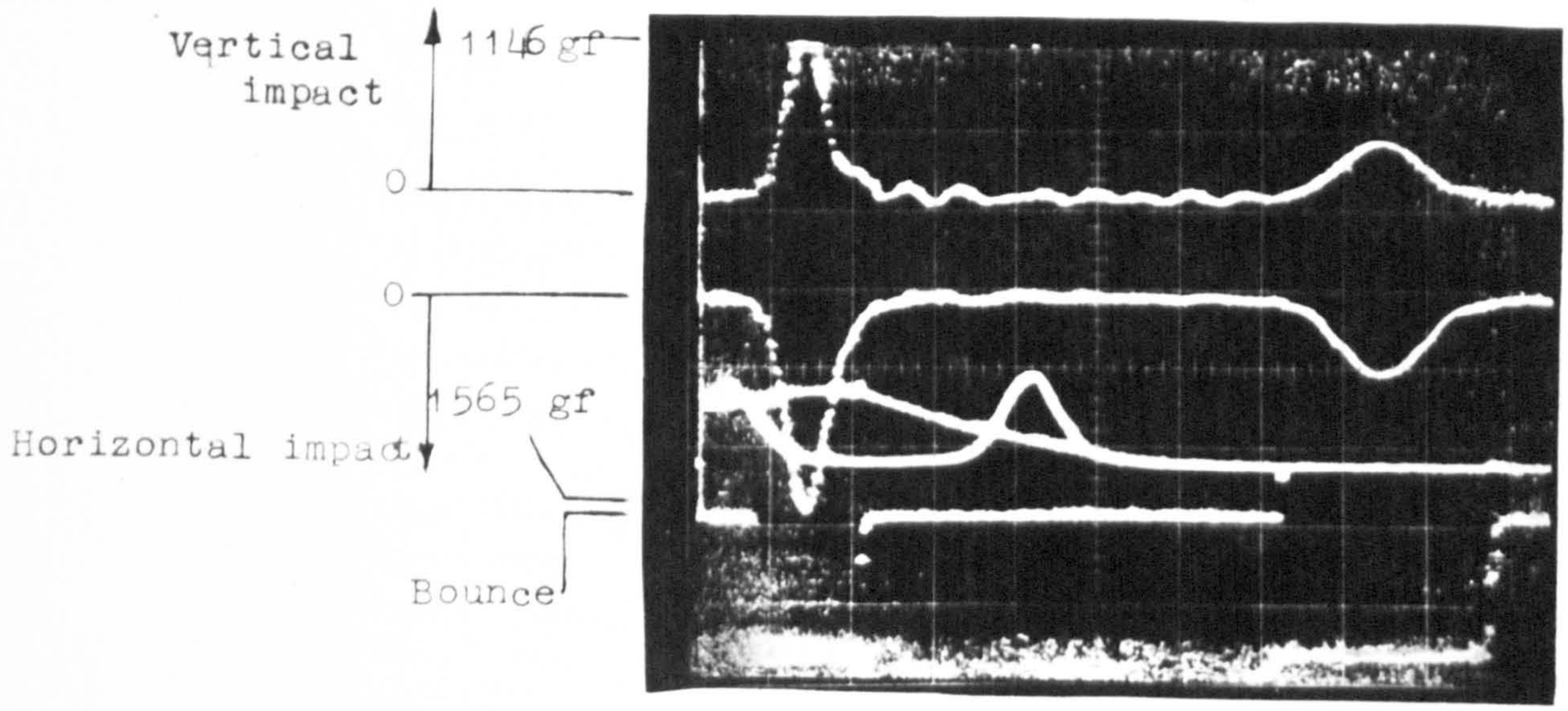

DIAGRAM III
Speed = 256 ft/min

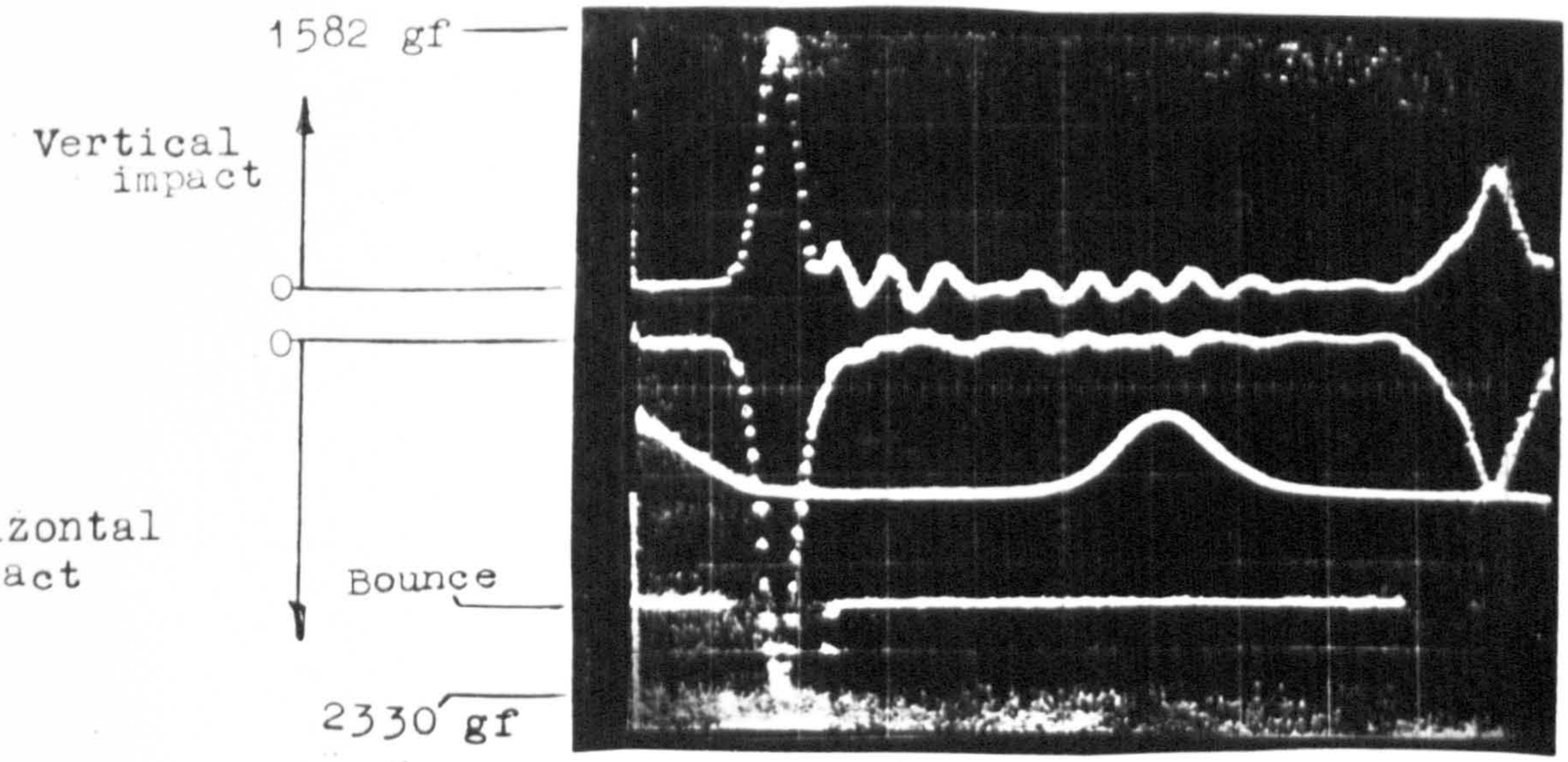

Effect of Machine Speed upon Impact Force

Fig 14.11(b)

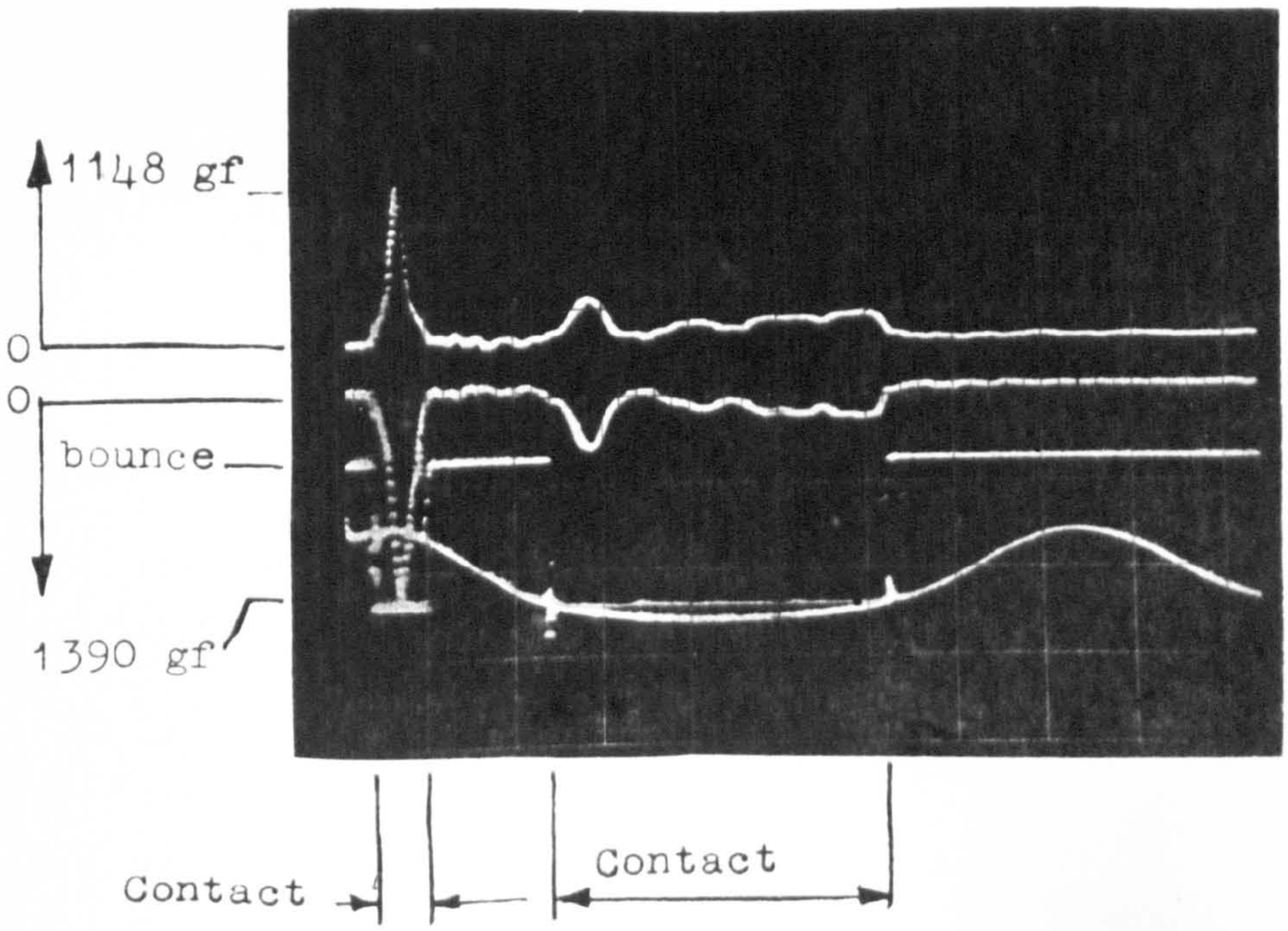

Machine Speed = 181 ft/min (0.92 m/sec)
49° Cam
Cam-cylinder clearance = 0.15 mm (0.006 in.)
Time = 0.5 X 10^{-3} secs/div (1div = 8.5 mm)
Horizontal impact = 69.4 gf/1 mm
Vertical impact = 76.5 gf/1 mm

STITCH-CAM IMPACT

Fig 14.12

Stitch-Cam Impact Crimped 0.406 mm Needle

Parameters

Cam-cylinder clearance	= 0.15 mm (0.006 in.)
Time	= 0.2×10^{-3} Secs/div (1 div = 8.5 mm)

Scales

Horizontal Impact		= 69.4 gf/1 mm
Vertical Impact		= 76.5 gf/1 mm
Diagram I	Speed	= 157.5 ft/min (0.8 m/min)
Diagram II	Speed	= 273 ft/min (1.38 m/min)

49^{o} Cam

Parameters for traces shown in Fig 14.13(b)

Fiv 14.13(a)

DIAGRAM I

157.5 ft/min

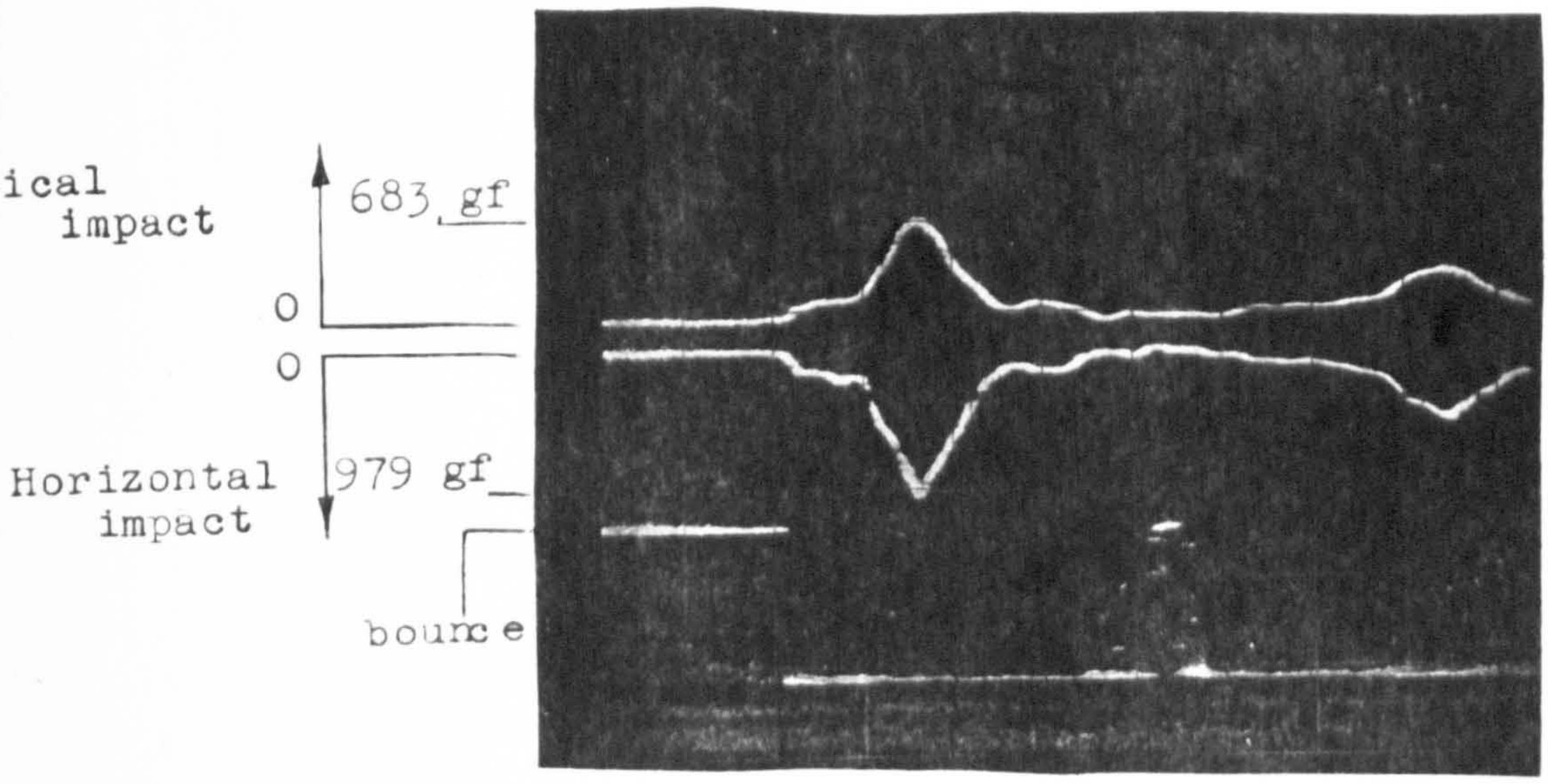

DIAGRAM II

273 ft/min

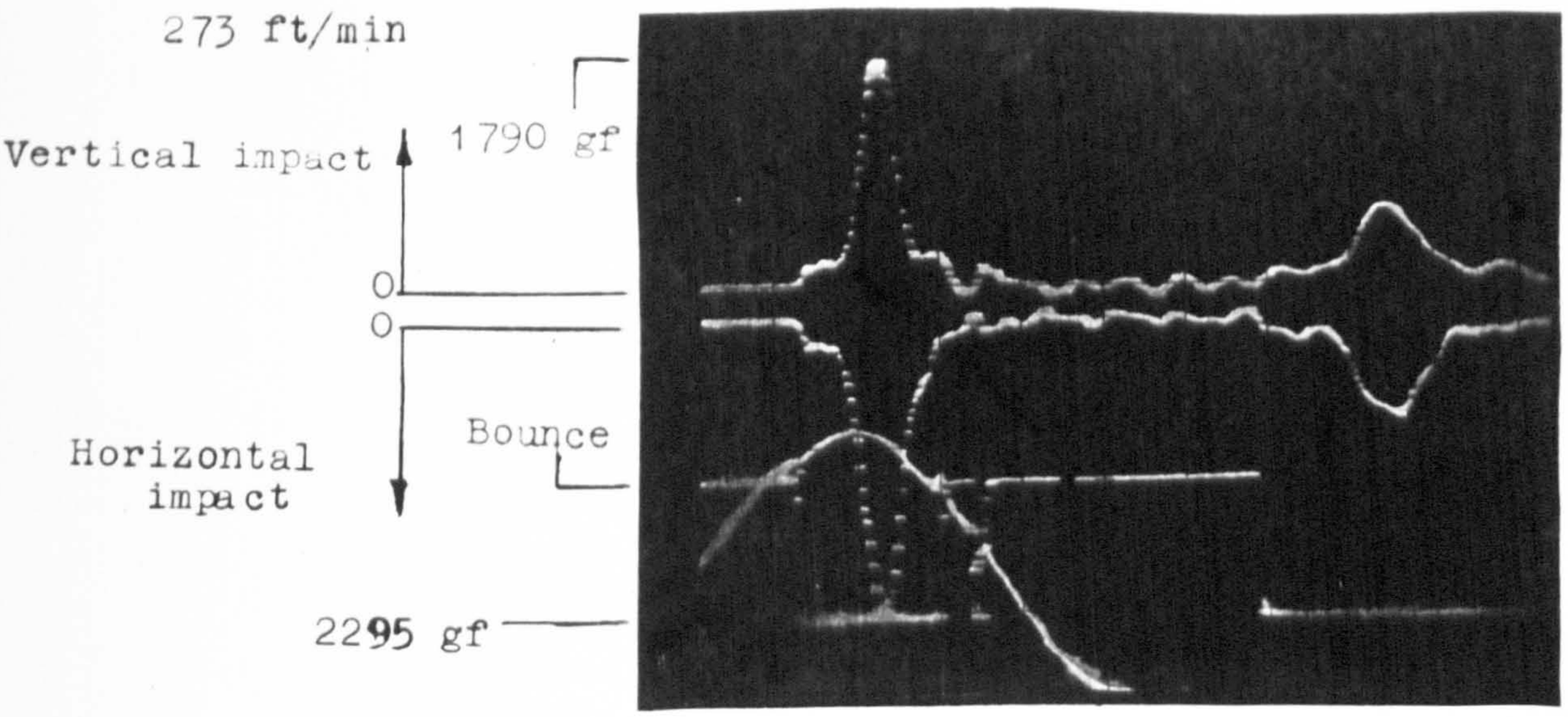

Stitch-Cam Impact

Crimped Needle

Fig 14.13(b)

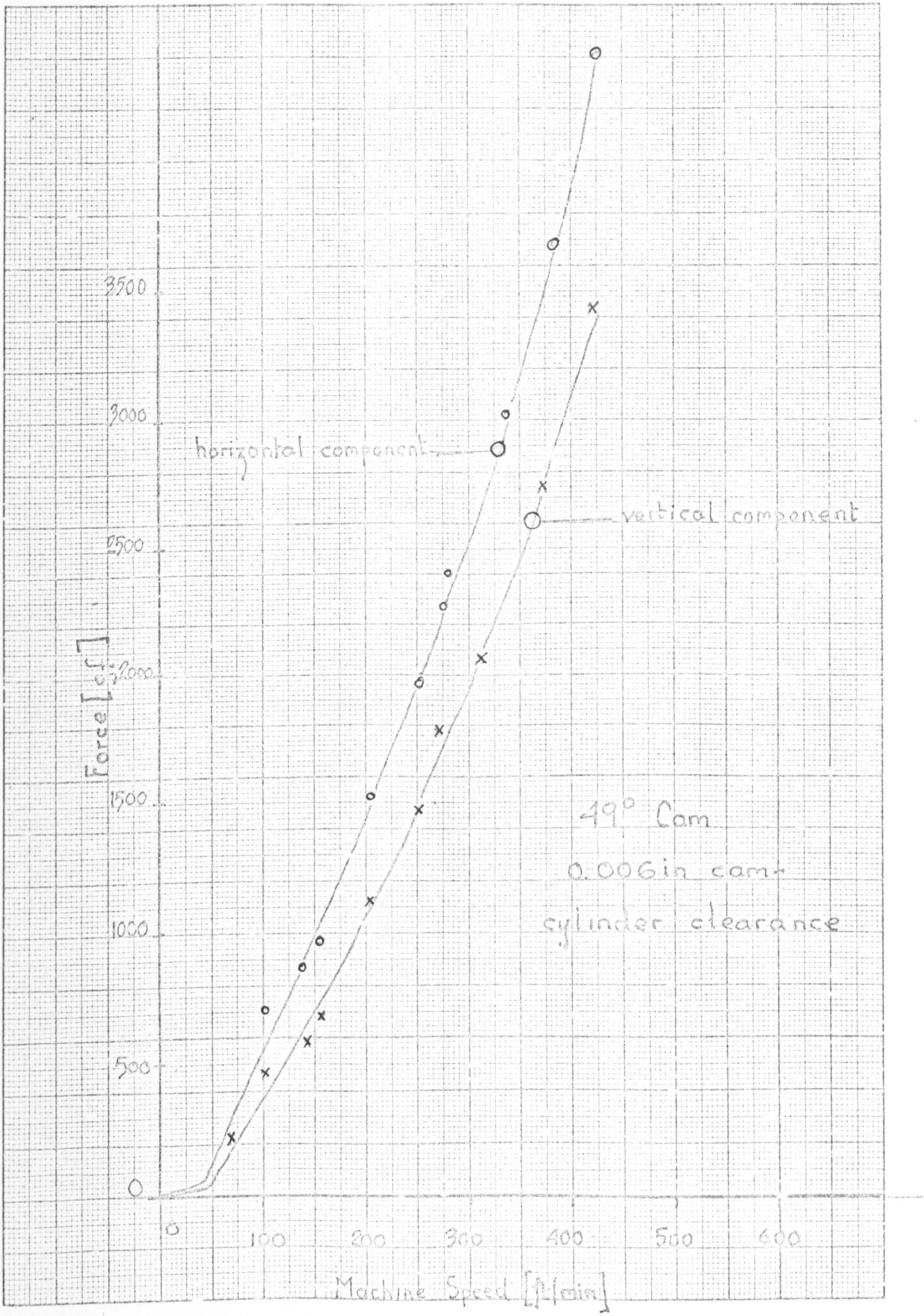

EXPERIMENTALLY MEASURED IMPACT MAGNITUDE
0.406 mm CRIMPED NEEDLE

FIG 14.14

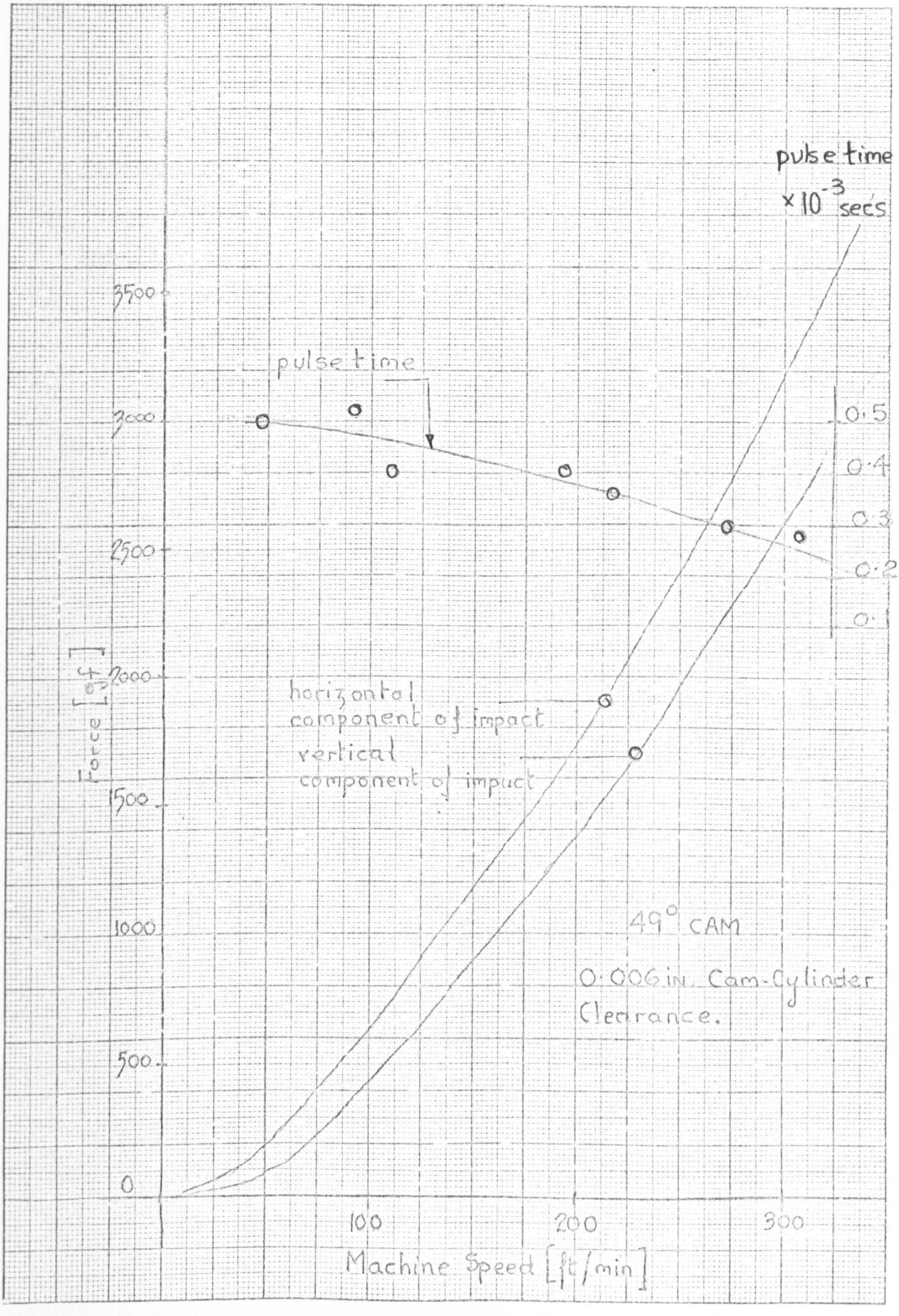

EXPERIMENTALLY MEASURED IMPACT MAGNITUDE
0·443 mm needle reduced butt (Diagram II Fig 12.8)

FIG 14.15

Effect of Trick Resistance to Needle Motion

Parameters

Cam-cylinder clearance = 0.15 mm (0.006 in.)

Scales

Horizontal Impact = 278 gf/mm

Vertical Impact = 306 gf/mm

Diagram I - speed = 200 ft/min (1 m/sec)

Diagram II - speed = 4 ft/min (0.02 m/sec)

Diagram III- speed = 359 ft/min (1.82 m/sec)

49^{o} Cam

Needle type - 0.443 mm see Fig 3.2

Parameter for traces

shown in Fig 14.16(b)

Fig 14.16(a)

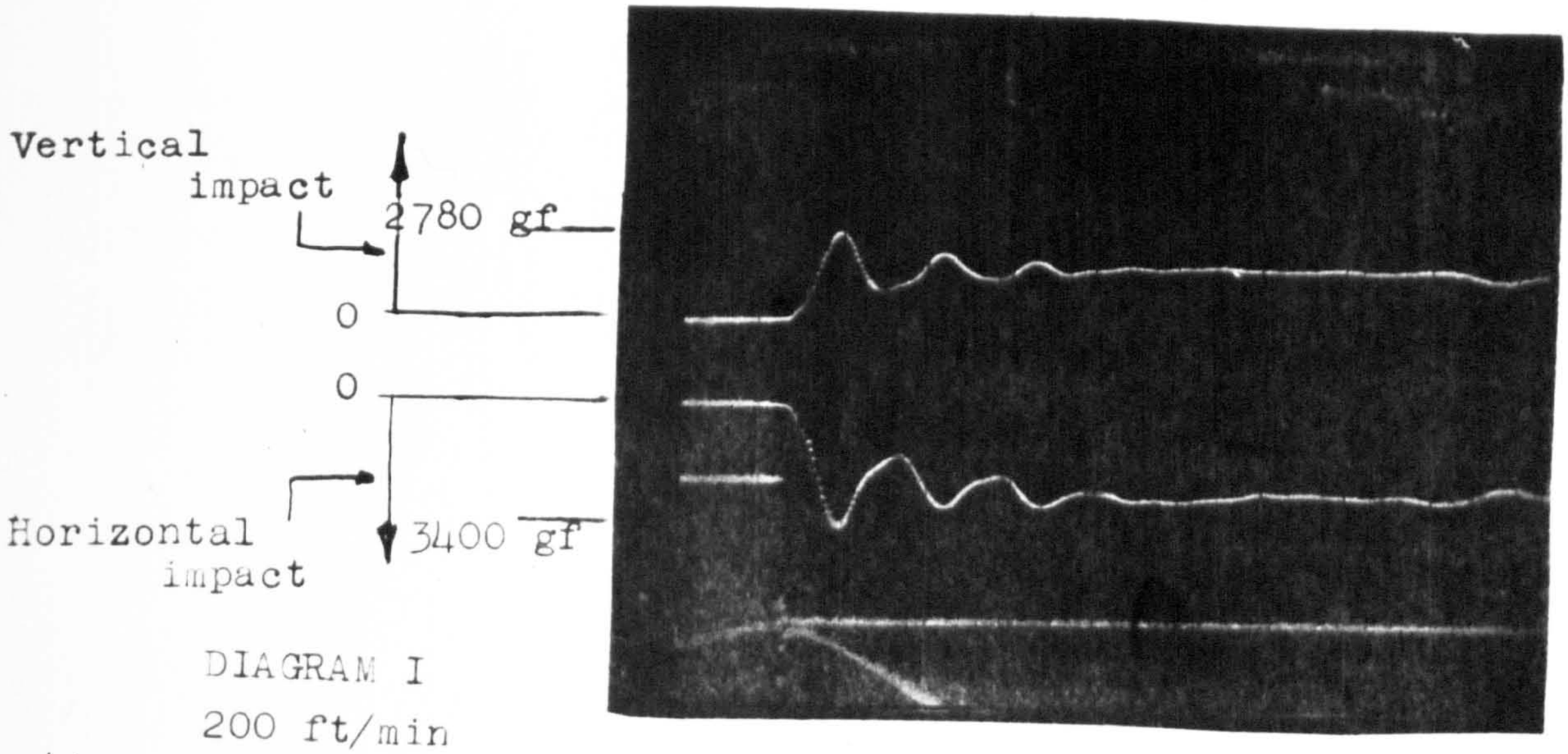

DIAGRAM I
200 ft/min

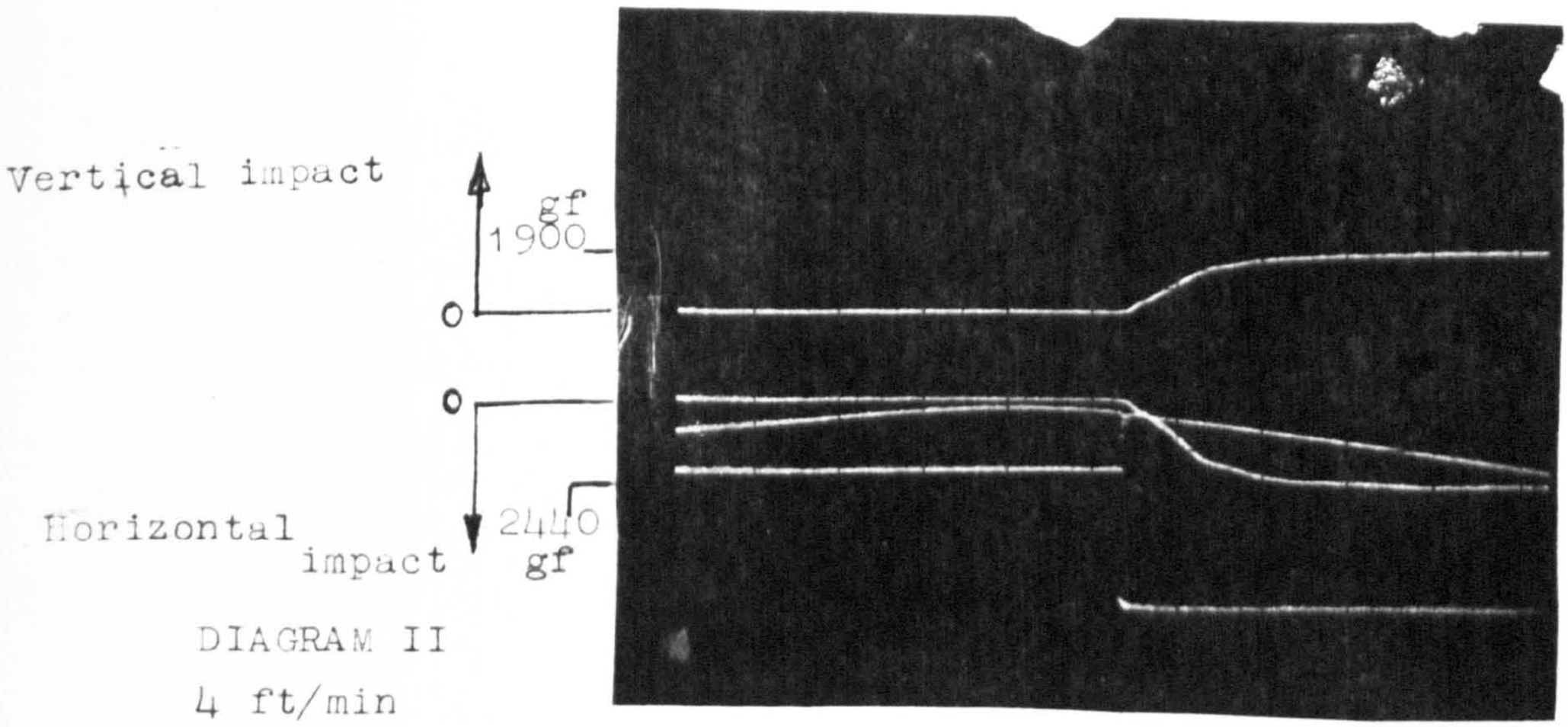

DIAGRAM II
4 ft/min

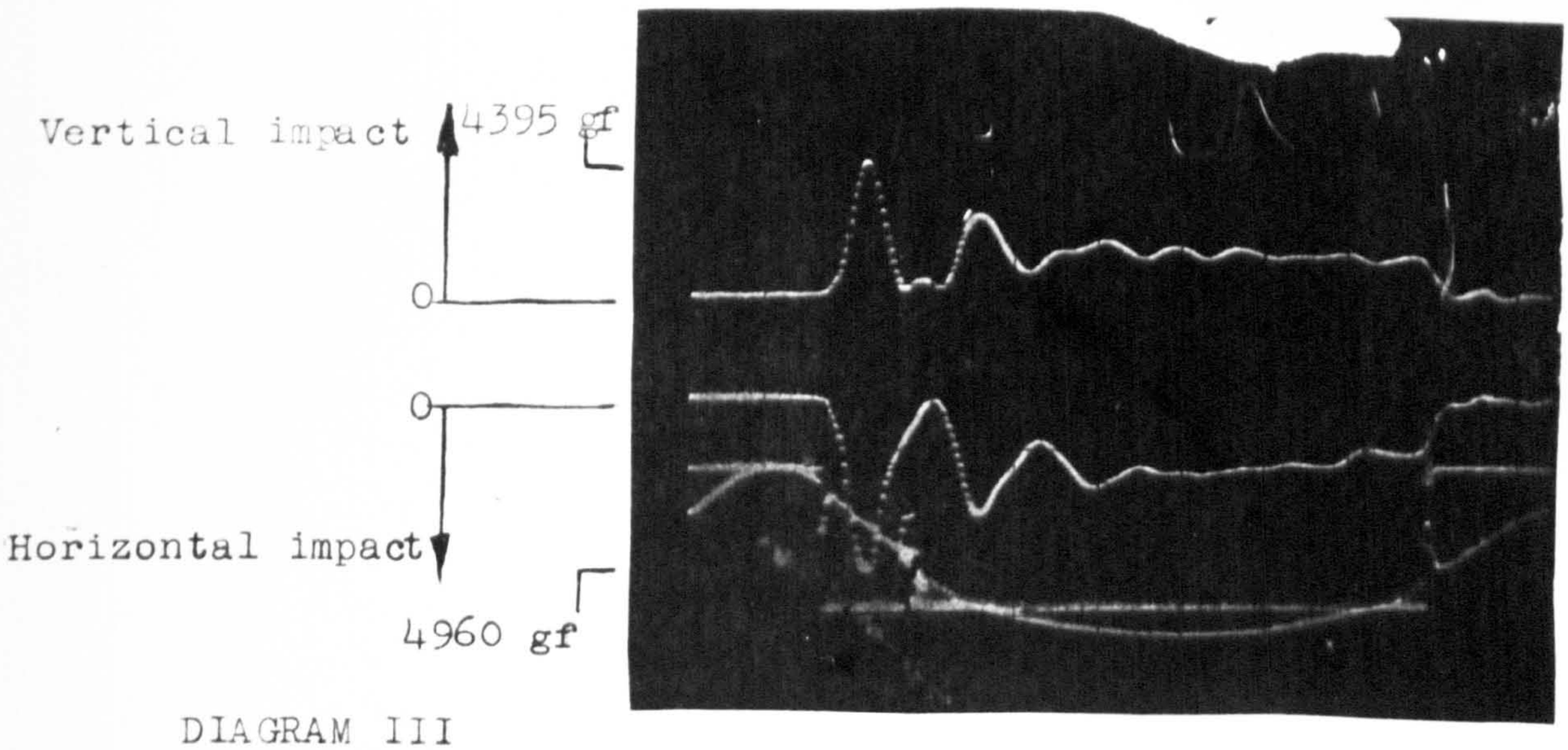

DIAGRAM III
359 ft/min

Effect of Trick
Resistance to Needle

Fig 14.16(b)

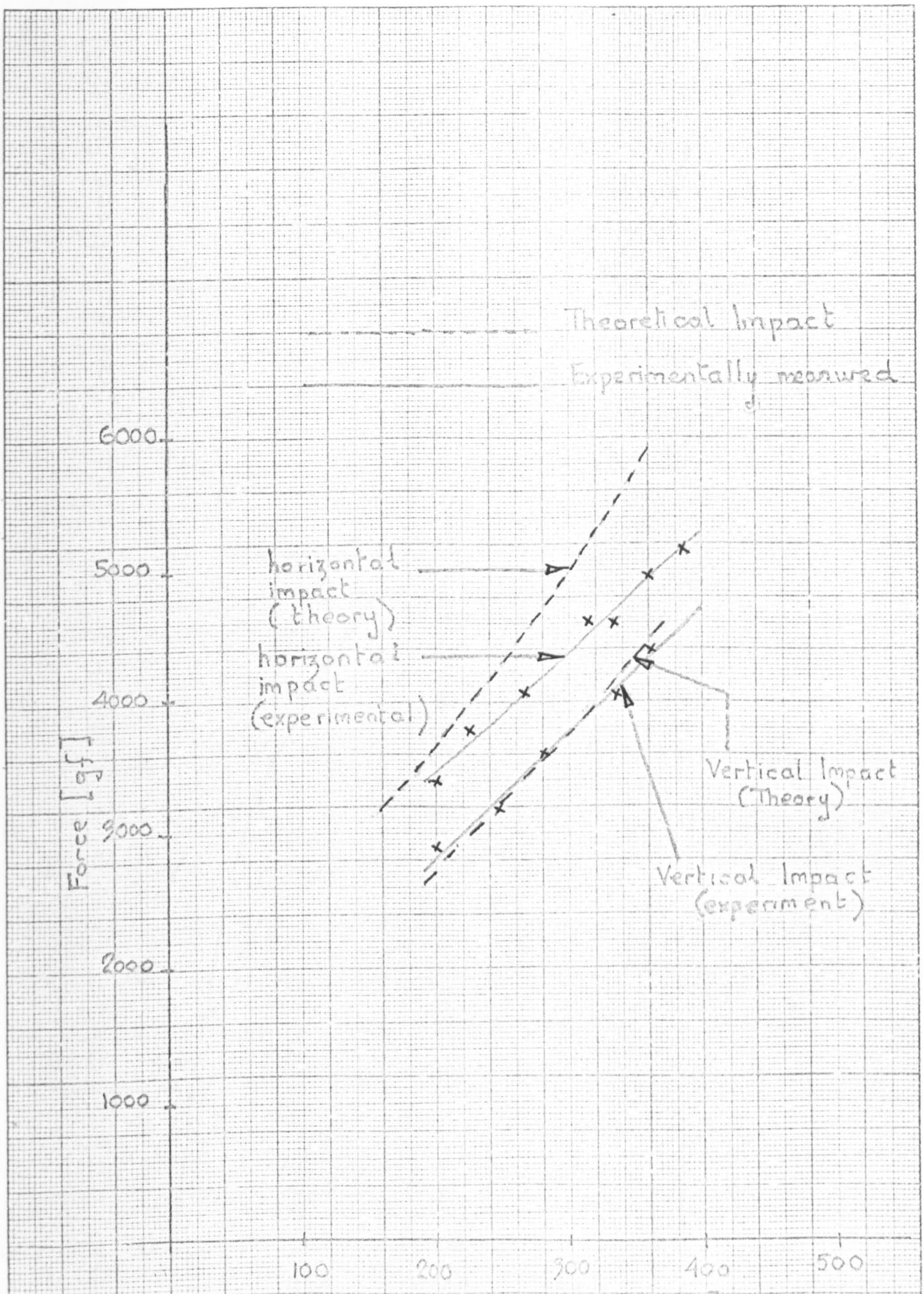

IMPACT MAGNITUDE, 49° CAM, 0.443 mm NEEDLE
HIGH TRICK RESISTANCE SEE SECTION 14.5.2

FIG 14.17

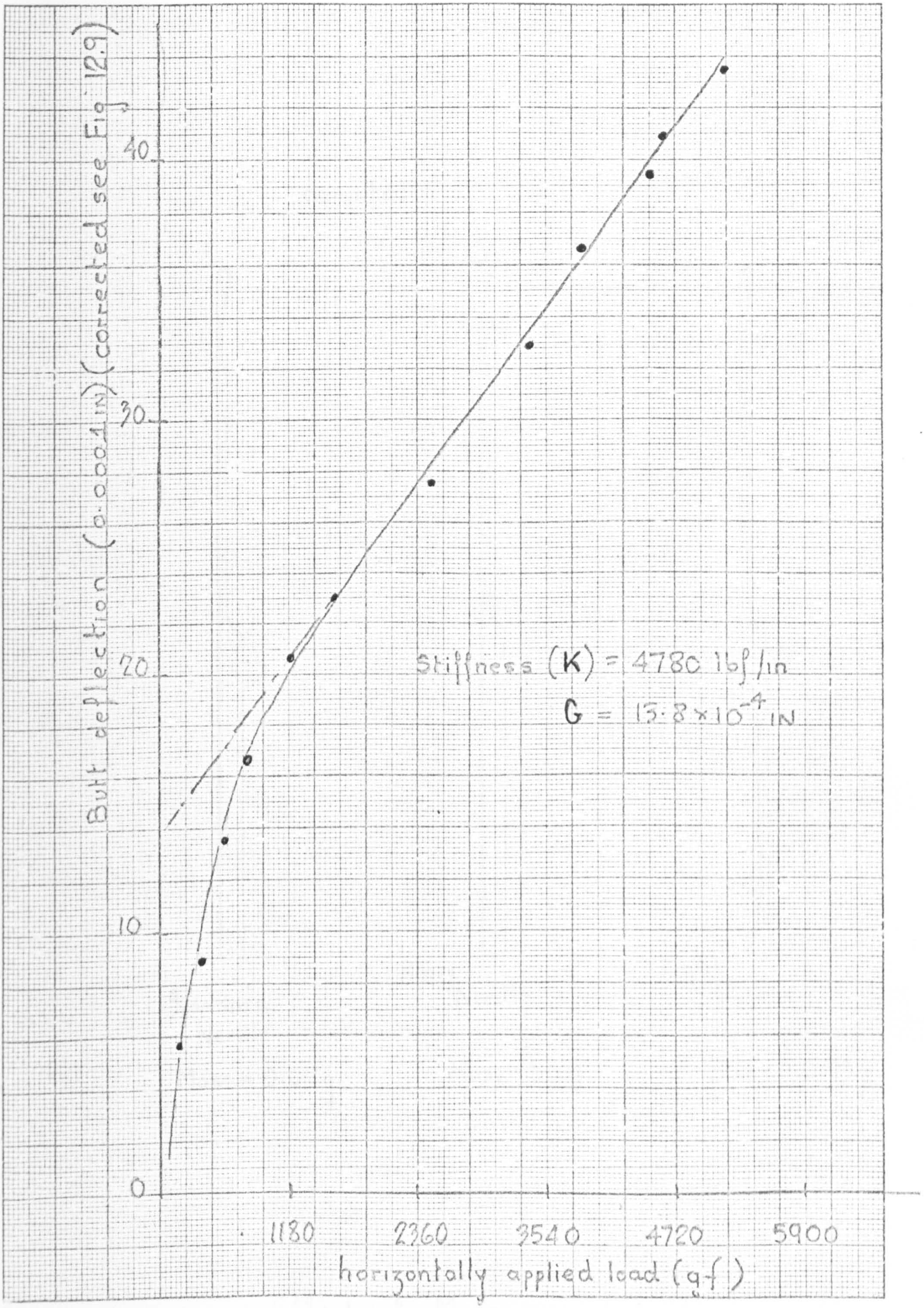

BUTT-DEFLECTION CHARACTERISTIC 0·443mm NEEDLE

FIG 14.18

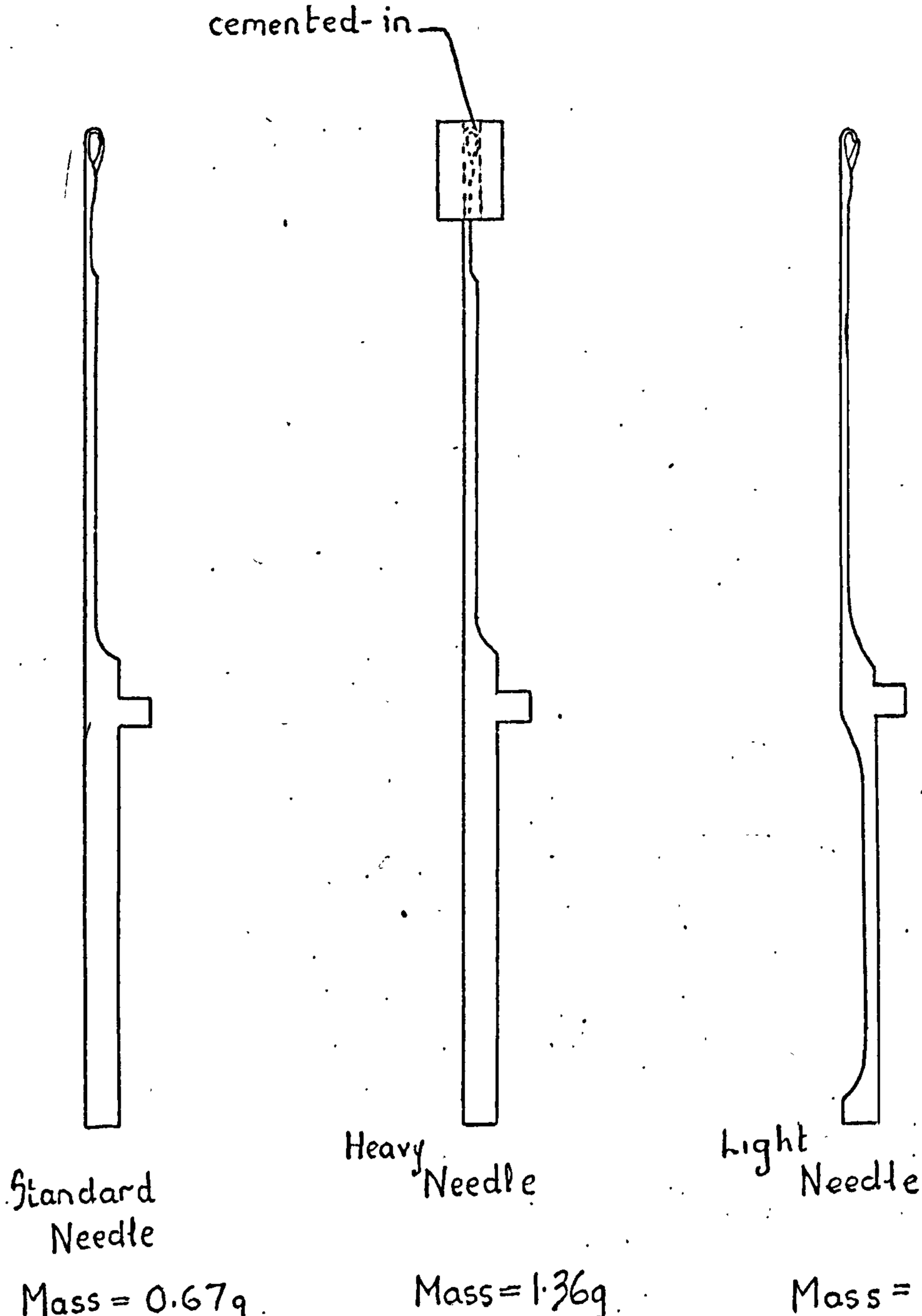

Effect of Mass upon Impact

Fig 14.19

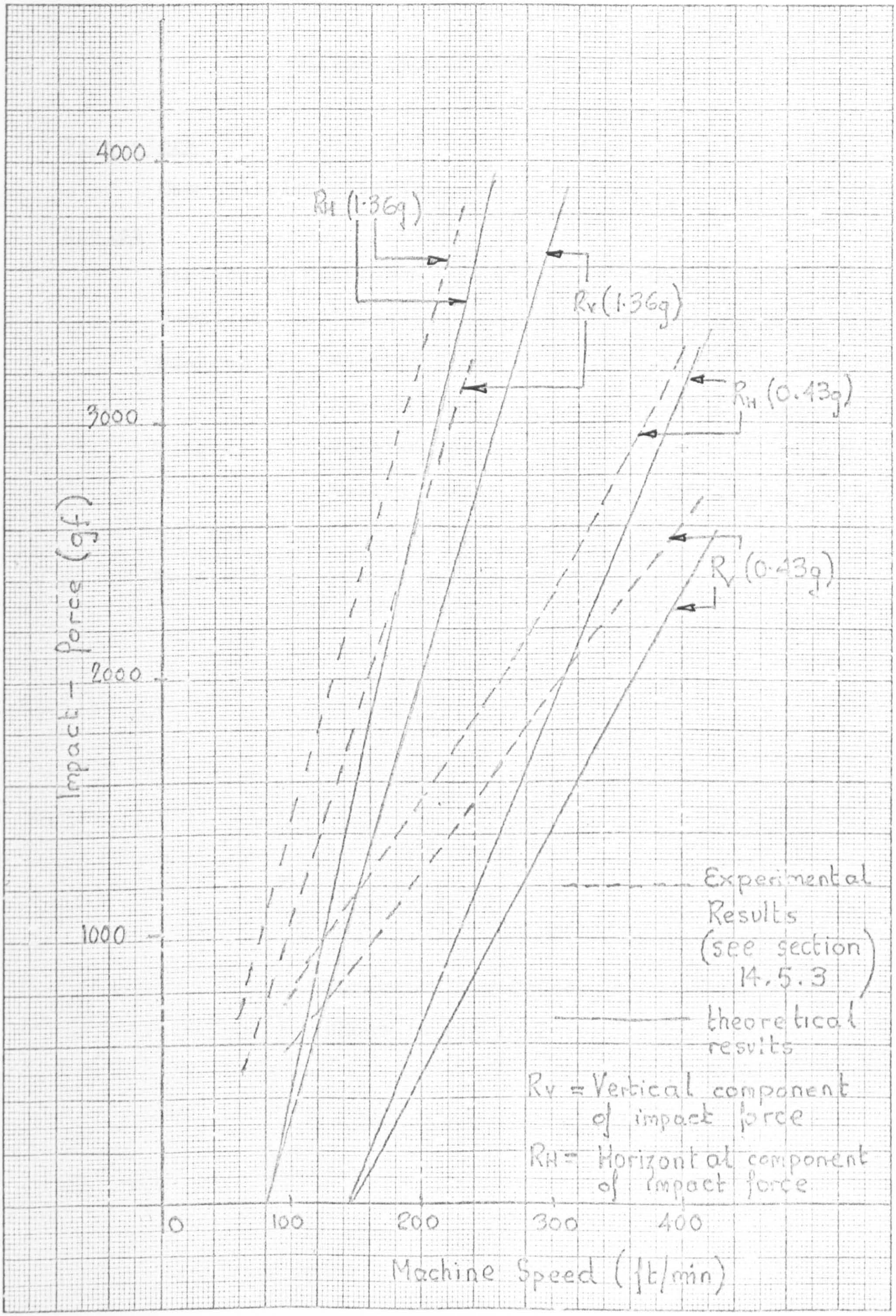

EFFECT OF NEEDLE MASS UPON THE IMPACT

FIG 14.20

Effect of Mass upon Impact

Parameters

Cam-cylinder clearance = 0.15 mm (0.006 in.)

Scales

Horizontal Cam-force = 69.4 gf/mm

Vertical Cam-force = 76.5 gf/mm

Diagram II Machine Speed = 116 ft/min (0.59 m/sec)

Needle mass = 0.67 g (standard)

Diagram I Machine speed = 116 ft/min (0.59 m/sec)

Needle Mass = 1.36 g

49° Cam

Needle type - 0.443 mm see Fig 3.2

Parameter for traces shown in Fig 14.21(b)

Fig 14.21(a)

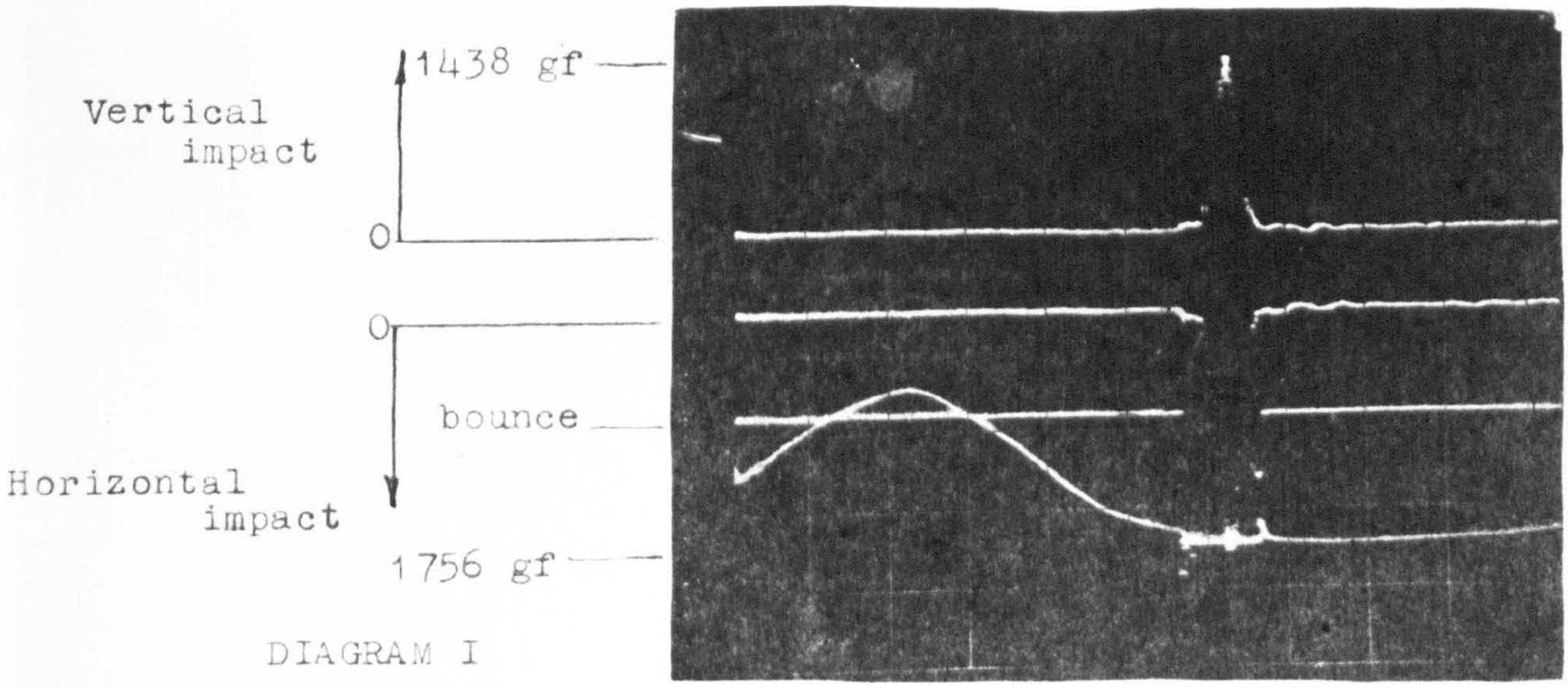

DIAGRAM I

Mass = 1.36 gf

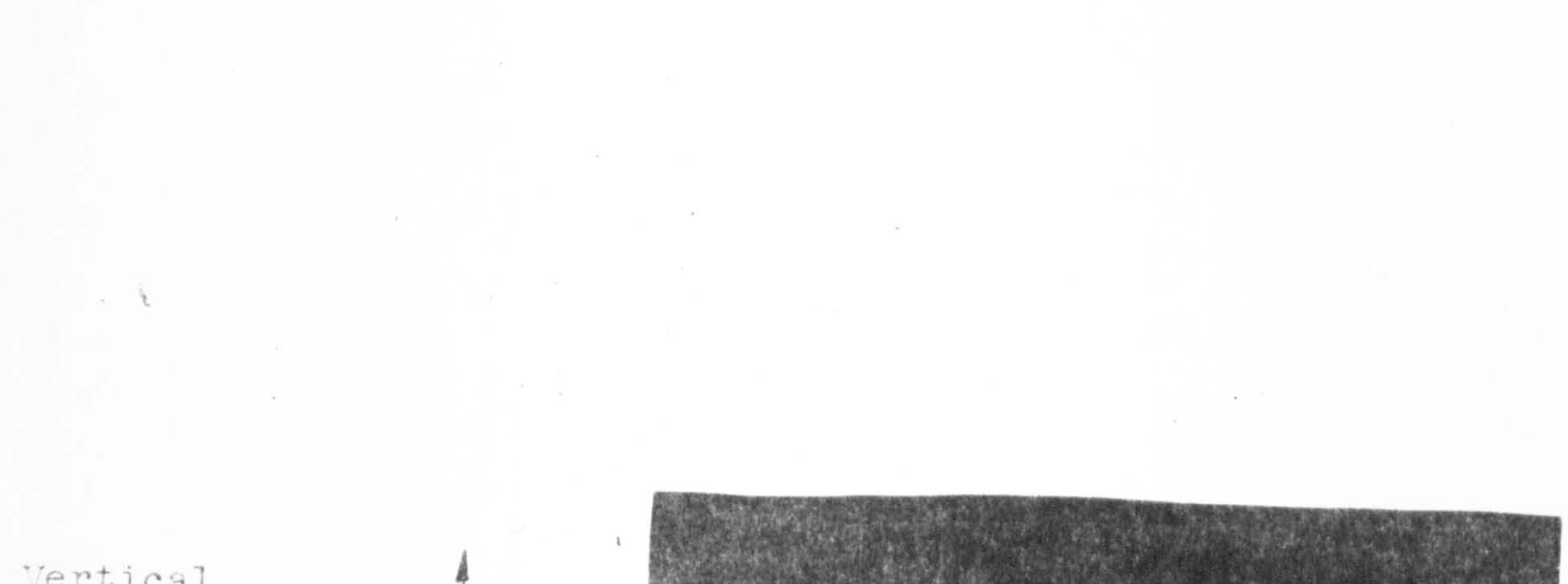

DIAGRAM II

Mass = 0.67 g

Effect of Needle Mass
upon the Impact

Fig 14.21(b)

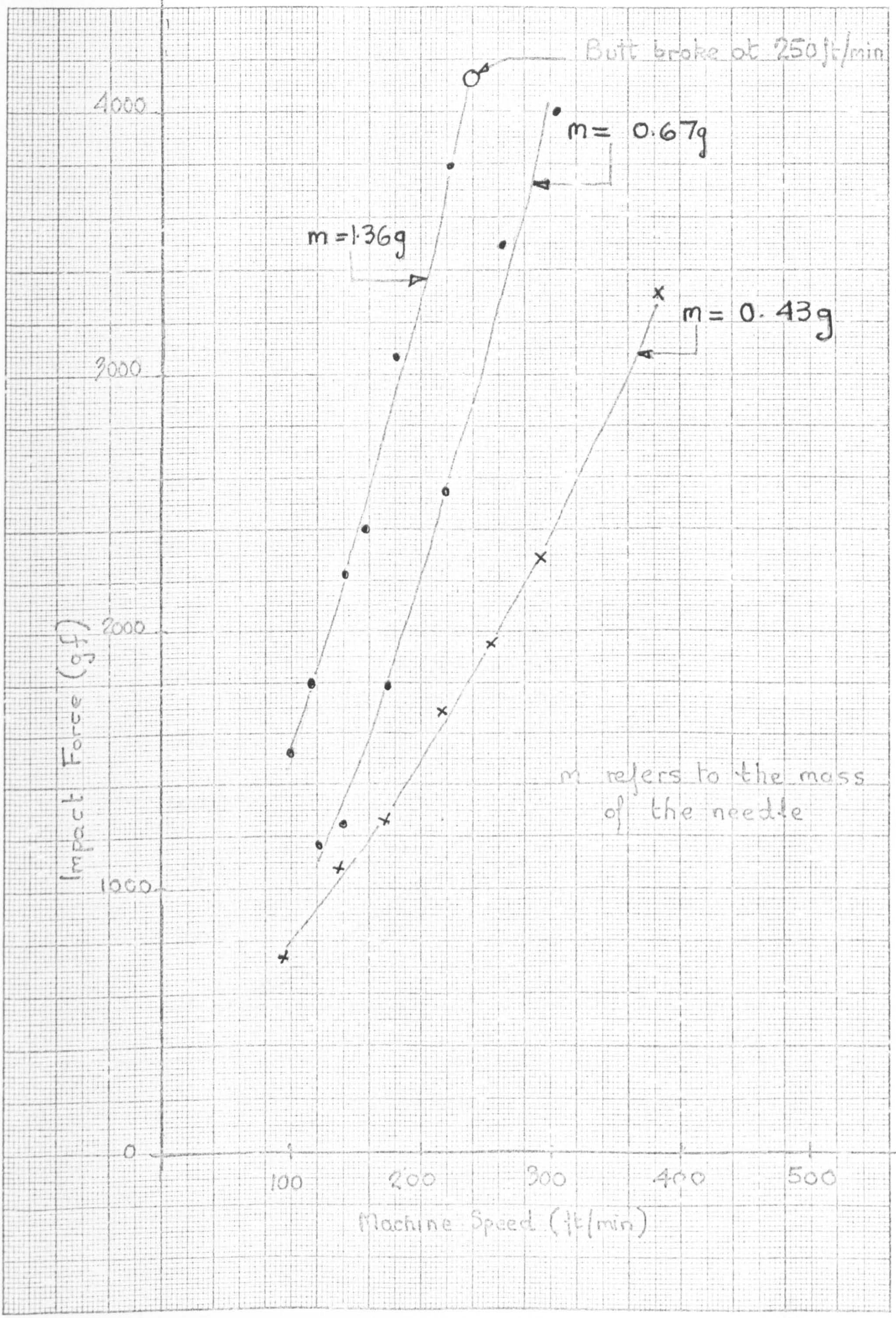

HORIZONTAL COMPONENT OF IMPACT, (EXPERIMENT)
EFFECT OF NEEDLE MASS.

FIG 14.22

R_H = horizontal component of impact force

R_V = vertical component of impact force

49° Cam

Cam-cylinder clearance ---- 0.006 INS (0.15 mm)

Cam-cylinder clearance ——— 0.015 INS (0.38 mm)

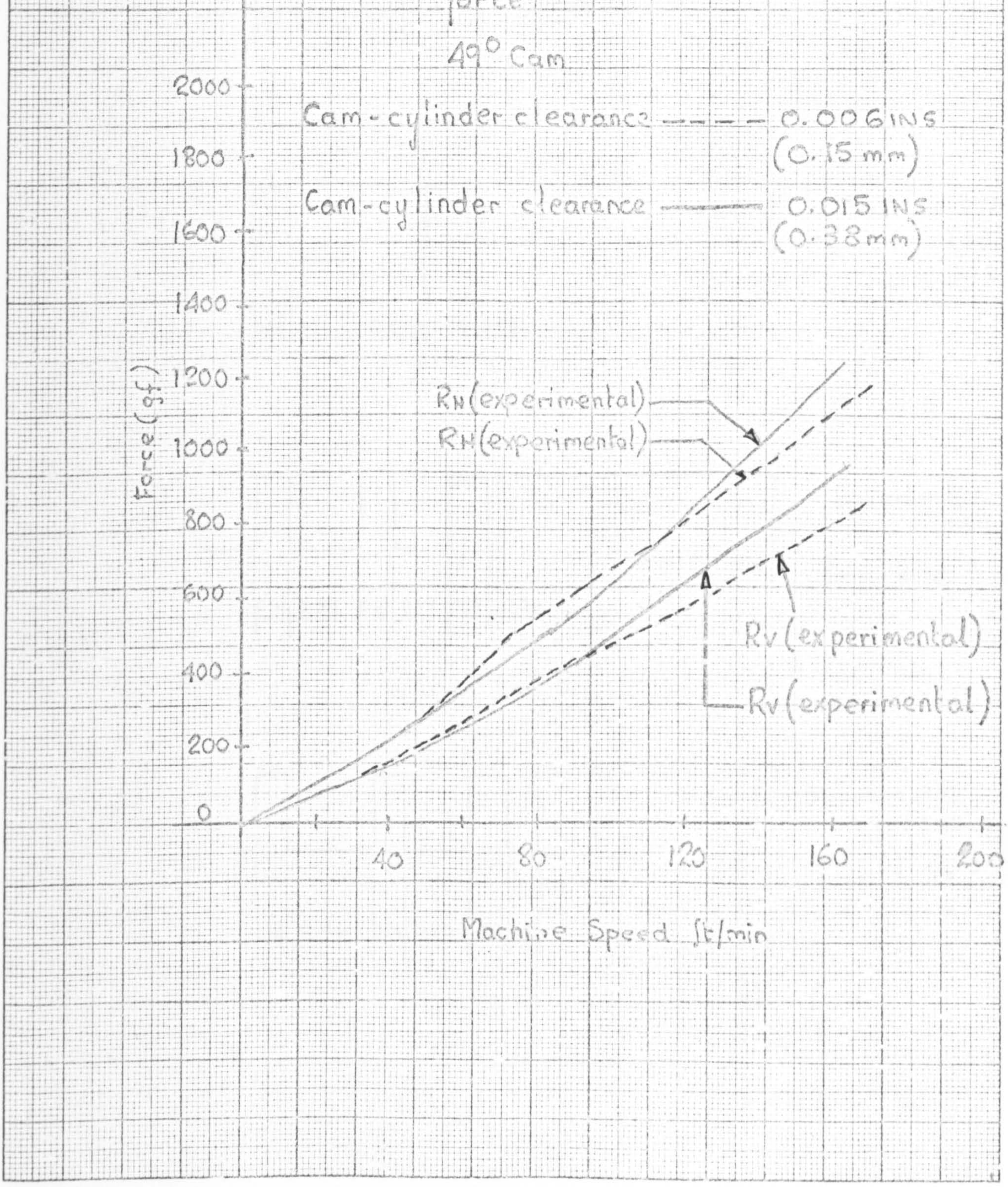

EFFECT OF A SMALL CHANGE IN CAM-CYLINDER CLEARANCE

Fig 14.23

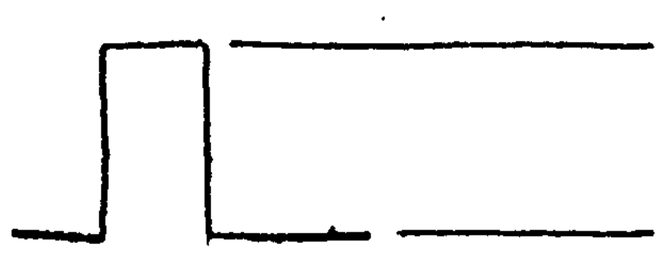

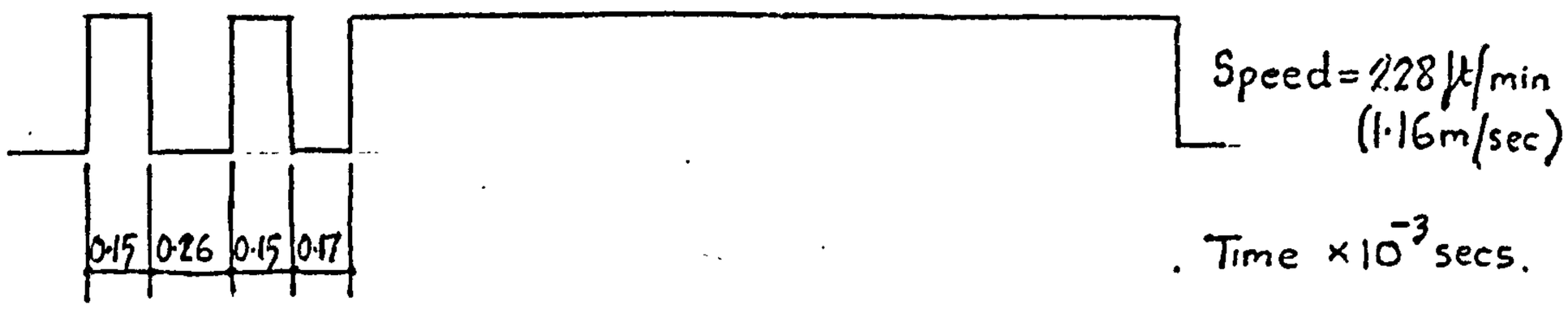

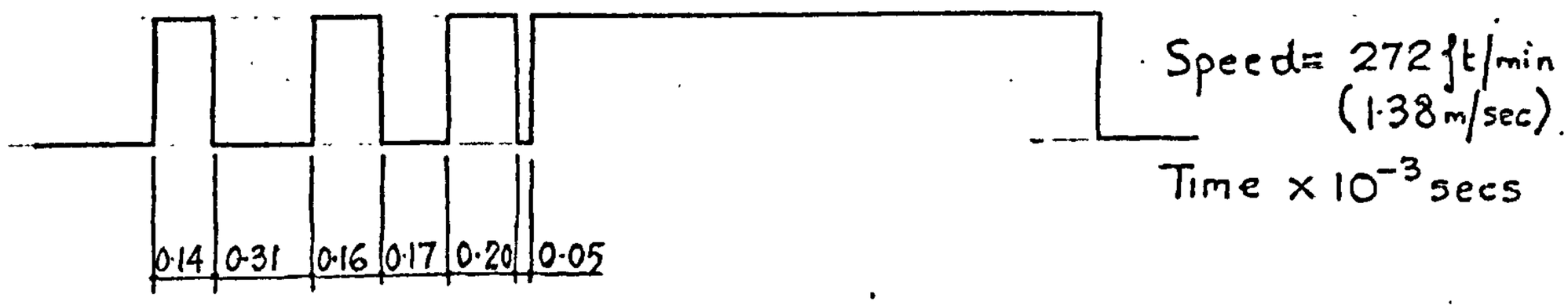

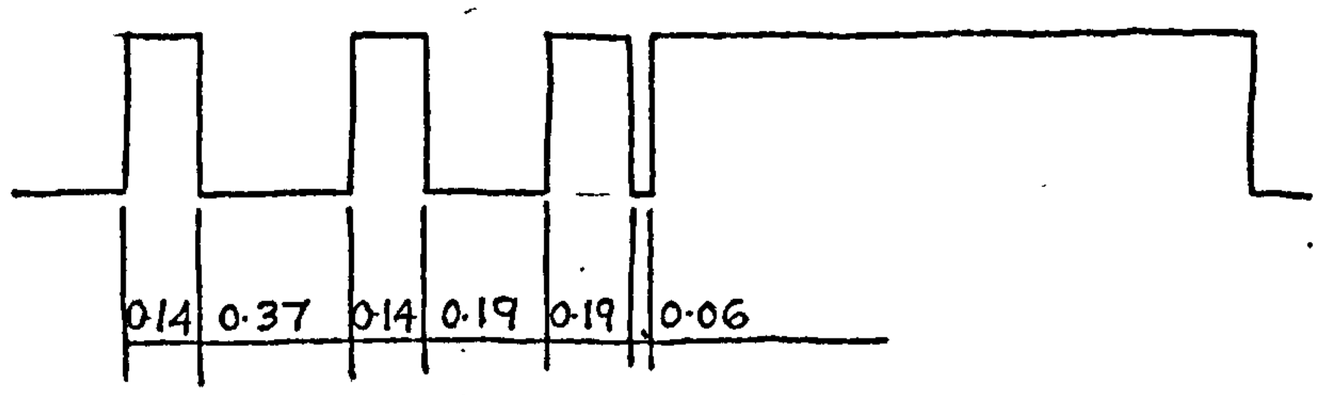

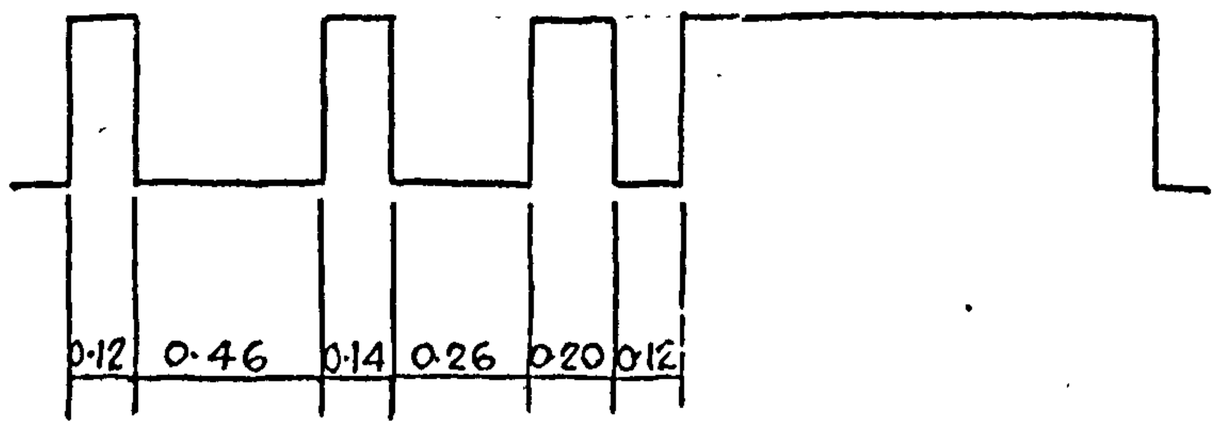

45° Cam
0·15 mm Clearance
0·443 mm Needle.

Needle Bounce on the Stitch Cam

Fig 14.24

0·006 IN cam cylinder clearance

1 Total horizontal projected cam length involved in the bounce region expressed as a length of time. 45° cam

5 Time interval between primary and secondary pulse, 45° cam.

2 As 1 60° cam

3 As 5 60° cam

6 As 1 30° cam

8 As 5 30° cam

4 As 1 45° cam (stiffened trick)

7 As 5 45° cam (stiffened trick)

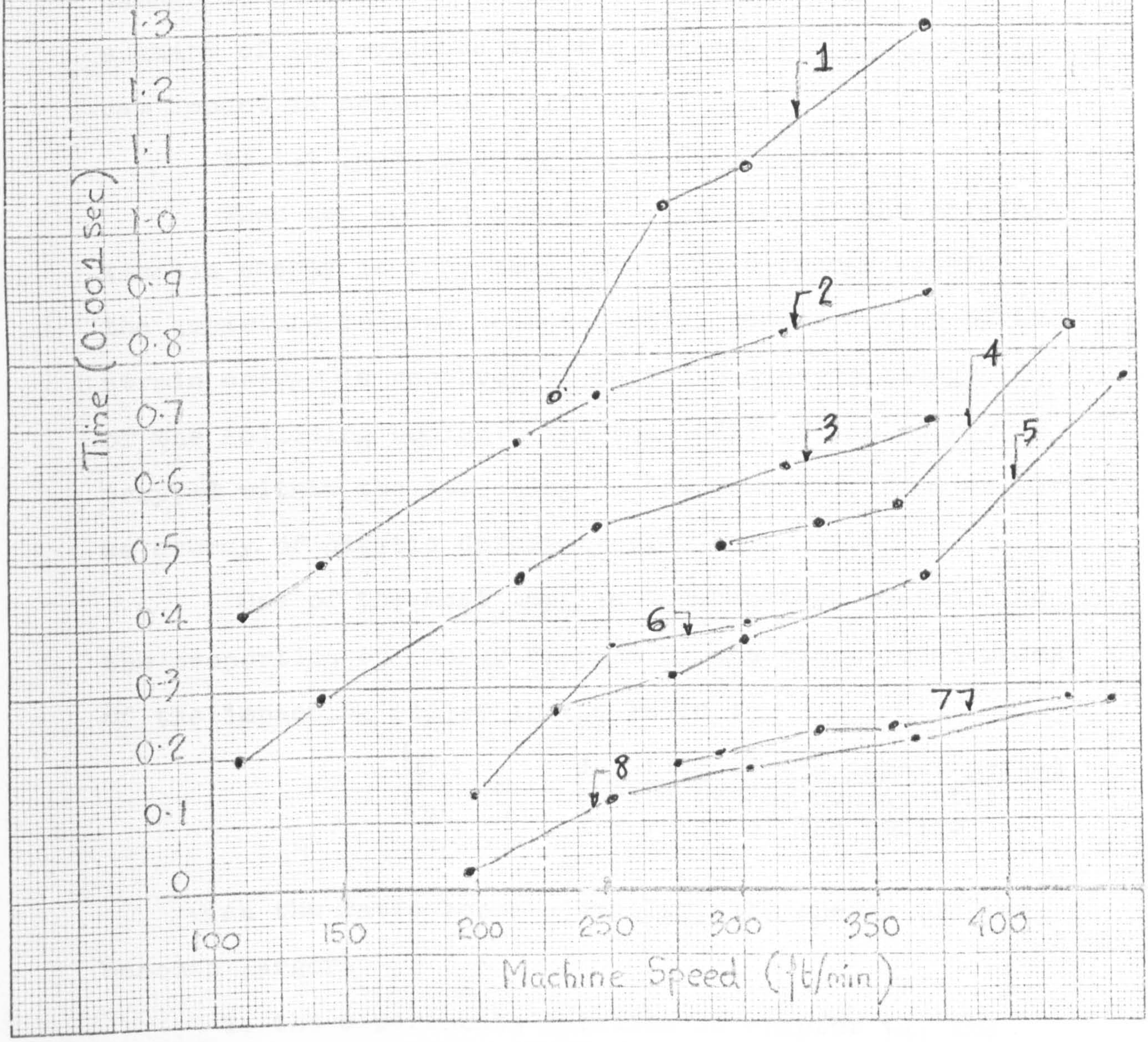

TIME INTERVAL AND CAM-LENGTH BETWEEN BOUNCES

FIG 14.25

CHAPTER 15

GUARD-CAM IMPACT INSTRUMENTATION

15.1 Introduction to Guard Cam Impact.

As the needle travels round the stitch-cam and the guard-cam as shown in Fig 15.1, there are two regions of major impact, i.e. at initial contact with the stitch-cam and also when the needle hits the guard-cam, The stitch-cam impact experiments, detailed in chapter 14, produced some evidence that stitch-cam impact was not responsible for needle-hook damage. More comprehensive work on needle damage is carried out in chapter 19; however, a brief summary of the evidence and the reasons for measuring guard-cam impact is presented below.

15.1.1 Importance of Guard Cam Impact.

When two bodies collide, a portion of the original kinetic energy is converted into strain-energy within the impacting bodies. Subsequently, some fraction of the strain energy is reconverted into the kinetic energy of the colliding bodies. The remainder of the energy is trapped within the impacting bodies as waves, or dissipated as energy of plastic deformation.

One of the most important parameters controlling the proportion of energy trapped by the vibrational modes of the impacting bodies is the ratio :-

$$\frac{t_f}{t_\eta} = \frac{\text{duration of the impact period}}{\text{period of the fundamental frequency of the bodies}}$$

As the ratio becomes smaller, the energy trapped becomes larger.

In the experiments detailed in chapter 14, the

minimum pulse duration was approximately 0.2×10^{-3} seconds and the traverse time for a wave to travel up and down the needle is approximately 17×10^{-6} seconds. The ratio is relatively large, and it is unlikely that much of the strain energy would be trapped in the needle longitudinal vibration modes.

Petrow's[33,34,35,36,37] analysis directly relates needle damage to the longitudinal wave process. It is probable that the stitch-cam impact would not have a sufficiently high frequency to generate waves. However, the pulse time is controlled by the butt flexibility, and the butt is much stiffer when vertically loaded,as with guard-cam impact, than when horizontally loaded, as with stitch-cam impact. It was considered that more energy would be trapped as waves, when following the guard-cam impact, because the duration of loading would be a much shorter interval of time.

During the experiments detailed in chapter 14 ,,a large number of tests were carried out under very adverse conditions, i.e. the needle running at 300 ft/min against 60^{o} cams. Although a considerable number of needle butts were broken, no heads were broken.

15.2 Theoretical Analysis of Guard-Cam Impact.

The theoretical analysis, based upon laws of conservation of momentum and energy, can provide information on the nett change in velocity of the needle, i.e. the nett impulse, and the energy exchange processes accompanying the impact. however, the method is incapable of describing the transient stresses, forces, or deformations produced. Nevertheless, the mathematical simplicity of the method renders it a valuable tool even if providing restricted information.

Nomenclature is contained in Fig 15.2, and Fig 15.3 is

a diagram illustrating some of the important parameters. From diagram II, Fig 15.3, the following equation can be derived :-

$$d - (b + Y) = X \tan\beta \quad . \quad . \quad . \quad (120).$$

From diagram I, Fig 15.3, the forces on the needle after it has left contact with the stitch-cam can be represented in the form :

$$\frac{d^2y}{dt^2} = -\frac{F}{m} \quad . \quad . \quad . \quad (121),$$

$$\frac{dy}{dt} = -\frac{F\,t}{m} + A \quad . \quad . \quad (122),$$

$$y = -\frac{F\,t^2}{2m} + At + B \quad . \quad . \quad (123).$$

In equation (121), (122), and (123), the viscous friction term was ignored to simplify the analysis. The effect of the oil upon the impact forces is examined in some detail in section 16.8.

From equation (120) :

$$d - (Y + b) = vT\tan\beta \quad . \quad . \quad . \quad (124),$$

$$\text{therefore} \quad Y = -vT\tan\beta + d - b \quad . \quad . \quad (125).$$

Substituting equation (125) for Y in equation (123) gives :-

$$-vT\tan\beta + (d-b) = vT\tan\delta - \frac{F\,T^2}{2m} \quad . \quad . \quad (126),$$

which simplifies to :

$$T^2 - \frac{2mv}{F}(\tan\delta + \tan\beta)T + \frac{2m}{F}(d-b) = 0.$$

If we define

$$L = \frac{2m}{F}(\tan\delta + \tan\beta),$$

$$\text{and} \quad M = \frac{2m}{F}(d-b),$$

then, $$T = \frac{Lv \pm \sqrt{(Lv)^2 - 4M}}{2} \quad . \quad . \quad (127),$$

As machine speed increases, the time, T, must become smaller, and this is only possible with the solution :-

$$T = \frac{Lv - \sqrt{(Lv)^2 - 4M}}{2} \quad . \quad . \quad (128).$$

At the point of leaving the stitch-cam :-

$$y = x = 0, \quad \text{and} \quad \frac{dy}{dt} = v \tan(\delta).$$

Therefore:

$$y = (v \tan \delta)t - \frac{F t^2}{2m} \quad . \quad . \quad (129),$$

and

$$\frac{dy}{dt} = (v \tan \delta) - \frac{F t}{m} \quad . \quad . \quad (130).$$

When the needle leaves the stitch-cam, the deceleration is controlled by the needle mass, m, and trick resistance to needle motion, F. The time taken for the needle vertical motion to reduce to zero, also depends upon the vertical velocity at the instant when the needle leaves the stitch-cam. Obviously, there is less chance of serious stitch-cam impact if m and v are both small, and, F, is large. The highest impact magnitudes would be generated if, m, and, v, were both large, and, F, small. An interesting conclusion is that whereas the trick resistance, F, increases the stitch-cam impact, it reduces guard-cam impact.

At guard cam impact :

$$X = vT \quad . \quad . \quad . \quad . \quad (131),$$

and:

$$Y = vT \tan \delta - \frac{F T^2}{2m} \quad . \quad . \quad (132).$$

Substituting equation (129) back in equation (131),

gives :- $$X = \frac{v}{2}\left(Lv - \sqrt{(Lv)^2 - 4M}\right) \quad . \quad . \quad (133).$$

An examination of this function shows that the impact point with the stitch-cam varies according to the machine speed V , and this is shown more fully in Fig 15.4.

Fig 15.5 is a diagram showing the forces at the instant of guard cam impact. The frictional force component, being small in comparison to the reaction-force, is neglected in this initial approximation.

From Fig 15.5, $\dot{U}_o$ is related to $\dot{U}_i$ by the expression:-

$$\dot{U}_o = -e\dot{U}_i \quad . \quad . \quad . \quad . \quad . \quad (134).$$

Where e is the coefficient of resitution.

The factor e may vary between zero and unity, and is the ratio of the relative velocity of separation to the relative velocity of approach. In the classical theory of impact, a coefficient of resitution of unity means an elastic impact with no loss of kinetic energy, and a coefficient of restitutiom of zero means an inelastic or plastic impact where the kinetic energy loss is a maximum.

From Fig 15.5, the following equations relating the impulse and momentum can be derived :-

$$I = \int_{t=T}^{t=T+\Delta T} R(t)dt = m\dot{U}_i(1+e) \quad . \quad . \quad (135),$$

where from Fig 15.5 $\dot{U}_i = \left(\sqrt{(\dot{X})^2+(\dot{Y})^2}\right)\cos\left(\frac{\pi}{2} - \left(\beta + \tan^{-1}\left(\frac{\dot{Y}}{\dot{X}}\right)\right)\right)$ (136).

An examination of equation(128),(129),(130), and(135) , shows that the worst case of impact occurs when :-

(i) $(d-b)$= is small,
(ii) F = is small,

and (ii) e is equal to 1.

Under these circumstances :

$$\dot{U}_i = \left(\sqrt{v^2\tan^2\theta + v^2}\right)\cos\left(\pi/2 - (\delta + \beta)\right) \quad . \quad (136),$$

which reduces to :-

$$\dot{U}_i = v\sec\delta\cos\left(\pi/2 - (\delta+\beta)\right) \quad . \quad (137),$$

then,

$$I = 2mv\sec\delta\cos\left(\pi/2 - (\delta+\beta)\right) \quad . \quad (138).$$

Equation (138) was evaluated under the conditions :-

$$m = 0.67\ g,$$
$$\delta = 50^o,$$
and $$\beta = 8^o.$$

the resulting graph is shown in Fig 15.6. An approximation based upon early measurements detailed in chapter 16 was made to the pulse shape, as shown in Fig 15.6, and the term

$$I = \int_{t=T}^{t=T+\Delta T} R(t)\,dt,$$

was evaluated.

The variation of R_{max} with machine speed is also shown on Fig 15.6. The force R_{max} varies linearly with machine speed but, in practice, it is unlikely that e, the coefficient of restitution, is constant and the experimental graph of max impact force may be far from linear.

15.2.1 Conclusions to Theoretical Analysis.

From equation (135), the needle mass evidently has a large effect upon the impact magnitude. When the trick resistance to needle motion is low, the reduction of impact is in the same ratio as the mass. When the trick resistance is increased, the effect of the change in mass is more pronounced, because it not only decreases the impact magnitude

but it also increases the needle deceleration when it leaves the stitch-cam.

High values of the trick resistance to needle motion has the advantage that it increases the deceleration after the needle leaves the stitch-cam, and therefore it reduces the needle vertical velocity component at impact with the guard-cam.

Butt modifications that increase the flexibility of the butt in the direction of guard-cam impact may increase the pulse time and decrease the force magnitude. The effect of butt modifications is detailed in section 16.7.

On Fig 15.4 it is shown that, when the butt leaves the stitch-cam, the needles follow different paths depending upon the trick-resistance to motion. Obviously, close clearance cam-tracks would have the distinct advantage that the needle would be controlled from one cam to the other, and irregularity in loop formation should be much less.

15.3 Measurements of Guard-Cam Impact Using the Stitch-Cam Impact Beam.

The analysis detailed in section 15.2 did not provide any information on the shape of the pulse, or on the length of time the impact force is applied. It was necessary to measure the guard-cam impact before an instrument could be designed, because without any knowledge of the pulse shape it would be very difficult to decide on the natural frequency and strain sensitivity of a guard-cam impact measuring device. Initially, measurements of the impact were carried out using the stitch-cam impact apparatus, and measurement of the force application time was made using the bounce detector.

Fig 15.7, shows a special attachment, for use with the stitch-cam impact transducer, which is essentially a rotatable

stitch cam for simulating varying angles. The cam, fitted to the end of the transducer beam, simulated a guard cam, and three cams were produced each with different angles. The spacers under the transducer were arranged so that, when the unit was clamped to the knitting machine, the needle initially hit the stitch-cam attachment, moved down, and then hit the guard-cam, as illustrated in Fig 15.8. The spacers were chosen so that needle impact with the guard-cam occurred when the underside of the hook was 1.7 mm below the level of the verge top; this simulated the same stitch-draw that was used for the majority of experiments detailed in chapter 8.

The method of carrying out measurements, and the calibration procedure, was very similar to that used for stitch-cam impact measurements. Backing needles without butts were placed on each side of a standard needle, and the lead-in and raising cams shown on Fig 14.1 were used for the guard cam impact measurements. Further details concerning the measuring method was given in section 14.2.

Impact measurements were carried out using a 0.443 mm standard needle fitted in a cleaned trick. The machine was lightly oiled, and the circuitry and the bounce detector were switched on and allowed to warm up. Before traces were taken, the machine was run for some time at the normal operating speed.

Traces were obtained for a range of speeds, and a typical sample is shown in Fig 15.9. The bounce traces revealed that the cam-needle contact time was approximately equal to 95×10^{-6} seconds and it did not change very much as the machine speed was altered. The traces obtained from the impact transducer showed a large amount of natural frequency

oscillation after the initial impact, and it was obvious that the impact transducer was incapable of accurately displaying the input pulse shape without severe distortion, due to the beam natural frequency being far too low to measure the high fequency impact.

From the measurements, it was concluded that the guard-cam impact pulse was of a considerably higher frequency than the stitch-cam impact and that a suitable measurement systcm would have to have a natural frequency considerably higher than the frequency of the existing impact transducer shown in Fig 15.7.

15.4 Design of a Guard-Cam Impact Instrumcnt.

The measurements detailed in section 15.3 showed that the impact duration was approximately 100×10^{-6} seconds. If the pulse shape was a pure sine-wave then the pulse frequency would be approximately 5000 Hz and, using the analysis detailed im section 11.3, the measuring system should have a natural frequency above 30,000 Hz. However, it was very unlikely that the impact pulse would be sinusoidal, and there would undoubtably be higher frequency components than 5000 Hz. It was concluded that the fundamental natural frequency of the measuring instrument should be 100,000 Hz ideally, if it was to record the guard-cam impact accurately.

Such a high natural frequency was completely beyond the capabilities of a practical transversely excited system, and the only possible practical device that could be used was one excited longitudinally. The fundamental natural frequency of a beam, in longitudinal excitation, is given by :-

$$f = \frac{c}{2l} \qquad (139)$$

where C = longitudinal wave speed,
and l = beam length.

For hardened steel, the wave speed is approximately 20,000 ft/sec (509 m/sec). If the beam length is one inch, then a fundamental frequency of 120,000 Hz can be achieved. For longitudinal excitation, the natural frequency does not greatly effect the strain sensitivity, because the beam dimensions can be varied, within limits, without changing the fundamental frequency. However, the beam section must be carefully chosen; if the section is very small, the response to bending may be so large as to overwhelm the longitudinal signal. Additionally, if the beam end is used as the guard cam surface, then obviously, if the section is too small, under particular circumstances the needle could entirely miss the beam end. There were also difficulties if the section was too large, because the strain sensitivity of a longitudinally excited beam is much less than a transversely excited beam, unless the cross-sectional dimensions are very small.

A suitable compromise was made, and a beam of dimensions 0.1 in. (2.5 mm) square by 0.8 in. (20.3 mm) long was manufactured out of a typical cam material, K200 steel, with a Rockwell hardness number of 60. The beam surface was polished smooth and this removed the risk of wave reflections at small discontinuities on the surface. Two strain-gauges were bonded to the side of the beam and arranged so that the bending response was cancelled out. With a 0.1 in. square beam, the strain sensitivity is approximately 1×10^{-6} strain per 200 gf, and this is adequate for high load measurements. A supporting structure was fitted at the top of the beam, and this restricted the transverse motion of the beam and therefore reduced the bending response further.

A diagram showing the positioning of the strain gauges and the design of the beam is given in Fig 15.10, and Fig 15.11 is a diagram showing the operational arrangement of the instrument on the knitting machine.

The experimental method used with the longitudinal impact instrument was the same as that detailed in section 14.2 using the stitch-cam impact transducer. Initially, a bench calibration was carried out and frequent spot checks were made on the machine during the experiments. The procedure for carrying out calibration tests on the machine was complicated by the fact that, in normal operation, the beam was inclined by a small amount to simulate the guard-cam angle. Before vertical calibration on the machine could be carried out, the instrument had to be tilted slightly so that the beam was vertical, and then the apparatus shown in Fig 4.10 could be used for calibration.

15.4.1 Electrical Circuitry.

Whereas there were eight strain-gauges bonded to the beams of the stitch-cam impact transducer and cam-force transducer mark III, there were only two gauges fitted to the beam of the longitudinal impact transducer. However, there were no basic changes in the circuitry. The two gauges were connected into a Wheatstone bridge circuit as shown in Fig 15.10 (a) and then connected to one of the amplifiers shown in Fig 4.5. The output from the amplifier was then passed to the Tektronix storage oscilloscope. The filter circuits, shown in Fig 5.5, were specifically designed for use with the cam-force transducer mark III and hence were disconnected from the circuitry when the longitudinal impact apparatus was used.

15.5 Initial Measurements.

A 0.443 mm standard needle was placed in a thoroughly cleaned trick and backing needles having no butts were placed each side of it. Initially, a few tests were carried out at various speeds and a typical trace is shown in Fig 15.12, this trace clearly shows that, at the instant of impact, there is a rapid increase in the force level occupying only 5 to 10 x 10^{-6} seconds, and then there is a slower reduction of the force occupying approximately 90 x 10^{-6} seconds. The essential shape of the pulse changed very little over a large number of tests, although the magnitude changed considerably as the machine speed was increased; this is discussed in more detail in section 16.3.

There was one serious disadvantage with the longitudinal impact instrument, in that, during the initial experimentation, it became apparent tha the instrument was very prone to damage at high speed. The beam had to be spaced very close to the cylinder to simulate the normal machine cam-cylinder clearance, and, at high speed, a needle had only to protrude slightly from the cylinder for it to hit the beam, which, being thin and relatively brittle, tended to break rather than either force the needle back in its trick, or alternatively break the needle. Needles protruding from tricks are rare, but over a wide range of experiments, where many different machine parameters were being varied, it did occur occasionally. Although extensive measures to reduce the risk of a needle hitting the instrument were carried out, and these are shown in Fig 15.11, the device was still far more prone to damage than the transverse beam instrument. During the experiments detailed in chapter 16, three longitudinal beam devices had to be manufactured and strain-gauged.

Due to the increased risk of damage, it was decided to re-examine the output from the stitch-cam impact transducer fitted with the special attachment shown in Fig 15.8. If a suitable correction could be discovered to relate the output from the instrument to the output from the longitudinal impact transducer, then the stitch-cam impact transducer could be used for the bulk of the experimental work. A suitable correction was discovered and this is detailed in the next sub-section. The procedure adopted during the majority of the experiments detailed in chapter 16 was for the stitch-cam impact transducer to be used for the majority of experimental measurements where force magnitudes were being examined, and for frequent spot checks to be carried out using the longitudinal impact transducer; this was to check the magnitude measured by the other instrument, and also to obtain a qualitative picture of the impact, showing pulse shape as well as magnitude.

15.5.1 Correction to the Output from the Stitch-Cam Impact Transducer to Enable it to be used for Guard-Cam Impact Measurements.

The guard-cam impact pulse differed from a pure sinusoidal pulse in that it contained higher frequency components and the shape more closely resembled a triangular pulse as shown in Fig 15.13. However, initially, it was decided to calculate the beam response to a pulse of sinusoidal form and of periodicity given by the period of the actual pulse measured by the longitudinal instrument. The analysis was carried out using the expression derived in section 11.3 for a simple spring mass system. The final expression had the form :-

$$y = \frac{F_o/k}{1-\left(\frac{\omega}{\omega_n}\right)^2}\left(\sin\omega t - \left(\omega/\omega_n\right)\sin\omega_n t\right) \quad . \quad (140)$$

where F_o = peak impulse force amplitude,
k = beam stiffness,
ω = pulse frequency,
and ω_n = beam naturalfrequency.

The beam response was evaluated for a pulse of frequency 5000 Hz, which is an impact duration of approximately 100×10^{-6} seconds. The beam natural frequency was measured as 11,500 Hz; this was lower than the natural frequency when stitch-cam impact measurements were carried out, and it's decrease must have been due to the slightly heavier guard cams fitted to the end of the beam. The response of the beam to the pulse of frequency 5,000 Hz, is illustrated in Fig 15.14.

From equation (140), the following relationship can be derived :-

$$y_{max} = \frac{F_o}{k}(\alpha) \quad . \quad . \quad . \quad . \quad . \quad (141),$$

where α = the maximum value of the expression:-

$$\frac{1}{1-\left(\omega/\omega_n\right)^2}\left(\sin\omega t - \left(\frac{\omega}{\omega_n}\right)\sin\omega_n t\right) \quad . \quad . \quad (142).$$

From Fig 15.5 α was measured, and for the particular pulse frequency 5000 Hz it equalled 1.6.

After the termination of the pulse, residual beam vibration continues. The ratio of the amplitude of the maximum natural frequency oscillation after the termination of the pulse, to the maximum response during the pulse, can

be evaluated from equation (140); this ratio was determined as 0.34.

From equation (141),

ky_{max} = the load to produce a static deflection of y_{max}, it is therefore directly related to the result obatined from a static calibration,

and therefore $1.6\,F_o = ky_{max}$ (static calibration). (143)

Experiments were carried out firstly with the longitudinal transducer fitted, and secondly with the stitch-cam impact transducer fitted and tested at the same speed. The impact magnitude, measured on the longitudinal instrument, agreed with the result obtained from the stitch-cam impact transducer, when corrected by using equation (143), An example demonstrating this agreement is illustrated in Fig 15.15.

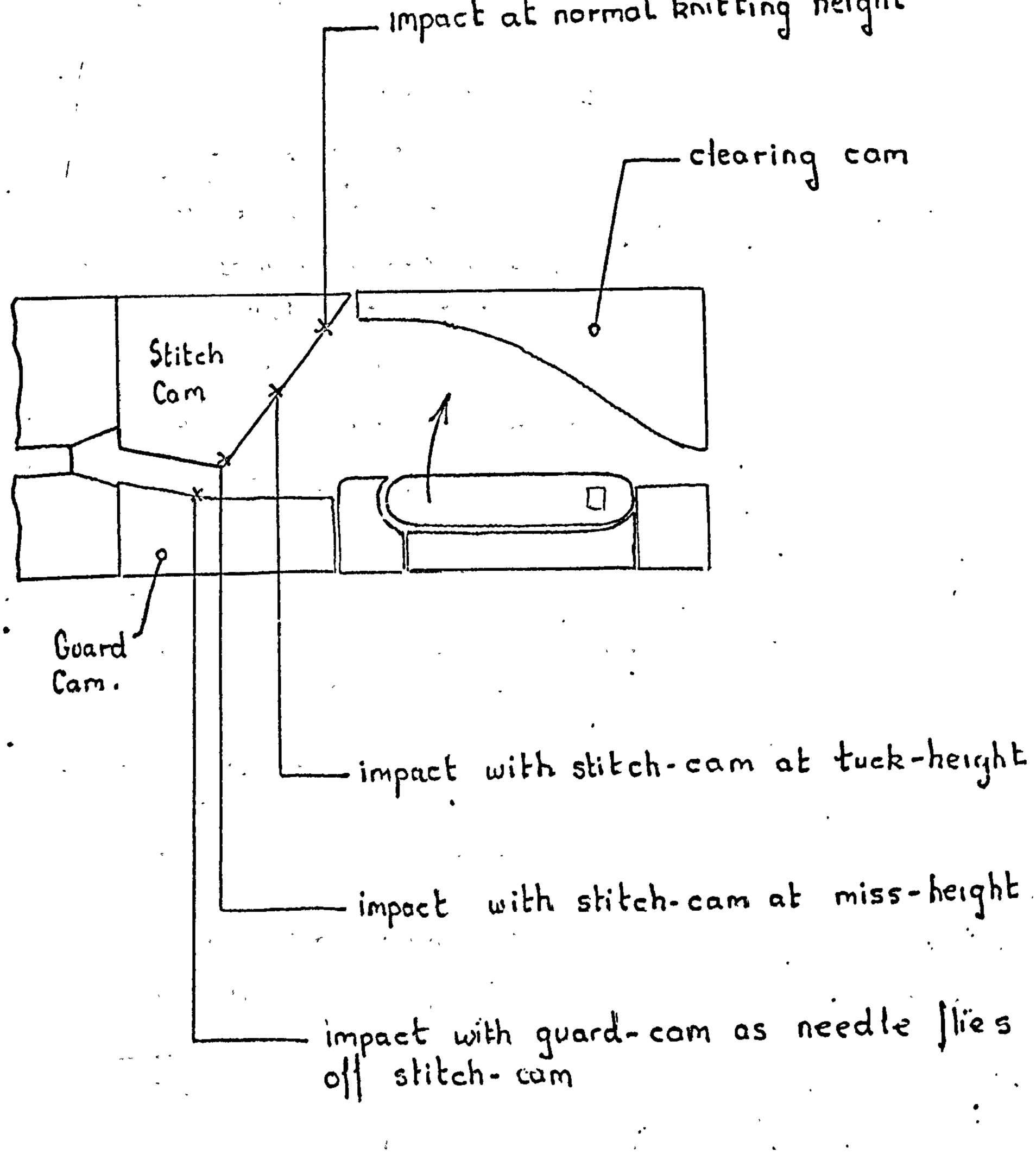

MAJOR IMPACT REGIONS ON KNITTING CAMS

FIG 15.1

Y = distance (vertically) from a point on the but when the needle is just about to leave cam contact, to the same point when the butt impacts the guard-cam. (see Fig 15.3).

X = as above, but distance measured horizontally.

F = total resistance to needle motion including trick resitance to motion and the yarn forces.

m = needle-mass.

δ = cam-angle at the point where the needle loses cam contact.

V = machine cylinder circumferential speed.

T = time taken for the needle to contact the guard cam from a datum taken as zero at the instant the butt leaves the stitch-cam.

x = horizontal displacement.
y = vertical displacement.
} co-ordinates defined on Fig 15.3

$\frac{dx}{dt}$ = horizontal needle velocity ($=V$).

$\frac{dy}{dt}$ = vertical needle velocity.

$\frac{d^2x}{dt^2}$ = horizontal needle acceleration.

$\frac{d^2y}{dt^2}$ = vertical needle acceleration.

β = guard-cam angle.

d = vertical distance from the point on the stitch-cam where the needle just loses contact with the guard-cam surface.

$\dot{X}$ = horizontal needle velocity at instant of impact with guard-cam.

$\dot{Y}$ = vertical needle velocity at instant of impact with guard-cam.

$R(t)$ = impact force magnitude expressed as a function of time.

I = impulse (lbf sec) at instant of contact with guard-cam.

$\dot{U}_i$ = velocity component just prior to impact resolved in the direction of the force.

$\dot{U}_o$ = as above, just follcwing impact.

θ = stitch-cam angle.

e = coefficient of restitution.

Δt = pulse duration.

b = butt width..

Nomenclature used in Guard-Cam Impact Analysis

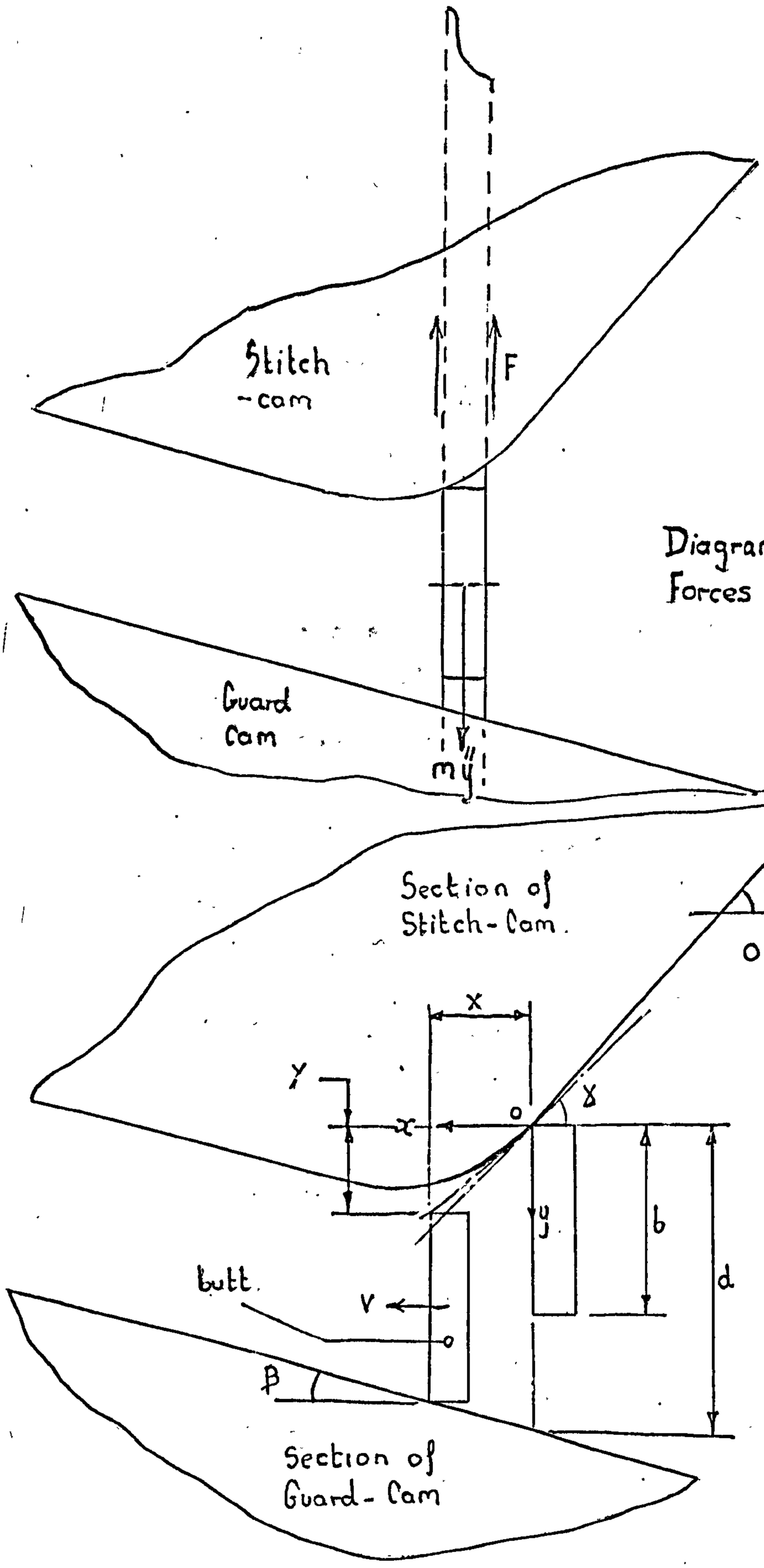

Diagram I
Forces on needle

o - defines the position on the stitch-cam where the butt first loses cam contact,

Diagram II

GUARD CAM IMPACT

FIG 15.3

After the needle lires off the stitch-cam the horizontal distance covered by the needle before it contacts the guard-cam is defined by the equation below:-

$$X = \frac{v}{2}\left[Lv - \sqrt{(Lv)^2 - 4M}\right]$$

where $L = \frac{2m}{F}(\tan\gamma + \tan\beta)$, All the terms of these equation in Fig 15.2 and Fig 15.3

and $M = \frac{2m}{F}(d-b)$.

From the above equations, as machine speed increases the impact point on the guard cam moves as shown below :-

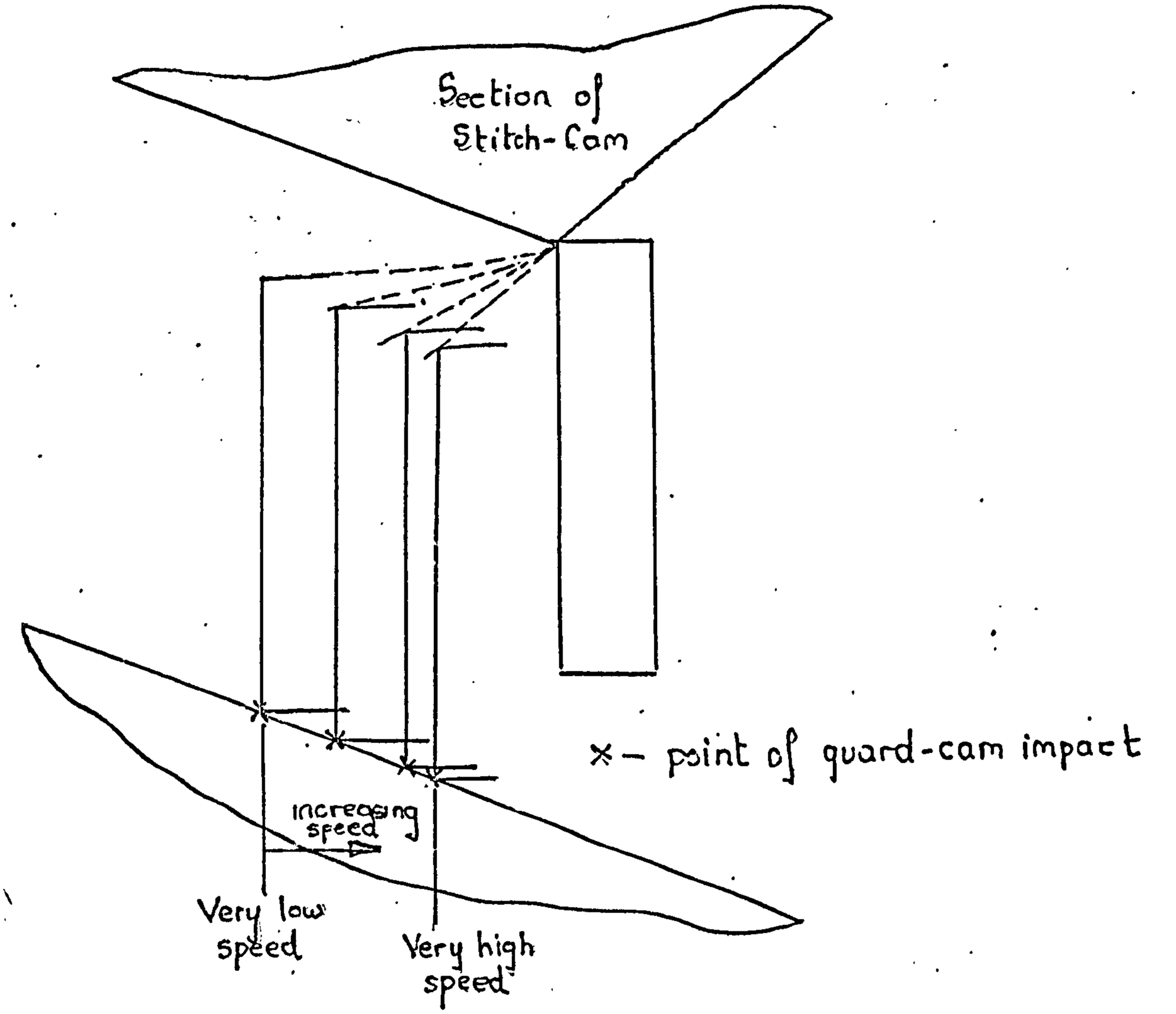

Effect of Machine Speed upon the position of Guard-Cam impact

Fig 15.4.

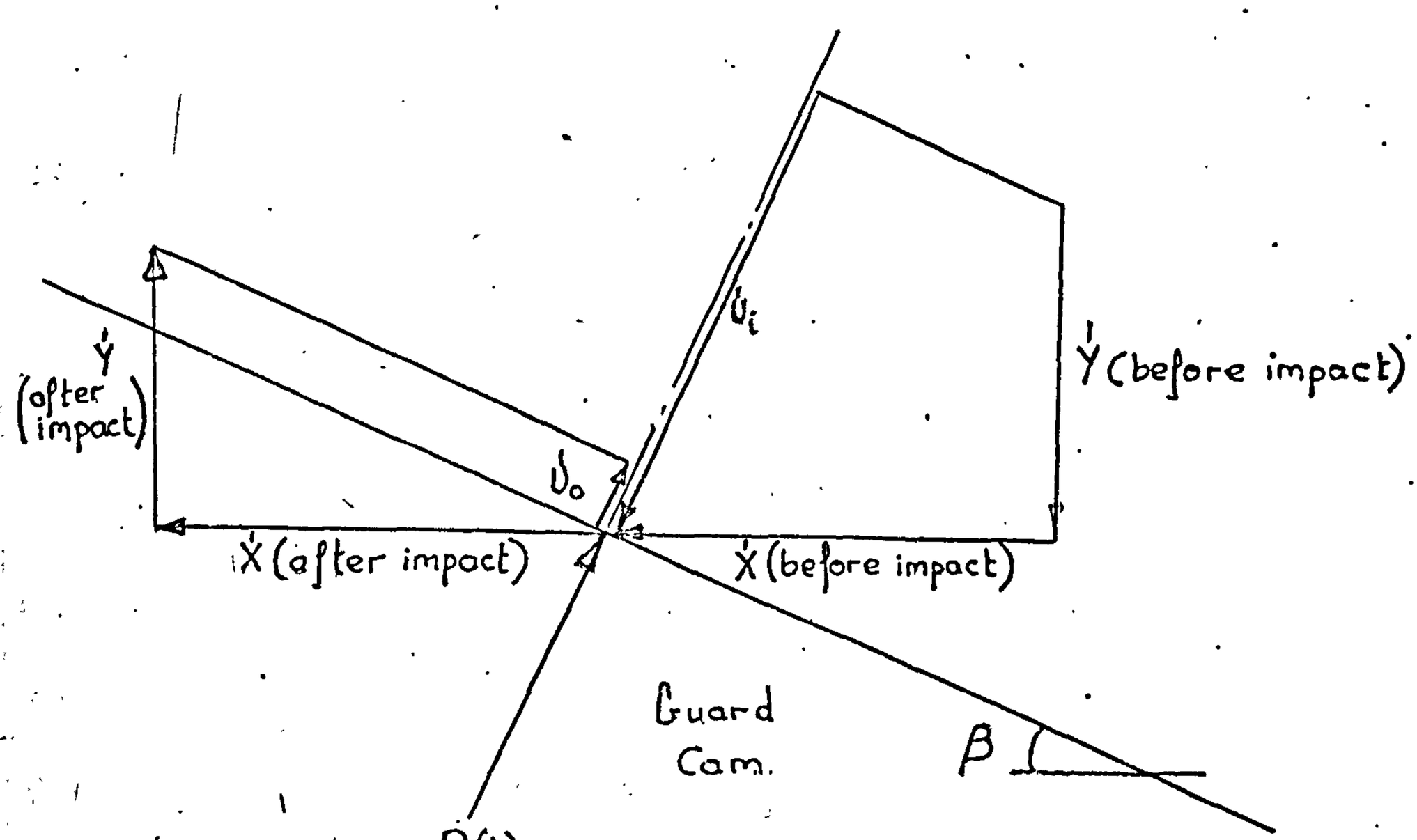

Nomenclature defined in Fig 15.2

IMPACT ON THE GUARD CAM (VELOCITIES) Fig 15.5

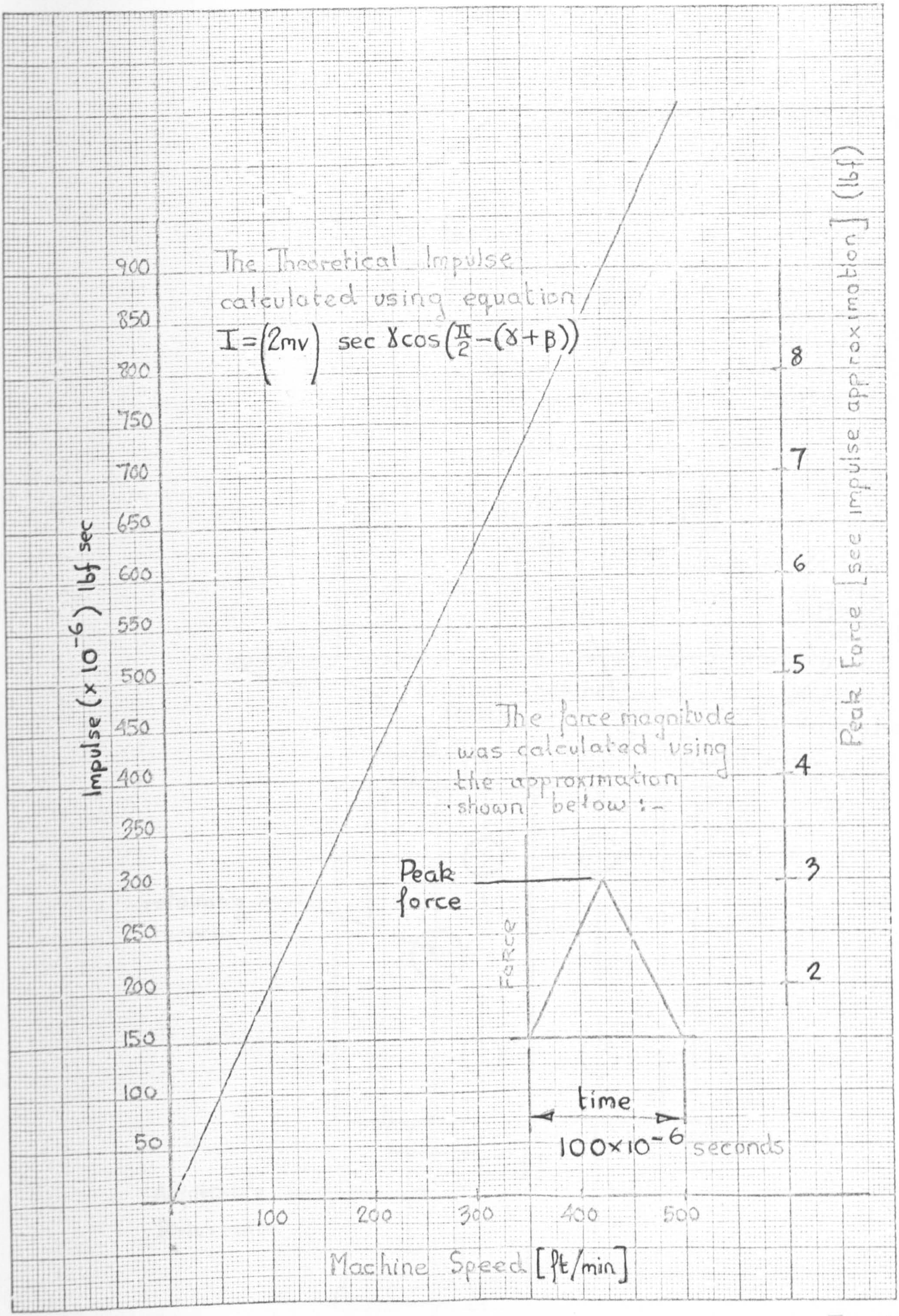

FIG 15.6

MAXIMUM THEORETICAL GUARD-CAM IMPACT USING EQUATION (138)

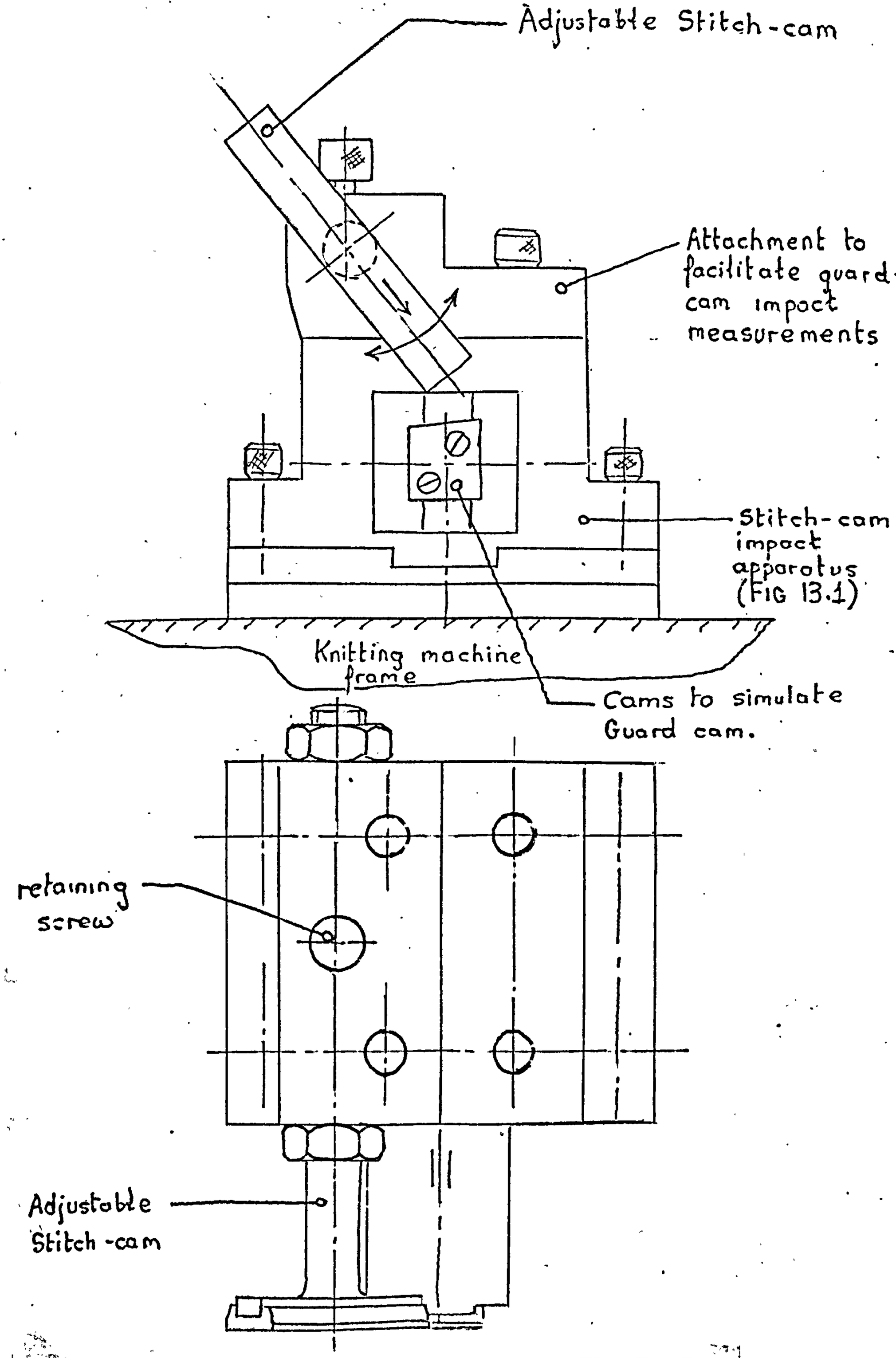

STITCH-CAM IMPACT TRANSDUCER FITTED WITH SPECIAL ATTACHMENT TO ADAPT IT FOR GUARD-CAM IMPACT MEASUREMENTS

FIG 15.7

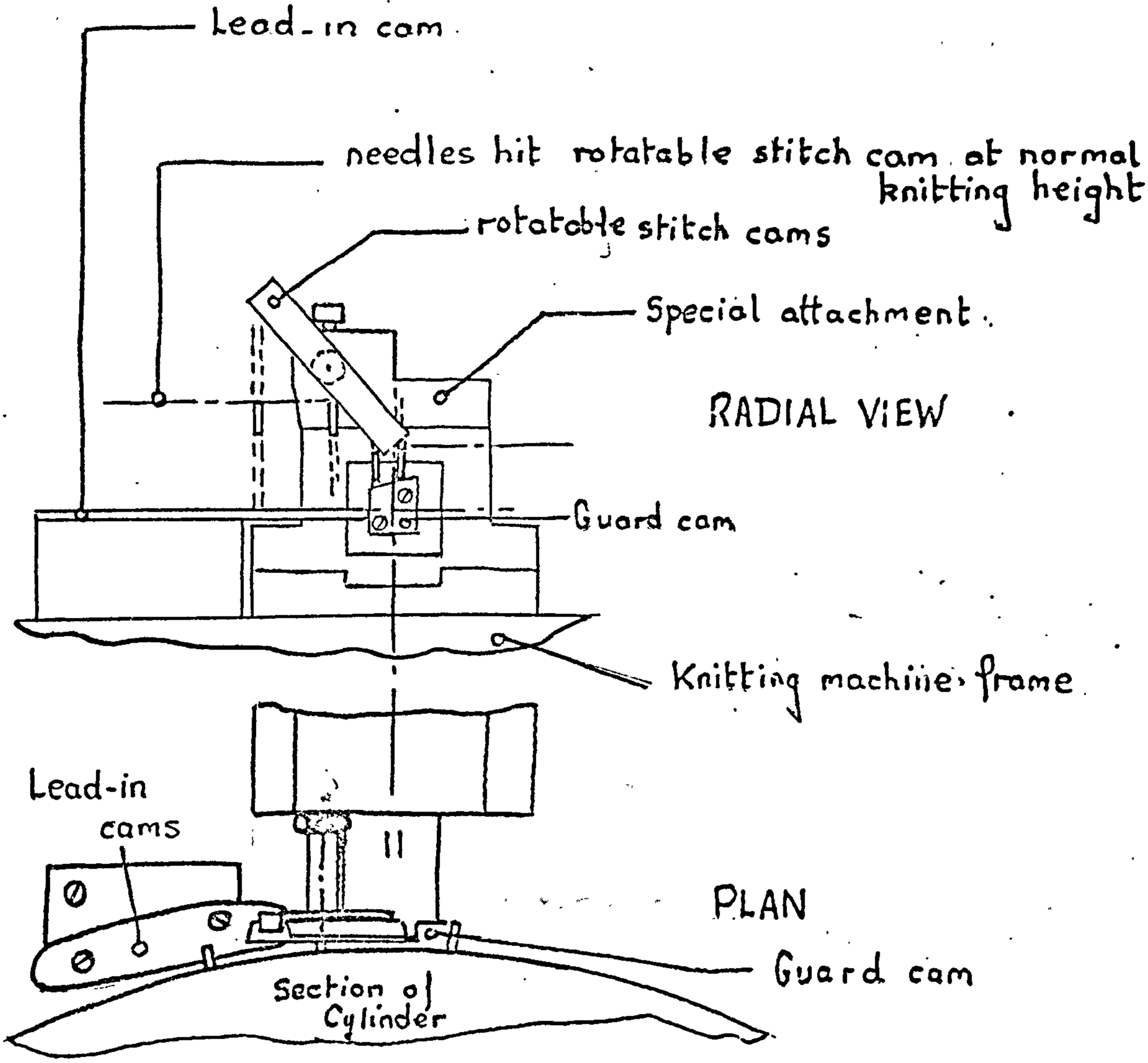

View of cylinder showing positions of transducer and cams.

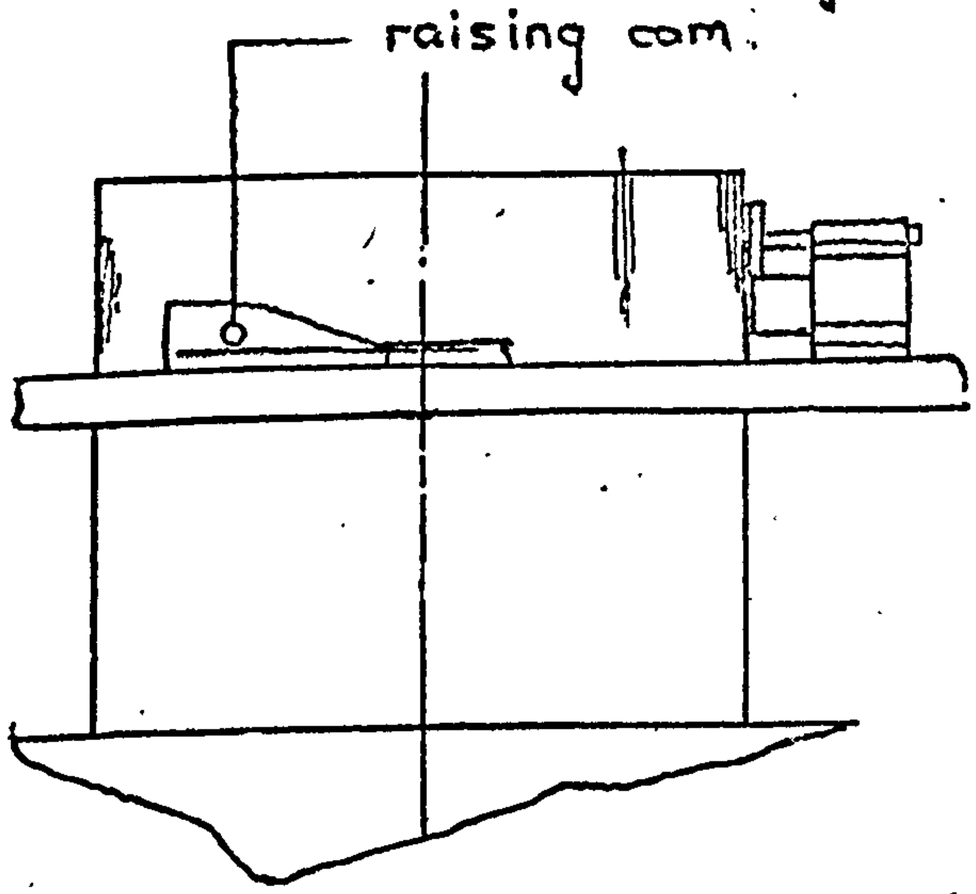

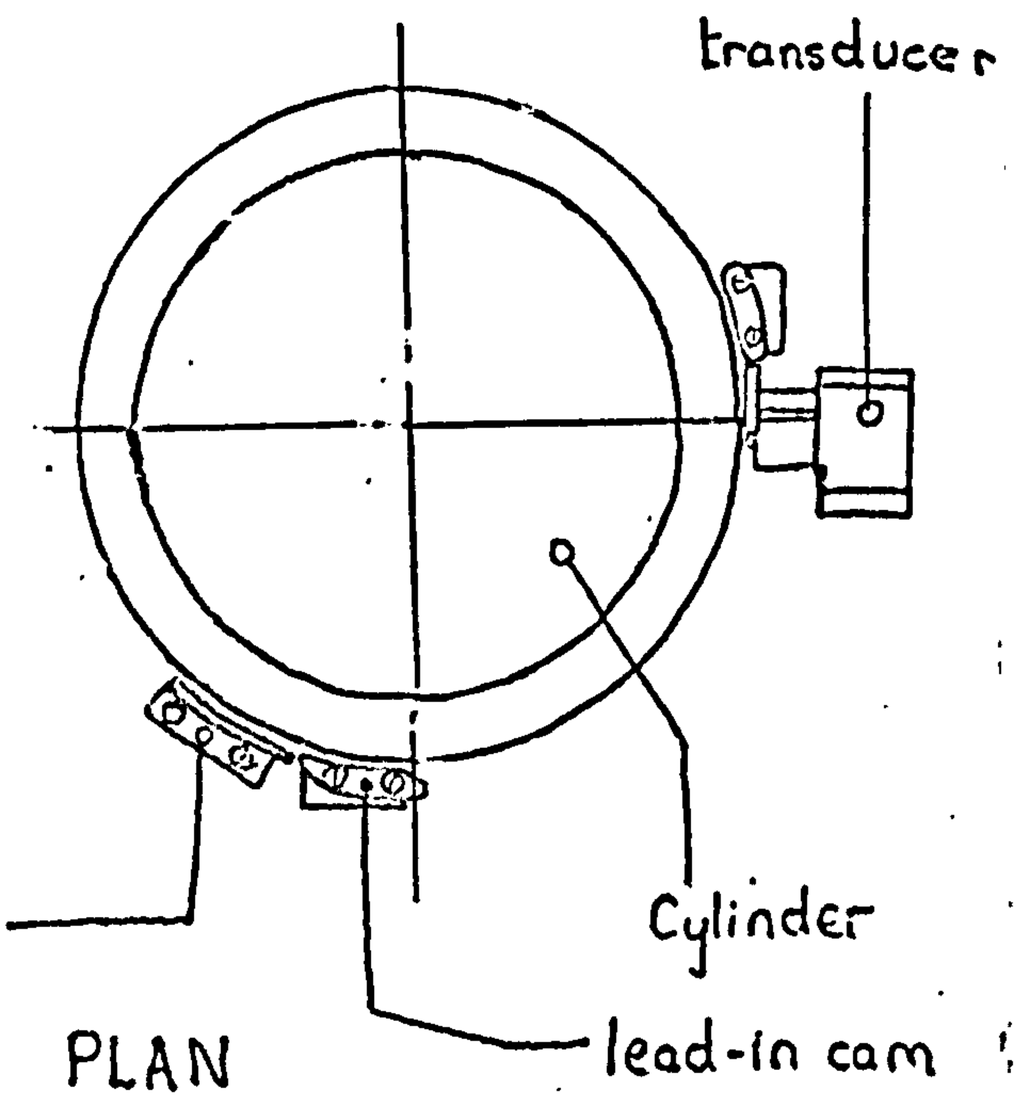

OPERATIONAL ARRANGEMENT OF STITCH-CAM IMPACT TRANSDUCER WHEN FITTED WITH SPECIAL ATTACHMENT AND USED FOR GUARD CAM IMPACT MEASUREMENTS

Fig 15.8

LOW SPEED (APPROXIMATELY 150 ft/min)
AMPLIFIER CAIN .05 V/div

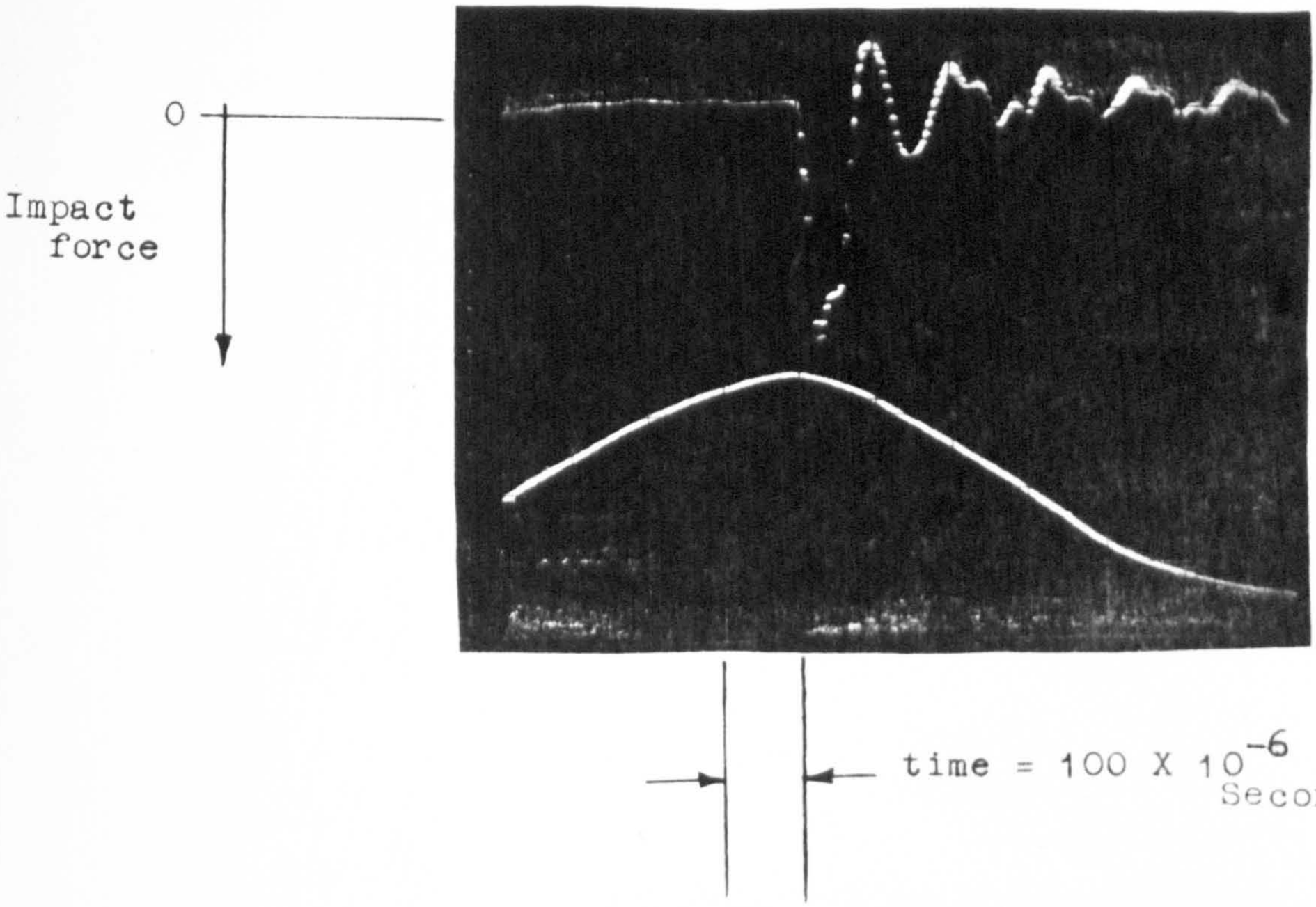

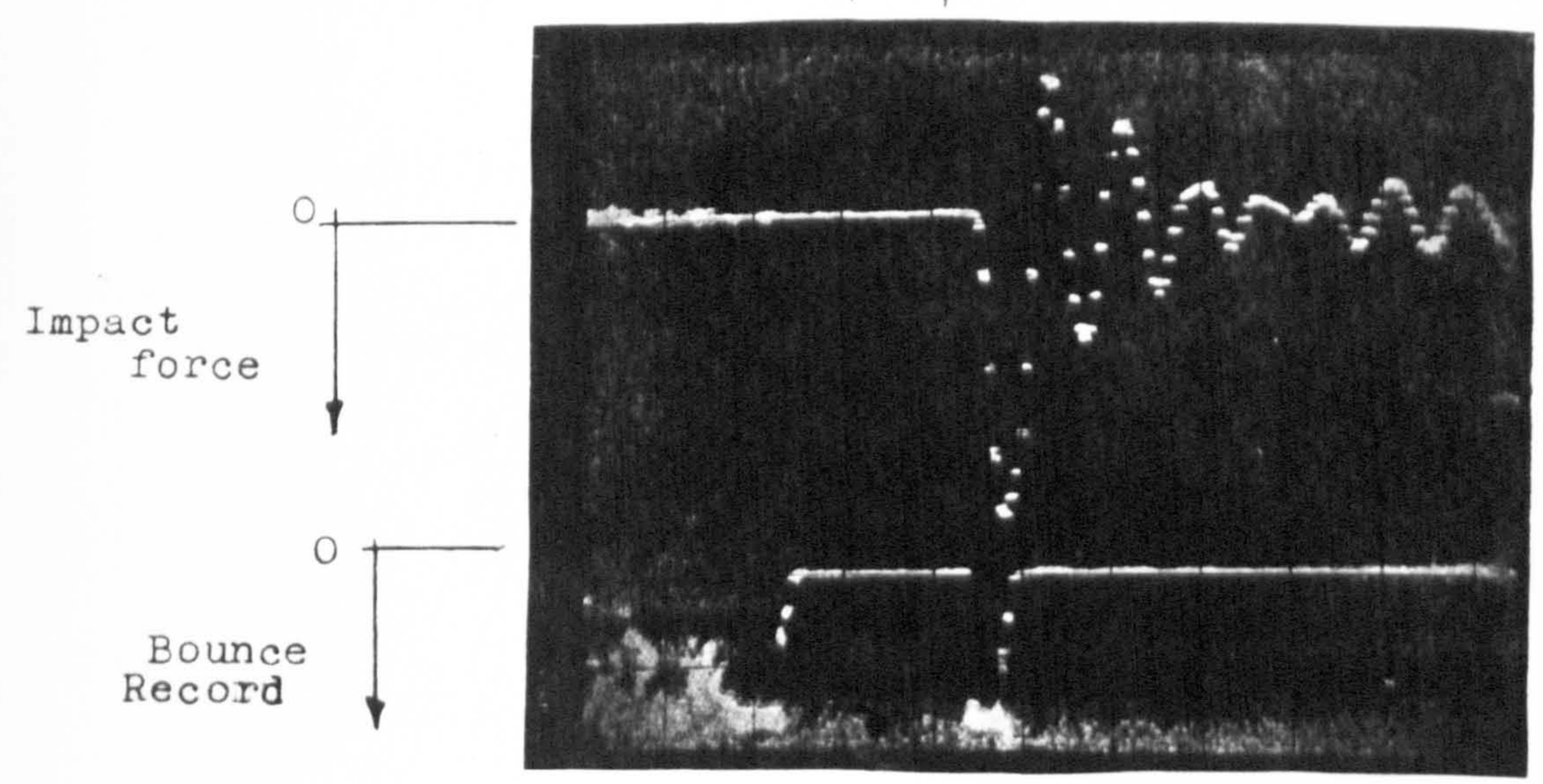

HIGH SPEED (APPROXIMATELY 350 ft/min)
AMPLIFIER GAIN .1V/div

INITIAL MEASUREMENTS OF GUARD-CAM IMPACT
(UNCALIBRATED) USING STITCH-CAM IMPACT TRANSDUCER
FITTED WITH SPECIAL ATTACHMENT

Fig 15.9

β = Guard-cam-angle

Beam manufactured out of cam material and hardened to the same extent.

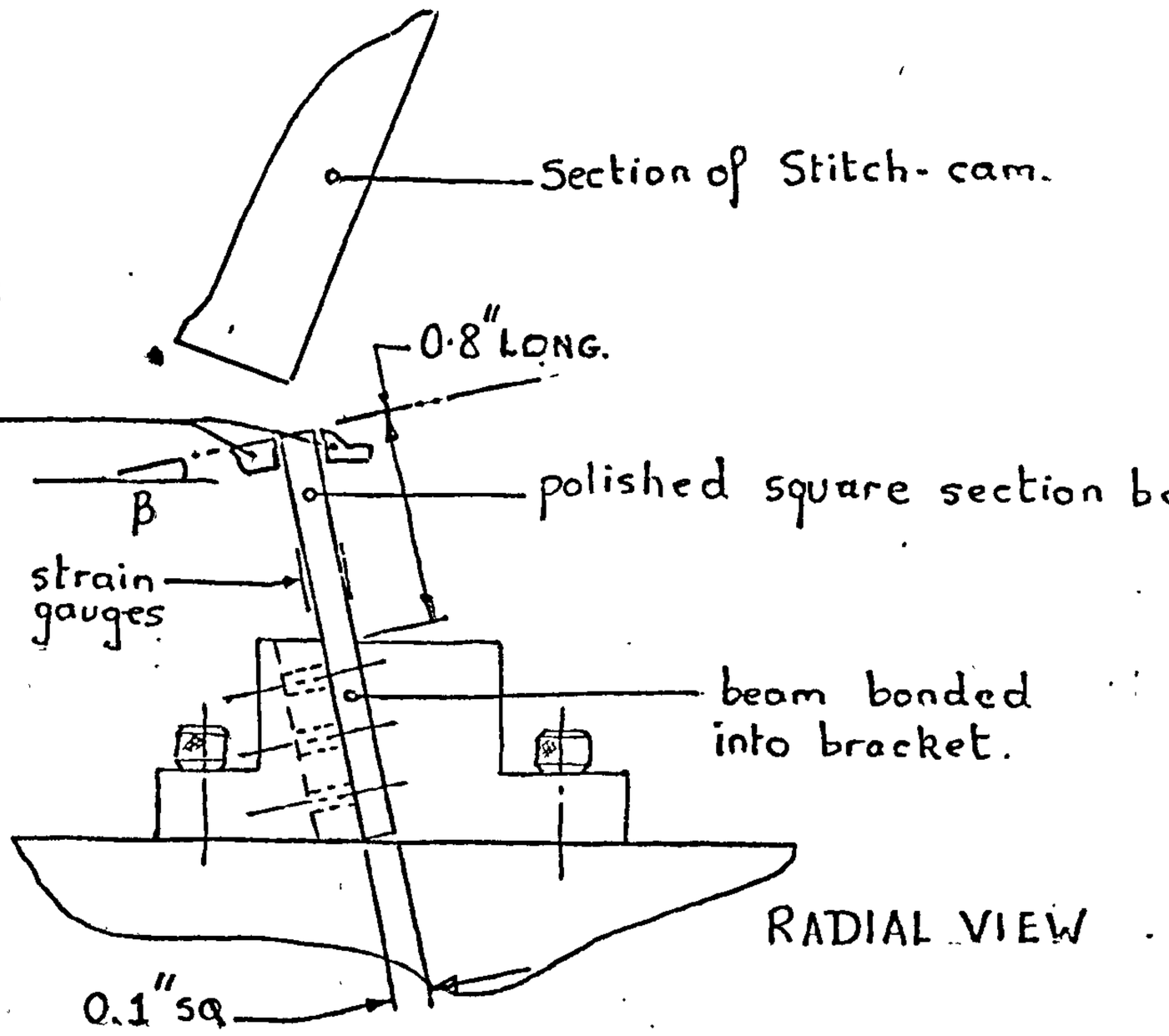

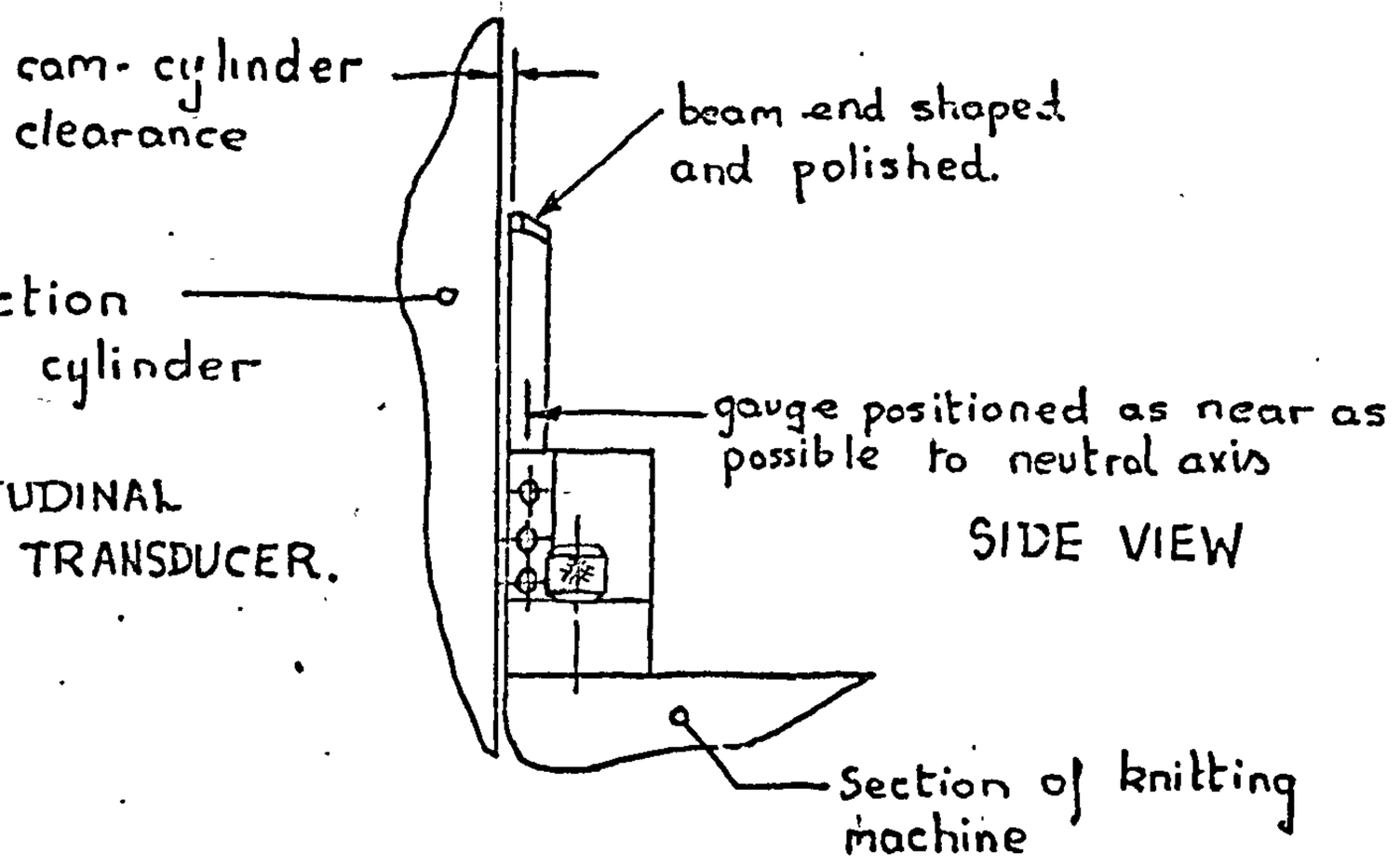

(b) LONGITUDINAL BEAM TRANSDUCER.

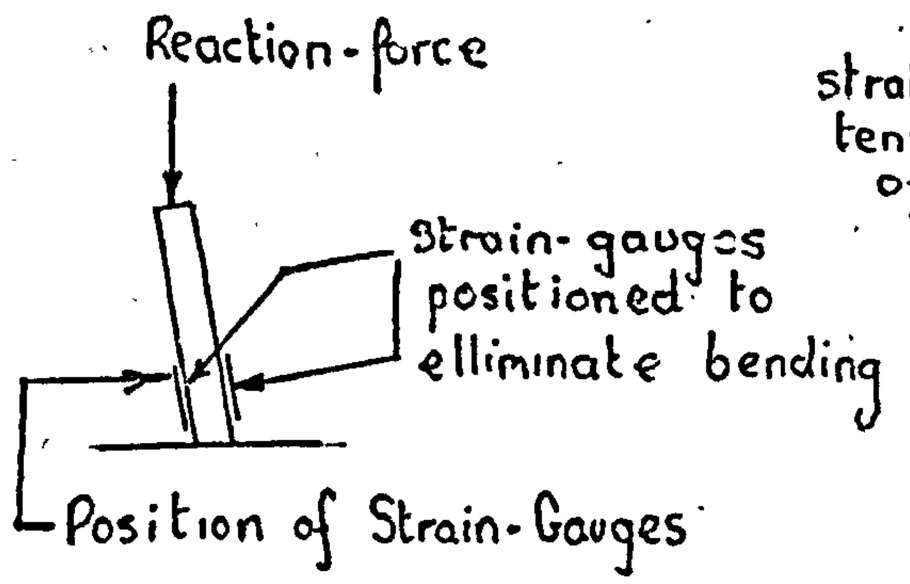

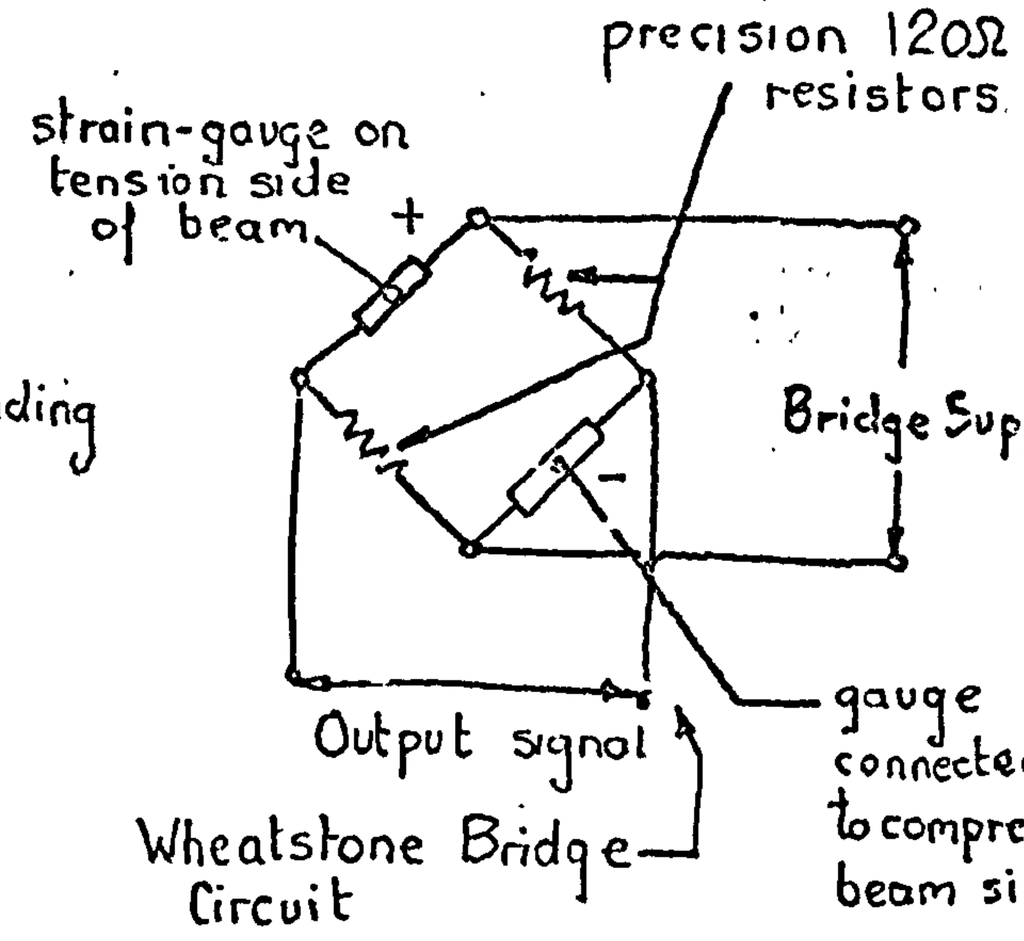

(a) POSITIONING OF GAUGES AND WHEATSTONE BRIDGE CIRCUIT

(a) LONGITUDINAL BEAM TRANSDUCER
(b) WHEATSTONE BRIDGE CIRCUIT

FIG 15.10

Needles hit stitch cam at normal knitting height (at stitch draw = 0.0668 INS)

rotatable stitch-cam.

Special Attachment

longitudinal transducer simulating guard-cont.

Close fitting guide to protect beam and minimise bending signal.

RADIAL VIEW

PLAN

lead-in cam and guide

transducer

Section of cylinder

cylinder

raising-cams

lead-in cam

SIDE VIEW (NOT TO SAME SCALE AS RADIAL VIEW)

LONGITUDINAL GUARD-CAM IMPACT TRANSDUCER OPERATIONAL ARRANGEMENT

FIG 15.11.

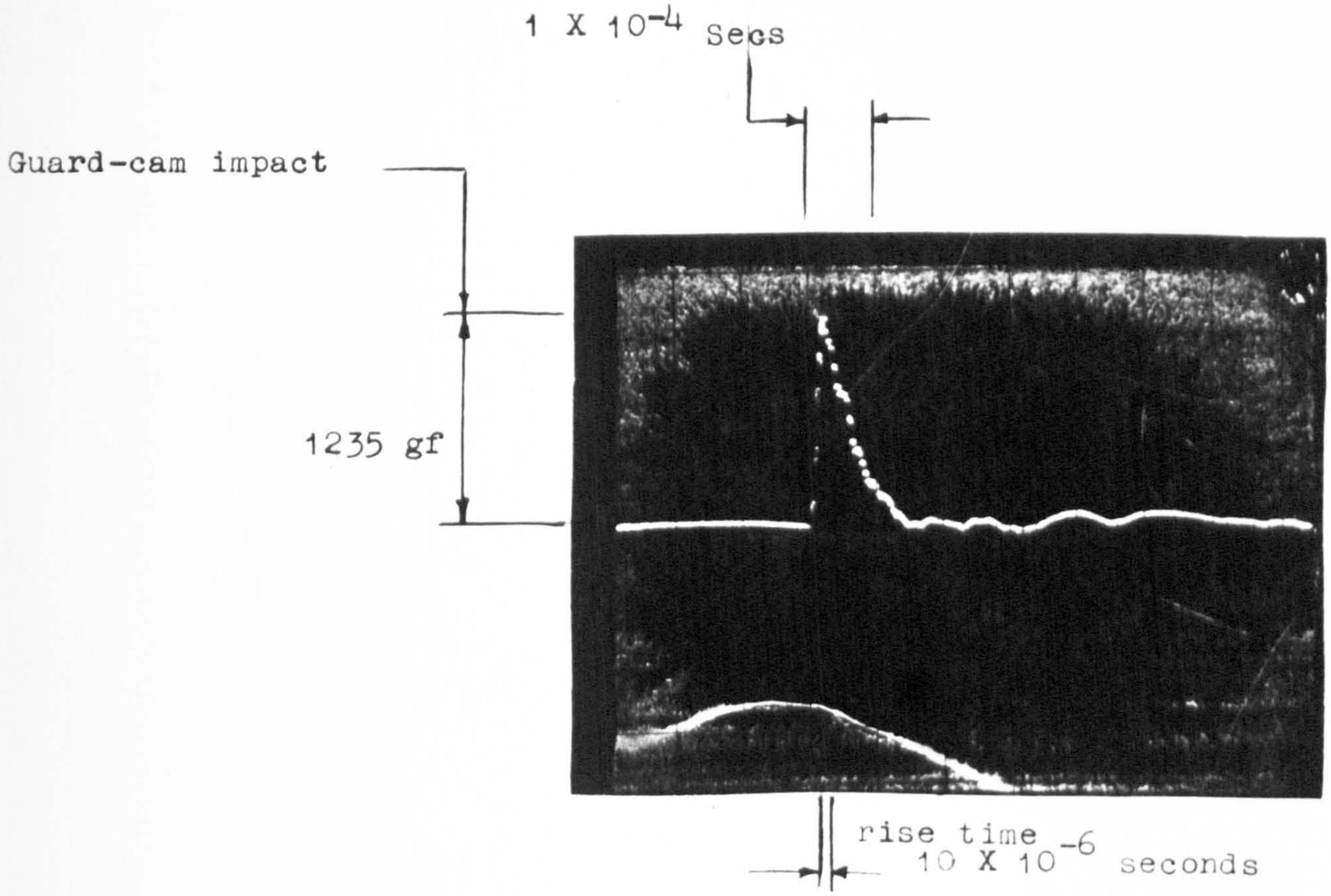

SPEED = 152.5 ft/min
GUARD-CAM ANGLE = 8°
CLEANED TRICK
46 gf/mm

A TYPICAL TRACE USING LONGITUDINAL BEAM TRANSDUCER

Fig 15.12

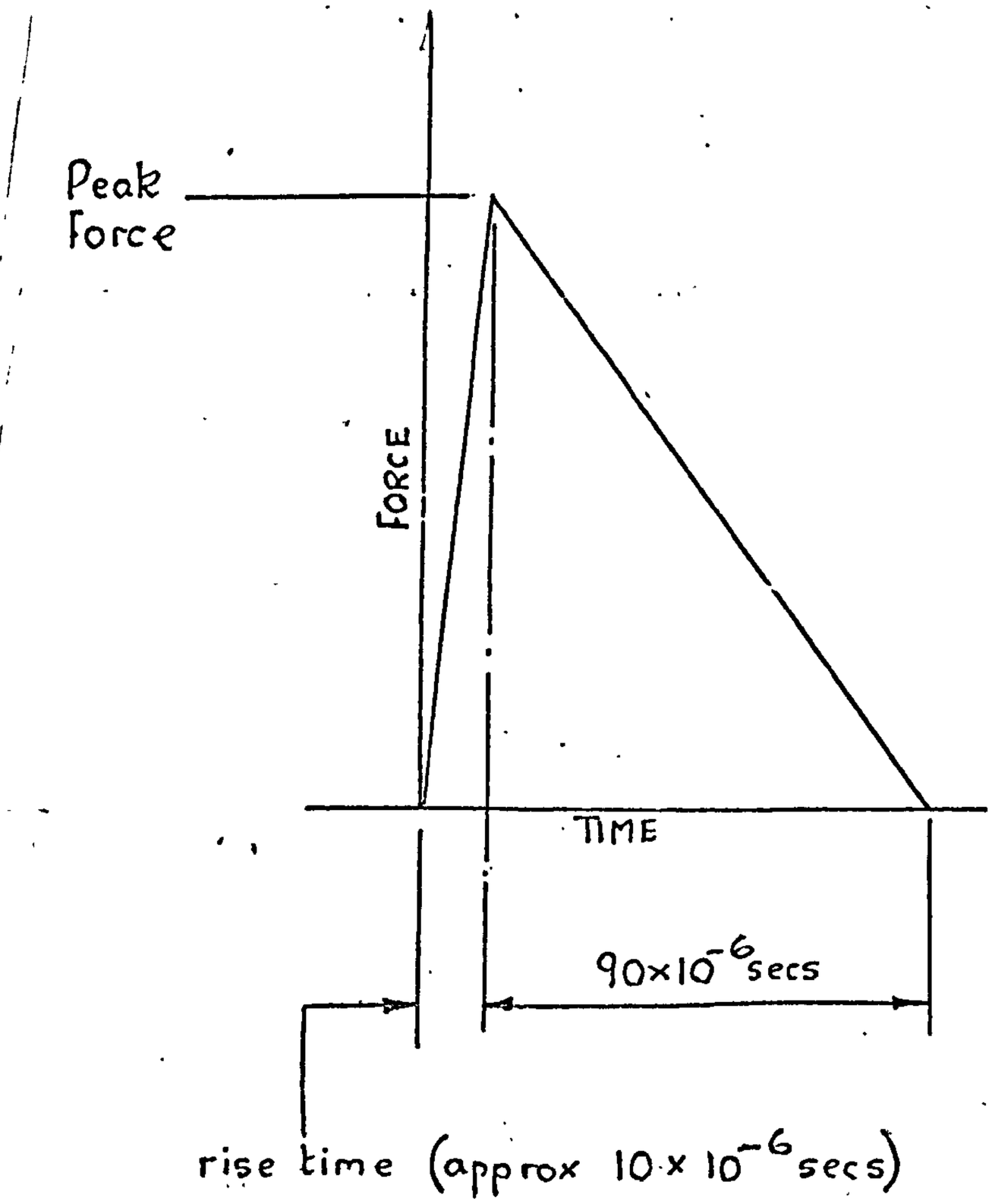

APPROXIMATION TO GUARD CAM IMPACT
REFER FIG 15.12

FIG 15.13

Equation $y = \dfrac{F_o/k}{1-\left(\frac{\omega}{p}\right)^2}\left[\sin\omega t - \frac{\omega}{p}\sin pt\right]$

$\omega = 5000$ Hz

$p = 11,500$ Hz

$y = \dfrac{1}{0.811}\dfrac{F_o}{k}\left[\sin\omega t - 0.435\sin pt\right)$

$$\alpha = \frac{1.3}{0.811} = 1.6$$

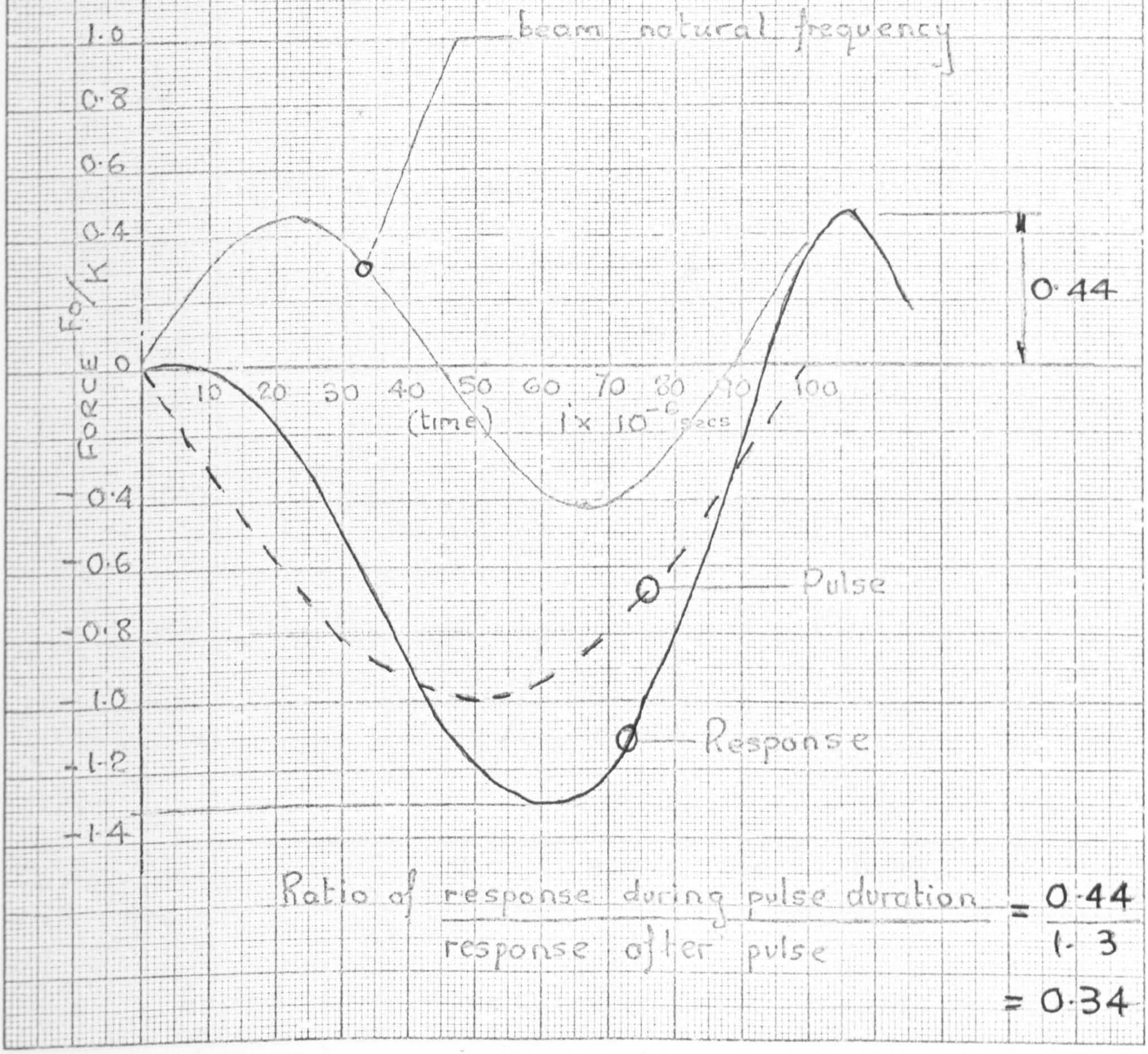

Ratio of $\dfrac{\text{response during pulse duration}}{\text{response after pulse}} = \dfrac{0.44}{1.3}$

$= 0.34$

NATURAL FREQUENCY = 11,500 Hz

BEAM RESPONSE TO A PULSE 5000 Hz

FIG 15. 14

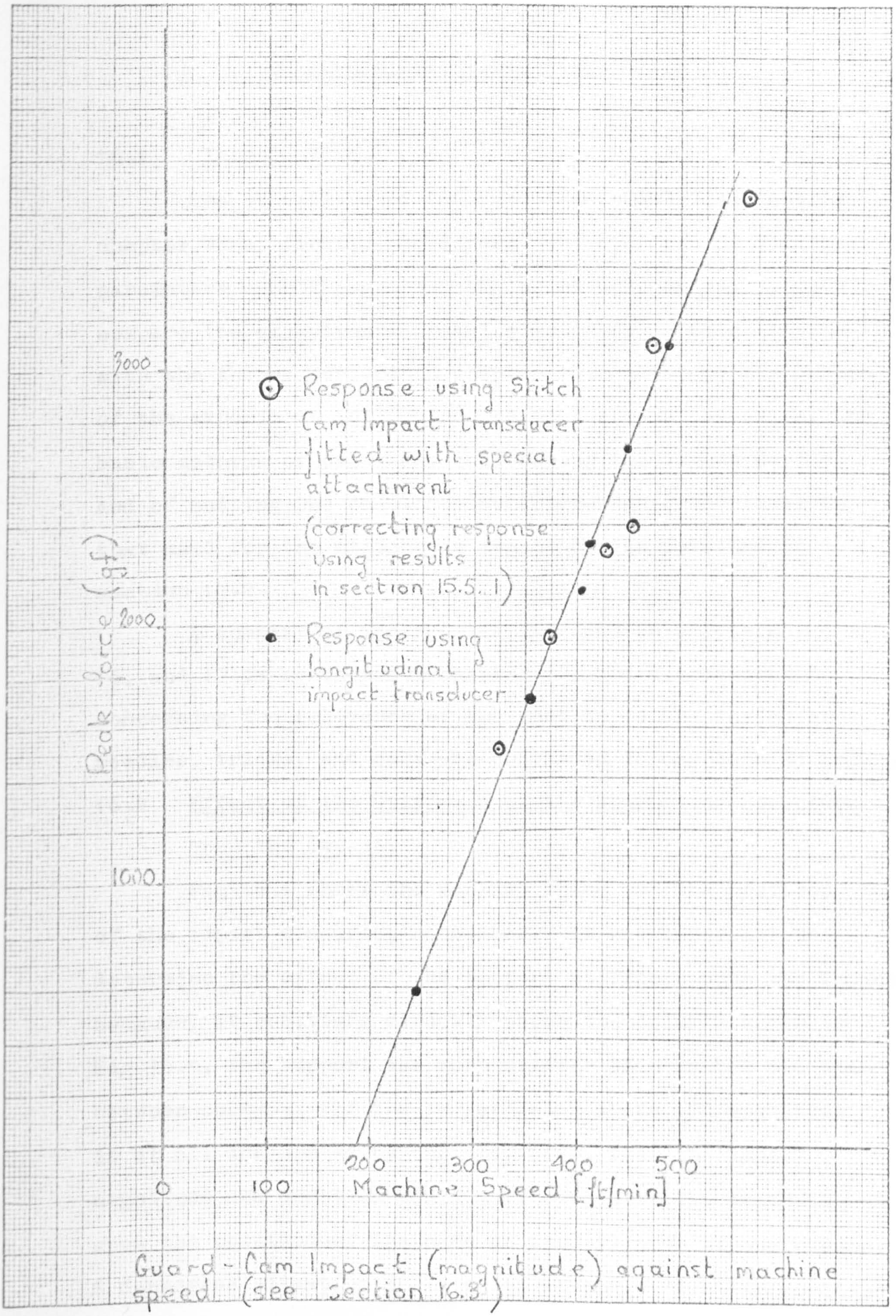

Guard - Cam Impact (magnitude) against machine speed (see Section 16.3)

COMPARISON OF OUTPUT FROM LONGITUDINAL TRANSDUCER AND STITCH CAM IMPACT TRANSDUCER

FIG 15.15

CHAPTER 16

GUARD-CAM IMPACT EXPERIMENTATION

16.1. Introduction.

The objectives of the experiments detailed in this chapter were, firstly, to determine the effect of various parameters upon the guard cam impact and, secondly, to compare the experimental results detailed in this chapter with the theory derived in chapter 15. Although the nature of the experiment influenced the measurement procedure, the basic methods of using and calibrating the impact device, and of setting the oscilloscope trigger were identical to that used for the stitch-cam impact device detailed in section 14.2.

A summary of the results detailed in chapters 14, 16, and 17 is contained in chapter 18, and discussions concerning the relevance of the results to the design of needles, tricks, and cams are contained in chapters 23 and 24.

16.2 Effect of the Stiffness of the Supporting Structure upon the Impact.

Fig 16.1 shows the machine frame and the position of the impact measuring transducer. It was important to determine the effect of the support stiffness upon the impact because, at positions directly above the columns shown in Fig 16.1, the support was much stiffer than in the mid-span between columns. If the impact pulse shape and magnitude is at all influenced by the stiffness, then the impact magnitude and duration would vary considerably, depending upon the position of the cams on the cylinder circumference. A dangerous situation could exist at one particular position

where high magnitude impacts are produced.

A standard 0.443 mm needle was inserted in a cleaned trick, and backing needles without butts were placed each side of it. Experimental traces of the impact magnitude were obtained at varying machine speeds.. Wedges were then forced underneath the supporting structure at the position where the transducer was fitted, and another set of impact traces was obtained. The method of stiffening the structure underneath the impact transducer is shown in more detail in Fig 16.1. The two sets of impact results are compared in Fig 16.2, and it can be clearly seen that the results are little different.

From the experimental results it is obvious that the stiffness of the supporting structure had a comparatively small effect upon the impact magnitude. It is likely that the major factors that control the shape and magnitude of the pulse are butt flexibility, and trick resistance to needle motion, as is later examined in the experiments detailed in this chapter.

16.3 Effect of the Yarn-Tension and Machine Speed upon the Impact.

During the knitting process, guard-cam impact occurs during the loop formation stage. The yarn, which at the instant of impact is being drawn into a loop, exerts a force upon the needle, and this force can be relatively large compared to the trick resistance to needle motion and other forces involved in the impact. It was thought highly probable that variation of the loop drawing tension would have some effect upon the impact magnitude. However, the design of the impact instruments, and the measurement requirements, were such that the normal knitting process

could not be carried out (see section 14.2). It was important to duplicate, in some way, the effect of the loop drawing tension, so that its effect upon the impact could be determined. A device which simulated the yarn tension variation was built and the essential details concerning the device are given below.

16.3.1 Design of a Yarn Tension Simulator.

Fig 16.3 Diagram I illustrates the essential construction of the apparatus, comprising a tension spring, a series of guides to duplicate the verge top, and a clamp. Diagram II, of Fig 16.3, shows the experimentally determined loop drawing force as analysed and detailed in section 9.6. The approximate position of the impact during the loop formation zone is shown by the cross in Diagram II of Fig 16.3, and the force exerted upon the needle by the yarn tension simulator is shown superimposed upon the experimental plot in Diagram II. Some features making the device particularly suitable for yarn tension simulation are summarised below :-

(i) The force imposed upon the needle by the yarn, at the instant of impact, was easily adjustable.

(ii) The yarn used with the simulator was the same as that used throughout the experiments detailed in chapter 8.

(iii) Yarn motion around the needle at the instant of impact was in the same direction as the yarn motion during the knitting process. This is further illustrated in diagram II of Fig 16.3.

16.3.2 Calibration of the Yarn Tension Simulator.

A needle was hooked into the yarn on the tension simulator, and a yarn loop was then tied around the butt of

the needle as shown in Fig 16.4. When this yarn was pulled, the needle moved down and extended the loop held in the hook. The force required to pull the needle down against the resistance offered by the simulator was measured by means of a Rothschild 0 to 100 gf head placed on yarn tied to the butt. The signal from the measuring head was passed to the Rothschild amplifier and then displayed on the Tektronix oscilloscope.

The force exerted upon the needle, by the yarn around the hook and connected to the spring and clamp of the simulator, was measured as 80 gf per 0.125 in. downward movement of the needle.

16.3.3 Method of Carrying out Measurements using the Yarn Tension Simulator.

The tension exerted upon the needle, at the instant of guard-cam impact, could be preset by controlling the amount of yarn between the spring and the clamp. For example, if a low tension was required at the instant of impact, then enough yarn would be present between the spring and clamp, to ensure that the position of the needle, at zero tension, was a small prescribed distance above the position of impact on the guard cam. Therefore, the extension of the loop around the hook at impact was small, and consequently the yarn force on the needle was also small.

The yarn tension simulator was bolted to the inside of the cylinder. A 0.443 mm needle was fitted in a thoroughly cleaned trick and the head was hooked into the yarn on the simulator. The device was then set to produce a particular force at guard-cam impact. Fig 16.5 illustrates the method of carrying out the measurements, most of the traces in this experiment were obtained using the stitch-cam impact

transducer fitted with the special attachment shown in Fig 15.7, but a few were obtained using the longitudinal beam instrument. Initially, results were obtained with a high tension on the simulator, then another set was obtained at a lower tension, and finally the yarn loop was removed altogether.

16.3.4 Experimental Results.

Fig 16.6 shows the experimental results plotted, together with the theoretical maximum guard cam impact derived in section 15.2. The results show that, as the tension increases, the machine peripheral velocity at which guard-cam impact just begins, also increases. At high speed, the difference between the impacts at zero and 167 gf yarn-force is relatively small. A typical sample of traces obtained using the longitudinal beam instrument is shown in Fig 16.7 (b). There was no noticeable change in the pulse shape throughout the experiments detailed in this section.

16.3.5 Comparison with the Theory.

Theoretically, the force exerted upon the needle by the yarn is defined in the term F, the trick resistance to needle motion; the yarn acts as an effective increase in the resistance.

The equations, derived in section 15.2, that govern the magnitude of the Impulse I are defined below :-

$$I = \int_{T}^{T+\Delta T} R(t)\,dt = m\dot{U}_i(1+e) \quad . \quad . \quad (144),$$

$$\dot{U}_i = \left(\sqrt{(\dot{x})^2 + (\dot{y})^2}\right) \cos\left(\pi/2 - \left(\beta + \tan^{-1}\left(\frac{\dot{y}}{\dot{x}}\right)\right)\right) \quad (145),$$

where:

$$\dot{x} = V \quad . \quad . \quad . \quad . \quad . \quad . \quad (146),$$

$$\dot{y} = v\tan\delta - \frac{F\,T}{m} \quad . \quad . \quad . \quad (147),$$

and $$T = \frac{Lv}{2} - \frac{\sqrt{(Lv)^2 - 4M}}{2} \quad \ldots \quad (148),$$

where L and M are defined in section 15.2, and all the remaining parameters are defined in Fig 15.2.

From equation (148), impact with the guard-cam occurs when,

$$(Lv)^2 \geqslant 4M$$

which simplifies to ,

$$v^2 \geqslant \frac{2F\ (d-b)}{m(\tan\gamma + \tan\beta)^2} \quad \ldots \quad (149).$$

If F is increased the minimum velocity at which guard cam impact just begins also increases. This is in agreement with the experimental results.

It is not immediately obvious from equation (147) whether the term $\frac{F \cdot T}{m}$ increases or decreases, when F is increased, because T is also a function of F . However, a few trial values were substituted into this equation, and it became obvious that as F increased the term $\frac{F \cdot T}{m}$ also increased. An examination of equation (145), shows that as the $\frac{F \cdot T}{m}$ term increases, the cosine term decreases and consequently the slope of the graph (Impulse I against machine speed) should decrease. The theoretical response for increasing F should be as shown in Fig 16.6. (a). The experimental results shown in Fig 16.6 indicated an increasing slope; however, the results were somewhat variable, and for the relatively small changes in F there would be only a small change in the theoretical slope. For the above reasons, it was considered that the experimental results followed the trend predicted from the theory derived in section 15.2.

16.3.6 Dimensional Analysis.

The impact force is dependent upon a large number of parameters. Although the representation of force against machine speed is convenient for a large number of circumstances, a more efficient method of presenting the results can be derived by carrying out a dimensional analysis. By means of the analysis, the maximum amount of information can be represented on the minimum number of graphs.

In section 15.2, it was shown that the

$$\text{Impulse } I = \phi(v, \gamma, \beta, d-b, m, e, F)$$

where $\phi(\ ) =$ a function derived in section 15.2.

Using the Buckingham π theorem[51] the best method of showing the inter-relationship between the parameters is to plot :-

$$\frac{I}{\sqrt{m(F)(d-b)}} \quad \text{against} \quad v\sqrt{\frac{m}{(F)(d-b)}} \quad . \qquad (150)$$

for constant e , γ , and β .

Before equations (150) could be plotted F , and $d-b$, had to be determined for the particular needle under test. The trick resistance to motion at zero yarn force given by:

$$P + \mu_1 Q - mg$$

where P = Trick clamping force,
μ_1 = Coefficient of trick-needle friction,
Q = Force exerted by band-spring,
and mg = needle weight.

The resistance was measured by steadily pulling a length of yarn that was tied around a needle hook. The Rothschild 0 to 100 gf measuring head was used to measure

the tension in the yarn, and the output from this was taken to the Rothschild Amplifier and then to the Tektronix oscilloscope. For the needle and trick used in the experiments (section 16.3.4) and using a method detailed in section 9.5 the trick resistance was measured as 35 gf. The distance d was measured using feeler gauges and the butt width b was then subtracted from the figure to give a value of :-

$$d - b = 0.006 \text{ ins. } (0.15 \text{ mm})$$

Using the experimental results detailed in section 16.3.4, the values of :-

$$\frac{I}{\sqrt{m(F)(d-b)}} \text{ were plotted against } V\sqrt{\frac{m}{(F)(d-b)}} \quad (151)$$

The graph is shown in Fig 16.8.

The terms defined in expression (151) were evaluated theoretically using the following parameters :-

$m = 0.67$ g,
$d - b = 0.15$ mm (0.006 in.)
$F = 35$ gf, 148 gf, and 202 gf (for three calculations),
$\gamma = 52^{\circ}$,
$\beta = 8^{\circ}$,
$e = 0$ and 1,
$V = 0.52$ m/s (100 ft/min), 1 m/s (200 ft/min), and 1.52 m/s (300 ft/min) (for three calculations).

I was evaluated from equations (144) to (148) in section 16.3.5, using the above values.

The results of the theoretical analysis, together with the experimental results is shown in Fig 16.8.

16.3.7 Brief Summary.

The experimental results show that, as the machine

speed is increased, the guard-cam impact increases in direct proportion. The effect of increasing the yarn-tension is to raise the speed at which impact first begins. The impact was compared with the predicticns from the theoretical analysis, and a reasonable degree of agreement between theory and experiment was achieved.

A non-dimensional method of plotting the results was derived in section 16.3.6 and this provided a means of displaying the information with the fewest graphs. The results obtained in this experiment are discussed further in section 18.2.1.

16.4 Effect of Stitch-Cam Incidence Angle upon the Magnitude of the Impact.

The special attachment used to simulate the stitch-cam, during guard-cam impact experiments, had the facility for changing the stitch-cam angle, and this is shown in more detail in Fig 15.7. An experiment was carried out by varying the stitch-cam angle, and, at each angle, obtaining a number of traces at various machine speeds. Traces were also obtained using the longitudinal impact apparatus at a cam-angle of 50^{o}. The experimental method, calibration, and oscilloscope trigger setting were identical to those detailed in section 14.2.

The parameters for the experiment measurements, and for subsequent theoretical analysis, are summarised below :-

Guard cam angle $\beta = 8^{o}$,

Cam-cylinder clearance = 0.15 mm (0.006 in.),

$d - b$ = 0.15 mm (0.006 in.),

and Standard 0.443 mm needle in a cleaned trick,

F = 35 gf.

It was shown, in section 16.3.4 and Fig 16.6, that

the maximum impact occurred when the needles were running through the cams without knitting. This experiment was carried out without the yarn simulator being fitted and therefore the loop-drawing tension was zero. During the normal knitting process, the yarn-force acting on the needle at the instant of impact is related to the stitch-cam angle. Obviously, for steeper angles the force will be less, and consequently, the velocity at which the impact just begins will be less than the velocity using shallower stitch-cam angles.

The experimental results are plotted in Fig 16.9, and Fig 16.10 shows the effect of cam angle upon the impact force at four different machine speeds.

A theoretical analysis was carried out at ,

$$\gamma = 56^{\circ} \text{ and } \gamma = 40^{\circ}$$

A typical comparisen between experimental and theoretical values is shown below :-

at $v = 250$ ft/min (1.27 m/sec),

experimental values were :

$\gamma = 56^{\circ}$, impact force = 2090 gf,

$\gamma = 40^{\circ}$, impact force = 1065 gf.

Theoretical values, assuming a triangular shaped impulse of duration 95 x 10^{-6} seconds, were calculated for e (coefficient of restitution), equal to 1.

then $\gamma = 56^{\circ}$, impact force = 2730 gf,

and $\gamma = 40^{\circ}$, impact force = 1750 gf.

and for $e = 0$,

then $\gamma = 56^{\circ}$, impact force = 1365 gf,

and $\gamma = 40^{\circ}$, impact force = 875 gf.

Additionally the non-dimensional parameters,

$$\frac{I}{\sqrt{m(F)(d-b)}} \quad \text{and} \quad v\sqrt{\frac{m}{(F)(d-b)}} \qquad (152)$$

were evaluated from the experimental results. The graph is shown in Fig 16.11.

The results clearly show that the stitch-cam angle has a large effect upon the impact magnitude.

16.5 Effect of a Large Change in the Guard Cam Angle.

An examination was carried out of the guard-cam impact for the cam arrangement shown in Fig 16.12. It was considered that the system shown may have some advantages. and these are summarised below :-

(i) A steep guard-cam would transform the guard-cam impact into what was effectively a stitch-cam impact with a consequently longer duration. Although at this stage of the project, little work had been carried out on needle damage, it was considered that a longer duration impact would reduce the risk of needle head damage.

(ii) As machine speed increased, the position of the impact on the guard-cam moved by an amount that depended on a large number of parameters, which varied from needle to needle. The movement of the impact point which could lead to stitch non-uniformity was restricted by the steeper guard-cam angle, shown in Fig 16.11.

The special guard cam (Fig 16.11) was fitted to the beam of the stitch-cam impact transducer, which was arranged for guard-cam impact measurements as shown in Fig 15.7. It was impossible to use the longitudinal impact instrument because the guard-cam angle on the device could not be varied.

The particular procedure adopted during the measurements for setting the oscilloscope trigger, and calibrating, were the same as detailed in section 14.2. The horizontal and vertical components of the impact on the transducer were recorded at various speeds and a typical sample of the experimental results is given in Fig 16.13. As can be seen, the pulse is considerably different in shape to that of the normal guard cam impact.

The pulse has a long time duration, i.e. almost 500×10^{-6} secs ; however it has a sharp high frequency peak. The magnitude of the force is shown plotted in Fig 16.14 in conjunction with the experimental results obtained with an 8^{o} guard cam. The results show much higher force magnitudes than those experienced with the shallow 8^{o} guard-cam, and indeed butt fracture occurred quite frequently when needles were run through the cam system at high machine speed.

16.5.1 Theoretical Effect of Guard-Cam Angle upon the Impact.

It was shown in section 15.2, that the worst case of impact occurred when $d-b$ was small, F was small, and e was equal to 1.

then $$I = \left(2mv\right) \sec\delta \cos\left(\pi/2 - (\delta + \beta)\right) \quad . \qquad (153).$$

The above equation was solved using a stitch-cam angle of $\delta = 45^{o}$. A graph of the impulse I against speed v , for varying guard cam angles, is shown in Fig 16.15. Although only one stitch-cam angle δ was used in the calculations, the essential characteristics of the response were the same no matter what angle was used. The analysis shows that minimum guard-cam impulse occurs when the guard-cam angle is small. However, it is likely that the shape

of the impact force changes as the guard cam angle is varied, and although the impulse at an angle of $\beta = 0^{\circ}$ is a minimum this does not mean that the maximum impact magnitude R_{max} is less at $\beta = 0^{\circ}$ than at other angles.

16.6 Effect of Cam-Cylinder Clearance upon Guard Cam Impact.

An experiment was carried out to examine the effect of the cam-cylinder clearance upon the impact magnitude. The stitch-cam impact transducer, fitted with the special attachment shown in Fig 15.7, was used for most of the tests although spot checks were occasionally made using the longitudinal beam instrument. A standard 0.443 mm needle used throughout the majority of the experiments detailed in this chapter was fitted in a thoroughly cleaned trick. Initially traces were obtained at a clearance of 0.15 mm, the clearance was then increased to 0.38 mm (0.015 in.), and finally to 0.86 mm (0.034 in.). The methods of carrying out the measurements, calibrating, and setting the oscilloscope trigger, were the same as that detailed in section 14.2.

The results were plotted as shown in Fig 16.16, and these show a small reduction in the impact magnitude as the clearance is increased.

16.7 Effect of Various Butt Modifications.

A number of experiments were carried out to examine the effect of various changes in the design of the needle butt, the butt shape being shown in Fig 16.17.

The modifications were aimed at either increasing the butt flexibility, or increasing the total surface of needle to cam contact at the instant of impact.

Initially, an experiment was carried out on a standard 0.443 mm needle, and traces were obtained at varying machine

speeds. After this, each modification was tested individually under the same conditions as the standard needle. The majority of the tests were carried out using the stitch-cam impact transducer fitted with the attachment shown in Fig 15.7. The method of carrying out the experiments was the same as that detailed in section 14.2. However, before each needle butt was fitted, the trick was cleaned and the cylinder and bearings were lightly oiled.

The experimcntal results are plotted in Fig 16.18, 16.19 and Fig 16.20. None of the modifications in butt shape produced much difference in the guard cam impact magnitude or the pulse shape. The minimum impact occurred with the butt modification shown as diagram I of Fig 16.17. However, the reduction in impact magnitude for this needle may have been due to the increased cam-cylinder clearance. The results obtained for needles with butts shaped as shown in Fig 16.17 showed a large degree of variability with machine speed. It was initially considered that this may have been due to the particular butt modification. However, at the end of the experiment the same standard 0.443 mm needle that had been used initially was again tested under exactly similar conditions to thcse used in the first test. The two results are shown superimposed in Fig 16.20. The test carried out at the end of the experiments showed a marked variability with force, although the pulse duration did not change significantly.

After a close examination of the cam surfaces, two fine horizontal scratches were noticed on the stitch-cam. The scratches were very fine and positioned approximately 0.5 mm from the lowest tip of the cam. It was considered

that the fine scratches may have been caused by a swiss-file that had been used during the experiment.

Before these scratches were removed from the cam surface, the longitudinal beam instrument was fitted, and a series of traces were recorded at variable speed using a standard 0.443 mm needle with a short butt; the traces showed a high degree of variability. The stitch-cam was then removed, the base of the cam polished until the scratches were completely removed, and impact was again measured using the same needle at similar conditions. The graphs are shown in Fig 16.21 and it can be seen that, after the scratches were removed the traces became much less variable. Finally, the trick resistance was greatly increased up to approx 450 gf and another set of results were obtained which are also shown on Fig 16.21.

16.7.1 Summary.

Although the needle butts were drastically modified, the magnitude of the impact for a particular machine speed did not change much for each needle tested. The results suggest that the shape of the butt has relatively little influence on the impact magnitude and duration.

When the base of the stitch cam was accidently marked with some fine horizontal scratches, the impact magnitude became very variable at high machine speed. It is possible that the fine marks produced a loss of cam contact before the bottom of the stitch cam. The loss of contact would have the effect of increasing the d-b term and also altering the angle of impact with the guard cam.

When the trick resistance to needle motion was increased to approximately 450 gf, the impact magnitude was reduced at high speed.

16.8 Effect of Oil upon the Guard Cam Impact.

The stitch-cam impact transducer was used to obtain the majority of the traces in this experiment, the methods of calibrating and using the instrument, and of setting the trigger being the same as that detailed in section 14.2. Initially, with no oil applied to the cylinder, a series of traces were obtained of impact against machine speed. After this initial test was completed, the machine was heavily oiled with Vickers Spotless B.N.O. oil and the test was repeated. The two graphs are shown in Fig 16.22. The parameters for this experiment are detailed below :-

Stitch-cam angle $\gamma = 51^{o}$,
Guard-cam angle $\beta = 8^{o}$,
Standard 0.443 mm needle used in cleaned trick,
and Cam-cylinder clearances 0.15 mm (0.006 in.)

The results show that the heavy addition of oil decreased the impact magnitude and also increased the minimum velocity at which impact just commenced. The results indicate that the effect of the oil upon the impact process is for the viscous forces to act so as to increase the total trick resistance to needle motion.

16.9 Effect of Needle Mass upon the Impact.

An experiment was undertaken to investigate the effect of needle mass upon the impact. Three 0.443 mm standard needles were prepared; material was removed from the shanks of two needles and the other was left unmodified. A diagram of the needles used in this experiment is shown in Fig 16.23. Initially, the stitch-cam impact apparatus, with the attachment fitted, was used; however most of the measurements were carried out using the longitudinal impact transducer. Initially, the 0.443 mm needle was inserted in

a thoroughly cleaned trick, and traces were recorded at a range of speeds. The 0.60 g needle was then inserted in the trick and tested and finally the 0.38 g needle was tested. A typical sample of the traces is shown in Fig 16.24, and 16.25, the results of the experimental measurements are plotted in Fig 16.26.

The experimental results clearly show that the mass of the needle has a large effect upon the impact magnitude, and has relatively little effect upon the impact duration.

16.9.1 Non-Dimensional Plotting.

As the results in this experiment were obtained for a similar stitch-cam and guard cam angle to that used in section 16.3, then, if the non-dimensional parameters derived in section 16.3.6 are calculated from the results detailed in section 16.8, they should lie on the curve shown in Fig 16.8. To demonstrate that the calculated values for a needle mass of 0.67 g and 0.38 g do lie on the curve, calculations were carried out using the following parameters :-

(i) $\beta = 8^{o}$,
$v = 40$ in/sec (1.02 m/sec),
and $m = 0.67$ g.
Impact force $= 1440$ gf,
$d-b = 0.006$ in. (0.015 mm)
$F = 35$ gf,
and $\gamma = 52^{o}$.

The calculated non-dimensional parameters are shown below :-

$$\frac{I}{\sqrt{m(F)(d-b)}} = 6.81;$$

and $$v\sqrt{\frac{m}{(F)(d-b)}} = 3.64.$$

(ii) $\gamma = 52^{\circ}$,
$V = 40$ in/sec (1.02 m/sec),
$m = 0.38$ g,
impact force $= 770$ gf,
$d - b = 0.006$ in. (0.015 mm),
$F = 35$ gf,
$\beta = 8^{\circ}$,

then,

$$\frac{I}{\sqrt{m(F)(d-b)}} = 4.82,$$

and

$$V\sqrt{\frac{m}{(F)(d-b)}} = 2.74.$$

If these results for the 0.38 g and 0.67 g needles are referred back to Fig 16.8 it can be clearly seen that they are still on the same experimental line for the particular conditions of $\gamma = 52^{\circ}$ and $\beta = 8^{\circ}$.

16.9.2 Theoretical Effect of Mass upon the Impact Magnitude.

When the trick resistance to needle motion is low, then equation(135) in section 15.2, shows that the reduction in the impact magnitude for constant impact duration varies in direct proportion to the mass reduction. For example, if the mass is halved the impact magnitude is also halved. When the trick resistance to needle motiom is higher, the effect of the needle mass upon the impact is even greater, because, not only is there the linear reduction, but there is also the increase in the $\frac{F}{m}$ term which means that the minimum velocity at which impact occurs is increased as the needle mass is reduced. Therefore if the mass is halved then, when

the trick resistance to needle motion is not negligible, the reduction in the impact magnitude is more than one half.

16.10 The Bounce of the Needle on the Guard Cam.

The bounce detector was connected to the stitch-cam impact transducer, as fitted with the special attachment to adapt it for guard-cam impact. An experiment was undertaken to measure the bounce of a 0.443 mm standard needle on the guard cam under the conditions specified below :-

$$\gamma = 52^{\circ},$$
$$\beta = 8^{\circ},$$
$$d-b = 0.006 \text{ in.},$$
and $$F = 35 \text{ gf.}$$

The method of using the impact transducer and the bounce detector was the same as that detailed in section 14.2. The results of the experiment are shown in Fig 16.27.

The yarn-tension simulator was then bolted to the cylinder, the yarn loop was connected to the needle hook and the yarn tension at the instant of impact was pre-set to approximately 90 gf. The experiment to measure the needle bounce was then repeated and a typical sample of the traces obtained are shown in Fig 16.28.

The results of the investigation clearly show that, for the particular needle tested, there was a second pulse closely following the first.

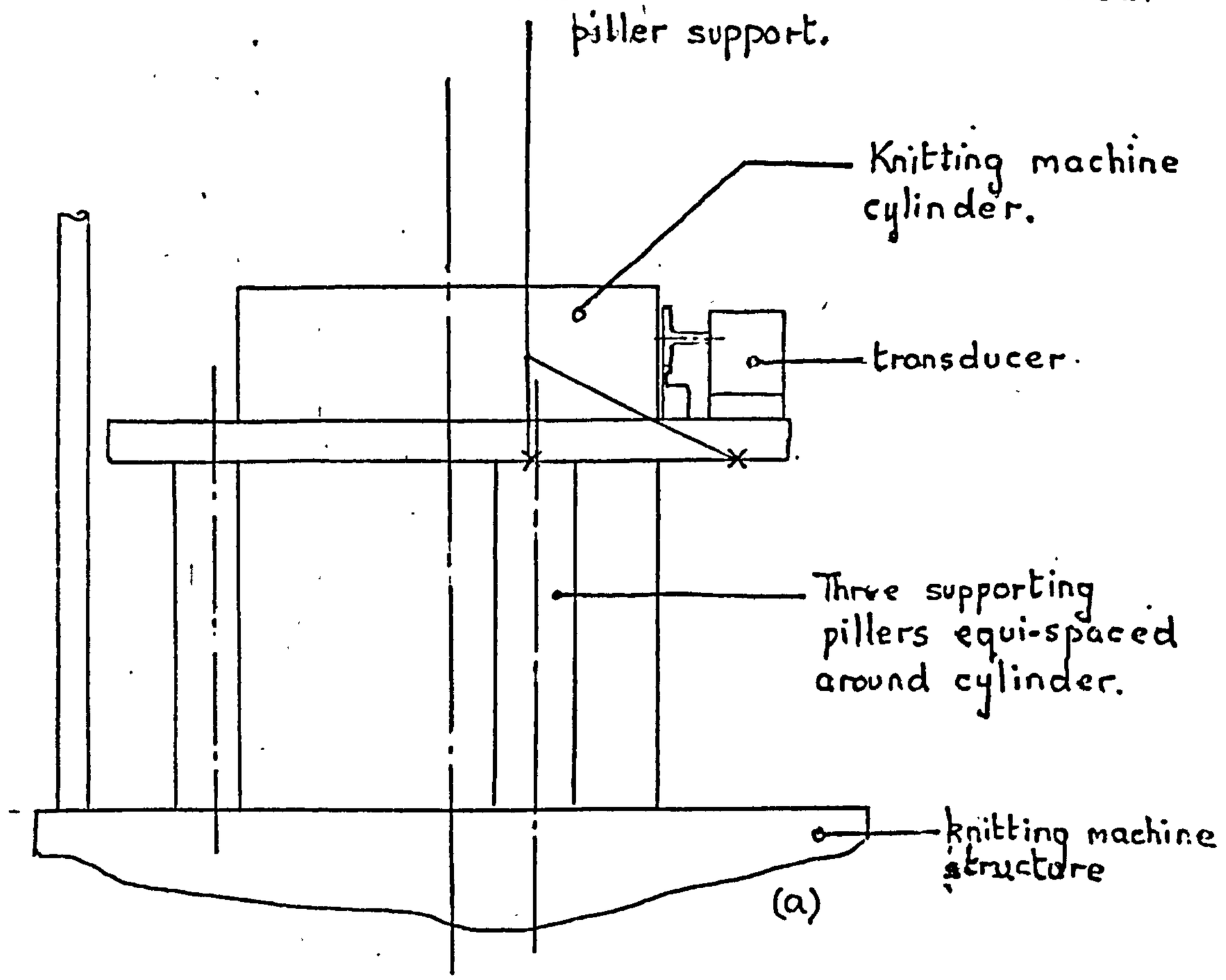

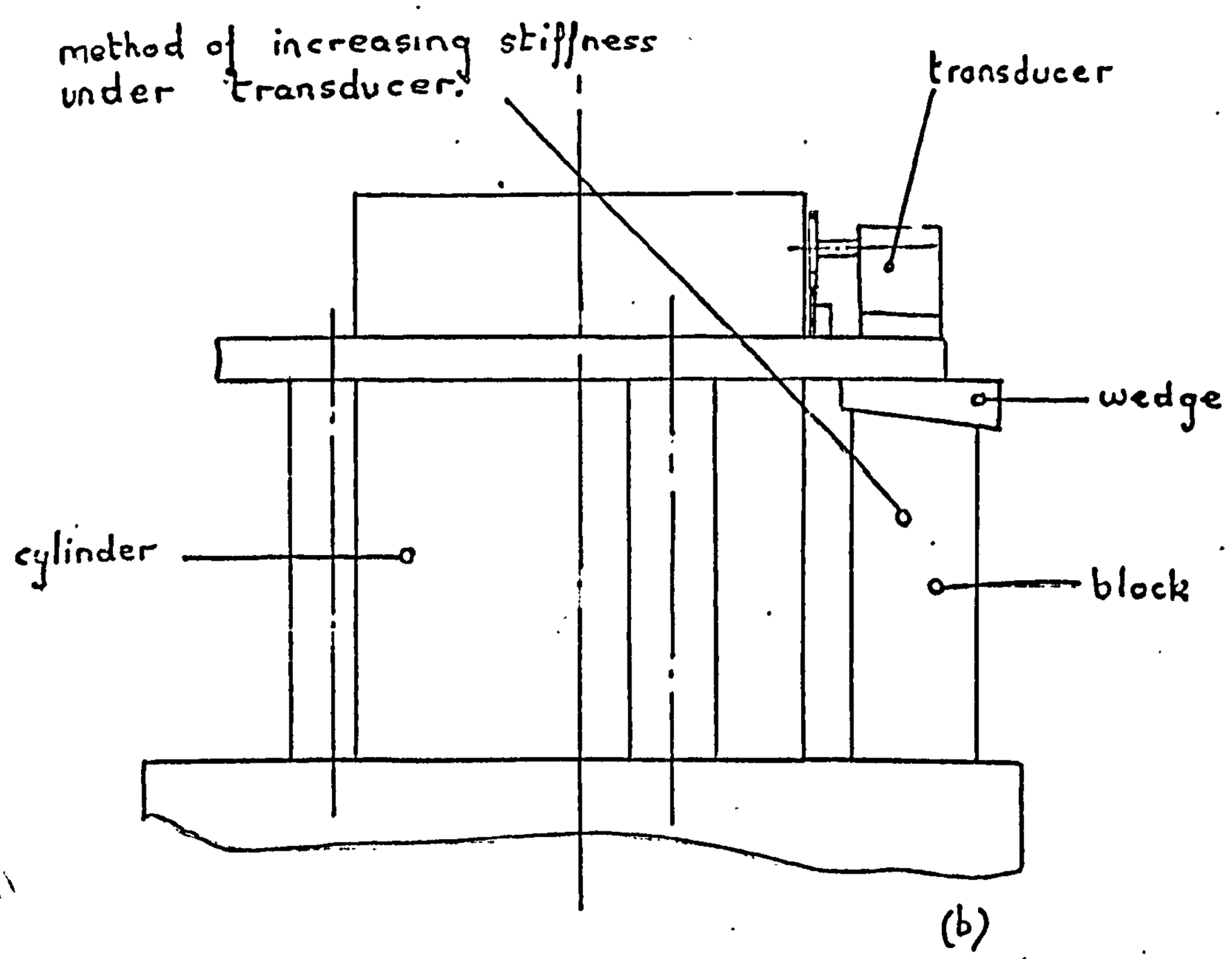

METHOD OF STIFFENING SUPPORTING STRUCTURE UNDERNEATH TRANSDUCER.

FIG 16.1.

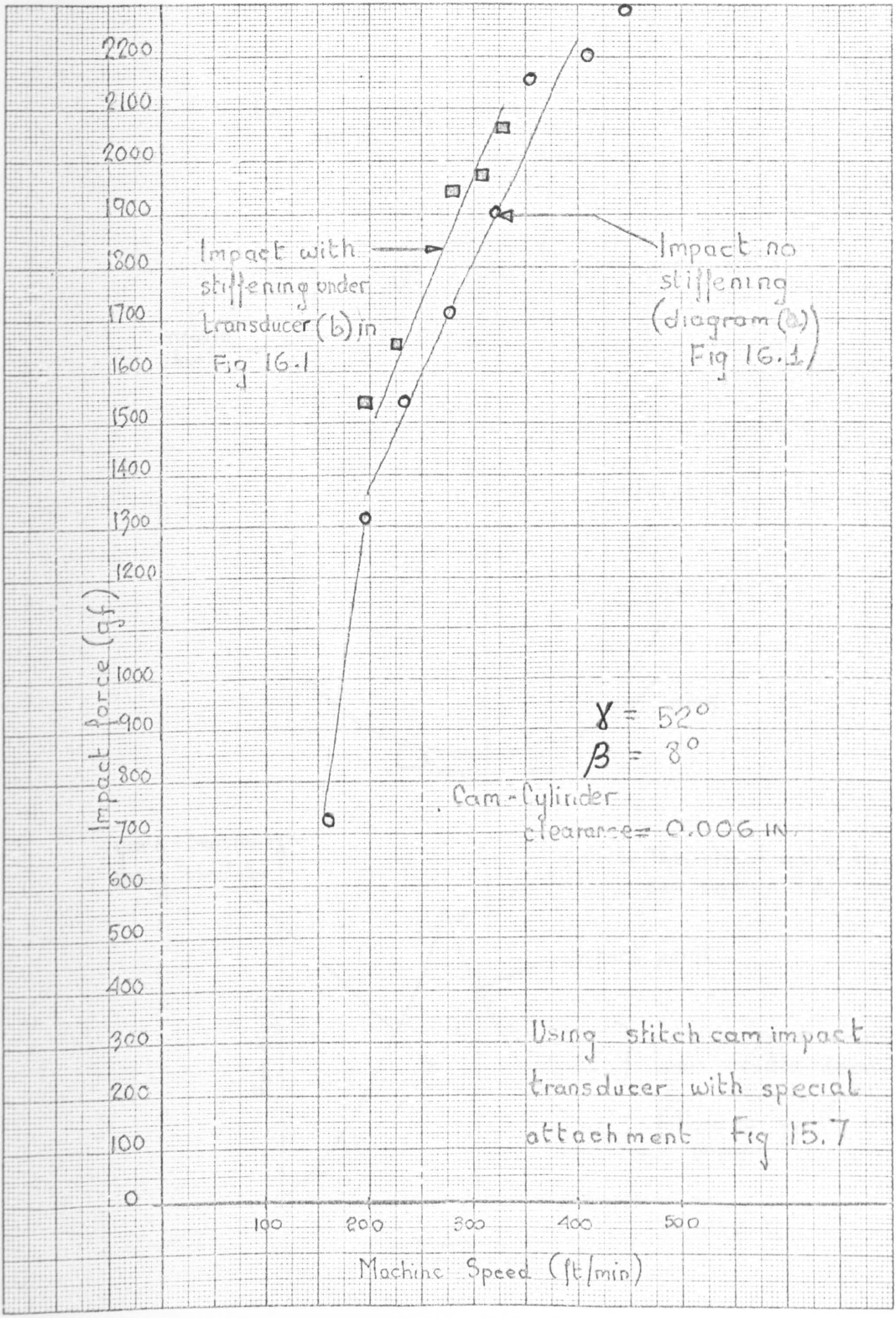

EFFECT OF THE STIFFNESS OF THE SUPPORTING STRUCTURE UPON THE IMPACT MAGNITUDE

FIG 16.2

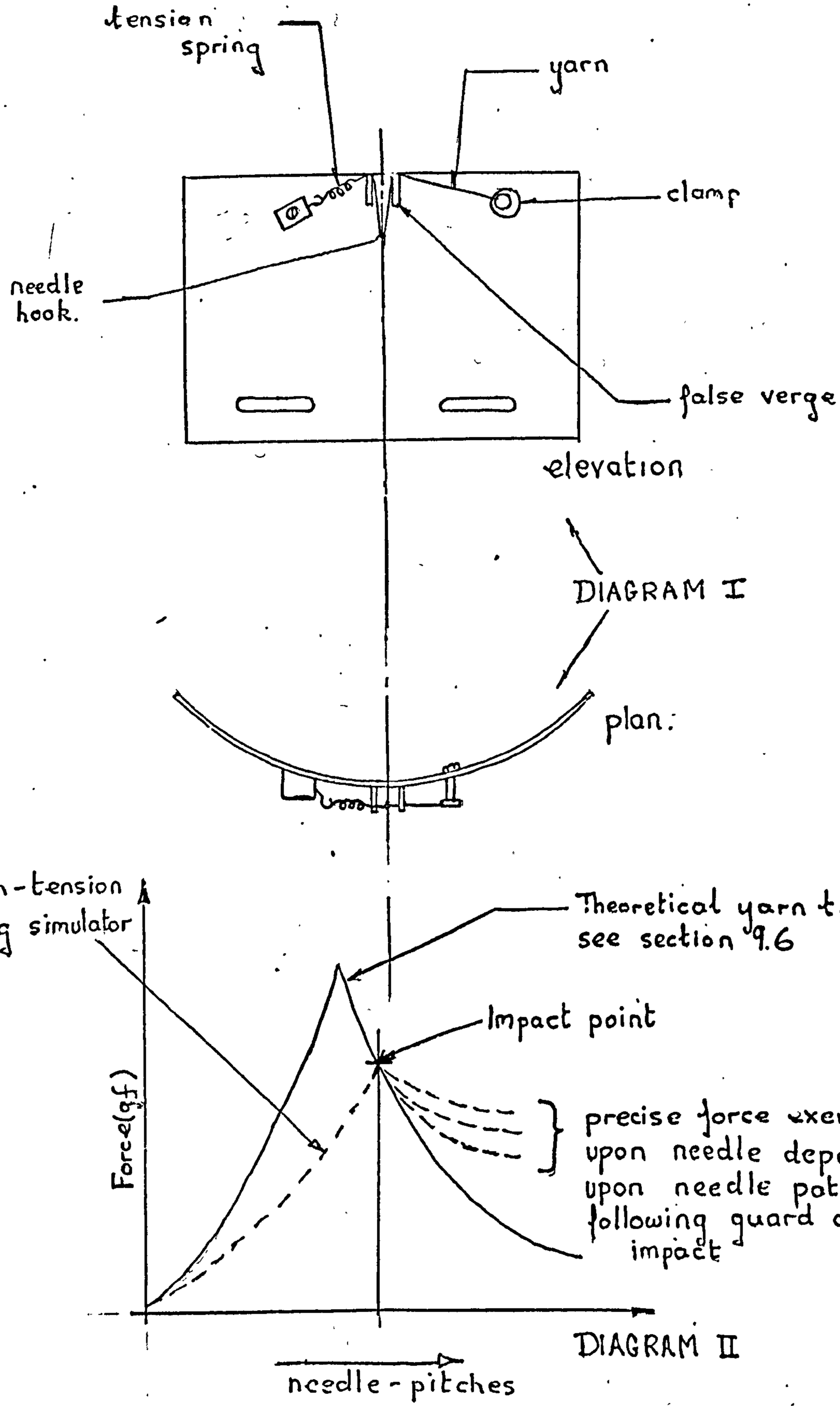

YARN- TENSION SIMULATOR

FIG 16.3

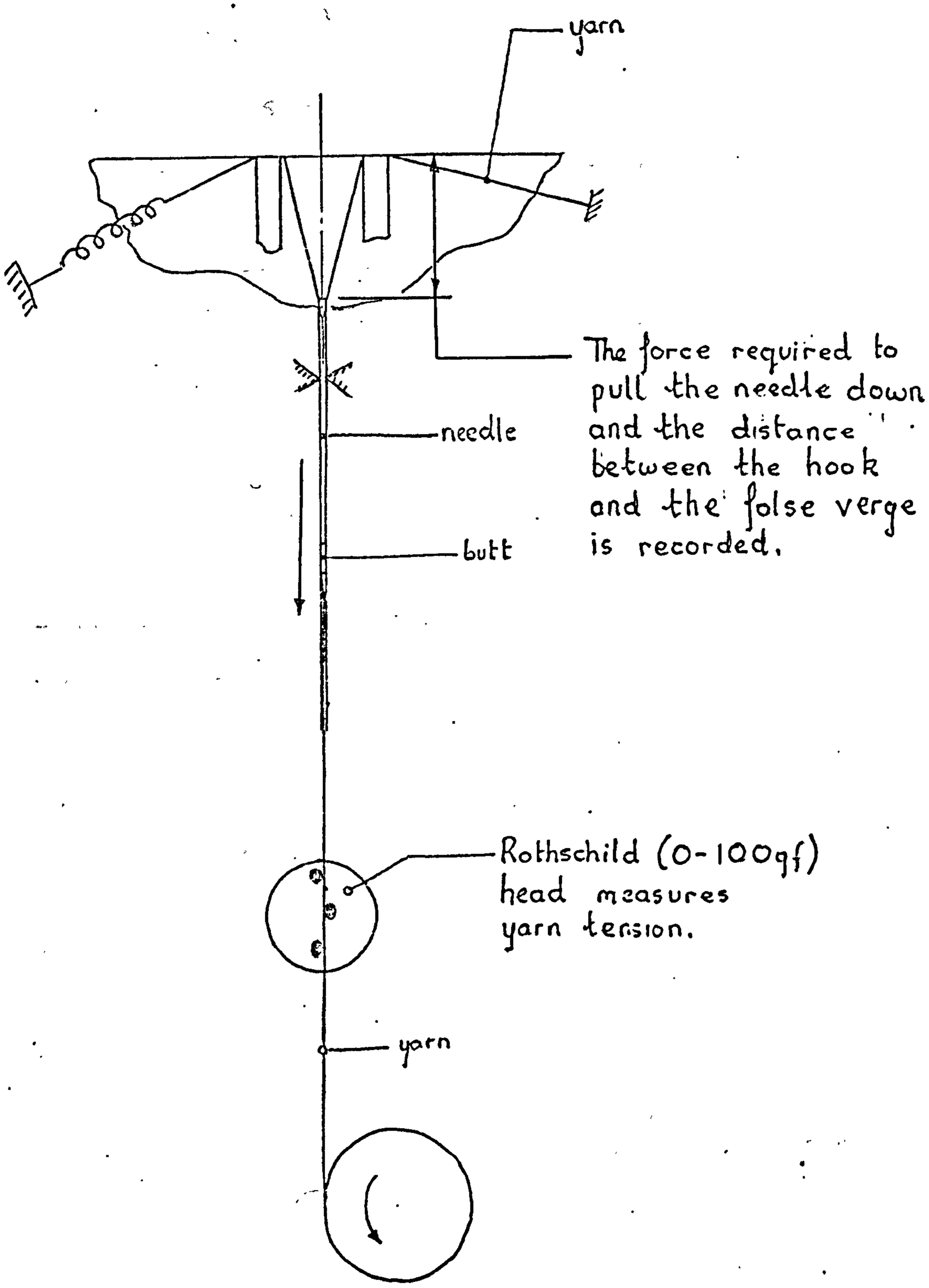

Method of calibrating Yarn Tension Simulator

FIG 16.4

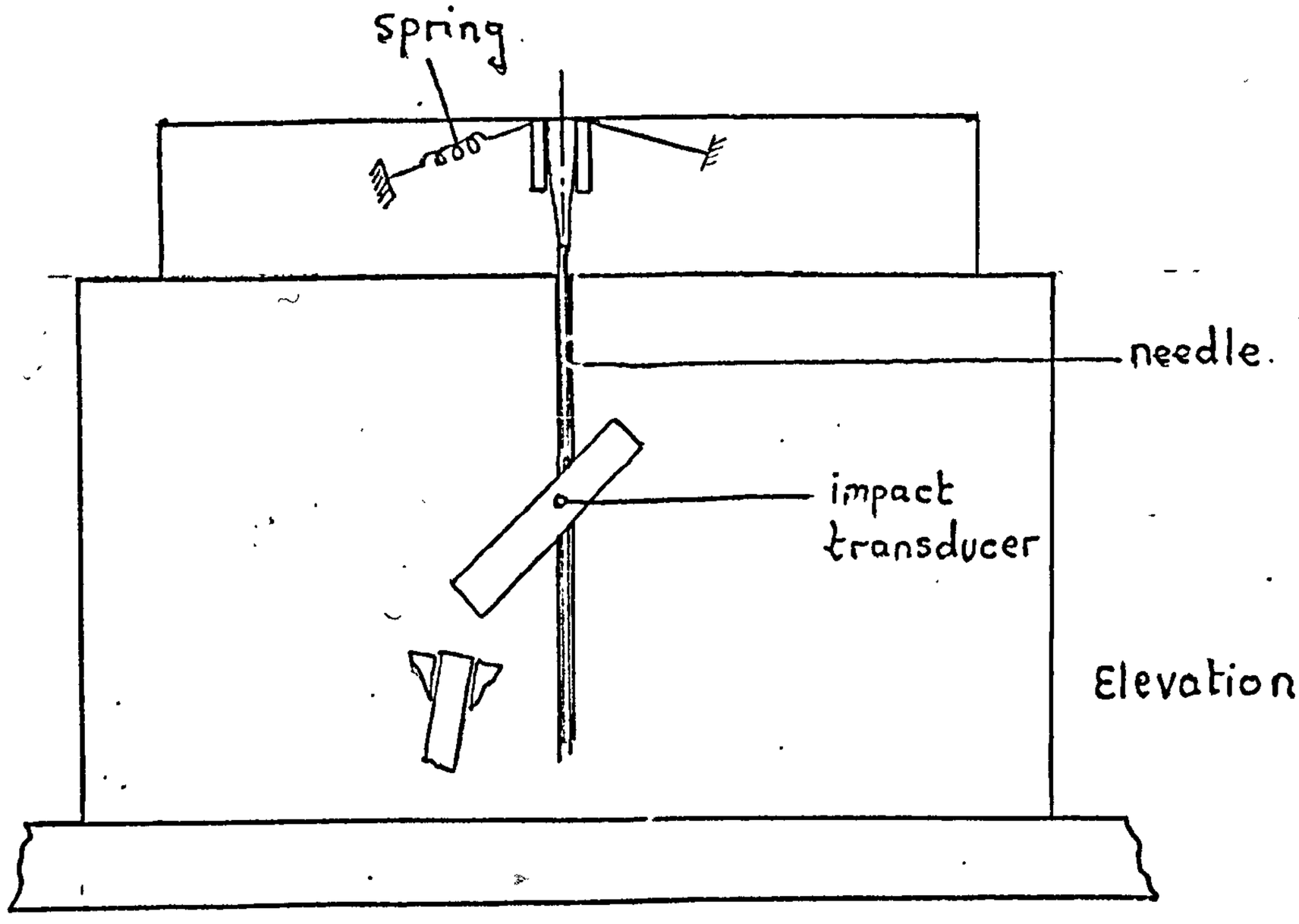

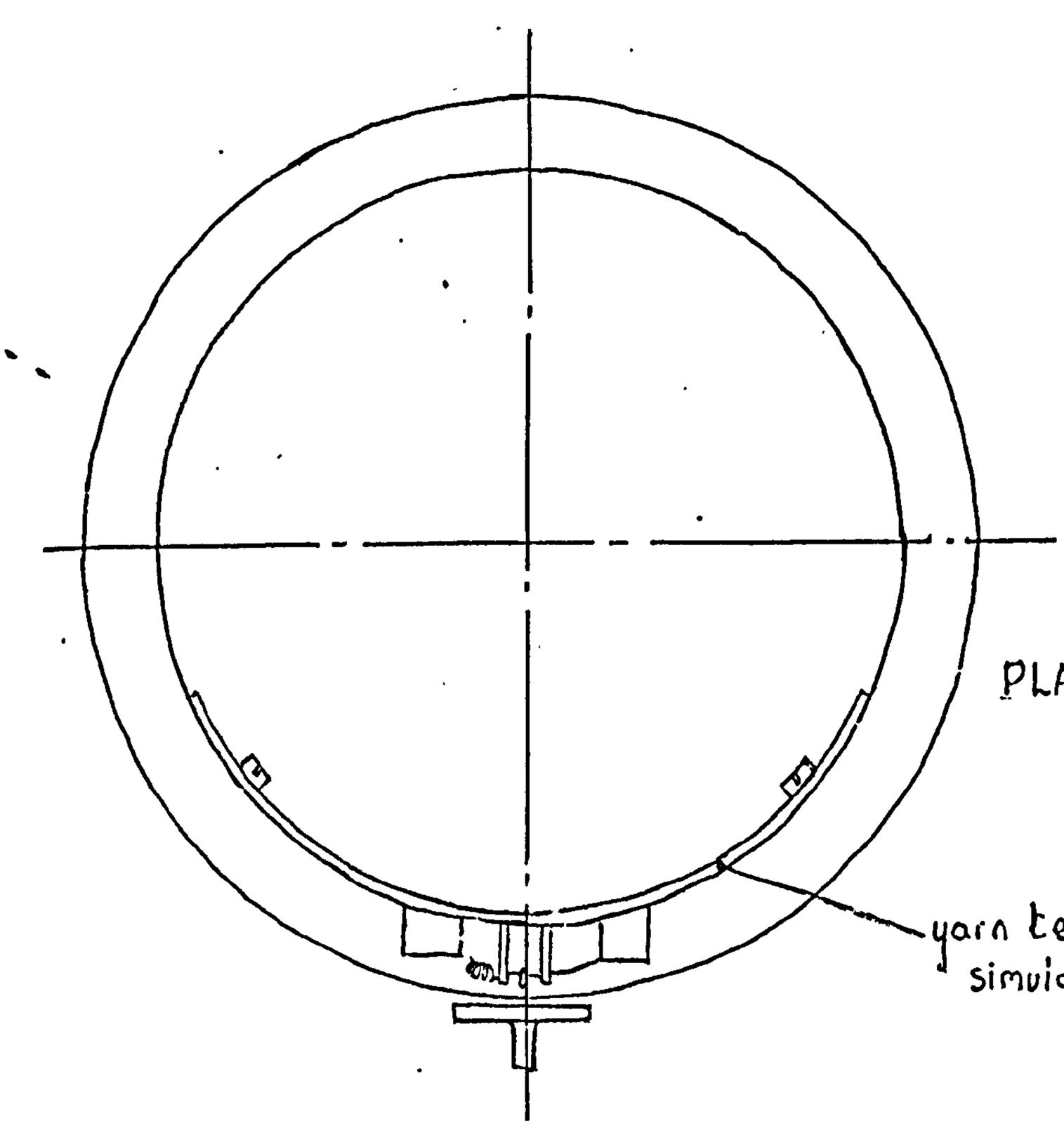

OPERATIONAL ARRANGEMENT.
YARN-TENSION SIMULATOR

FIG 16.5

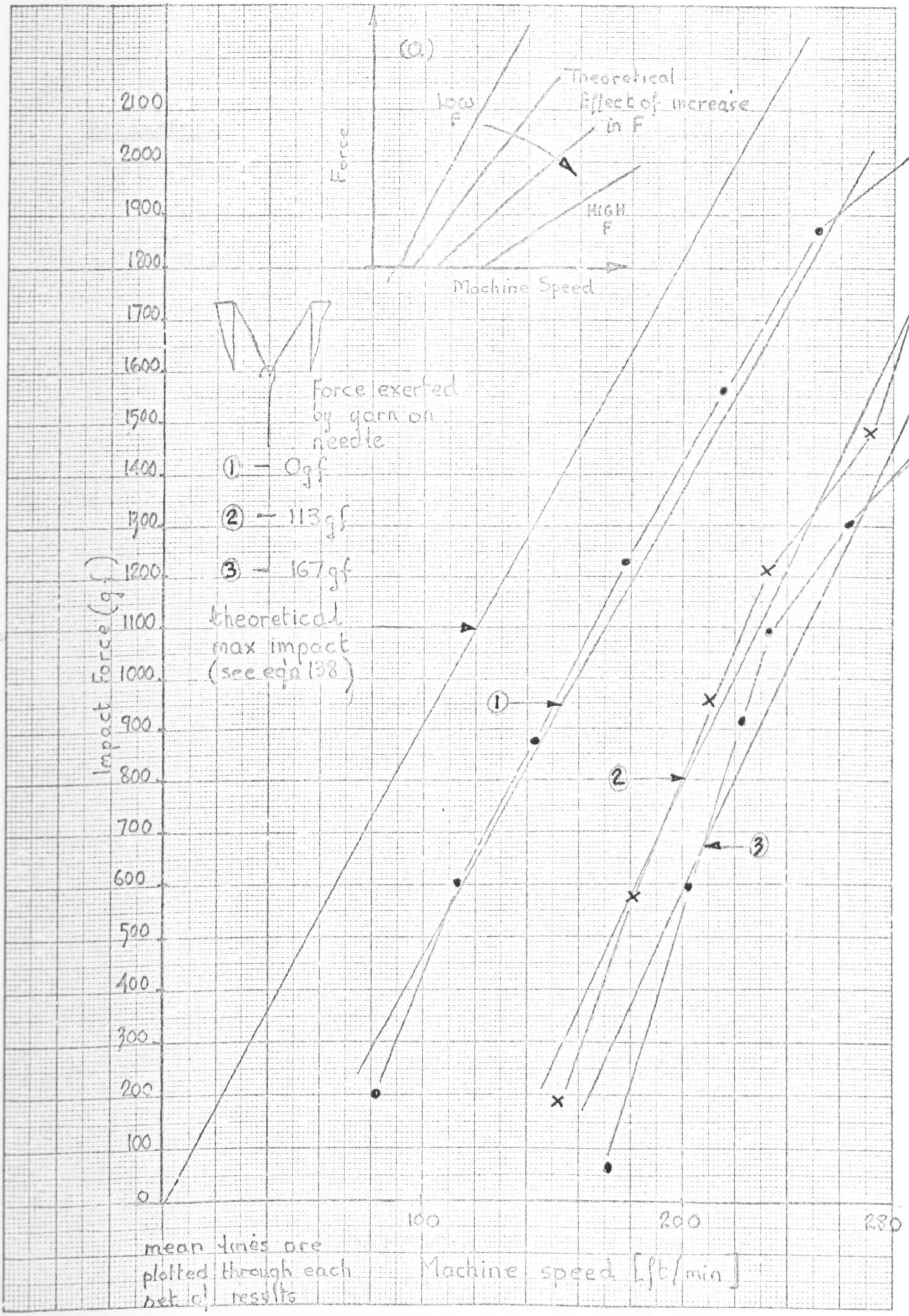

IMPACT MAGNITUDE AGAINST MACHINE SPEED
VARYING YARN-DRAW FORCE 0gf 113gf 167gf

FIG 16.6

Effect of Yarn Tension upon the Impact

Parameters

Yarn-force at impact	= 120 gf
Stitch Cam-angle	= 52^{o}
Guard Cam-angle	= 8^{o}
Cam-cylinder clearance	= 0.006 in.
Free in trick	
Calibration	= 65 gf/mm on trace

Parameters for traces showin in Fig 16.7(b) (using longitudinal beam instrument)

Fig 16.7(a)

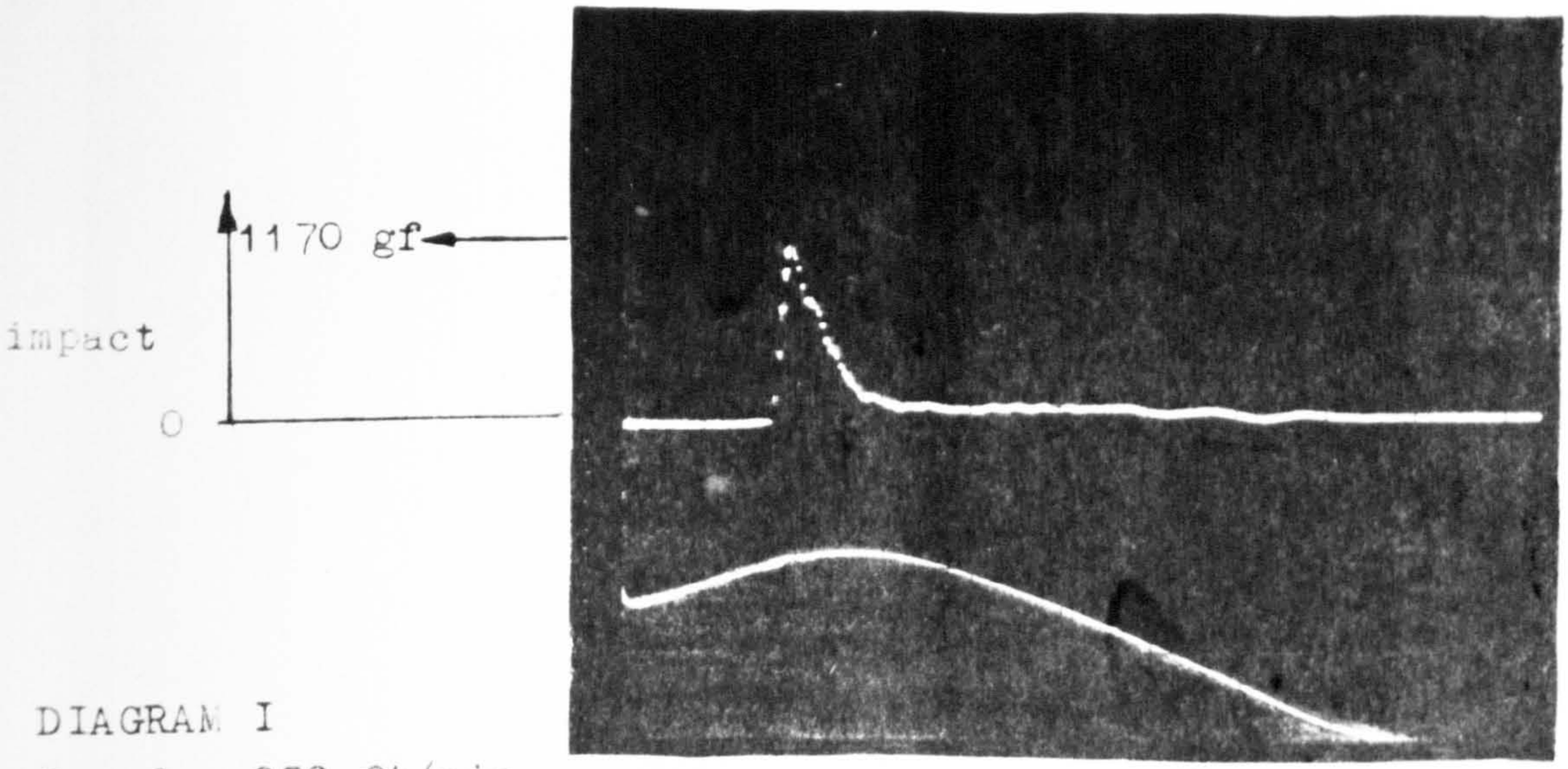

DIAGRAM I
Speed = 250 ft/min
100 X 10^{-6} secs /8.5 mm

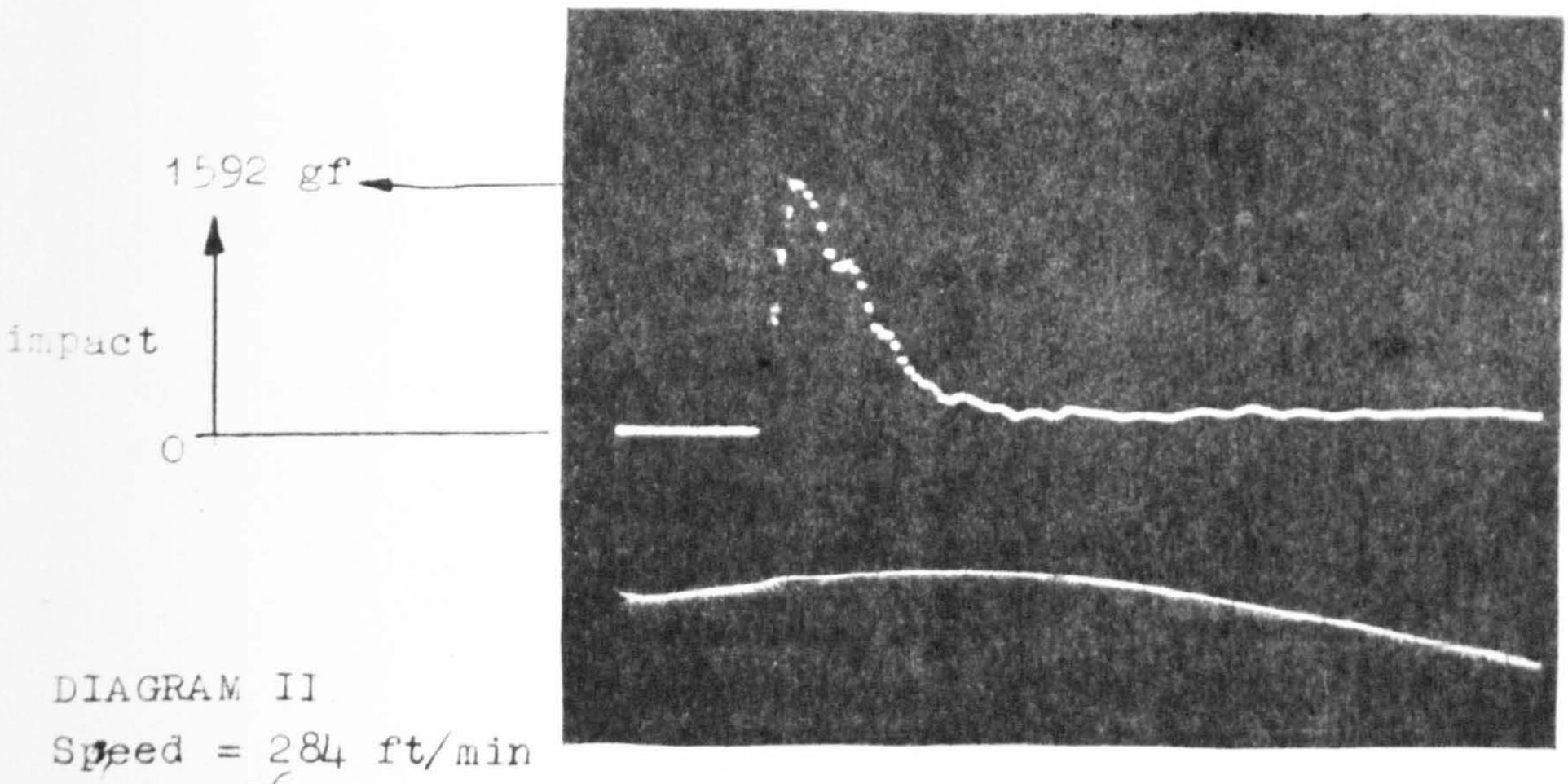

DIAGRAM II
Speed = 284 ft/min
50 X 10^{-6} secs/8.5 mm

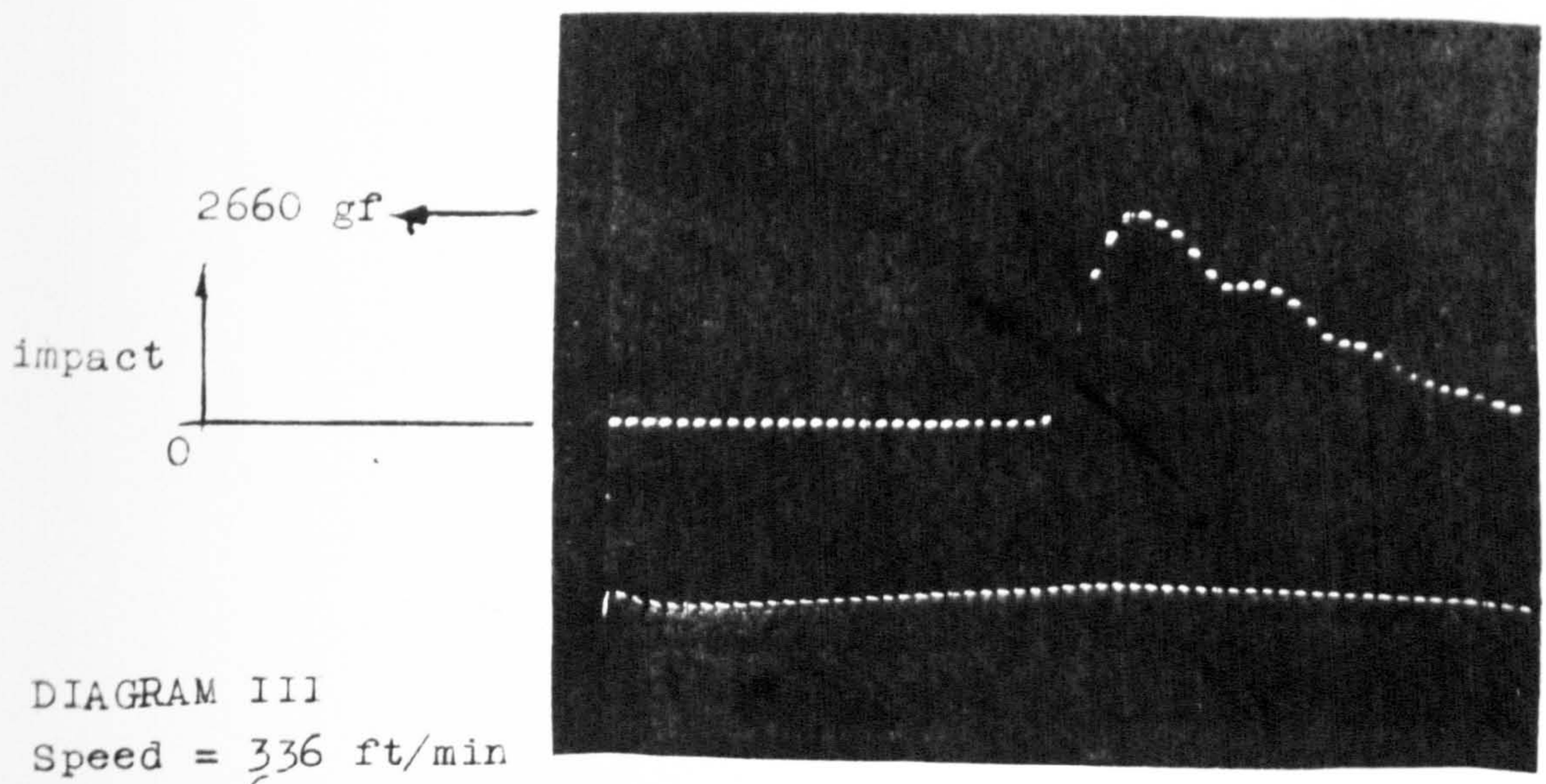

DIAGRAM III
Speed = 336 ft/min
20 X 10^{-6} secs/8.5 mm

Effect of Yarn-Force upon Impact
Yarn-force = 120 gf

Fig 16.7(b)

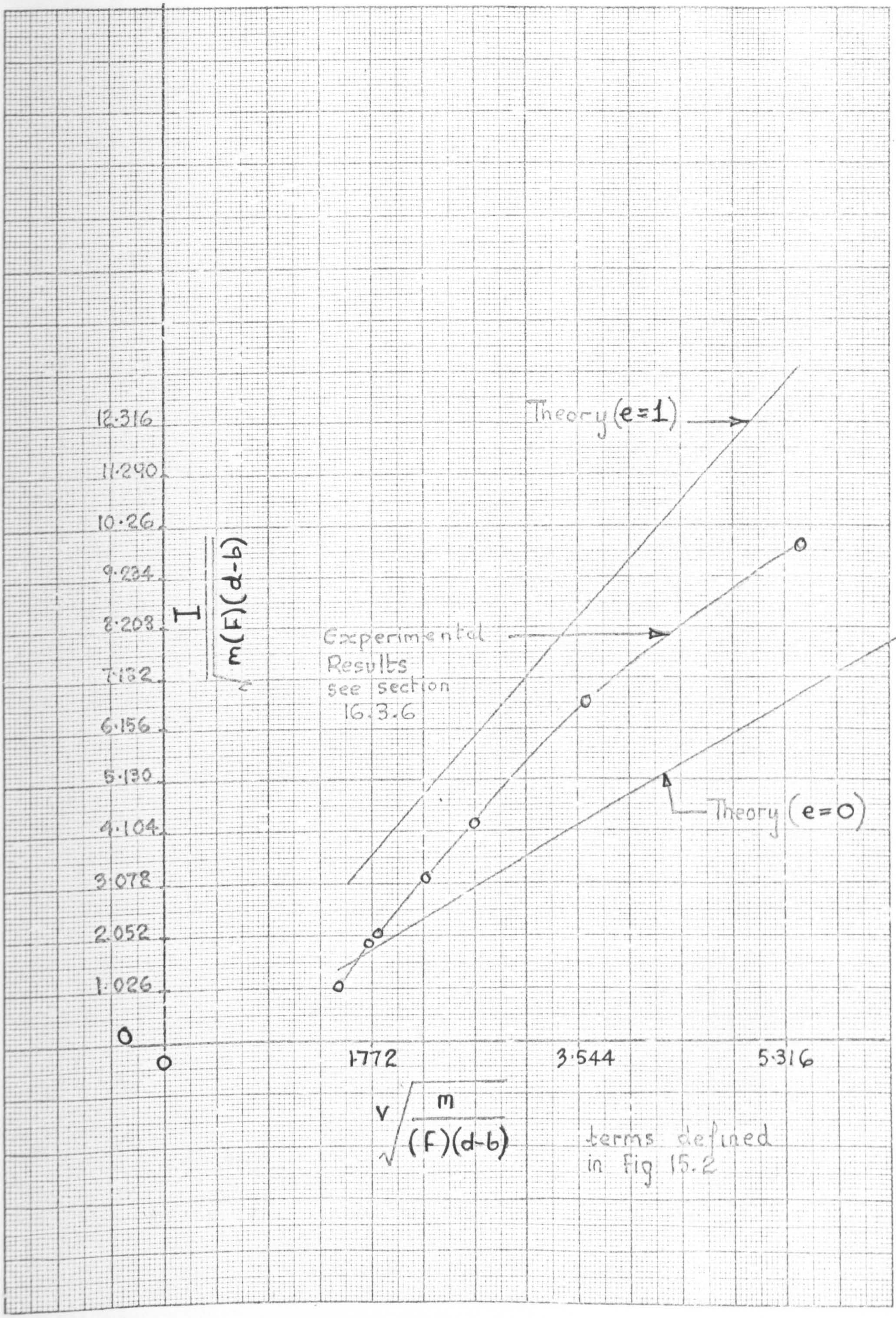

NON-DIMENSIONAL PLOTTING (SECTION 16.3.6) FIG 16.8

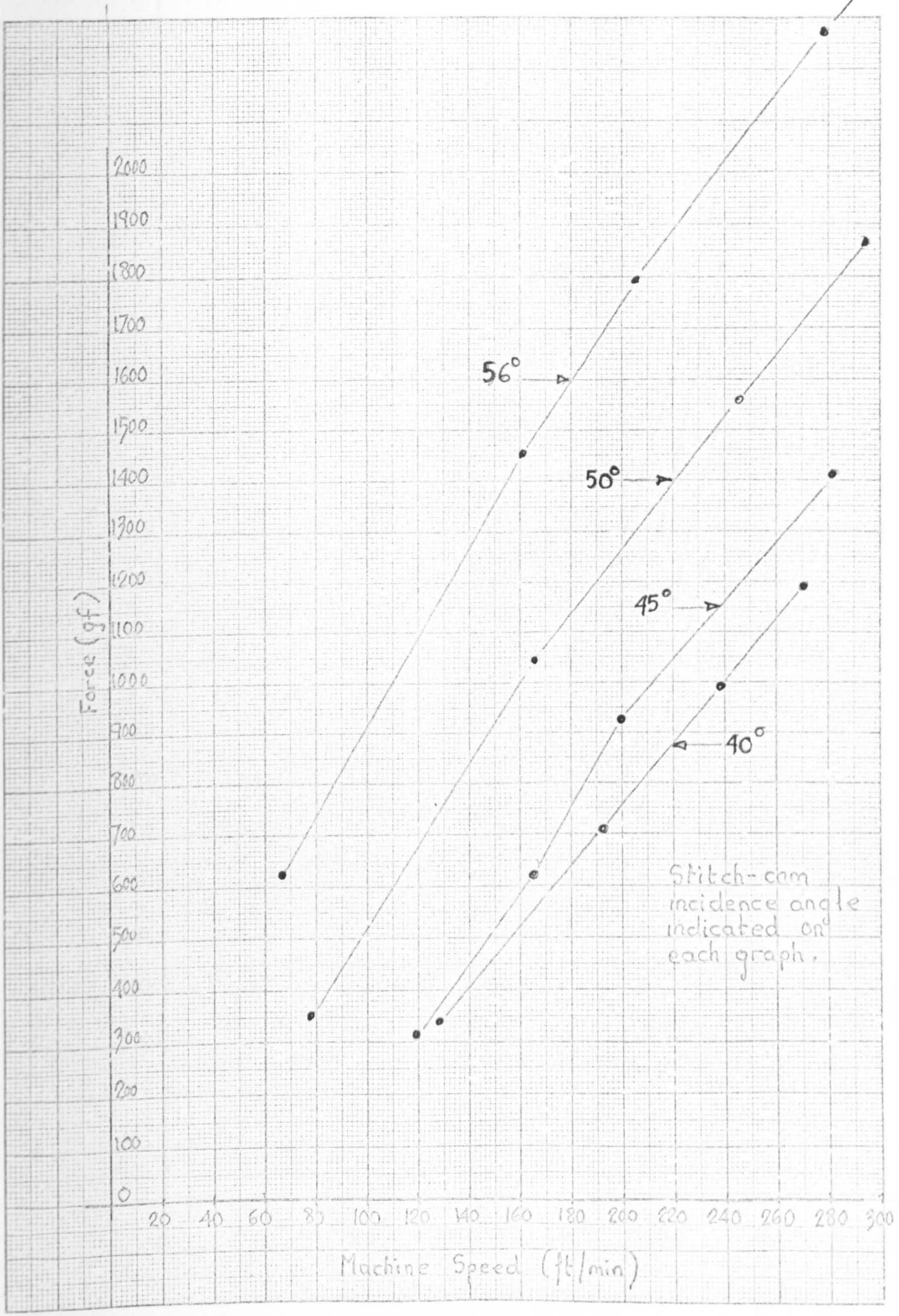

Effect of Stitch-Cam Incidence Angle upon Impact Magnitude

FIG 16.9

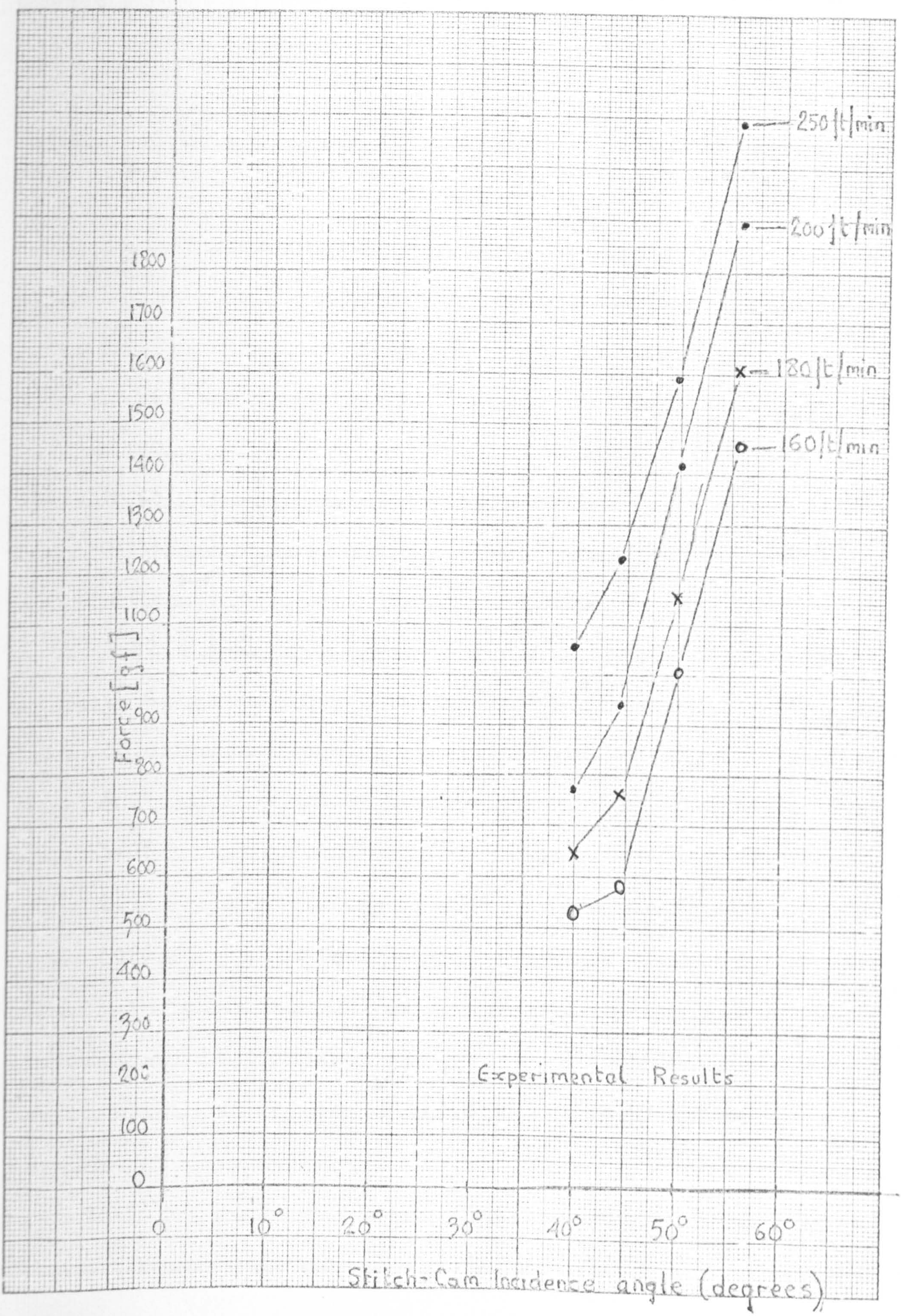

EFFECT OF STITCH-CAM INCIDENCE ANGLE UPON IMPACT MAGNITUDE AT 160, 180, 200, AND 250 ft/min

FIG 16.10

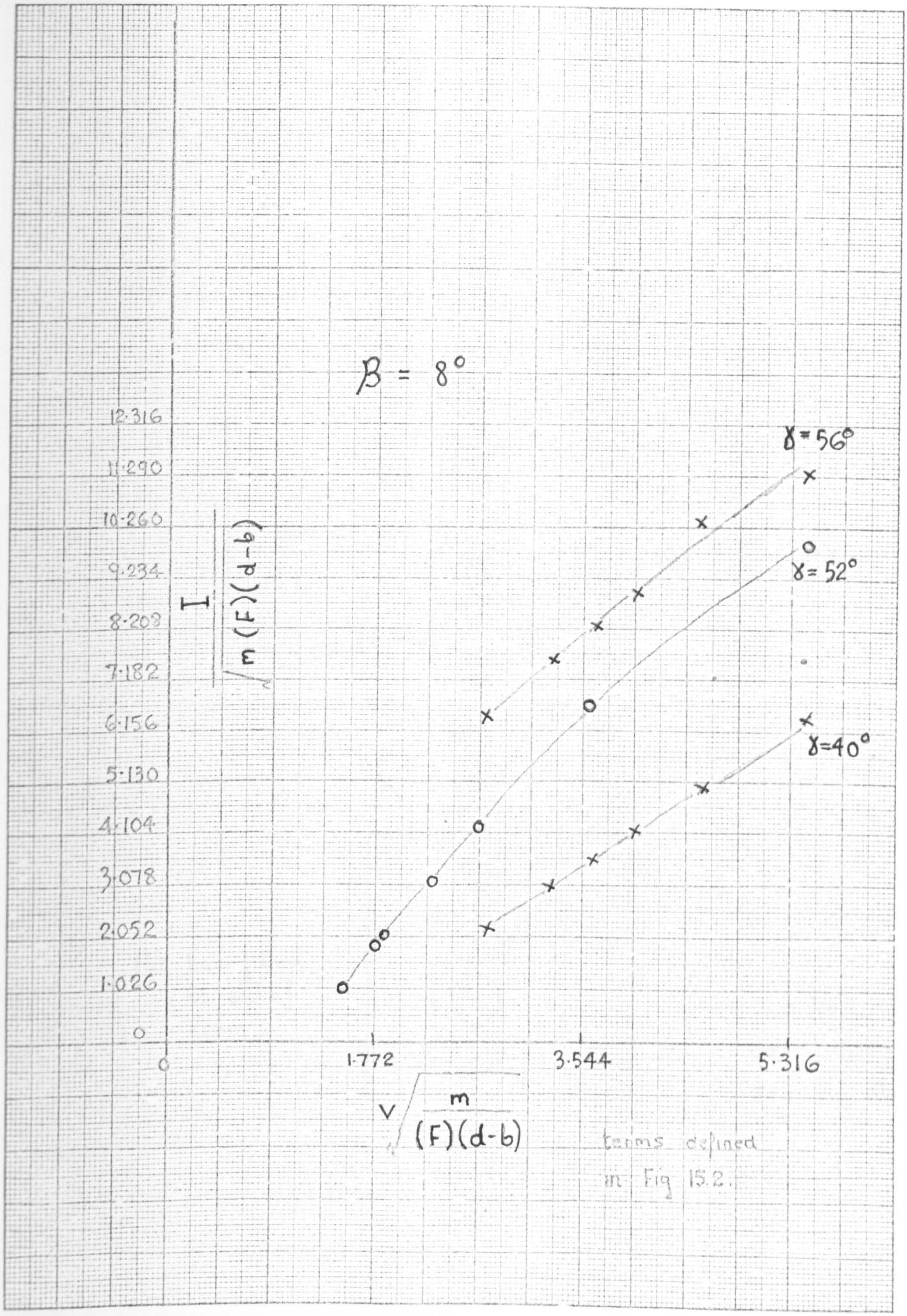

EFFECT OF VARIATION IN STITCH-CAM ANGLE UPON THE NON-DIMENSIONAL PARAMETERS

FIG 16.11

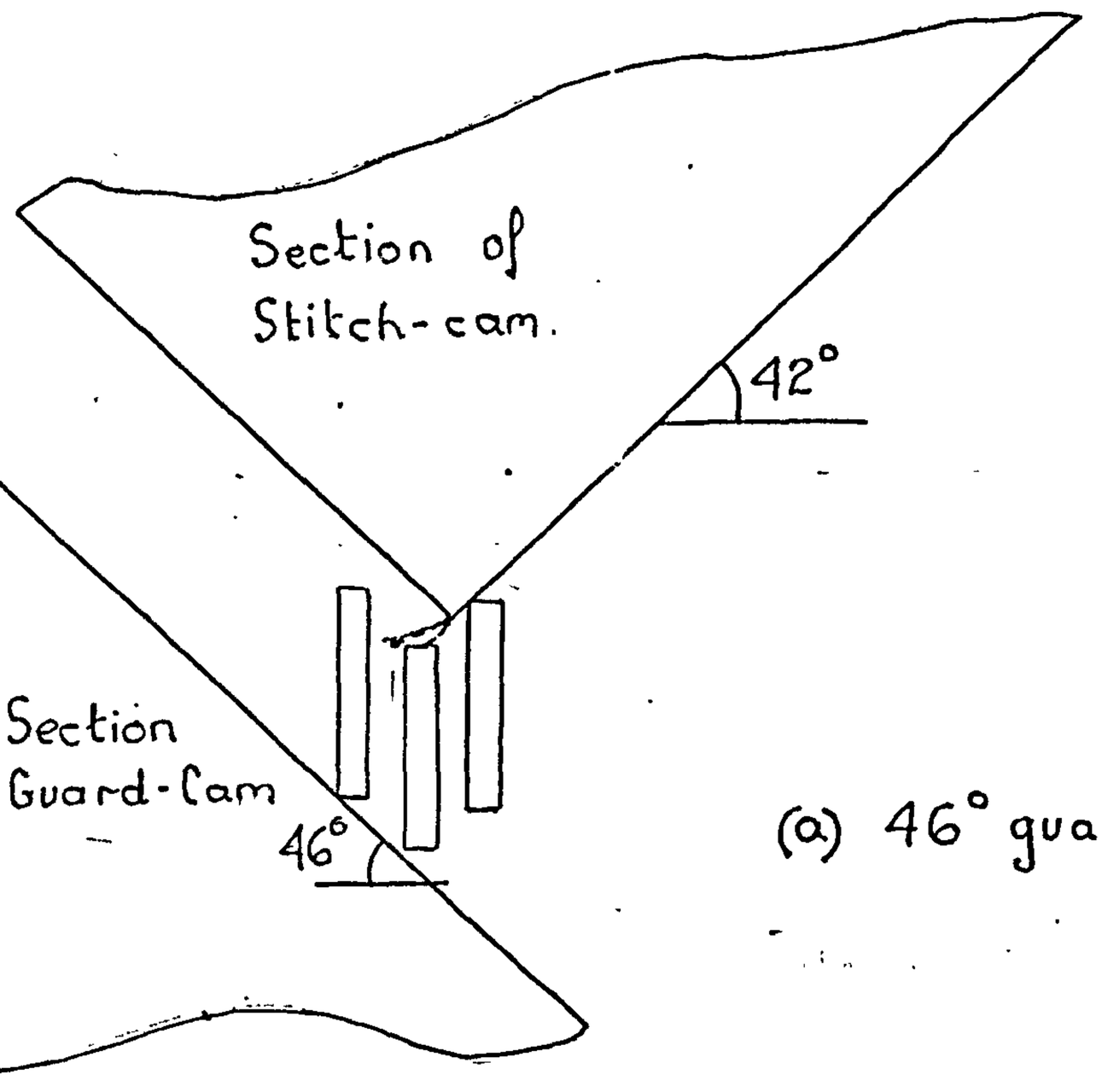

(a) 46° guard-cam.

(b) Cam fitted to end of beam.

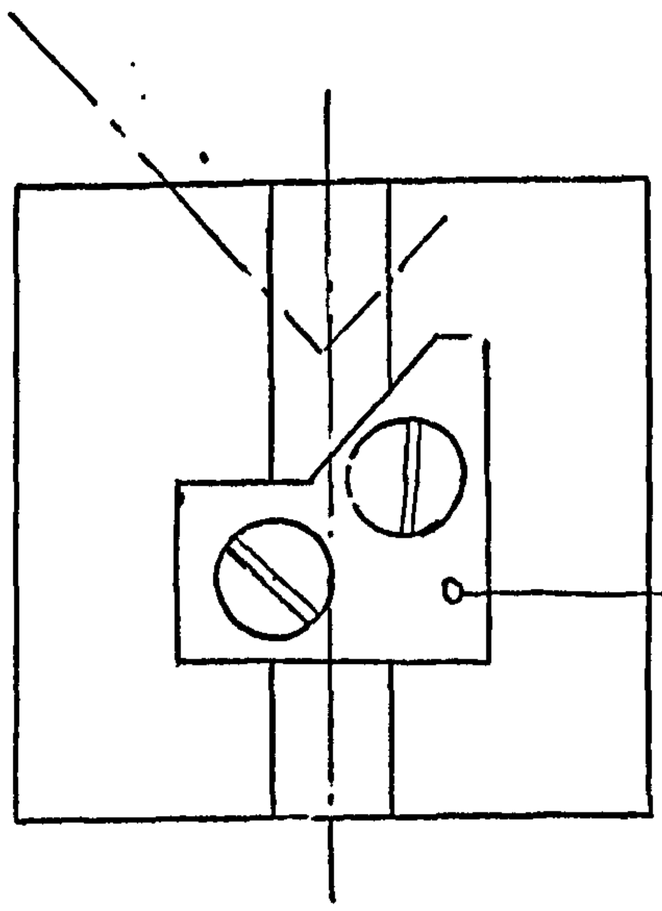

The 46° Guard-cam (Section 16.5)

FIG 16.12

Forces calculated using calibration factor

65 gf/mm

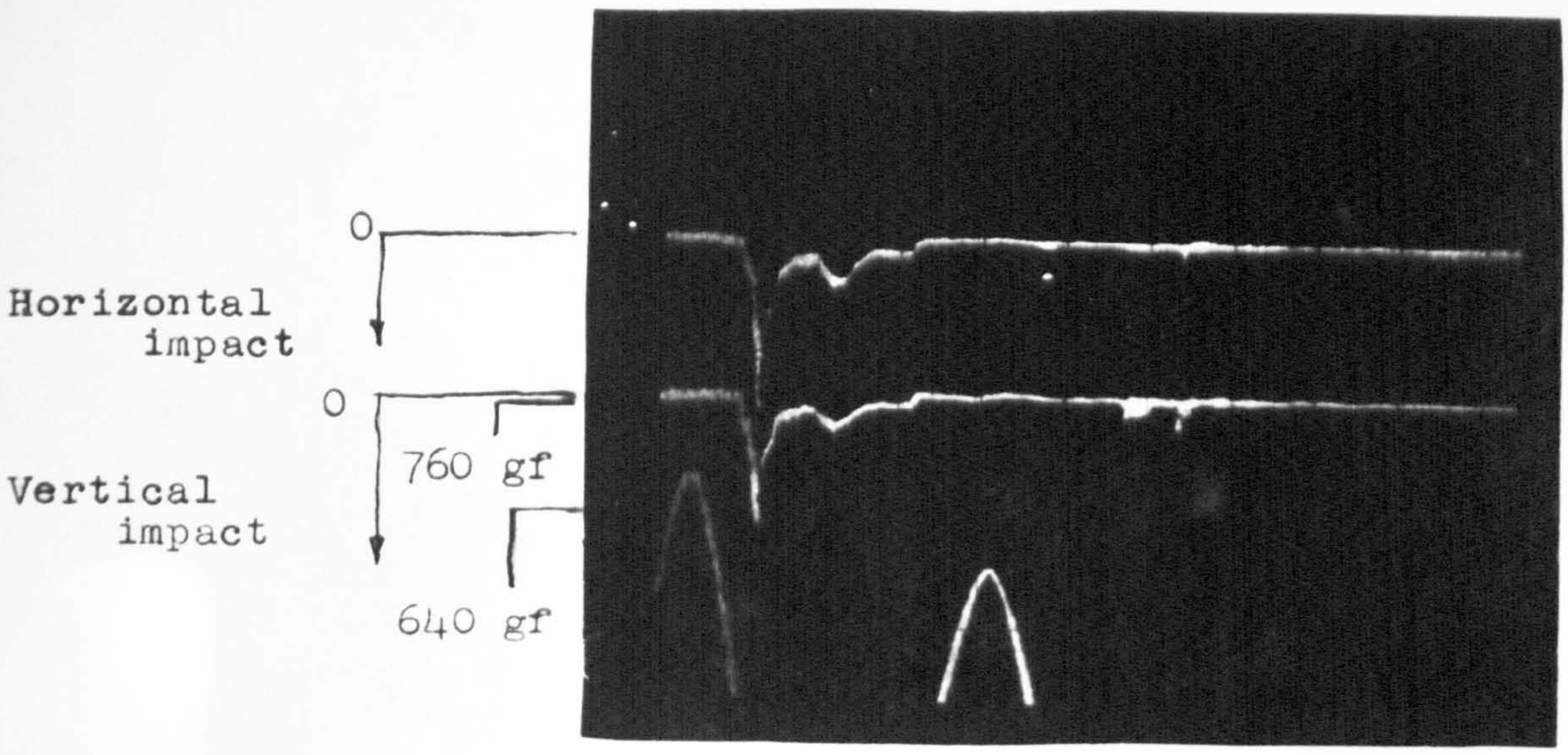

Machine Speed = 204 ft/min

7 experiments were carried out
each experiment with a new standard
0.443 mm needle. In each case butt
fracture occurred at approximately 250 ft/min

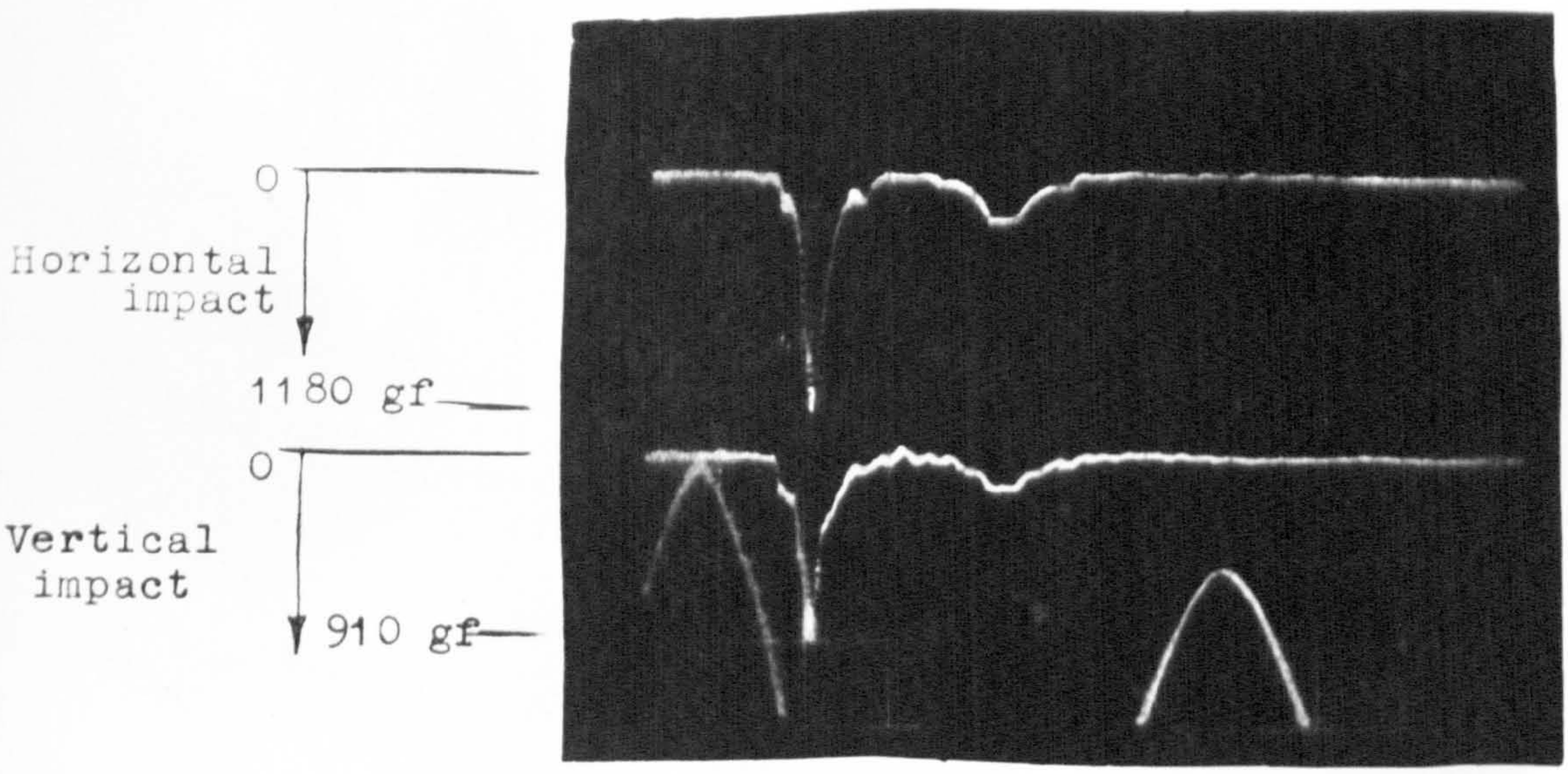

Machine Speed = 241 ft/min

HORIZONTAL AND VERTICAL COMPONENT
OF IMPACT

STITCH - CAM ANGLE = 42°
GUARD - CAM ANGLE = 46°

Fig 16.13

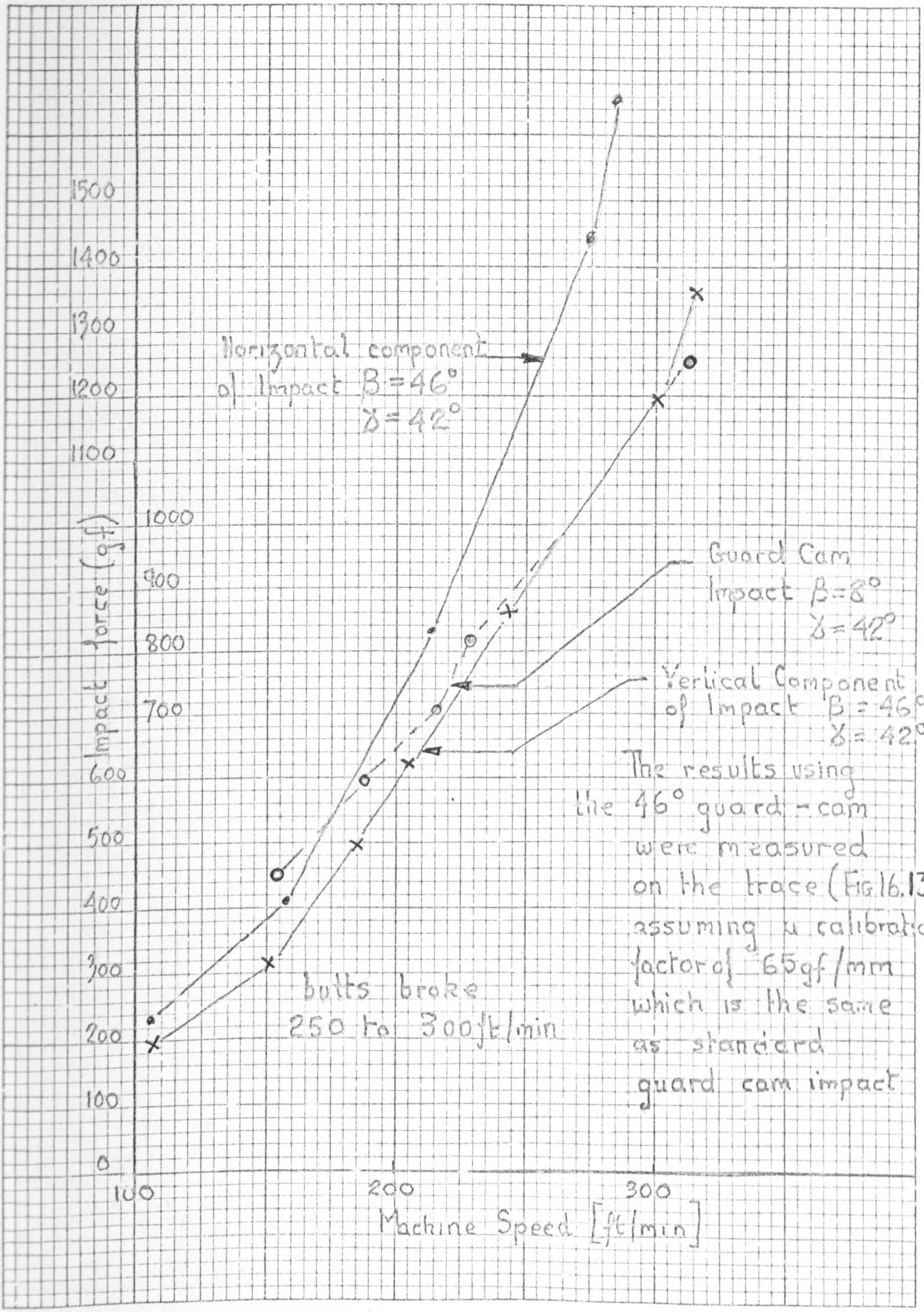

HORIZONTAL AND VERTICAL COMPONENT OF IMPACT AGAINST MACHINE SPEED ($\delta = 42° \beta = 46°$) FIG 16.14

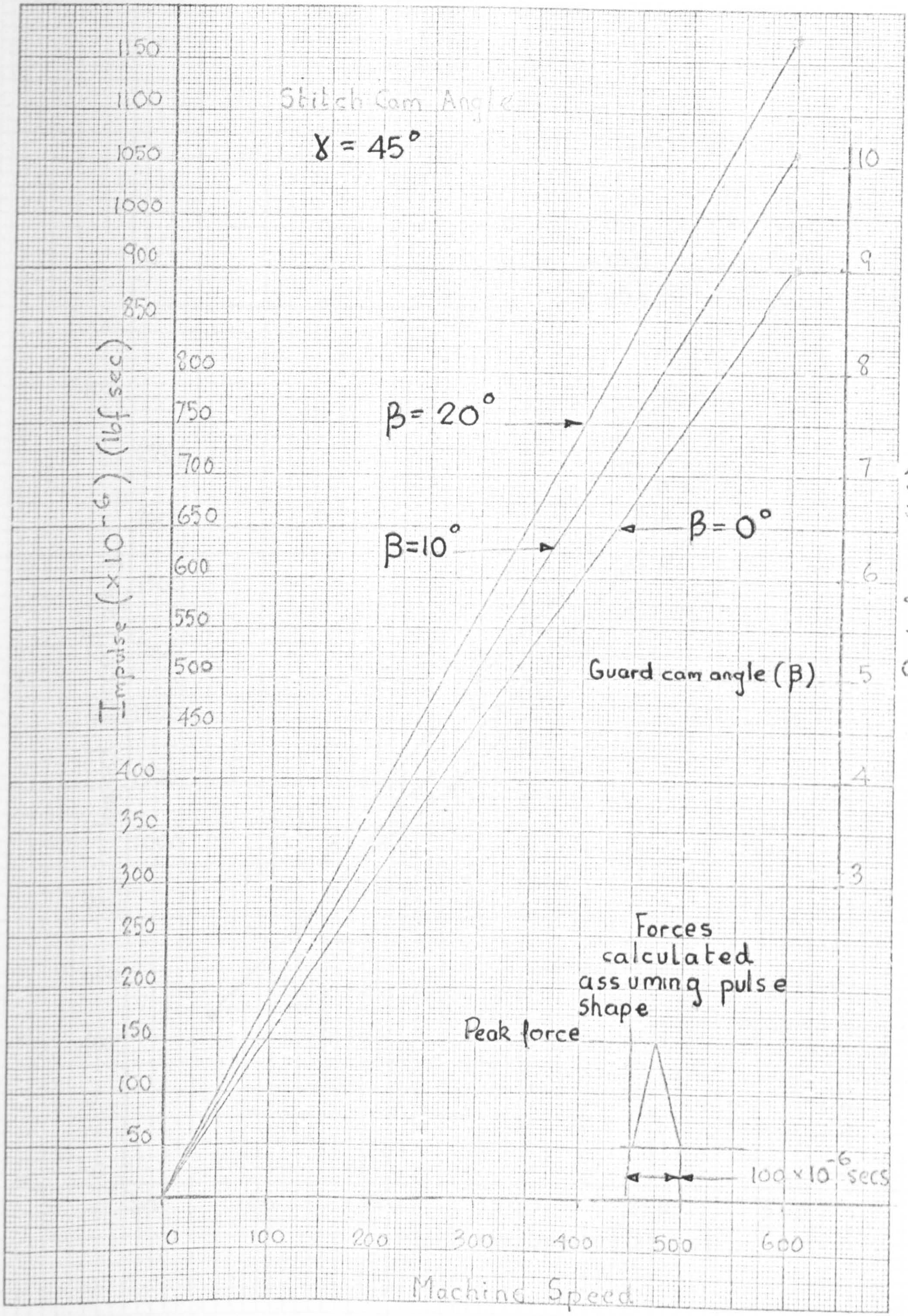

EFFECT OF GUARD CAM-ANGLE UPON THE THEORETICAL MAXIMUM IMPACT

FIG 16.15

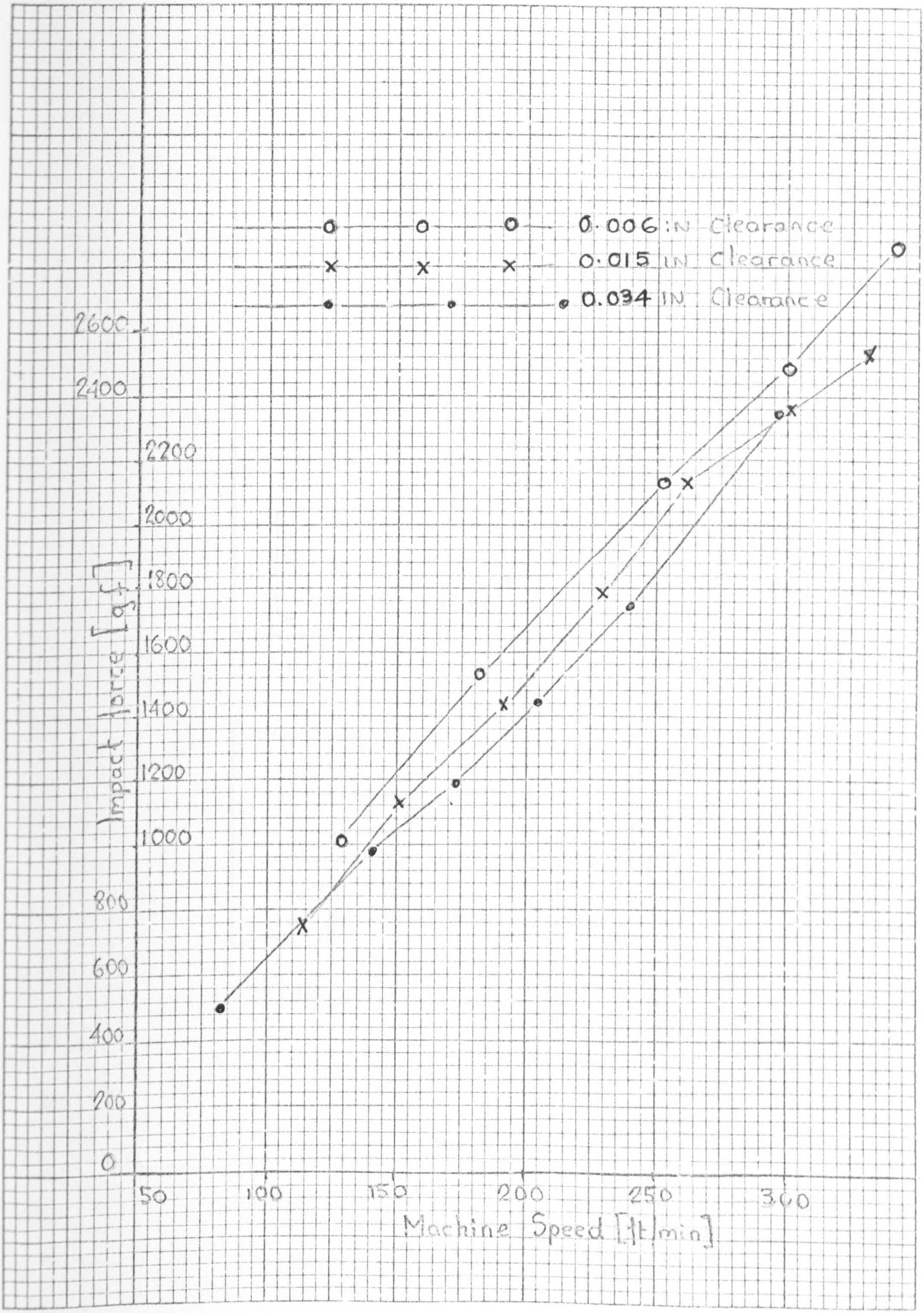

EFFECT OF CAM-CYLINDER CLEARANCE UPON IMPACT

FIG 16.16

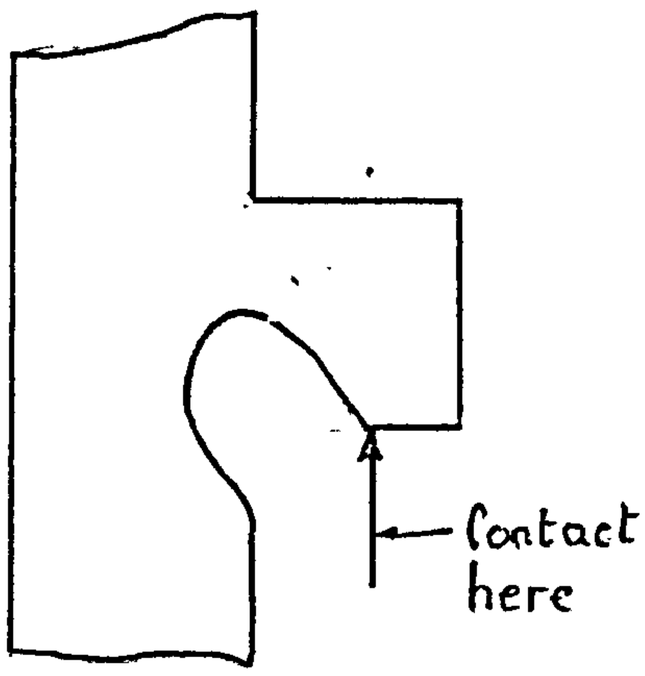

diagram I

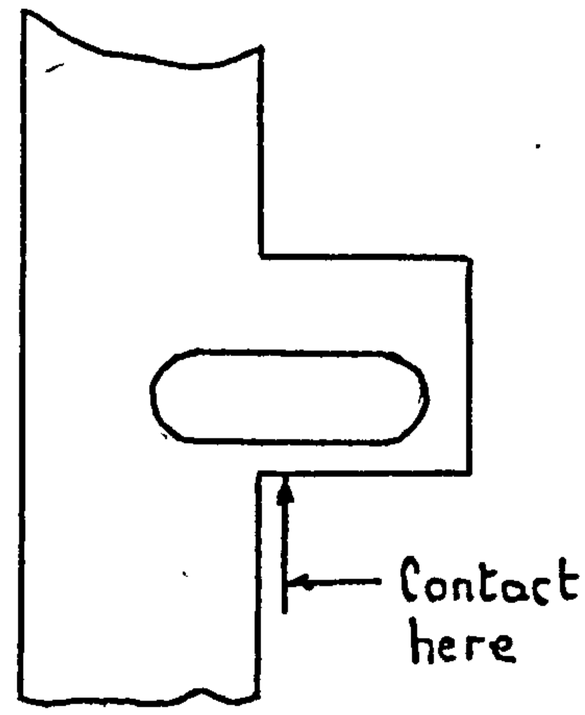

diagram II

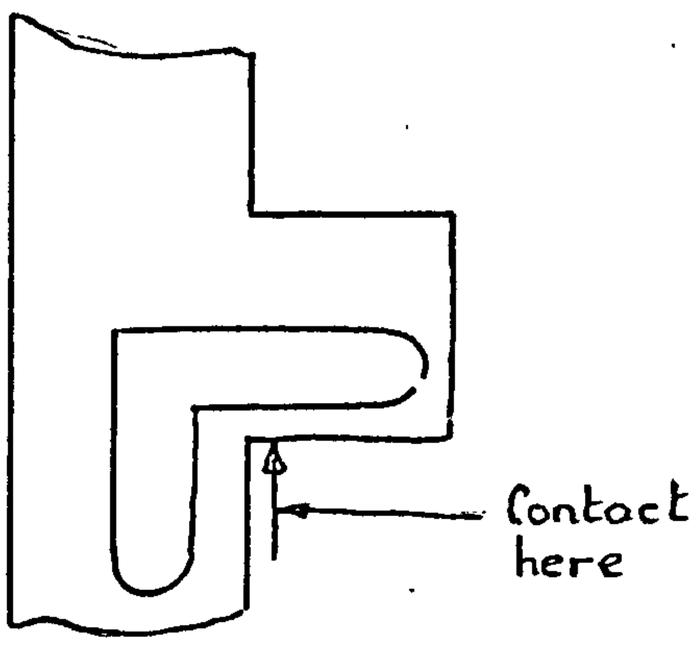

diagram III

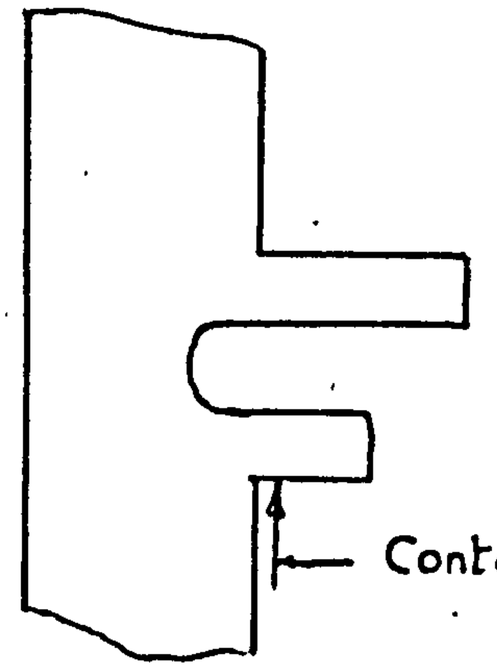

diagram IV

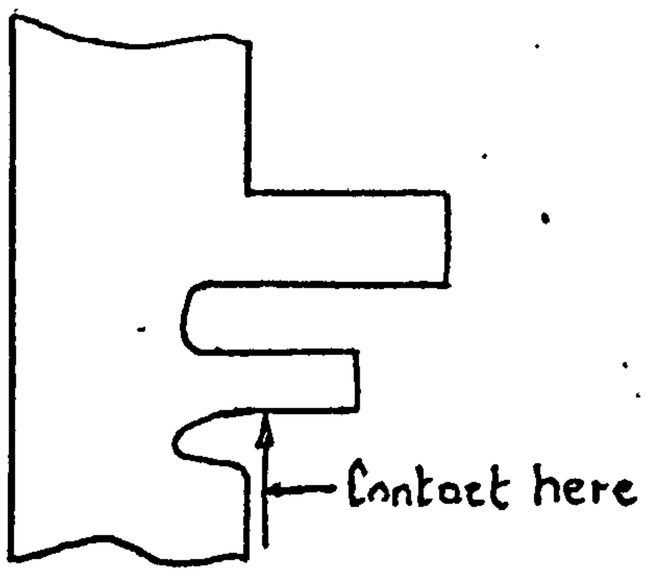

diagram V

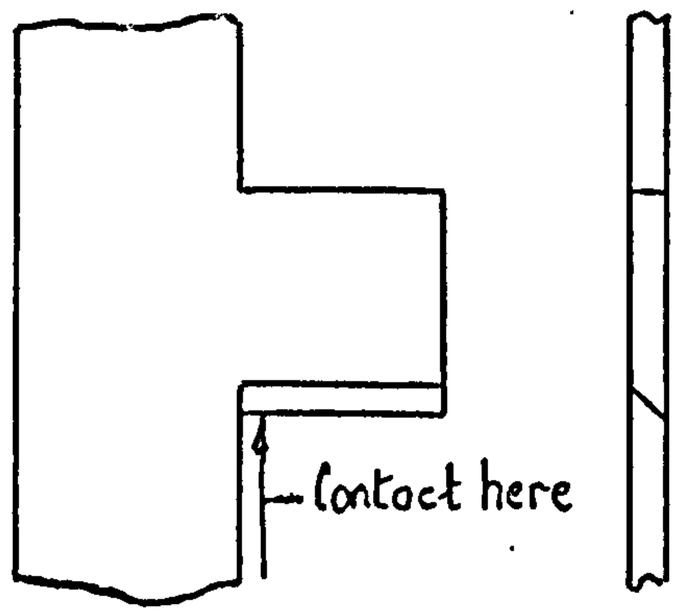

diagram VI

BUTT-MODIFICATIONS (SECTION 16.7)

FIG 16.17

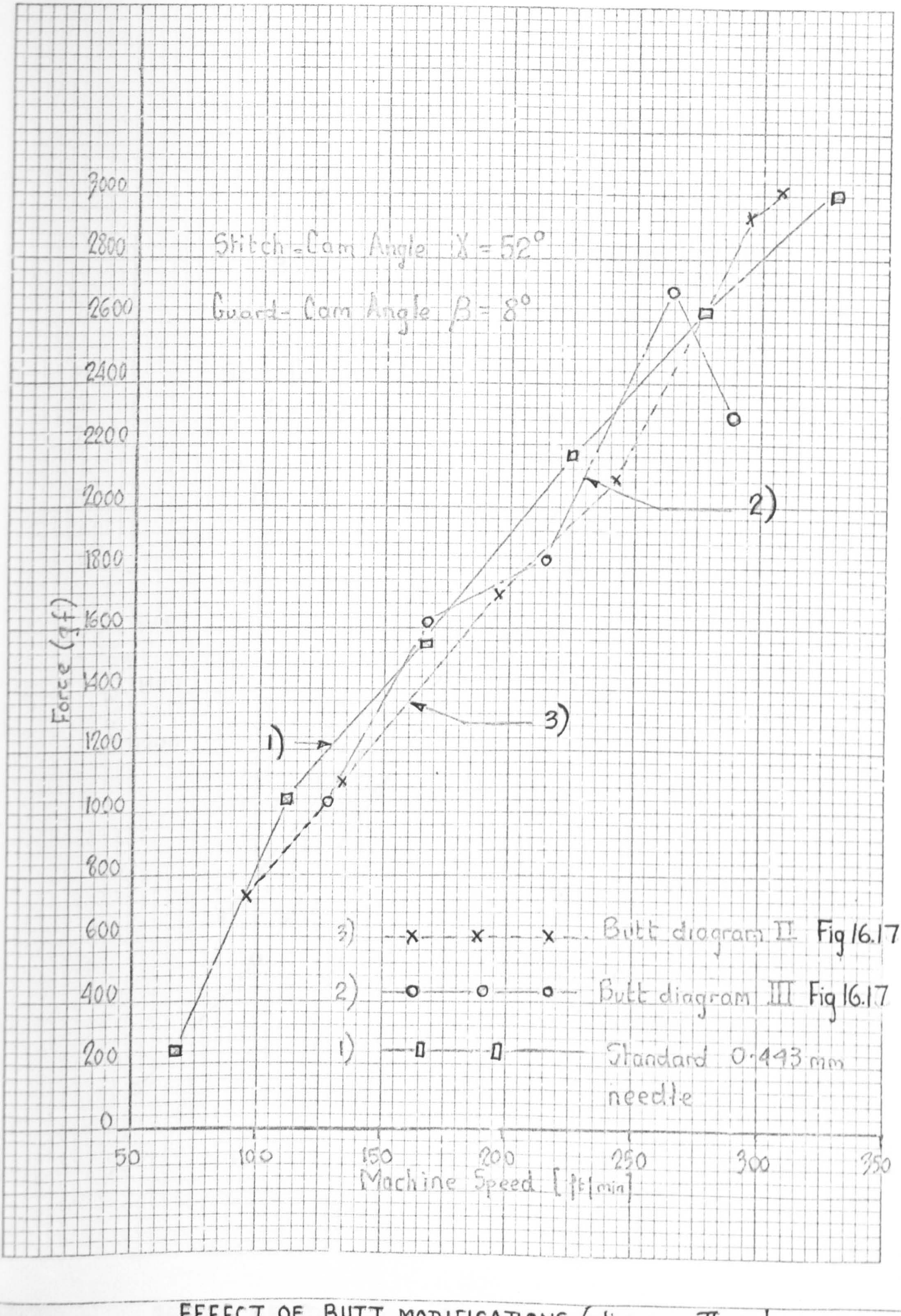

EFFECT OF BUTT MODIFICATIONS (diagram II and III FIG 16.17) ON GUARD CAM IMPACT

FIG 16.18

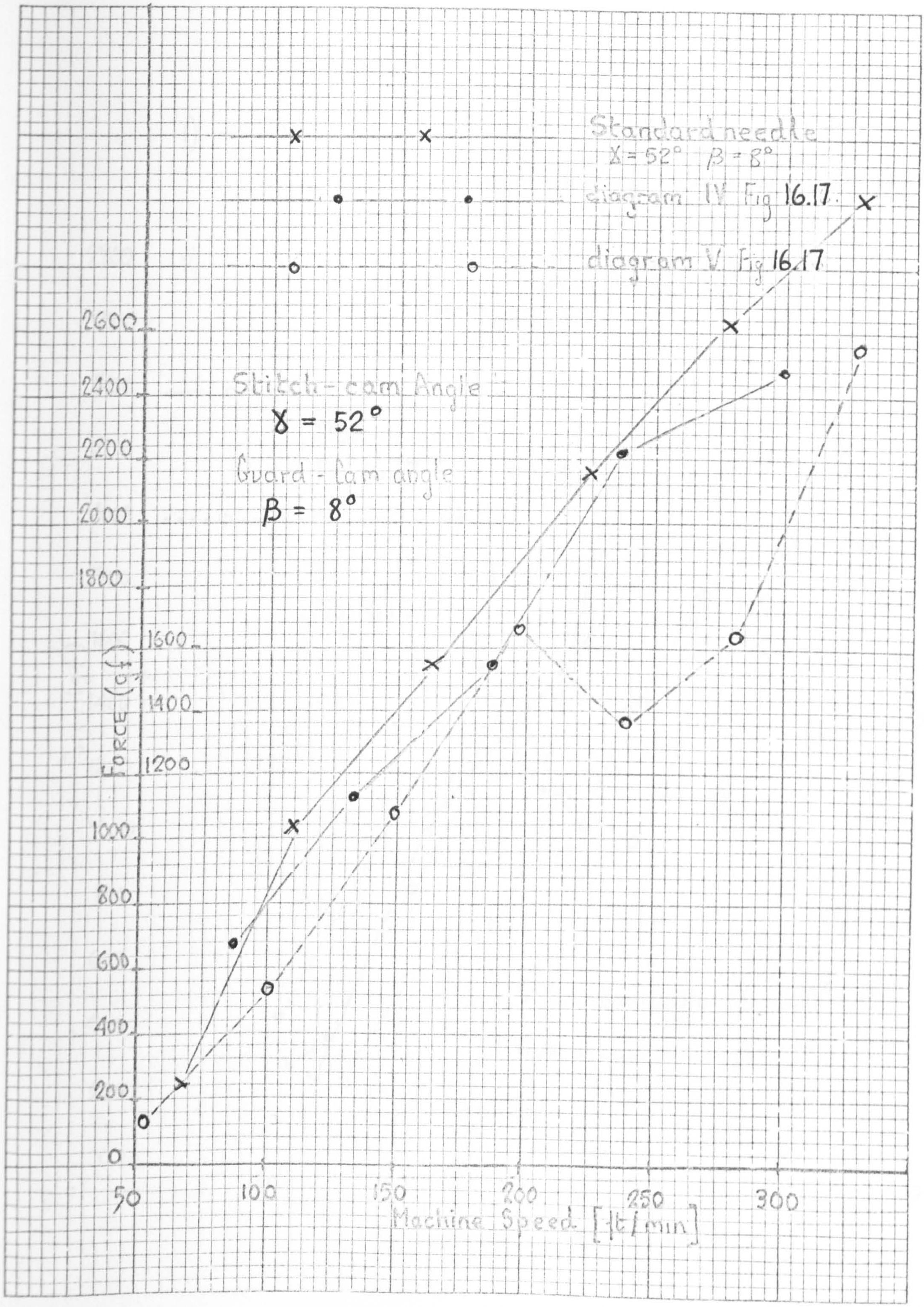

EFFECT OF BUTT MODIFICATIONS (DIAGRAM IV AND V FIG 16.17) ON GUARD-CAM IMPACT

FIG 16.19

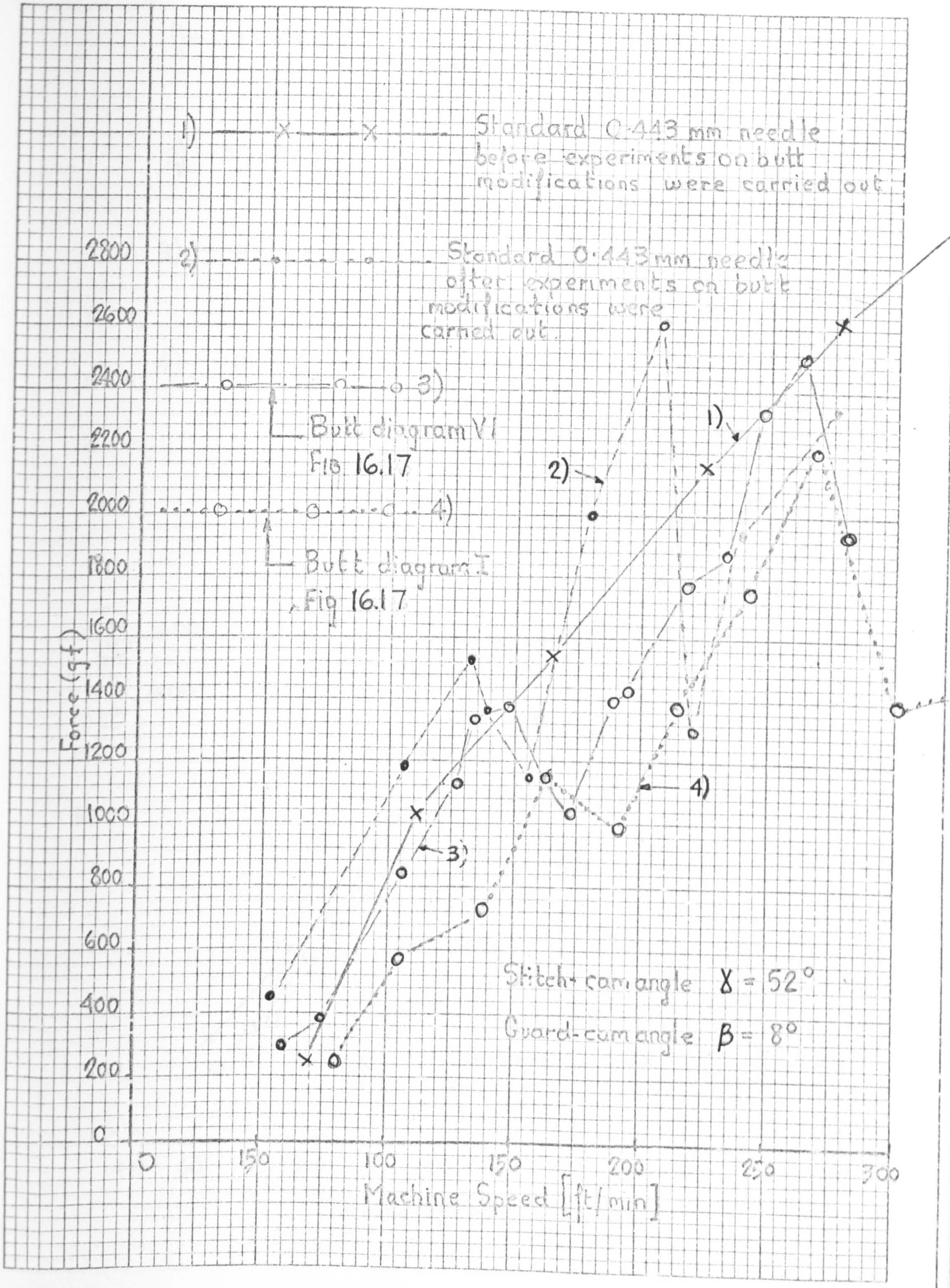

EFFECT OF BUTT MODIFICATIONS (diagram I and VI FIG 16.17 ON GUARD-CAM IMPACT FIG 16.20

1) Standard needle (0·443 mm) after butt experiments, before the base of the stitch cam was polished (using longitudinal instrument).

2) Standard needle (0·443mm) after butt experiments, after the base of the cam was polished (using stitch-cam impact apparatus)

3) Standard needle (0·443mm) before butt modification experiments were carried out

4) Standard needle (0·443mm) after butt modification experiments were carried out and after polishing the base of the stitch-cam. (using longitudinal instrument)

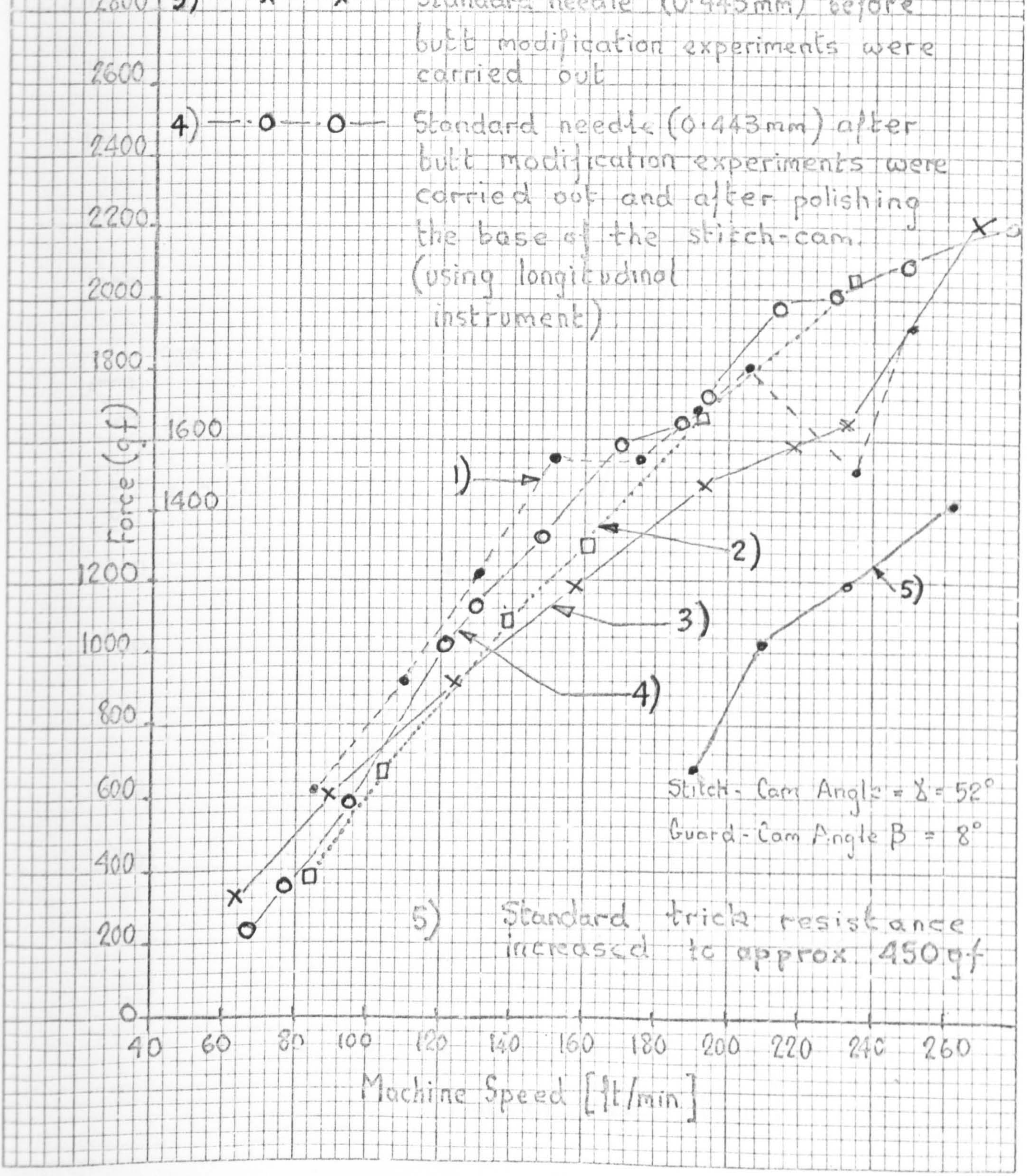

EFFECT OF POLISHING THE BASE OF THE STITCH-CAM

FIG 16.21

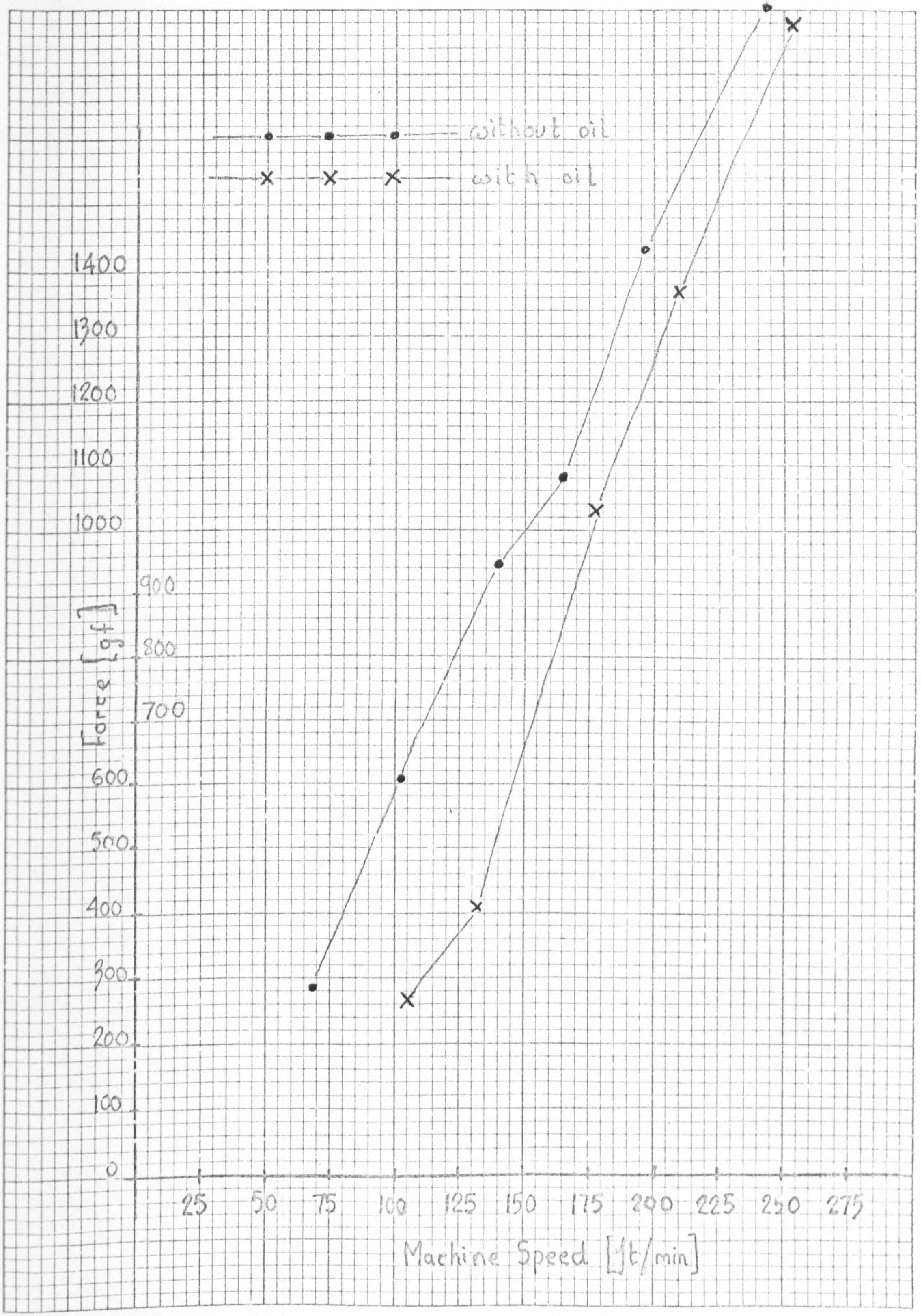

EFFECT OF OIL UPON THE GUARD CAM IMPACT

FIG 16.22

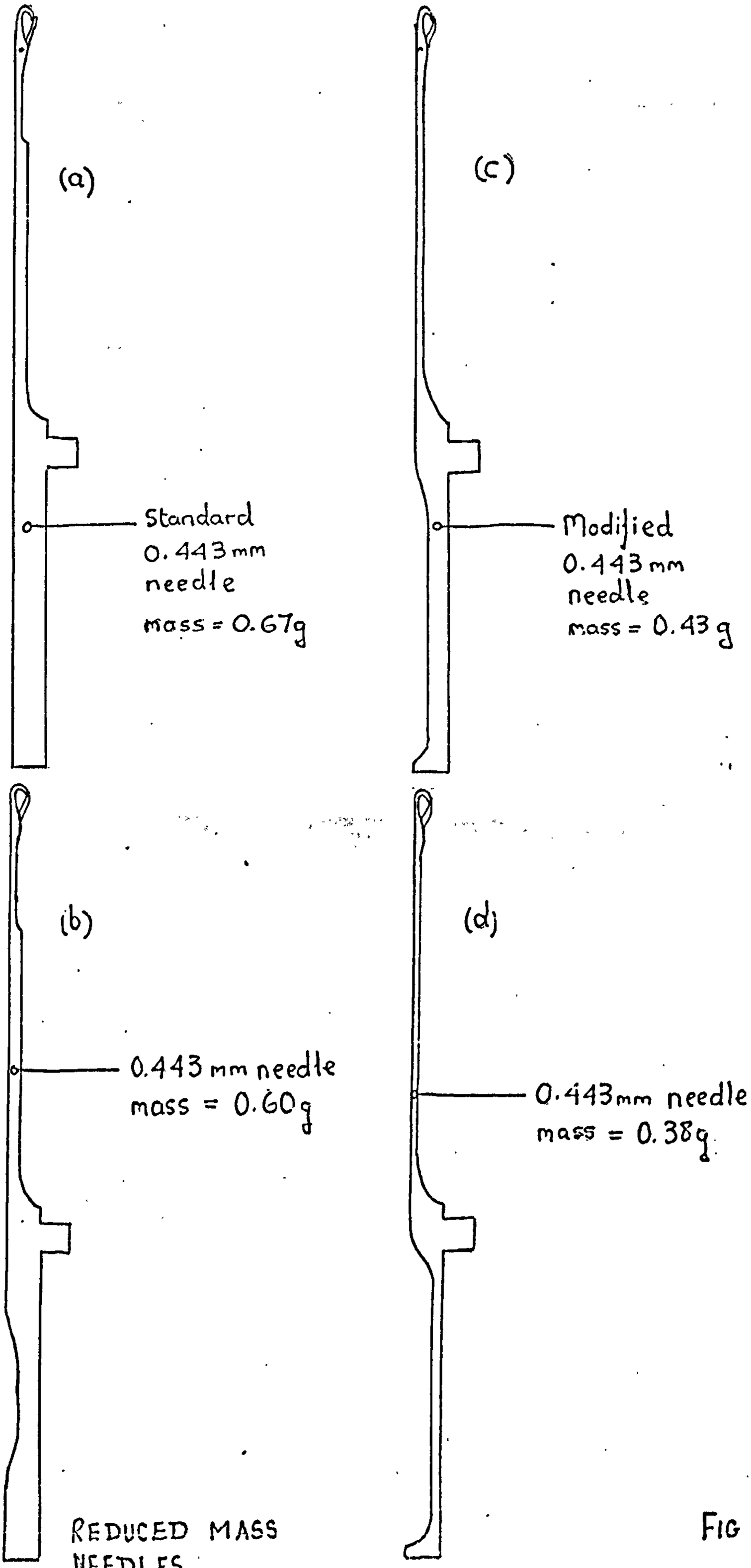

REDUCED MASS
NEEDLES

FIG 16.23

Calibration factor 39 gf/mm
Time = 100 X 10^{-6} seconds per division
Stitch Cam angle = 52^{o}
Guard Cam angle = 8^{o}

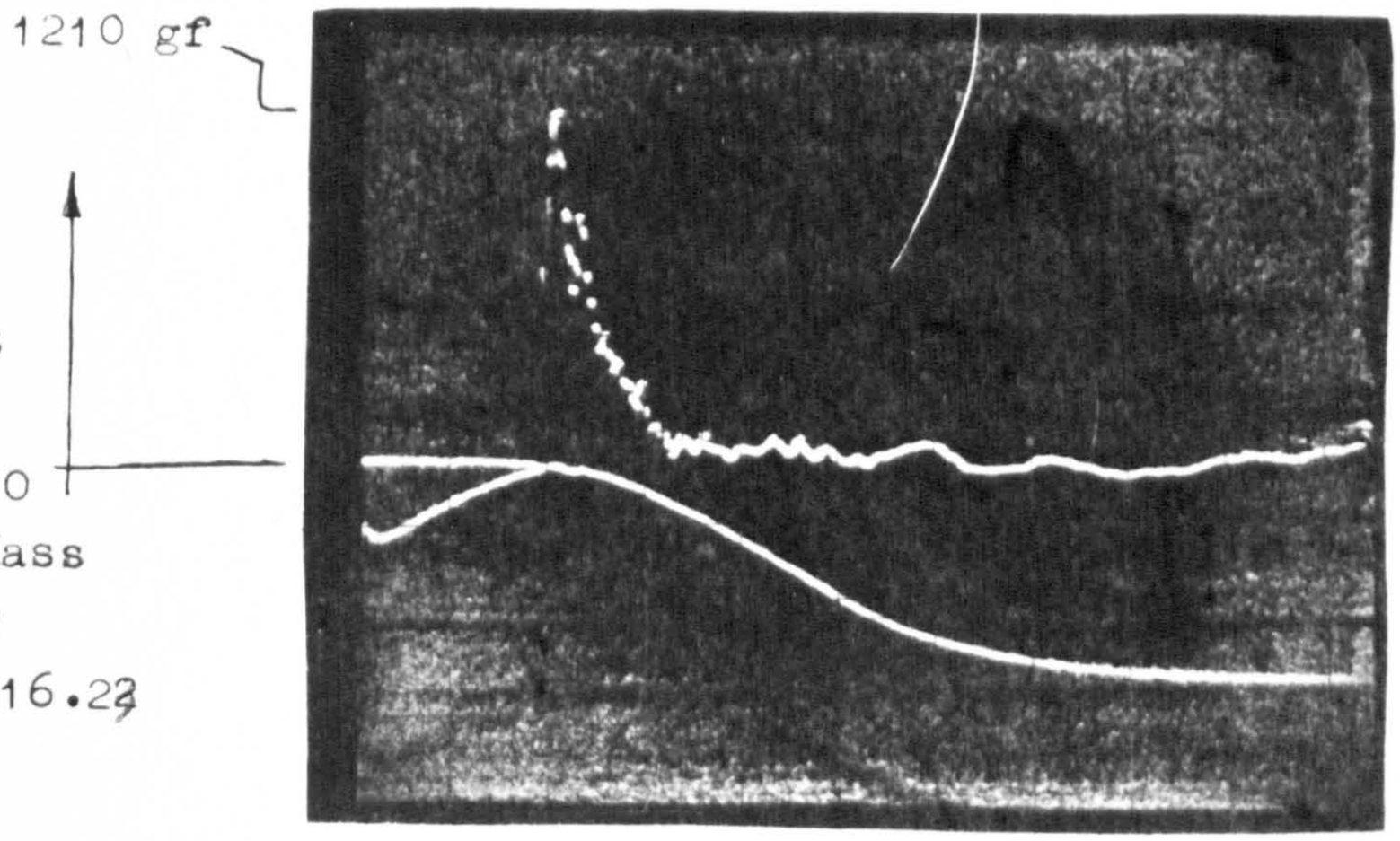

Needle Mass
0.67 g
(a) Fig 16.23

Machine Speed = 152 ft/min

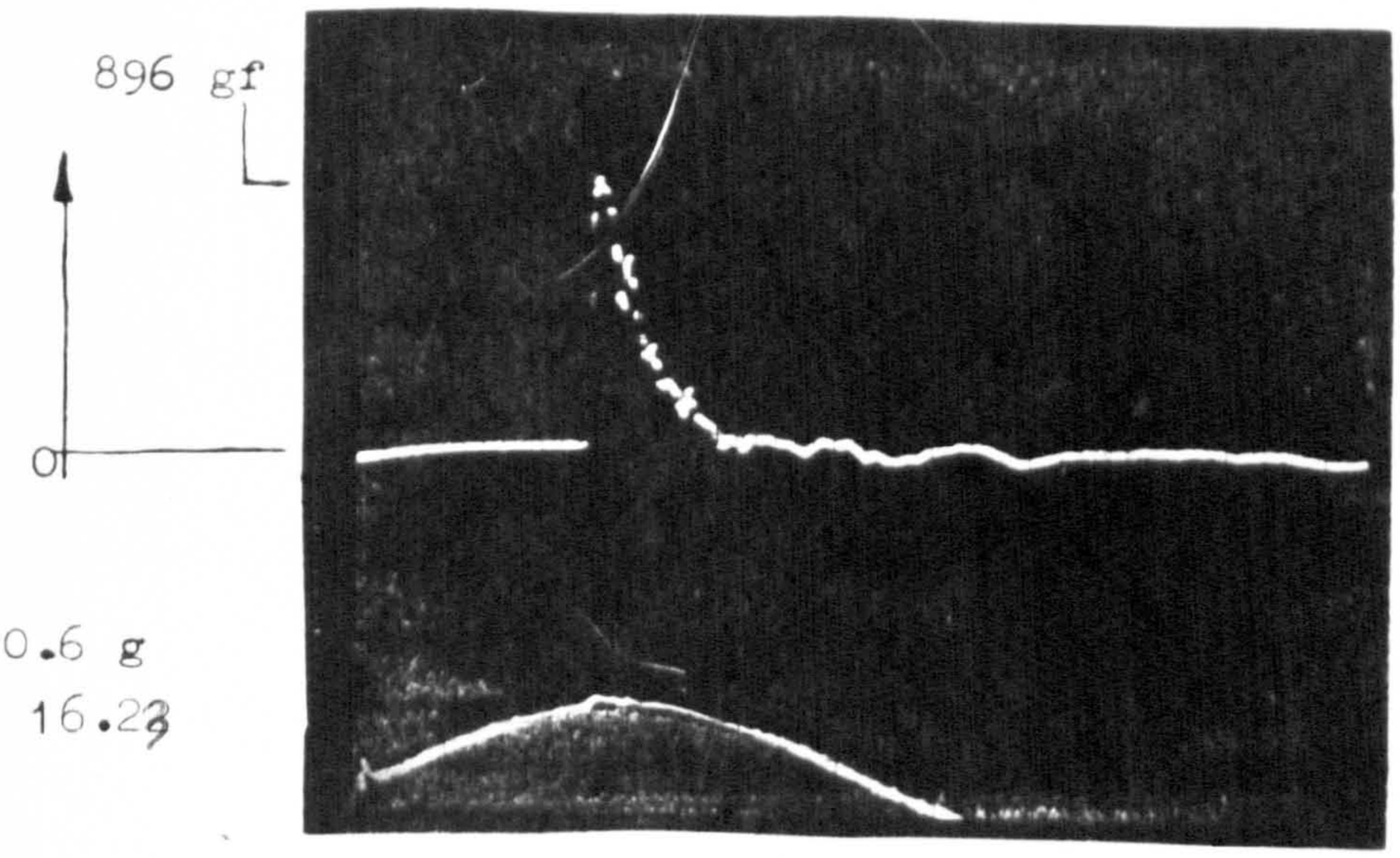

Needle
Mass = 0.6 g
(b) Fig 16.23

EFFECT OF MASS ON GUARD CAM IMPACT
USING LONGITUDINAL IMPACT TRANSDUCER

Fig 16.24

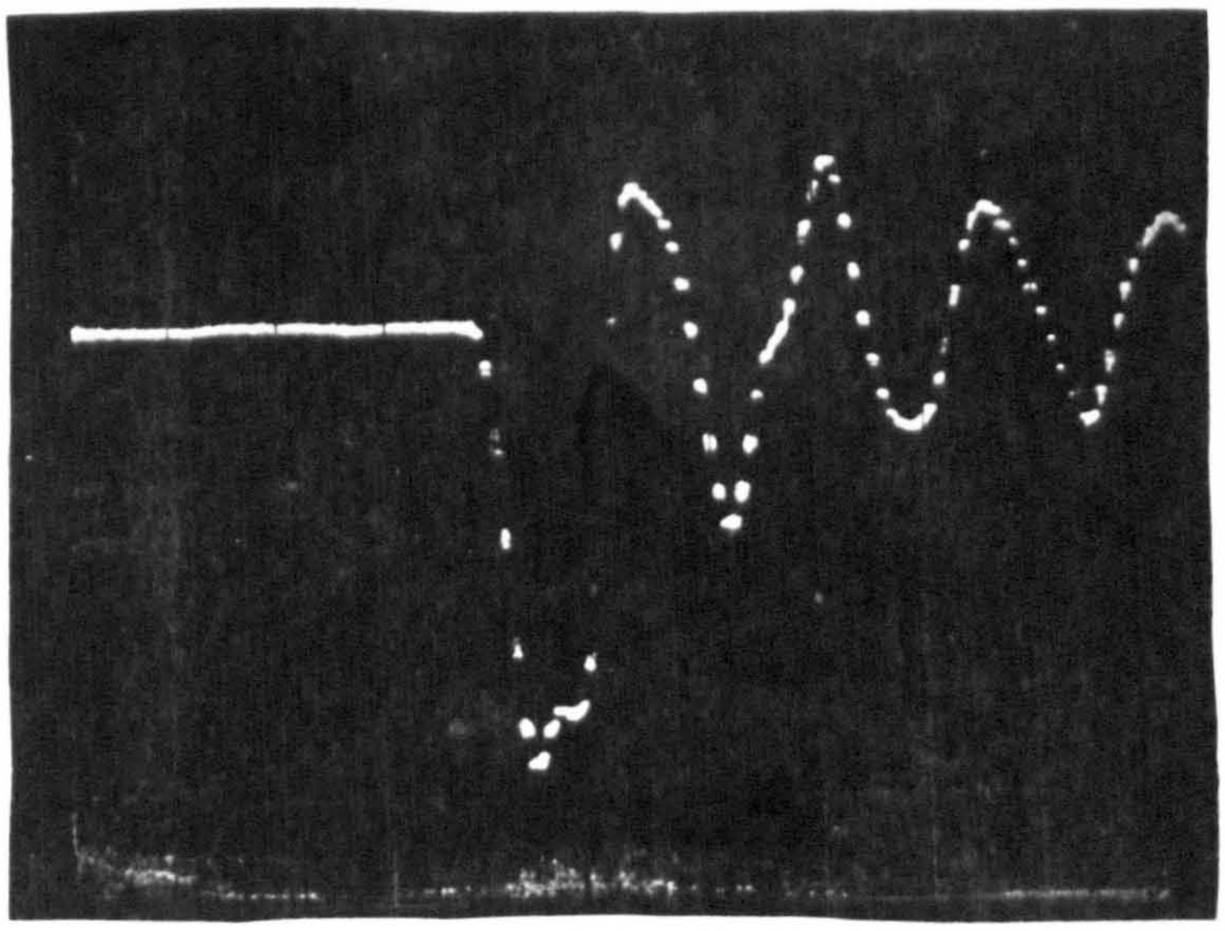

Needle (a) Fig 16.23
Standard 0.433 mm

Time 50 $\times 10^{-6}$ Secs/8.5 mm

Machine Speed - 258 ft/min

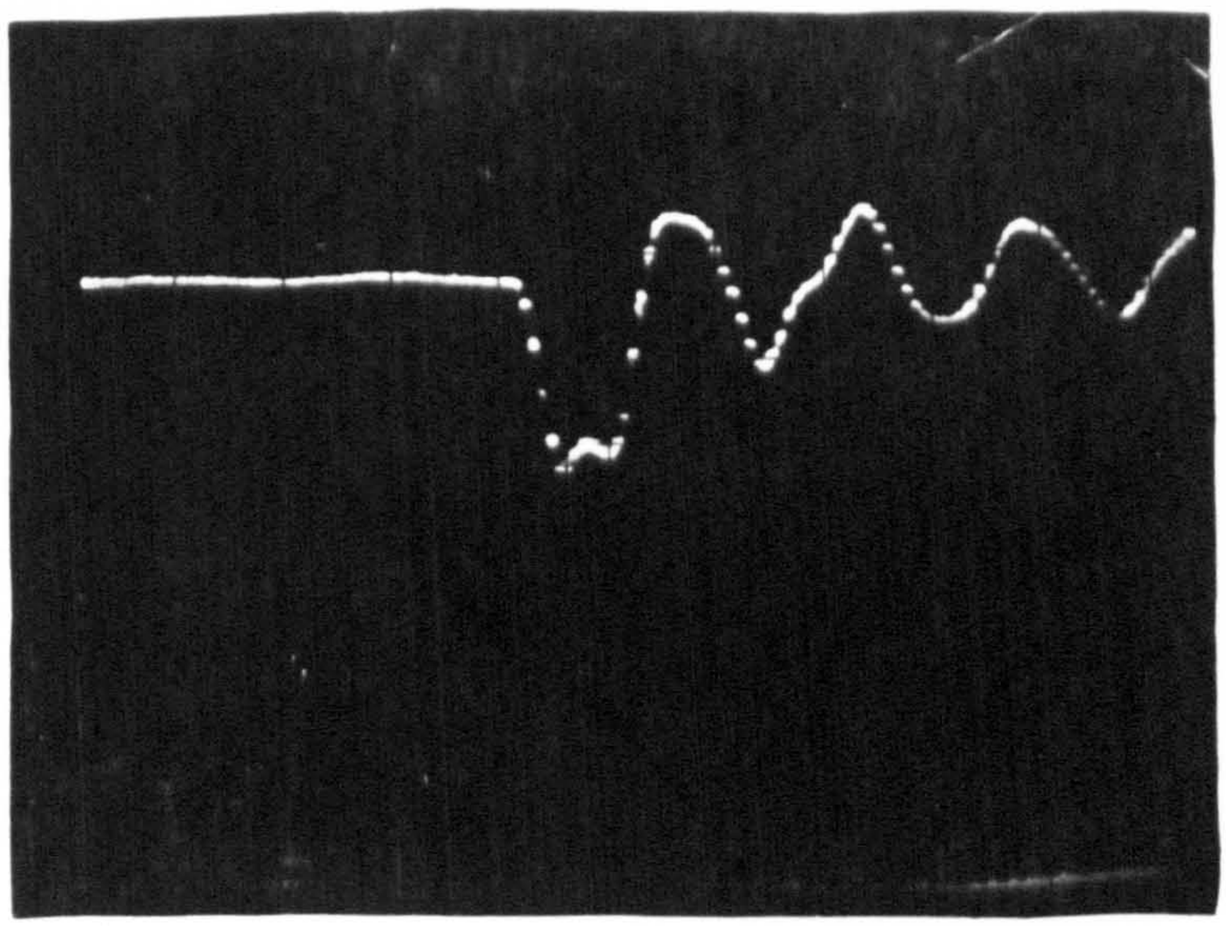

Needle (d) Fig 16.23
mass = 0.38 g

EFFECT OF NEEDLE MASS ON GUARD CAM IMPACT
USING STITCH-CAM IMPACT TRANSDUCER (Fig 15.7)

Fig 16.25

Impact Magnitude

1) 0·67g standard 0·433mm needle (a) Fig 16.23.
2) 0·60g needle (b) Fig 16.23
3) 0.38g needle (d) Fig 16.23

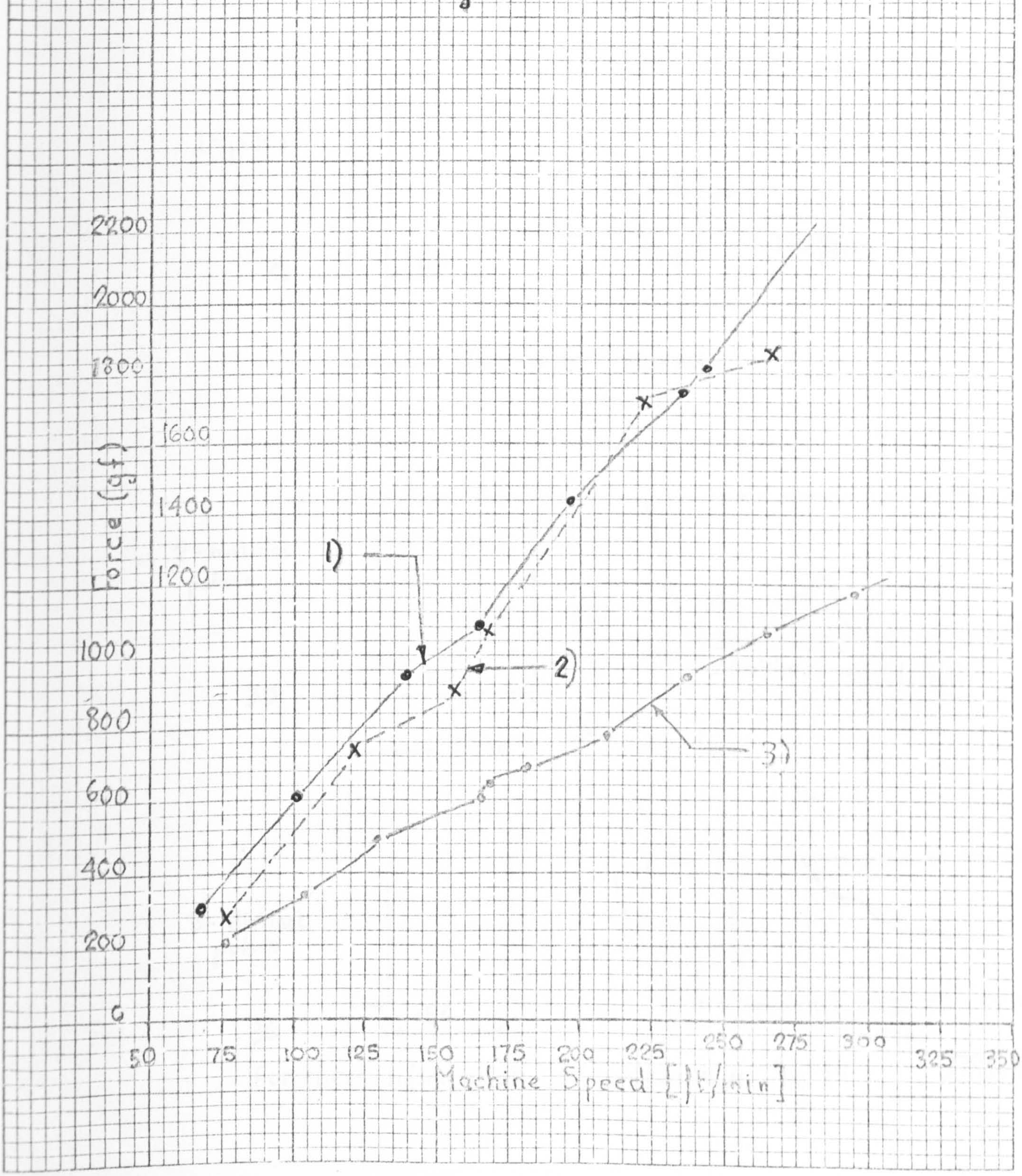

EFFECT OF NEEDLE MASS ON GUARD CAM IMPACT USING LONGITUDINAL TRANSDUCER

FIG 16.26

Stitch-cam angle = 43°

Guard-cam angle = 8°

0.443 mm standard needle.

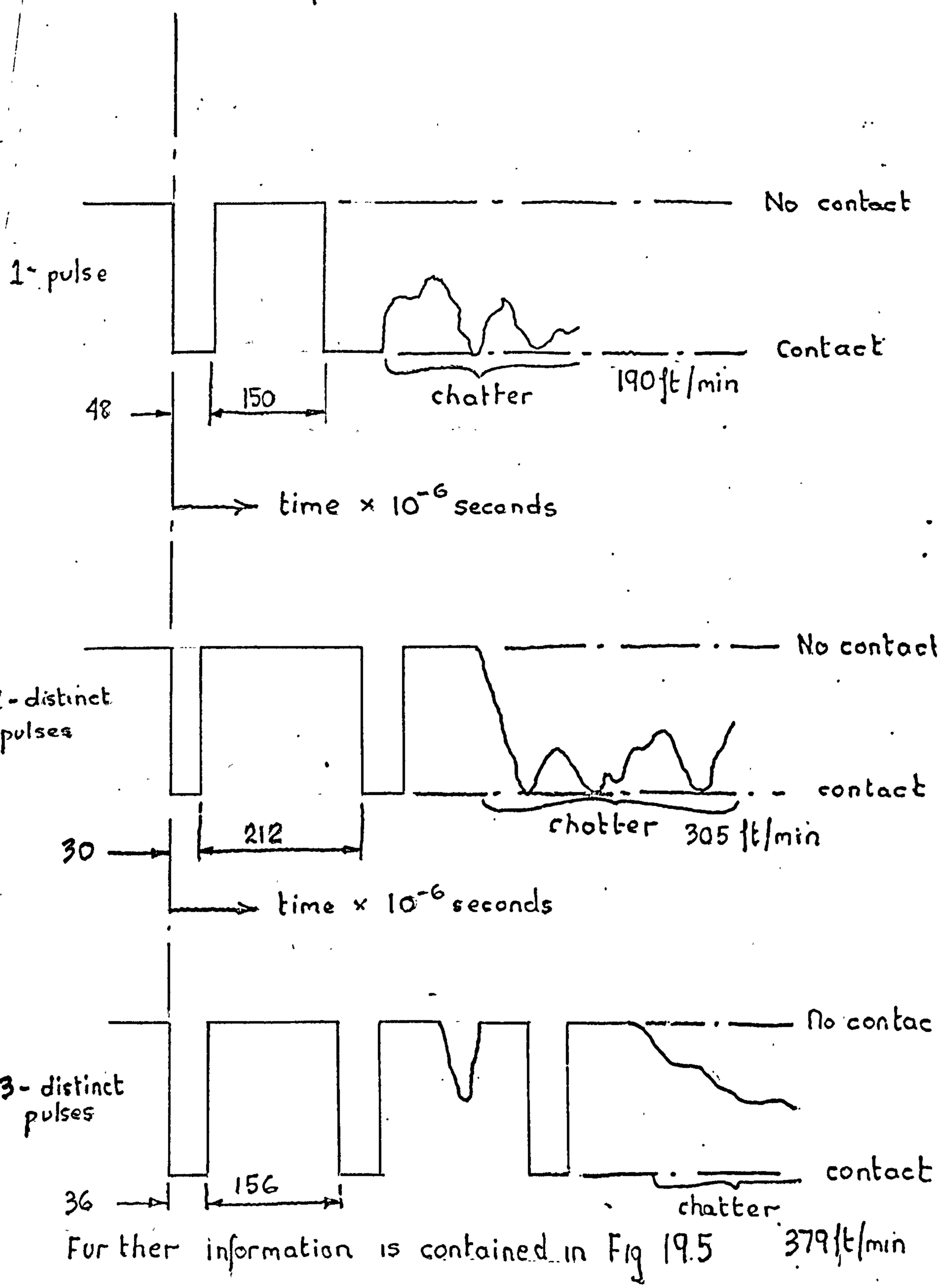

Further information is contained in Fig 19.5

BOUNCE ON THE GUARD-CAM
YARN-FORCE = 0 gf

FIG 16.27

Stitch - cam angle = 43°

Guard - cam angle = 8°

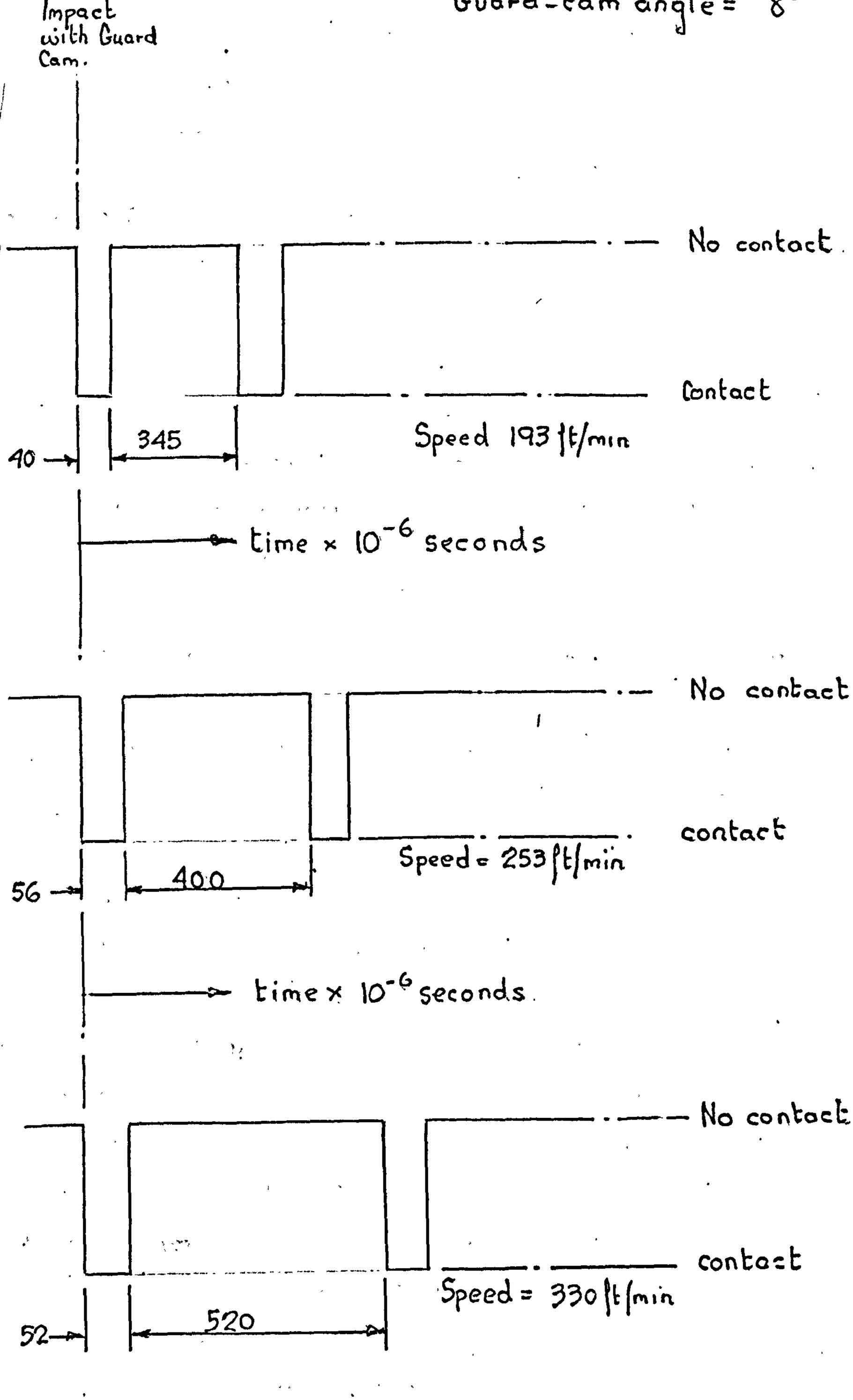

BOUNCE ON THE GUARD-CAM
YARN - FORCE = 90 gf

FIG 16.28

CHAPTER 17

LATCH IMPACT

17.1 Introduction.

Maximum latch impact with the needle hook occurs when the needle is passing through the loop drawing region, and the old loop shown in Fig 8.4 is rising up the stem of the needle. At the instant the loop contacts the latch base there is rapid closure of the latch which then impacts the hook. However, fracture often occurs at the hook bend even when the needle is passing through the cam system without pulling a yarn loop; this indicates that the major factor influencing hook fracture is the impact with the knitting cams. Petrow[33 to 37 inc] does predict dangerous stresses at the hook bend arising from a stress wave originating from impact with the cams. It is quite likely, however, that the latch impact has a contributary influence upon needle hook fracture, and at high machine speed the magnitude of the latch impact could rise to such proportions as to cause head damage.

When the needle rises to clearing height, the old loop, as it moves down the shank, forces the latch open at considerable speed, and a damaging impact occurs on the needle shank. Recent high-speed tests on multi-feeder commercial machines undertaken at Bentley Machine Development Company Limited, revealed considerable damage to the needle shanks. Fig 17.1 is a diagram illustrating the damage and the major impacts occurring at the hook and on the shank.

It is very important to have an understanding of latch impact, because controlling the stitch-cam and guard cam impact may be of little value if the latch impact reaches

such magnitudes that it alone could cause serious needle damage. Unfortunately none of the instruments developed for guard-cam or stitch-cam impact were of any use for latch-impact measurement, and time precluded any detailed experimental work on this topic.

Detailed in the following section is some very simple theoretical analysis. Further discussion concerning possible methods of reducing the impact, following on from the theoretical analysis, is contained in chapter 24.

17.2 Theoretical Analysis.

As the needle moves down the stitch-cam, the old loop rises up the shank. The mean velocity at which the yarn rises up the shank is given by :

$$V \tan \theta$$

where V = Cylinder rotational speed,
and θ = Stitch-cam angle.

The term $V \tan \theta$ is a constant for a linear cam.
The time for the old yarn loop to move by 1 mm up the shank is equal to :-

$$\frac{1}{V \tan \theta}$$

where V is measured in mm/sec.

As the old loop moves up the shank, it forces the latch open at high speed. Two conditions exist, firstly the latch can acquire sufficient kinetic energy for it to lose contact with the yarn and, secondly, contact is maintained and latch motion is dictated by the position of the yarn on the shank. Both cases of latch motion are considered in the following two sub-sections.

17.2.1 Latch Motion Controlled by the Position of the Yarn on the Shank.

If contact is maintained between the latch and the yarn

as the old loop moves up the shank, then the position of the latch in relation to the yarn loop can be easily evaluated. A scale drawing was made of the needle, and at successive positions of the loop on the shank the resulting position of the latch was evaluated. Fig 17.2 is a reproduction of a drawing showing the relationship between yarn position and latch motion, and Fig 17.3 is a graph of latch angular rotation against time.

From Fig 17.3, a reasonable approximation to the graph is :-

$$\gamma = Kt^5 \quad . \quad . \quad . \quad . \quad (154),$$

$$\text{and} \quad t = \frac{d}{v \tan\theta},$$

where γ = Latch rotation angle see Fig 17.2,
K = Constant,
d = distance measured up shank from position 1 in Fig 17.2,
v = machine peripheral speed,
θ = stitch cam angle,
and t = time (from datum at 1).

From Fig 17.3, K , can be evaluated and is equal to :-

$$K = 0.00154 (v \tan\theta)^5$$

$$\text{and hence} \quad \gamma = 0.00154 (v \tan\theta)^5 t^5 \quad . \quad (155),$$

$$\omega = \frac{d\gamma}{dt} = 0.0077 (v \tan\theta)^5 t^4 \quad . \quad (156),$$

$$\text{and} \quad \alpha = \frac{d^2\gamma}{dt^2} = 0.0308 (v \tan\theta)^5 t^3 \quad . \quad (157).$$

At the instant of impact :

$$t = \frac{4.5}{v \tan\theta},$$

where, V, is measured in mm/sec,

$$\text{therefore} \quad \omega = 0.0077 (v \tan\theta)^5 \left(\frac{4.5}{v \tan\theta}\right)^4,$$

which reduces to :-

$$\omega = 3.16 v \tan\theta$$

and, by similar arguments: -

$$\propto = 2.8 (v \tan\theta)^2.$$

From simple impact theory

$$k \int_0^{\Delta t} R(t)dt = I_o \omega (1+e),$$

where k = The distance from the impact point to the pivot see Fig 17.2,

$\int_0^{\Delta t} R(t)dt$ = Impulse N of duration Δt,

I_o = moment of inertial about pivot O on Fig 17.2,

and e = the coefficient of restitution of the latch on the needle hook.

If the shape of the latch is approximated to a rod of length l, width b, and mass m.

Then $$kN = \frac{ml^2}{3}(3.16 v \tan\theta)(1+e) \quad . \quad (158),$$

where V is measured in mm/sec,

and $$N = \frac{ml^2}{k}(1+e)(1.053 v \tan\theta) \quad . \quad (159).$$

As k is very nearly equal to l :

then $$N = ml(1+e)(1.053 v \tan\theta) \quad . \quad (160).$$

For a latch mass m = 0.01 g :

$\theta = 60^\circ$,

l = 4 mm,

and $e = 1$.

The units of $1.053 v \tan\theta$ are rads/sec.

$N = \frac{5.06}{386} \times 25.4 \times 10^{-6}$, where V is in inch/sec.

$N = 0.836 \times 10^{-6}$ lbf sec,

where V is in inches/sec.

The peak force magnitude of the impact depends upon the duration of the impact, and the manner in which the machine speed affects the duration.

If we assume a triangular shaped impulse of duration 60×10^{-6} seconds, which is comparable to the duration of the guard-cam impact.

Then as 100 in/sec. (2.54 m/sec):

$$R_{max} = \frac{0.836 \times 10^{-6} \times 10^{+6} \times 100.}{60} ,$$

or $$R_{max} = 1.39 \text{ lbf } (632 \text{ gf}).$$

17.2.2 Latch Motion unrelated to the Position of the Yarn on the Shank.

When the resistance to motion at the pivot is small, it is possible that the latch moves ahead of the old loop, which is moving up the shank, and contacts the hook before the loop has reached a point opposite the latch pivot. It has been predicted, by analysis carried out at Bentley Machine Development Co. Ltd., that the actual motion of the old loop over the needle head is a series of stick-slip motions. When the yarn is moving forward rapidly after sticking for a short time, the latch can acquire sufficient energy to leave the yarn when it reaches the next stick position. When the latch has left the yarn, the subsequent motion is defined by the following equation :

$$M = -I_o \alpha \quad . \quad . \quad . \quad . \quad (161)$$

where M = the pivot clamping force expressed as a resisting moment,

I_o = moment of inertia of latch about position O in Fig 17.4,

and α = angular acceleration.

Fig. 17.4 is a diagram illustrating the forces on the latch, the stick-slip motion, and the subsequent motion.

of the latch; Fig 17.5 is a graph of latch rotation against time.

Obviously the highest magnitude impact would occur when M was very small. There is no information on the velocity of the yarn during stick-slip motion, and it is impossible to determine the angular velocity of the latch as it leaves the yarn. The slip velocity of the yarn after a stick region will be higher than the vertical velocity of the needle, but certainly not instantaneous. An initial calculation was carried out assuming that M is negligible, and the latch motion is completed while the old yarn loop moves only 0.5 mm up the shank:

$$\text{therefore } \frac{d\gamma}{dt} = \frac{2.84 v \tan\theta}{0.5} \quad \cdots \quad (162)$$

$$\text{and } \omega = \frac{d\gamma}{dt} = 5.68 v \tan\theta \quad \cdots \quad (163)$$

v in mm/sec

This is higher than the latch velocity as calculated in section 17.2.1 :-

$$\text{i.e. } \omega = \frac{d\gamma}{dt} = 3.16 v \tan\theta.$$

v in mm/sec

It can be concluded, therefore, that the magnitude of the impact, if the latch loses contact with the old loop can be higher than the impact if the latch maintains contact with the yarn. The parameters controlling the subsequent velocity of the latch are :-

(i) the clamping moment at the latch pivot,

and (ii) the vertical velocity of the old loop during the slip part of the stick-slip motion.

17.3 Methods of reducing Latch Impact.

Based upon the theoretical analysis, a brief summary of methods for reducing the magnitude of latch impact is presented below :-

(i) Enlarging of the cheek height could reduce the latch velocity at impact, but it would mean increased yarn stretch as the old loop passed over the needle. Fig 17.6 shows the effect of increasing the cheek height by 10%. For the example at the end of section 17.2.1, the peak impact magnitude equalled 1.39 lbf at 100 ins/sec; at similar conditions, when the cheek height was increased, the impact force = 1.021 lbf.

(ii) Use of energy absorbing latch material to reduce the coefficient of restitution.

(iii) Reduction of cam-angle when the latch is being closed.

(iv) Reduction of latch-mass.

(v) Reduction of latch-length.

(vi) Elimination of stick-slip yarn motion over the needle head.

(vii) Increase in the latch-clamping moment at the pivot. However, this would mean increased loading imposed upon the old loop (see section 8.5.7, and Fig 8.22 (b)).

(viii) Alteration to latch design, as shown in Fig 17.7. The graph of latch angular rotation δ against time is shown in Fig 17.8.

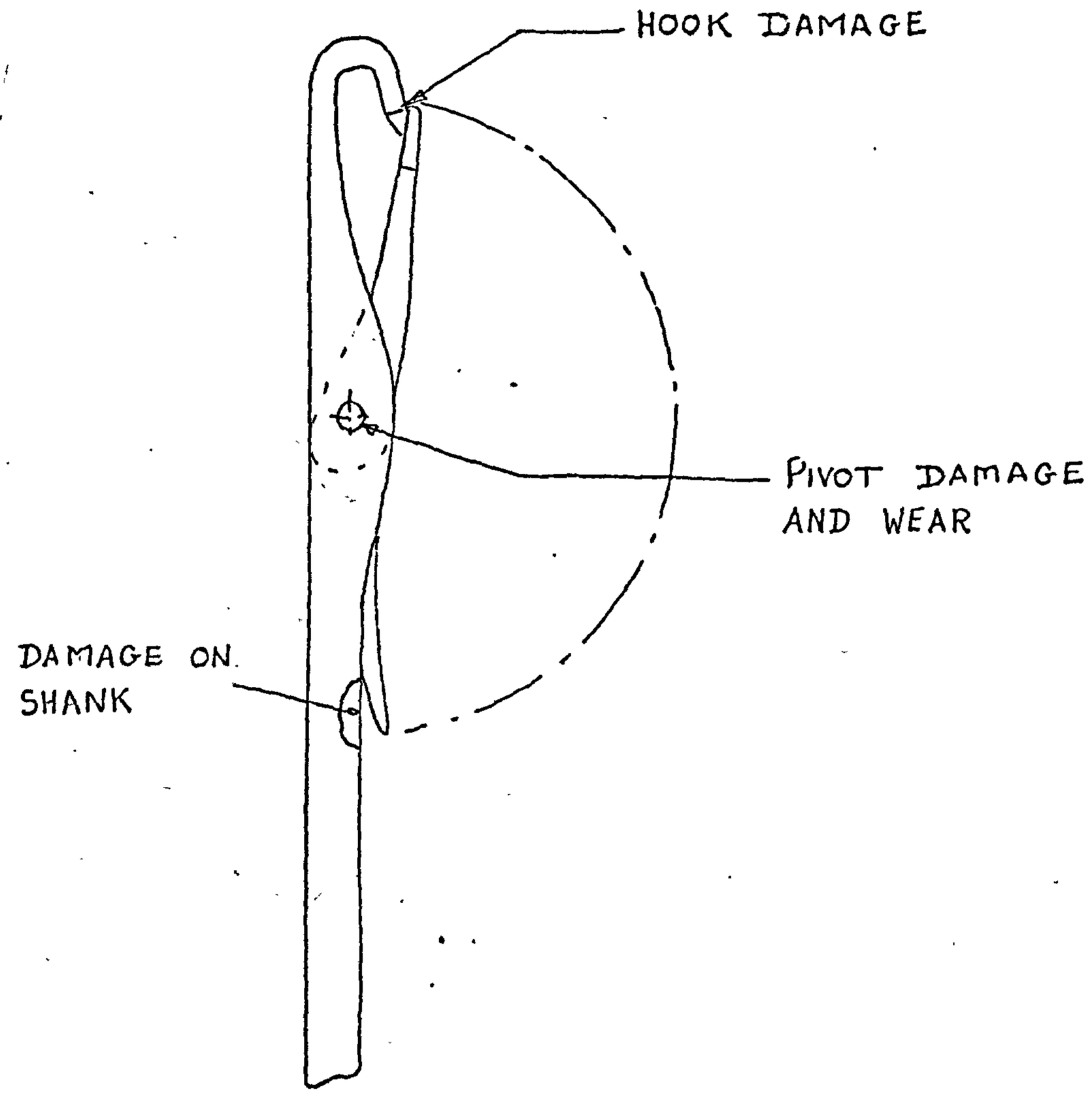

DAMAGE RESULTING FROM LATCH IMPACT.

Fig 17.1

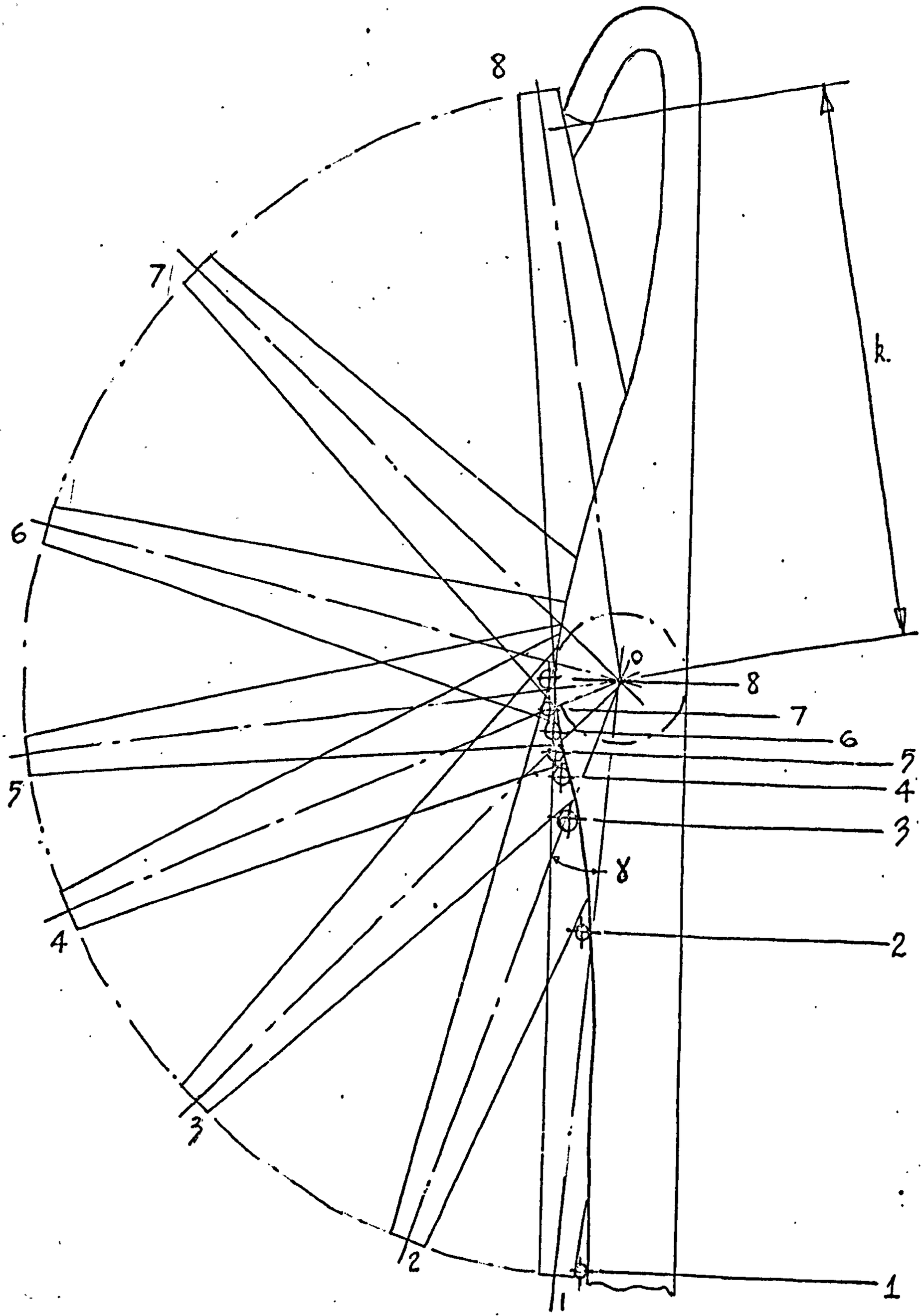

LATCH- MOTION

Fig 17.2

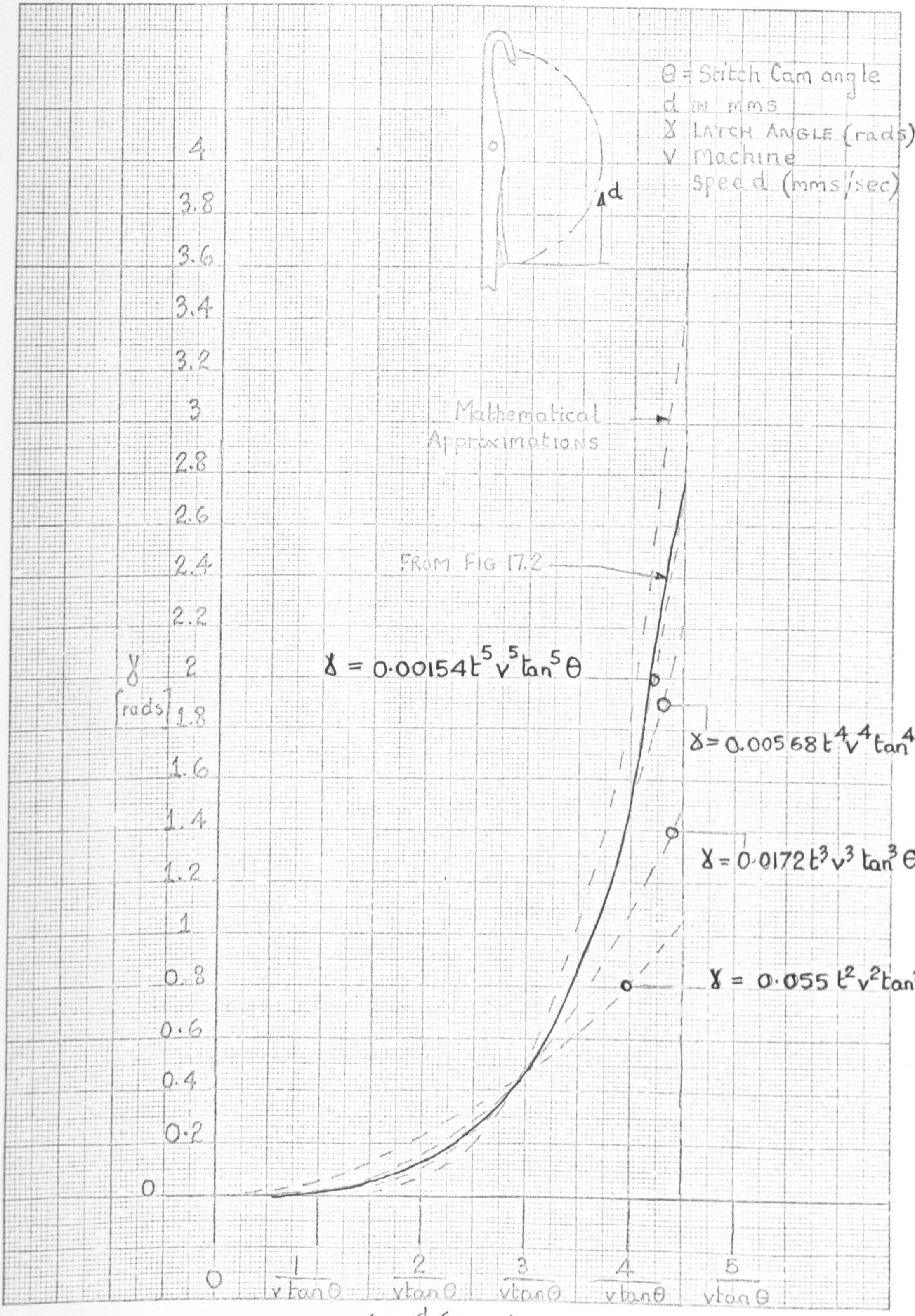

Latch Motion

Fig 17.3

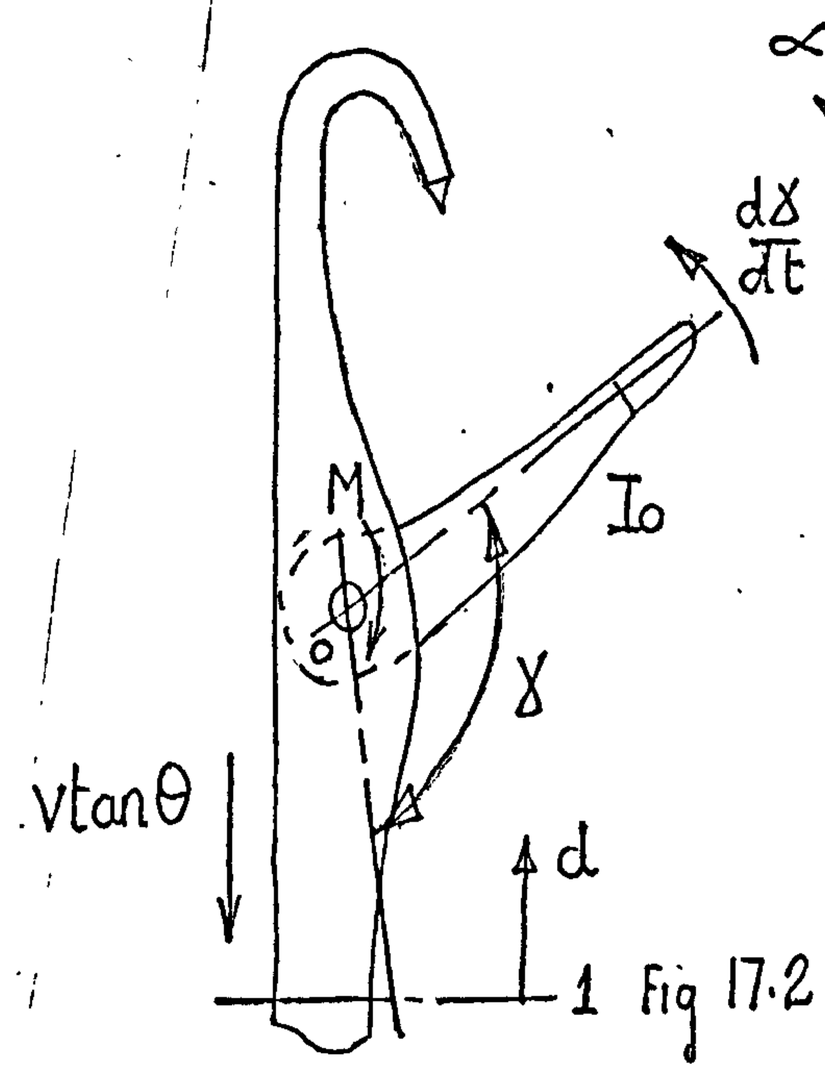

Forces on latch

Fig 17.2

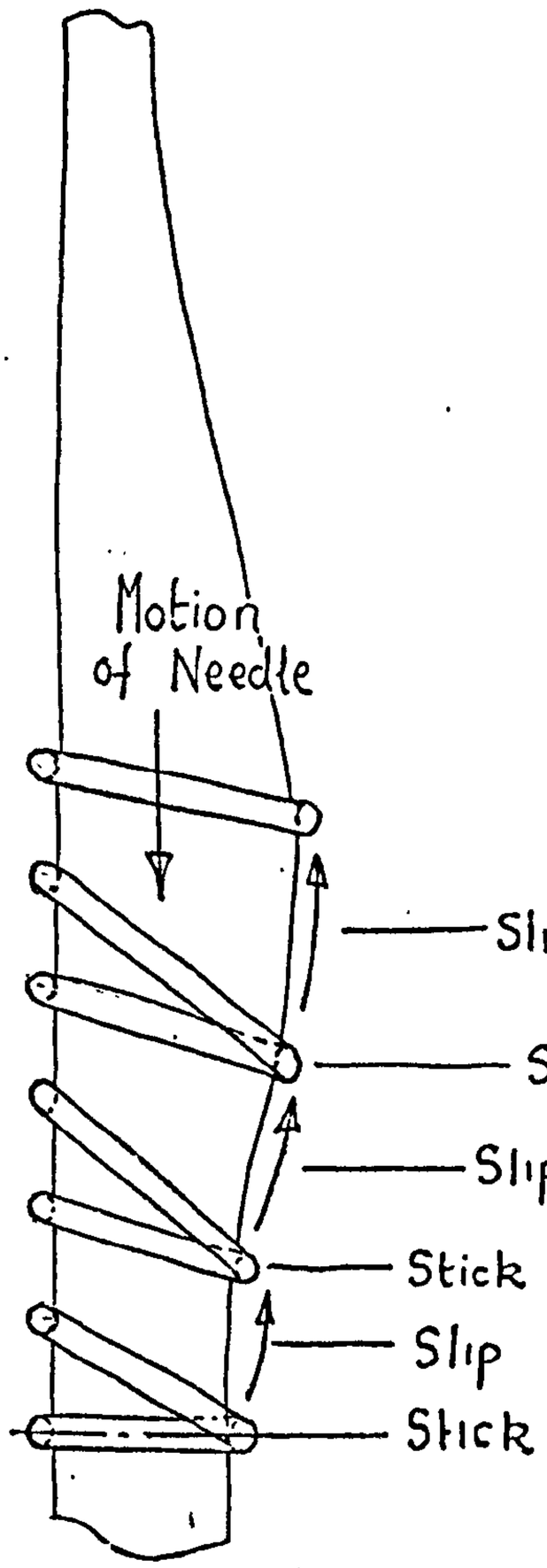

Stick-Slip Motion
[Greatly enlarged]

Stick-Slip Motion

Fig 17.4

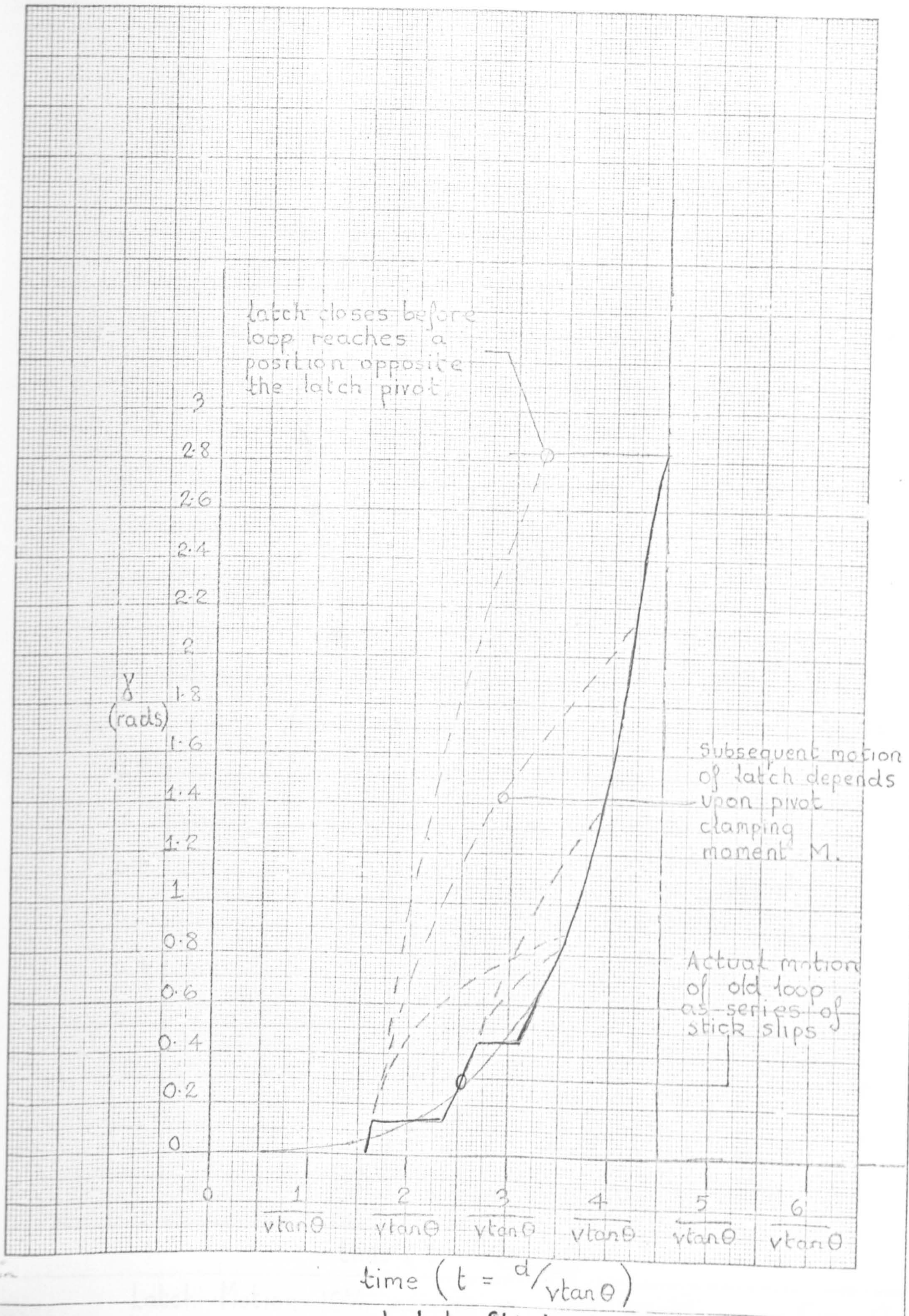

Latch Stick-Slip Motion FIG 17.5

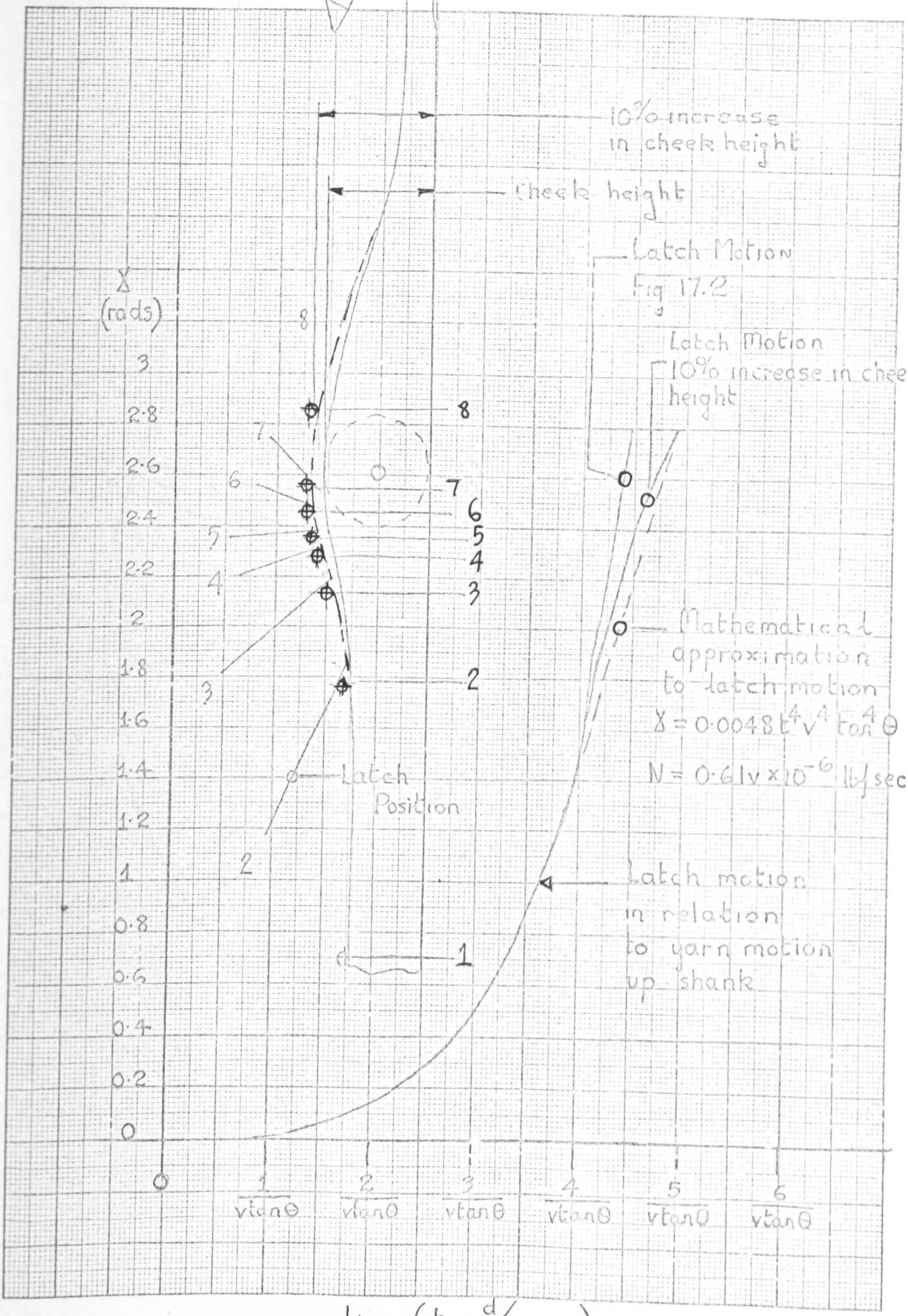

Latch Motion 10% increase in cheek height

FIG 17.6

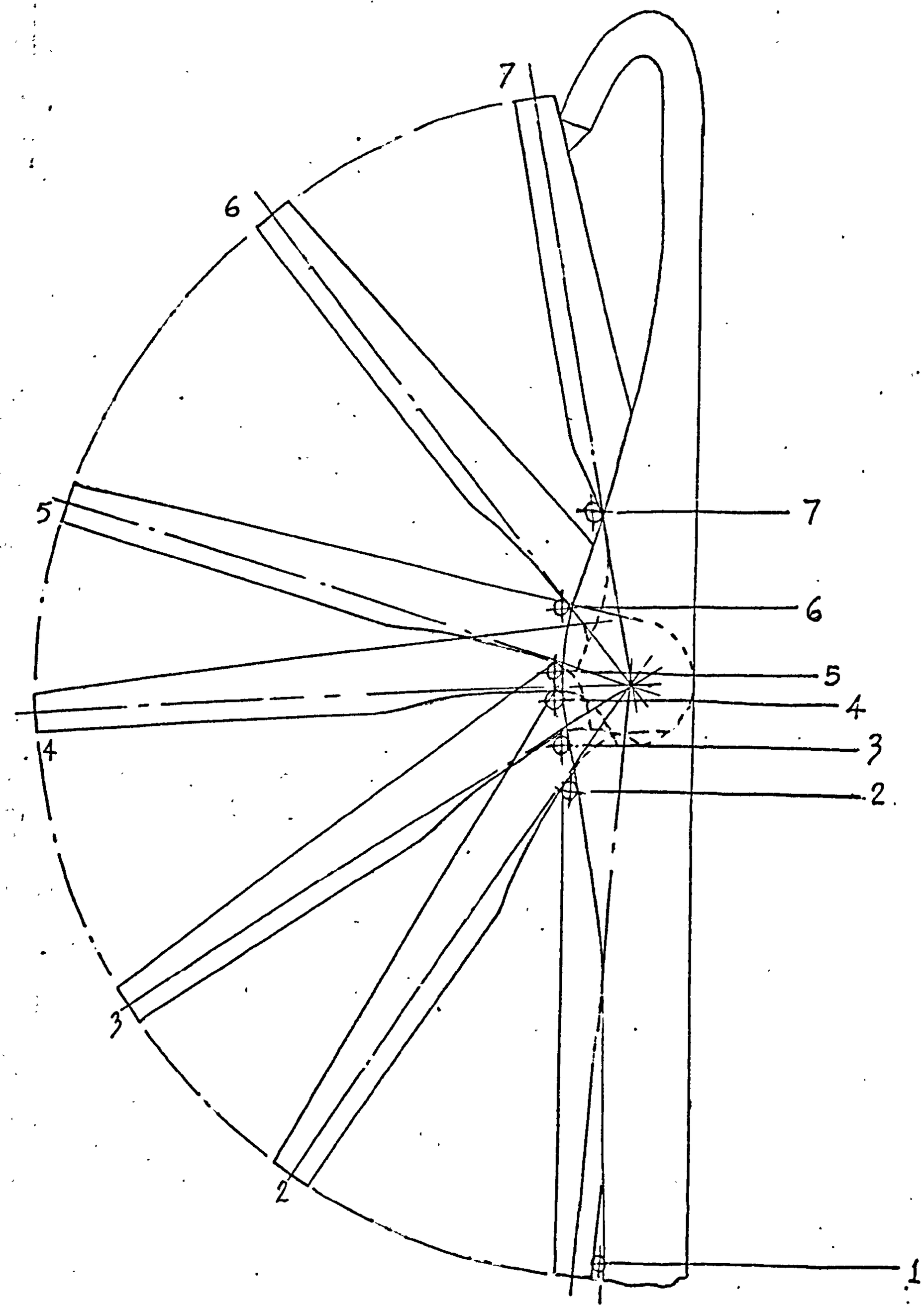

MODIFIED LATCH DESIGN

FIG. 17.7

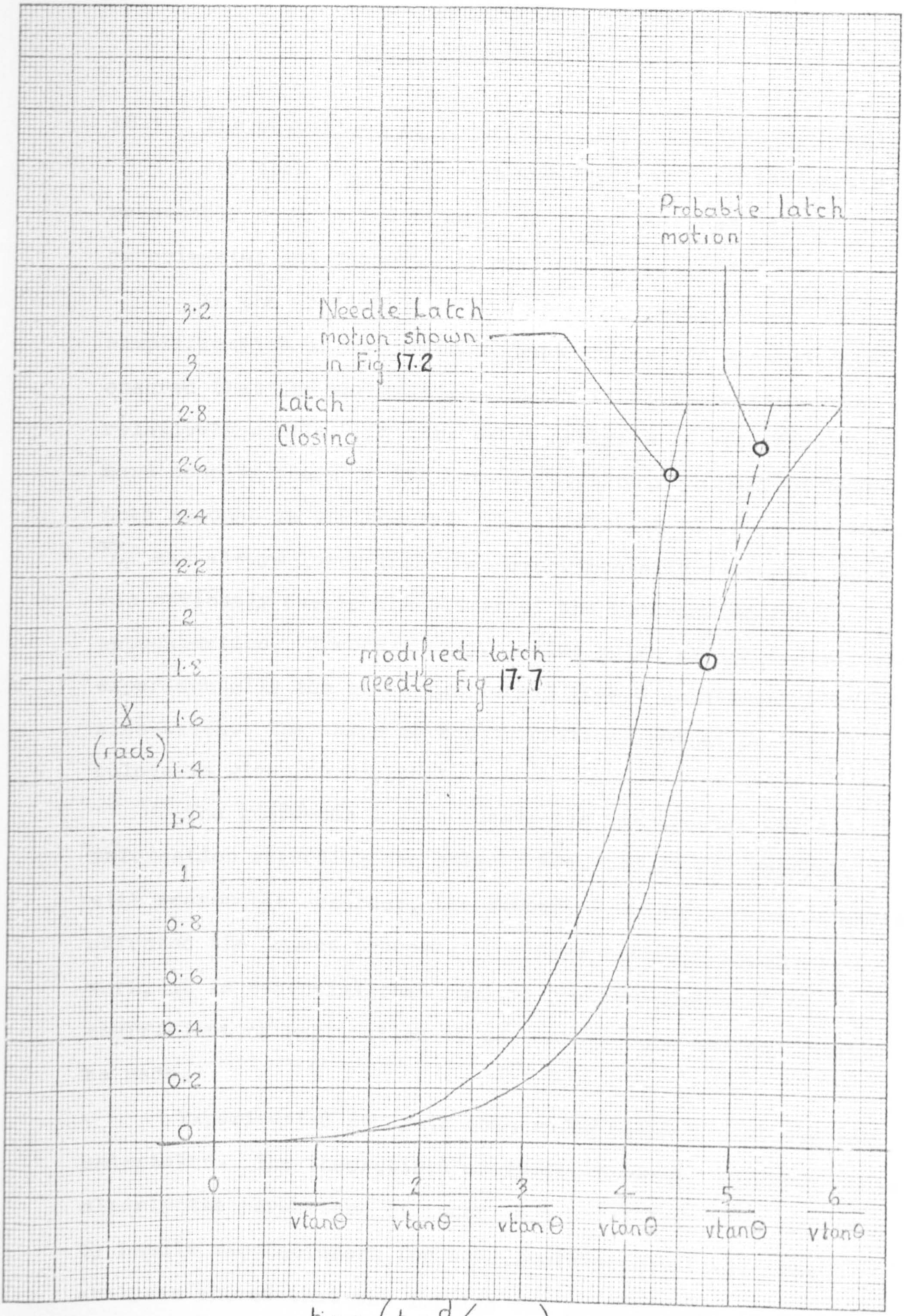

Latch Motion - modified latch needle FIG 17.8

CHAPTER 18

CONCLUSIONS TO PART D

18.1 The comparison of Theoretical and Experimental Results.

For both the stitch-cam and the guard-cam impacts, a reasonably good degree of agreement was obtained between the experimental and theoretical results.

In the prediction of stitch-cam impact, the simplification of the graph of butt-deflection against load ensured that the mathematics and the final expression were relatively simple. If more exact analysis is required, the more complex shape of the butt-deflection graph must be taken into account in the theory. The prediction of the pulse time π/n was always lower than that experimentally measured; this was obviously due to the nature of the butt-deflection approximation. Theoretically, a sine pulse was predicted, and experimentally the pulse was formed from a superimposition of sine-waves. The shape of the theoretical and experimental pulses, is given on Fig 18.1.

The guard-cam impact theory did not provide any information regarding the pulse shape, but it did predict, with reasonable accuracy, the manner in which various parameters affected the impact process. For more detailed theoretical work, it is essential that realistic measurements of the coefficient of restitution of the needle upon the cam surface be made.

Experimental analysis concerning latch impact was not undertaken. The theoretical analysis, however, revealed quite clearly the parameters of importance which have been examined by needle manufacturers for some considerable time. The analysis showed that the impulse was proportional to machine

peripheral speed if the other parameters were held constant, and if the duration of impact is a constant no matter what the machine speed:

18.2 Brief Summary of the Experimental Results Contained in Chapters 14,16 and 17.

18.2.1 Effect of Machine Speed.

Stitch-cam impact (section 14.4.2).

Guard-cam impact (section 16.3).

Latch impact (section 17.2).

As machine speed increases, the stitch-cam impact also increases. For example, when a standard 0.443 mm needle impacted a 60^{o} stitch-cam, the peak impact force increased from 1600 gf to 8750 gf, for a machine speed increase from 100 ft/min (0.50 m/s) to 400 ft/min (2.00 m/sec).

For this particular test, butt failure occured at 420 ft/min (2.13 m/s). The guard-cam impact increased with machine speed; for example when a 0.443 mm standard needle impacted a 8^{o} guard cam, after firing off a 52^{o} stitch-cam, the impact increased from 440 gf at 100 ft/min to 2110 gf at 300 ft/min. In this particular example there was no yarn around the needle hook. The pulse duration for guard-cam impact was much shcrter than the duration for stitch-cam impact, i.e. 95×10^{-6} seconds compared to a figure varying between 300 and 700×10^{-6} seconds.

The theoretical analysis predicted a linear increase in latch impact for a varying machine speed.

18.2.2 Effect of Stitch Cam Angle.

Stitch cam impact (section 14.4.2).

Guard cam impact (section 16.4).

Latch impact (section 17.2).

The stitch cam impact increased when the cam angle was steepened. For example, when the machine speed was 200 ft/min.(1 m/sec), impact of a 0.443 mm standard needle against a 30^{o} cam resulted in a peak force magnitude of 560 gf, while impact at the same speed but against a 60^{o} cam resulted in a peak force of 3,800 gf.

The angle at which the needle "fired-off" the stitch-cam had a large effect upon guard-cam impact. For example, when the stitch-cam angle was 40^{o} and the guard cam angle 8^{o}, then at 250 ft/min (1.27 m/sec) the peak impact force was 1050 gf; for a stitch-cam angle of 55^{o}, the peak impact force was 2020 gf.

The latch impact theory predicted that, when the angle of the stitch-cam at the latch closing position increased, the impulse also increased.

18.2.3 Effect of Yarn Tension.

Stitch cam impact (section 14.4.1).

Guard cam impact (section 16.3).

The yarn-loop held around the needle shank at the instant of stitch-cam impact had very little effect upon the impact magnitude.

The yarn-tension, acting on the needle during loop formation, had a large effect upon guard-cam impact. For example when the yarn tension, at the instant of impact, was increased from 10 gf to 176 gf, the peak impact force at 200 ft/min decreased from 1,430 gf to 550 gf (in this example the stitch-cam angle was 52^{o} and the guard-cam angle 8^{o}).

18.2.4 Effect of Needle Mass.

Stitch-cam impact (section 14.5.3).

Guard-cam impact (section 16.9).

Latch impact (section 17.2).

The needle mass had a large effect upon all three impacts; generally, if the mass was reduced by one-half, the impacts all reduced by more than one-half depending upon the trick resistance to needle motion.

For impact against a 49° stitch-cam at 200 ft/min, the horizontal component of stitch-cam impact decreased from 3,300 gf, for a 1.36 g needle, to 1,540 gf, for a 0.43 g needle. Similarly, guard-cam impact decreased from 1,440 gf to 760 gf when the mass was reduced for 0.67 g to 0.38 g. For these examples the stitch-cam angle was 52°, guard-cam angle 8° and machine speed 200 ft/min (1 m/sec).

The theoretical analysis carried out on latch impact showed that, if the needle mass was reduced by one-half, the impulse should also reduce by one-half.

18.2.5 Effect of Oil.

Stitch-cam impact (section 12.3.2).

Guard-cam impact (section 16.8).

The oil used throughout the experiments was Vickers Spotless B.N.O. oil.

The oil had no appreciable effect upon the magnitude of the primary stitch-cam impact. However a heavy soaking of oil did effect needle bounce, since it shortened the period of time between bounces and generally inhibited the bounce process.

A heavy addition of oil reduced guard-cam impact. For example, for impact at 200 ft/min (1 m/sec) of a 0.443 mm standard needle against an 8° cam, firing of a 51° stitch-cam, the impact decreased from 1470 gf to 1280 gf, after a heavy addition of oil.

18.2.6 Effect of Trick Resistance to Needle Motion.

Stitch-cam impact (section 14.5.2).

Guard-cam impact (sections 16.3 and 16.7).

The trick resistance to needle motion had a large effect upon the impact forces. For the stitch-cam impact of a 0.443 mm needle against a 49° cam at 200 ft/min (1.00 m/sec), the peak horizontal component of impact increases from 1200 gf to 3,400 gf when the trick resistance is increased from 35 to 1650 gf. When the trick resistance to needle motion was increased from 35 gf to approximately 450 gf, the guard-cam impact at 200 ft/min, against an 8° guard cam, decreased from 1440 gf to 760 gf. As trick resistance to needle motion was increased, so did the minimum velocity at which guard cam impact just commenced.

18.2.7 Effect of Cam-Cylinder Clearance.

Stitch-cam impact (section 14.5.4).

Guard-cam impact (section 16.6).

Small changes in the cam-cylinder clearance, i.e. from 0.006 in. (0.15 mm) to 0.015 in. (0.37 mm), have very little effect upon stitch-cam impact. Very little experimental work was undertaken upon the effect of large changes in the clearance. However, it seems likely from the theory that the impact increases as the cam-cylinder clearance is increased.

Guard-cam impact decreased a small amount when the cam-cylinder clearance was increased. For example, guard cam impact, of a standard 0.443mm needle at 200 ft/min, changed from 1640 gf to 1400 gf when the clearance was increased from 0.006 in. (0.15 mm) to 0.034 in. (8.6 mm).

18.2.8 Effect of Butt Modifications.

Stitch-cam impact (section 14.5.1).

Guard-cam impact (section 16.7).

Many severe modifications were made to the butt design

of a selected range of needles. Although there was variation between one needle and another, none of the modifications showed significant improvement upon stitch-cam or guard cam impact.

18.2.9 Effect of Various Parameters upon Guard Cam Impact.

(i) Supporting Structure Stiffness. (section 16.2)

Although the knitting machine structure where the impact transducer was fitted was considerably stiffened, it had very little effect upon guard-cam impact.

(ii) Guard-Cam Angle. (section 16.5)

A special guard-cam was designed with a very steep guard-cam angle. The experiments carriedout to investigate the impact magnitude upon the steep cam showed that, at high-speed, although the impact duration is somewhat longer (approximately 500×10^{-6} secs), the impact magnitude at high speed soon rises to such a high value that the butt breaks.

(iii) Marks on the Stitch-Cam. (section 16.7)

Very fine horizontall marks at the base of the stitch cam led to some very irregular impact force results at high machine speed. It was possible that, as the speed increased, the corresponding impact magnitude decreased.

18.3 Methods of Reducing Impact.

The needle mass has a large effect upon the impact magnitude, so that, if a low mass needle where to be used in the knitting machine, the stitch cam impact, guard-cam impact, and latch impact would all be substantially reduced.

The trick resistance to motion should not be so large that high stitch-cam impact results, ncr so free that high guard-cam impacts result. The cam angle at stitch-cam impact should be small, and if possible the cam angle when

the latch is closing should also be small. The angle at which the needle fires off the stitch cam should be as nearly as possible parallel to the guard camangle at the point of cam-needle contact.

The cam-cylinder clearance at stitch-cam impact should be small, but the clearance at guard cam impact could be usefully increased by a small amount. A diagram illustrating an increased width of land on a guard cam designed to reduce the impact is shown in Fig 18.2.

Heavy addition of oil reduces the bouncing phenonemon down the stitch-cam and also reduces the guard-cam impact.

A tentative idea for reducing the stiffness term, in section 12.2, and hence stitch-cam impact by modification of the trick wall is shown in Fig 18.3. However, this idea was never examined experimentally and there is the attendant danger of increased bouncing down the stitch-cam.

An examination of equation(102) of section 14.4.2, shows that, if the frequency term n is large, then the stitch cam impact force R is small. The frequency n is large when the term, $1 - \alpha\mu_1\mu_2$ is large and the term $\mu_2 + \alpha\mu_1$, is small; these are only possible when μ_1 and μ_2 are both small. However, frequency n is small if, $\sin\theta + \mu_2\cos\theta$, is large. It is obviously an advantage to have both μ_1 and μ_2 small, but to keep μ_1 considerably smaller than μ_2.

A similar argument can be applied to the guard-cam impact. If the impact duration, at the instant of contact, could be lengthened then the force magnitude would be reduced. Methods of increasing the cam flexibility at the instant of impact would lengthen the pulse time and some tentative ideas are shown in Fig 18.4.

Methods of reducing latch impact, based upon the

results of the theoretical analysis, are contained in section 17.3. A further discussion concerning the relevance of the measurements to the design of the needles, tricks, and cams, is contained in chapters 23 and 24.

18.4 Effect of Needle Bounce on the Knitting Process.

Recently, a patent[52] for a knitting machine with vibrating cams has been applied for. The idea behind the device is that the needle makes reduced contact on the vibrating cams and therefore less heat is generated at high speed. However, the vibrations may lead to impacts of a larger magnitude, because, combined with needle motion, the cam is also moving, and if the two components are moving towards each other at the instant of contact the impact could be very large. The phasing of the cam motion should be arranged so that the cam is always receeding from the needle at the instant of contact. The horizontal frequency of cam motion must be controlled by the needle passing frequency. However, although the phasing of cam vibration could be controlled to reduce primary impact, the motion of the needle on the cam would have to be rigidly controlled so that the secondary impact was also reduced in magnitude.

There is no evidence that bouncing in itself leads to any form of needle damage; however, if the bouncing extends to the portion of the cam where the latch is moving, then it could possibly have an effect upon latch motion. Bouncing on the stitch cam could have some advantages from the view-points of decreased contact and reduced heating; however, bouncing is evidence of an increased number of impacts. Since free needles tended to bounce more than tighter needles, and tight needles had impacts of higher magnitude on the stitch-cam, then bouncing is indicative of primary impacts of lower

magnitude. It is also very important that bouncing should not extend into the loop formation region.

Measurement of guard cam-bounce revealed that, under most conditions, there was a loss of contact after initial impact followed by a recontact. Guard-cam bounce could lead to irregular loop formation, and a too higher number of impacts, which consequently could lead to a rapid fatigue situation..Guard-cam bouncc could be largely removed if an energy absorbing material was used for the cam,,or in the cam support construction, and this would act so as to reduce the coefficient of restitution.

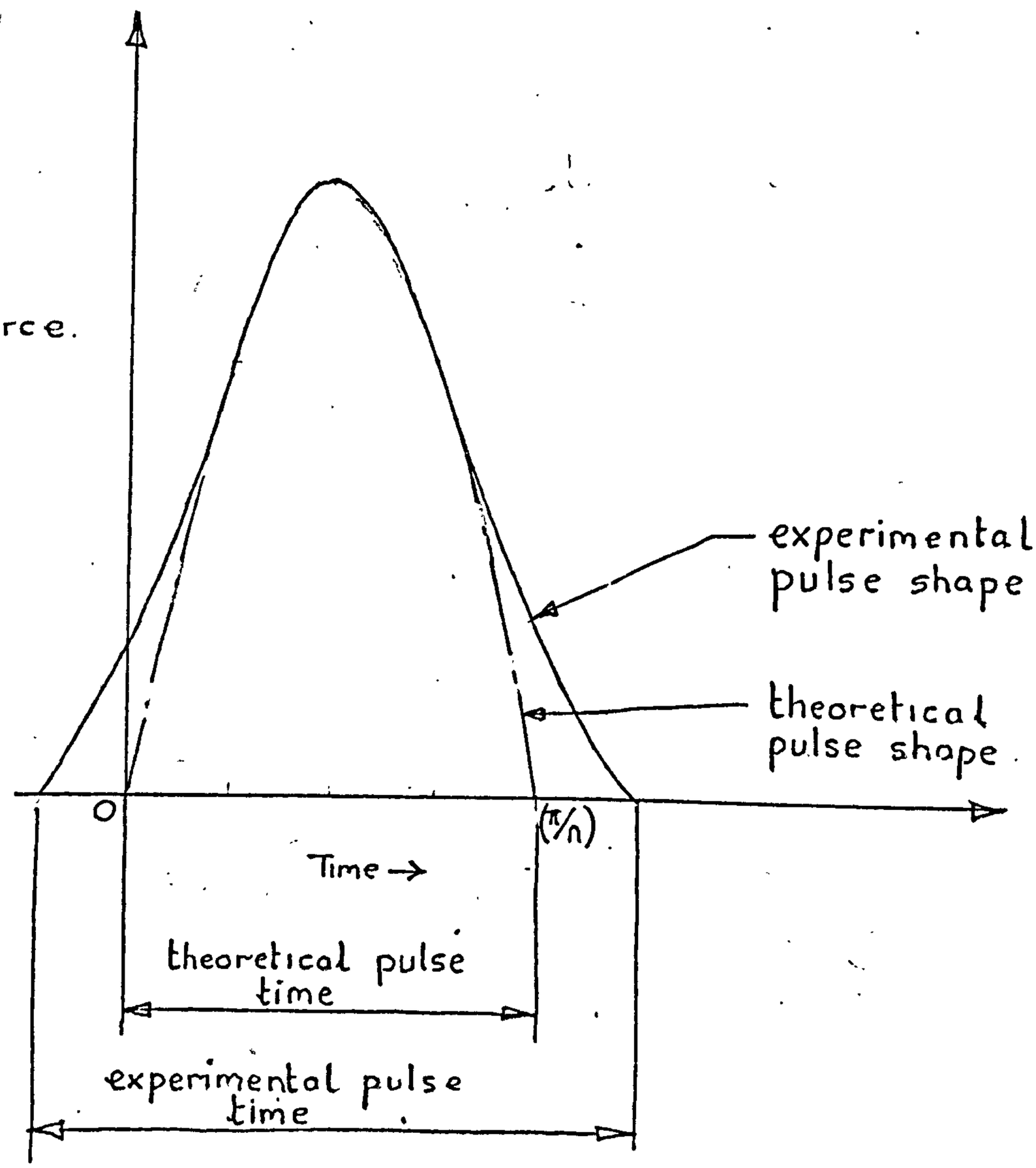

Stitch - Cam Impact pulse shape.

FIG 18.1

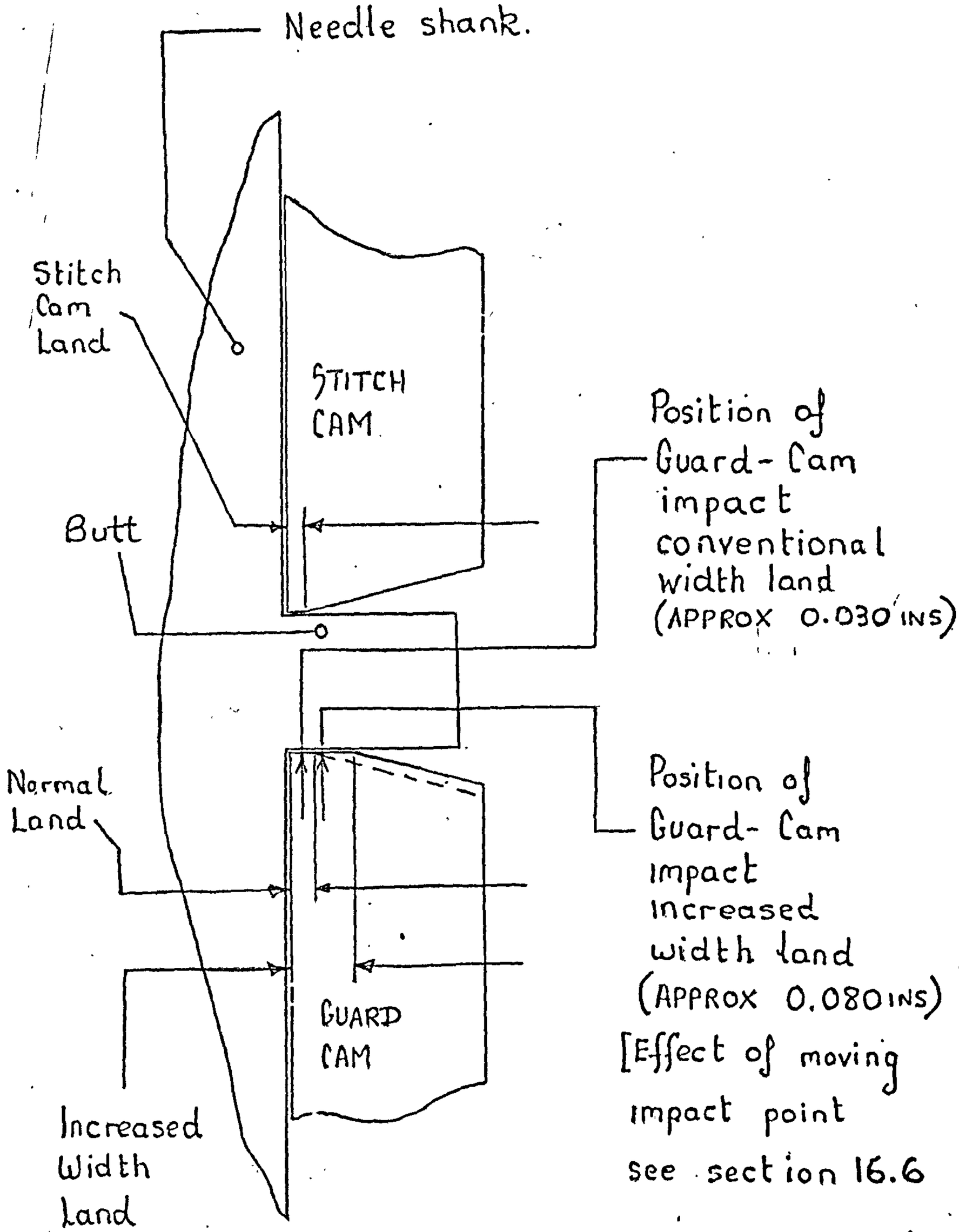

Effect of increased Land-width on Guard-Cam.

FIG 18.2

Section of machine cylinder

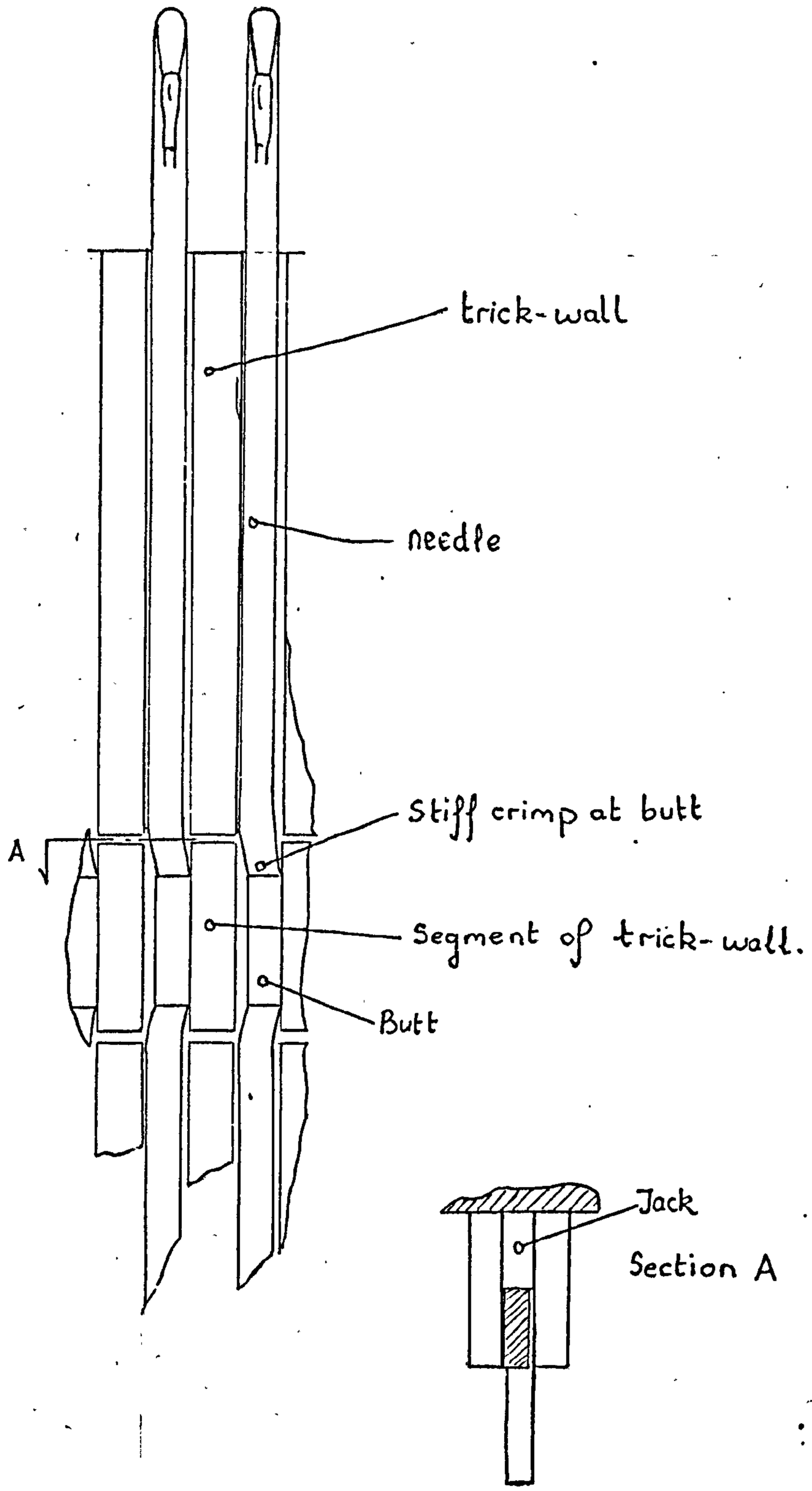

TENTATIVE IDEA FOR REDUCING IMPACT
BY REDUCING TRICK WALL STIFFNESS

FIG 18.3

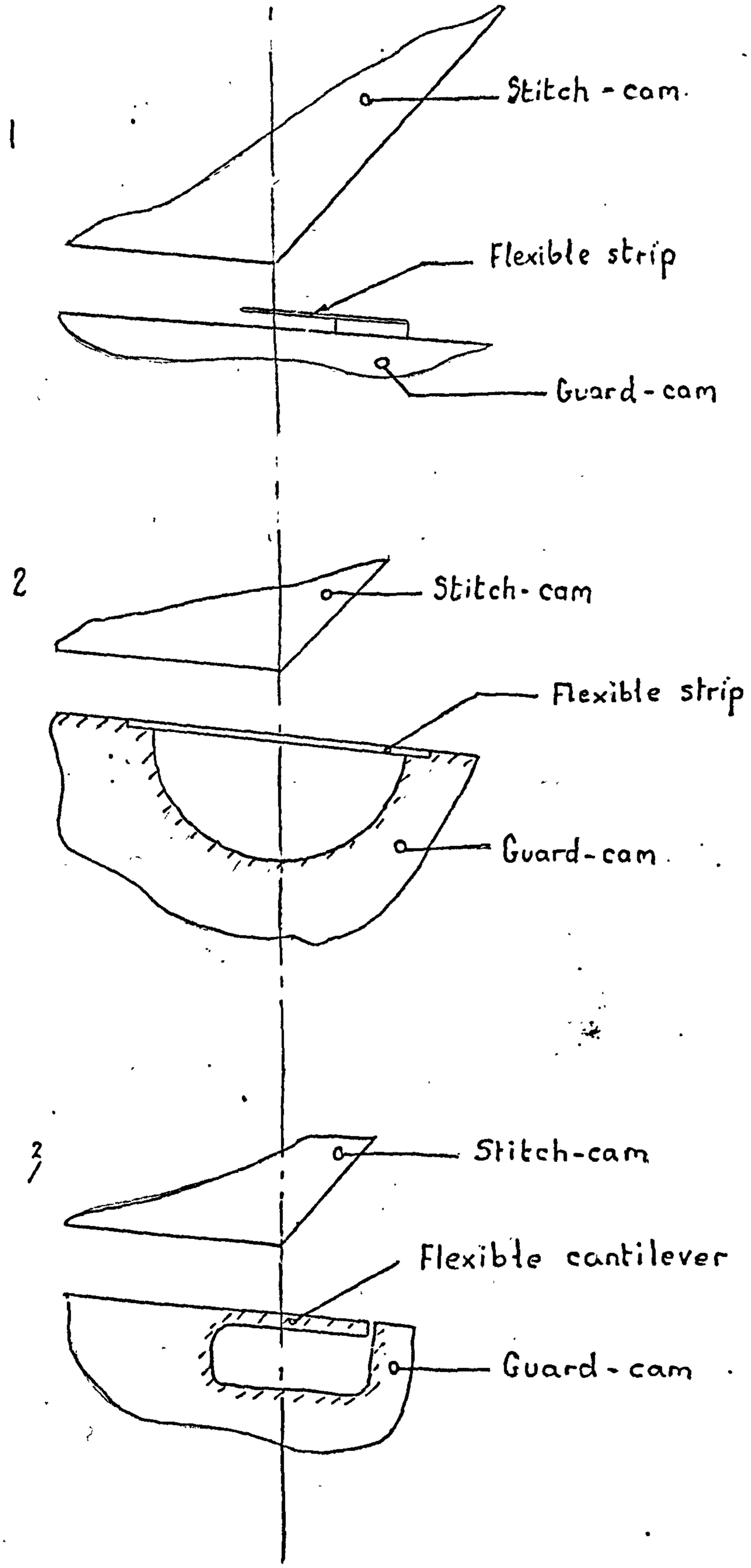

INCREASING CAM FLEXIBILITY AT IMPACT POINT (THREE EXAMPLES)

Fig 18.4

PART E

STRESS-WAVE PROPAGATION IN THE NEEDLE

CHAPTER 19

PRELIMINARY

19.1 Theoretical and Practical Aspects of Stress-Wave Propagation.

When two bodies moving towards each other collide, an impact force exists at the instant of contact. The duration and magnitude of the force depend upon several parameters, such as the masses dimensions, and flexibilities of the impacting bodies. Effects of stress wave propagation, following an impact becomes important, when the applied impact force changes significantly during the time required for the propagation of the wave throughout the system. At the beginning of impact, remote portions remain unstressed while large stresses develop near the point of impact and propagate through the medium at a finite velocity. When the wave reaches a discontinuity, or a free end, or rigidly fixed end, wave reflection occurs. The reflected waves and incident waves all add together and, depending upon their respective phases, very high stresses can result, i.e. much higher than the stress predicted from static loading conditions.

The most common types of waves generated are :-

(i) Longitudinal waves which transmit compressive and tensile stresses. The velocity of propagation of such waves through a medium is given by :-

$$C_L = \left(\frac{E}{\rho}\right)^{1/2} \quad . \quad . \quad . \quad . \quad . \quad (164),$$

where E = youngs modulus of elasticity,

ρ = density of medium.

and C_L = wave speed.

(ii) Torsional waves which transmit shear waves.

The velocity of propagation of such waves through a medium is given by :-

$$C_T = \left(\frac{G}{\rho}\right)^{1/2} \quad \cdots \quad (165)$$

where G = the shear modulus,
ρ = density of medium,
and C_T = wave speed.

(iii) Bending waves such as are encountered in the transverse impact of beams. The velocity of propagation of such waves is very dependent upon the frequency.

A brief description is given below of the most probable type of wave propagated at each of the principal needle-cam impacts, namely, guard-cam impact, latch impact, and stitch-cam impact; this also generally includes impact at tuck and miss height, and, if the cam is non-linearly shaped, impacts at changes of profile.

(i) Stitch-Cam Impact.

The longitudinal wave speed is approximately 20,000 ft/sec, and the time for the wave to travel from the butt up to the top of the needle and back to the butt is approximately 17×10^{-6} seconds. Stitch-cam impact force was approximately of 250×10^{-6} seconds duration, and it was a relatively slow changing pulse, not greatly different from a plane sine wave of frequency 2000 Hs. Since the ratio of the duration of the impact to the period of the fundamental natural frequency is large, it is unlikely that longitudinal waves will be generated by the impact. Similarly, it is also unlikely that shear waves, which have a traverse time of approximately 25×10^{-6} seconds, will be generated by the stitch-cam impact. However, it is likely that the horizontal component of stitch-cam impact will propagate high frequency bending waves. The lower frequency waves, with larger amplitudes would be restricted

by the trick walls.

(ii) Guard-Cam Impact.

The guard cam impact pulse is sharp and has a fast rise time, from zero-force, level to maximum force level, of the order of 5 to 10 x 10^{-6} seconds. It is highly likely that longitudinal stress waves propagate through the medium following this impact. It is also possible that the very rapid deceleration of the needle at guard-cam impact could generate hook bending vibrations, as shown in Fig 19.1 Diagram I. It is unlikely that guard cam impact generates any bending waves, simply because there is very little horizontally applied load to the butt.

(iii) Latch Impact.

The actual duration of the latch impact pulse is unknown. However, it is highly likely that latch impact generates hook bending vibrations, as shown in Fig 19.1 diagram II, and it is also possible, depending upon the pulse time, that the latch impact generates longitudinal stress waves.

19.1.1 Properties of Plane Longitudinal Waves.

At a free end, an incident wave is reflected back as a wave of equal and opposite magnitude, i.e. an incident compressive wave is reflected back as a tensile wave.

When an incident plane wave reaches a perfectly rigid, fixed end, the wave is reflected without change in sign or magnitude.

When an incident longitudinal plane-wave, σ_I , passes through a discontinuity in a medium, either as a result of a change of material, or geometry, there will arise a reflected wave, σ_R , and a transmitted wave, σ_T . The equations relating the magnitudes of the waves are as follows :-

$$\frac{\sigma_T}{\sigma_I} = \frac{2A_1\rho_2 c_2}{A_1\rho_1 c_1 + A_2\rho_2 c_2} \quad \cdots \quad (166),$$

and

$$\frac{\sigma_R}{\sigma_I} = \frac{A_2\rho_2 c_2 - A_1\rho_1 c_1}{A_2\rho_2 c_2 + A_1\rho_1 c_1} \quad \cdots \quad (167),$$

where all the terms in equations (166) and (167) are defined in Fig 19.2.

Davids and Kesti[40] have shown that a gradual reduction in area (such as a tapered section) can result in stress magnifications higher than that experienced during wave contact with a step reduction in area. They derived an equation of the form :-

$$\frac{\sigma_T}{\sigma_I} = \left(\frac{A_1}{A_2}\right)^{1/2}, \quad \text{for } c_1 = c_2, \text{ and } \rho_1 = \rho_2, \quad \cdots \quad (168).$$

The terms in equation (168) are defined in Fig 19.2.

19.1.2 Wave Attenuation.

The wedge and square cut-out shown in Fig 19.3 can be used to reduce the amplitude of a wave propagated through a medium which contains the cut-out. Referring to Fig 19.2 diagram I, when an incident wave contacts a sudden change of section, the magnitude of the transmitted wave is controlled by equation (166). If, for this particular example, the incident wave propagating through a medium of cross-sectional area A_1 suddenly contacts a discontinuity of area A_2 :-

then

$$\frac{\sigma_2}{\sigma_1} = \frac{2A_1}{A_1 + A_2} \quad \cdots \quad (169)$$

where σ_2 = the magnitude of the transmitted wave from the discontinuity,

and σ_1 = the magnitude of the incident wave at the discontinuity.

if the area A_2 is gradually opened out to an area A_3 ,

as shown in diagram I Fig 19.3.

then

$$\frac{\sigma_3}{\sigma_2} = \left(\frac{A_2}{A_3}\right)^{1/2} \quad . \quad . \quad . \quad . \quad (170),$$

where σ_3 = the magnitude of the transmitted wave from area A_3,

and σ_2 = the magnitude of the incident wave at area A_3.

From equation (169) and (170),

$$\frac{\sigma_3}{\sigma_1} = \frac{2A_1}{A_1+A_2}\left(\frac{A_2}{A_3}\right)^{1/2} \quad . \quad . \quad . \quad (171).$$

For the example shown in Fig 19.3 diagram I :-

if $A_1 = 2A_2 = A_3$,

then $\frac{\sigma_3}{\sigma_1} = \frac{4}{3}\left(\frac{1}{2}\right)^{1/2} = 0.94.$

Using the same method as above, the equation for the square cut-out has the form :-

$$\frac{\sigma_3}{\sigma_1} = \frac{2A_1}{A_1+A_2}\left(\frac{2A_2}{A_2+A_3}\right) \quad . \quad . \quad (172).$$

For the example shown in Fig 19.3 diagram II :

if $A_1 \doteq 2A_2 \doteq A_3$,

then $\frac{\sigma_3}{\sigma_1} = \frac{4}{3}\left(\frac{2}{3}\right) = 0.89.$

If six wedge cut outs were positioned on the needle shank, as shown in diagram III Fig 19.3:-

then $\frac{\sigma_T}{\sigma_I} = 0.94^6 = 0.69,$

where σ_T = the transmitted wave from the six wedge cut outs,

and σ_I = the incident wave on the six wedge cut outs.

If six square cut outs are positioned as shown in diagram IV Fig 19.3:

$$\text{then } \frac{\sigma_T}{\sigma_I} = 0.89^6 = 0.496.$$

The disadvantage of the wedge and square sections is the increased risk of fracture at the sharp corners due to high stress concentrations; a small radius should be provided at the corner to reduce this risk.

19.1.3 Summary of the important conclusions contained in Petrow's work.

An introductory summary of the work carried out by J.I. and E.I. Petrow[33 to 27 inc] is contained in chapter 2 (section 2.1.4). A list of some of the important results and conclusions contained in the papers is summarised below :-

(i) Theoretical considerations showed that the needle hook was destroyed by a strain wave that originated at the impact of the needle butt with the cams.

(ii) The theory is specifically concerned with the tapered sections of the needle. Neglecting dispersion the prismatic parts of the needle do not change the amplitudes and the shape of the impact impulses.

(iii) A certain time after the initial propagation of the impact wave, the load sign at a particular needle cross-section will reverse, i.e. a compressive pulse changes to a tensile pulse.

(iv) As the impact wave advances towards the top of a conical section, the pressure zone narrows and a stress-strain wake remains. The stress is greater in the wake of the impact wave, and can exceed the ultimate strength of the material.

(v) In every wedge-shaped part of the needle, the

load from the impact wave increases and the duration shortens.

(vi) Petrow calculated that the most dangerous cross-section of the needle was just at the beginning of the hook bend. At this position, there are repeated alternating high-intensity stress waves due to the load sign reversal.

(vii) The number of hook breakages not only depends upon the speed, but also depends upon the number of cam impacts.

19.2 Characteristics of Needle Failure at High Machine Speed.

Before embarking upon detailed measurements of the wave process, it was essential that the important characteristics of needle breakage should be examined.

The knitting machine was set-up in a manner suitable for guard-cam impact experiments, i.e. with the special lead-in, and raising cams fitted, and with the majority of the needles in the cylinder removed, as was described in detail in section 15.3.

Thirty needles were placed in adjacent tricks; the majority of the needles were of standard 0.443 mm thickness, and the remainder were 0.406 mm thick. Most of the thinner needles were very free, and it took only a small force to raise and lower the needles vertically in the tricks. However, some of the needles were very tight and it took considerable force to move them. Throughout the experiments, the machine was run at 450 ft/min (2.29 m/sec), the stitch cam angle was 50^{o}, the guard cam angle 8^{o}, the cam-cylinder clearance equal to 0.006 in. (0.15 mm). After every 1,000 revolutions the machine was stopped and fractured needles were removed; the location of the fracture, and the conditions under which the particular fractured needle was running in the trick, were carefully noted. Another needle was then inserted in the

trick, and the machine was re-run for another 1,000 revolutions before being examined.

19.2.1 Experimental Results.

The results are summarised below :-

(i) None of the 0.443 mm standard needles broke at the hooks, even after several thousand revolutions. However, when the hook thickness for a group of these needles was reduced to 0.006 in. as shown in Fig 19.4, hook fracture occurred frequently. The hook breakage rate was nearly in direct proportion to the resistance to needle motion in the trick. The needles which were very free broke after only a few hundred rvolutions, while the needles that were tight did not fracture at the hook until many thousands of revolutions were completed, and some did not fracture at all.

(ii) The free 0.406 mm needles fractured at the hook bend after only a few hundred revolutions. If a broken needle was replaced by a similar needle then in general, this needle also fractured at the hook after a few hundred revolutions.

(iii) The butts of the 0.443 mm needles, that were tight in their tricks broke frequently. When the machine was stopped, the butt fracture on a particular needle was sometimes caught in a transition stage, i.e. before it had completely seperated from the shank; it then showed a characteristic bending at the top, as shown in Fig 11.2. Often the butts of needles that were free in their tricks failed at high speed; however, this time the transition stage showed that fracture originated from the base of the butt; this particular form of failure was reduced when a light smear of oil was applied to the surfaces of the guard, stitch and raising cams. Before the oil was applied, the

bounce detector was switched on, a particular needle that was free in its trick was selected for a test, and approximately ten needles on each side of it were removed from their tricks. The bounce trace of the test needle as it passed along the guard-cam is shown in diagram I of Fig 19.5. Similarly, the trace of a tighter, but otherwise similar, needle is shown in diagram II. The traces clearly show the excessive amount of "chatter", as the free needle passed along the surface of the guard cam. A light smear of oil was then applied to the cam surfaces, and the free needle was re-run and bounce traces again recorded. Although diagram III of Fig 19.5 shows that there was still an excessive amount of chatter on the guard-cam surface ; the oil certainly reduced the number of the fractures which initially started at the bottom of the butt, but it had little effect upon the number of fractures which initially started at the top of the butt.

(iv) The breakage rate was very sensitive to changes in the cross-sectional area of the needle hook and it appeared that failure occurred slightly more readily if the depth rather than the width was reduced, as shown in diagram I Fig 19.6. The method of reducing the thickness of the needle hook was carefully controlled so as to avoid any stress concentrations that could act as crack starters; this is shown in diagram II Fig 19.6. If the cross-sectional area of any particular part of the needle shank was reduced to approximately the same area as a standard needle hook then fracture occurred quite frequently across the reduced section.

(v) Several shaped needles were produced, and these are shown in Fig 19.7. The needle shown in diagram I had a sharp termination near the hook and, during the high speed

tests of a sample of these needles it was found that, instead of breaking at the hook bend, they tended to break across the section A-A . The failure rate was approximately the same as the hook failure rate of similar standard needles. The hooks of a group of needles were removed as shown in diagram II of Fig 19.7, and, just below the position of fracture, a fine cut-out was made in the shank; care was taken to see that the cut-out was carefully polished to remove scratches that could possibly act as stress raisers. During subsequent tests, fracture occurred across the cut-out at approximately the same rate as hook failure of standard needles in the same tricks. Many tests were made with a range of needle shapes with cut-outs at various positions, these being indicated in diagrams III to V Fig 19.7. Sometimes failure still occurred at the hook, but generally the needle fractured across the shank at the position of the cut-out.

(vi) A needle was modified by cutting seven wedges in the shank. The position of the wedges is shown in diagram VI Fig 19.7 and, according to the theory derived in section 19.1.2, the reduction of amplitude through the wedges is governed by the equation :-

$$\frac{\sigma_T}{\sigma_I} = 0.94^7 = 0.646,$$

where σ_T = the magnitude of the wave transmitted to the needle head,

and σ_I = the magnitude of the incident wave propagated up the shank.

There were no hook breakages during the high speed tests but the shanks of the needles fractured several times at section B-B in diagram VI Fig 19.7. The breakage rate, for fractures across the shank, was approximately the same as the rate of hook breakages when 0.443 mm standard needles were

inserted in the same tricks. However, this experiment did not prove that needles with wedge cut-outs are incapable of reducing hook failure by reducing the transmitted wave amplitude; it only proved that the wedges need to be very carefully designed to avoid stress concentration at the corners.

(vii) The guard-cam was removed, so that the needles only impacted the stitch-cam. During a test involving several thousand machine revolutions, none of the free needles either broke at the butt or the hook. However there was considerable butt damage to the needles that were tight in their tricks. As soon as the guard-cam was refitted, the free needles showed signs of hook and butt damage.

(viii) Sometimes when needles were fitted in a particular trick, hook failure occurred very frequently, even though the needle in question did not appear to be particularly free in the trick. There were often many similar needles in adjacent tricks that were very free by comparison, but these did not fracture at anything near the same rate. The stitch-cam impact transducer, using the special attachment for guard cam impact measurements, was connected into the circuitry and switched on. The method of using the instrument to obtain traces was the same as that detailed in section 14.2. The vertical and horizontal component of guard-cam impact was measured for each of the needles in turn and in all approximately thirty traces were obtained. Without exception, the frequency of hook fracture showed a direct relationship to the magnitude of guard-cam impact. Samples of the traces obtained are shown in Fig 19.8, and the type of needle fitted in the trick and the number of machine revolutions to fracture.

are shown next to each diagram. The needle-trick combination with the highest rate of hook failures corresponded to the largest impact magnitude, and the second highest rate to the second largest magnitude impact, and so on, until the needle-trick combination with the minimum fracture rate was seen to correspond to the minimum impact.

(ix) Throughout the tests, the majority of the fractures occurred at the hook and butt, but sometimes fractures occurred at a point below the latch pivot, as shown in Fig 11.2. When all the needles that had fractured at this position were compared, it was observed that the fracture surface, and position of the fracture, were almost identical for every needle. A microscopic examination showed that the cross-sectional area of the needle at this fracture surface was scarcely different from the area of the needle at the hook bend, where the majority of fractures occurred. It was also noted that the hook bend, and the fracture position below the pivot, were each points of minimum cross-sectional area on the shank of the needle. During high-speed knitting, it is unlikely that fracture would occur below the latch pivot, because the yarn tension acting upon the hook would impose a bending stress on the hook in addition to the stress transmitted by the wave process; this would make the hook bend a far more likely position of failure.

19.3 Conclusions.

Throughout the experiments detailed in section 9.2.1 the three most common positions of needle breakage were at the butt, at the hook, and just below the latch pivot. Evidence concerning the mechanism of fracture, as obtained from the experiments, is briefly summarised as follows :-

(i) Breakage of the butt, with the fracture initially

originating from the top of the butt; this form of fracture occurred in needles that were tight in their tricks, and from the results (vii) of section 19.2.1, was due to stitch cam impact.

(ii) Breakage of the butt, with the fracture initially originating from the bottom of the butt; this form of fracture occurred in needles that were free in their tricks. The results of the experiments, particularly those detailed in (ii) and (vii) of section 19.2.1 indicates that this form of fracture was probably caused by either guard-cam impact, or high-frequency chatter on the guard and raising cams.

(iii) Breakage of the head occurred in needles that were free in their tricks. The breakage rate was very sensitive to the cross-section area of the hook; if the area was reduced slightly, the incidence of fracture increased appreciably. The results of the experiments, and particularly those detailed in (i), (iv) and (vii) of section 19.2.1, indicate that the most likely cause of fracture is the guard-cam impact, and those detailed in part (v) section 19.2.1, proved that the incidence of fracture was directly related to the magnitude of the guard-cam impact. During the knitting process, it is probable that the destructive stress acting upon the hook is a combination of the high magnitude impact stress and a bending stress imposed by the yarn.

(iv) The experiments gave no clear indication concerning the reasons for the breakage of the needle shank at a position approximately 1 mm below the latch pivot, except that it appeared to be caused by the same mechanism as hook breakage. It was also noticeable that the area of the hook and shank breakage was a minimum in each case. Hook

destruction could be caused either by the plane transmission of a stress pulse along the needle shank, or by an unfavourable combination of reflected and incident waves whose respective phases are such that, when the wave intensities are added together, very high stress magnitudes result. The evidence of the experiments detailed in section 19.2.1 (v) and (vi), pointed towards the plane transmission of a high magnitude stress pulse as being responsible for failure rather than an addition of waves. The evidence is briefly summarised below :-

(i) Needle fracture occurred wherever the area of the needle was reduced to a cross-section comparable to the hook.

(ii) The breakage rate was dependent completely upon impact magnitude, and was not very sensitive to changes in the needle geometry.

(iii) When a small reduction of area was made just below the original hook fracture, the needle, during subsequent tests, fractured at the reduced area.

The needle modified with wedge sections did not reduce the number of fractures, but the majority of the breakages occurred across the stress concentration at the base of the wedge.

The machine could not be run for sufficient time to test for fatigue. However, it was noted that the tighter the needle in the trick, the longer the time to hook failure, and most of the very tight needles failed at the butt before there was any discernable head damage.

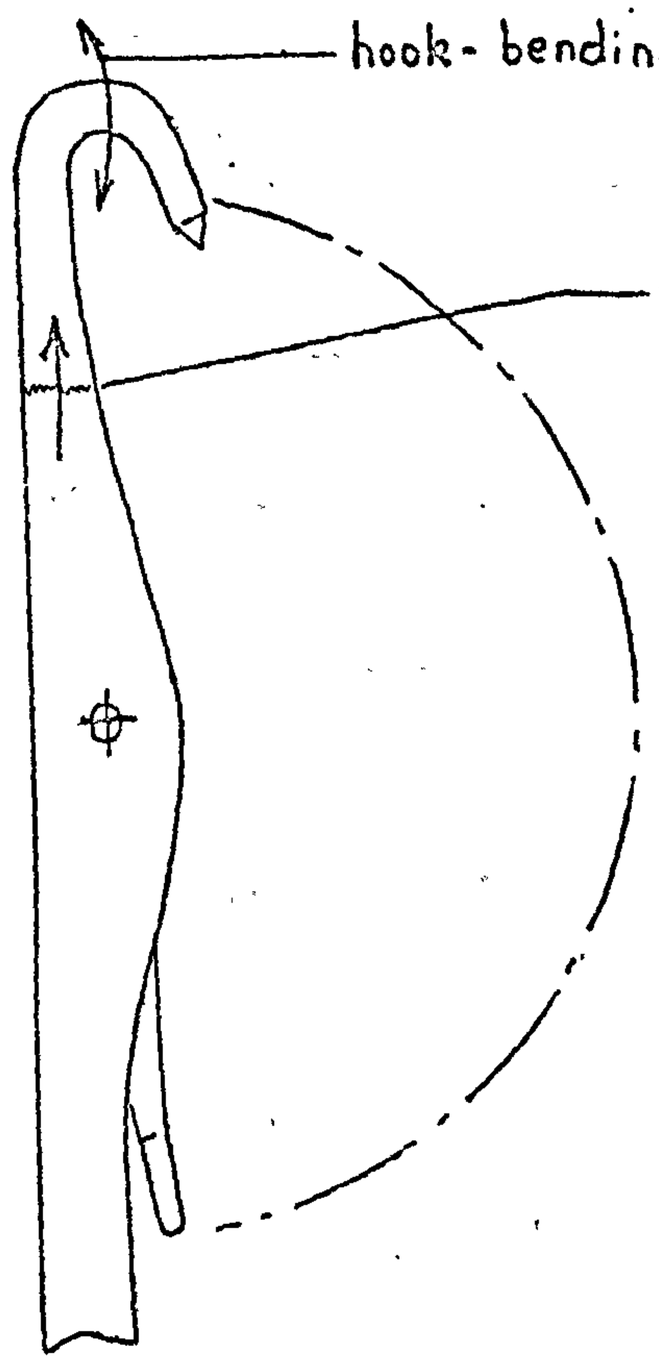

Diagram I

Instant of time after guard-cam impact.

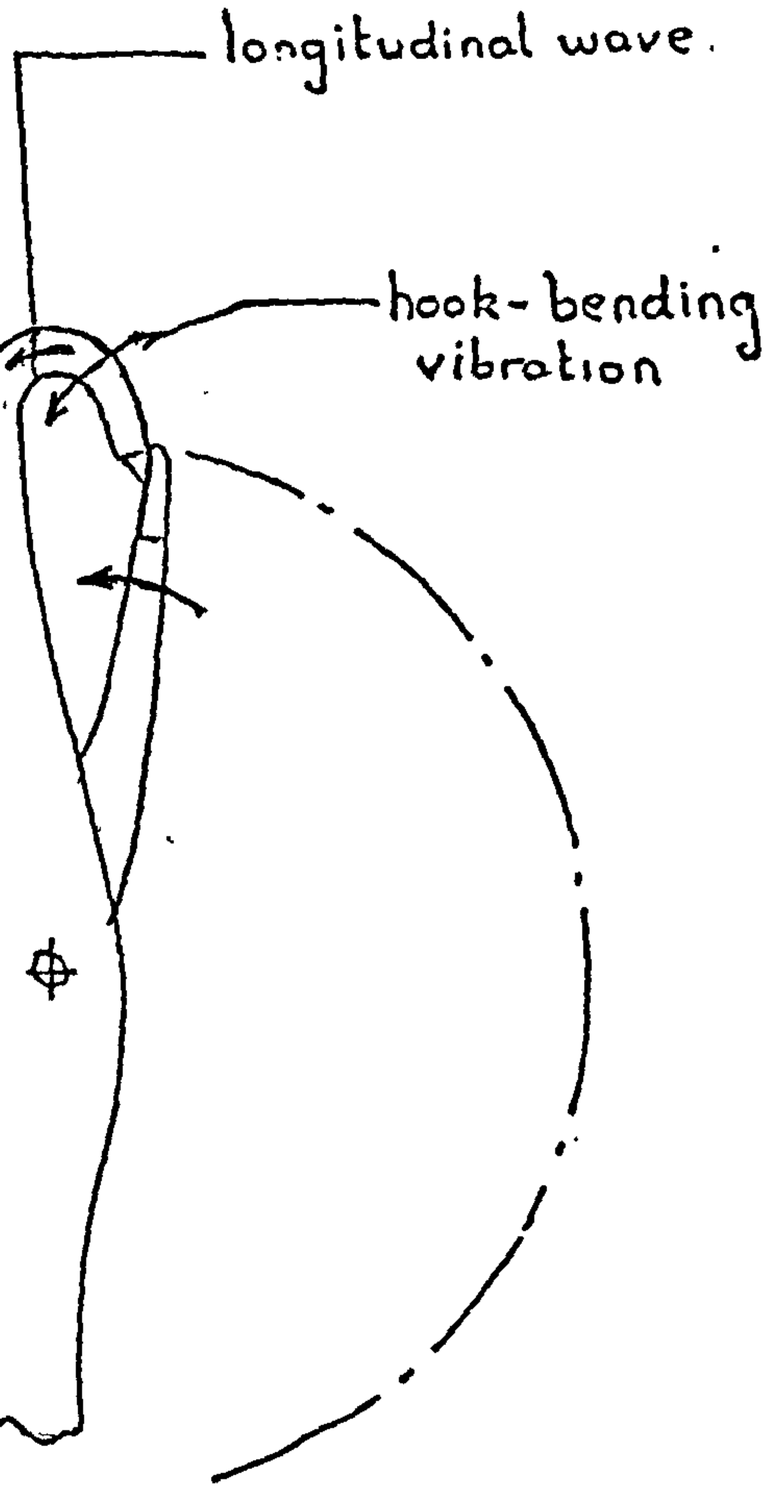

Diagram II

Instant of time after latch impact

STRESSES RESULTING FROM GUARD-CAM AND LATCH IMPACT

Fig 19.1

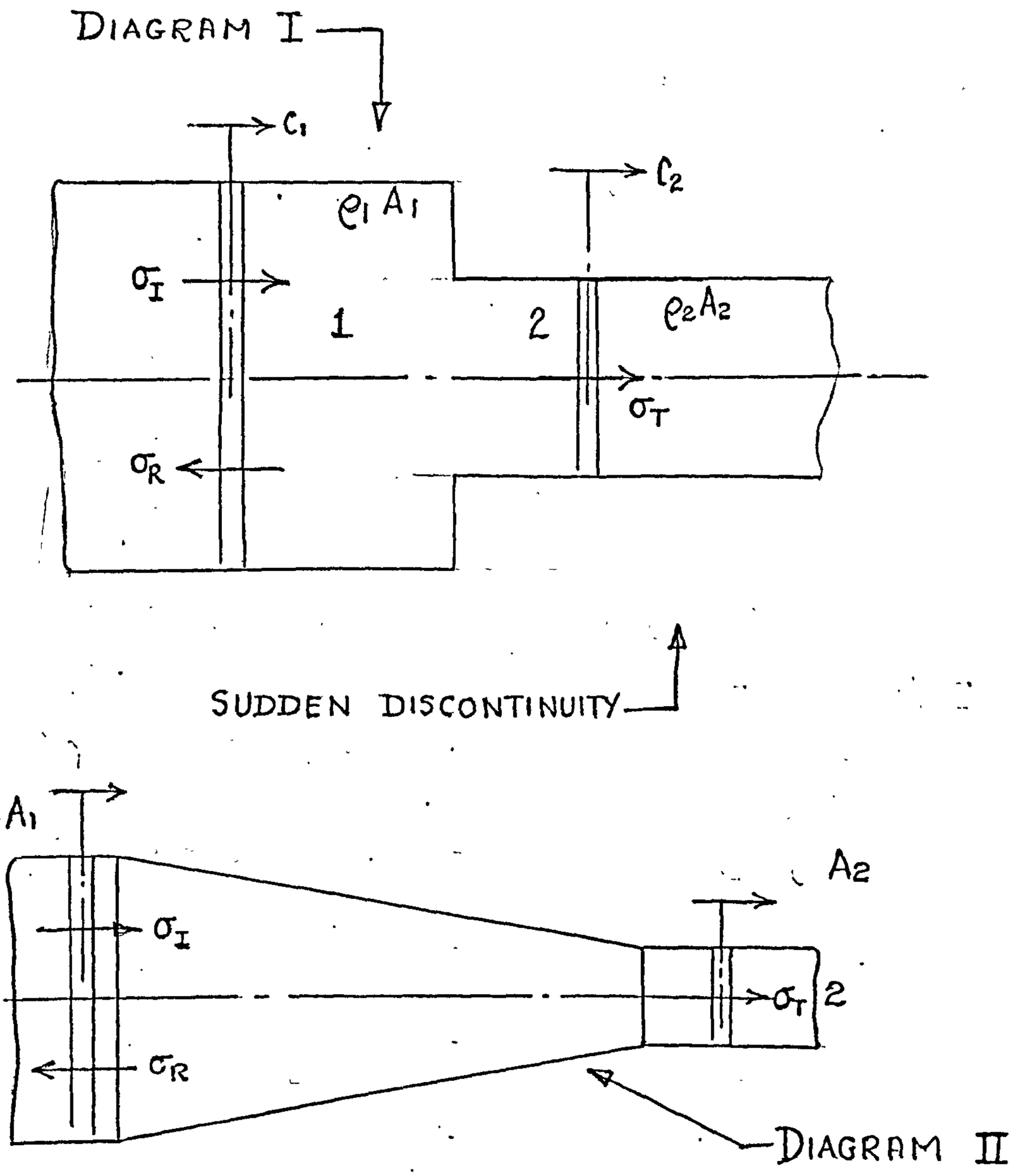

GRADUAL REDUCTION IN AREA

A_1	Area section 1	σ_I	Incident stress-wave
A_2	Area section 2	σ_T	Transmitted stress wave
ρ_1	Density section 1	σ_R	Reflected stress wave
ρ_2	Density section 2		
c_1	Wave speed section 1		
c_2	Wave speed section 2		

PROPERTIES OF PLANE WAVES

FIG. 19.2

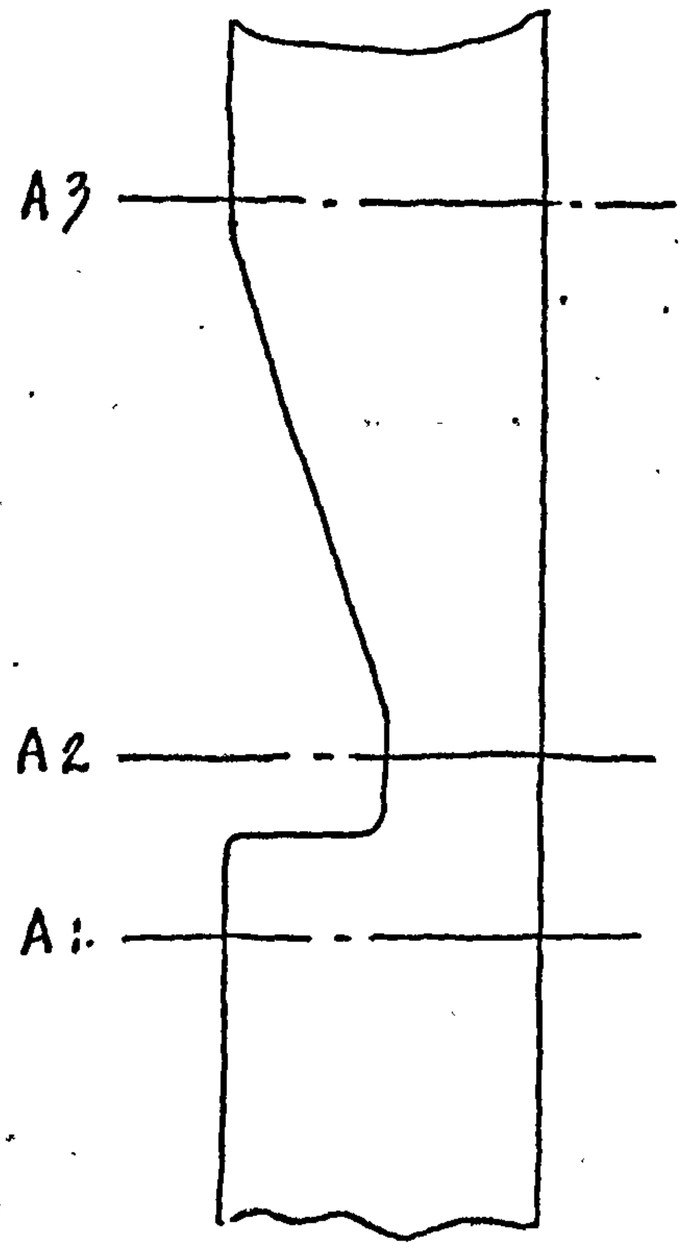

Wedge section
Diagram I

$\frac{\sigma_3}{\sigma} = 0.94$

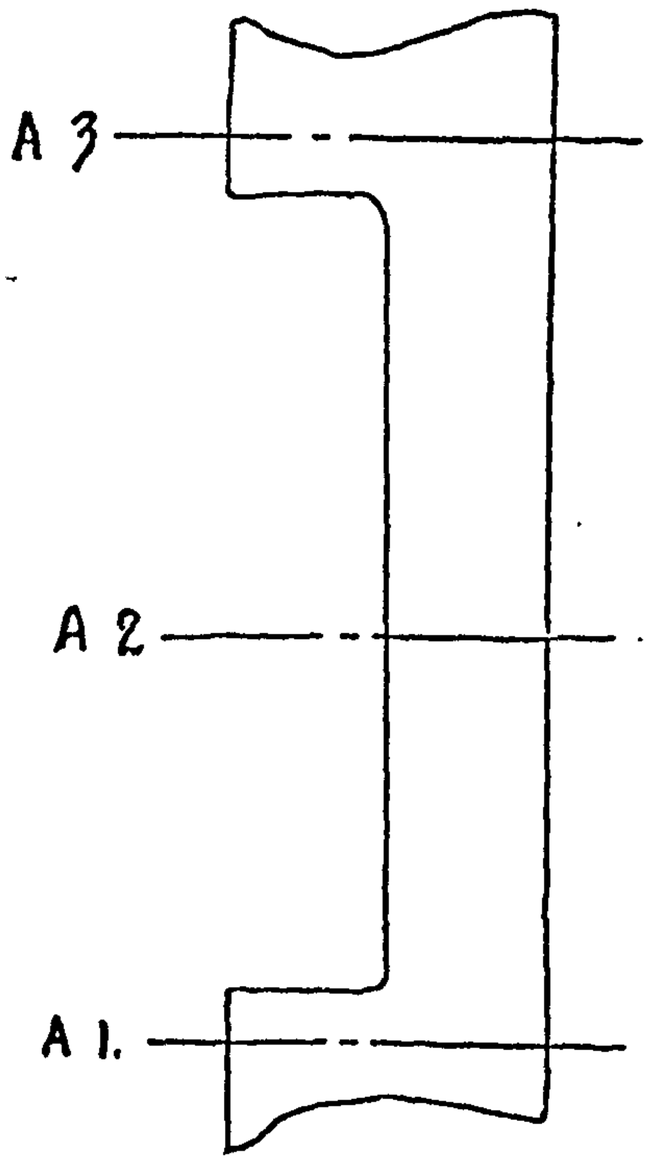

Square section
Diagram II

$\frac{\sigma_3}{\sigma} = 0.89.$

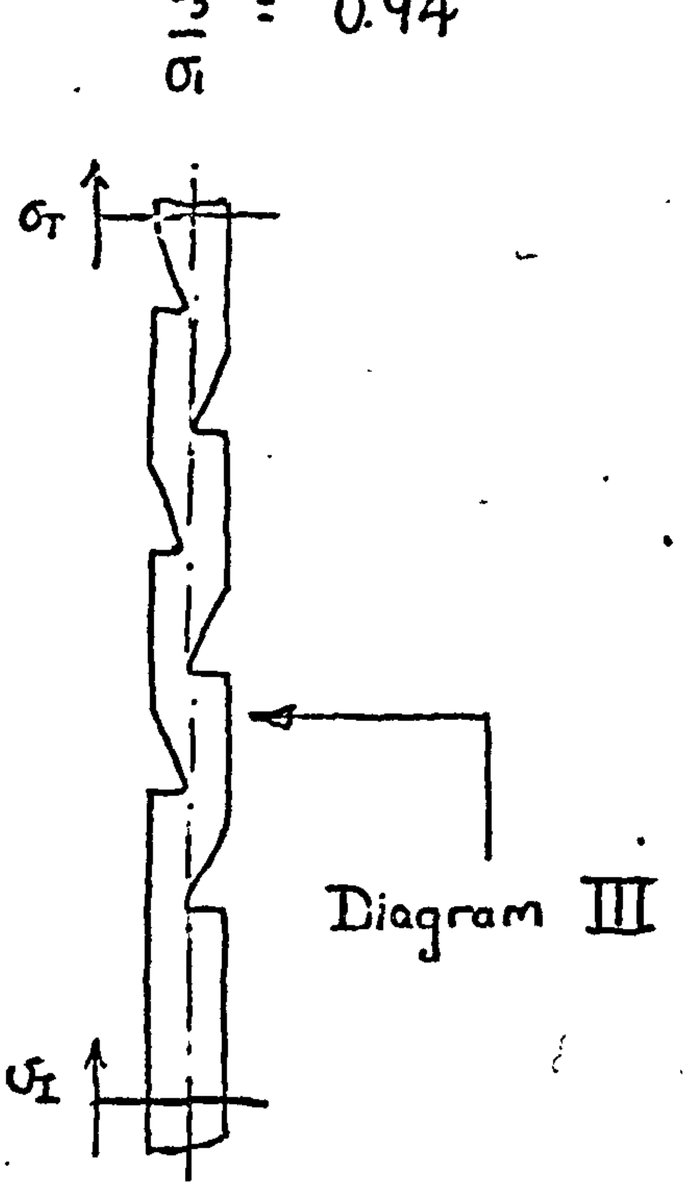

6 wedge cut-outs

$\frac{\sigma_T}{\sigma_I} = 0.69.$

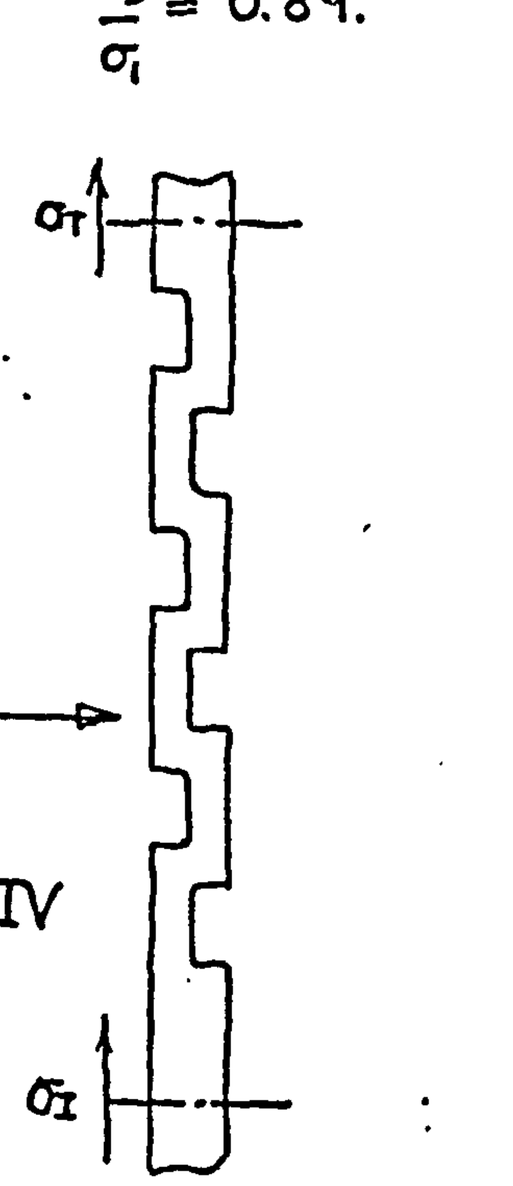

6 square cut-outs

$\frac{\sigma_T}{\sigma_I} = 0.496$

WEDGE AND SQUARE CUT OUTS.

Fig 19.3

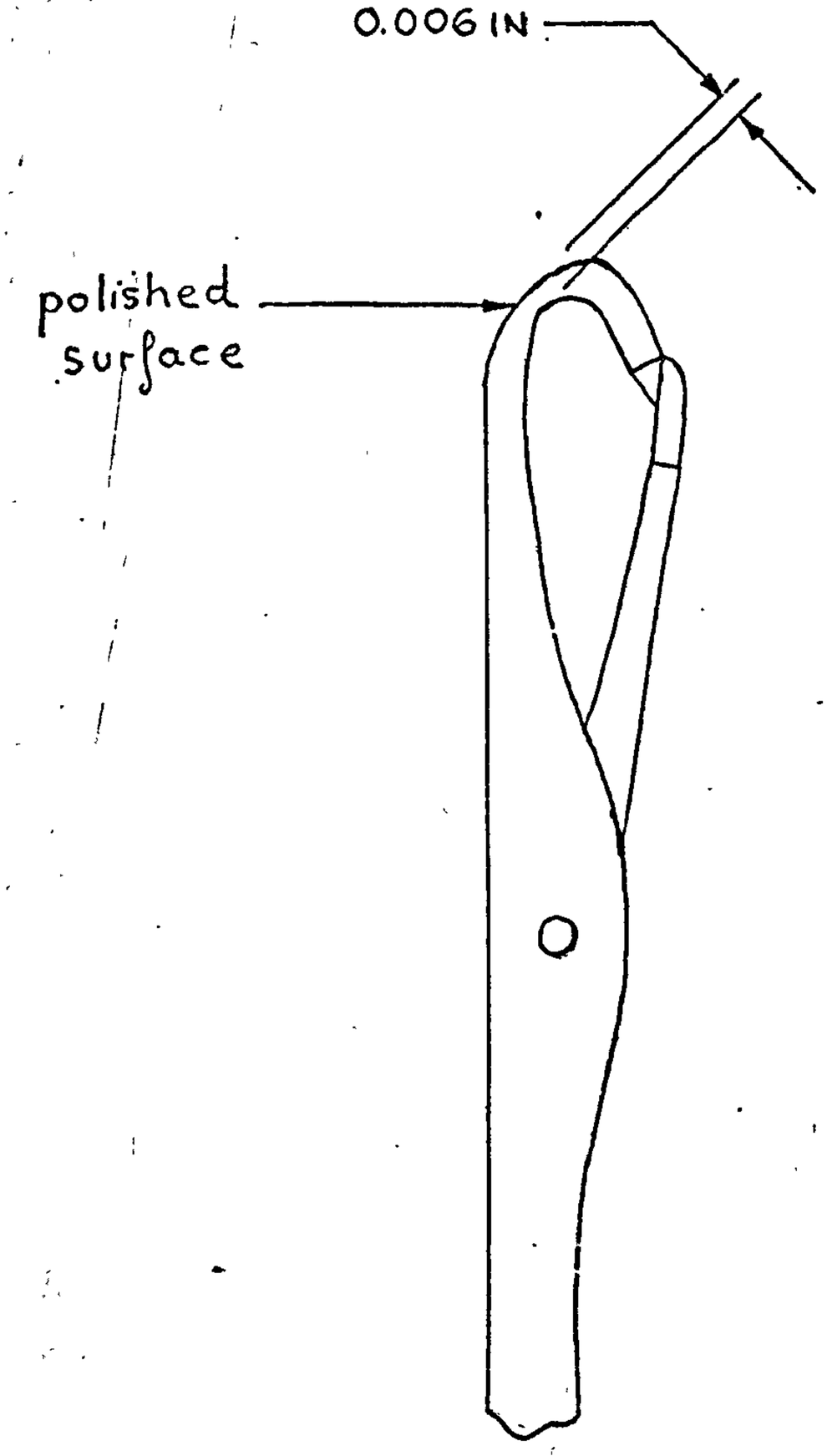

NEEDLE HEAD

0·443 mm NEEDLE HOOK WIDTH REDUCED TO 0.006 IN.

FIG 19.4.

DIAGRAM I
No oil free
needle

No Contact ————————

Contact ————————

Approx 200 ft/min
500 secs/div

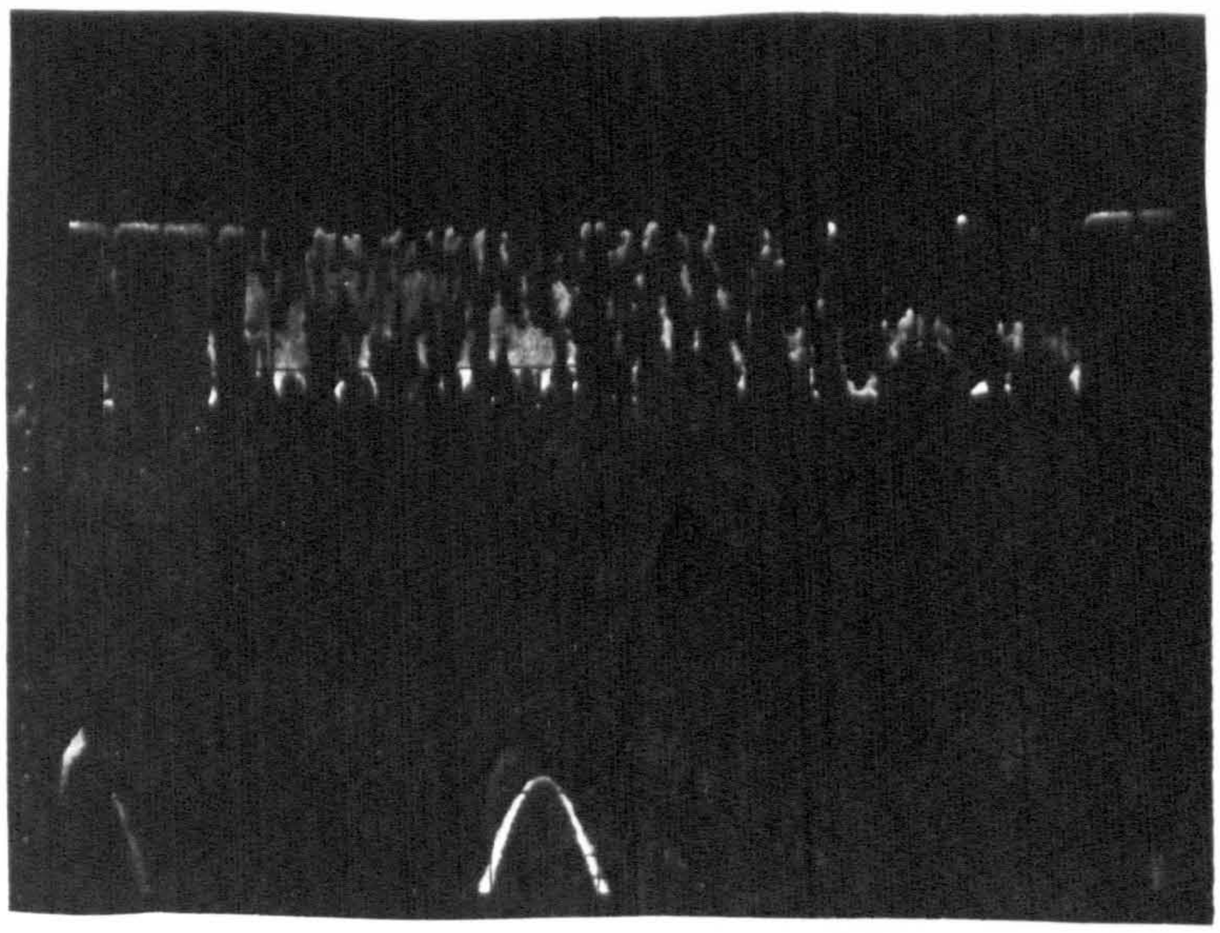

DIAGRAM II
Tighter needle
No oil
No Contact ————————

Contact ————————

Approx 200 ft/min
200 secs/div

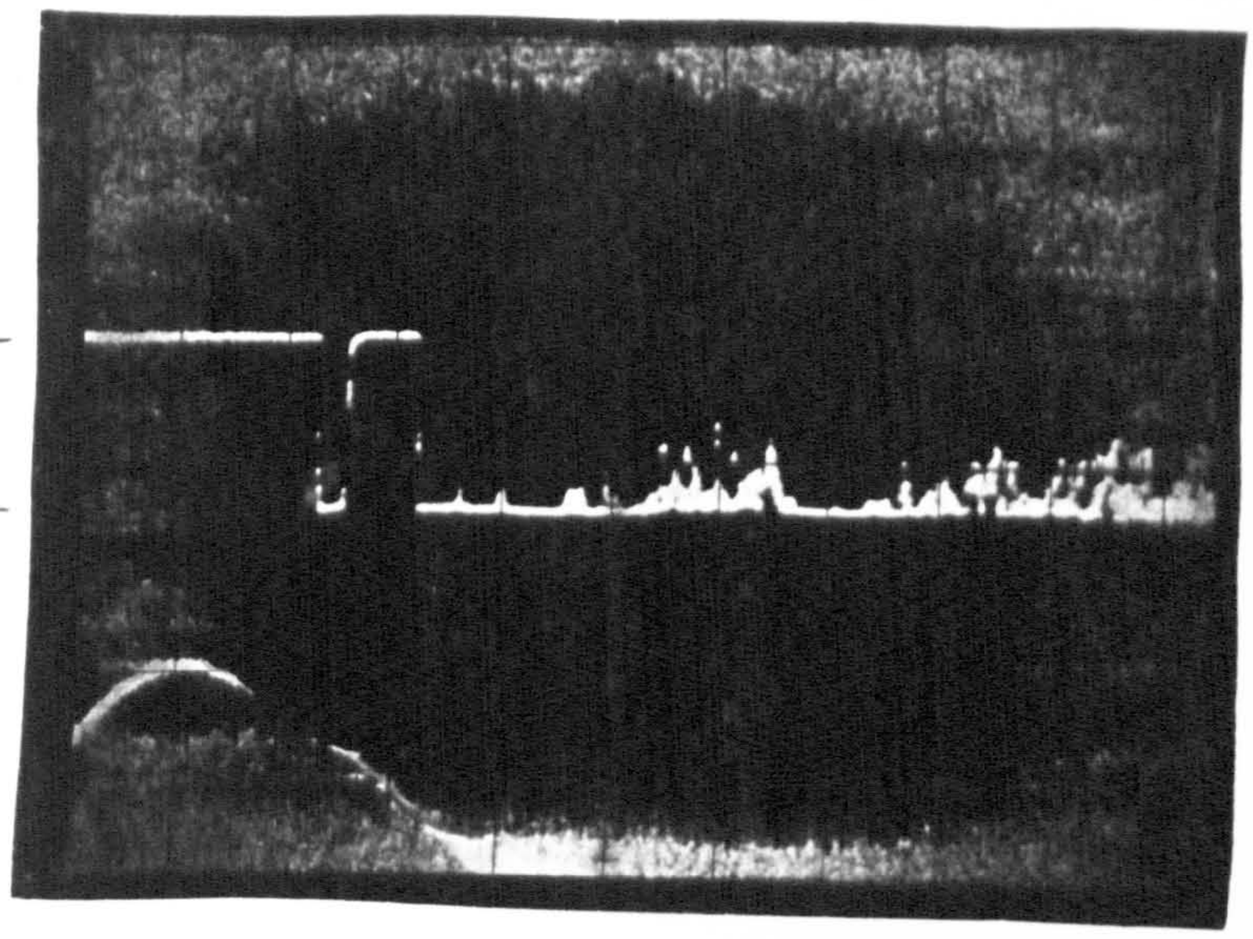

DIAGRAM III
Light oil
Free needle

No Contact ————————

Contact ————————

Approx 200 ft/min
500 secs/div

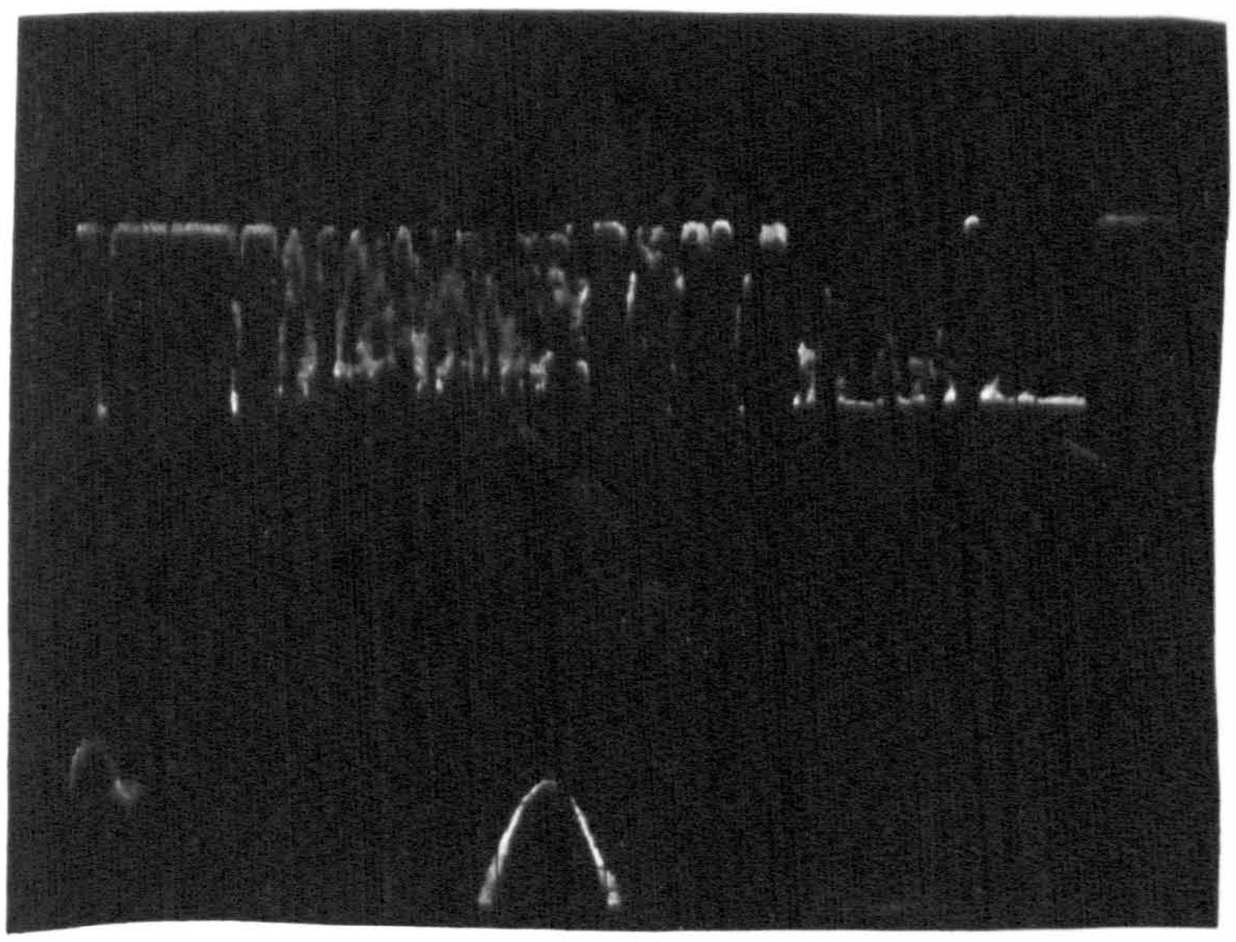

NEEDLE BOUNCE ON GUARD CAM

Fig 19.5

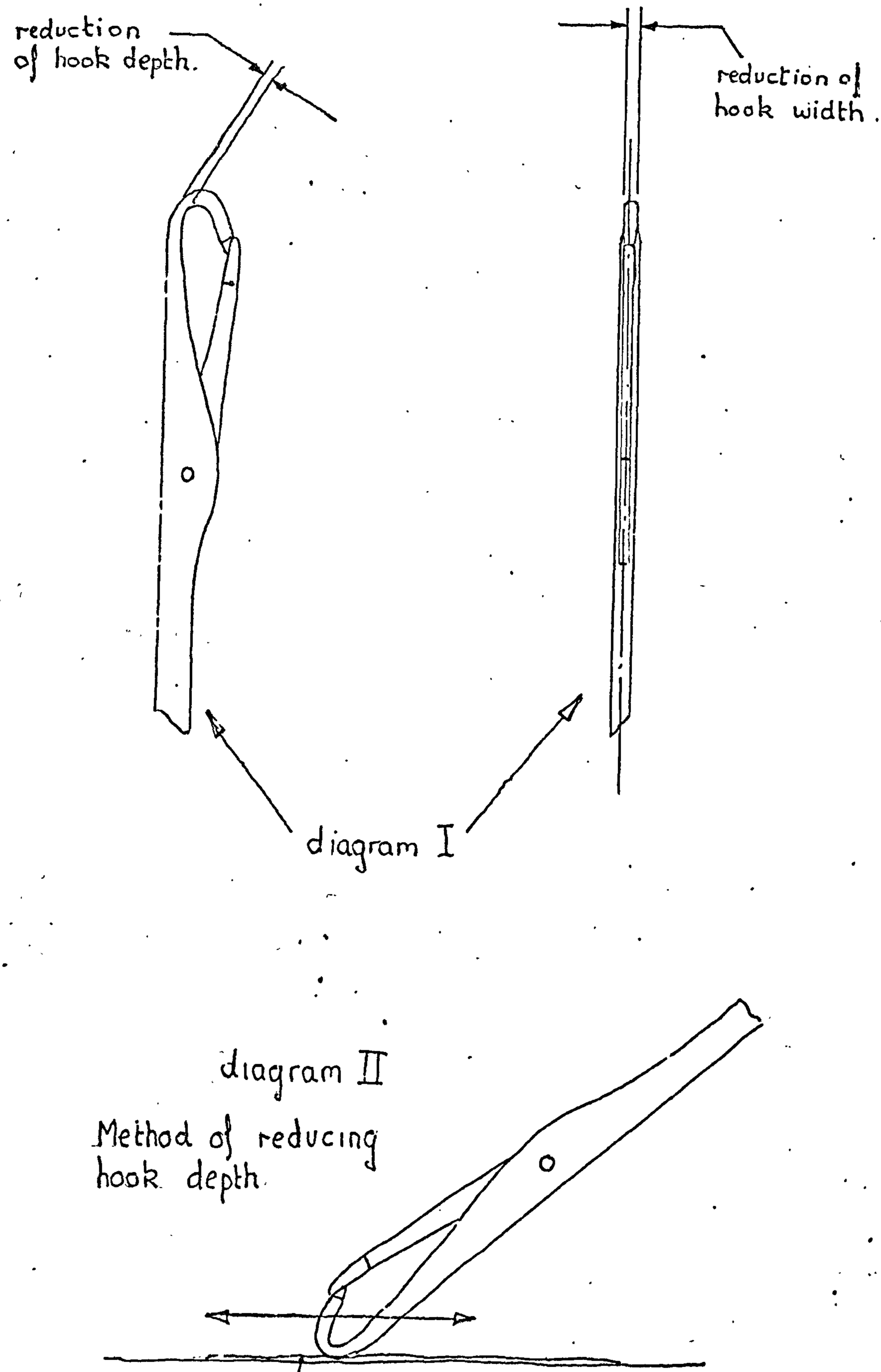

REDUCTION OF HOOK DEPTH AND WIDTH
(SEE SECTION 19.2.1 (iv))

FIG 19.6

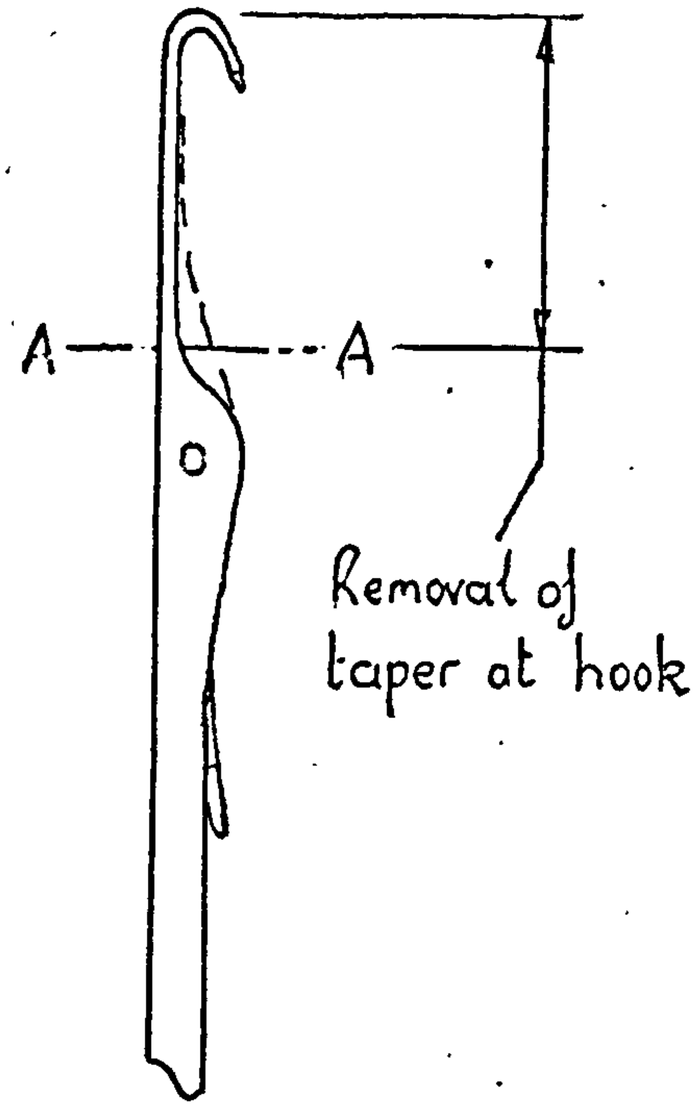

diagram I

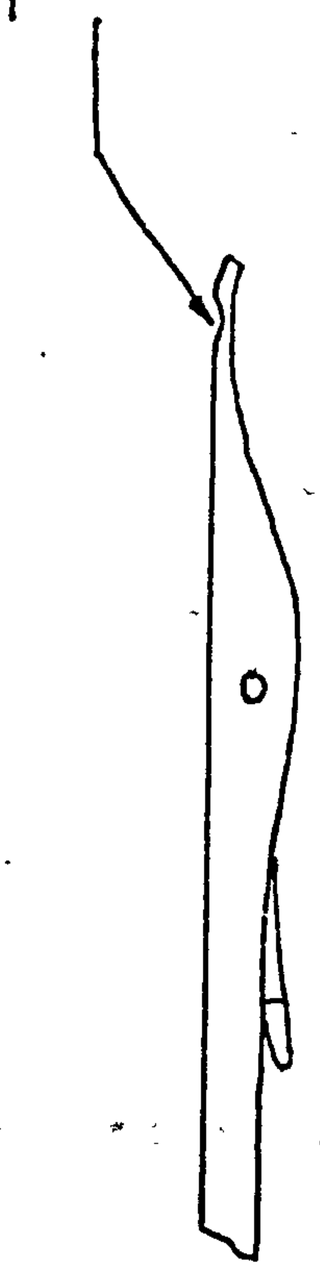

diagram II

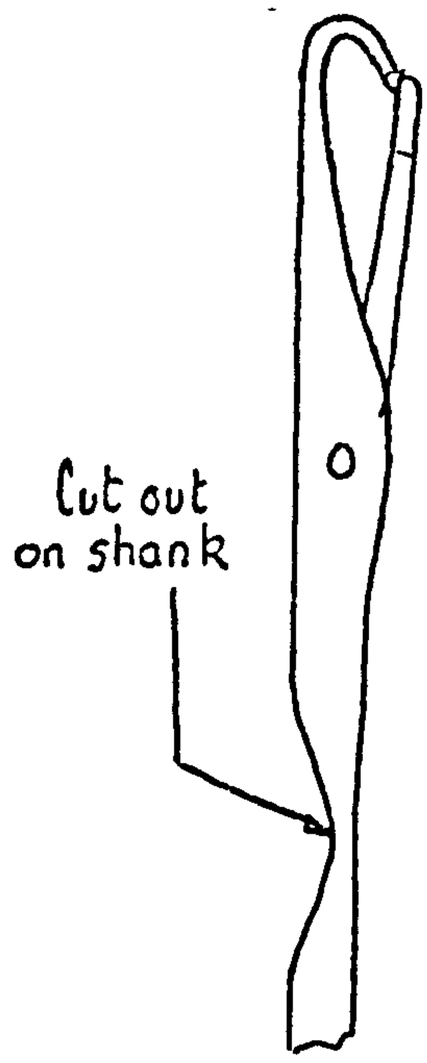

diagram III

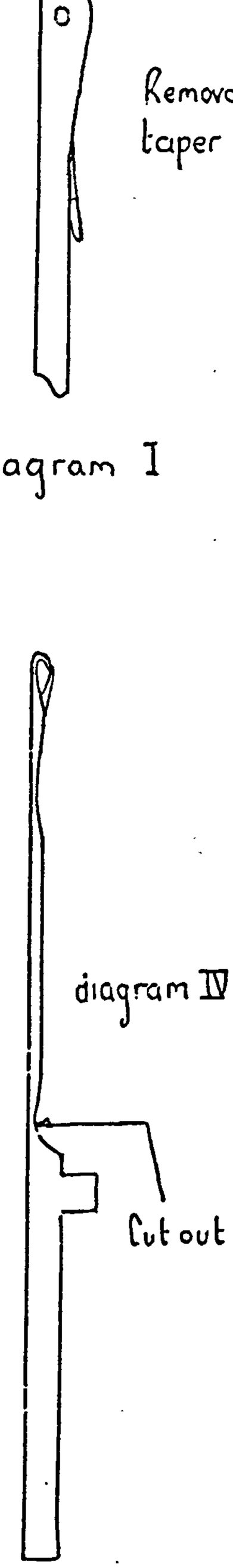

diagram IV

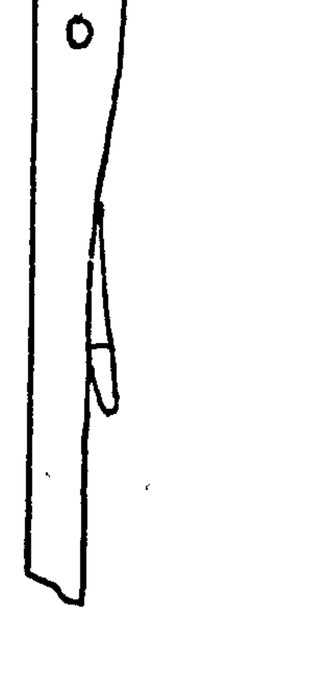

diagram V

diagram VI

MODIFICATIONS TO NEEDLE SHAPE

FIG 19.7

0.443 mm needle
free in trick
broke once after
10,000 revs

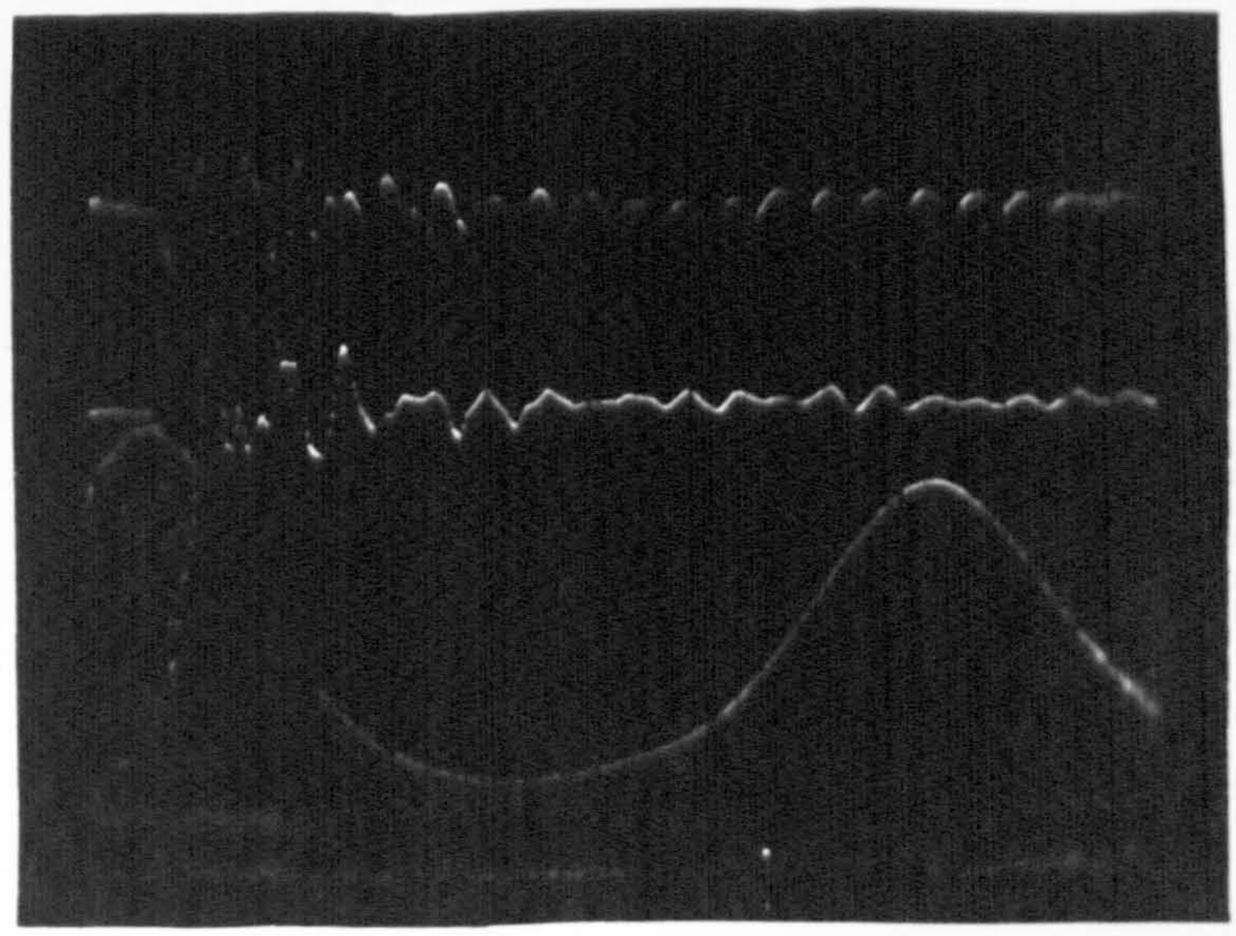

DIAGRAM I
49° Stitch-Cam
8° Guard-Cam
200 X10^{-6} Secs
per 8.5 mm

0.406 mm needle
free in trick
broke after
400 revs

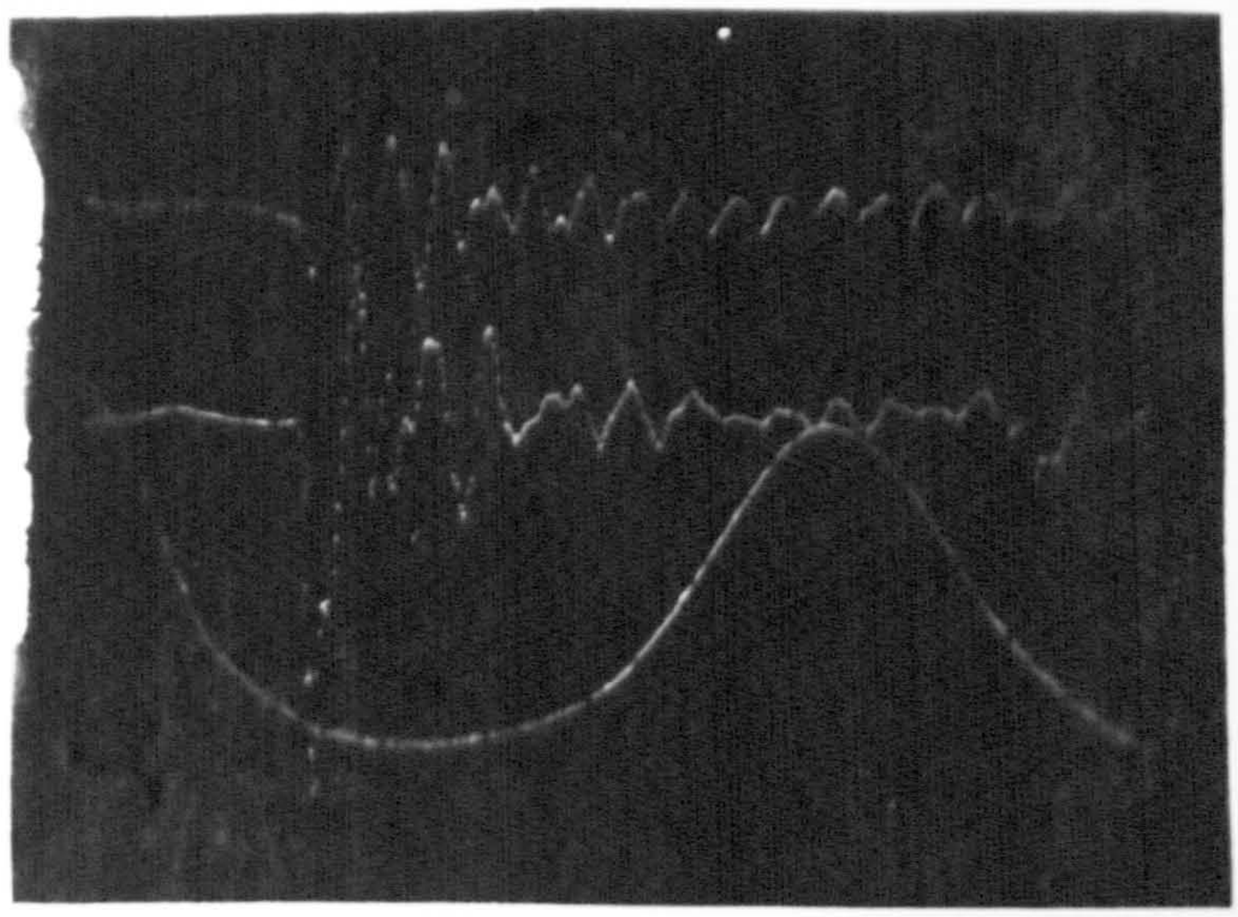

DIAGRAM II
49° Stitch-Cam
8° Guard-Cam

0.406 mm needle
free in trick
broke after 5000 revs

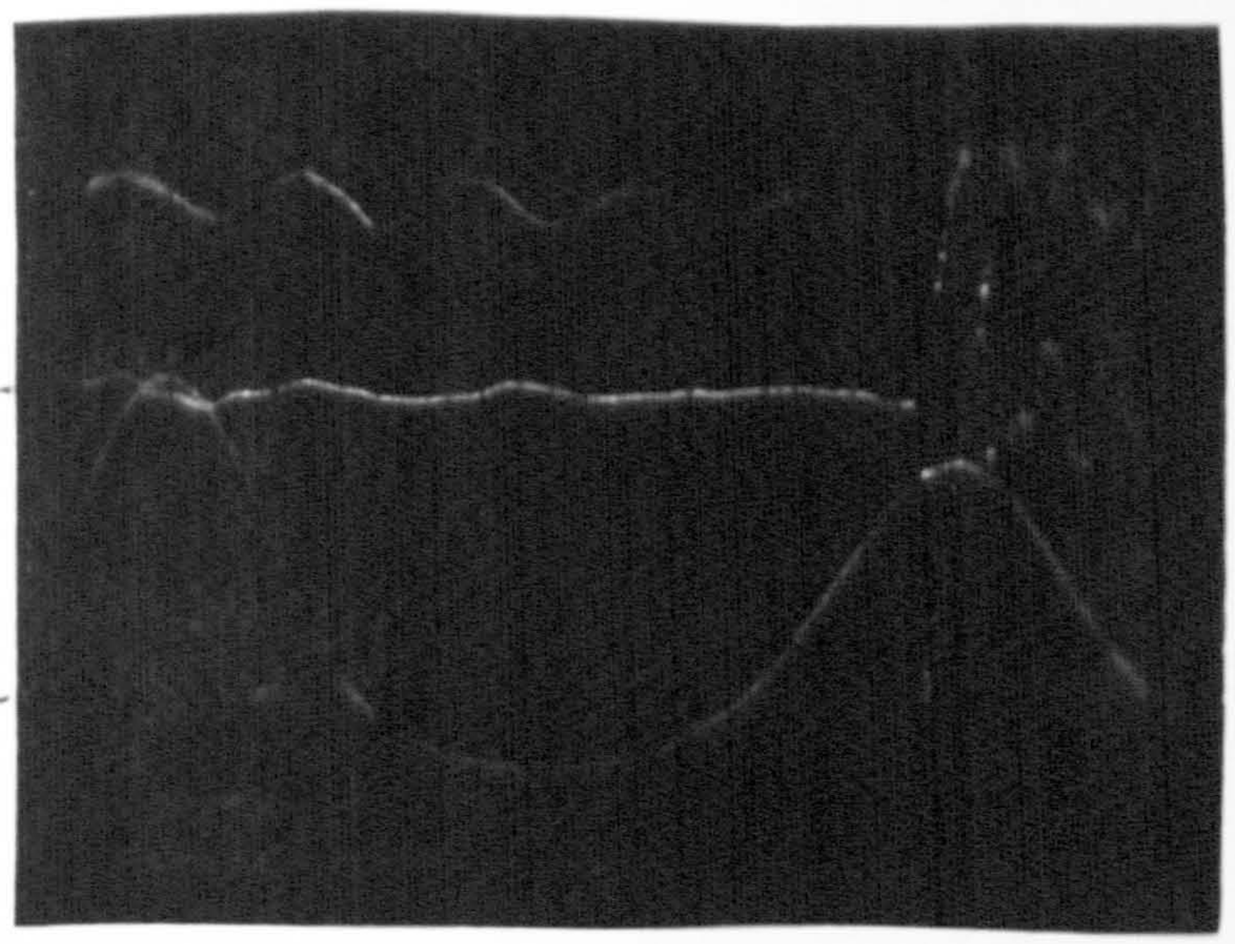

DIAGRAM III
49° Stitch-Cam
8° Guard Cam

GUARD-CAM IMPACT (USING STITCH-CAM IMPACT TRANSDUCER) AT 450 ft/min

Fig 19.8

CHAPTER 20

STRAIN-MEASUREMENTS ON THE NEEDLE

20.1 Introduction.

Knitting machine needles are designed to meet complex knitting requirements, and consequently relatively little attention has been given to the problem of minimising the destructive effect of the dynamic forces generated during the knitting process. If a succesful high-speed knitting machine is to be produced then the needle design, from both the knitting and dynamic aspects, must be carefully optimised. A large amount of theoretical work, concerning the wave process in the needle, has been carried out by J.I. and E.I. Petrow[33 to 37 inc]. At this stage it was considered essential to obtain experimental measurements of the transmitted wave because, without such experimental knowledge, the existing theories cannot be verified or modified, thus limiting future progress.

The ultimate objective is to determine the needle's response to high speed loading, by using either experimental or reliable theoretical techniques, and then to use such results to optimise needle design prior to their mass production. Two techniques were developed with the purpose of determining the magnitude and form of the pressure wave; the first was by means of strain gauges, as detailed in this chapter, and the second was by means of dynamic photoelasticity, as is detailed in chapter 21. Both methods had inherent advantages and disadvantages, and these are outlined in the respective sections of each chapter.

20.2 Advantages and Disadvantages of using Strain Gauges Mounted on the Needle.

Strain gauges are probably the only method of obtaining measurements from a needle as it passes through the knitting cams. However, apart from bonding problems, they have two basic disadvantages for this type of work, namely :-

(i) They can only give point measurements, and thus cannot give a complete picture of the stress-wave pattern over the complete needle.

(ii) Even the smallest strain-gauges available are relatively large compared to the needle sections near the hook. It is highly likely that complex strain patterns exist at the hook, but the gauges can indicate only an average strain intensity on the area under the sensitive element.

However, strain gauges possess the important advantage that they can be used on the actual needle while it is moving through the knitting-process. The photoelastic technique, detailed in chapter 21 basically overcame the disadvantages of the strain-gauges, but it had the disadvantage that it could only be used on a transparent model material. It was hoped that the features of the two techniques, photoelasticity and strain-gauges, would compensate each other, and together provide a powerful experimental technique for measuring wave propagation.

20.2.1 Micro-Miniature Strain Gauges.

As the needle hook cross-section is very small, it is essential that the strain gauges bonded to the shank should also be as small as possible. The miniature semi-conductor strain-gauge, as used throughout the experimentation in the previous chapters, were far too large for this application. The strain gauge selected for the measurements was a micro-miniature foil gauge, with a grid length of only 0.010 in. Obviously, with such a tiny element, there were

severe bonding problems and these are detailed in the next section.

20.3 Positioning and Bonding the Strain Gauges.

During the knitting process the needle shank is enclosed within the trick walls, and it is very difficult to fit the gauge on the shank, because there is very little clearance between the needle and the walls, and the gauge would be quickly rubbed off. Fortunately, however, there was a recess in the trick wall, as shown in diagram I Fig 20.1, and, if the gauges were bonded to the shank at this position, then, provided the total vertical movement of the needle was controlled, no damage would occur to the gauges during the needle's passage through the cams. The maximum vertical motion of the needle was controlled to a value equivalent to the slot height (see Fig 20.1) minus the total length of the strain gauges and tabs; this was approximately 0.18 in., (4.6 mm). The positioning of the gauges, including the bridge circuit, is shown in diagram II Fig 20.1. Two gauges were bonded to the needle, one on each side of the shank. It was probable that there would be a large amount of bending vibration after the impact and, if only one gauge had been fitted, it would have been impossible to separate the longitudinal component of signal from the bending component.

Additional to the two gauges fitted on the needle shank, a gauge was also bonded to the hook bend of another 0.443 mm standard needle, as shown in diagram I Fig 20.2. A special apparatus (see diagram II Fig 20.2) was built to facilitate gauge bonding, consisting of a means of holding the needle while the gauge was applied to the surface and also of a means of applying a uniform pressure to the gauge after bonding.

20.4 Electrical Circuitry.

The stain gauges bonded to the needle shank were connected into a Wheatstone bridge circuit as shown in diagram II Fig 20.1. As the needle is fitted in the trick on the rotating cylinder it was necessary to transmit the signal from the rotating system to a stationary signal display instrument. Fortunately, this problem had been solved during the design of the yarn force transducer, shown in Fig 6.1, and the yarn transducer was therefore disconnected from the amplifier and the two minature foil gauges connected into the circuitry in its place. The circuitry associated with the yarn-force transducer is shown in Fig 6.5, and a description of the operating method is given in section 8.1. The amplifiers needed slight modification to suit the different current requirements of the foil gauges, and this meant a change of the resistance values on the bridge supply side of the amplifier.

The gauge bonded to the needle head was connected into a Wheatstone bridge circuit as shown in diagram III Fig 20.2. To use the device it was only necessary to disconnect the bridge circuit containing the two gauges bonded to the needle shank, and then connect the bridge to the gauge bonded to the needle hook.

20.5 Calibration.

The needle shank's gauges were calibrated in the manner shown in Fig 20.3. The test needle was clamped in a supporting bracket, weights were applied to the needle hook, and the output signal from the gauges was amplified and stored on the Tektronix oscilloscope. The circuitry used in the calibration was identical to that used in normal measurements.

The needle hook's gauge was only used for qualitative

measurements, because it was extremely difficult to calibrate due to it's being fitted to a curved portion of the needle hook.

20.6 Experimental Method.

The method of obtaining measurements using the needles with the gauges bonded to the shank and hook was very similar to that used to obtain guard-cam impact measurements. In adjacent tricks, needles without butts were fitted as shown in Fig 14.1, and the stitch-cam impact transducer, together with the attachment to adapt it for guard cam impact measurements, was fitted to the knitting machine and set so that the cams were only 0.15 mm from the cylinder.

The method of setting up the trigger to fire the oscilloscope just when the needle hits either the stitch cam or the guard-cam was identical to that detailed in section 14.2 and 8.1.1. The method of operating the circuitry originally associated with the yarn-force transducer is described in section 8.1.

The gauges bonded to the needle sides were arranged so that the bending component of stress was minimised. However, if the bending signal was considerably larger than that of the longitudinal stress, then differences between strain sensitivity of the two gauges could result in a bending signal as large as the longitudinal strain signal and it would be difficult to separate them. Initial measurements, which are detailed in subsection 20.7, showed that there was a large bending component of strain, and a technique was developed to separate the bending component of the signal from the longitudinal component. The strain-gauges were individually calibrated to determine precisely the strain

sensitivity of each gauge. Initially, the gauge resistance was measured as accurately as possible; then it was disconnected from the Wheatstone bridge circuit and a resistance equal to the gauge resistance was substituted in its place. With just one active gauge on the shank, the calibration was carried out as shown in Fig 20.3. After both strain gauges had been calibrated individually, the gauge-factor of the most sensitive gauge was reduced so that the strain-sensitivity of both gauges corresponded exactly. The method of reducing the gauge factor was by the insertion of resistances in series with the gauges,

20.7 Measurements obtained from the Gauges on the Needle Shank.

Before embarking upon this experiment, some care was taken to ensure that the strain sensitivities of both gauges were carefully matched to eliminate the bending component of the signal. The method of carrying out the particular tests was discussed in section 20.6, and the initial experiment consisted of measuring the effect of machine speed upon the impact wave. Samples of the traces obtained are given in Figs 20.4 (b), (c), and (d); Fig 20.4 (a) defined the experimental parameters.

The results clearly show a high magnitude pulse at the exact location of guard cam impact; they also show two stitch cam impact pulses. A considerable amount of disturbance is evident after the guard cam impact and this becomes more prominent as the machine speed is increased. It is also apparent, from the trace, that the guard cam impact pulse is compressive. A graph of the impact magnitude against machine speed is shown in Fig 20.5.

20.7.1 The Bending Stresses on the Needle.

One of the strain gauges bonded to the needle shank was disconnected from the Wheatstone bridge circuit and a resistance equivalent to the gauge resistance was substituted. An experimental trace, using the one active gauge, was obtained and this is shown in Fig 20.6 diagram I. The other gauge was then re-connected into the circuitry, the gauge used for the measurement in diagram I being disconnected, and another trace was obtained at the same speed, (see diagram II Fig 20.6). As the different strain sensitivities of each gauge had been measured during calibration the output from the least sensitive gauge was multiplied up graphically by the ratio of the two sensitivities, thus ensuring that the gauges were equally responsive to the same load. For the gauge on one side of the shank, the strain approximates to :-

$$\varepsilon = \varepsilon_L + \varepsilon_b$$

where ε = strain recorded by gauge,

ε_L = tensile or compressive strain,

and ε_b = bending strain.

On the other side of the shank, the strain is given by :-

$$\varepsilon = \varepsilon_L - \varepsilon_b$$

If the trace from one of the gauges is subtracted from the trace obtained from the other, then the resulting strain is:-

$$(\varepsilon_L + \varepsilon_b) - (\varepsilon_L - \varepsilon_b)$$

$$= 2\varepsilon_b$$

The above equations were used to graphically derive the bending strain. The analysis for a machine speed of 248 ft/min (1.26 m/sec) is shown in Fig 20.7.

Many tests were carried out at varying machine speeds, and it was evident that the intensity of the bending strain increased as machine speed increased. It was also obvious

that the peak bending stresses occurred in the region of the two stitch-cam impact pulses. The shift of the D.C. level, shown on Fig 20.6, indicates that as the needle is moved vertically in the trick it is deformed slightly to increase the mean level of bending strain.

20.8 Measurements obtained from the gauges on the Needle Hook.

At varying machine speeds, tests were carried out to measure the strain in the needle hook resulting from the impact process. The method of obtaining the measurements and of setting the oscilloscope trigger was discussed in more detail in section 14.2 and 8.1.1. A sample of the traces obtained, including details of the important parameters, is given in Figs 20.8 (a), (b), and (c).

Further discussion concerning the shape of the response is included in section 20.9.

20.9 Conclusions.

The gauges bonded to the needle shank responded to a bending component and a longitudinal component of strain. At the instant of guard cam impact, a large sharp compressive pulse was evident and this became more prominent as machine speed was increased. The compressive pulse had a larger magnitude than the two pulses originating at the instant of stitch-cam impact. Following the large compressive pulse, there was a considerable amount of wave disturbance which grew in magnitude as the machine speed was further increased. There was also evidence of a large bending component of strain, which originated from the stitch-cam impact.

The gauges mounted close to the needle hook indicated an equal distribution of compressive and tensile strain. The two initial stress oscillations change little in shape as

speed was increased; however there was evidence of a pulse, reaching large magnitudes, occurring soon after the instant of guard-cam impact. The high magnitude pulse shown on diagram II of Fig 20.9 (b) was not evidenced on all the traces, even at higher machine speeds, but what was evident was the increasing amount of wave disturbance. An interesting feature of the traces obtained from the gauge mounted on the needle hock is the large number of stress reversals, tensile to compressive and vice-versa. At 402 ft/min (2.00 m/sec), following stitch and guard cam impact, there are at least fifteen clearly discernable stress reversals shown on diagram II of Fig 20.8 (b). On a commercial machine, where there are a large number of impacts over a relatively short time interval, there would be a considerable number of stress reversals after a few days normal operation. Stress reversal is compatible to a fatigue mechanism for fracture, where impact magnitude, machine speed, and the number of cams, could all be important parameters affecting needle life. Combined with stress reversal, there is the clear evidence of a high magnitude pulse at the instant of guard-cam impact.

A considerable quantity of work could still be usefully carried out using strain-gauges mounted on the needles. However, it was decided to combine further measurements with the photoelastic analysis, so that both techniques should augment each other. For example, if a successful modification was evident from the photoelastic analysis, it could be subsequently tested by means of strain gauges mounted on the shank and hook.

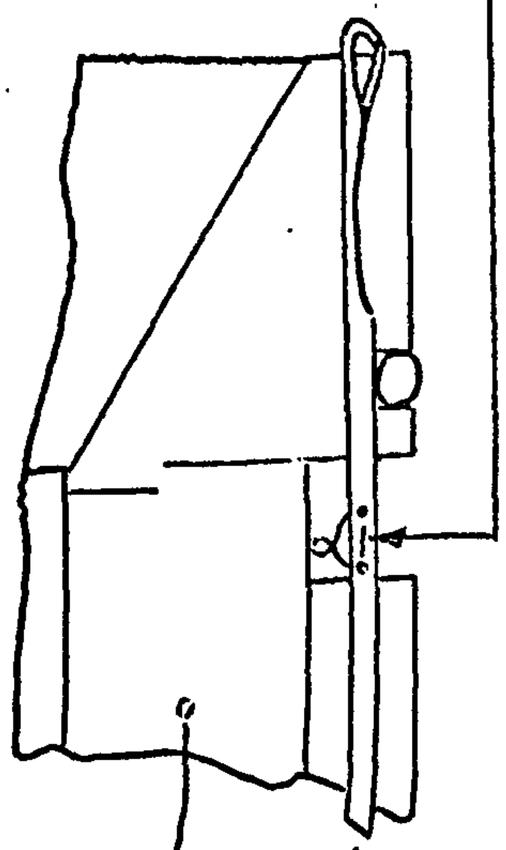

Section shewing gauges fitted to needle

Strain-gauges

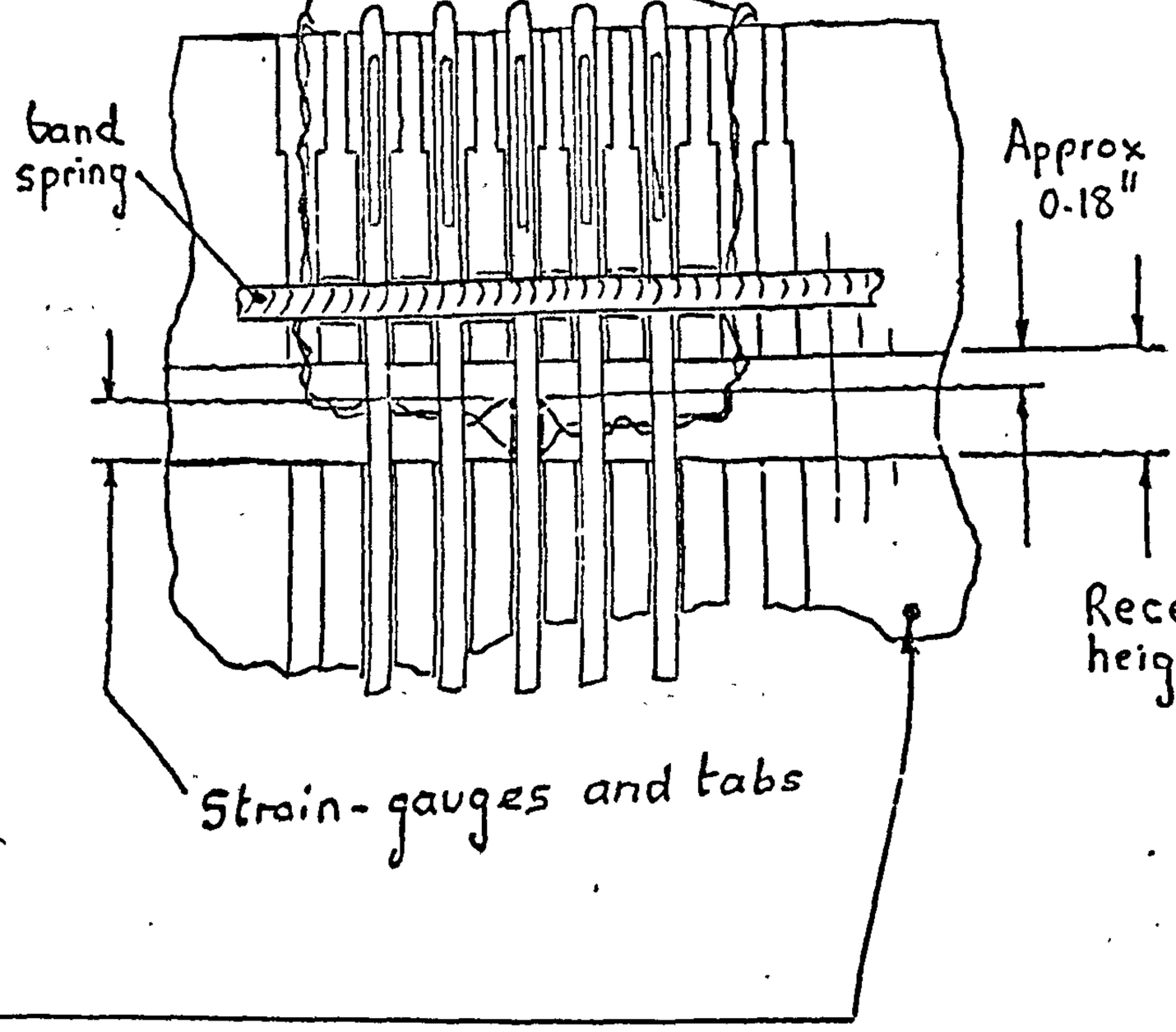

Diagram I (section of cylinder showing strain gauged needle in position)

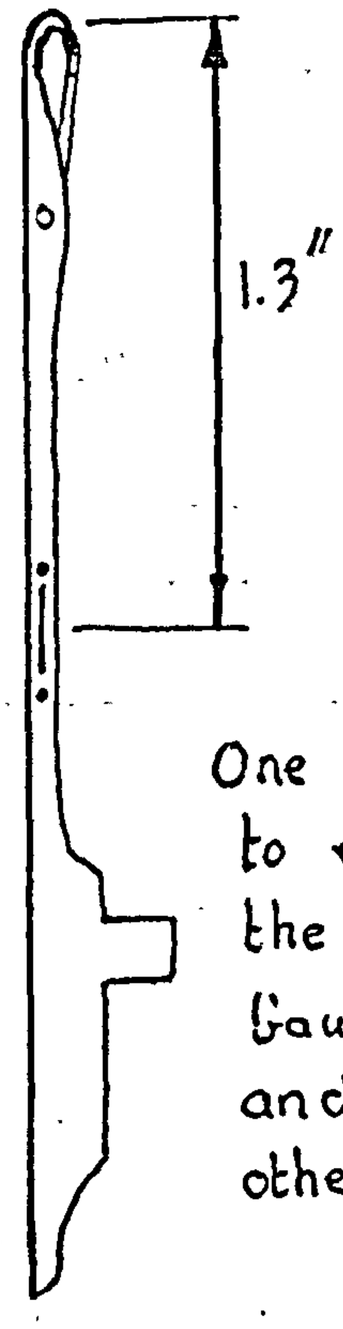

One gauge attached to each side of the needle.
Gauge ① to one side and Gauge ② to the other.

③ and ④ precision 120Ω resistors

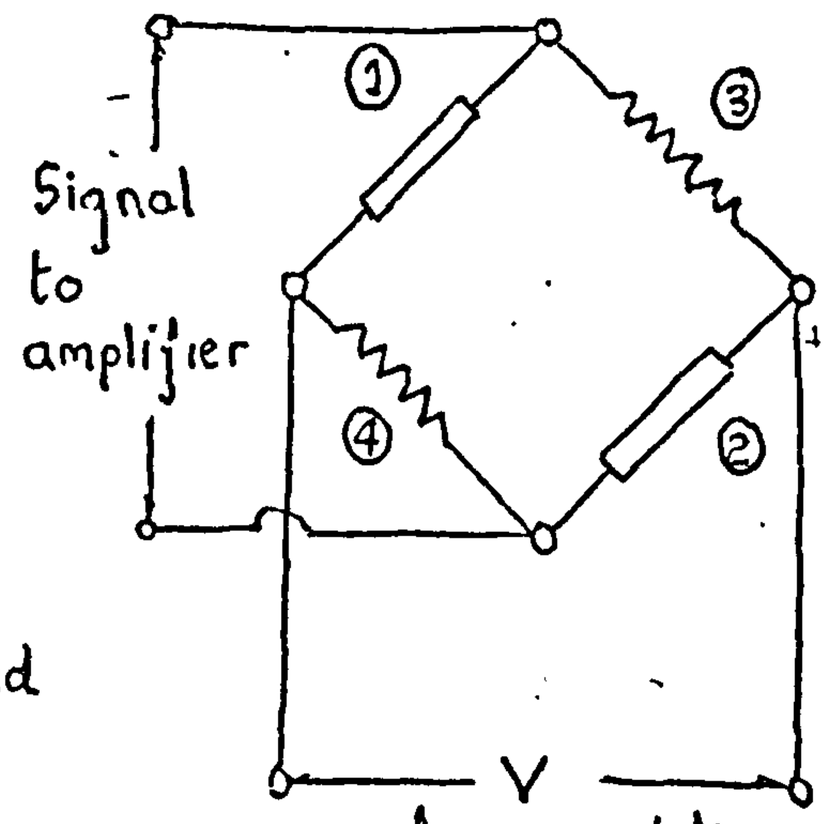

Diagram II position of strain gauges and Wheatstor bridge circuit.

BONDING MICRO MINIATURE STRAIN-GAUGES TO NEEDLE SHANK

FIG 20. 1.

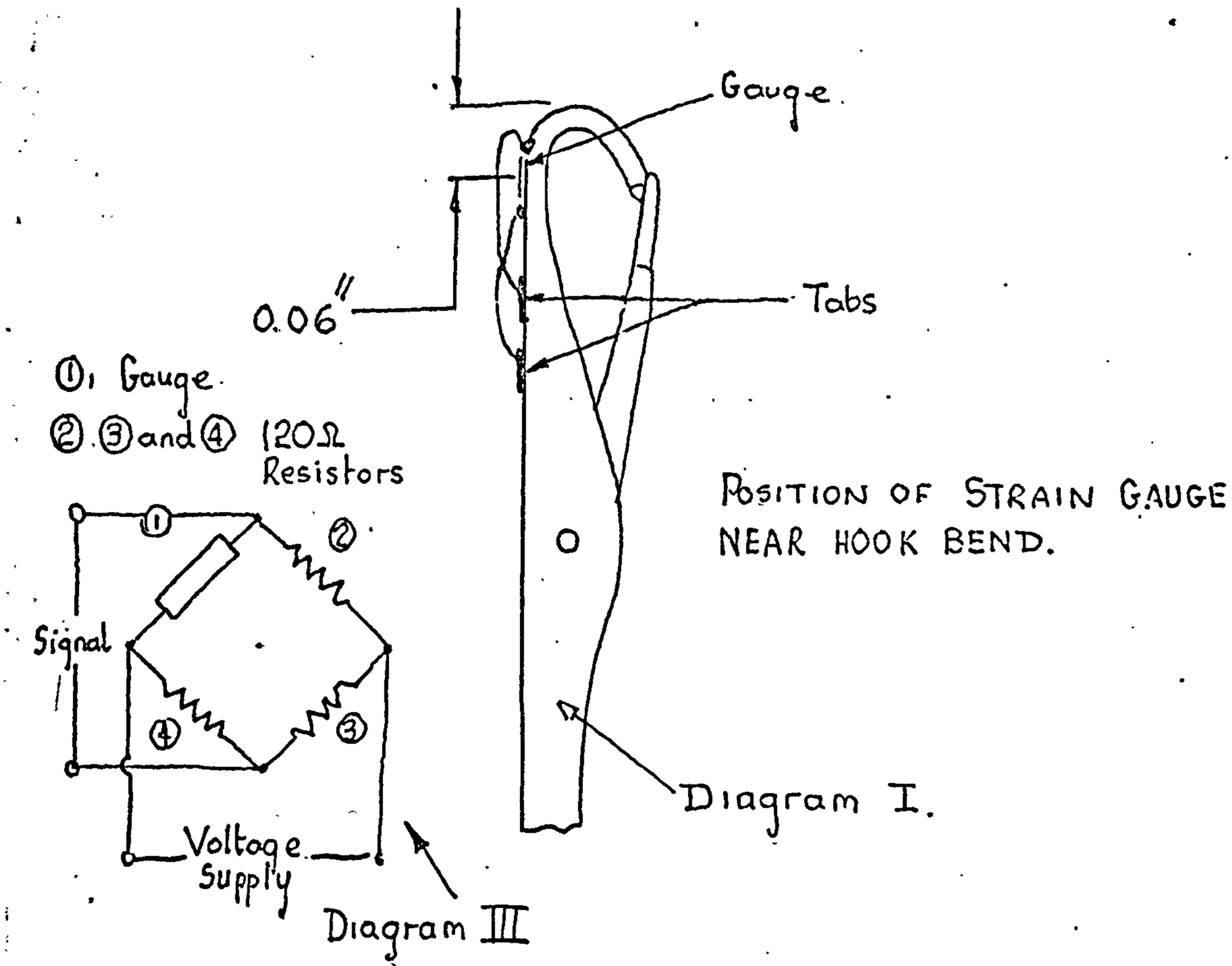

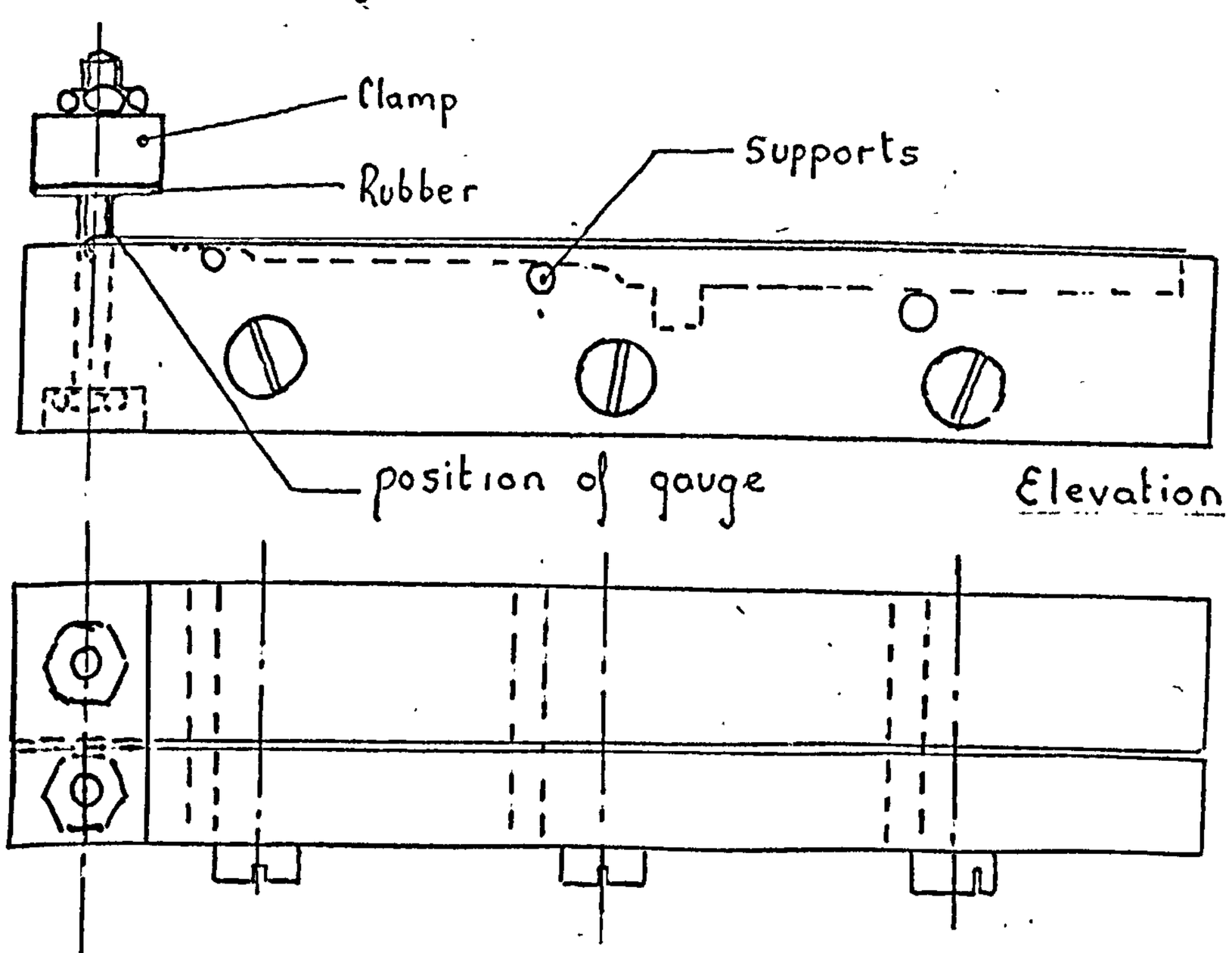

THE POSITIONING OF THE MICRO-MINIATURE STRAIN-GAUGE ON NEEDLE HOOK

FIG 20.2

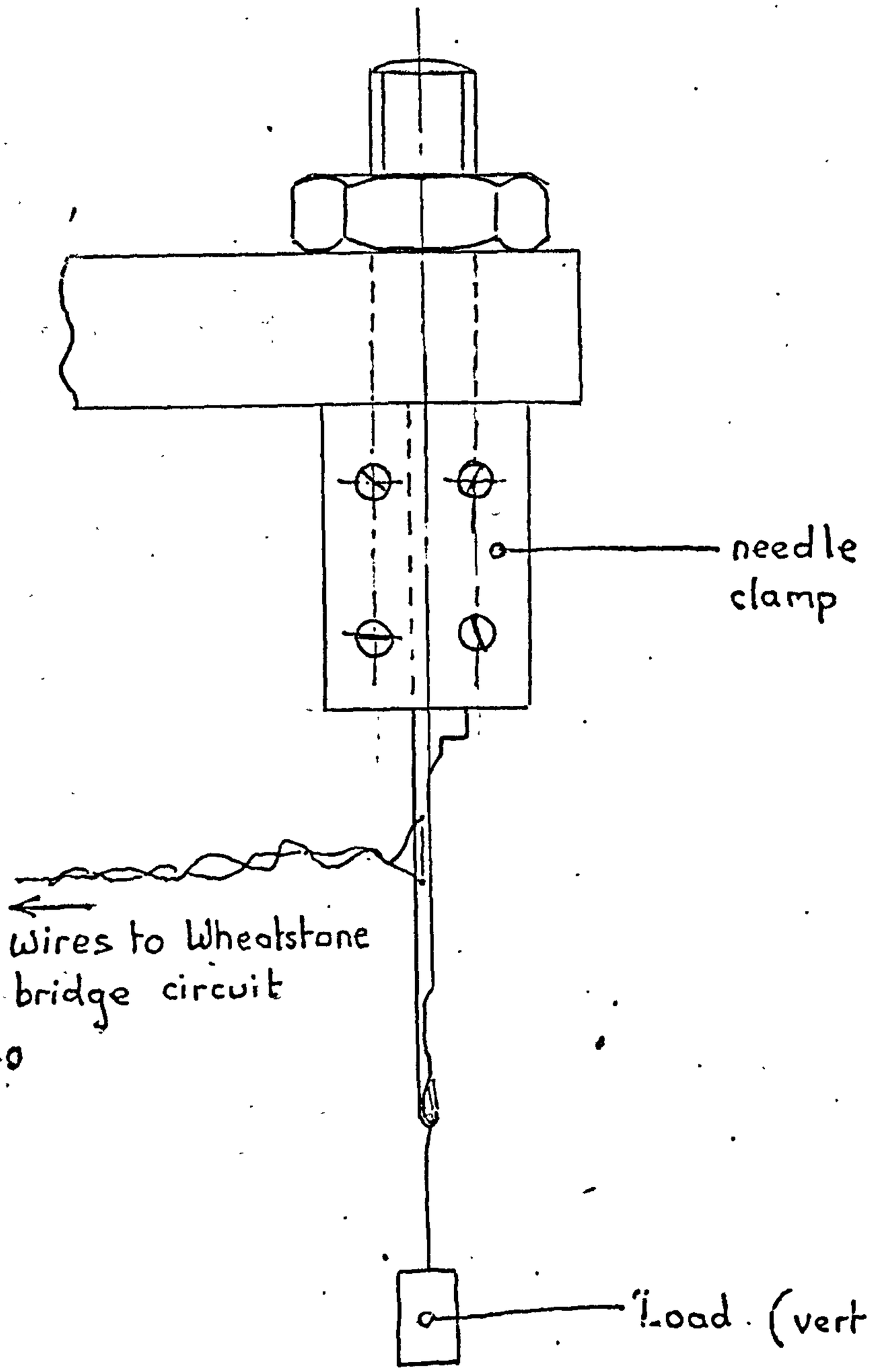

CALIBRATION OF STRAIN-GAUGES BONDED TO NEEDLE SIDES

FIG 20.3

Effect of Machine Speed upon the Wave propagated up the Needle Shank

Parameters

Cam-Cylinder Clearance = 0.15 mm (0.006 in.)

Scales

Diagrams I to Iv = 98 gf/mm

Diagram V toVii = 245 gf/mm

Time

Diagram I = 100×10^{-6} secs/8.5 mm

Diagram II = " " " "

Diagram III = " " " "

Diagram IV = " " " "

Diagram V = 50×10^{-6} secs/8.5 mm

Diagram VI = " " " "

Diagram VII = " " " "

Needle type - 0.443 mm see Fig 3.2

Parameters for traces shown in Fig 20.4(b),(c), and (d)

Fig 20.4(a)

DIAGRAM I
169 ft/min

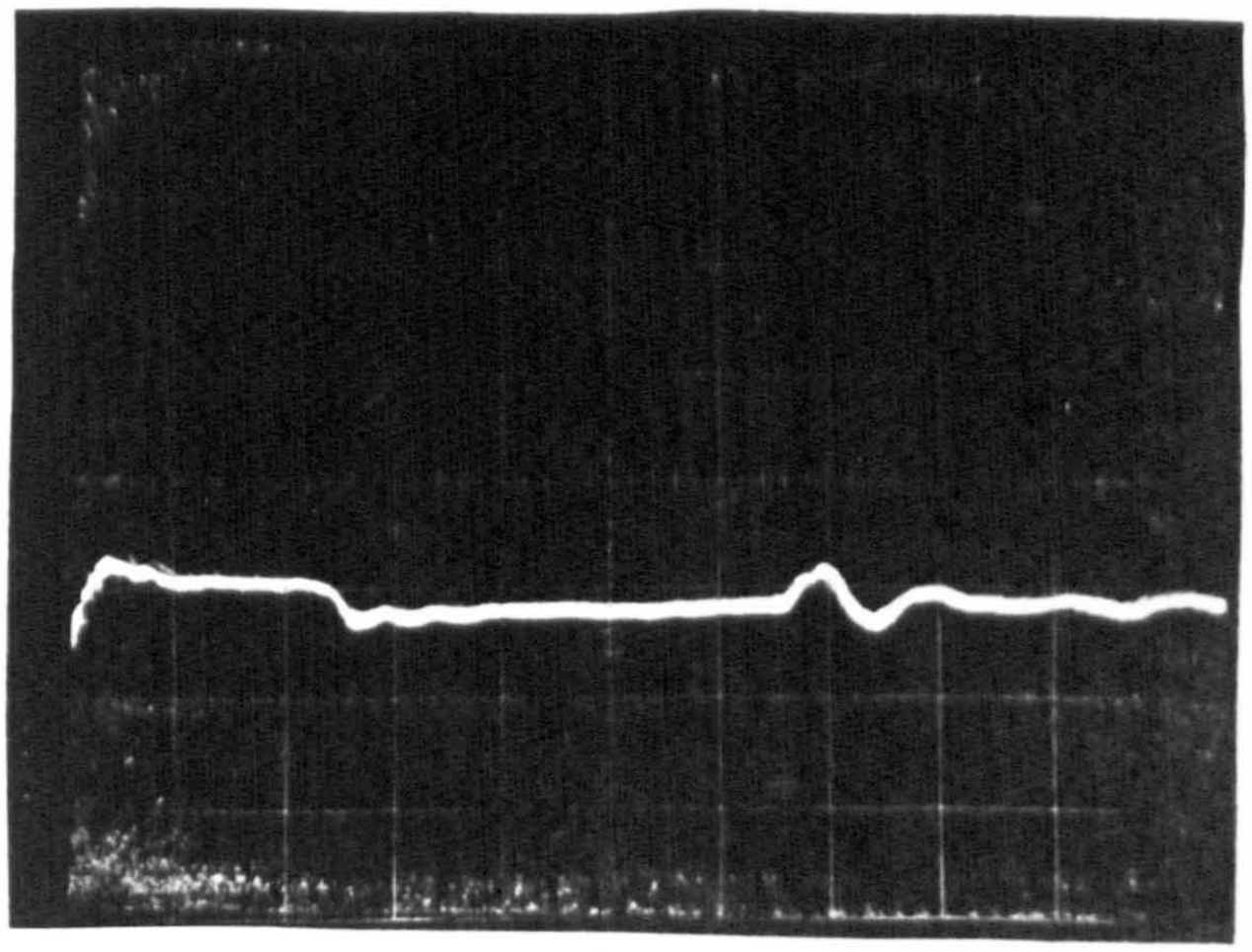

DIAGRAM II
222 ft/min

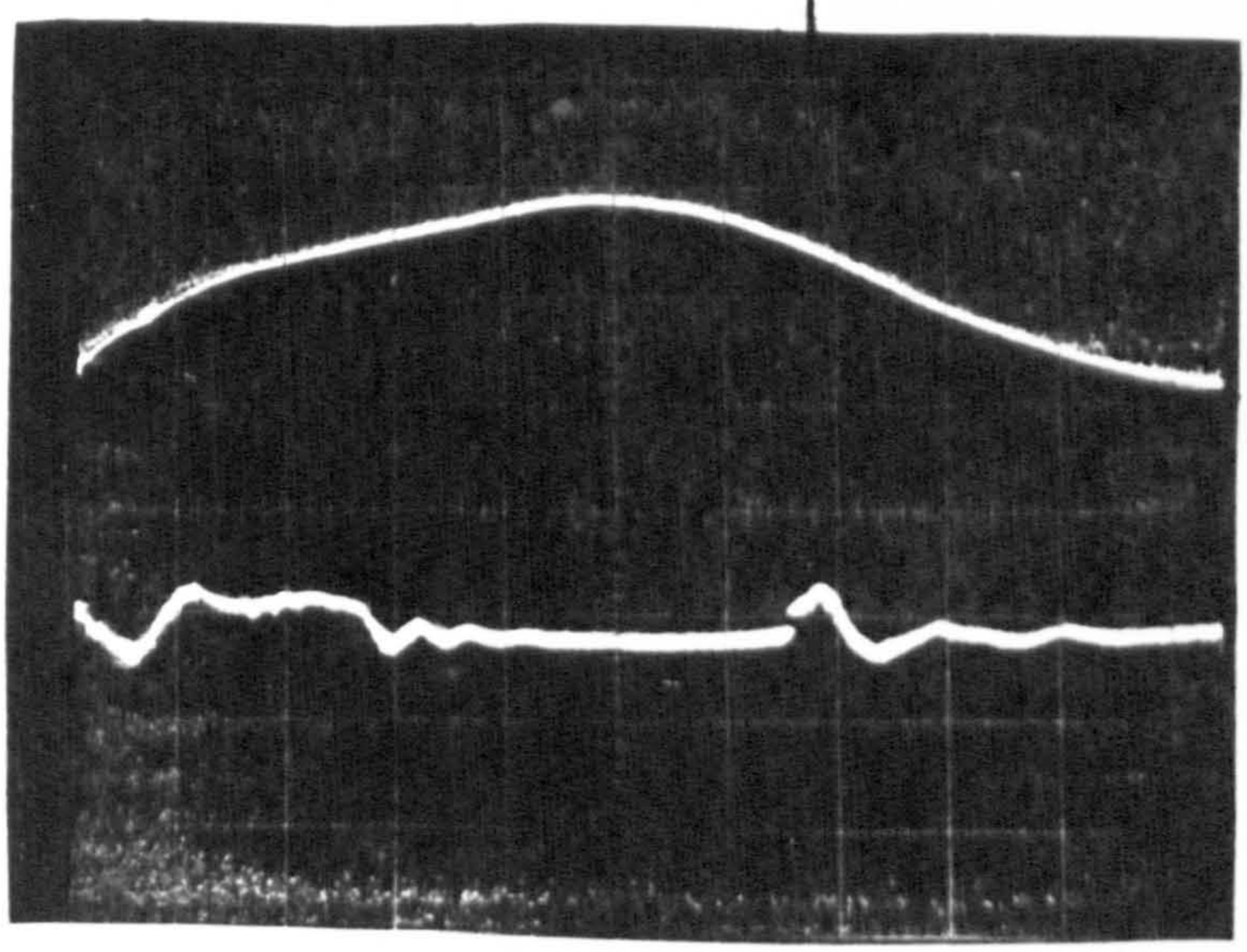

DIAGRAM III
267 ft/min

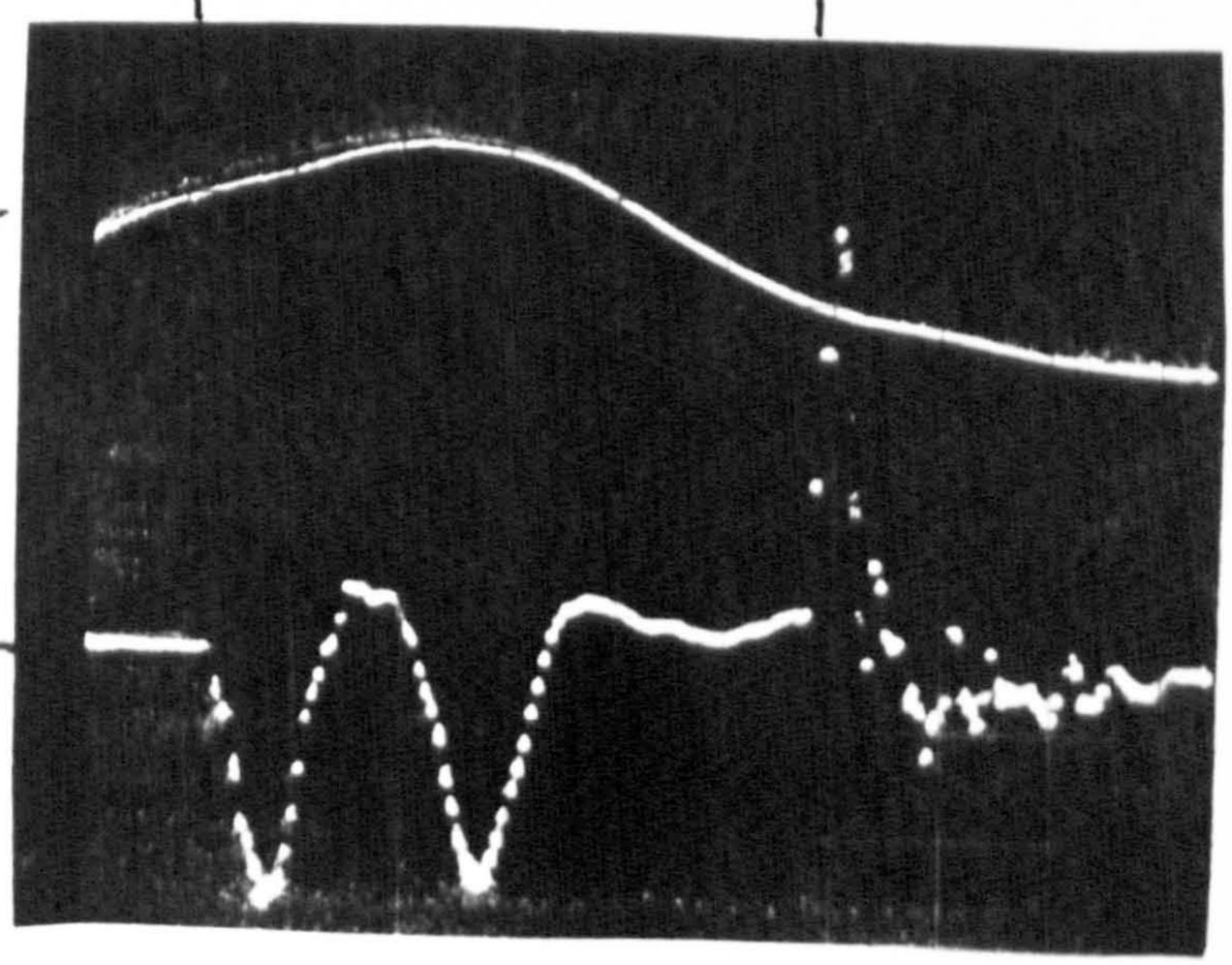

EFFECT OF MACHINE SPEED UPON THE WAVE

PROPAGATED UP THE NEEDLE SHANK(169,222 **and** 267 **ft/min**)

Fig 20.4(b)

DIAGRAM IV
325 ft/min

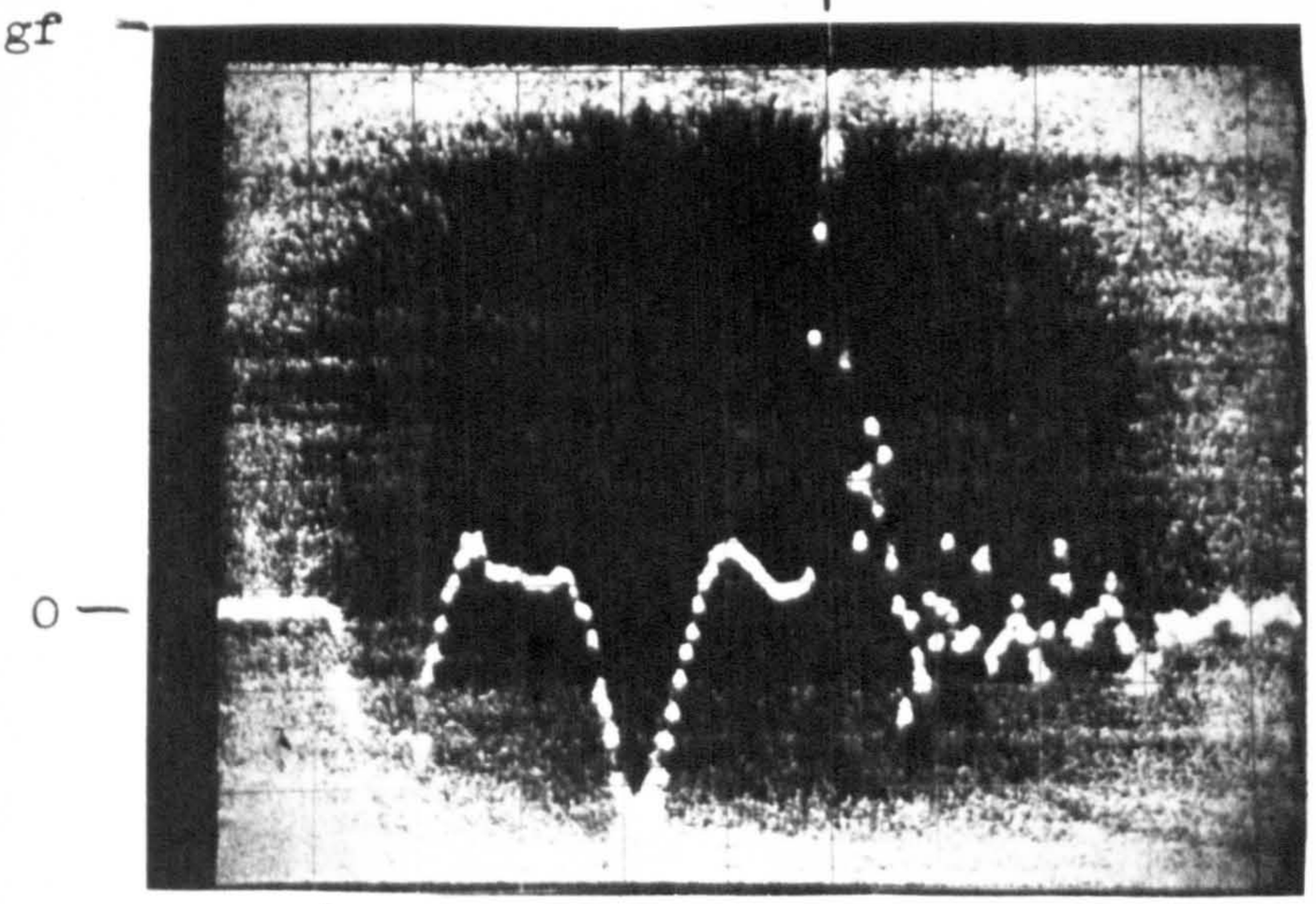

DIAGRAM V
377 ft/min

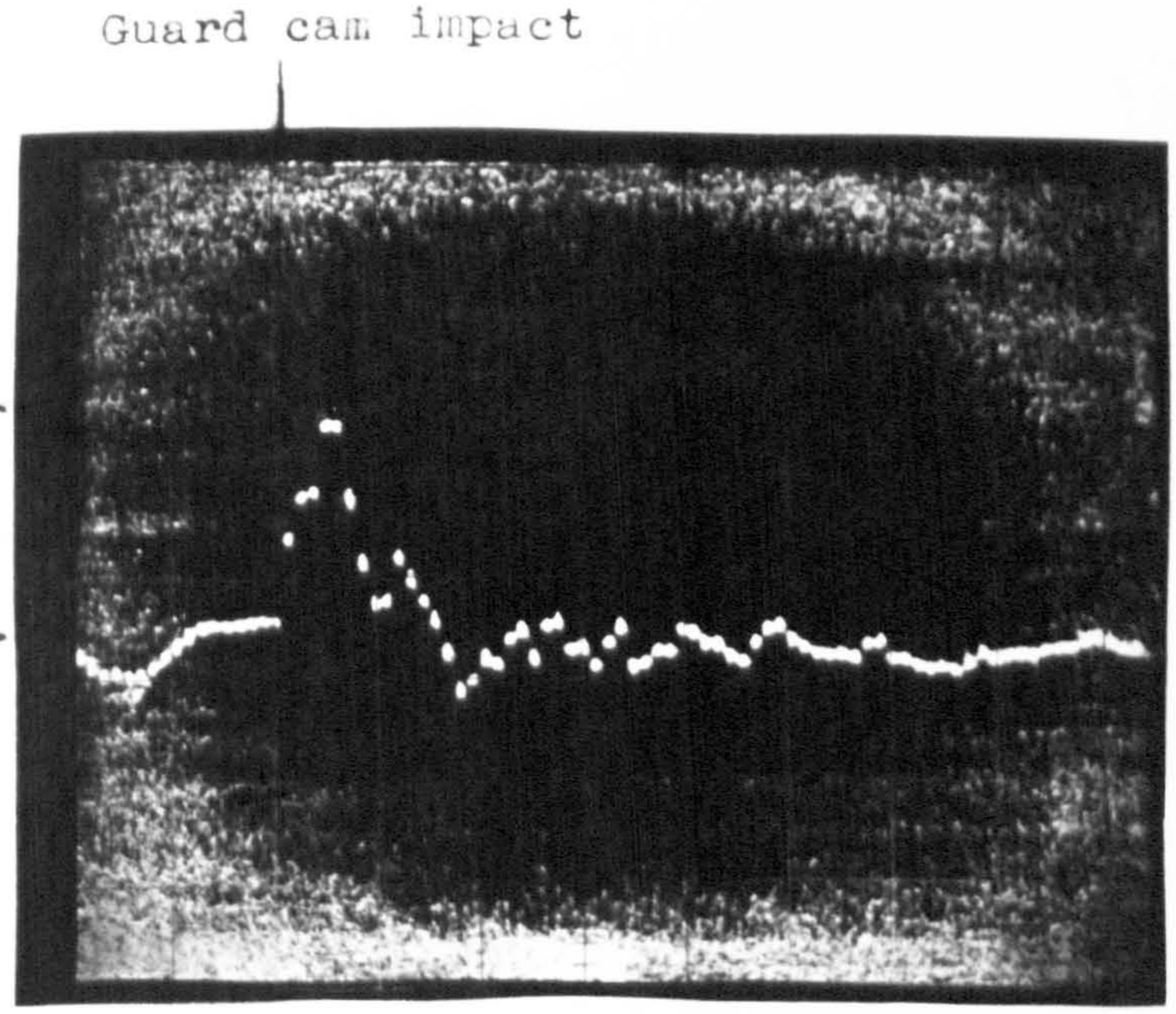

EFFECT OF MACHINE SPEED ON THE WAVE PROPAGATED UP THE NEEDLE SHANK(325 and 377 ft/min)

Fig 20.4(c)

DIAGRAM VI

430 ft/min

5080 gf

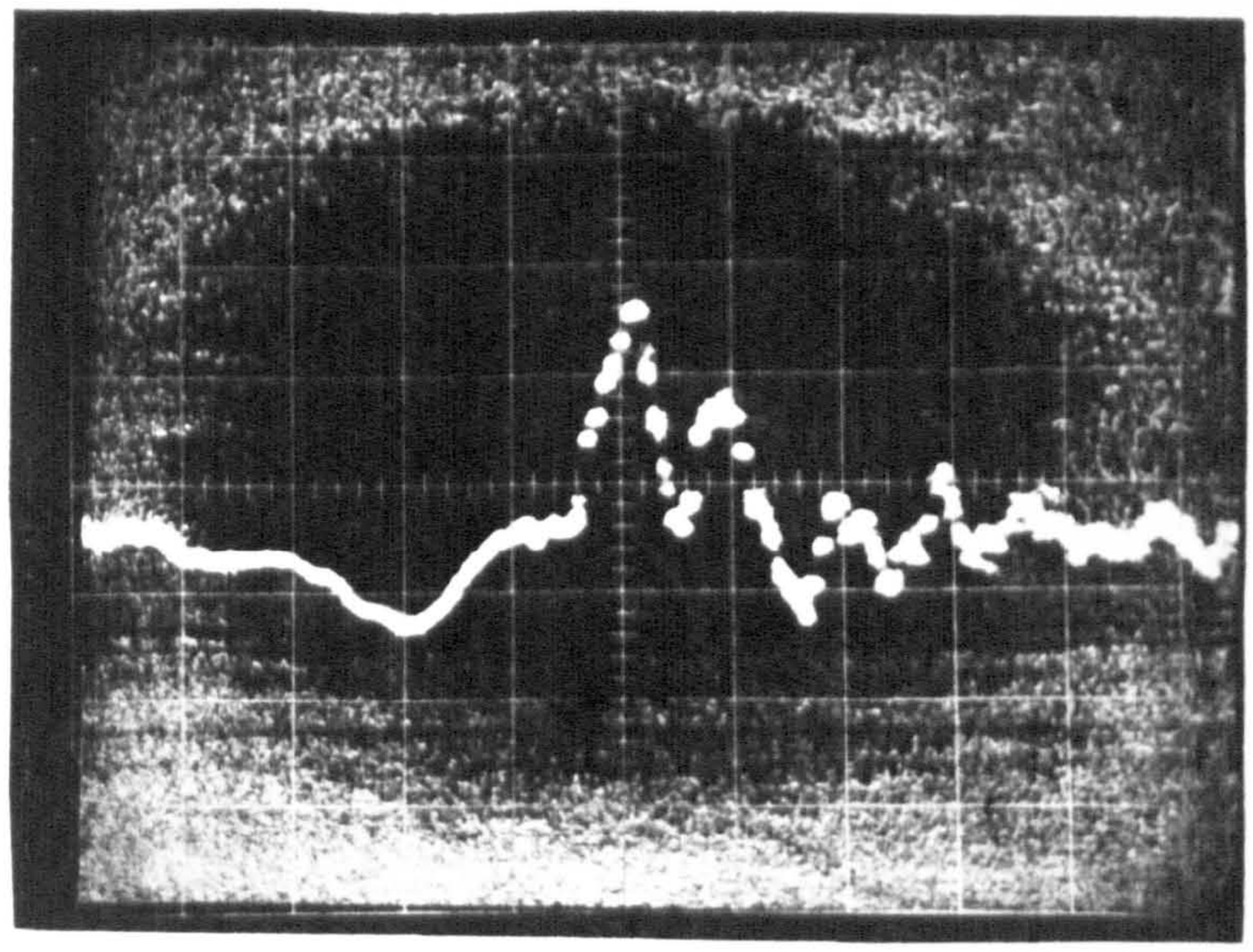

0

DIAGRAM VII

405 ft/min

4510 gf

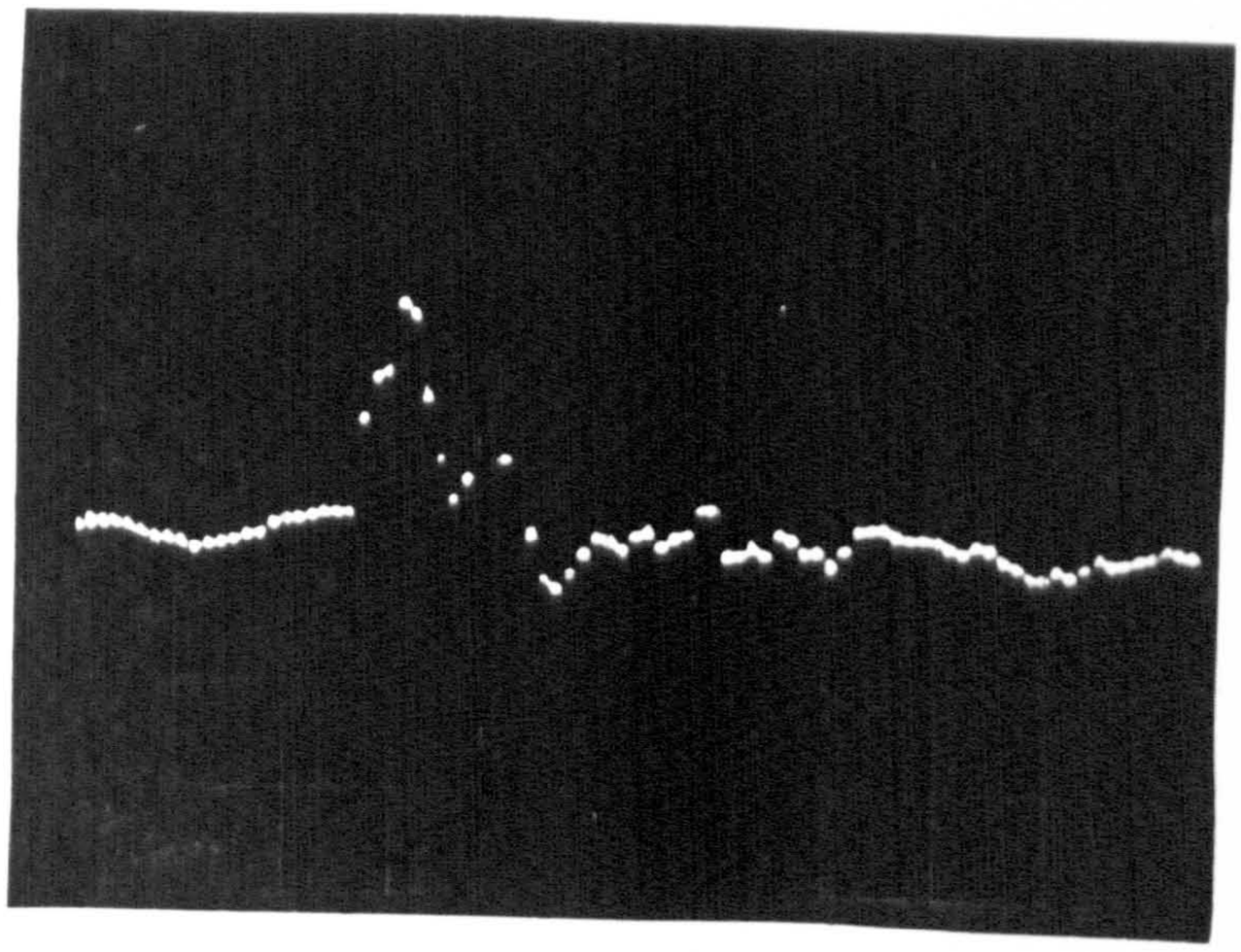

0

EFFECT OF MACHINE SPEED ON THE WAVE PROPAGATED UP THE NEEDLE SHANK(430 and 405 ft/min)

Fig 20.4(d)

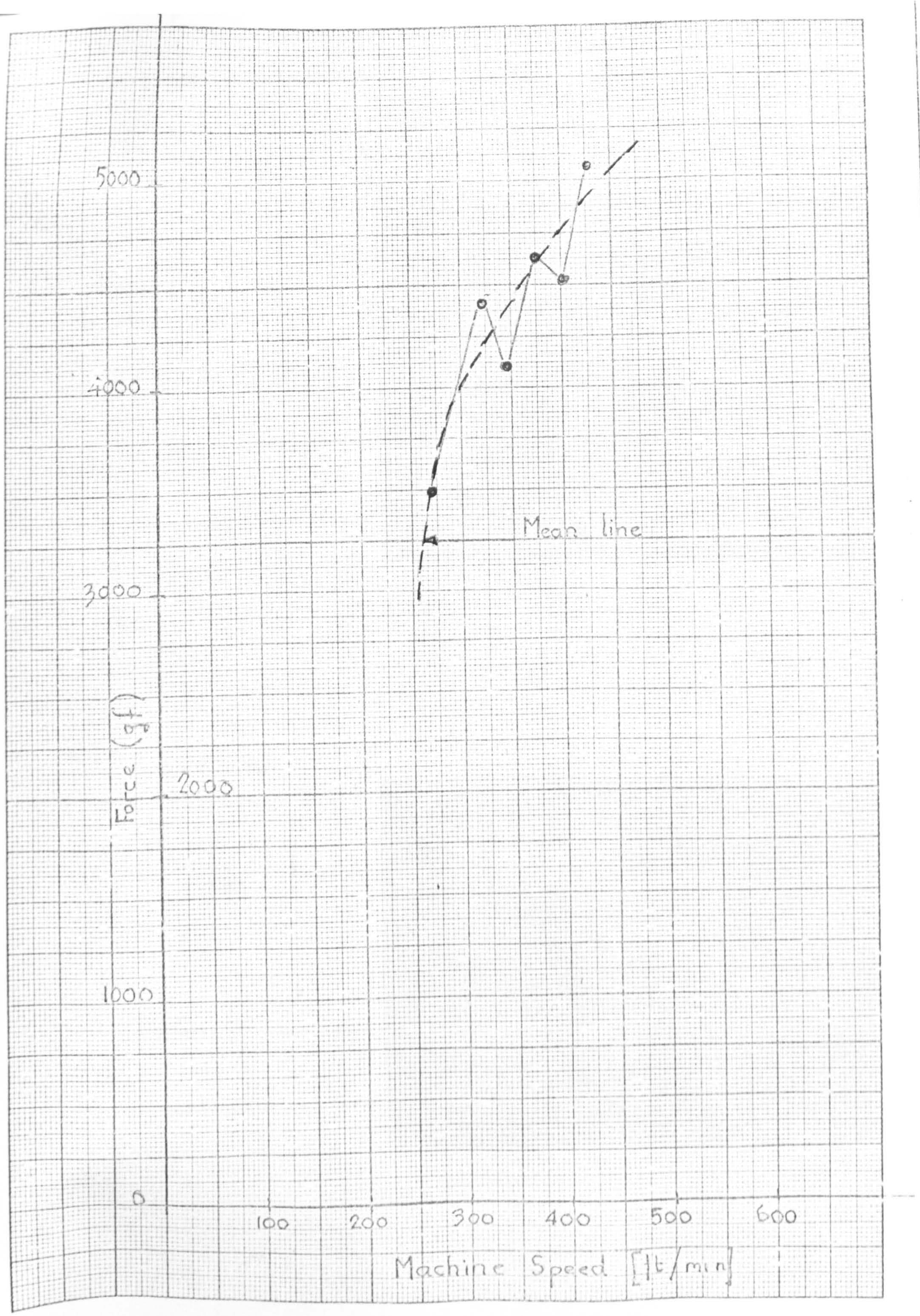

FORCE MAGNITUDE MEASURED BY STRAIN GAUGES ON NEEDLE SHANK

FIG 20.5

Time, both traces 200 x 10^{-6} secs/8.5 mm Horiz scale

Calibration factor 82 gf/mm

Machine speed 248 ft/min

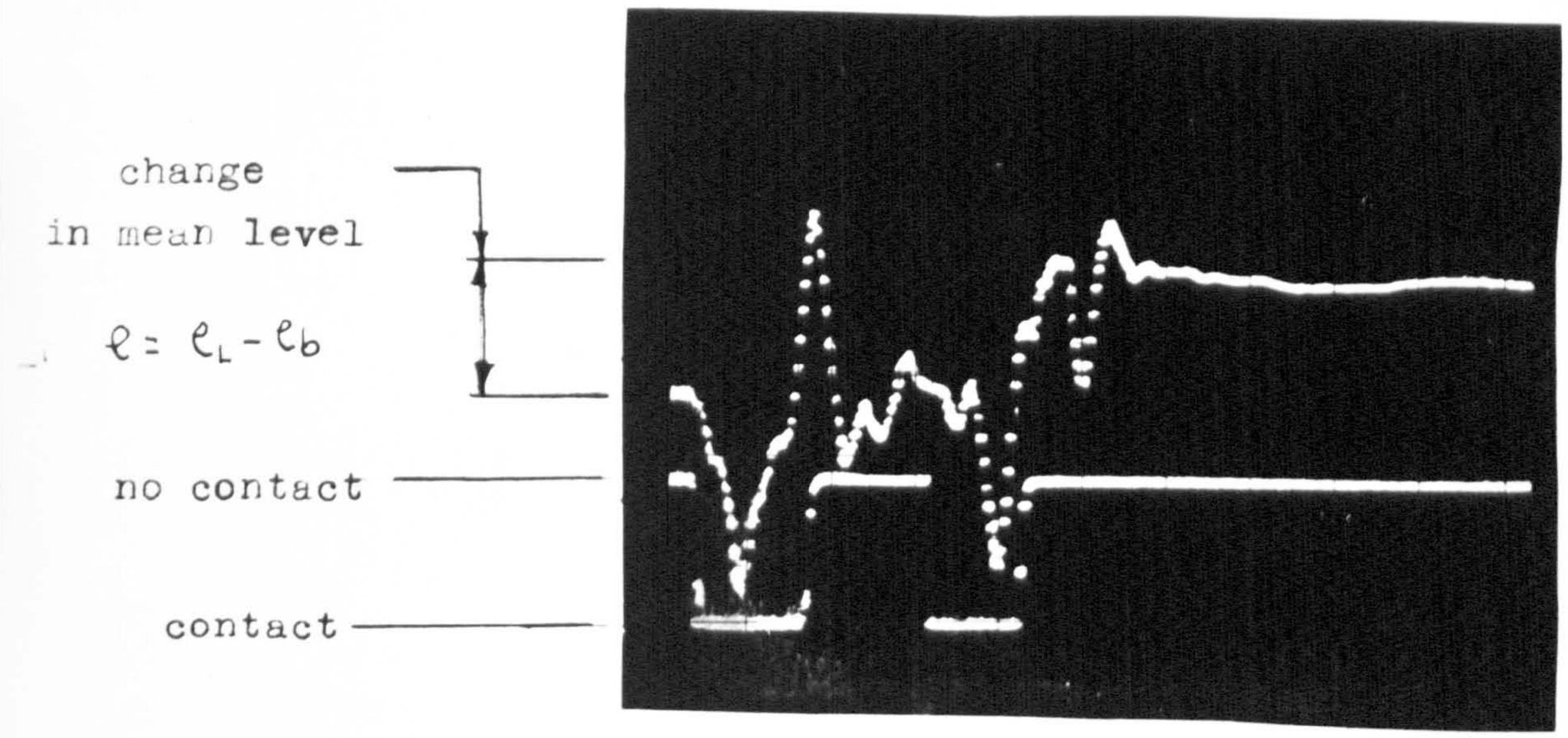

DIAGRAM I

$e = e_L + e_b$

(Terms defined in text)

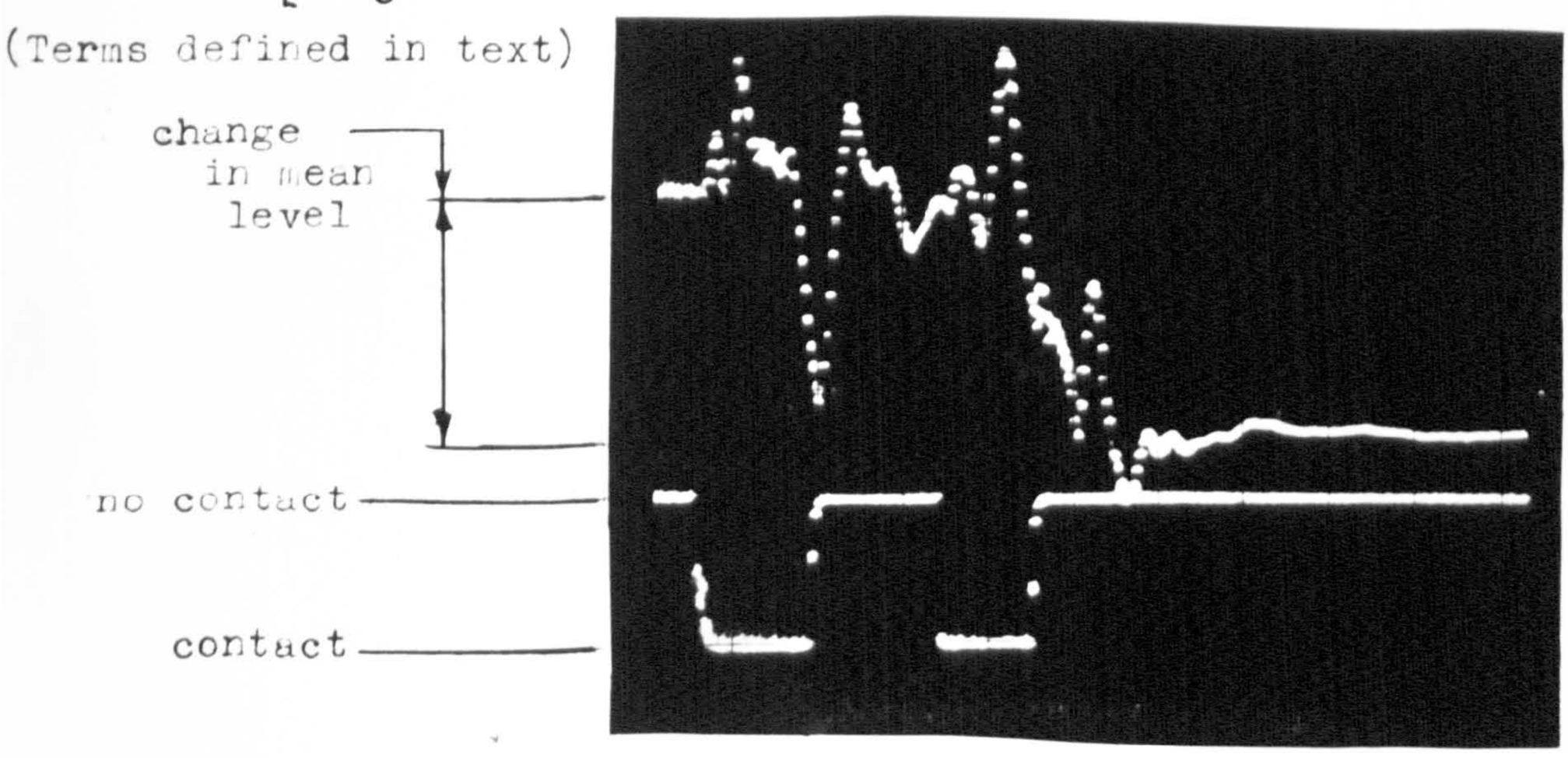

DIAGRAM II

MEASUREMENTS OF BENDING STRAINS IN THE NEEDLE SHANK

Fig 20.6

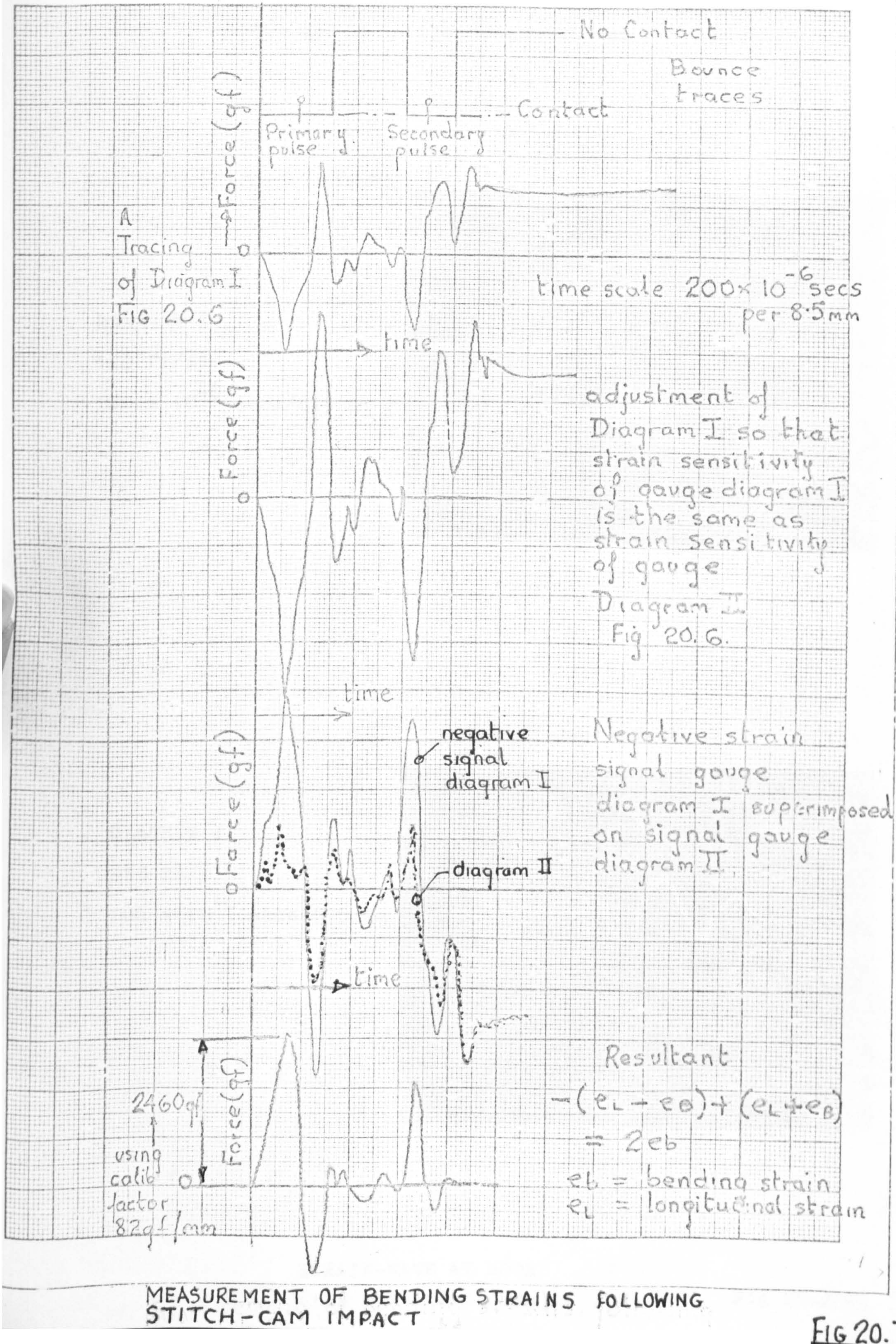

MEASUREMENT OF BENDING STRAINS FOLLOWING STITCH-CAM IMPACT

FIG 20.7

49° Cam Fig 4.3
0.443 mm needle
Cam-Cylinder Clearance 0.15 mm

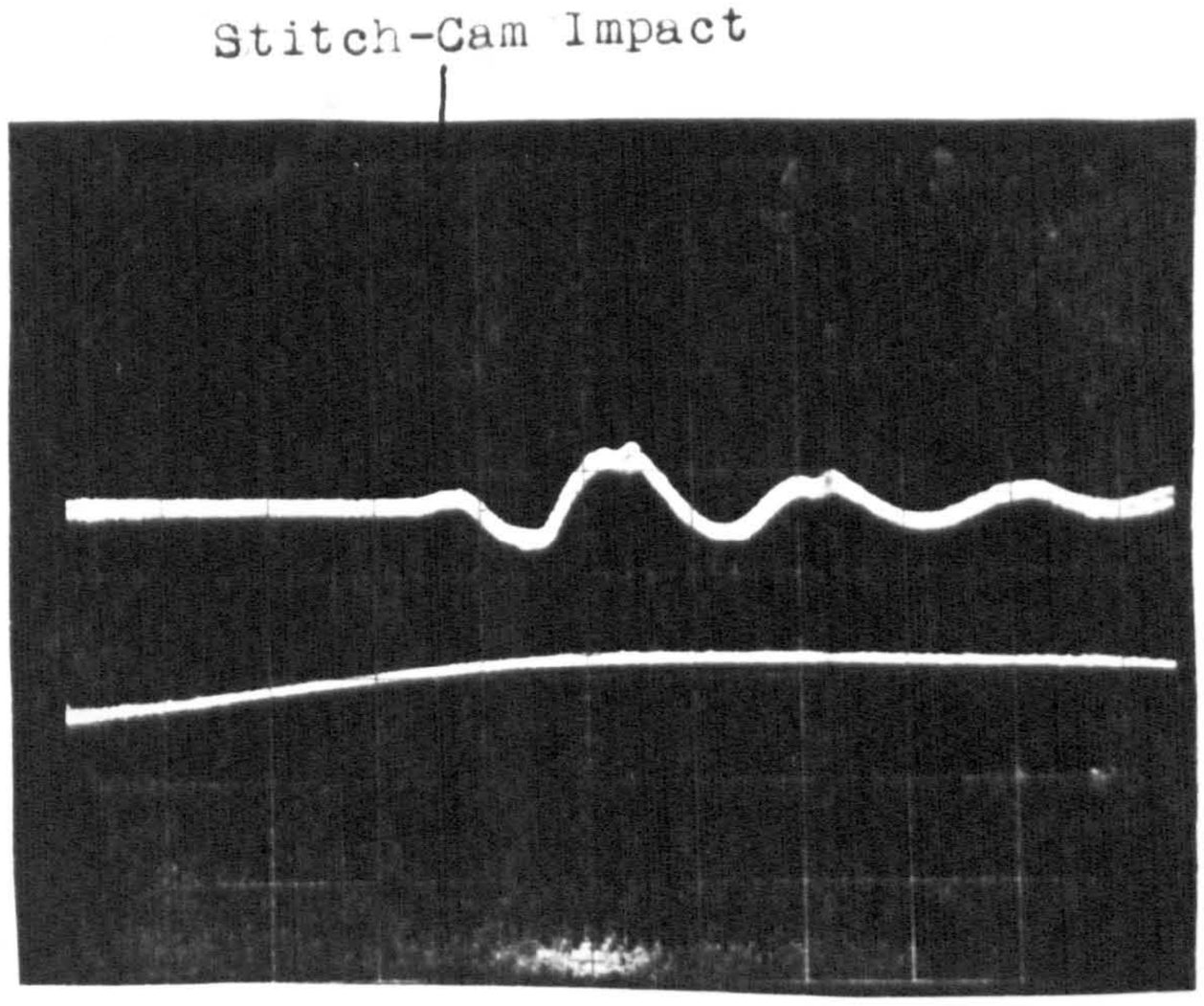

DIAGRAM I

129 ft/min

100 x 10^{-6} secs/8.5 mm

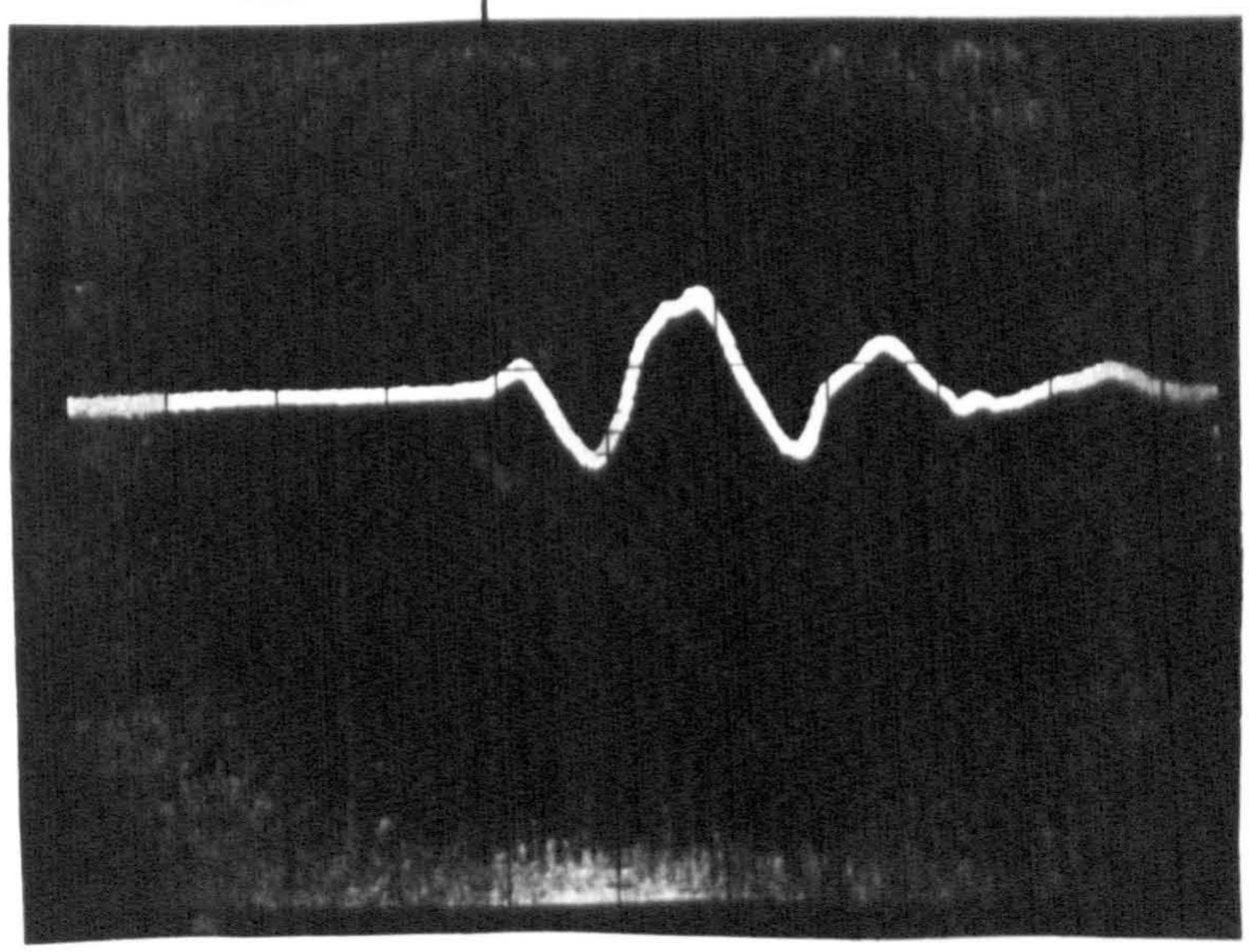

DIAGRAM II

210 ft/min

100 x 10^{-6} secs/8.5 mm

STRAIN-WAVE AT HOOK
(129 and 210 ft/min)

Fig 20.8(a)

Guard cam impact

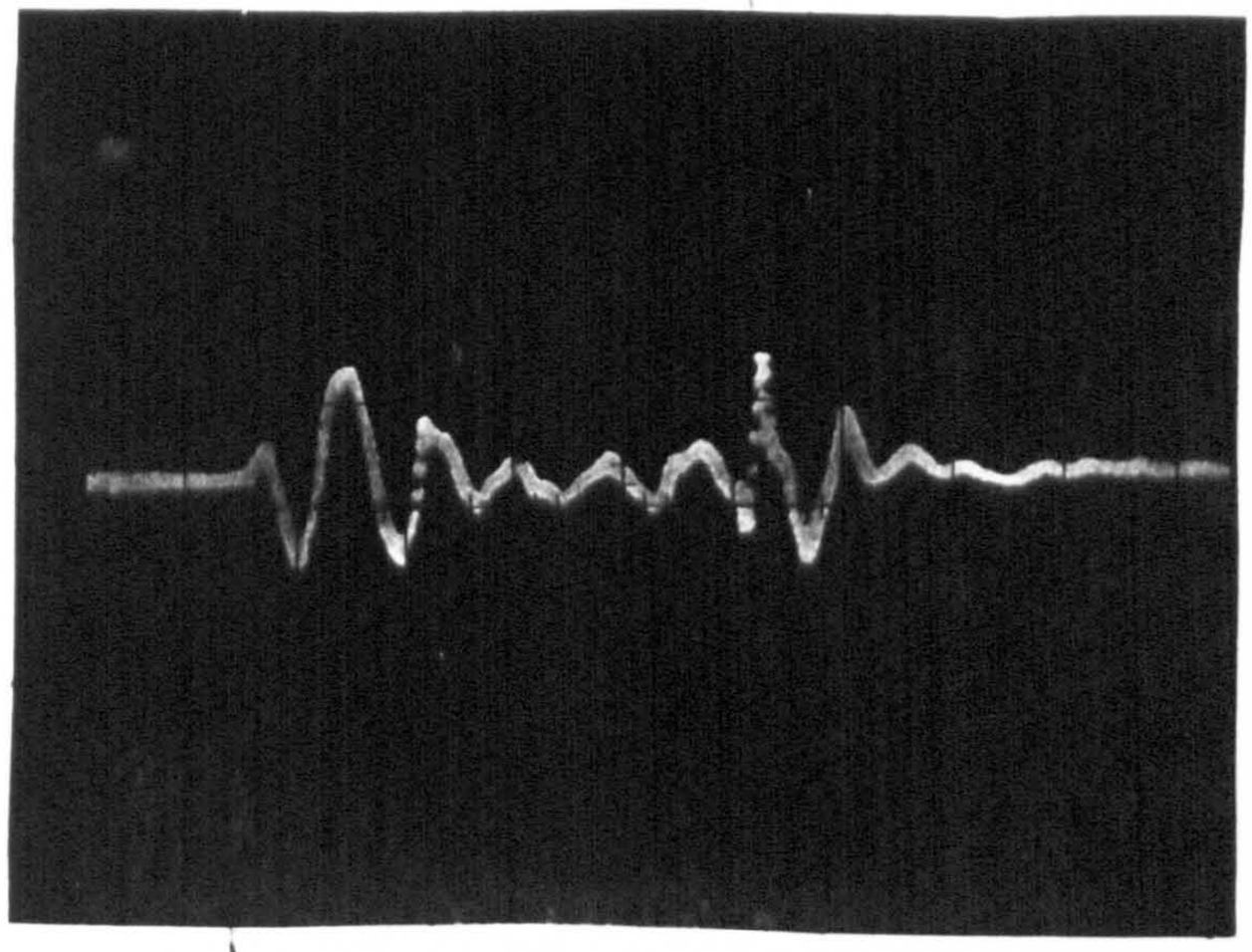

DIAGRAM III
264 ft/min
200 secs/div

Stitch cam impact

Guard cam impact

4000 gf

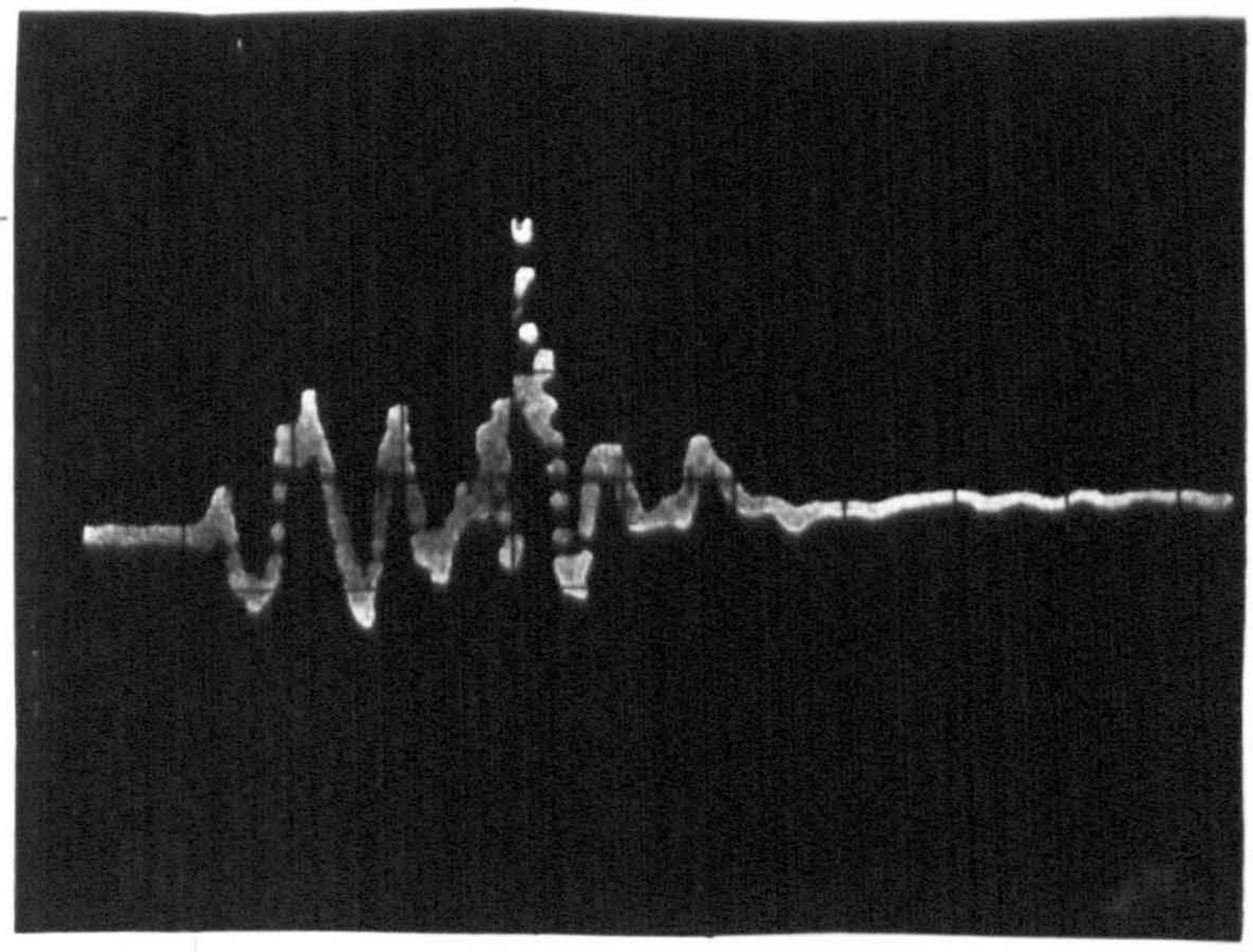

DIAGRAM IV
402 ft/min
200 secs/div

Stitch cam impact

49^{o} Cam Fig 4.3
0.443 mm needle
Cam-Cylinder Clearance 0.15 mm

STRAIN-WAVE AT HOOK
(264 and 402 ft/min)

Fig 20.8(b)

DIAGRAM V
432 ft/min
200 sec

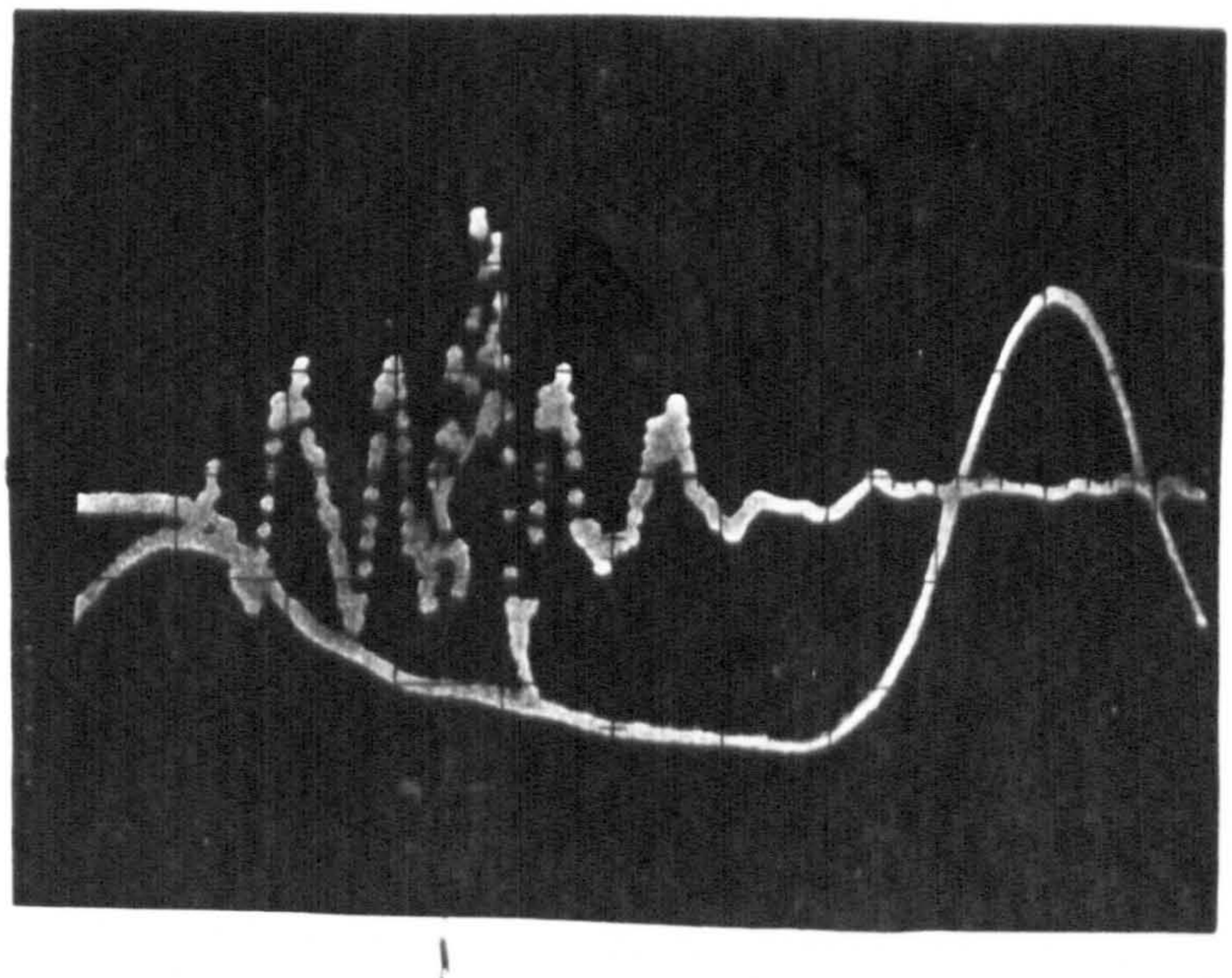

DIAGRAM VI
443 ft/min
100 secs

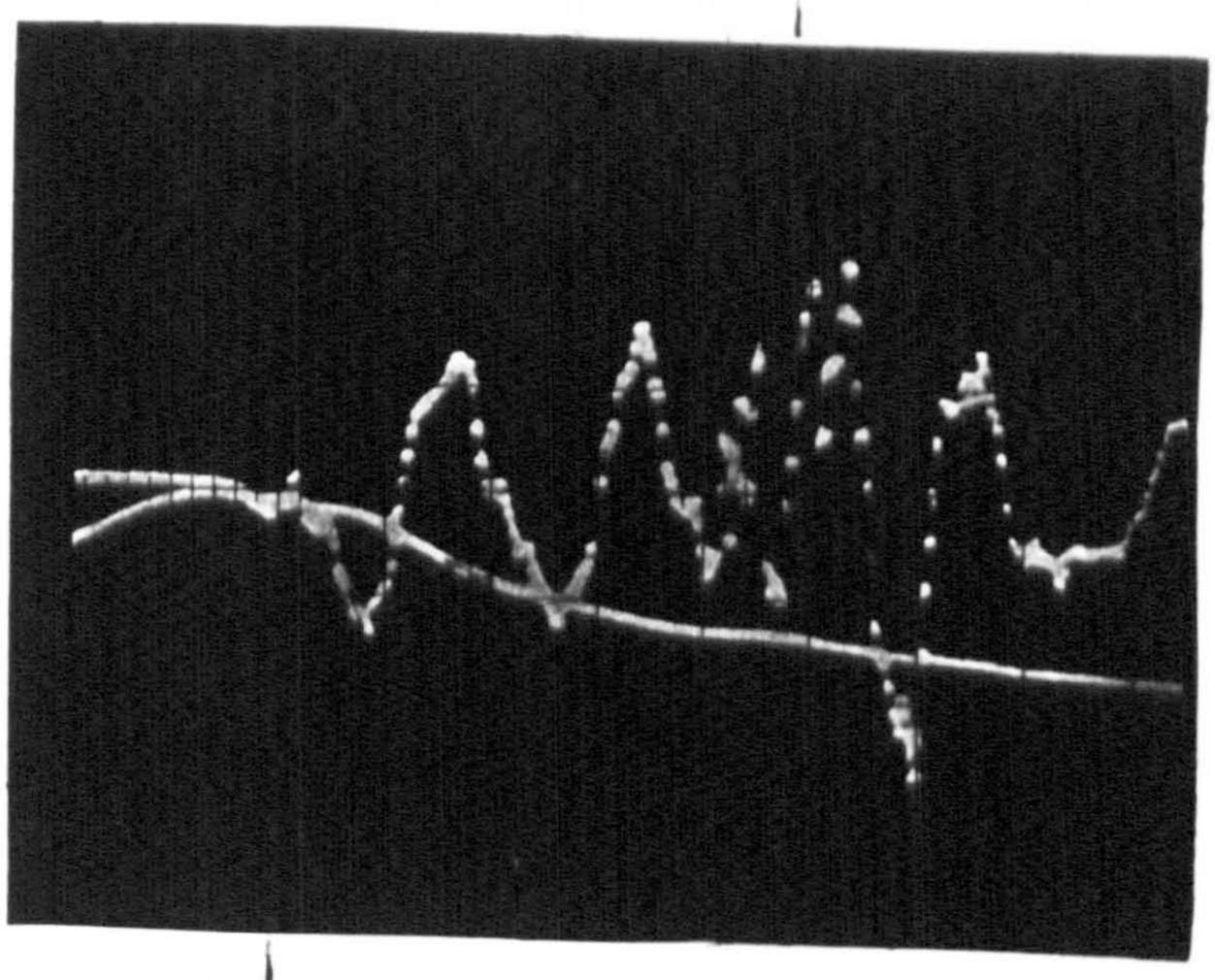

49° Cam Fig 4.3
0.443 mm needle
Cam-Cylinder clearance 0.15 mm

STRAIN-WAVE AT HOOK
(432 and 443 ft/min)

Fig 20.8(c)

CHAPTER 21

DYNAMIC PHOTOELASTICITY

21.1 Introduction.

Dynamic Photoelasticity[53 to 62 inc] is a technique which uses polarised monochromatic or white light to observe the process of stress wave propagation through structural components.

Used for the measurement of impact propagation through the needle, the technique has some important advantages but it also possesses some severe limitations, and these are each summarised below :-

(i) As photoelasticity is a whole-field measuring technique, it has a distinct advantage over strain gauging techniques (chapter 20) in that it provides a complete and continuous picture of stress-wave propagation through the needle.

(ii) It is relatively easy to examine wave propagation at any time interval after the initial impact.

(iii) It is difficult to quantitatively determine stress magnitudes, because the normal static photoelastic techniques for determining the principal stresses cannot be used.

(iv) For stress-wave considerations the most important region of the needle is the hook; unfortunately this is far to small for detailed photoelastic analysis, and the model must be considerably enlarged. Unfortunately, with such differences in scale between model and needle, the problem of dynamic similarity and the relationship between the responses becomes very difficult to interpret.

(v) It is difficult to ensure dynamic simalarity between the pulse applied to the plastic model and the impact applied to the needle during the knitting process.

At the time of writing this thesis, the work carried out on dynamic photoelasticity is at an early stage and no experimental measurements have been obtained; however an experimental technique has been evolved and many of the technical problems have been solved.

21.2 Dimensional Analysis.

The shape of the pulse applied to the model should be similar to that applied to the prototype (i.e. the actual needle), and should have the same scale factor as that used for the linear dimensions of the model. For example :-

$$\frac{F_P}{x_P} = \frac{F_m}{x_m} \qquad (173)$$

where F_p = Force applied to the protoype
F_m = Force applied to the model
and x_p/x_m = Linear prototype to model scale factor.

Similarly, for the shape of the pulse to be the same for the prototype and model :-

$$\frac{\delta F_p}{\delta x_p} = \frac{\delta F_m}{\delta x_m} \qquad (174)$$

Corresponding stress distributions exist in both model and prototype when the stress waves have travelled corresponding distances, i.e. when :-

$$\frac{t_m}{t_p} = \frac{L_m c_p}{L_p c_m} = \frac{L_m}{L_p}\left(\frac{E_p}{E_m}\right)^{1/2}\left(\frac{\rho_m}{\rho_p}\right) \qquad (175)$$

for rods, and similar cases, when :

$$\nu_m = \nu_p$$

and where

L_m = model distance,

L_p = prototype distance,
c_p = propagation velocity for prototype
c_m = propagation velocity for model,
E_p = Youngs Modulus for material of prototype
E_m = Youngs Modulus for material of model,
ρ_m = density of model material,
ρ_p = density of prototype material,
ν_m = poissons ratio of model material,
and ν_p = poissons ratio of prototype material.

Due to the high viscoelastic damping of model materials, however, quantitative interpretation must be restritced to the initial phases of the response to impact only.

21.3 Apparatus and Circuitry.

Fig 21.1 is a diagram showing the circuitry, and Fig 21.2 shows the essential construction of the measuring apparatus which is based upon a technique suggested by H. Becker[54].

A pendulum hammer impacts the plastic model which is constrained horizontally between two transparent plastic walls to simulate the trick constraint. At the instant of impact with the plastic model, a circuit is closed and a signal is transmitted to the retard circuit. Depending on the particular settings on the retard circuit, the input signal is delayed for a controlled time interval which can be adjusted between 1×10^{-9} seconds and 1×10^{-3} seconds.

The delayed output signal then triggers the carbon-arc unit which produces a high intensity flash. The light from the flash passes through a polariser, the model, and analyser. The image showing the photoelastic fringes is recorded by an open-shutter camera. The major advantage of the technique is that, by adjusting the time-delay, the wave motion can be photographed at any pre-set time interval after

the initial impact. However, the technique depends upon the absolute repeatability of the input force, the delay time, and the triggering position.

A major limitation to the experimental method is that the needle must be capable of free vertical motion in the plastic guides. If there was any vertical constraint in the guides, then the experiment would be unrepresentative because the needle, during the knitting process, is free to move vertically in its trick. If the needle was indeed constrained vertically in the trick a much better system could be used; this would involve impacting the needle at a high frequency, by a bell mechanism or something similar. The flash would be at the same frequency but delayed by a fixed amount depending upon the settings on the retard circuit. A stationary image could then be displayed on a screen before a photograph was taken and, simply by adjusting the delay, the position of the wave could be observed at any instant of time after the impact.

The apparatus used in the photoelastic examination is discussed below.

21.3.1 The Triggering Method.

The retard circuit is designed so that, when a junction is closed between the two input terminals of the circuit, a voltage signal is generated inside the device. A thin small steel shim was glued to the model needle very near to the position of impact and one wire from the retard circuit was connected to this shim. The other wire was connected to the hammer and, when the hammer made contact with the model and shim, it closed the junction.

21.3.2 The Retard Circuit.

The retard circuit transmits a nine volt signal to

the flash unit, at an adjustable time-delay, after generating the input voltage signal from the trigger circuit.

21.3.3 The Flash Units.

To arrest the wave motion and record a distinct photograph it is essential that the flash has a very short duration, i.e. approximately 0.4×10^{-6} secs. The major problem with t is type of work is the amount of light that can be concentrated into the model during the flash duration. The amount of energy released should be at least 100 Joules, to obtain a reasonably detailed photograph. Unfortunately the flash unit shown in Fig 21.1, while satisfying the time requirement, provided insufficient energy, and the initial photographs did not develop succesfully. At the time of writing the thesis, the circuitry is being adapted to use a ruby pulsed laser; this has a very short flash duration with an output energy of approximately 100 Joules.

21.3.4 Ultimate Objective of Photoelastic Analysis.

Eventually, it should be possible to use this technique to examine and test needle design before commercial needles are mass-produced. Obviously, the measuring technique would have to be optimised before it could be used commercially, and this might necessitate a cheaper alternative light source, or method of increasing the light intensity, to replace the expensive pulsed laser. However, as the latter was available for use with other research in the Department, it was adopted for this application.

In the future it should be possible to manufacture a plastic model of the needle, test it under impact conditions, modify it if necessary, and test each stage of the design process. Finally, a commercial needle could then be produced,

having been designed specificully to withstand the dynamic conditions simulated during the test.

A photo-diode trigger can be used to produce an input signal into the delay signal; however it has the disadvantage that a square fronted pulse cannot easily be produced.

A contacting trigger is shown where a metal based paint is painted to the butt surface. One wire is connected to the butt and the other to the load. A square fronted pulse is produced when the load contacts the butt

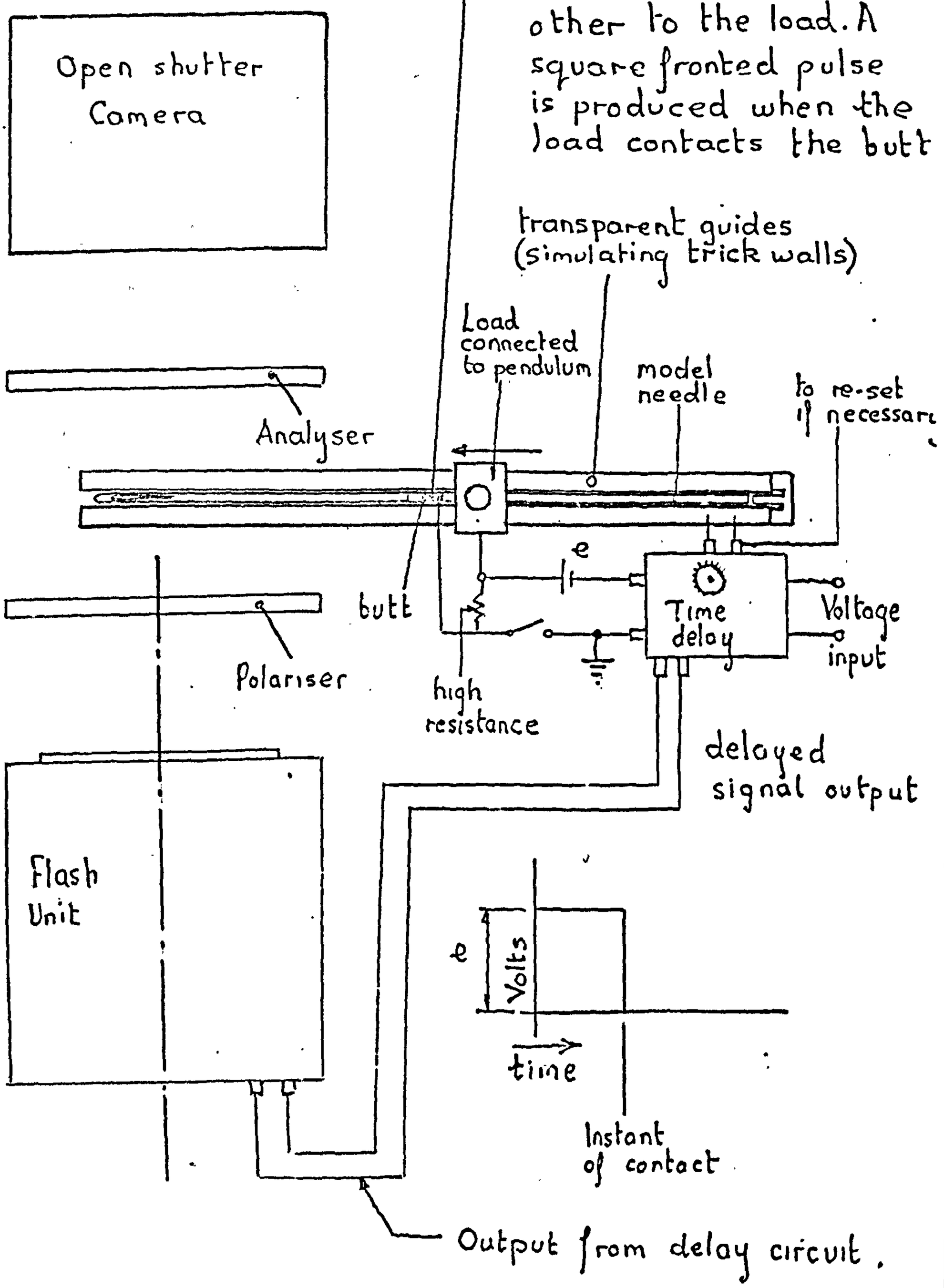

DYNAMIC PHOTO-ELASTIC EXAMINATION OF STRESS-WAVES (APPARATUS AND CIRCUITRY)

FIG 21.1

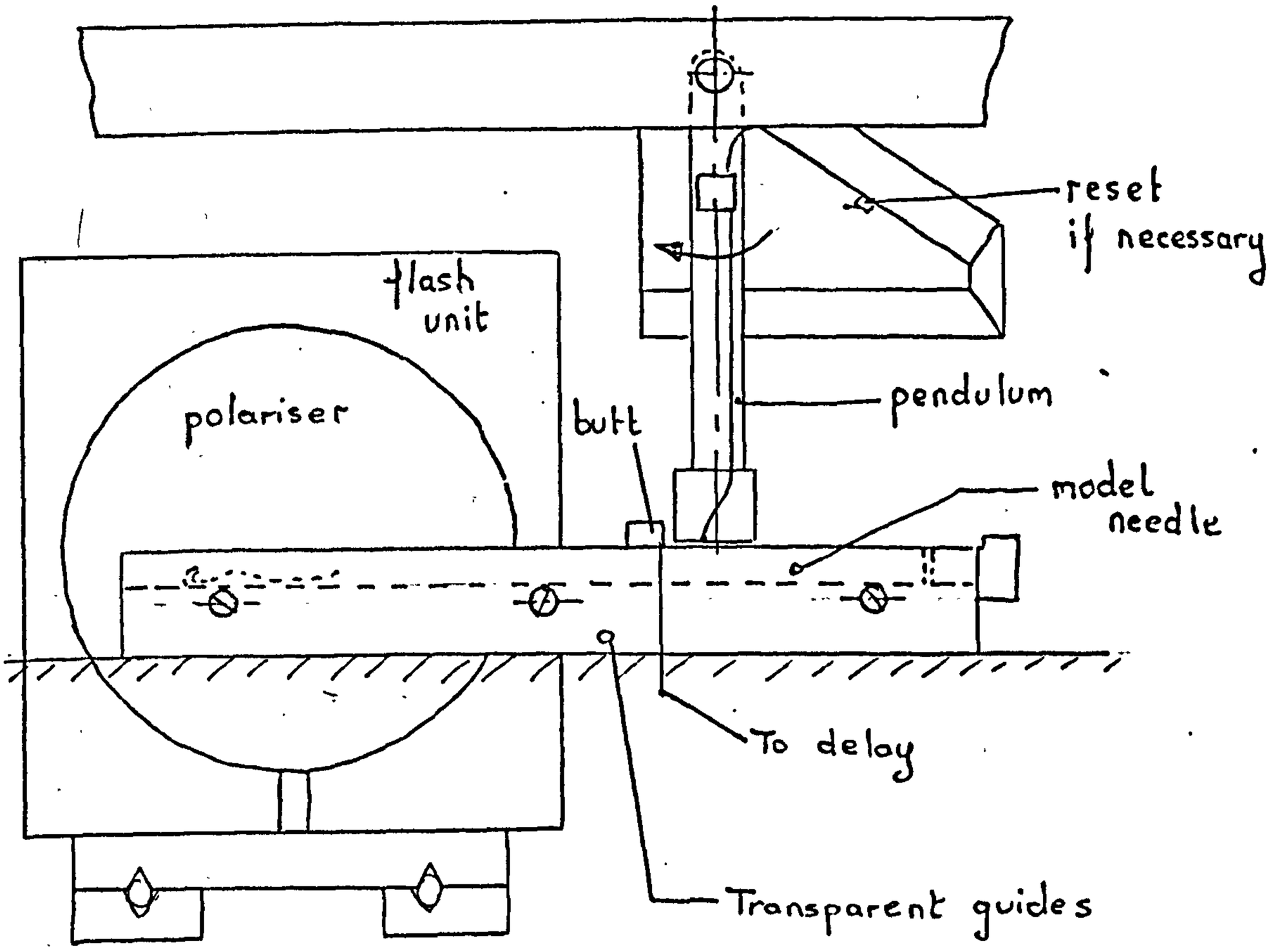

DYNAMIC PHOTOELASTIC APPARATUS

FIG 21.2

CHAPTER 22

CONCLUSIONS TO PART E

22.1 Introductory Discussion.

Experimental measurements, using the dynamic photoelastic technique, have not been obtained at the time of submitting the thesis. Obviously, when the analysis is completed, a wide range of important conclusions concerning the wave propagation through the needle will be available, but at the moment the results are somewhat incomplete. However, a summary of the other results, contained in chapters 19 and 20, is presented below.

22.2 Summary of Conclusions contained in Chapters 19 and 20.

(i) Butt fractures were common for needles, tight in their tricks, when they impacted relatively steep stitch-cams at high speed.

(ii) Butt fractures often occurred at high speed impact with the guard-cam, if the trick resistance to needle motion was low, and if the stitch-cam firing angle was steep. It was not clear, during the experimentation detailed in chapter 19, whether it was the magnitude of the impact, or needle chatter on the guard-cam, or a combination of both, that was responsible for butt fracture.

(iii) Needle hook fracture was dependent upon the magnitude of guard-cam impact. Fracture occurred more readily if needles that were free in their tricks were fired off steep stitch-cam angles at high machine speed. The breakage rate is very sensitive to changes in the needle cross-sectional area at the hook; if the area is reduced the incidence of fracture increases.

(iv) Needle breakage occurs anywhere on the shank where the area of the needle is reduced to small proportions; this tends to contradict the suggestion of a wave addition process being responsible for failure.

(v) Results using the needle with the cut-out just below the normal fracture position, as detailed in section 19.2.1 section (v), suggested that hook vibration was not a significant cause of fracture.

(vi) There was a time scale in the needle destruction process. Needles with the highest magnitude guard-cam impacts broke at the hook more rapidly than needles with progressively lower magnitude impacts.

(vii) Measurements using strain gauges bonded to the needle shank clearly showed a high magnitude strain pulse transmitted up the needle shank at the instant of guard-cam impact. The results also showed a high proportion of vibration or wave disturbance following the pulse. Additional to the longitudinal disturbance there was a large bending strain at the instant of stitch cam impact.

(viii) Measurements, using the strain gauge bonded to the needle hook, showed a large number of high magnitude stress reversals combined with a pulse that increased in magnitude as machine speed increased. It appeared that the first four or five reversals resulted from stitch-cam impact, and the remainder from guard-cam impact. The result suggests a possible fatigue mechanism where the fracture rate would depend upon the number of cams, and on impact magnitude and machine speed.

(ix) Measurements carried out using a needle with seven of the wedge cut-outs detailed in section 19.1.2 were inconclusive; however it did seem that there was an

increased risk of fracture across the corner of the wedge.

22.2.1 An Alternative Measurement Technique.

Another possible technique for measuring the wave propagation, might be developed as future work, particularly if the current photoelastic technique does not live up to expectations. This involves building an enlarged steel model of the needle which would be strain-gauged. A catapult device could be used to propel the needle at high velocity against a hard cam, and the strain-gauge output could be recorded.

PART F

RECOMMENDATIONS FOR THE REDESIGN OF THE NEEDIE-CAM SYSTEM

CHAPTER 23

DESIGN OF KNITTING CAMS

23.1 Introduction.

The sponsors of this project were particularly interested in applying the results obtained during the research, to the design of stitch and guard-cams for use on a future high-speed knitting machine. Further details of the design brief, issued by the company, concerning the dimensions and operational requirements of the cams is contained in section 23.3. The cams are intended for a particular speed and knitting machine, and for any other application they would need to be redesigned; however, the techniques detailed in this chapter could be used for the design of any cams used for knitting operations.

23.1.1 Important Considerations in Cam Design.

The design of cams to operate at high machine speeds must, as far as is possible, satisfy the important criteria given below :-

(i) Short-circumferential length.

To increase the production rate and to obtain a large pattern area, it is important to maximise the number of cams around the machine circumference; this can only be accomplished if the circumferential cam-length is small.

(ii) Stitch-cam impact.

It is important that the stitch-cam impact should be minimised. Impact with the cams can occur at the normal knitting height, at the tuck-height, and at the miss-height, as shown in Fig 15.1.

(iii) Guard-cam impact.

Means must be provided to minimise the impact when

the needle leaves the stitch-cam and hits the guard-cam.

(iv) Latch-impact.

To minimise latch impact, it is important to reduce the vertical velocity of the needle at the instant when the latch is flicking upwards to enclose the new yarn. The only obvious method of reducing the latch closing velocity at present is to minimise the stitch cam angle.

(v) Loss of cam-contact.

Loss of contact at the base of the stitch-cam can lead to non-uniform loop formation. The cam profile should be designed so that all the needles lose contact at the same precise position on the profile; the subsequent motion of the needles can be controlled by blending the guard-cam and stitch-cam profiles to provide a smooth transition from one cam to the other.

(vi) Needle Bounce.

Under particular circumstances needle-bounce, originating from stitch-cam impact, can extend to the loop formation zone; if possible this should be prevented, because it can lead to stitch non-uniformity.

(vii) Vertical Adjustment.

A commercial cam system must satisfy the practical requirements of the knitting process. One of these is that the stitch-draw should be variable, and usually this is achieved by s. vertical adjustments to the stitch and guard-cams.

(viii) Wear Resistance.

Over a period of time, the cam-profile will change due to wear. It is important, especially for mathematically shaped profiles, to minimise such wear, because the

inherent advantages designed into the profile can be completely lost as it is slowly worn away.

(ix) Machine "Lock".

If steep cam angles are used on a commercial machine with a large number of cam-stations around the circumference, then, when the machine is started, it can "lock" and this tends to break the needle butts rather than drive the needles through the knitting process.

(x) Manufacturing Considerations.

If at all possible, the cam profiles should be relatively easy to machine and unexpensive to produce.

(xi) Smooth transition.

The cam profile must be designed so that there are no rapid changes of a needle's acceleration at it passes through the system. Such a rapid change in acceleration produces a high magnitude impact.

(xii) Cam length in the loop drawing region.

To minimise the number of yarn-needle and yarn-verge contacts it is important that as few needles as possible be used in the loop-forming zone. The number of needles drawing the yarn loop depends upon cam width at the verge height, see Fig 23.1.

23.2 The Circular Stitch Cam Termination.

It is common practice in cam manufacture to provide a radial base to the stitch-cam, and the cam profile Fig 4.3 used for the majority of the experiments detailed in chapter 8 is a typical example. The circular cam profile was analysed in some detail in section 9.2.1. The inertial force was defined by equation (26), and Fig 9.3 defines the cam co-ordinates. The equation had the form :-

$$T = mv^2 \frac{d^2y}{dx^2} \quad . \quad . \quad . \quad . \quad (176),$$

$$\text{and } \frac{d^2y}{dx^2} = -\left(\frac{(y-y_c)^2 + (x_c - x)^2}{(y-y_c)^3} \right) \quad . \quad . \quad (177),$$

where $T =$ Inertial force,
$m =$ needle mass,
$v =$ machine speed,
and, x_c, y_c are as defined in Fig 9.3.

The equation for the reaction force between a needle butt and linear cam was derived in section 9.2 and had the form :-

$$R = \frac{F + P + \mu_1 Q + f(x) - mg}{\cos\theta(1 - \alpha\mu_1\mu_2) - \sin\theta(\mu_2 + \alpha\mu_1)} \quad . \quad (178),$$

(All the terms are defined in Fig 9.2).

When the needle is on the circular stitch-cam termination then :-

$$R = \frac{F + P + \mu_1 Q - mg + mv^2\left(\frac{d^2y}{dx^2}\right) + f(x)}{\cos\theta(1 - \alpha\mu_1\mu_2) - \sin\theta(\mu_2 + \alpha\mu_1)} \quad . \quad (179).$$

Loss of cam needle contact occurs when the reaction-force :-

$$R = 0,$$

i.e., when,

$$mv^2\left(\frac{d^2y}{dx^2}\right) = -\left(F + P + \mu_1 Q - mg + f(x)\right) \quad . \quad (180).$$

Using equation (24) and (25) of section 9.2.1, expressions for the maximum and minimum needle acceleration.

on the radial cam termination were determined. The analysis used the equation given below :-

$$\frac{d^2y}{dt^2} = v^2 \frac{d^2y}{dx^2} \quad . \quad . \quad . \quad . \quad (181),$$

where $\frac{d^2y}{dx^2}$ is defined in equation (177),

also $$\frac{dy}{dt} = v \frac{dy}{dx},$$

and $$\frac{dy}{dx} = \frac{(x_c - x)}{(y - y_c)}.$$

From Fig 9.3 :-

$$r^2 = (y - y_c)^2 + (x_c - x)^2 \quad .$$

therefore,

$$\frac{d^2y}{dt^2} = -v^2 \left(\frac{r^2}{(y - y_c)} \right) \quad . \quad . \quad . \quad (182).$$

Maximum deceleration occurs when $(y - y_c)$ is a minimum on the circular profile, and then :-

$$(y - y_c) = r\cos\Theta$$

where: Θ = linear cam angle

and Maximum Deceleration = $-v^2 \left(\frac{1}{r\cos^3\Theta} \right) \quad . \quad . \quad (183)$

For example, when $\Theta = 55^0$, and V = 250 ft/min,

for r = 0.05 in. (1.27 mm), maximum deceleration = -22,200 ft/sec^2,

and for

r = 0.2 in. (5.07 mm), maximum deceleration = -5,500 ft/sec^2.

Minimum deceleration is when $(y - y_c) = r$

and therefore :

minimum deceleration $= -\frac{v^2}{r}$

The highest magnitude deceleration occurs when the needle first contacts the radial cam termination. Depending upon the trick clamping and yarn-force for each needle,

there is a particular machine speed above which the needle will separate from the cam at the instant of contact with the circular termination, and below which the needle will maintain cam contact down to the very base of the cam.

From equations(180)and(181), seperation occurs when :

$$\frac{d^2y}{dt^2} = -\frac{(F + P + \mu_1 Q - mg + f(x))}{m} . \qquad (184).$$

For example, if the needle is free in its trick, and the term $F + P + \mu Q - mg$ is only equivalent to 20 gf, and if the yarn tension term is 50 gf, then seperation occurs when : $\frac{d^2y}{dt^2} = 2{,}884$ ft/sec^2 (879 m/sec^2).

For there to be no separation on a 55° cam at 250 ft/min (1.27 m/sec), then the radius must be approximately 0.4 in. (10.1 mm).

23.2.1 Conclusions.

The radial termination to the stitch-cam has three important disadvantages.

(i) Because trick resistance to needle motion varies considerably from one trick to the other, some needles will leave the cam at the beginning of the radial termination, where the cam has a maximum magnitude deceleration, and the others will maintain cam contact to the very bottom of the radius. Consequently, such different needle paths will produce considerable stitch non-uniformity.

(ii) To ensure that all the needles maintain cam contact at high machine speeds, the radius must be large compared to the dimensions of the cam. For example, at speeds of 250 ft/min (1.27 m/sec), the radius must be greater than 0.4 in. (10.1 mm).

(iii) At the instant the needle transfers from the

linear to the radial profile, there is an impact resulting from the rapid change in acceleration.

23.3 Introduction-Design of a Practical Cam System.

The brief from the sponsoring company was for a stitch-guard cam system designed to reduce the incidence of needle damage and produce a more uniform stitch formation when used at a speed of 30 revs/min on a 30 in. diameter machine (235 ft/min). The system had to be designed within the dimensions specified on Fig 23.2, which corresponded to a 55^{o} linear cam. It had to be capable of accepting needles at various heights i.e. tuck height, miss height, etc, and it had to be vertically adjustable to alter the stitch-draw.

23.3.1 Calculations.

From equation (184), separation occurs when :-

$$\frac{d^2y}{dt^2} = -\frac{1}{m}\left(F + P + \mu_1 Q - mg + f(x)\right) . \qquad (185)$$

On a commercial machine the trick resistance to needle motion varies considerably from one trick to an other. However, separation occurs earlier on the cam profile if the term $P + \mu_1 Q - mg + f(x) + F$ is small. If there is very little oil in the trick, the F term can be considered to be zero. The term $P + \mu_1 Q - mg$ can be approximated by measuring the force required to lift the needle vertically in its trick at a steady low velocity. The procedure for measuring $P + \mu_1 Q - mg$ was described in more detail in section 9.5, and for the 0.443 mm standard needle the value was 46 gf; this was assumed to be normal trick resistance, although considerable variation was evidenced. A low value of trick resistance is 20 gf, and this figure was used in the subsequent analysis. It is possible that the trick

resistance could be smaller but this would be rare and would probably only be as a result of trick damage. A low value of the term $f(x)$ occurs, when small yarn loops are being drawn.

The force exerted upon the needle by the yarn depends upon the cam-profile in the loop formation zone, and it is impossible to define the tensions before a particular profile is designed. The results contained in chapter 8 showed that low yarn-force occurs when the input yarn tension, take-down tension, and stitch-draw are all small. The yarn-force magnitudes measured in chapter 8 cannot be used for the design of the cams, firstly because a particular cam profile was used, and secondly because a high speed machine would probably not use the square section verges shown in Fig 9.8.

In the design of the cams, the value chosen for $f(x)$ was 70gf, it is immaterial what value is chosen provided that, during the normal machine operation, it seldom falls below 70 gf. The theoretical analysis, examined in chapter 9, can be used to define the minimum values of yarn-tension, take-down tension, and stitch-draw, to ensure that the force $P + \mu_1 Q - mg + f(x)$ does not fall below the chosen value on the cam-profile.

From equation (185) :-

$$\frac{d^2y}{dt^2} = -32.2 \times \frac{(70 + 20)}{0.67} \text{ ft/sec}^2,$$

and hence $$\frac{d^2y}{dt^2} = -4,320 \text{ ft/sec}^2 \quad . \quad . \quad . \quad (186)$$

The cams detailed in section 23.3.2 below, were designed so that the needle deceleration on the cam profile was less than -4,320 ft/sec^2 at a machine speed of 234 ft/min (1.19 m/sec).

23.3.2 Sine-Sine Cam Profile.

A group of cams were designed, all from the junction of two basic mathematical curves. None of the cams completely satisfied all the requirements specified in section 23.1.1, and generally a compromise was made. The most restrictive specification is cam-length, and, if the stitch cam could be longer than the limit specified on Fig 23.2, then the design problem would be simplified; this, however, would mean fewer knitting stations around the machine.

A typical sine-to-sine profile is shown in Fig 23.3. The sine curve at the bottom of the cam was designed using the condition that the maximum magnitude deceleration just reaches the value specified in section 23.3.1 at the cam-base.

Using the co-ordinates shown in Fig 23.4, the profile of the cam is defined by the equations :-

$$y = a \sin\left(\frac{\pi x}{b}\right) \quad \frac{3b}{2} \leqslant x \leqslant 2b \quad . \quad . \quad (187),$$

$$y = d \sin\left(\frac{\pi(x-2b)}{c}\right) \quad 2b \leqslant x \leqslant 2b + \frac{c}{2} \quad . \quad (188),$$

$$\frac{dy}{dt} = \frac{va\pi}{b} \cos\left(\frac{\pi x}{b}\right) \quad \frac{3b}{2} \leqslant x \leqslant 2b \quad . \quad (189),$$

$$\frac{dy}{dt} = \frac{vd\pi}{c} \cos\left(\frac{\pi(x-2b)}{c}\right) \quad 2b \leqslant x \leqslant 2b + \frac{c}{2} \quad (190),$$

$$\frac{d^2y}{dt^2} = -\frac{v^2a\pi^2}{b^2} \sin\left(\frac{\pi x}{b}\right) \quad \frac{3b}{2} \leqslant x \leqslant 2b \quad . \quad (191),$$

and

$$\frac{d^2y}{dt^2} = -\frac{v^2d\pi^2}{c^2} \sin\left(\frac{\pi(x-2b)}{c}\right) \quad 2b \leqslant x \leqslant 2b + \frac{c}{2} \quad (192).$$

An additional requirement is that when :-

$$x = 2b \quad \frac{dy}{dt} = v \tan\eta \quad . \quad . \quad (193)$$

where η is the cam angle at the junction of the two curves.

From equation (189) and (193)

when $x = 2b$,

$$\frac{va\pi}{b} = v\tan\eta,$$

therefore : $$\frac{a}{b} = \frac{\tan\eta}{\pi} \quad . \quad . \quad . \quad . \quad . \quad (194).$$

Similarly from equations (190) and (193)

when $x = 2b$

$$\frac{d}{c} = \frac{\tan\eta}{\pi} \quad . \quad . \quad . \quad . \quad (195).$$

Two cam profiles were designed, the first with an angle η of 60° and the second with an η of 65°. At the bottom of both cams, the deceleration just reached a magnitude of $-4,320$ ft/sec^2, i.e. the figure evaluated in section 23.3.1. Cam-needle separation during knitting will, for the vast majority of the needles, occur at exactly the same position on the profile, and only very free needles will separate just prior to reaching the base. However, as the closed track between guard and stitch-cam was extended to cover the possibility of an early separation, as shown in Fig 23.5, all the needles should follow the same path :-

From the co-ordinates defined in Fig 23.4 the base of the stitch-cam is at position ① :-

where $x = \frac{3b}{2}$,

then from equation (191)

$$\frac{dy}{dt} = \frac{v^2a\pi^2}{b^2} \quad . \quad . \quad . \quad . \quad (196)$$

Using equation (186) and noting from the co-ordinates Fig 23.5 that $\frac{v^2a\pi^2}{b^2}$ (equation (196)) is a deceleration.

then $$\frac{v^2a\pi^2}{b^2} = 4320 \quad . \quad . \quad . \quad . \quad (197)$$

and when V = 235 ft/min (1.19 m/sec),

$$\frac{a}{b^2} = 2.42 \quad . \quad . \quad . \quad . \quad (198)$$

Also as the designed cam depth is a known quantity, thus, from Fig 23.5 :-

$$a + d = B \quad . \quad . \quad . \quad . \quad (199)$$

where B equals the total cam depth.

Combining equation (194), (195), (198) and (199), a, b, c, and d can be calculated.

For the cam $\eta = 60^{\circ}$:

$a = 0.124$ in.,
$b = 0.225$ in.,
$c = 0.562$ in.,
and $d = 0.310$ in.;

and, for the cam $\eta = 65^{\circ}$:

$a = 0.187$ in.,
$b = 0.28$ in.,
$c = 0.316$ in.,
and $d = 0.248$ in.

The two stitch-cams are shown in Fig 23.5 and Fig 23.3 respectively.

If it is important that the cam-length should be a defined quantity, this requires that :-

$$b + c = 2A \quad . \quad . \quad . \quad . \quad (200)$$

where A = the length of the Stitch-cam.

Using equation (200) in conjunction with the four equations (194), (195), (198) and (199), the cam angle η can also be evaluated.

One stitch-cam and guard cam with an angle of $\eta = 60^{\circ}$ was manufactured. Fig 23.6 diagram I shows the cam track, and some important features of the design are the closed-tracking at the cam-base to ensure stitch-uniformity, and the continued sine curve profile at the base to remove an impact caused by a sudden change of acceleration when the needle

leaves the stitch-cam.

Another feature of the guard-cam design shown in diagram II of Fig 23.6 is the increased land-width. The experimental results detailed in section 16.6, showed that increasing the cam cylinder clearance decreased the magnitude of the guard-cam impact. Increasing the land width distributes the impact over a large butt area and effectively increases the cam-cylinder clearance.

23.3.3 Features of the Sine-Sine Profile.

The 65^{o} and the 60^{o} sine-sine cams do not satisfy all the requirements stipulated in section 23.1.1. The important features of the curves are illustrated below :-

(i) The 60^{o} cam :-

Cam-length	25% longer than 55^{o} linear cam.
Stitch-cam impact	40 to 45 depending upon stitch-draw.
Guard-cam impact	non-existant up to a machine speed of 235 ft/min.
Latch-impact	55^{o} cam angle.
Tuck-height impact	55^{o} cam angle.
Total draw length	0.08 in. (2.03 mm).

(ii) The 65^{o} cam :-

Cam-length	2% shorter than 55^{o} linear cam.
Stitch-cam impact	48 to 58o depending upon stitch-draw.
Guard-cam impact	non-existant up to 235 ft/min.
Latch-impact	60o.
Tuck-height impact	60o
Total draw length	0.075 in.

The 65^{o} cam would be unsuitable for high-speed operation due to the steep angles at tuck and latch-closing height.

23.3.4 Sine-Circular Cam Profile.

This cam profile was designed to overcome the basic disadvantages with the sine-sine cams. The angles of stitch-cam impact, latch closing, and tuck height impact, are all much less than the angles for the sine-sine curves. However, the basic disadvantage of the curve is that there is a step

change in acceleration where the circular profile joins the sinusoidal profile. However, the impact resulting from the change in profile will be considerably less than the primary impact when the needle hits the stitch-cam.

The cams were designed using exactly the same procedure as detailed in section 23.3.2. Figs 23.7 and 23.8 are diagrams showing both cams with radii of 0.675 in. (17.2 mm) and 0.585 in. (14.85 mm) respectively. The guard-cam was also designed following the method desribed in section 23.3.2. However a flat-portion was provided at the bottom of the 0.675 in. radius stitch-cam. In the subsequent experiments,, the flat portion and its effect upon the loop-drawing force was determined. For further information concerning future work see section 23.3.6.

23.3.5 Features of the Sine-Circular Profile.

The imprtant features of the 0.585 in. and 0.675 in. cams are presented below :-

(i) The 0.585 in. radius cam.

Cam-length	10% longer than 55° linear cam.
Stitch-cam impact	35 to 40° depending upon stitch-draw.
Guard-cam impact	non-existent up to a machine speed of 235 ft/min.
Latch-impact	50°
Tuck-height impact	45° to 50°.
Total draw length	0.08 in. (2.03 mm)

(ii) The 0.675 in. radius cam.

Cam-length	5% longer than 55° linear cam.
Stitch-cam impact	40 to 45° depending upon stitch-draw.
Guard-cam impact	non-existent up to a machine speed of 235 ft/min.
Latch impact	55°.
Tuck-height impact	50 to 55°.
Total draw length	0.08 in. (2.03 mm)

23.3.6 Future Work.

At the time of writing this thesis, experimental work to examine the non-linear profiles, at high speed, using the cam-force transducer markIII has not been completed.

However, measurement of the forces will be obtained in the near future and, if necessary, the recommendations contained in the experimental results will be used to modify the cams. The effect of the flat-termination on the base of the 0.675 in. stitch-cam will provide some useful results concerning the process of loop-formation. Finally, it is hoped to combine all the results in the design of cams to be fitted to a commercial 30 in. diameter dial-and cylinder machine and test them under normal working conditions.

23.4 Further Discussion on Cam Design.

The best form of cam-track is one that is continuous, closed-tracked, and involves no step changes in acceleration; such a form is given by a continuous sine-curve and this has the basic advantage of simple manufacture and easy stitch-draw adjustment. However, the system has a basic disadvantage in that it cannot readily cope with tuck and miss stitches. Two possible suggested methods for transmitting the motion of the basic curves from the guide to the motion of the needle, by means of some intermediate linkage, so as to allow for tuck and miss stitches to be accommodated are indicated schematically in Fig 23.9.

23.5 Conclusions.

Although detailed mathematical analysis of the stitch-cam and guard-cam profiles has not been undertaken to date, it is doubtful if any non-linear form could possibly satisfy all the requirements specified in section 23.1.1. The sine-sine profile and the sine-circular profile are simple mathematical shapes and they satisfy many of these. However, if cams are designed for machine speeds of 50 to 100% above those of current operational speeds, it is inevitable that they will be longer than conventional linear cams, and there

will be fewer feeding stations around the machine. If non-linear cams are designed, the mathematical properties of the profile could be destroyed by cam wear, after a period of normal service, and consequently very hard materials are preferable providing these are compatable with machining capabilities. Guard-cam impact occurs when the needle leaves the stitch cam and moves over to contact the guard-cam, and if this is to be avoided, the closed tracking should be used, and the shape of the stitch-cam termination should be so designed that at the operational speed, all the needles leave the stitch-cam at one particular position on the profile where a smooth transition from one cam to the other can be provided. However, at high speed, the cam termination must inevitably become wider if cam-needle separation is to be avoided, and this means that more needles will be held in the loop formation zone; consequently, the yarn tensions will be higher due to the increased number of yarn to metal contacts. At high speed the yarn-tensions must be minimised; two possible methods of doing this are to round and polish the verge tops, and to supply a constant yarn supply at very low input tension.

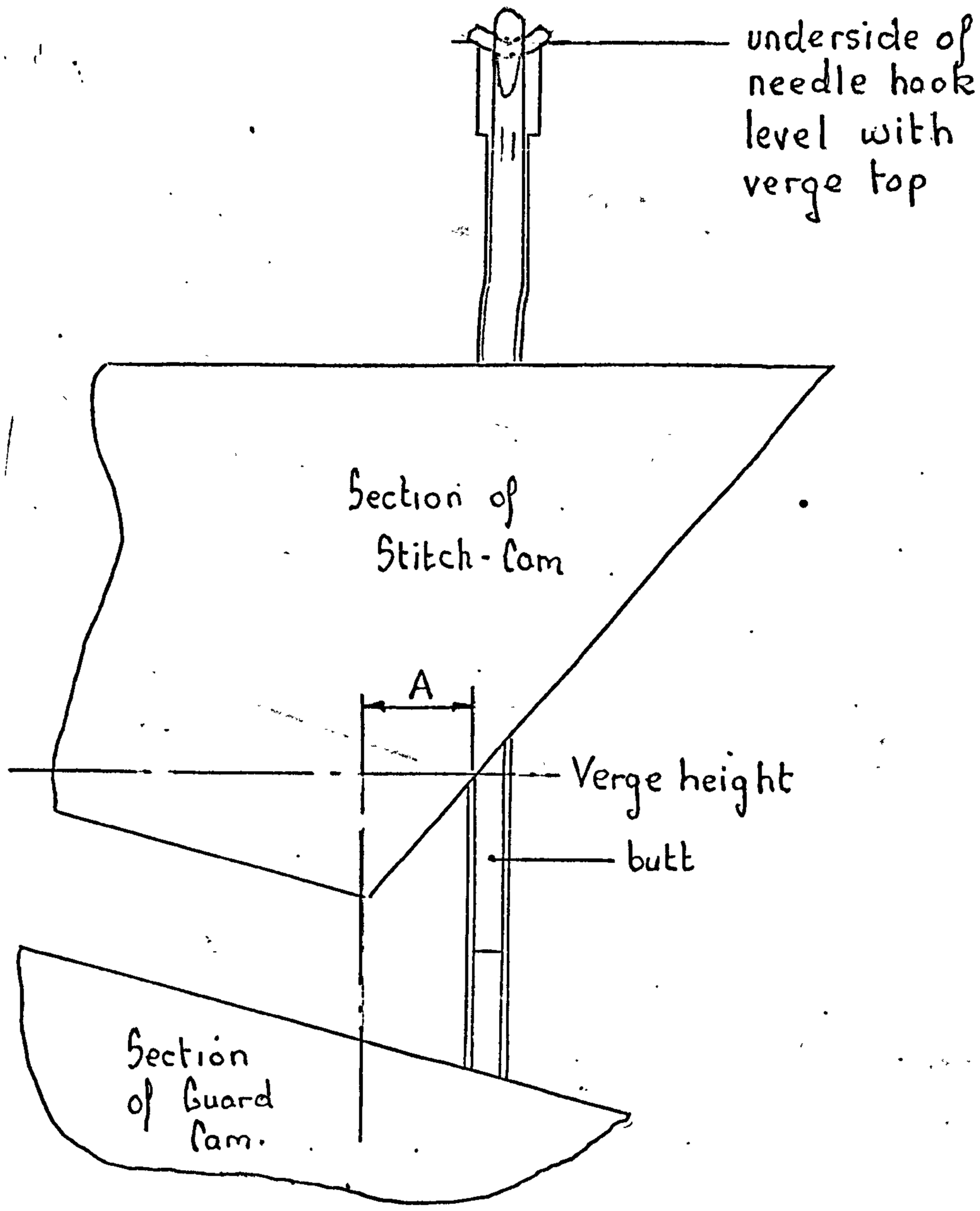

When the needle butt reaches the verge height the needle hook is level with the verge top. If dimension A is small the number of yarn metal contacts is minimised and consequently the yarn-tension build-up is lessened.

CAM-WIDTH AT VERGE HEIGHT

Fig 23.1

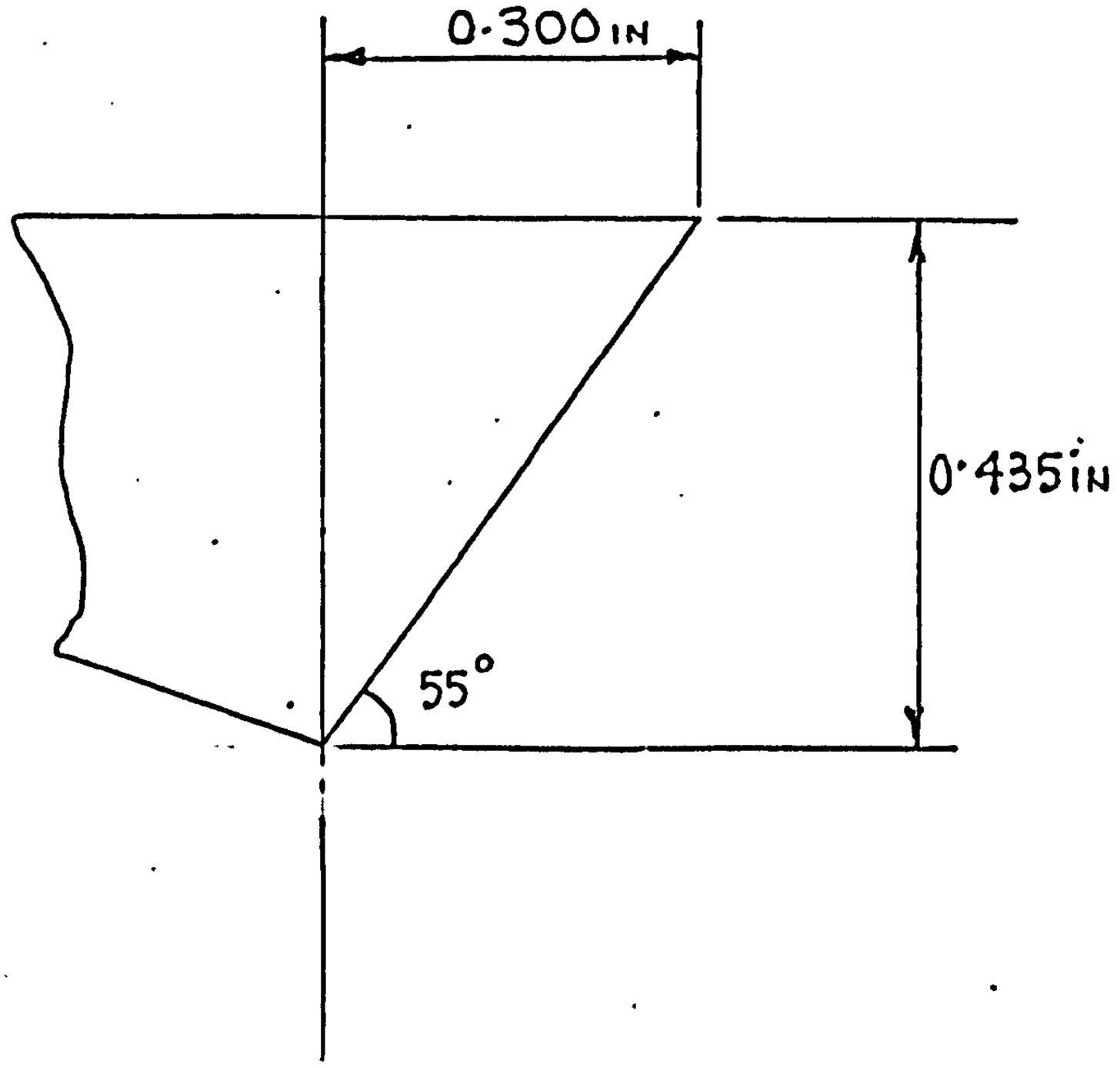

The dimensions of the non-linear cam must be within the limits specified above. (55° linear cam).

DIMENSIONS FOR NON LINEAR CAMS FIG 23.2

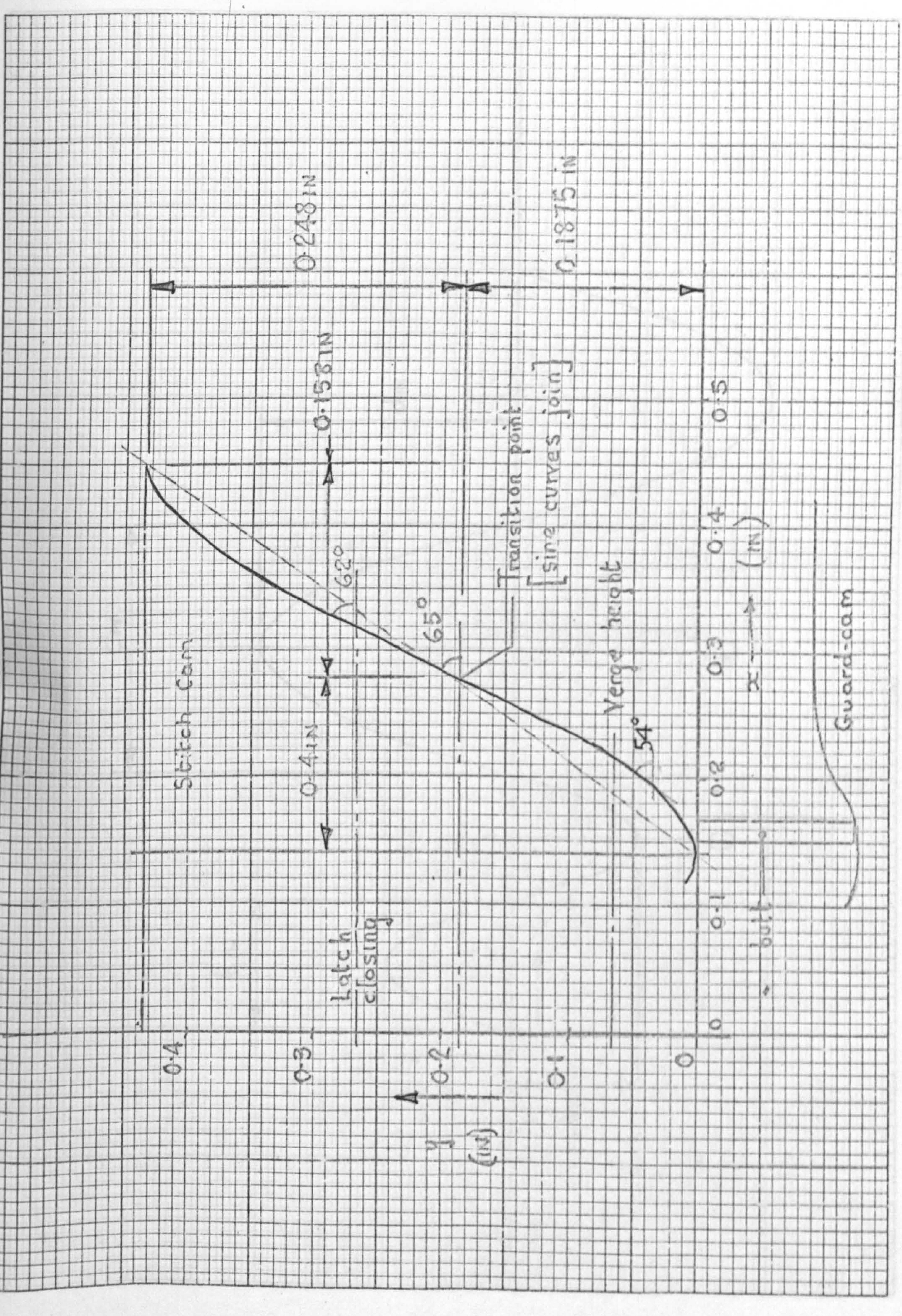

THE $\eta = 65°$ SINE-SINE CAM PROFILE

FIG 23.3

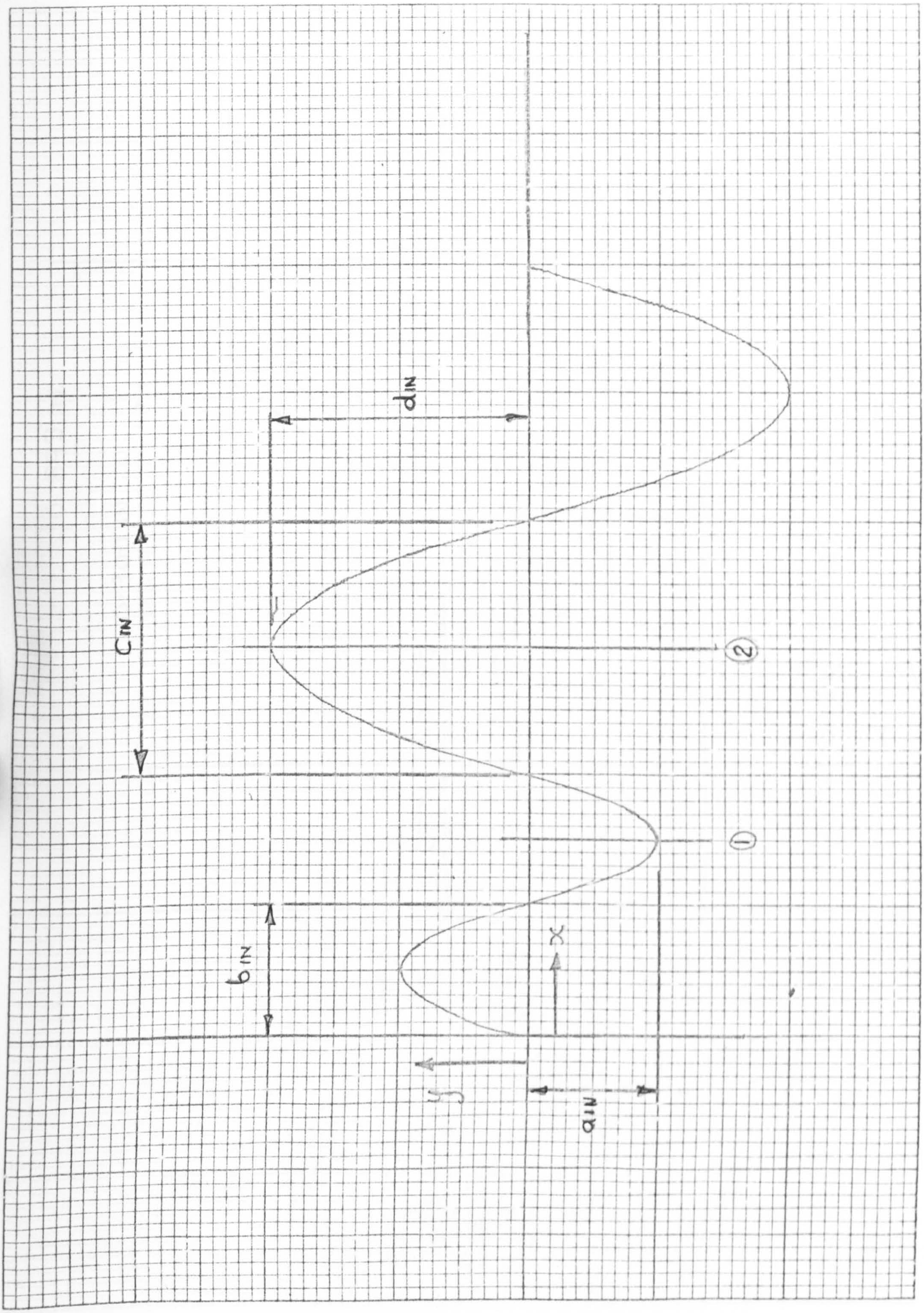

CO-ORDINATES FOR SINE - SINE CAMS

FIG 23.4

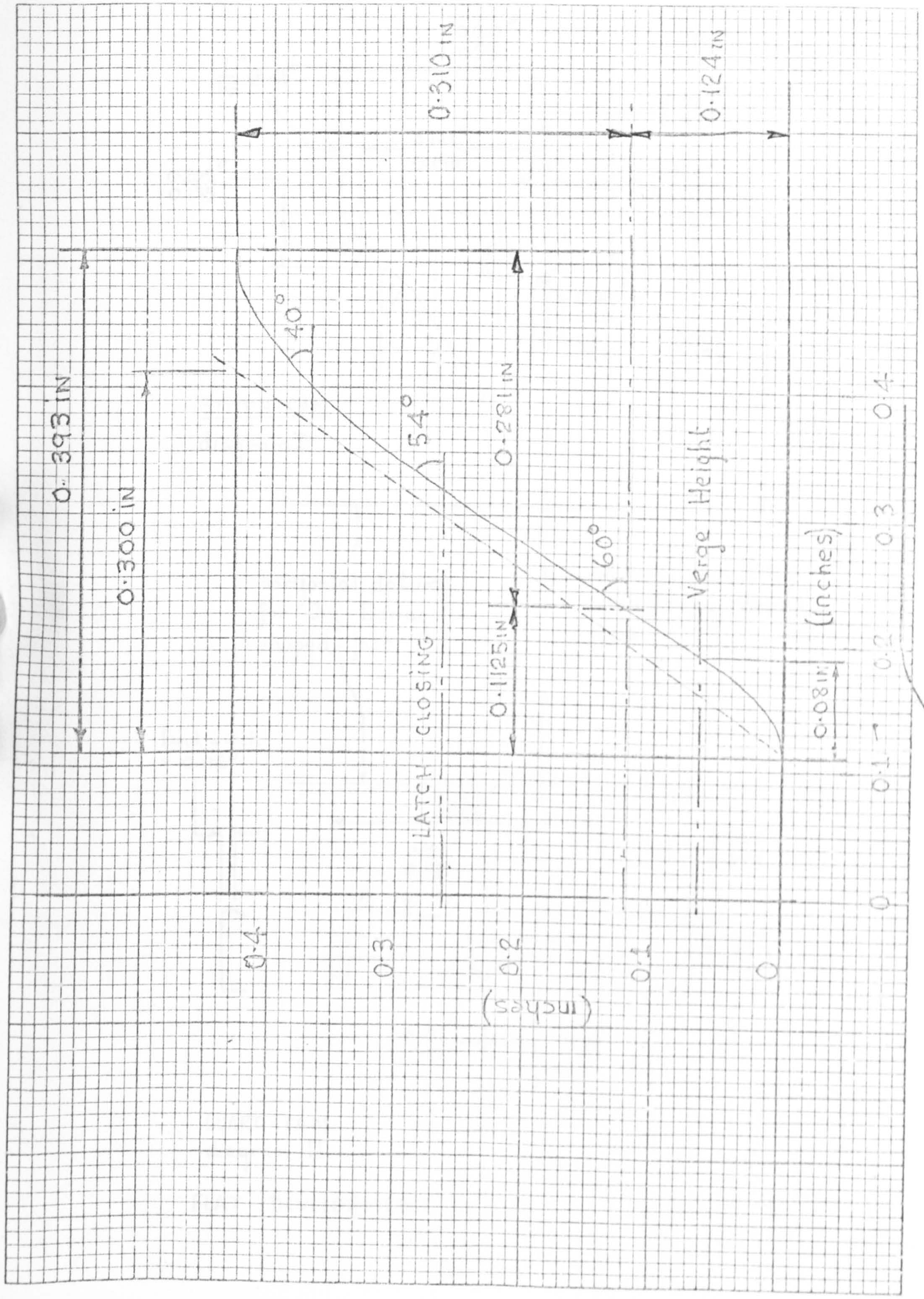

THE $\eta = 60°$ SINE – SINE CURVES

FIG 23.5

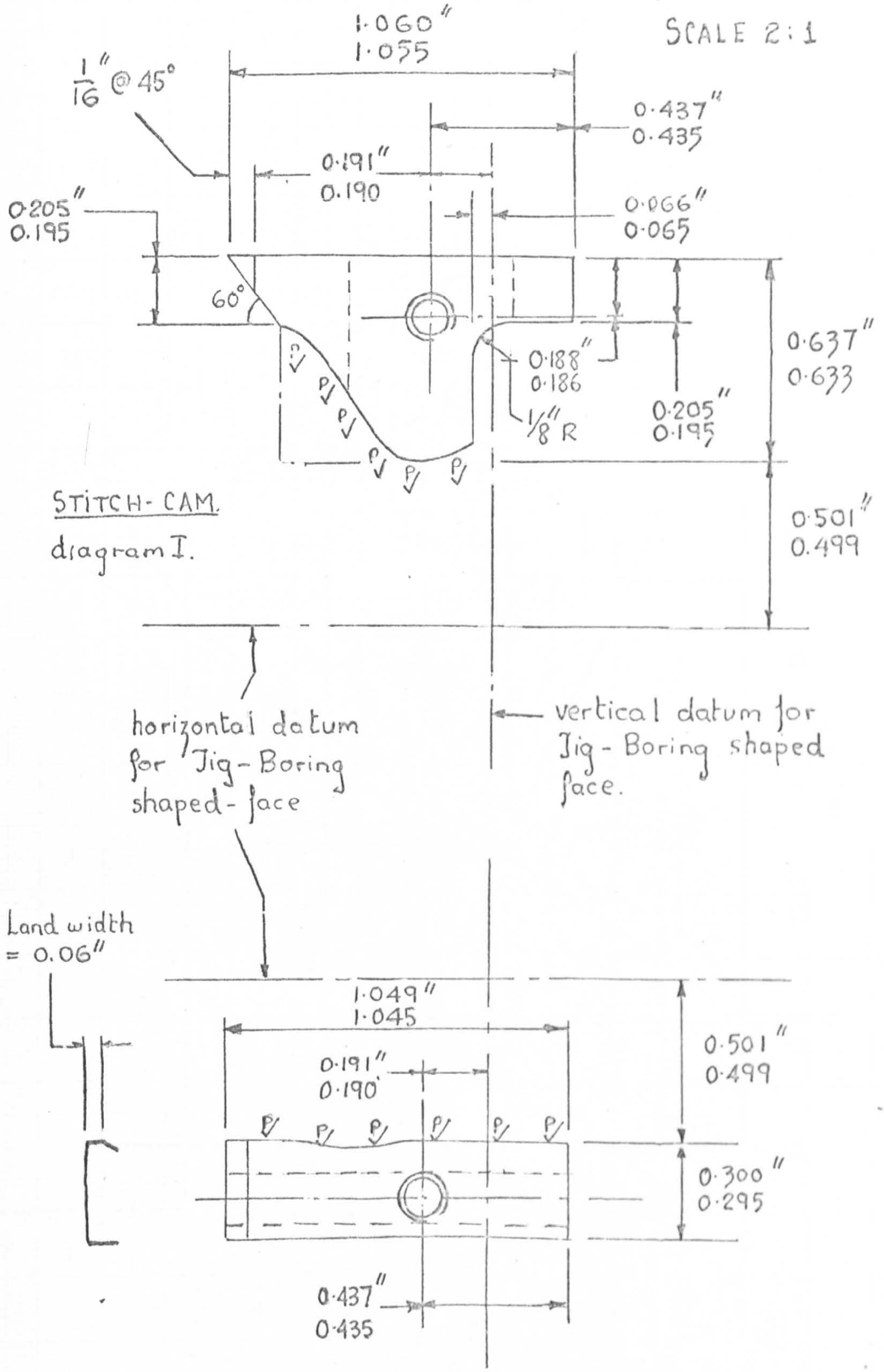

FLAT - DEVELOPMENT

(η = 60°) SINE-SINE CAMS DESIGNED FOR CAM-FORCE TRANSDUCER MARK III

FIG 23.6

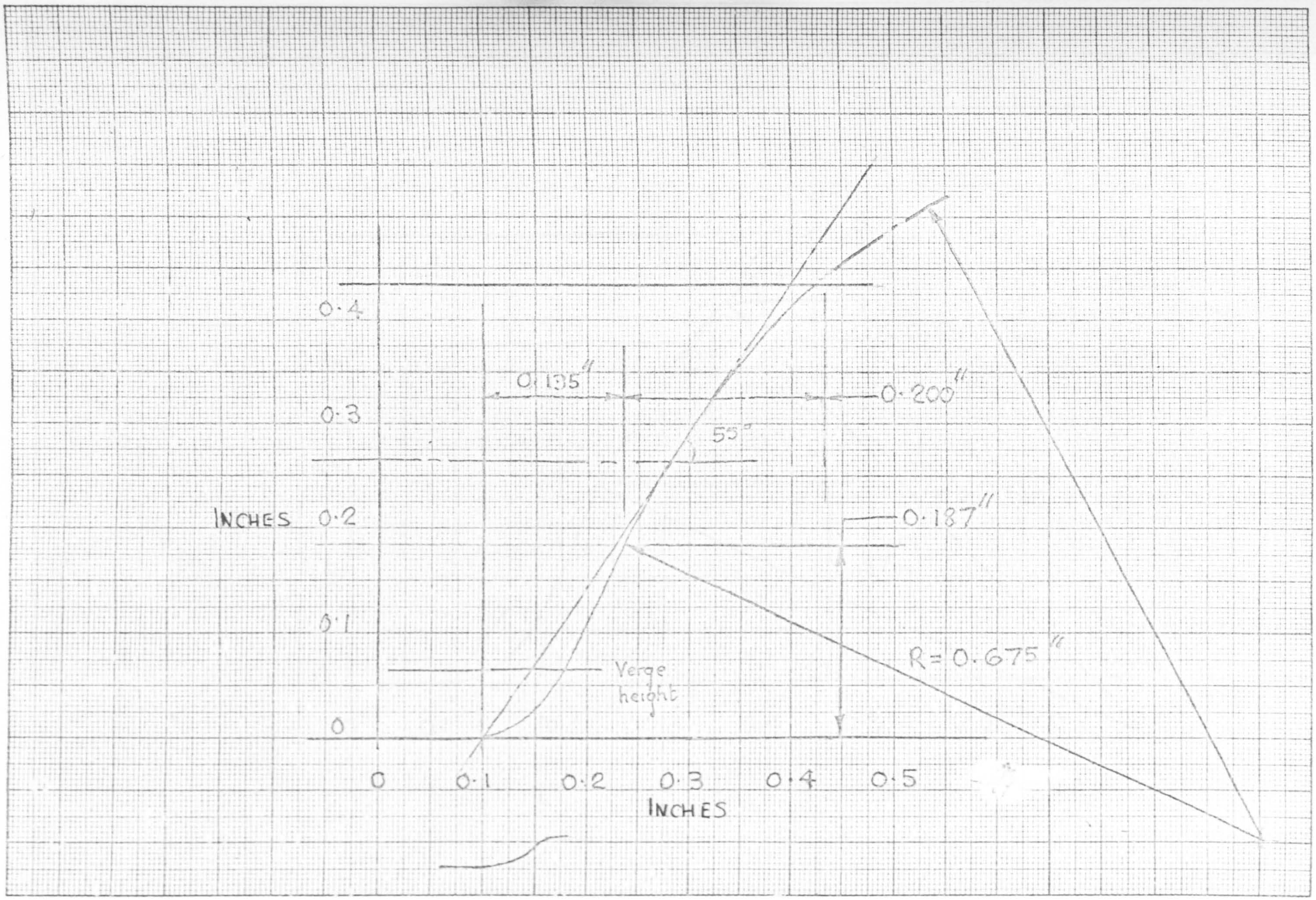

0·675 IN SINE-CIRCULAR CAM.

FIG 23.7

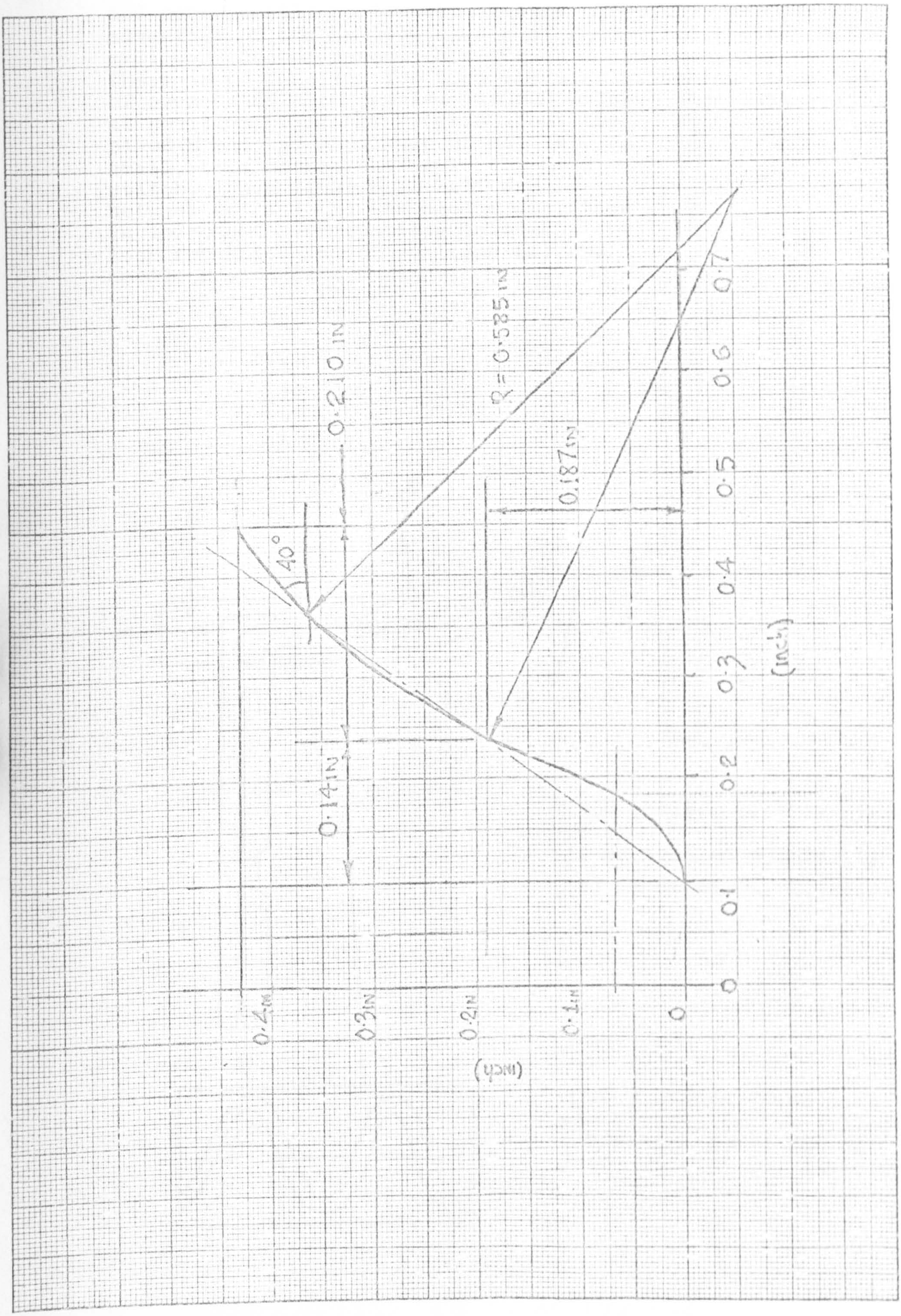

0·585 IN SINE · CIRCULAR CAM.

FIG 23.8

When a needle passes through a closed sine curved cam track there is no sudden changes in needle acceleration and consequently no impact. A sine curve also has the advantage of the maximum number of feeds distributed on the cylinder circumference. However, on a continuous closed track there is no facility for tuck and miss stitches. A method of overcoming this problem is shown below. When link A is at position (b) link K rotates about the pivot E and the amplitude of needle D is small, this corresponding to the miss stitch. When pivot E is half way between (a) and (b) the needle amplitude is increased corresponding to tuck loop formation and at position (a) the needle motion is a maximum.

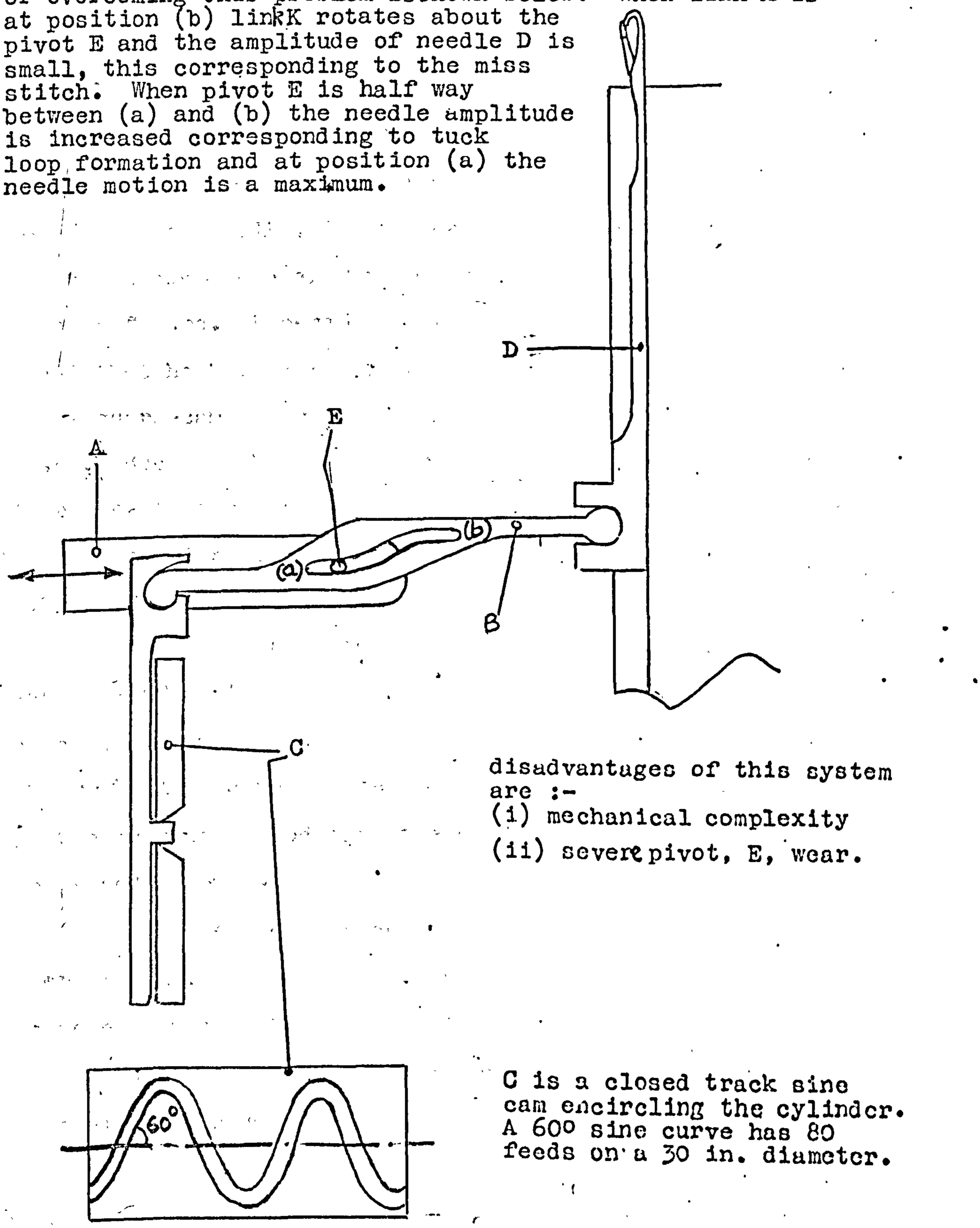

disadvantages of this system are :-
(i) mechanical complexity
(ii) severe pivot, E, wear.

C is a closed track sine cam encircling the cylinder. A 60° sine curve has 80 feeds on a 30 in. diameter.

A 60° CONTINUOUS SINE CURVED CAM TRACK WITH TUCK AND MISS-STITCH FACILITY

FIG 23.9

CHAPTER 24

NEEDLE AND TRICK DESIGN

24.1 Introduction.

The work, aimed at determining the effect of the impact upon the needle structure and wave propagation process in the needle, is uncompleted at the time of submitting the thesis; however further work will be carried out in the near future. Experiments, detailed in chapter 19, proved that hook failure was directly related to the magnitude of the guard-cam impact, and butt-failure to the stitch-cam impact. Much can be done towards reducing this impact by alteration to the needle design, and this is discussed more fully in section 24.2.

24.2 Needle Design.

The mass of the needle has a large effect upon the magnitude of stitch and guard-cam impact. If the mass is reduced, the impact, especially on the guard-cam can be substantially reduced, see sections 16.9 and 14.5.3. There are two methods of reducing the needle mass and these are summarised below :-

(i) Needle mass can be reduced by using lighter material. Approaches were made to Imperial Metal Industries Limited concerning the use of a low mass, but high strength Titanium alloy. After consultation they considered that a Titanium alloy might be used, but the wear resistance could be a problem and some form of surface coating would be necessary. As to the practical aspects, i.e. whether the needle could indeed be made in Titanium and the likely cost, more consultation would be necessary with the needle manufacturers. However, from mass considerations alone,

Titanium, with a density approximately a half that of steel could substantially reduce guard-cam, stitch-cam and latch impact.

(ii) The impacts can be reduced if the amount of material used in the needle construction is minimised, as shown by the needle designs in Fig 24.1.

In section 9.8.2, it was shown that, when the old loop (as defined in Fig 9.8) nears the top of the needle, the high yarn tension is relieved by casting off a loop from the adjacent needle which is one verge pitch (0.058 in.) further advanced into the loop drawing process. Consequently, there seems to be no practical restriction to increasing the needle section near the top of the needle, other than the possibility of manufacturing difficulties; further more, and as detailed in section 19.2.1, the incidence of hook fracture decreases when the cross-sectional area of the needle hook is increased.

Combined with the increased hook section, the tentative idea for a needle drawing a small yarn loop, Fig 10.1, and the latch designed to reduce impact, Fig 17.5, are combined in Fig 24.2.

24.3 <u>Needle Design to Reduce the Effect of the Impact.</u>

Petrow[33] to 27 inc used wedges to reduce the amplitude of the stress wave propagated up the needle shank. A diagram of his modified Groz-Beckert needle is shown in Fig 2.2, and analysis of the wedge section is given in section 19.1.1. Experiments, as detailed in chapter 19, investigated the effects of wedge terminations, and the results indicated that, instead of failure occurring across the hook, it occurred across the shank originating from the sharp corner of the wedge cut-out. Obviously, the wedges

would need to be designed very carefully to eliminate high stress concentrations at the corners.

The dynamic photoelastic technique is at an early stage of development at the moment, but it is hoped that, in the near future, the wave propagation process will be studied by this method and that, ultimately, a technique will be evolved to test model needles under realistic conditions; modifications could then be made before improved commercial needles are tooled up for mass-production.

24.4 Trick Design.

Stitch-cam impact is high if the needle is tight in its trick, and guard cam-impact is high if the needle is free in its trick. It is difficult to control the trick properties, and inevitably after a period of normal operation there will be a large variation in the trick's resistance to motion. For a high machine speed, both very free and very stiff tricks should be avoided, and frequent checks of the condition of the tricks should be made.

A high speed machine will undoubtedly have a cooling problem, and probably also a noise problem. The oil, of low viscosity to minimise the viscous drag at high machine speed, could be used to dissipate the heat, to reduce any guard cam impact (see section 16.8), and to limit the extent of the bounce (see section 12.3.2). Another method of cooling might be to use a refrigerated water jacket fitted inside the cylinder. The noise problem might not be severe if the cams and needles were to be designed properly so that the impacts are minimised, and if careful consideration be given to bearing design.

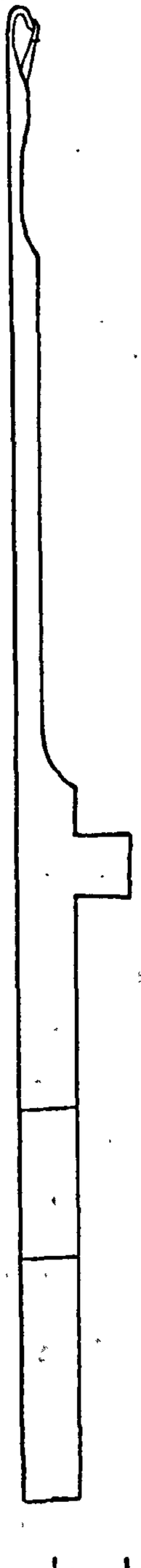

Standard
0·443mm
Needle
Steel

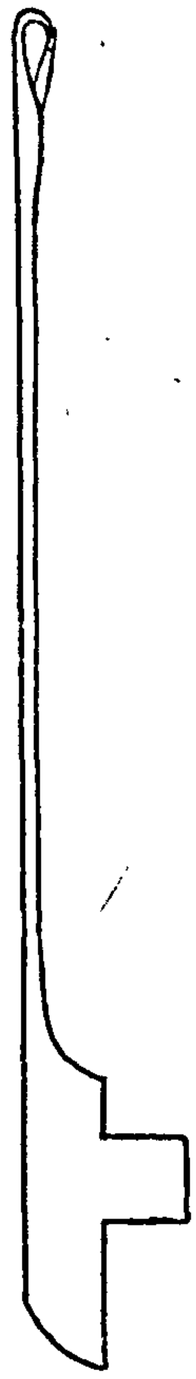

Reduced
Mass
Titanium
Alloy

If possible
raise butt
as high as
possible
Titanium
Alloy.

LOW MASS NEEDLES.

FIG 24.1

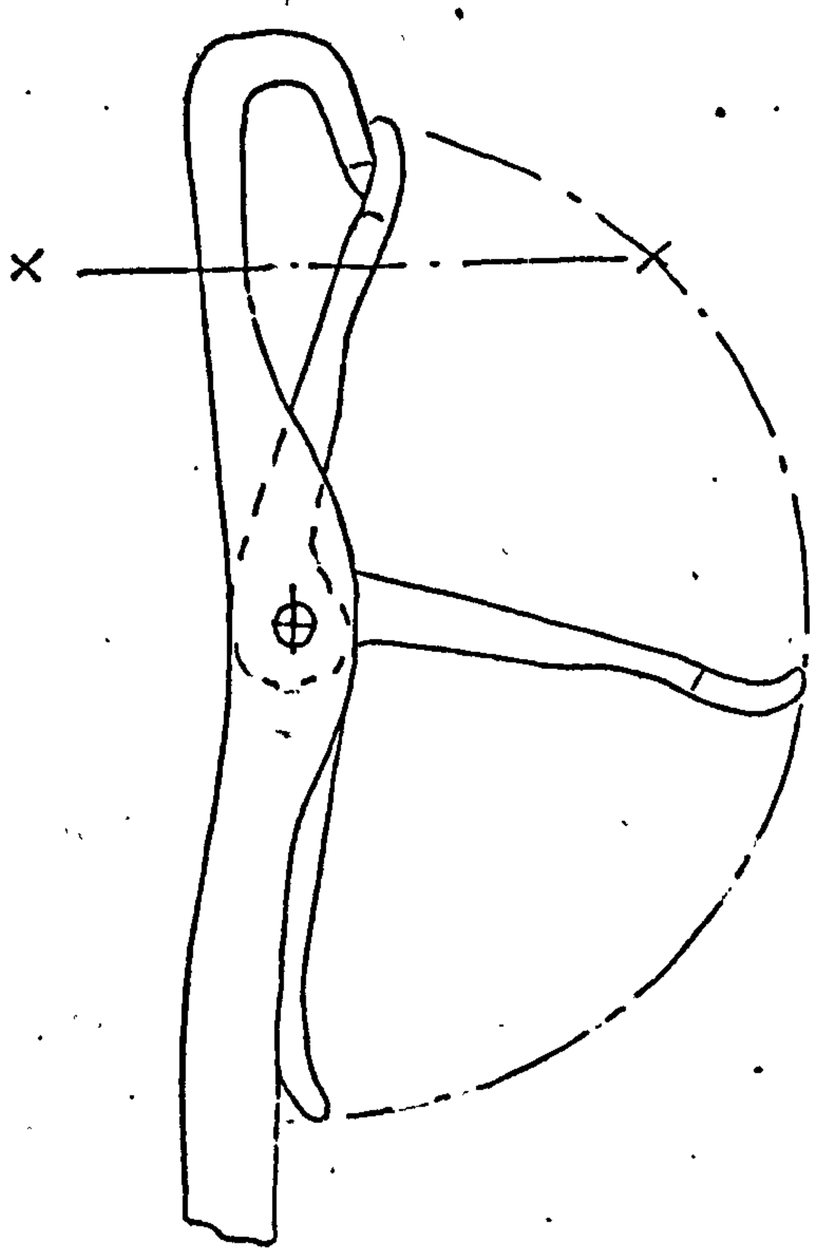

Section X-X
yarn expansion
controlled to
rob yarn from cast-off
loop at one needle-pitch
further into the loop drawing
process.

Needle head
Swan necked to :-

① Reduce yarn stretch
as old loop passes
over head.

② Decrease latch-length.

③ Remove taper above
pivot (as much as possible)

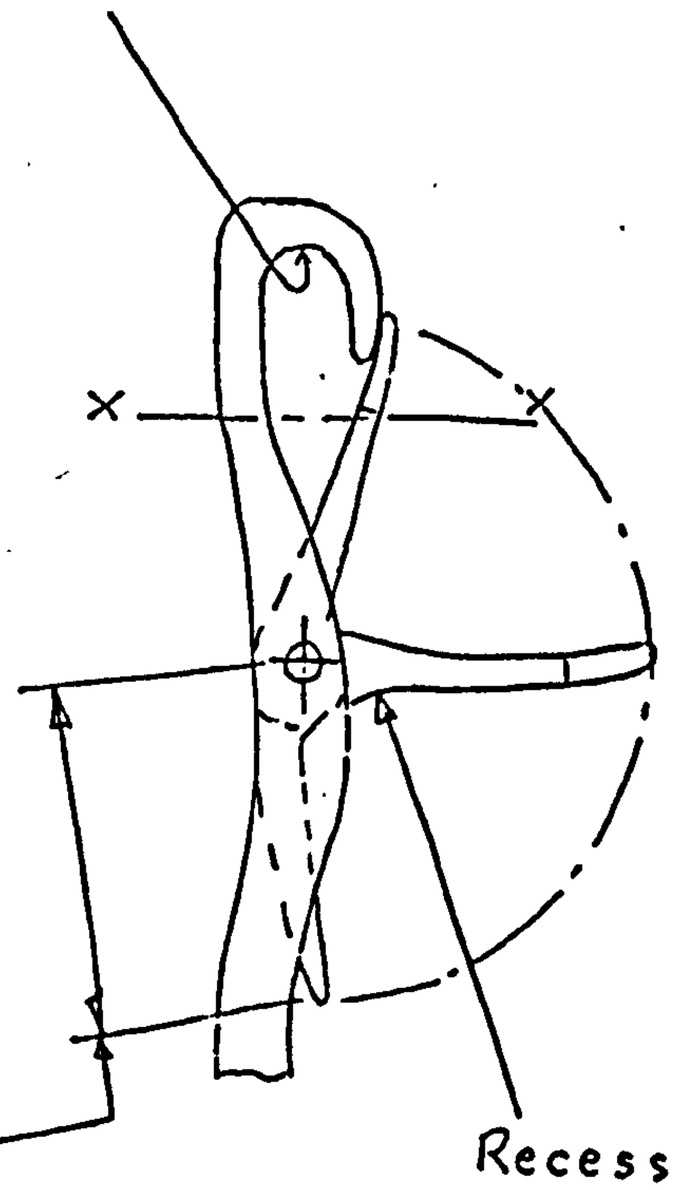

Needle Head
Design

Fig 24.2

CHAPTER 25

COMPENDIUM OF THE WHOLE INVESTIGATION

25.1 Summary of the Work and General Conclusions.

Because the investigation has been described under six distinct parts in this Thesis, each with its own conclusions section, it has been considered advisable to state as a brief summary the following resumé of the most important experimental findings :-

1) When the cam-needle impact point was moved radially away from the cylinder the cam-needle force increased. (Sections 4.6.4 and 8.5.6).

2) As stitch-draw was increased, the yarn-force and cam-force increases non-linearly in the region where the new loop was being drawn, e.g. when the stitch-draw increased from 0.0668 in. to 0.1077 in., the cam-force increased from 180 gf to 540 gf, and the yarn-force 140 gf to 300 gf. (Section 8.5.1).

3) During casting-off the old yarn loop, it has to stretch considerably in order to pass over the needle head; consquently the cam-force is high. (Section 8.5.1).

4) As the input yarn tension is increased the peak vertical cam-force and yarn-force increased, e.g. changing the tension from 1.5 gf to 5.5 gf the peak vertical cam-force increased from 90 gf to 160 gf, while the yarn-force increased from 50 gf to 118 gf. (Section 8.5.2).

5) Increasing the fabric take down tension increases the yarn-force, e.g. changing the total fabric load from 1,477 gf to 3,757 gf increases the force from 69 gf to 83 gf. (Section 8.5.3).

6) When the needle and trick were soaked in oil

the cam-force increased with the machine speed,. e.g. at 35 ft/min, after heavy oiling, the force was 100 gf approx., and it increased to 200 gf when the speed was 180 ft/min. For only slight oiling, the cam-force does not change with machine speed.(Section 8.5.4 and 8.5.9).

7) When the needle width was increased from 0.0155 in. to 0.0178 in., the maximum vertical non-knitting cam-force rose from 56.5 gf to 141 gf. (Section 8.5.5).

8) When the latch resistance to motion is increased the cam-force also increases.(Section 8.5.7).

9) Very wide variations in the force level were noted when a needle was transfered from one trick to another. (Section 8.5.8).

10) The frictional tension increase over the square section verge top was large, but was considerably reduced when the verge tops were rounded.(Sections 9.4.2 and 9.4.3).

11) Stitch cam impact was measured at the instant of stitch-cam needle contact. A primary impact occurred, whereupon the needle lost contact and a secondary impact occurred when contact was re-established with the cam. (Chapters 12,13 and 14).

12) A high frequency guard cam impact occurred when the needle "fired-off" the stitch-cam and collided with the guard-cam. (Chapters 15 and 16).

13) As machine speed increases, the magnitude of stitch-cam and guard cam impacts also increase e.g. when a 0.443 needle hits a 60^{o} stitch-cam, the peak horizontal stitch-cam impact increasd from 600 gf to 8,750 gf when the machine speed increased from 100 ft/min to 400 ft/min, similarly when the needle "fires off" a 52^{o} stitch-cam and impacted an 8^{o} guard-cam, the force magnitude increased

from 440 gf at 100 ft/min speed to 2110 gf at 300 ft/min. (Sections 16.3 and 14.4.2).

14) The yarn-loop held around the needle shank at the instant of stitch-cam impact had very little effect upon this impact. The yarn tension acting on the needle during loop formation, reduced the guard-cam impact force. (Section 18.2.3).

15) The needle mass had a large effect upon both impacts; if the mass was reduced by one-half, the stitch cam and guard cam impact all decreased by more than one-half, depending upon the trick resistance to needle motion. (Sections 14.5.3 and 16.9).

16) Oil has a negligible effect upon primary stitch-cam impact but shortens the bounce time and decays the impact oscillation. (Section 12.3.2). A heavy addition of oil reduced guard-cam impact, e.g. at 200 ft/min the impact decreased from 1,470 gf to 1,280 gf after a heavy application of oil. (Section 16.8).

17) The trick resistance to needle motion had a large effect upon the impact forces. When the resistance increased, the stitch cam impact also increased but the guard cam impact decreased. (Sections 14.5.4, 16.3 and 16.7).

18) Small changes in the cam-cylinder clearance, e.g. from 0.006 in. to 0.015 in., have very little effect upon stitch-cam impact; however guard-cam impact decreased by a small amount. (Sections 14.5.4 and 16.6).

19) Many severe modifications were made to the butt design of a selected range of needles but none of the modifications showed significant reductions in either stitch-cam or guard-cam impact. (Sections 14.5.1 and 16.7).

20) Fine horizontal marks at the base of the stitch-

cam led to very irregular impact force results at high machine speed.(Section 16.7).

21) Hook fracture was closely dependent upon the magnitude of guard cam impact. A major parameter influencing the breakage rate was the tightness of the needle in the trick and, as it decreased, the fracture rate increased. (Section 19.2, item (i)).

22) Butt fracture was influenced by the magnitude of stitch cam impact. A major parameter influencing the breakage rate was the tightness of the needle in the trick, and as it increased the fracture rate also increased, (Section 19.2.1., item (vii)).

23) The hook failure rate depended greatly upon the hook sectional area; if this area was reduced the fracture rate increased.(Section 19.2., items (i) and (iv)).

24) If the area of any part of the needle was reduced to comparable dimensions of the hook, then breakage usually occurred across the area reduction instead of at the hook.(Section 19.2.1., item (v)).

25) A needle was manufactured with seven wedge cut-outs designed to reduce the amplitude of the stress-wave transmitted up to the needle hook. Subsequent experiments were inconclusive, but they demonstrated that the corners of the wedges must be carefully designed to avoid stress concentrations.(Section 19.2.1., item (vi)).

26) Butt fracture also occurred as a result of guard-cam impact, but the incidence of fracture was substantially reduced when a light smear of oil was applied to the guard-cam surface.(Section 19.2.1., item (iii)).

27) Strain gauges bonded to the needle shank

responded to a longitudinal component of strain; a large sharp compressive pulse was evident at the instant of guard cam impact and this became more prominent at machine speed was increased. (Section 20.7).

28) Strain gauges bonded to the needle shank registered high frequency bending strain at the instant of guard cam impact.(Section 20.7.1).

29) Strain gauges mounted close to the needle hook indicated an equal distribution of compressive and tensile strain following both stitch-cam and guard cam-impacts. (Section 20.8).

30) Following the guard-cam impact, the strain-gauge mounted close to the needle hook registered a large number of tensile to compressive stress reversals.(Section 20.8).

Apart from the above-mentioned experimental findings, a major part of the work has been the development of the various instruments used for such findings, and these are also intended for further work. This is all described in chapters 4,5,6,13 and 15.

Moreover, various theoretical analyses were derived at each particular stage of the experimentation, and as occasion demanded, these were modified in line with the experimental findings. The major sections of the thesis containing such analyses are chapter 9 and sections 12.2 and 15.2.

25.2 Further Recommendations for Good-Quality Fabric Production at High Machine Speeds.

The prospect of a high-speed knitting machine with a much higher production rate than present-day conventional machines may have some disadvantages from the manufacturer's

point of view, because one machine might effectively replace two or three conventional machines. However, this research has shown that a great deal can be done to the knitting elements to facilitate higher machine speeds. A considerable amount of high quality research is being undertaken into the topic in various parts of the world, it seems only a matter of time before somebody somewhere manufactures an economical high-speed machine producing good quality fabric.

This project has been fundamentally concerned with an investigation of the forces involved in knitting, and the control of knitting elements. However, before high-speed machines can be successfully designed, there are other problems that must be solved; some of these exist on conventional machinery, but others are likely to be a direct result of higher machine speeds. A summary of these is presented below :-

(i) Bearings :- The design of the bearings is important especially at high speed. Further information concerning bearing design is contained in Black's thesis[29].

(ii) Cooling :- A knitting machine will generate considerable heat at high speed. It is debatable just what effect high temperature will have upon the knitting process; but some control might be necessary to protect both the operator and the fabric.

(iii) Yarn-Supply :- The yarn-supply system must be capable of providing low tension yarn to the knitting elements at higher machine speeds.

(iv) Noise :- The noise emitted by a high-speed machine must be within statutory noise limits..

(v) Take-down Tension :- It is important that a

constant take-down tension device be used on a high-speed machine.

(vi) Oil :- At high machine speed, a low-viscosity oil supply should be applied at a uniform rate all round the cylinder.

25.3 The Scope and Usefulness of the Specialised Instruments Developed for the Investigation.

The instruments developed, during the course of this work, were capable of recording the knitting force between (i) the cams and needles, (ii) the bounce, (iii) the force exerted by the yarn upon the needle during knitting, and (iv) the impacts. All the experiments were carried out on the 10 in. diameter knitting machine shown in Fig 3.1. Although the theory derived during this work can be used for any cam-needle system, further measurements ought to be carried out on more typical commercial machinery, to determine the effects of delayed and synchrosised timing, different stitch formations, etc. Fortunately, the instrumentation can be used as the basis for further design of measuring suitable for such commercial machinery and the circuitry developed in this project can be used without basic modification on any machine.

For measurements on a cylinder-and-dial machine, an instrument similar to the transducer Mark II (shown in Fig 5.1) could be used. A yarn force transducer, of the type shown in Fig 6.1, would be difficult to fit to a commercial machine; the cantilever principle could not be used because there are no verges on a cylinder and dial machine since the cylinder yarn loop is formed over the dial needle shank. The results in section 9.8.1 shows that, under particular circumstances,

i.e. low trick resistance, and very little oil, the cam-force transducer can be used to measure the yarn-force.

25.3.1 Possible Improvement in the Instrument System.

A few particular improvements can be made to the design of the cam-force transducer Mark II as follows :-

(i) The beam natural frequency could be increased from approximately 2,000 Hz to 6,000 Hz; this will reduce the natural frequency oscillation and should remove the need for the filter circuits shown in Fig 5.5. The strain sensitivity using semi-conductor strain-gauges would still be adequate for detailed measurements.

(ii) The beam could be manufactured from Aluminum and in one piece as discussed in section 10.3.

Some worthwile improvements could be made in the yarn input tension measuring system. The Rothschild measuring head was too large to fit in the confined area where the yarn enters the needle. The final yarn guide, shown in Fig 7.2, had to be modified in order to facilitate measurements, and there is a need for a very small measuring head, no longer than 0.125 in. wide. A system using semi-conductor strain gauges is in the process of manufacture at the time of submission of this thesis. One of the amplifiers of the cam-force transducer will be used, in conjunction with the circuitry shown in Fig 4.5.

25.4 Future Work.

In the near future, measurements using techniques established in this thesis will be obtained from instruments mounted on a commercial cylinder-and -dial machine. The theories derived in this work could be further investigated together with needle and cam modifications under realistic practical conditions. Measurements on commercial machines

will additionally provide information on cylinder and dial timing relationships, and the effects of complex stitch formations. The cams detailed in chapter 23, and any subsequent re-designed needle, will be tested on cylinder and dial machines under industrial conditions.

A considerable amount of experimental work is to be carried out using the dynamic photoelastic technique, and it is hoped that the technique will be capable of providing detailed information enabling a needle to be designed to suit both dynamic loading and knitting conditions.

Work is to be carried out on the rig shown in Fig 3.1 to measure the frictional properties of a wide range of knitting yarns. The transducers constructed during the course of this work will then be used to measure the knitting forces under a wide range of conditions for each yarn type.